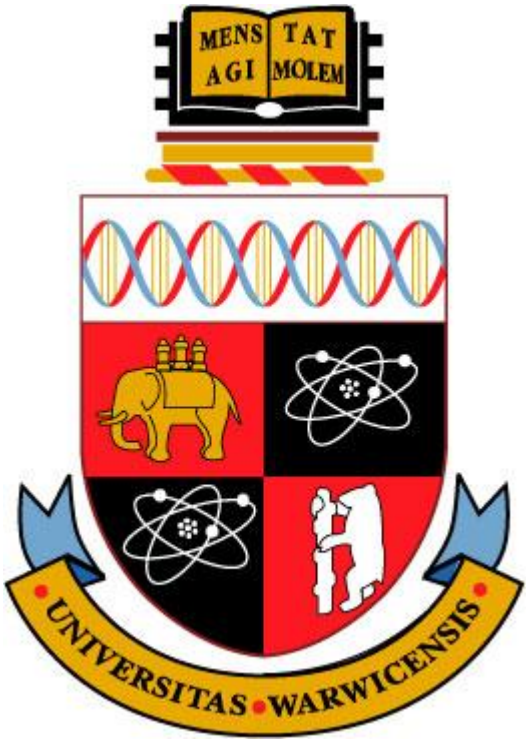

An Investigation into the Effects of Hybrid Electric Vehicle Power-trains on Ride and Handling

By

Matthew Bastin

A thesis submitted in partial fulfilment of the requirements for the degree of

Doctor of Philosophy in Engineering

University of Warwick, School of Engineering

November 2014

Table of Contents

Table of Figures

Table of Tables

Acknowledgements

I would firstly like to thank my supervisor Dr R Peter Jones, whose knowledge, guidance and help throughout this work were second to none, and proved invaluable. Further to the professional support provided I would also like to extend my most grateful thanks to him, in helping me find a role within WMG, without the financial support of which I would not have been able to complete this study.

I am grateful to all in the Embedded Systems Group in WMG, who provided me with a place to work and the facilities and equipment to conduct my research.

To my wife Kornelia, I would like to say dziękuję bardzo (thank you very much), as it was you who persuaded me to apply to Warwick, to conduct my Ph.D. in the first place, and without your continued encouragement, support (emotional and financial) and patience, the completion of this study would have not been possible.

I would also like to extend my gratitude to my parents Dave and Christine, who have always given me great encouragement and support throughout all of my studies.

Finally I would like to thank the School of Engineering for allowing me to conduct this study, and providing me with the financial benefit of a bursary to cover my tuition fees, and to everyone else within the school, both academic and administrative who have helped and encouraged me in some way over the last few years, thank you.

Declaration

I confirm that the work contained in this thesis is my own work, data and texts that have been taken from other sources have been referenced. Furthermore the material presented here has not been submitted for a degree at any other University.

Material within this thesis has been presented and discussed at conferences and as such are listed below.

1. Bastin, M. Shah, M. Cheng, C. Jones, R, P. 2011. Physical modelling of vehicle systems dynamics for drivability and handling studies. Vehicle Dynamics and Control 2011. Cambridge University.

2. Bastin, M. Jones, R, P. 2013. The effects on ride and handling due to modified mass distribution arising in hybrid electric vehicles. Vehicle Dynamics and Control 2013. Cambridge University.

Summary

Hybrid electric vehicles are becoming increasingly common within the automotive market. Whilst there have been a large number of studies investigating hybrid electric vehicle drive-train control, for efficiency and active safety purposes, there is little work reflecting the effects of such technologies on pure vehicle dynamics.

This thesis investigates the effects of hybrid drive-trains on vehicle ride and handling. A specific case study based on the hybridisation of a conventionally powered vehicle into a series hybrid electric vehicle is utilised as a means of doing so.

In order to investigate the effects of the hybrid drive-train components on the vehicle's ride and handling responses, detailed multibody models of both the Standard Vehicle (SV) and the hybrid General Technology Vehicle (GTV) were produced. As work was conducted in parallel with the Low Carbon Vehicle Technology Project (LCVTP), these models were created in a modular and physical fashion, as to allow for their easy parameterisation and adaption into other hybrid vehicle architectures. Prior to detailed investigation the standard vehicle model was successfully validated against real world test data collected as part of this work.

Model responses for both the standard and hybrid vehicle models were investigated and analysed in the ride and handling domain.

Ride analysis focused on statistical investigation of contact patch load and occupant comfort levels inside the vehicle. It was shown that there was a higher comfort region within both vehicles around the Cog and spring centre, as these two

vehicle parameters moved with changes that were made to the GTV, the occupants within were subjected to different comfort levels. As the weight shifted rearwards in the GTV, occupants seated at the front were subjected to higher levels of discomfort, however those in the rear actually saw a slight increase in comfort levels. Levels of vertical acceleration within the GTV were found to generally be slightly larger, resulting from increased pitch and bounce motions due to an increase in coupling between these modes. Furthermore levels of low speed damping on the GTV were shown to be incorrect for its new mass parameters, which led to a further deterioration in ride quality.

The handling analysis took on a novel form of investigating trends in specific handling metrics over the entire vehicle operating range. Said trends were then investigated further through more detailed model outputs. The GTV was shown to have a lower understeer gradient than the SV, due to the rearward shift in mass distribution and stiffer rear suspension. Transient handling responses were shown to be quite speed and manoeuvre specific, but all differences between the two vehicles could be explained by the differences in their dynamic indices and understeer gradients. Lateral acceleration response times were governed by the dynamic index and were always slower for the GTV, the magnitude of these responses were speed dependant, below the GTV's tangent speed they were smaller than the SV's, however above this speed they were larger. Yaw rate responses were more mixed, but were also seen to be governed by the dynamics index, at lower speeds or during simple unidirectional manoeuvres the GTV could obtain large faster yaw rates than the SV, during a transient to transient manoeuvre the GTV's yaw rate responses were generally smaller, this was seen to be due to the way in which a higher dynamic

index effects rear tyre slip angle generation having a larger effect at low speeds but a smaller effect when large slip angles are already present at the rear tyres.

The results obtained have given a clear picture of how the inclusion of hybrid drive-trains can affect vehicle ride and handling. Something that was re-enforced by the results being generalised and applied to a few types of hybrid vehicle architecture in order to make recommendations on layout/packaging of these vehicles and highlight areas of importance for future hybrid vehicle design in terms of ride and handling.

Abbreviations

2WD	Two Wheel Drive
4WD	Four Wheel Drive
ABS	Anti-lock Braking System
ARB	Anti Roll Bar
CAD	Computer Aided Design
Cog	Centre of gravity
Cop	Centre of Percussion
DC	Direct Current
DI	Dynamic Index
DOF	Degree of Freedom
DYC	Direct Yaw Moment Control
ECU	Electronic Control Unit
EGR	Exhaust Gas Recirculation
EM	Electric Motor
EMF	Electromotive Force
ESC	Electronic Stability Control
EV	Electric Vehicle
FCEV	Fuel Cell Electric Vehicle
FE	Finite Element
FWD	Front Wheel Drive
g	Acceleration expressed in gravitational units
GUI	Graphical User Interface
GTV	General Technology Vehicle

HEV	Hybrid Electric Vehicle
High g	High lateral acceleration
HMI	Human Machine Interface
ICE	Internal Combustion Engine
IM	Inductance Motor
K&C	Kinematics and Compliance
KPI	Kingpin Inclination
LCVTP	Low Carbon Vehicle Technology Project
LHS	Left Hand Side
Low g	Low lateral acceleration
OEM	Original Equipment Manufacturer
PHEV	Parallel Hybrid Electric Vehicle
PI-HEV	Plug-in Hybrid Electric Vehicle
PMM	Permanent Magnet Motor
REEV	Range Extended Electric Vehicle
RGB	Regenerative Braking
RHS	Right Hand Side
RSD	Roll Stiffness Distribution (% Front)
SHEV	Series Hybrid Electric Vehicle
SOC	State of Charge
SPHEV	Series Parallel Hybrid Electric Vehicle
SRM	Switched Reluctance Motor
SV	Standard Vehicle
TCS	Traction Control System
USG	Understeer Gradient

Notation

α_f	[rad]	Front tyre slip angle
α_r	[rad]	Rear tyre slip angle
a	[m]	Distance between front axle centreline and Cog
β	[rad]	Body slip angle at Cog
b	[m]	Distance between rear axle centreline and Cog
c	[m]	Distance between spring centre and Cog
c_f	[N/rad]	Front axle cornering stiffness
c_r	[N/rad]	Rear axle cornering stiffness
δ	[rad]	Steer angle at road wheels
d_t	[s]	Delta time
e	[m]	Distance between pitch centre and Cog
f	[m]	Distance between bounce centre and Cog
F_{Hz}	[Hz]	Ride frequency of sprung mass on front springs
F_{yf}	[N]	Lateral force at front axle
F_{yr}	[N]	Lateral force at rear axle
g	[g]	Acceleration due to gravity
I_{xx}	[Kg.m2]	Moment of inertia about x-axis
I_{yy}	[Kg.m2]	Moment of inertia about y-axis
I_{zz}	[Kg.m2]	Moment of inertia about z-axis
K_{cog}	[N/m]	Linear rate at Cog
K_f	[N/m]	Front spring rate
K_o	[N/m]	Linear rate at spring centre

K_r	[N/m]	Rear Spring rate
K_{tcog}	[Nm/rad]	Torsional rate at Cog
K_{to}	[Nm/rad]	Torsional rate at spring centre
l	[m]	Wheelbase
m	[Kg]	Mass
m_s	[Kg]	Sprung mass
P	[m]	Distance between centre of percussion and Cog
P_f	[s]	Period of sprung mass oscillating on front springs
P_r	[s]	Period of sprung mass oscillating on rear springs
R_{Hz}	[Hz]	Ride frequency of sprung mass on rear springs
r	[rad/s]	Yaw rate
$\dot{r}$	[rad/s^2]	Yaw acceleration
R	[m]	Turn radius
ω	[rad/s]	Natural frequency about pitch and/or bounce centres
v	[m/s]	Vehicle velocity
v_x	[m/s]	Vehicle velocity x axis component
v_y	[m/s]	Vehicle velocity y axis component
Ψ	[rad]	Yaw Angle

N.B Units above used unless otherwise stated in text.

Chapter 1 Introduction

Since the beginning of the 20th century automotive engineers have worked towards creating safer, more comfortable and more efficient transport (Gillespie, 1992). It was in the first half of this century that the foundations of vehicle dynamics were laid by the engineers within large automotive companies and research labs of the time, Ford, Rolls Royce, GM and Cornel Aeronautical Laboratory (CAL) to name a few (Genta, 2006, Olley et al., 2002, Milliken and Milliken, 1995). The concepts and techniques developed during this time remain largely unchanged and are still used throughout the automotive industry today. Despite this, since the early 1900's there have been huge steps made in all areas of technology relating to road vehicles, from, the move from mechanical to electrical control of fuel injection systems to the introduction of active safety systems. All the advancements are too numerous to mention. The latest step forward, which has become present in the last decade is the electrification of vehicle power-trains. Electric and hybrid electric vehicles are the next evolutionary step of the automobile. Whilst such vehicles may have been born out of the need to produce what are seen as cleaner and more efficient vehicles, the use of electric drive is proving to have many other advantages in terms of vehicle dynamics control strategies. But as with any new technology it needs to be investigated from a number of standpoints and not just viewed in one context.

1.1 Overview of Vehicle Dynamics of Hybrid Vehicles

Despite huge advances in technology leading vehicles of today to look a world away from vehicles of the early 20th century they are in effect extremely similar, not much

has really changed. Of course the internal combustion engine (ICE) has become more refined, more powerful, the human machine interface (HMI) has also become more advanced, there are electronics and control systems that cars of the early 1900's did not have, but in effect, the car of today is still very similar to those early vehicles. New vehicles are still driven by ICE's, there remains the same mechanical coupling systems between ICE and wheels, the ICE's are still in one of three locations (front, mid, rear) and the car still consists of the majority of components being sprung on top of the four wheels. It could be that car design has been stifled for the last 100 years by the constraint of the ICE, but with changes that are reverberating around the automotive industry of today this could all be set to change (Andreasson, 2007). With the increasing presence of electrical propulsion systems in new vehicles and the seemingly endless possibilities of vehicle power-train architectures that this brings, it could be quite conceivable that vehicles of the near future will be very different from current vehicles in terms of their construction and architecture. Such trends are already starting to be seen in concepts such as the GM Hy-Wire which has the entire hybrid power-train packaged very low on a flat floor, and the Siemens E-corner or Michelin Active wheel, which are self contained single point attachment wheel, electric motor (EM), suspension and braking systems (Andreasson, 2007, Bobier et al., 2008, Perry, 2004, Mitchell and Schmitt, 2007).

With such significant changes being made to vehicle architectures it is quite likely that equally significant changes will be seen in the vehicle's mass and inertia properties (Bobier et al., 2008, Beiker and Vachenauer, 2009). Vehicles such as the GM Autonomy concept car, shown in Figure 1-1, which has in wheel motors and integral suspension and braking systems (similar to the Siemens E-Corner), with other power-train components located within its flat floor (skateboard) chassis are a

clear example of this (Automotive Intelligence, 2003). With the use of components like the E-Corner un-sprung mass is likely to be larger, suspension geometry and the associated characteristics will be completely different to current vehicles and sprung mass and inertia properties are likely to lie outside of what is currently considered a normal range. Such changes are certain to have ramifications on the vehicle's ride and handling characteristics. Even with the acknowledgment that the GM Autonomy concept is an extreme case, consideration of more conventional hybrids still yields the same hypothesis. A series hybrid electric vehicle (SHEV) based on a conventional vehicle still needs to house additional hybrid power-train components, EM's, power electronics, and large battery packs need to be packaged somewhere within the vehicle. The inclusion of such components will have an effect on the vehicle's mass and inertia properties which will subsequently affect its ride and handling characteristics. Furthermore it should not be overlooked that the energy transfer path through such vehicles is also now considerably different. The aforementioned GM concept car and the SHEV that were just considered are now driven by electric motors and have hugely different power-trains to conventional vehicles, this will also likely lead to large differences in the vehicles' driveability (Crolla et al., 2008, Shah, 2013).

Further to the passive effects of hybrid systems on vehicle dynamics are the ways in which such systems can be used to actively control vehicle dynamics. The high torque capability coupled with the ease of control of EM's means that they lend themselves to being utilised in vehicle stability control systems. Certain hybrid architectures have the ability to control axles or even wheels independently, which of course opens up a world of possibilities for lateral response manipulation such as in

electronic stability control (ESC). There are numerous works currently being conducted in this area on varying types of hybrid architecture.

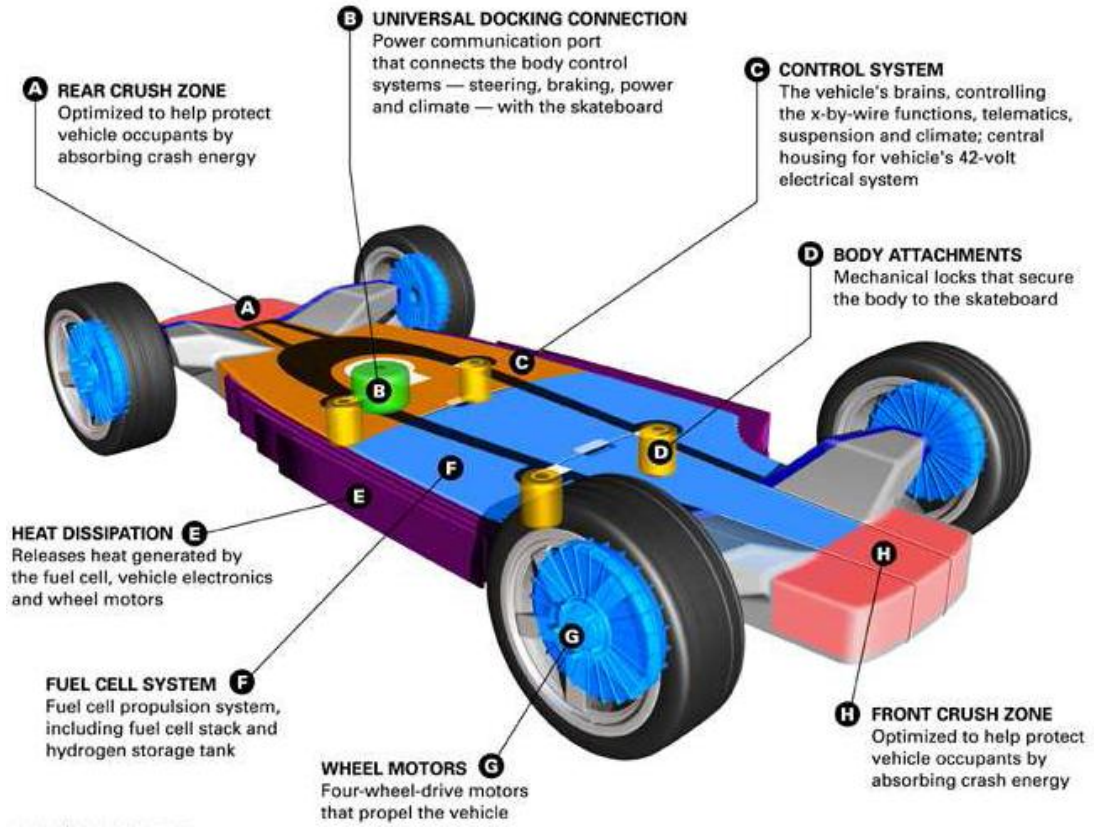

Figure 1-1 GM AUTOnomy Concept (Andreasson, 2007)

The use of electric propulsion, through the ability to implement bi-directional energy flow, also gives rise to the possibility of regenerative braking (RGB). Whilst regenerative braking is primarily an energy capture strategy it is also shown to have profound effects on vehicle handling. Assadian and Hancock (2006) showed that the presence of regenerative braking during a turn increased driver workload along with the ESC workload to maintain the desired heading. Beiker and Vachenauer (2009) considered the effects of regenerative braking on a number of hybrid vehicle configurations and concluded that regenerative braking can heavily effect lateral responses in brake and turn events, furthermore the control of such a system and its interaction with other control systems, such as ESC and Anti-Lock Braking Systems

(ABS) need to be carefully considered. Moreover it was also hypothesised by the authors that due to the difference in suspension anti-force angles, resulting from the use of two different braking systems, body motions could be affected which would alter driver perception, ride and handling.

1.2 Summary

The overview of vehicle dynamics of hybrid vehicles has highlighted a number of areas for further work within the field, these can be summarised as;

- Whilst a significant amount of research is being conducted on how electric and hybrid electric power-trains can capitalize on the use of EM's for handling and stability control, due to the number of possible architectures and implementations of such systems which has been opened up there is still scope for further investigation.
- Regenerative braking has been shown to effect vehicle handling and so the control over its use and its integration with other vehicle control systems in different hybrid architectures should be further considered.
- It is also hypothesised that regenerative braking can effect a vehicles ride and handling through how anti-forces will vary depending on which braking system is used (RGB or conventional), such changes effect force transfer through suspension springs and linkages and so is likely to affect body pitch motions which could affect driver perception as well as ride and handling.
- The increasing number of differing power-train components and their packaging within the vehicle will affect mass and inertia properties which will ultimately affect the vehicle's lateral and longitudinal capabilities along with its ride.

1.3 Research Objectives

The material outlined in the previous section illustrated that HEV's, due to the inclusion of new power-train components, and the differing architectures that are made possible by hybrid propulsion are likely to possess what can be considered atypical mass and inertia characteristics. Furthermore due to this, and the inclusion of different technological methods, such as regenerative braking, hybrid vehicles are likely to require special attention in relation to their vehicle dynamics properties.

What has become clear from this is that whilst hybrid power-trains bring increased fuel economy and the ability to improve vehicle handling and stability through control system approaches, consideration must be given to the effects of such systems on a vehicles passive vehicle dynamics properties.

From the areas that have been brought to attention here and in the previous section, it is appropriate that the research in this thesis will investigate the effects of hybrid power-trains on vehicle dynamics by consideration of how a vehicles mass and inertia properties are changed by the introduction of such hybrid power-train systems. Due to the large number of possible hybrid power-train architectures, and the broadness this brings to such a study, one specific case study will be focussed upon in order to conduct research of the required detail, findings can then of course be applied more generally to all hybrid architectures by making appropriate assumptions.

In conducting this research the following aims and objectives will be pursued;

1. Investigate areas where hybrid power-trains influence passive vehicle dynamics.
2. Based on a specific case study, create a modular flexible architecture multibody model, which can be utilised to investigate aim No.1. The

model should be created in a modular fashion to allow easy adaption of the model to extend it to other hybrid architectures and allow for addition of complexity for extension of this work.

3. Derive comprehensive data analysis techniques which will aid in the analysis of both ride and handling data across the entire vehicle operating range.
4. Utilise vehicle model(s) to investigate areas uncovered by aim No.1.
5. Based on the approach developed, outline specific areas where future hybrid vehicles may need attention in terms of their vehicle dynamics characteristics.

1.4 The Case Study

Due to the broadness in types and degrees of hybrid vehicle currently, and possibly available in the future, there was a need for this study to specify a type of vehicle to be used, in order to hone the scope and not allow the focus to become too broad.

It was decided that the case study to be utilised would be that of one of the development vehicles of the Low Carbon Vehicle Technology Project (LCVTP). Such a choice was made as this study was conducted closely with said project with interests of one of the industrial partners.

The vehicle under investigation in this study is a standard sports utility vehicle and its adaption into a range extended, series hybrid electric concept vehicle. This exact vehicle is utilised due to the specific interest of one of the industrial partners of the LCVTP, and also thereby easy access will be available to all required data. Whilst a more complete description of the vehicle will be given in chapter three, here it is useful to mention that the use of this vehicle for this study imposes certain

directions for the research, regardless of the scope defined by the literature review, these are;

- The study will focus solely on a range extended, series hybrid electric vehicle that is being developed as part of the LCVTP.
- Changes that are implemented on the real vehicle likewise need to be implemented in this study in the modelling domain in order for it to have inherent real world value.
- The effects of vehicle dynamics control systems, such as Electronic Stability Control (ESC) or Regenerative Braking (RGB) control will not be included as they are not present on the vehicle that is being developed. Whilst the standard vehicle does have an ESC system it is not possible to model it due to lack of data regarding the control model, to mitigate the effect of this not being included in the vehicle model, all testing for validation and subsequently all further analysis of the two vehicles will be conducted sub limit handling. Validation of the model below limit handling will ensure no interaction of the ESC, and further analysis of the two models will be kept in this validated range.
- This study focuses specifically on lateral and vertical dynamics of the vehicle. As there is no regenerative braking present on the vehicle braking events will not be considered. Longitudinal dynamics and driveability are the focus of another study conducted on the same vehicle by Shah (2013).

Such collaboration with the LCVTP has also placed certain restraints on the way in which parts of this work have to be conducted, perhaps the most significant of which relates to the modelling platform and modelling methodology used. One of the main focuses of the LCVTP was to investigate the adoption of the object

orientated, acausel, physical modelling facilitated by Dymola. Emphasis is to be placed on full use of Dymola's physical modelling capabilities to show how it can be used to simultaneously track real world development of the actual vehicle. Furthermore as one of the key targets for the LCVTP was to produce a generic, modular vehicle model that could be easily altered to represent different vehicle architectures and interface with a modular control system, it has been decided that the modelling conducted in this study should also follow this same approach. Such an approach will also allow the models developed within this study to be easily adapted/extended and/or interfaced with other models to represent other forms of hybrid vehicle and be used as a basis for further investigation into the dynamics of hybrid vehicles. One example of this is that the chassis models produced in this study could be easily combined with the compliant drive-train models created in the aforementioned study by Shah (2013).

1.5 Research Methodology

The aims and objectives laid out in the previous section will be achieved through modelling of the standard and hybrid vehicles, differences in the responses of the two vehicle models will be analysed in detail in both ride and handling domains.

Vehicle models constructed for this study, as mentioned, are done so in Dymola (DYnamic MOdelling LAboratory) using a mixture of the standard Modellica, Modelon Vehicle Dynamics, and Vehicle Interfaces libraries. The two vehicle models are of multibody type and consist of independent front and rear suspensions with linear springs and anti-roll bars, non-linear dampers and bushes, and Magic Formula tyre models. The suspension units are mounted to the chassis through a rigid subframe with non-linear mounting bushes. The chassis itself is rigid and has a detailed mass model. A simplified power-train model is included as a means of

realistically driving the vehicle model. The models are controlled via open loop inputs or via interfacing with a number of closed loop driver models. The two models are used to directly compare the differences in ride and handling responses of the two vehicles, during specifically designed manoeuvres.

Ride domain analysis will focus on occupant comfort levels arising from road unevenness. Statistical analysis is utilised to investigate forces and motions arising in the tyres and vehicle body. Occupant comfort levels are obtained through the utilisation of standards relating statistical data to comfort levels. The ultimate aim is to identify root causes of differences in ride characteristics of the two vehicles.

Handling domain analysis is formed of two main parts, firstly trends and differences in specific handling metrics between the two vehicles are identified, secondly these trends and differences are investigated through instigating directly the vehicle responses. The ultimate aim is to identify the root causes of differences in handling characteristics of the two vehicles.

1.6 Thesis Outline

Chapter two discusses the origin and need for hybrid vehicles along with their major design philosophy. Current works in the field of the vehicle dynamics of hybrid vehicles are discussed to give background and set the context for this thesis.

Chapter three discusses the specific vehicle modelling that has been conducted for this study. The model of the standard vehicle is developed and introduced, this model is then validated. Validation is carried out in two parts, the first is component based and uses model based test rigs to obtain Kinematics and Compliance (K&C) and chassis inertial parameters for comparison against real world data. The second part of the validation compares full vehicle model responses to those obtained from the real vehicle at a proving ground. Following this the alterations that are made to

the standard vehicle in order to produce the hybrid vehicle are introduced and discussed, these are then implemented to create the hybrid vehicle model. Finally an initial basic comparison of the differences between the two vehicle model responses is illustrated.

Chapter four introduces vehicle dynamics principles which illustrate the problem posed by hybrid vehicles. Detailed explanations of model and real world based tests are also given along with a discussion of the data analysis techniques to be used.

Chapter five is the first of the two results chapters, and concerns ride domain results. Model outputs from rough road inputs obtained over the entire vehicle speed range form the basis of discussion, with the analysis taking a statistical form. The force path from road input to occupant comfort is investigated by considering contact patch loads and body motions. Occupant comfort is rated based on defined industry standards. Conclusions which explain the differences in the two vehicles' ride characteristics are presented at the close.

Chapter six presents handling results. Initially steady state handling simulations are conducted based on a number of constant radii tests. Differences between the two vehicles' steady state steering responses are discussed and are used for construction of the dynamic handling simulations. The dynamic handling simulations comprise two manoeuvres, a ramp to step steer and a sinusoidal steer. Such manoeuvres are again conducted over the entire vehicle speed range. The presentation and analysis of the dynamic handling results has two parts, initially response metrics that were introduced in chapter four are investigated, trends in these results are then identified and consolidated, further investigation of these trends is conducted via direct comparison of the model outputs. Finally conclusions are

drawn that explain the differences in the two vehicles steady state and dynamic handling.

Chapter seven provides final conclusions. Conclusions from the two results chapters are consolidated and used to illustrate the overall changes in the vehicle ride and handling characteristics. The findings of this study are used to make general recommendations for future vehicles of how hybridisation can affect their ride and handling. The contribution made by this study is also given. Finally Opportunities for further work are presented.

Chapter 2 Review of Hybrid Electric Vehicles and Vehicle Dynamics

2.1 Introduction

The study of vehicle dynamics has been around almost as long as the wheel itself. Whilst the origins of the wheel cannot be certain it is thought to have come from southern Mesopotamia where evidence of wheels being used as far back as 3500 BC has been found (Genta, 2006). The wheel slowly diffused across the globe and as it did so it evolved. First of all the solid wheel became a spoked wheel, making it lighter and more efficient. Rigid spokes, in some places, were eventually upgraded to flexible spokes to improve comfort for the occupant/rider, and so it continued. Whilst these changes probably took centuries to conceive and now seem extremely primitive, they were in fact the beginning of vehicle dynamics. Clearly vehicle dynamics studies have come a long way since the inception of the wheel, but the basic principles are still the same, to make transport more efficient, more comfortable, safer and quicker. The foundations of modern vehicle dynamics were laid at the beginning of the 20th century with the invention of the pneumatic tyre and the beginning of private road vehicle mass production, and it was at this time that a lot of the principles that are still used today within the field of vehicle dynamics were developed.

It is important to remember that over a century of research and development has been conducted for us to arrive at where we are today. And so to develop new ideas and theories in the field of vehicle dynamics, it is important to appreciate and understand what has been done before. This chapter will investigate previous work

in related areas to this study which should aid in giving an overview of the field and setting the context for this thesis.

2.2 The Current State

In recent years the automotive industry has been the focus of much attention regarding world pollution levels and "global warming". It is estimated that road transport as a whole contributes 25% of Europe's total greenhouse gas emissions, making it the second largest contributor after the energy sector. Private road vehicles make the largest contribution to this and in terms of their carbon dioxide emissions make up 15% of the EU's total emissions (ECCC, 2012).

Emissions of nitrogen oxides (NOx), total hydrocarbons (THC), non-methane hydrocarbons (NMHC), carbon monoxide (CO) and particulate matter (PM) are regulated by European directives. The allowable levels of these in exhaust emissions has been reduced drastically over the past 20 years through the use of tightening legislation, and this trend looks likely to continue with the introduction of the latest Euro 6 directive due in 2014 (Jeuland and Ubrich, 2007). Carbon dioxide (CO2) emissions are not regulated by law, however there exists a voluntary agreement between European vehicle manufactures and the European commission that aims to reduce CO2 emissions from passenger cars sold within Europe. Current targets are for vehicle fleets to omit on average 130 g/Km of CO2 or less by 2015, this is down from 195 g/Km in 1995 when first agreements were launched (ACEA, 2004).

Table 2-1, shows emissions levels set out by the Euro directives, it can be seen that PM emissions in diesel engines have been reduced by 97% from Euro 1 to Euro 6, and CO emissions have likewise had to be reduced by 82%. Such reductions are set to continue through the use of legislation, however with vehicles becoming more efficient, diminishing returns in emissions improvements are obtained from

technological advancements and so vehicle manufacturers are putting more resources into searching for greener technologies.

Categories reference mass (RM)[a] (kg)	Carbon monoxide (CO) (mg/km)		Total hydrocarbons (THC) (mg/km)		Non-methane hydrocarbons (NMHCs) (mg/km)		Nitrogen oxides (NOx) (mg/km)		Combined mass (THC + NOx) (mg/km)		Particle mass (PM) (mg/km)		Number of particles/km	
	SI	CI	SI	CI	SI	CI	SI	CI	SI	CI	SI	CI	SI	CI
Euro 1 01.07.1992	2,720	2,720							970	970		140		
Euro 2[b] 01.01.1996	2,200	1,000							500	700		80		
Euro 3 01.01.2000	2,300	640	200				150	500		560		50		
Euro 4 01.01.2005	1,000	500	100				80	250		300		25		
Euro 5 01.09.2009	1,000	500	100		68		60	180		230	5.0	5.0		
Euro 5+ 01.09.2011	1,000	500	100		68		60	180		230	4.5	4.5		6.10^{11}
Euro 6 01.09.2014	1,000	500	100		68		60	80		170	4.5	4.5	c	6.10^{11}

SI Spark ignition (gasoline, LPG, Natural Gas).
CI Compression ignition (diesel).
a Effective dates for new vehicle types. For all types of vehicles: one year after the new types.
b Values for IDI engines (from 10.01.1999, DI engines must comply with IDI limits).
c Value to be determined before 2014 based on inter-laboratory testing.

Table 2-1 Euro directive emissions levels (Jeuland and Ubrich, 2007)

Whilst such emissions standards can be viewed as technologically neutral, meaning that vehicle manufacturers can implement technologies of their choosing to meet the required emissions levels, it must be seen that such restrictions force technologies in certain directions. Examples of this are the invention and usage of catalytic converters to enable vehicles to meet Euro 1 emissions levels (Jeuland and Ubrich, 2007), and similarly the inclusion of EGR valves to successfully reduce NOx emissions for diesel engines to meet Euro 4 emissions levels (Yu and Jing, 2011). Perhaps the increasing number of hybrid and hybrid electric vehicles that are being produced currently will be seen in the future as being conceived from Euro 6 legislation.

2.3 Hybrid Electric Vehicle History

In 1834, the first battery powered electric vehicle was born, it was a tricycle built by Thomas Davenport. The first vehicle to ever travel faster than 100 Km/h was also an

EV, it was called ‘Jamais Contente’ meaning ‘Never Satisfied’ and was driven by Camille Jenatzy in 1899 (Chau and Wong, 2002). However it was Dr Ferdinand Porsche who also in 1899 built the world’s first hybrid vehicle. It was the second car Porsche ever built and used an ICE to turn a generator which provided power to two motors located inside the front wheel hubs (Chan, 2007, HybridVehicleOrg, 2005).

At the first National Automobile show held in New York in 1900, a poll suggested that patrons favoured future vehicles to be powered firstly by electric and secondly by steam. Also in 1900 the Belgian car maker Pieper created the first form of a PHEV, where a small ICE was mounted coaxially with an electric motor which both charged batteries and drove the car when extra performance was needed. The patents from this vehicle were utilised by another Belgian car maker Auto-Mixte who commercially produced and sold the car from 1906-1912.

It was Henry Ford in 1904 who started the beginning of the end for hybrid vehicles of the time. Ford successfully managed to overcome the then flaws of the ICE powered vehicle, namely noise, vibration and odour. A production line creating Ford’s light, cheap and higher performance ICE powered vehicles was set up and saw the rapid decline of hybrid vehicles. Despite attempts by other car makers to re-introduce different forms of hybrid such as Woods and Leveland, who produced a hybrid which boasted a fuel economy of 48 mpg, they could not compete with the more powerful purely ICE powered vehicles.

Despite hybrid vehicles fading out of public view work continued to be done on hybrid vehicle design and technology, most notably GM researched and produced a number of electric and hybrid electric vehicles from 1916 all the way through to the present day. In what GM calls its search for better propulsion systems it researched

and developed vehicles ranging from hybrid adaptations of its normal cars and vans to buses and even military vehicles (Rajashekara, 1994).

In the mid 70's hybrid vehicles were given a small resurgence in the United States due to rapidly increasing fossil fuel prices, however very little commercial output was seen. It was in 1997 that the automotive industry began down its current route, as the Toyota Prius was put on sale in Japan, a year later it was available in the United States and Europe, this was followed by the release of the Honda insight and the Honda Civic hybrids (Chan, 2007, Kirsch, 2000, Rajashekara, 1994). The introduction of such vehicles marked a change in the types of vehicle being offered to the public, hybrid vehicles now included all the refinement and conveniences of modern vehicles, combined with the fiscal gains of increased fuel economy and tax breaks from owning a lower emission car (Gallaghera and Muehleggerb, 2011). Since the introduction of the Toyota Prius, more and more hybrid vehicles have emerged onto the market. World sales of hybrid vehicles continue to increase, and whether this is due to true consumer demand, or consumer demand that is being driven by the aforementioned financial benefits, introduced by governments and legislators as a need to address the issue of global warming, one cannot be certain. What is certain is that for the foreseeable future hybrid vehicles look set to become an even larger part of the world's automotive markets.

2.4 Hybrid Electric Vehicles (HEV's)

A hybrid electric vehicle is one in which propulsion energy is available from two or more kinds or types of energy stores, sources or converters, of which at least one delivers electrical energy (Chau and Wong, 2002, Hermance and Shinichi, 2006). Perhaps a more straightforward explanation is that a HEV is a combination of two power sources; one unidirectional based upon an internal combustion engine (ICE)

and the other bidirectional based on electrical energy storage systems and electric machines (Chen et al., 2009).

HEV's can be divided into three main categories defining hybrid architectures in use today; these are as follows; series, parallel and series-parallel (Lo, 2009).

2.4.1 Series Hybrid Electric Vehicles (SHEV's)

A series hybrid electric vehicle uses a conventional ICE to drive a generator which in turn creates electrical energy, this electrical energy is either stored in a set of batteries or if needed can be used to directly power the electric motor and drive the vehicle (Supplier Business LTD, 2008). In a SHEV there is no mechanical connection between the ICE and the wheels; it is used purely to drive the generator and create the electrical energy required to power the electric motor which in turn drives the vehicle. Due to this arrangement the SHEV has a simpler drive-train than other HEV's, and in some ways is easier to package. As the ICE doesnt drive the wheels directly, it could be located anywhere within the vehicle, however the need for a generator unit can make the assembly bulky (Bayindir et al., 2011). As the ICE has no mechanical connection to the wheels, theoretically it can be run at its optimal operating point constatntly, thus producing minimal emissions for the energy produced (Brown et al., 2002). One of the main disadvantages of a SHEV however is that the electrical components of the drive-train need to be sized for the maximum load conditions that will be imposed; for example a large enough generator and electric motor need to be installed to allow the vehicle to climb a long steep hill, as such operating conditions are not likely to be encounterd very often, the majority of the time the vehicle will be carrying larger than required components which is not optimal for efficiency (Chan, 2007).

Generally series hybrid configurations are found in buses, millitary vehicles and even locamotives, mainly as the size of these vehicles allows them to take advantage of the packaging options offered by such an architectire (Gao et al., 2005).

2.4.2 Parallel Hybrid Electric Vehicles (PHEV's)

A parallel hybrid electric vehicle again uses both an ICE and an electric motor, however in this architecture they are both capable of providing drive to the wheels, individually or simultaneously (Chan, 2007, Maggetto and Van Mierlo, 2000). This is achieved as the ICE and the electric motor are connected to the drive shaft of the wheels by clutches, gears, chains/belts or even directly via a solid axle, allowing them to be used as the power demand dictates. A PHEV can be run in a number of different modes, if the power demanded is higher than can be achieved by the ICE then the EM assists, if the power demanded is lower than the ICE output then the EM acts as a generator and recharges the batteries, depending on driving requirements they can also be run in pure electric or pure ICE mode (Gao et al., 2005, Chan, 2007).

As both power sources are connected to the wheels, component sizing is less of an issue compared with the SHEV as both sources can drive the vehicle, generally speaking both the ICE and EM can be smaller and be used together to produce the same performance as a larger ICE powered vehicle. The PHEV also does not need a generator unit like the SHEV so could prove easier to package in smaller vehicles. One major drawback of the PHEV is that due to the engine being coupled to the wheels it can't be run in such a narrow, efficient operating window as in the SHEV (Bayindir et al., 2011, Chau and Wong, 2002). Due to the PHEV architecture there are two distinct ways in which it can be implemented, the first being to downsize the ICE and supplement it with an EM, this can be thought of as an emissions reduction

approach. The second option is to not downsize the ICE and supplement it with an EM, this is termed a power hybrid, as the EM increases the performance of the vehicle, an example of this is the Toyota Highlander (Chan, 2007).

2.4.3 Series-Parallel Hybrid Electric Vehicles

A series-parallel hybrid, as the name suggests, is a mixture of both series and parallel hybrid vehicles. The power-train is more complicated than the other two variations as it comprises of two electric motors, an ICE and a planetary gear set. Its ability to run as either a SHEV or a PHEV is achieved through the use of the planetary gear set which allows one of the electric motors to connect to the planetary ring gear, the ICE to connect to a carrier gear in the centre and the second electric motor to connect to a sun gear (Chen et al., 2009). Using such a configuration allows the EM connected to the ring gear to be utilised with the ICE as a generator unit, its speed is adjusted to ensure that the engine is always operating at its most optimum speed. This part forms the series power flow route. If the ICE outputs more power than is needed then it is split, some being used to drive the vehicle and the rest used via the EM/generator to charge the batteries, the EM/generator can also be used to drive the vehicle with the ICE when the latter's output alone is not sufficient. The EM/generator unit can be locked and not powered and then the planetary gear set becomes a simple fixed ratio gearbox. The second EM works in parallel with the ICE and EM just mentioned to form the parallel power flow route (Gao et al., 2005).

The series-parallel hybrid poses advantages from both series and parallel hybrids in terms of emissions reduction, although it is a lot more complex and costly to produce, as well as being far more complex to control with a plethora of possible control strategies (Chau and Wong, 2002). Despite its cost and complexity the

SPHEV seems to be quickly becoming the standard in hybrid passenger vehicles (Bayindir et al., 2011, Emadi, 2005). The Toyota Prius is an example of a SPHEV.

2.4.4 Hybrid Vehicle Variants

Whilst the majority of hybrid vehicles on the market fit into the previous three categories, there are variants of each with subtle differences.

There are Fuel Cell Electric Vehicles FCEV's, these use hydrogen fuel cells as the electrical source to charge batteries and/or power EM's, such vehicles are thought to be in good stead for the future as they boast zero emissions, however they rely on the supply of hydrogen which currently is very energy intensive to obtain (Chan, 2007).

Micro hybrids take the form of a standard ICE vehicle with a larger starter motor and alternator, the motor allows stop/start capabilities during city driving. The cost of micro hybrids are only fractionally more than a standard vehicle and a significant fuel saving in urban driving can be obtained (Chan, 2007).

Mild hybrids generally replace the flywheel in the ICE with a high profile EM. The EM can be used to boost performance under acceleration conditions and be utilised for regenerative braking. Such a hybrid is slightly more costly to produce than the micro hybrid but fuel efficiency is slightly better (Chan et al., 2010).

Full hybrids are vehicles that have the ability to drive in a full electric mode, fully conventional mode or combination of the two (Chan et al., 2010).

Plug in hybrid vehicles can be any variant of hybrid vehicle, which has the capability of plugging in and re-charging its batteries from the grid. For city drivers the PI-HEV can offer fully electrical usage with no need to use an ICE as it can be charged overnight at home or during the day at place of work (Amjada et al., 2010, Chan et al., 2010).

All of the aforementioned vehicles whilst being slightly different variants fall under the three main types of hybrid vehicle discussed in the previous section. It is also important to note that within the three main types of hybrid vehicles, power-train architecture can be quite different, numbers of electric motors can vary along with their installation. For instance a parallel hybrid can consist of an ICE and an EM, but it can also consist of an ICE and four EM's that can drive each wheel independently.

2.5 Technological Advances of Hybrid Electric Vehicles

With the knowledge of where HEV's have come from, what is driving their research and development, and the different types of these vehicles that are currently available, it is appropriate to introduce directions of work which are being pursued with current HEV's. Before doing so it is important to outline the fundamental philosophy of HEV's to be able to put certain works into context. The philosophy of a HEV can be thought of as the summation of two sets of technologies, where their sum is of greater worth than their individual parts. Meaning that in a HEV, the electrical and conventional parts of the vehicle's drive-train complement each other in such a way as to make up for/overcome each other's flaws. In simplest terms this can be shown by the consideration of a SHEV, the ICE performance is enhanced as it is able to run at an optimal operating point, the electric vehicle performance is enhanced as its range is extended. There are of course numerous ways to achieve and implement this philosophy, as was shown in previous sections, then of course there are even more ways such implementations can be controlled for greater performance. However whilst focussing on optimising performance in one area, the effect on others should not be overlooked, what may create a 15% gain in fuel efficiency could cause a 20% loss in driveability, ride comfort or handling. The

above philosophy should be applied to the whole vehicle and not limited to certain systems within it.

The majority of work that has been conducted in the field of HEV's over recent years has primarily been with concern to their efficiency, in terms of energy consumption and emissions. Within the context of this work this relates to control strategies of the hybrid systems. The increasing interest in hybrid vehicles has also driven development in hardware, such as EM's, power electronics and energy storage devices.

2.5.1 HEV Control Development

It is no surprise when considering the HEV philosophy that there is a vast amount of work being conducted with HEV control strategies. The controller is central in HEV design as it manages the energy and energy flow between the two main systems (EM and ICE) to ensure some level of optimal efficiency is obtained. Due to the large number of studies being conducted on HEV power-train control a number of reviews have been issued in an attempt to consolidate understanding and give a clearer overview of the big picture (Crolla et al., 2008, Wei et al., 2010, Emadi and Wirasingha, 2011). These reviews all look at the current state of HEV control strategies, within them the most commonly used control techniques are introduced and discussed. Also a large numbers of current works are presented to illustrate the direction and variety of control techniques currently being investigated. Whilst some studies (Crolla et al., 2008) do mention that the implementation of EM's in vehicle power-trains is likely to affect vehicle drivability and driver perception, and that future works should investigate such areas, there is still little work being conducted along such lines and the hybrid vehicle research problem is seen to be heavily power-train based.

The current trends in vehicle dynamics research in HEV's can be summed up by considering that in hybrid vehicles different components within the vehicle may perform similar tasks (Fredriksson et al., 2004). Meaning that the controllability and response times of electric motors lend themselves to being used not only to drive the wheels but also to brake them. Electric motors and wheel components should not be seen as a means of driving or braking but rather as a means of applying forces to ground. Such thoughts give rise to the majority of works being conducted on hybrid vehicle handling and stability. Certain hybrid architectures make such control applications easier than others, for example in a hybrid vehicle which has more than one EM, there becomes the possibility of controlling axles or even wheels independently from one another. Such control opens up numerous possibilities and further extension to the study of Direct Yaw Moment Control (DYC) (Waltermann, 1996, Chu, 2001), and also the integration of other vehicle control systems such as Electronic Stability Control (ESC), Anti-lock Braking Systems (ABS) and Traction Control Systems (TCS) (Fredriksson et al., 2004, Yim et al., 2012).

DYC through utilizing a hybrid power-train is demonstrated by Liu et al (2011) who present a vehicle model of a PHEV with two EM's on the front axle controlling each wheel, and the ICE driving the rear axle. By using a control system based on a single Lyapunov function, the front axle motor torques are controlled to directly affect the yaw responses of the vehicle, it is illustrated how such wheel torque manipulation, known as torque vectoring can be used to make vehicle yaw responses more closely match those demanded by the driver. Similarly the work of Pusca et al (2004) illustrates that for a hybrid vehicle with four independently driven wheels, the utilisation of a fuzzy logic based control system allows control of each wheel torque independently, which can be used to increase vehicle lateral and longitudinal

stability in critical/limit handling situations, in much the same way as current TCS and ESC systems do.

There are again large numbers of works that investigate control systems for DYC in hybrid vehicles, based on different control theories and applications to different hybrid architectures, which all bring their own subtle differences, advantages and disadvantages. Once again the focus is primarily on control systems modelling, the majority of studies use simplified, low degree of freedom vehicle models as a base for the work, and references to changes that arise in vehicles passive vehicle dynamics as a result of the hybrid systems are neglected.

2.5.2 HEV Hardware Development

Whilst on the fringe of the context of this work, hardware development within HEV's forms a significant portion of the current work being conducted in the field of HEV's and so is included for completeness. With increasing development of HEV's the technology within them such as batteries, EM's, power controllers, even power steering and air conditioning are all becoming the focus of increasing studies.

Batteries are probably receiving the most attention with respect to HEV hardware, as energy storage is seen as one of, if not the most important factor in current HEV's (Amjada et al., 2010). It is shown that significant developments in battery technology have been made, for example the Nickel Metal Hydride batteries used in the Toyota Prius almost halved in weight and doubled their specific power between 1998 and 2004 (Hermance and Shinichi, 2006). Whilst most HEV's have traditionally utilised the Nickel Metal Hydride batteries there has been considerable development of Lithium Ion batteries which are beginning to be used in more recent EV's and HEV's (Burke, 2007, Maggetto and Van Mierlo, 2000). A discussion of the different types of batteries used in HEV's and technological advances being

made in such areas is given by Amjad et al (2010), and Maggetto and Van Mierlo (2000). It is shown that a large number of technologies are being researched, everything from the common lead-acid to more exotic lithium-polymer batteries are being considered, this is shown to be the case as battery selection is specific to vehicle type, usage and expectation of performance, and so with the wide variety of HEV's there is likewise a wide variety of battery technologies being worked upon. Research on battery technology is also extremely wide reaching, it spans materials science, mechanical, chemical and electrical engineering, and it is seen that research for HEV batteries is being conducted on all of these fronts.

Supercapacitors are also receiving more attention as an energy storage device in HEV's due to their very high power density. However as they possess a very low energy density their implementation currently is to supplement the battery pack not as a replacement (Burke, 2007, Chan, 2007).

EM development has also been subject to a lot of attention with respect to HEV's, like batteries, the EM requirements are driven by its usage and so there are again quite diverse areas of work being conducted on EM's (Maggetto and Van Mierlo, 2000). The three main types of EM currently used in HEV's are; Permanent Magnet (PMM) (Synchronous and Brushless), Induction (IM) and Switched Reluctance motors (SRM) (Chan, 2007). Permanent magnet motors are classed as having high efficiency, high torque and high power density, their downside is that they possess a short constant power range due to their limited field weakening ability, they also produce high back emf which can cause issues for the power electronics. Toyota uses PM motors in all of its hybrid vehicles and puts the choice down to improvements it has made in their power, efficiency and rotational speed (Hermance and Shinichi, 2006). Induction motors are seen as simple and robust, due

to this they are common in EV's and HEV's, however they are generally less efficient than PM motors and as such are larger than a PM machine with equivalent power and speed rating. SRM are capable of high speeds and have a wide constant power region, they also possess a high starting torque and a high torque/inertia ratio, although manufacturing costs of SRM's are currently high. Within the HEV EM field a lot of effort is being used to investigate the manufacturing of components as cost is seen as a major factor slowing the development of HEV's. Despite this it is currently permanent magnet and switched reluctance motors that are preferred choices in HEV's (Amjad et al., 2010, Hermance and Shinichi, 2006).

Power electronics such as converters, inverters, semiconductor devices, switches and switching strategies, is also seen as a crucial area in optimisation of HEV's and faces a large number of technical challenges that are being addressed in the fields of materials science, electrical engineering and manufacturing (Emadi et al., 2008). Furthermore with the hybridisation of vehicles more electrical systems are being introduced into the vehicle, examples are electric power steering and air-conditioning (as these can no longer be run from ICE), meaning that electrical systems on vehicles are becoming more complex and as such the focus of more work.

One final area where it has been found there is significant contribution to the research and development of HEV's is within modelling and simulation of vehicle systems, and especially model and hardware in the loop simulations (MIL and HIL simulations). The increased complexity of HEV's through the introduction of extra technologies (software and hardware) as discussed in this section, is leading to a greater requirement for model based testing and validation. HIL simulations give the ability to run new hardware (EM's, batteries, power electronics) or software (control

strategies) on a test rig with all other systems (plant) represented in the modelling domain. Such platforms will expedite the design and development of new hardware and control strategies as well as aiding in their integration into the vehicle (Hung et al., 2010, Sung, 2005). A consequence of such needs is that more resource is also being put into the design and development of modelling and simulation platforms that are capable of meeting the requirements of HEV modelling and simulation. Similarly this can also be said for the computer and test rig hardware used for such HIL rigs (Zhong et al., 2006).

Other more niche areas of HEV technology research and development are discussed by Chan and Chau (2002), who discuss transmission technologies as well as the possibility of thermal recovery systems to recuperate lost thermal energy, which are thought to be the next focus in the search for ever more efficient vehicles.

In the push for more efficient, cleaner vehicles of the future, automotive engineering is becoming a multi-domain discipline. It has been shown here that HEV technology spans, mechanical, chemical and electrical engineering as well as materials science and manufacturing. Due to this there are significant amounts of work being conducted in all of these fields on HEV's.

2.5.3 Regenerative Braking

The culmination of HEV hardware and HEV control systems leads to technologies that are not possible to implement in conventional vehicles being common place in HEV's. Such a technology is regenerative braking.

Regenerative braking is an effective way to increase fuel economy and lower emissions (Li et al., 2009). When a conventional vehicle is braked, the kinetic energy that is possesses is dissipated as heat. In a hybrid vehicle the opportunity arises to utilise the EM('s) for braking, in doing so the kinetic energy can be

converted via the EM('s) into electrical potential energy in the batteries which can later be used to propel the vehicle (Gao and Ehsani, 2001). It has been shown that in city driving due to the large number of stop start conditions, up to 50% of the energy output by the motor is wasted in braking, and so the use of regenerative braking can increase the fuel economy of a hybrid vehicle between 8% – 25% (depending on its usage) (Gao and Ehsani, 1999, Yoong et al., 2010, Liu et al., 2011).

While it has been shown that the majority of publications focus on top level vehicle control techniques, there is not an insignificant amount of work being conducted on regenerative braking control. Again whilst the emphasis seems to be primarily on overall vehicle energy efficiency (Gao et al., 2007, Yoong et al., 2010), here there is at least a little more consideration given to vehicle dynamics. The main vehicle dynamics concerns with regenerative braking, relate, firstly to driver perception and secondly to vehicle stability. Driver perception of regenerative braking is brought about by the need to use such energy recovery to re-capture as much lost braking energy as possible, but at the same time the EM is inadequate/unsuitable to provide braking in all conditions. Shang et al (2010), look at how conventional friction braking and EM braking can be utilised together during braking events to ensure the desired overall braking profile demanded by the driver is obtained, such control is needed as the EM is not suited to all braking conditions and can result in excessive or insufficient braking torques, depending on the vehicle operating parameters. Assadian and Hancock (2006) discuss the second aspect, vehicle stability. Here it is illustrated through braking on a constant radius turn with and without regenerative braking, that the addition of the regenerative braking (at the rear axle) increases rear slip sufficiently to increase driver workload. This problem will diversify further with the consideration of different power-train architectures,

clearly regenerative braking on front wheels, rear wheels or all four wheels will produce different handling characteristics, some of which will be more stable than others. Han et al (2011) go one step further and develop a regenerative braking control system that derives the optimum distribution of braking torques to avoid limit handling events brought about by regenerative braking.

The two aspects of driver perception and vehicle stability are actually quite interrelated, driver perception/feel of the regenerative braking is caused by the conventional friction brakes and the regenerative braking having to interact to obtain the required braking torque, such interaction requires blending of the two braking systems which can result in varying total levels of brake torque, varying levels of vehicle acceleration and different brake pedal feel. Such circumstances can be encountered due to battery state of charge (SOC) not allowing for additional regenerative braking, vehicle state not permitting for and/or terminating regenerative braking (limit handling conditions), and the interaction of other vehicle control systems, such as ESC (Assadian and Hancock, 2006, Beiker and Vachenauer, 2009).

With regard to comments made in the previous section, it should once again be noted that here the majority of work conducted on regenerative braking takes the form of a power-train problem. There are a small number of studies that look at the effects of the systems from a vehicle dynamics and control viewpoint, but even fewer that consider the effects of such systems on pure/passive vehicle dynamics.

2.6 Effects of HEV Systems on Passive Vehicle Dynamics

Whilst it has been shown a large amount of work has and is being conducted in the control areas of hybrid vehicles, mainly with views on increasing energy efficiency, but also to a smaller extent in terms of influencing vehicles' stability, there is very little mention of the effects of hybrid vehicle systems on pure/passive vehicle

dynamics. In fact this study only uncovered a small handful of papers that make reference to such factors. It seems that this is raising concern as the work by Beiker and Vachenauer (2009) was aimed purely at starting a discussion on the effects of hybrid vehicle systems on vehicle dynamics. The authors touch upon previously discussed matters such as the interaction of regenerative braking and other control systems, and the use of EM's to control vehicle stability, but they also make important statements regarding the increased number of hybrid systems within the vehicle, these being;

- With increasing power-train complexity comes increased sprung mass, this alone will effect body motions during ride and handling events along with reduced overall lateral and longitudinal capabilities.
- The effects of regenerative braking on body motions needs to be considered. When conventional friction brakes are used, vehicle body pitch motion is controlled through the use of geometric effects such as anti-dive/squat, with the use of regenerative braking the anti-dive/squat angles are different to those when conventional friction brakes are used and the interaction between the two systems could lead to irregular body motions being felt by the occupants.

Whilst the aforementioned theories relating to how hybrid power-trains can effect vehicle dynamics properties are introduced by the authors, no major work has been conducted, and it is left to the reader to instigate further studies.

More conclusive work within the specific area of vehicle inertial properties conducted by Bobier et al (2008) considers the effects of such atypical properties possibly arising in hybrid vehicles, on lateral vehicle responses. It is quite rightly pointed out that due to differing hybrid power-train architectures, it is possible that

future hybrids will have mass and inertia properties far outside the realms of those seen in today's vehicles. Through the use of a vehicle model and test vehicle, the effects of the position of the vehicle rotation centre, (a metric that in this study is referred to as the Dynamic index (DI)), on the vehicle's lateral responses is investigated. It is shown that only small changes in a vehicle's yaw and roll inertia have profound effects on the vehicle's transient lateral responses through the changes that are imposed on rear slip angle generation at the instant of steering angle application. It is concluded that more consideration should be given to future vehicles' mass and inertia properties as they will become more influential on vehicle handling, it is also suggested that such properties will become increasingly used as tuneable parameters at the vehicle design stage. The previously mentioned study specifically focuses on the influence of the rotation centre on vehicle handling, and leaves clear scope for a more comprehensive study of other factors introduced by the addition of hybrid power-trains. Complimentary to the work of Bobier et al (2008) are studies by Olley et al (2002) and unpublished work by Prodrive, and the author of this thesis, that have also considered the effect of the vehicle rotation centre or DI, on vehicle lateral responses, although these are not specific to hybrid vehicles. These works also showed that small changes in the position of the DI had significant effects on vehicle lateral responses, and driver perception during transient and post limit handling events. Bringing this into the context of hybrid vehicles, it can be surmised that with the level of difference in mass and inertia properties predicted by Bobier et al (2008) that the position of the DI will be a useful indicator and possible tuning metric for hybrid vehicle handling analysis.

The work of Akhgari et al (2008) illustrates to some extent how the hybridisation of a conventional vehicle can alter its handling characteristics. Here the vehicle in

question is a city bus which has undergone hybridisation to create a series hybrid vehicle. Using multibody models of the standard and hybrid vehicle, the lateral responses of the latter were investigated and shown to be considerably different to its standard counterpart. Changes to mass distribution, springs and anti-roll bars were tested in an attempt to re-tune the handling properties of the hybrid vehicle, which was achieved to what is said to be a 'satisfactory' level. Whilst informative, the analysis of the two vehicles is very limited, only two manoeuvres were conducted for objective comparison, inertial properties were not considered, there was no comparative measure of the difference in handling seen between the two vehicles (standard and hybrid), and furthermore fundamental changes in the vehicles' steady state handling were neglected during test manoeuvres and in the analysis of the vehicle's re-tuned state. The analysis of the two vehicles also only considers the handling domain, no reference to how such changes may affect the vehicles ride is given.

A more complete consideration of the effects of vehicle hybridisation is given by Hamedi et al (2007), who look at the differences in ride and handling between a conventional ICE powered vehicle and a bi-fuel hybrid vehicle using compressed natural gas. Whilst not a HEV, the remit of the work is very similar. Once again a multibody model of the vehicle is created and used for objective analysis of the vehicle, as well as optimization of springs, bars and dampers in the modelling domain. Vehicle testing and subjective analysis are conducted to match the hybrid vehicle's handling as closely as possible to the standard vehicle. Work is concentrated around improvement of the hybrid vehicle's handling, subjective analysis of the vehicle seems comprehensive and the overall aim of obtaining similar levels of ride and handling as the standard vehicle are met via tuning of the springs,

anti-roll bars and dampers. The purpose of the work is more concerned with obtaining the required characteristics of the new vehicle, rather than where and why differences between the two arise. Analysis of the two vehicles is primarily conducted through subjective testing, and objective differences between the two vehicles are not discussed. The study does however also cover the ride domain, although the analysis is somewhat limited as only body motion control resulting from handling manoeuvres is considered, and is again purely subjective.

The works specifically focussing on ride and handling of hybrid vehicles (Akhgari et al., 2008, Hamedi et al., 2007), give an overview into how one might expect vehicle characteristics to change in such specific examples. However as previously mentioned no attempt to identify the root causes of ride and handling differences brought about by the hybridisation are made, and no measure of the vehicles ride and handling differences are quantified. It is not possible to draw conclusions from these studies that may be applied to future hybrid vehicles, and therefore both leave significant scope for further work.

Outside of the realms of vehicle dynamics control systems, based on the works reviewed in this section, it can be said that the introduction of hybrid power-trains is likely to affect vehicle dynamics properties of a vehicle through the following mechanisms;

- Changing mass and mass distribution
- Changing inertia properties
- Interaction of regenerative braking with suspension geometry (anti-dive/squat geometry)

These mechanisms are top level changes and the effects of each will filter down and effect both vehicle ride and handling in numerous ways. There is a need to fully

understand generally how such parameters change within hybrid vehicles and then specifically how such changes affect ride and handling characteristics. Through and understanding of this, areas that may need special attention in future hybrid vehicles can be highlighted.

2.7 Conclusion

The previous sections have discussed past works and current trends in the vehicle dynamics of hybrid vehicles. It has been shown that whilst considerable work is being conducted, and considerable achievements being made with regard to improving vehicle handling and stability in hybrid vehicles, such steps are being made in the field of vehicle dynamics control systems. A very small number of studies have highlighted the need to investigate the effects of hybrid power-trains on passive vehicle dynamics, and as such have proposed areas of research, although as of the time of writing, no studies have taken up these proposals. Two case studies were found and reviewed, however both left scope for further work. Both studies simply discussed re-tuning to account for the changes in vehicle responses incurred by the hybrid power-trains, root causes of such differences were not investigated and so the ability to draw conclusions or make recommendations on the design of future hybrid vehicles was not possible.

From review of the literature in the past sections it has become clear that ways in which hybrid power-trains will affect a vehicles ride and handling, are through changes in mass and inertia properties. So this study will concentrate on the ways in which hybrid power-trains affect the vehicles mass and inertia properties, then consequently how these affect a vehicles ride and handling at a root level. Such a study is needed in order to fulfil the philosophy of HEV's stated earlier in this chapter, there is no point in optimising the efficiency of the vehicle if in doing so the

compromises made to its ride and handling make the vehicle, uncomfortable or dangerous to drive. Furthermore, with respect to the work being conducted on vehicle dynamics control strategies of HEV's, it seems of little worth to focus on the control system of a vehicle with poor underlying vehicle dynamics properties brought about by the inclusion of the very technologies which are being implemented to enhance its vehicle dynamics characteristics. Some level of analysis and/or optimisation of the lower levels of the vehicle chassis need performing otherwise such control systems will be rendered neutral as they will simply mitigate their own effects.

Chapter 3 Vehicle Modelling

3.1 Introduction

This chapter will outline in detail, the make-up of the Standard Vehicle (SV) and General Technology Vehicle (GTV) models which form the crux of the modelling portion of this study. Initially the SV model will be considered, an overview of the vehicle itself will be given, the modelling methodology followed will be explained and illustrated in detail, and finally the model will be validated against model outputs obtained from the OEM, and real vehicle test data collected as a part of this study. Following this it is appropriate to introduce the GTV, in terms of how it differs from the SV and how such changes are implemented in the modelling domain. Finally the two vehicle models will be compared statically and dynamically to illustrate fundamental differences between the two.

3.2 Modelling Approach

Within the case study section of chapter 1 it was explained that Dymola/Modelica would be used as the modelling environment, firstly, in order to keep commonality with the aims and outputs of the LCVTP, and secondly to make use of Dymola's object orientated, acausal modelling capabilities, which prove useful for one of the main aims of this research and that of the LCVTP, which is to create a modular flexible architecture multibody model, for use in this study and perhaps as a base for others in the future.

Throughout the modelling activities of this research, models have been created in such a way as to maximise their flexibility in how they can be utilised, and also to

allow ease of modifications and adaption to form other variants of hybrid vehicle model based on this modelling architecture.

Taking a front suspension corner as an example, this is one of the lowest levels of modelling implemented here. This model has been created by defining a front suspension corner base class. This base class simply sets up inputs and outputs for the corner model, it is analogous to a container for the model, any format model can be within it as long as the requirements for inputs and outputs are satisfied. This base class for the front suspension can be instantiated to create a specific model, the previously defined inputs and outputs (mechanical connections to chassis and tyre model) are fixed by the base class, but the models of the mechanical linkages within can be arranged in any format, to represent any type of suspension system, here a MacPherson strut. Once the MacPherson strut model was created it too can be instantiated, now connections between the links are fixed as they have been inherited from the MacPherson strut class, so whilst this model will always represent a MacPherson strut, as the connect statements are inherited, the geometry of this suspension can be freely edited by the user, something that is made even simpler in Dymola via the functionality of propagating parameters up the hierarchical tree of the model. For example, hard point geometry can be propagated from a linkage level within the suspension corner model, up one level to the top of the suspension corner model, meaning the user does not have to delve into the model to set parameters. Taking this further, if it was desired these parameters could be propagated higher in the model, once the suspension model has been used within a chassis model.

This model of a MacPherson strut can now be used in any number of situations as long as the constraints of the input and outputs are met (it is connected in the correct way), for example it, can be connected to subframe model, with another

instance of itself to represent the opposite corner, it can be used in model based test rigs and in other vehicle models etc, with no requirement to re-arrange the model based on its application.

The process that was discussed here, has also been implemented for all other components of the model, the engine, drive-train, chassis, all have base classes that define the format of the model at a basic level, its inputs and outputs. Defining the components of the model in such a way means that they can easily be interchanged and/or upgraded, any model that fits the format of the base class can simply be 'dragged and dropped' into place, with no need to re-arrange the model. For example a model of a series hybrid electric vehicle can be changed to a parallel hybrid electric vehicle simply by swapping the drive-train component model. Further examples of this will be shown throughout this chapter when detailing each component model.

There are however drawbacks to object orientated modelling, two of the main ones are size of the modelling package and effort needed to create the model. At the outset of modelling a great deal of time is needed to plan the structure of the model. Creating base classes, and instances of different component models also makes model packages large and sometimes quite complex.

Given that one of the desired outcomes of this research is a flexible architecture, modular, multi-body model, that can be used here and possibly in the future, the effort in model planning is justified, also on modern computers model size should not become an issue, and therefore the object orientated modelling approach facilitated by Dymola fits the purpose of the this research, and the benefits it brings in terms of model flexibility, and in some areas a reduction in modelling time, outweigh the drawbacks of the object orientated modelling approach.

3.3 The Standard Vehicle (SV)

The standard vehicle can be classed as a luxury, four wheel drive (4wd) sports utility vehicle. It has a 3-litre V6 diesel internal combustion engine mounted at the front, which connects to a Haldex 4wd system. It is a five door vehicle and can accommodate up to five occupants, with luggage space at the rear. A schematic diagram of, and top level data for this vehicle are shown in Figure 3-1 and Table 3-1.

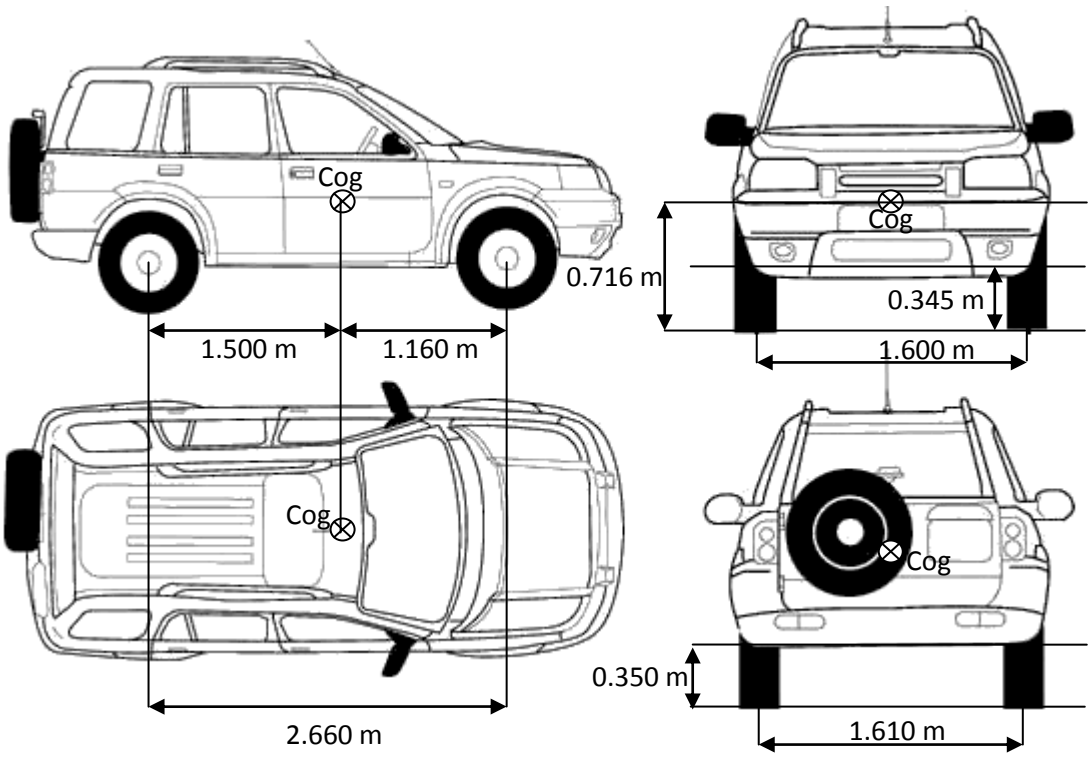

Figure 3-1 Vehicle schematic diagram

Total Mass [Kg]	2150.00
Roll Inertia [Kg.mm2]	859.4
Pitch Inertia [Kg.mm2]	3471.7
Yaw Inertia [Kg.mm2]	3776.5

Table 3-1 Chassis level vehicle data

3.3.1 Front Suspension Overview

For the models used in this study the lowest level of modelling occurs for the suspension corner models. Corner models of the front and rear suspension where created using a mixture of template parts, simple linkages and force elements from the vehicle dynamics library of Dymola.

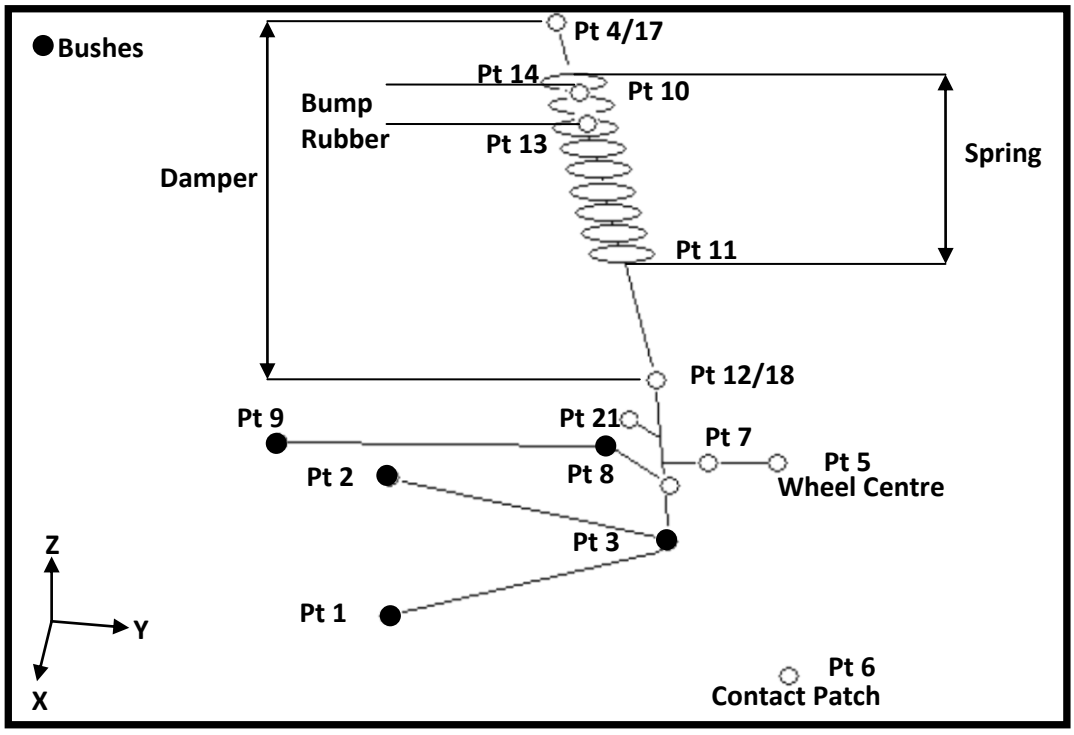

Figure 3-2 Front left suspension linkage

The front suspension of the SV is of MacPherson strut type, and so has a lower wishbone connecting the bottom of the upright/hub (pt 3) to the subframe (pt 1 and 2), a steering tie-rod which connects the upright, rearward of the wheel centre (pt 21) to the steering rack (pt 9), and a damper/strut that connects directly and rigidly to the top of the upright/hub at its lower end Pt 12/28), and to the vehicle body at its upper end (pt 4/17). The model diagram is shown in Figure 3-2 and its representation in the Dymola modelling package in Figure 3-7

The links of the model are rigid, and incorporate mass and inertia properties, the inclusion of these individual mass and inertia properties allow the un-sprung mass effects to be captured and a more accurate representation of the vehicle mass and inertia properties obtained. The joints between the links consist of bushes with six degrees of freedom, this allows translation along, and rotation about each of the three orthogonal axes, and allows for compliances to be accurately captured and their effect on the overall performance of the vehicle to be incorporated.

The spring and damper units that make up the strut are modelled separately, both by prismatic joints allowing translation and rotation along and about one of their local axis, the difference being one is acted upon by a damping element which acts on the relative velocity between the two ends of the joint and the other is acted upon by a spring element which acts on the relative displacement between either end of the joint. Whilst in Figure 3-7 it looks as if the two prismatic joints are not aligned, their geometry data ensures that the top and bottom points of both are constrained to be equal, ensuring equal motion ratios. The mass and inertia properties of the damper/strut are incorporated by the addition of two separate multi-body mass elements mounted in the correct place to represent the Cog of the bottom of the strut (un-sprung) and the Cog of the top of the strut (sprung), again the separation of these two masses allows a more accurate picture of the sprung and un-sprung masses to be acquired, which should ultimately lead to better correlation between model and test data.

Once the general layout and construction of the corner model had been completed it could be parameterised with geometry, mass, inertia, stiffness and damping properties. This data was extracted from a pre-existing MSC ADAMS model of the vehicle, which had been constructed in house by the OEM. The force

displacement data for the spring element was linear and so was implemented as a single rate. The force velocity data for the damper on the other hand is non-linear, and so is implemented in tabular format which allows interpolation. The stiffness and damping properties of the bushes were also highly non-linear and so again were implemented in tabular format within bush data files. All data for geometry, stiffness and damping properties are given in Appendix A.

Having successfully constructed and parameterised one corner of the front suspension, the other corner was accomplished by creating another instance of this corner model and the geometry reflected with a single modifier on the y coordinates, which had the effect of reflecting the corner to create the opposite side.

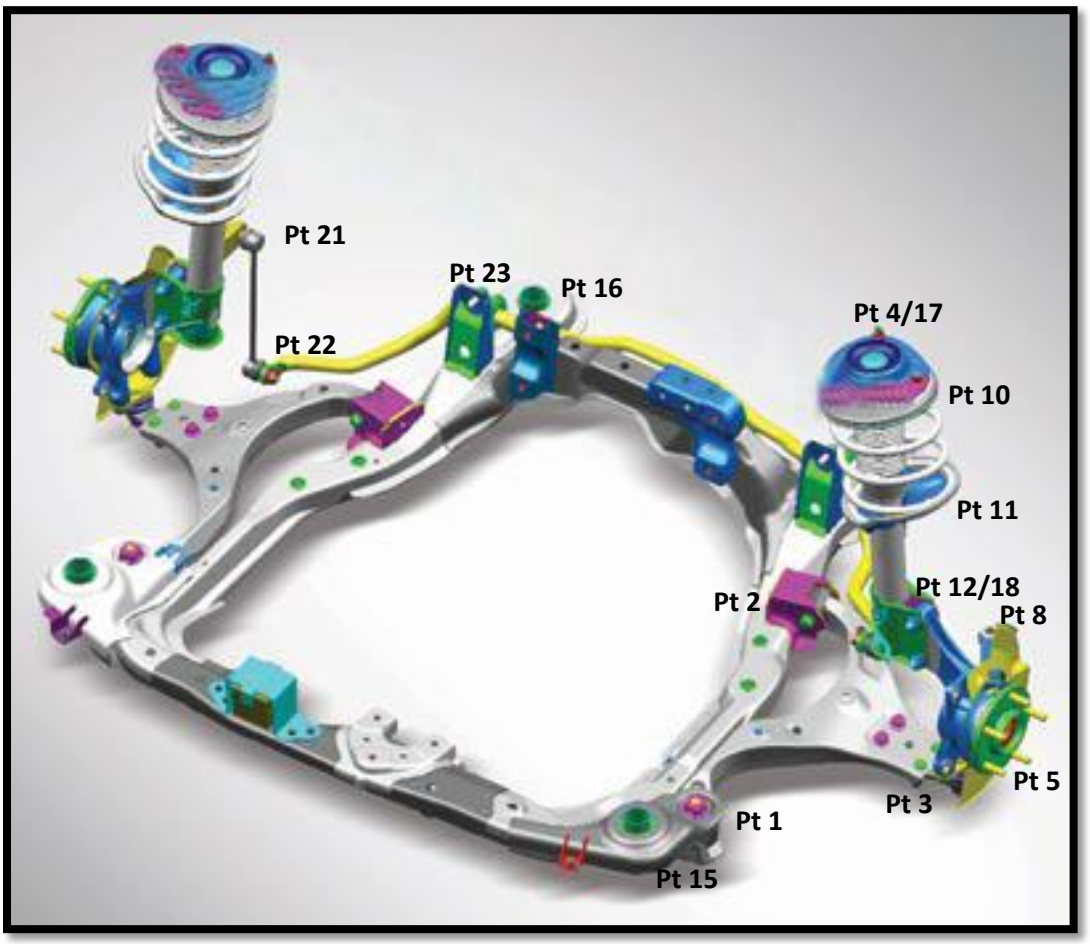

Figure 3-3 Front axle construction

The two front corners are connected by a rigid subframe, anti-roll bar and steering rack. Whilst the subframe is rigid, it is connected to the vehicle body via four, six degree of freedom bushes, again with non-linear stiffness and damping properties. The subframe also contains its own mass and inertia data. The anti-roll bar rate is linear, and the component itself joins the uprights/hubs of the left and right corners. The steering rack is a library component representing a simple rack and pinion system, although it has been adapted, again with the addition of a multi-body mass to reflect its mass and inertia properties. The front axle model is shown in Figure 3-3 with all point numbers referring to the geometry data, and as it is represented in Dymola in the centre of Figure 3-7. Again all geometry, mass and inertia, stiffness and damping data for the front axle model is included in Appendix A.

3.3.2 Rear Suspension

The rear suspension of the standard vehicle is of multi-link type, which was built from its own rear corner base class. It consists of three lower links, two transverse connecting the upright/hub (pts 28 and 29) to the rear subframe (pts 26 and 27), and one almost purely longitudinal that connects forward of the wheel centre (pt 30) to the vehicle body (pt31). The damper/strut connects directly and rigidly to the upright/hub at its lower end (pt 25) and to the vehicle body at its upper end (pt 41). The model schematic of this system is shown in the lower part in Figure 3-4 and as it is represented in the modelling environment in the lower part of Figure 3-8.

As with the front suspension the links are rigid, but connected via six degree of freedom bushes with non-linear stiffness and damping properties, the spring and damper elements also follow the same principles outlined in the previous section for the front suspension.

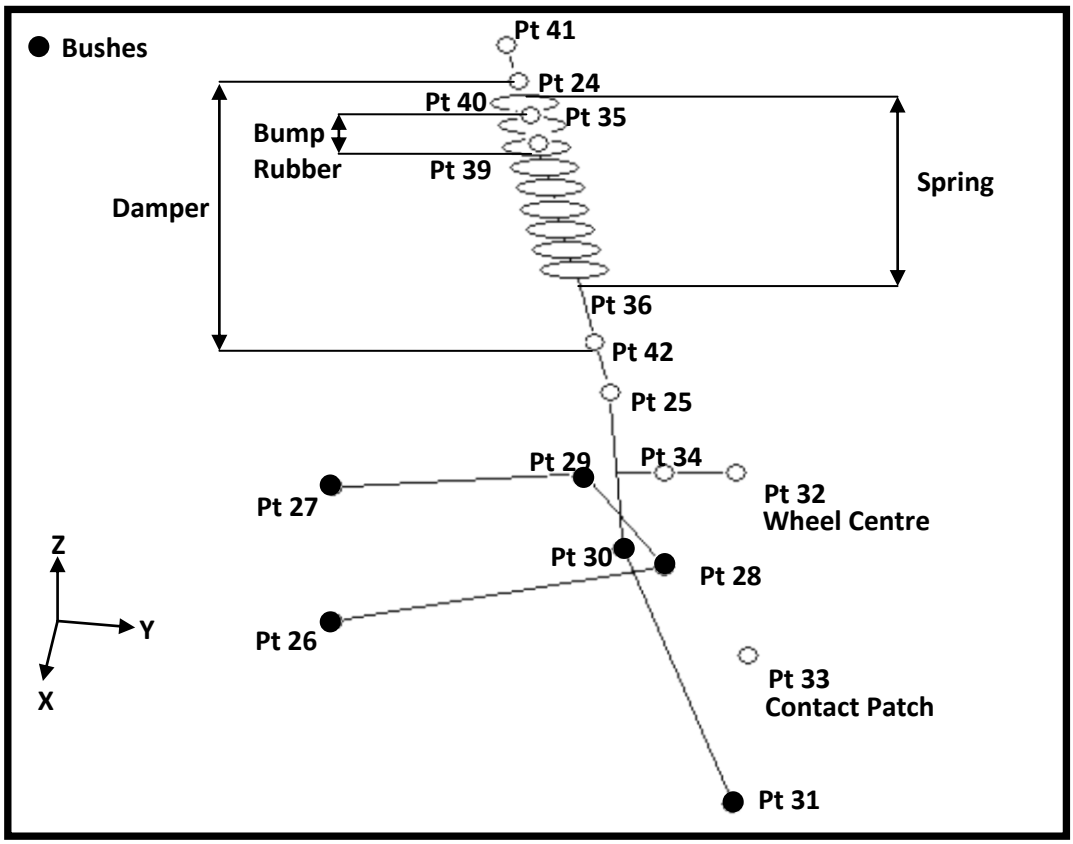

Figure 3-4 Rear left suspension linkage

Once again, with just one corner linkage created a second was instantiated and reflected to create its opposite corner.

At the rear the two corner models are connected via a rigid subframe and an anti-roll bar. The subframe again houses its own mass and inertia properties and is connected to the vehicle body by four, six degree of freedom bushes. As with the front suspension the anti-roll bar has a linear rate and connects the two uprights/hubs of each corner. The rear axle model is shown at the top of Figure 3-8. As with the front axle, all geometry, mass and inertia and stiffness and damping properties for the rear axle are given in Appendix A.

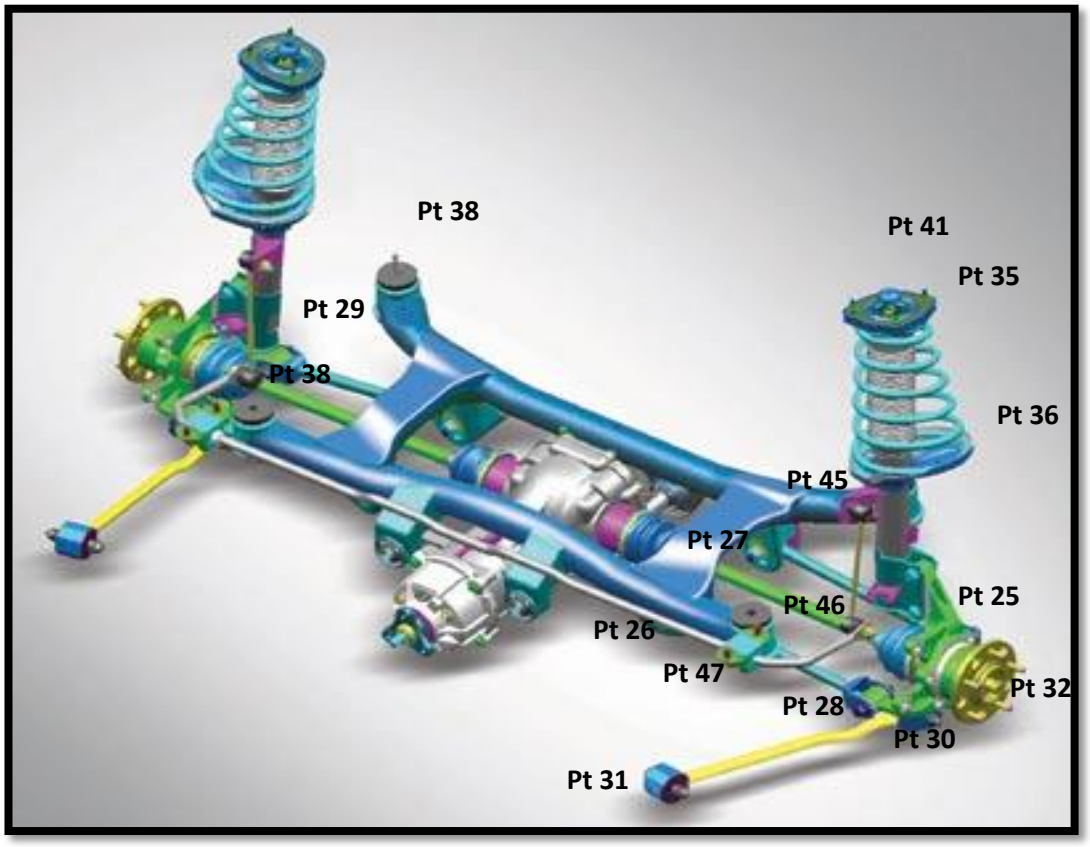

Figure 3-5 Rear axle construction

It can be seen in Figure 3-7 and Figure 3-8 there are a number of sensors connected to the wheel centres, these allow the steer angles and positions of the wheels centres to be easily extracted for use in future analysis.

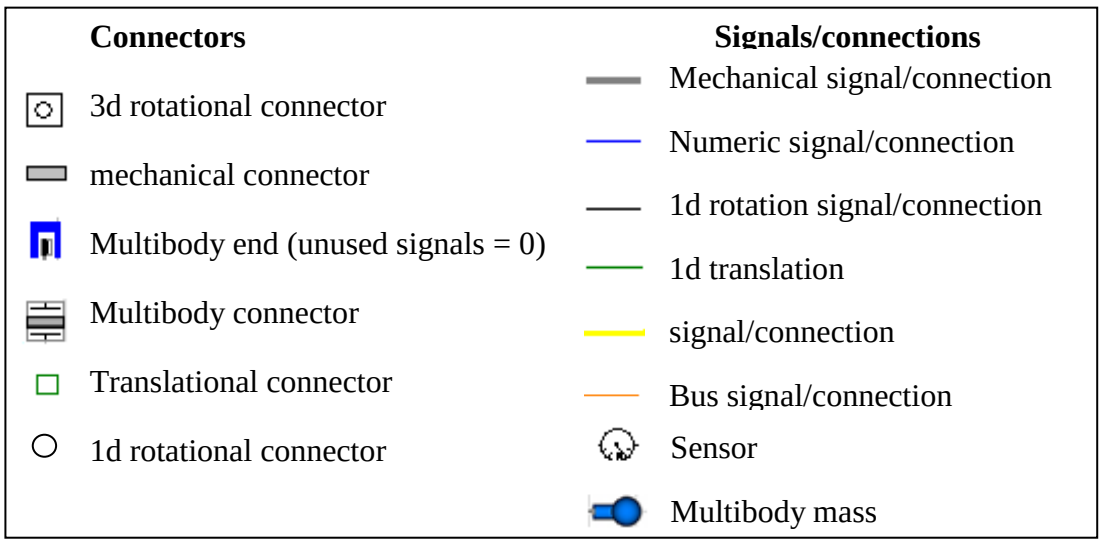

Figure 3-6 Dymola model symbol key

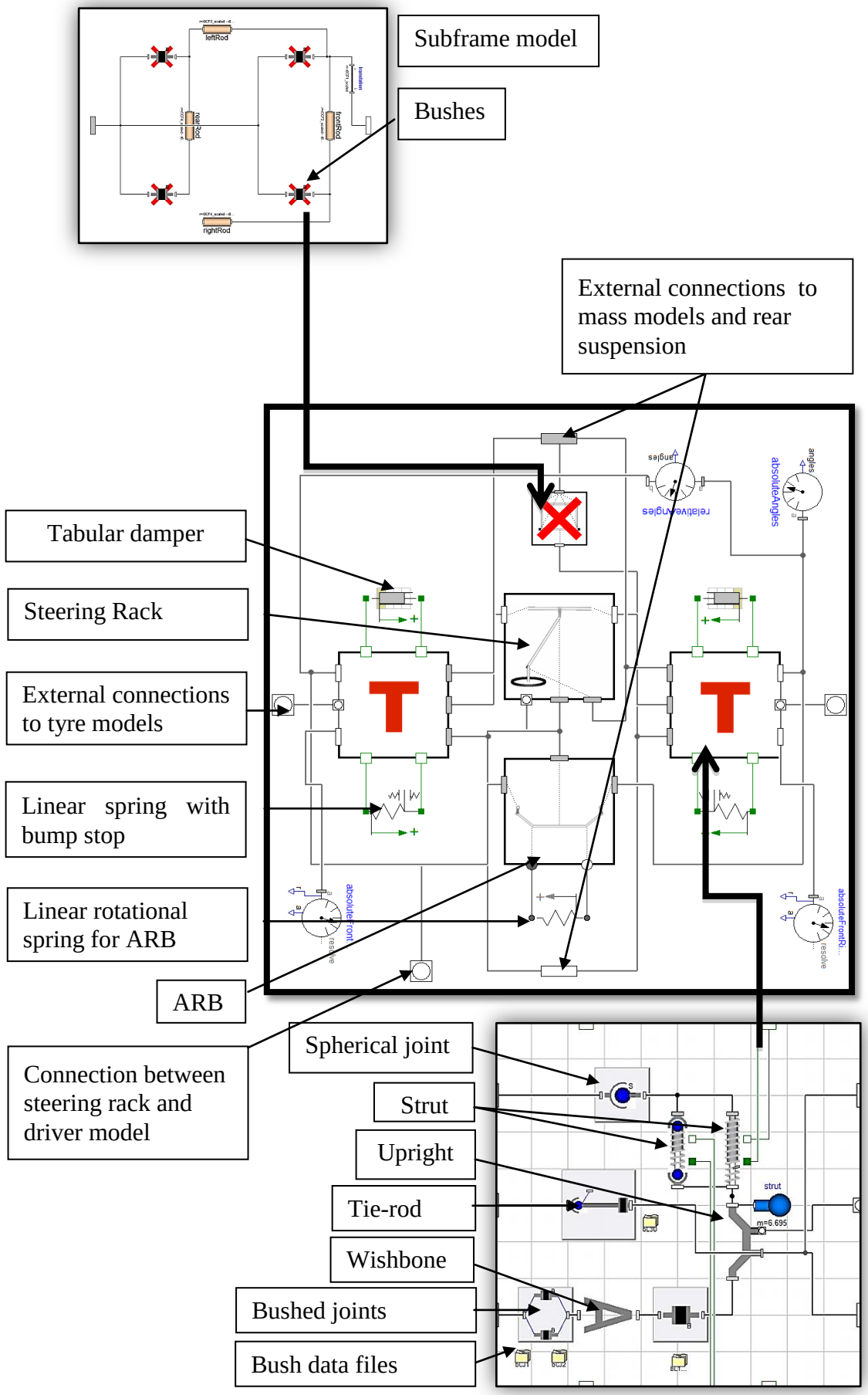

Figure 3-7 Front axle components

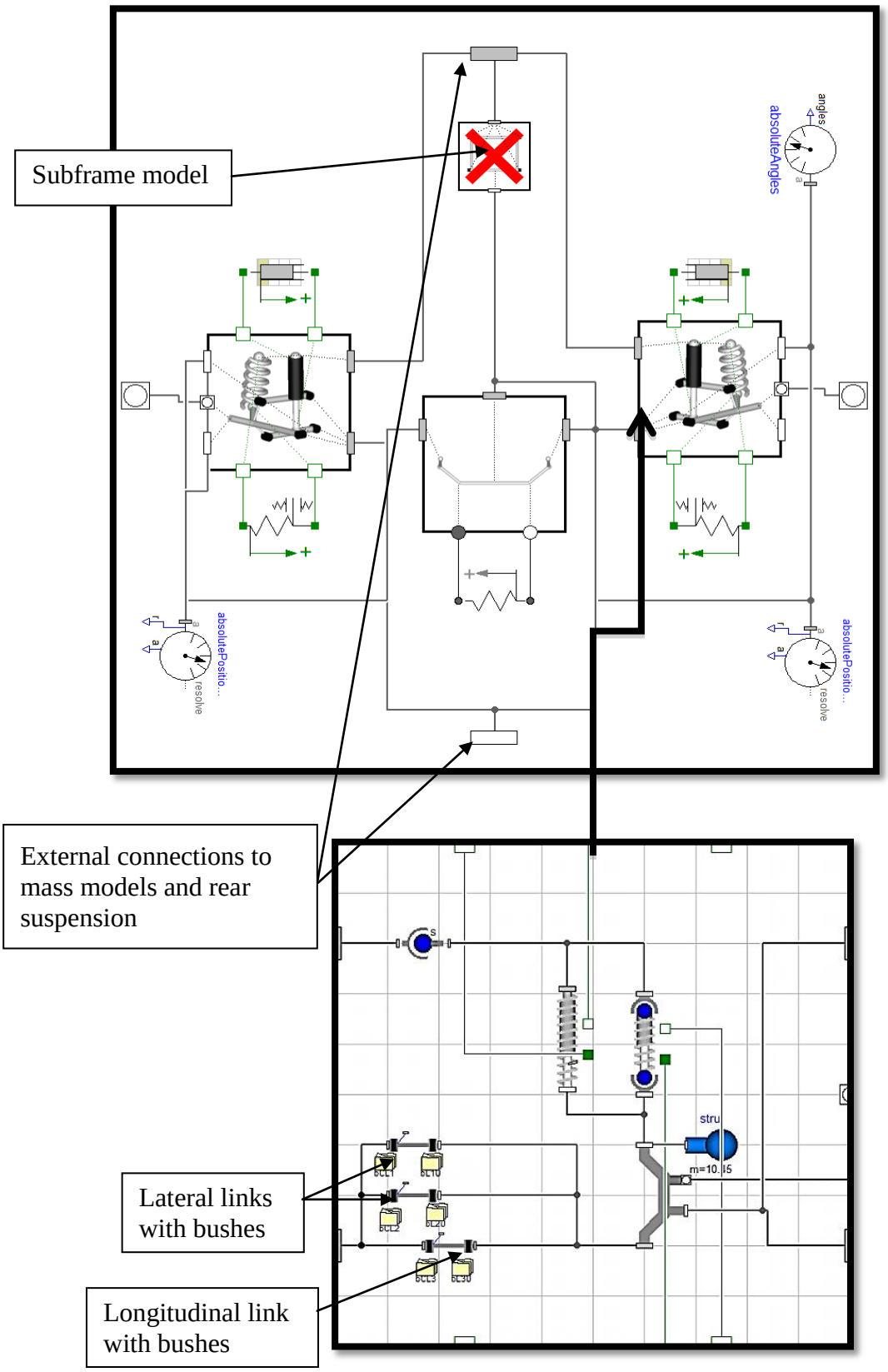

Figure 3-8 Rear axle components

3.3.3 Suspension Kinematics

Following the modelling and parameterisation of the suspension and axle models validation was conducted to ensure that they represent the actual systems. This was carried out via examination of the linkages kinematics during bump/rebound and steer motion. By moving the wheel centre through prescribed motion from full rebound (wheel centre at its lowest point) to full bump (wheel centre at its highest point) a number of kinematic metrics can be plotted. The same metrics can also be plotted over the full steering range.

Within the Modelon vehicle dynamics library there exists a number of modelled test rigs. One of these rigs allows the mounting of a complete axle model (so long as the model fits the axle linkage class definition in terms of inputs and outputs) and then articulation of the wheel by prescribing a motion in the z-axis. By doing this the corresponding metrics can be measured from the wheel centre. The model setup used to conduct such a test is shown in Figure 3-9.

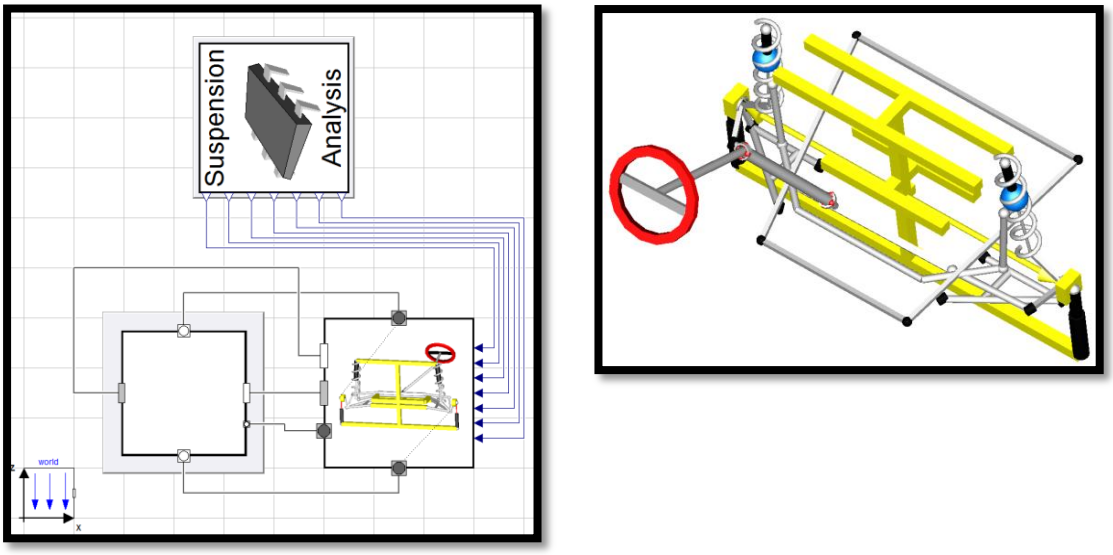

Figure 3-9 Front suspension rig test

The kinematics obtained from these test are shown in Figure 3-10 to Figure 3-12. The first shows caster, camber and toe change during two wheel combined bump motion. Figure 3-11 shows the same metrics, although this time plotted against steer motion. Finally Figure 3-12 illustrates the spring motion during both bump and steer inputs. Plotting wheel centre motion against spring motion yields the motion ratio between the wheel centre and the spring/damper unit. Here the motion of the spring/damper is less than that of the wheel, indicating that the motion ratio is less than 1. The vertical line shown in (b) at zero steer angle is due to the spring motion that accompanies the two wheel bump input test carried out when the steering is centred. It is also seen in (b) that spring deflection is induced by steering, this indicates that due to the caster angle and kingpin inclination, the wheel centre is displaced in the z-axis due to steering and so a roll angle and an additional weight transfer will be induced by steering inputs. This roll angle is shown in (c). The non-symmetric shape of the spring curves illustrate the compliance in the suspension bushes.

The same tests shown here, and the same metrics obtained (with the exception of the steering metrics) were obtained for the rear suspension. These are shown in Figure 3-13 and Figure 3-14.

Metric		Dymola Model		OEM Model	
	Unit	Front	Rear	Front	Rear
Camber gain	deg/m	-13.67	-16.77	-13.00	-16.00
Bump steer	deg/m	7.60	-0.04	7.40	-0.05
Motion ratio	m/m	0.95	0.95	0.95	0.95
Wheel centre recession	m/m	-0.01	0.15	-0.01	0.16
Kinematic jacking	deg/deg	0.0003	-	-	-
Static KPI	deg	13.1	-	13.1	-
Caster Trail	m	0.025	-	0.025	-

Table 3-2 Suspension kinematics metrics comparison

Table 3-2 summarises the metrics that can be obtained from the kinematic rig tests. All values are given for the vehicle at design ride height (as it would sit at rest). The two sets of results shown relate to the Dymola model presented here and data supplied by the OEM. Only single values for the vehicle in a static steady state condition are supplied by the OEM, so it is not possible to comment completely on the correlation of the two sets of results, however it can be said that the values obtained from the Dymola model at this point agree well with those supplied by the OEM.

3.4 Tyre Model

A lot of effort has gone into creating accurate representations of the suspension linkages and mass and inertia properties of the vehicle, however none of this would matter if the tyre was not accurately represented. The tyres being the only points of contact between the vehicle and ground are the elements which generate all the necessary forces that ultimately dictate the vehicles ride and handling characteristics. As such the tyre model is of vital importance for the overall vehicle model.

3.4.1 Types of Tyre Model

The last two decades have yielded a big step forward in the understanding of tyres and so with it has come a large variety of tyre models that can be utilised for vehicle dynamics modelling. Models range in type and complexity, from those that are based purely on experimental data, implemented into models as tables which can be interpolated depending on the tyre operating condition, these models are aptly named interpolation models; to finite element (FE) models of the tyre structure with hundreds of degrees of freedom.

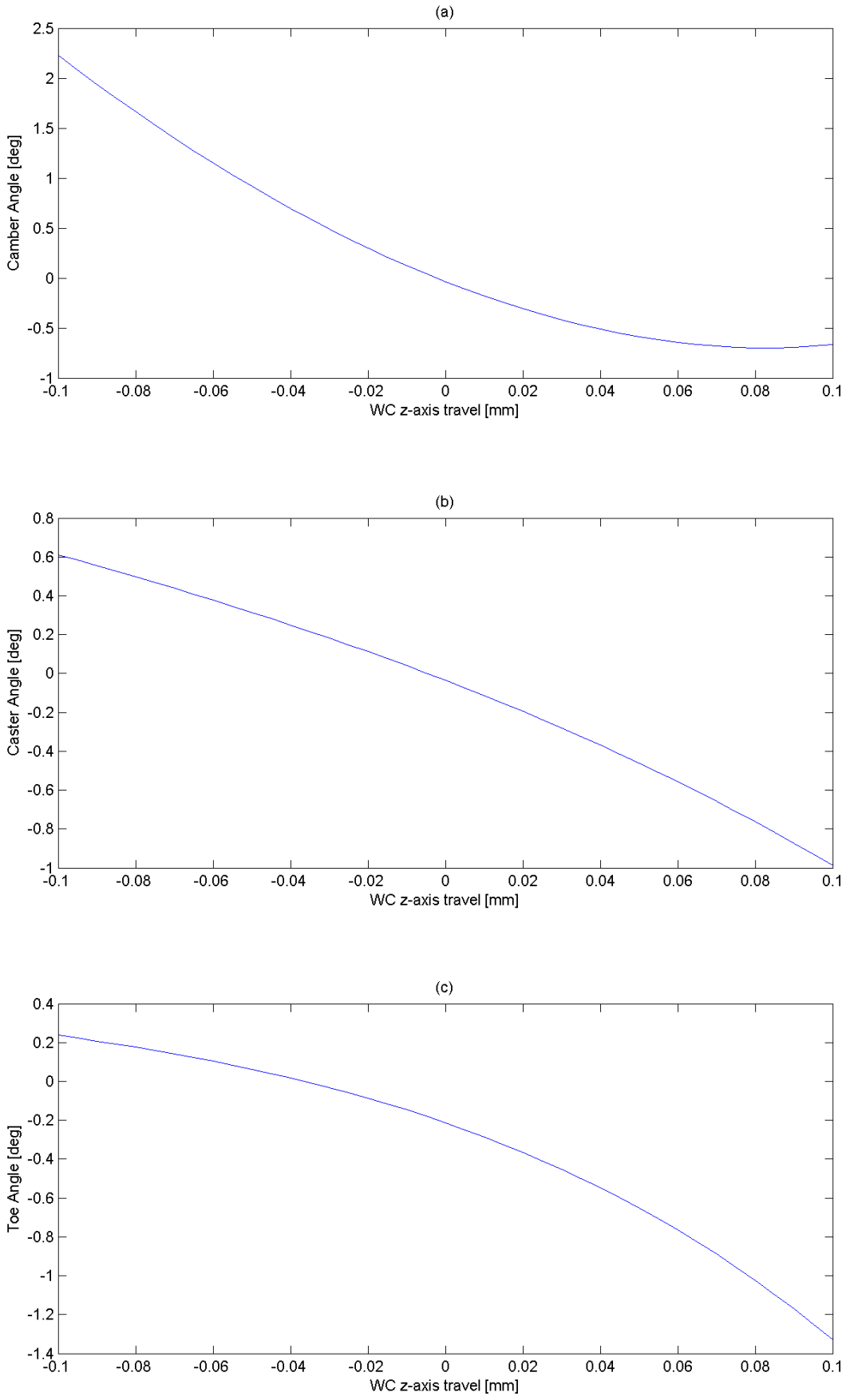

Figure 3-10 Front suspension caster, camber and toe change in bump

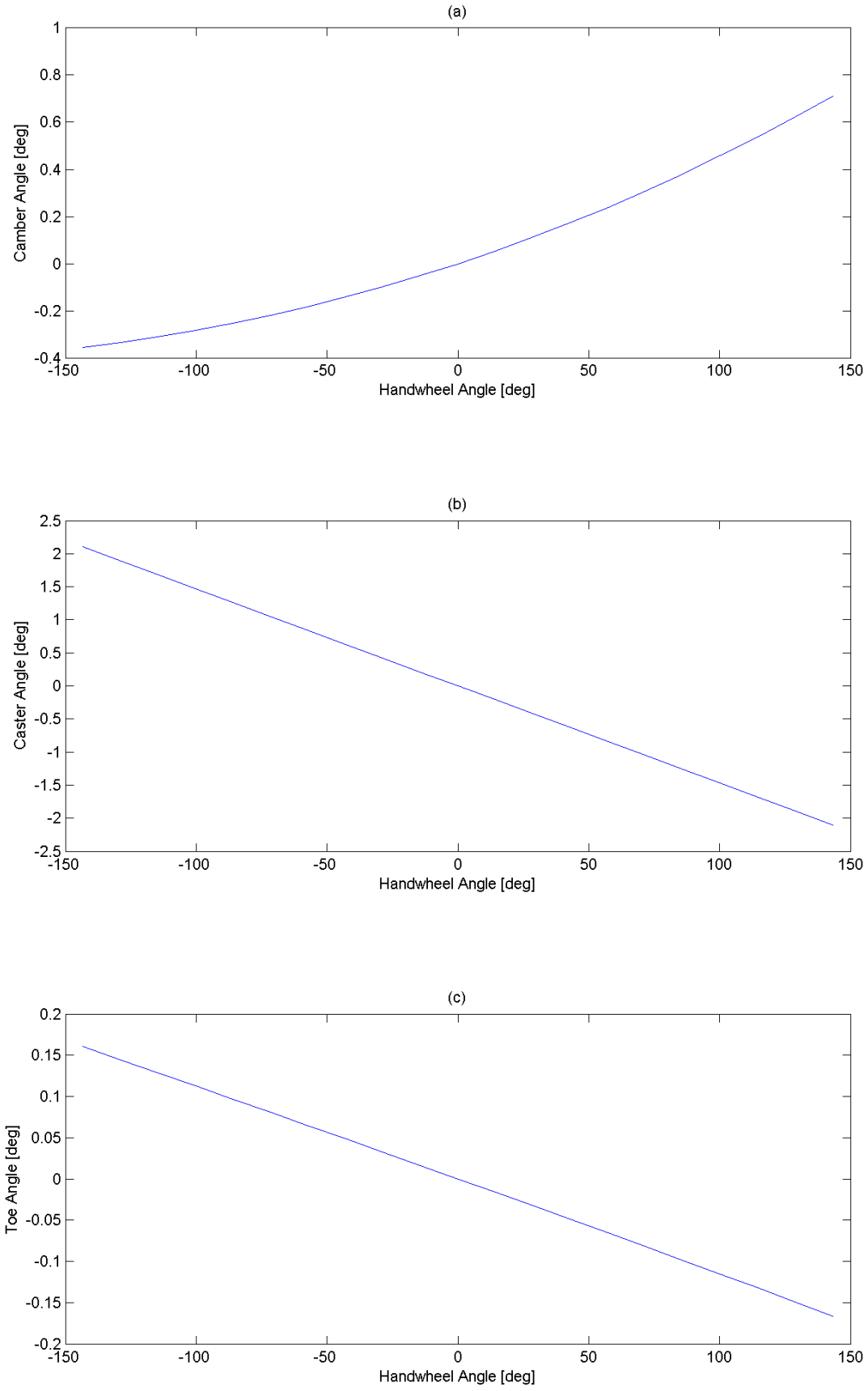

Figure 3-11 Front suspension caster, camber and toe change with steer motion

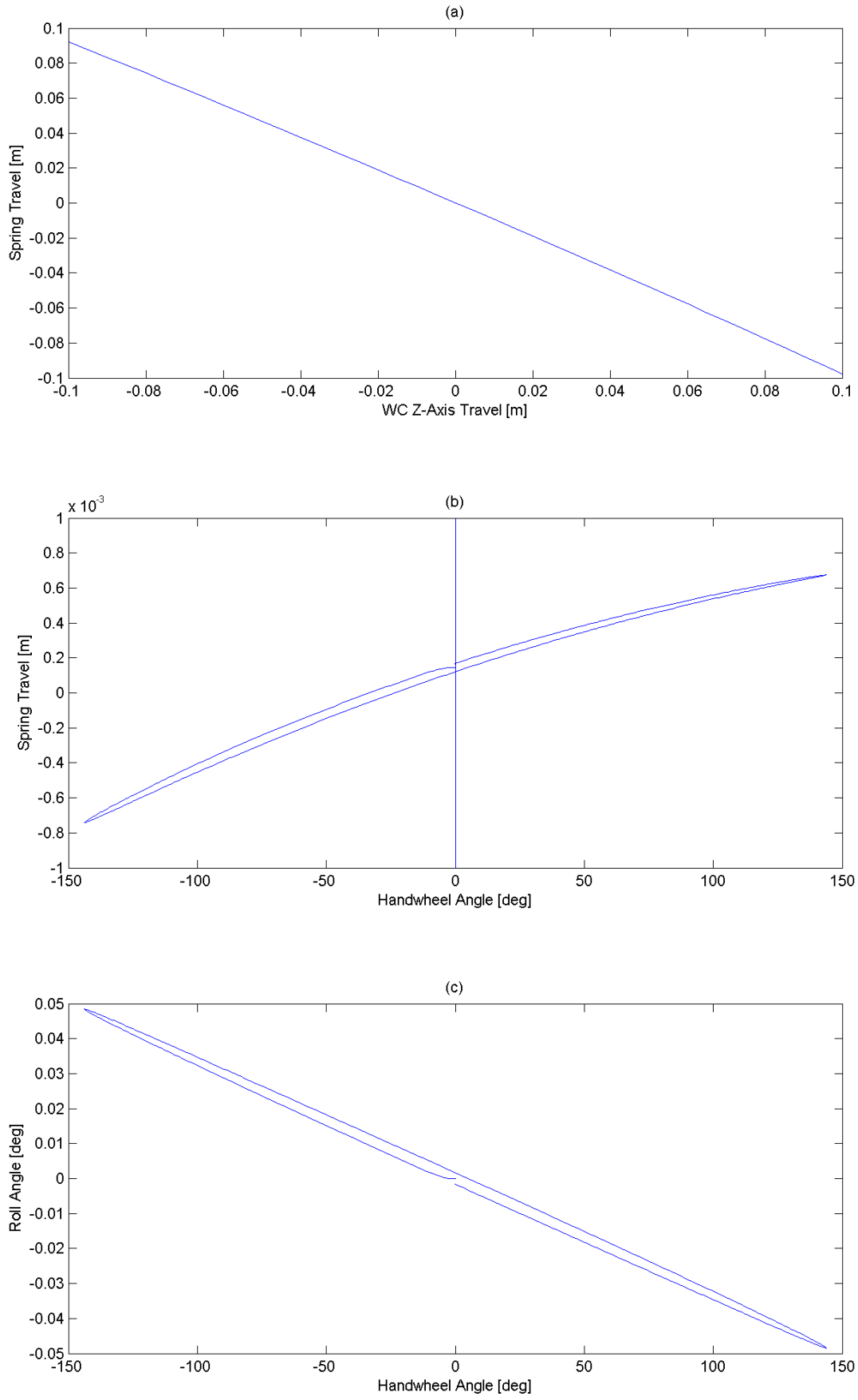

Figure 3-12 Front suspension spring motions

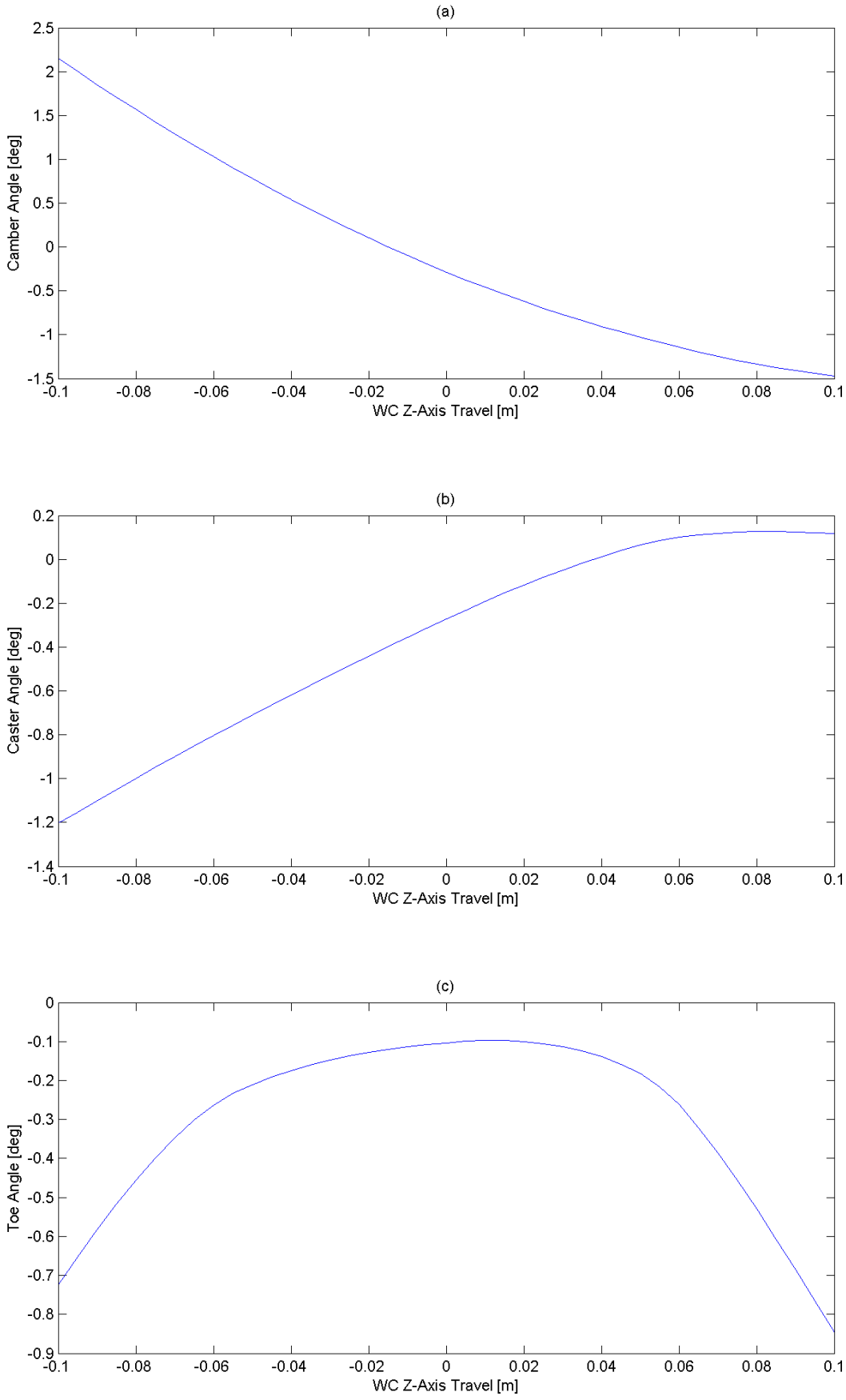

Figure 3-13 Rear suspension caster, camber and toe change in bump

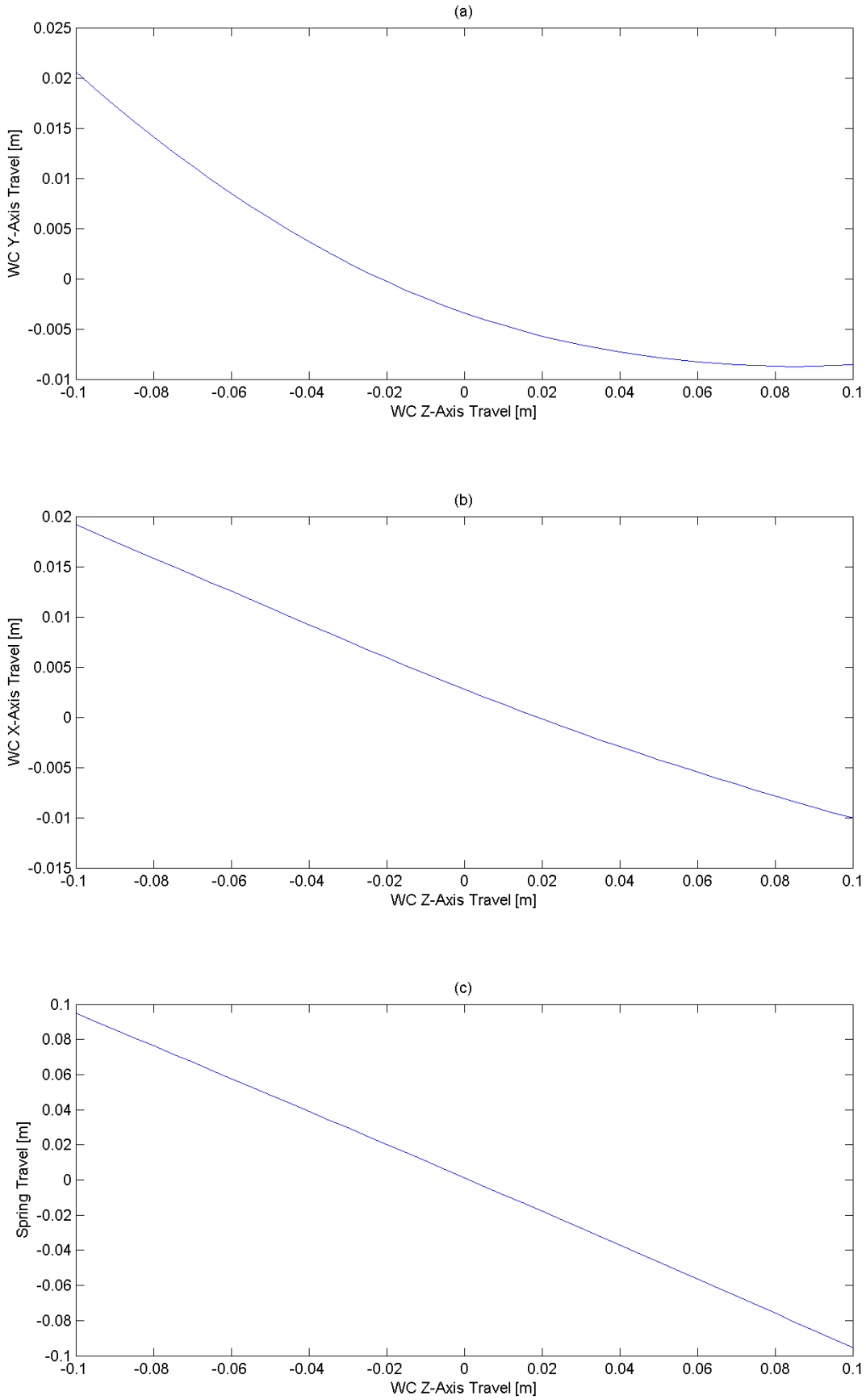

Figure 3-14 Rear suspension x and y axis translation and spring motion in bump

Interpolation models, their use and advantages and disadvantages are discussed by Browne and Arambagas (1981). Such models are useful for their ease of implementation, their simplicity and the fact that the data that comprises the model has a physical meaning, they are also very computationally efficient and so can be used in situations where quick simulation times are required. On the other hand interpolation models tend to be very large as they are made up entirely of tables of measured data, because of this they are only useable over a small range of operation conditions, as to fully map the relationship between all slip, orientation and load conditions would not only require hours of testing, but would lead to vast amounts of data that would not be feasible to implement. In recent years interpolation models have started to become obsolete due their capabilities compared to other types of tyre model.

In the 60's and 70's more physically based tyre models were produced, one of the most well known of these is called the Brush model (Dugoff et al., 1970, Pacejka, 2002). The model itself is based on the physics of a tyre and so has meaning and is easy to understand. The tyre model describes the forces by assuming two regions within the contact patch, the adhesion region based on the elasticity properties of the tyre and the sliding region governed by frictional forces. The model is referred to as the Brush model as it is obtained by considering the rubber volume in the contact patch as brush elements which can stretch to create the tyre forces. The Brush model was very popular and widely used until the introduction of empirical tyre models (Svendenius, 2007).

Somewhere in between interpolation and physical models lie empirical and semi-empirical models. Empirical models can be described as sets of formulae possessing parameters that are usually evaluated with the aid of regression techniques in order to

find a best fit to measured data (Pacejka, 2002). The most common empirical model is probably the Magic Formula. The Magic Formula was conceived in the mid eighties in a partnership between TU-Delft and Volvo, numerous versions have been developed over the years, each version adding complexity or configuring the model to a slightly different purpose. Despite this variation, all Magic Formula tyre models posses the same basic form composed from a sine of an arctangent which is used to fit test data, and comprises numerous coefficients relating to shaping, peak values, curvature and stiffness etc (Pacejka and Bakker, 1991, Zegelaar, 1998). With its increased complexity it has the ability to handle both pure and combined slip conditions. As complexity is added to empirical models the number of coefficients they contain increases, the Pacejka 94 model which is based on the Magic Formula consists of 68 coefficients, newer versions consist of over 150. Empirical models should be used when tyre forces are needed in a combination of pure and combined slip conditions, and where the idealized representation of experimental data is deemed acceptable (Pauwelussen and Schmeitz, 2001).

Semi-empirical tyre models are an intermediate step between empirical and physical models. Most are again an adaption of the magic formula but with extra coefficients coming from tyre measurement and construction data, the model focuses more on representation of the actual tyre as a system. One of the most well known tyre models of this type is the Short Wavelength Intermediate Frequency Tyre (SWIFT). The SWIFT model is an enveloping tyre model, meaning it models translations and rotations in all three axis as a result of road irregularities up to 100Hz, (Pauwelussen and Schmeitz, 2001). Semi empirical models sit on the boundary between use in lateral dynamics and ride dynamics, the SWIFT model was originally designed for studying tyre performance at high frequencies over short sets

of road obstacles for ride assessment, however with increasing computing power semi-empirical models such as SWIFT are beginning to be utilised for handling studies.

Physical tyre models are based on a purely mathematical approach and focus on finite element methods which describe in detail the interaction between the tyre and ground (Hall et al., 2004b, Hall et al., 2004a). Work carried out by Palmer, Farahani and Zhang (1998) explains detailed finite element methods using implicit and explicit integration techniques to create FE models of tyres that predict interactions to cleat impacts and other road irregularities. Due to the complexity of the models, and the integration methods used, physical models require a large amount of computational power and as a result are very slow to run. Two of the most recent physical models to be developed are known as F-Tire and CD-Tire, (Dorfi et al., 2005). F-Tire is based on similar principles to the SWIFT model, however it has in the order of a few hundred degrees of freedom and has a much more complex model of the contact patch which is modelled as individual tread blocks which allow shear deformation and compression between them. The latest versions of F-Tire also includes factors which account for tyre wear, tyre temperature and even tyre imperfections, (Gipser, 2008). Physical models such as F-Tire can be used for both ride and handling studies, although simulation times are very slow compared to less sophisticated empirical or interpolation models, and so use is most commonly kept to ride and comfort or tyre studies where a more detailed picture of what is happening within the tyre is needed.

Despite there being a large number of tyre models to choose from, tyre data is notoriously difficult to come across and is closely guarded by tyre manufacturers and OEM's. Due to this there was not much choice in the type of tyre model utilised. It

was possible to obtain coefficients for a tyre of the same size and construction as the ones on the vehicle in question. The tyre model utilised in this study is of a Michelin Latitude Tour 235/65/R17 at 2.21 BAR (32 psi). This data, like the stiffness and geometry data, was obtained directly from the OEM. The tyre model .tir file and lateral and longitudinal force plots are shown in Appendix A.

The model utilised for the vehicle model is of MF02 format. The MF 02 model is based on the Magic Formula type tyre model discussed earlier in this section and contains 160 coefficients describing the shape of test data.

The method of implementing the tyre model into the vehicle model was one that was particularly straight forward as the Modelon vehicle dynamics library offers a template for recent Pacejka and MF models. The MF02 sets of equations are pre written, with a GUI that enables data entry.

The four tyres on the vehicle are identical so again, one tyre model was created and parameterised and then instantiated to create the three other tyres. These tyre models where then connected to the uprights/hubs of the suspension models.

3.5 Chassis Model

The chassis connects the front and rear suspension linkages. The models utilised here employ a rigid chassis, meaning there are no degrees of freedom between the front and rear suspensions, the two are simply offset in the x-axis by the wheelbase. This approach is the simplest and most feasible given the data at hand. Chassis models including varying degrees of freedom can be developed and included if need be, ranging from simple torsional models which just incorporate a torsional stiffness, to full FE models of physically modelled chassis'.

The chassis model houses the detailed mass and inertia data for the vehicle. As with the development of the real vehicle, the model of the standard vehicle is going

to undergo changes to its architecture and setup in order to create the model of the GTV. To enable this, all components of the real vehicle that are to be altered are modelled separately in the standard vehicle model. Components such as the engine and gearbox all the way down to the rear seats and carpet are included in the model as separate multi-body masses, enabling their individual mass and inertia effects to be captured. In the adaption of the SV model into the GTV model, these components are simply removed, and similarly added for components such as the EM and battery pack. This allows the mass and inertia properties to be accurately captured by the models without the need for testing of the real vehicle to obtain such data. The data required for this section of modelling was again obtained from the OEM, the data for the parts of interest were extracted from a detailed CAD model, these parts were then removed from the CAD model and the parts that were not of interest left in and lumped together with the mass and inertia data given for the vehicle body.

Also incorporated with the chassis model is the body model, this houses specific data regarding the body in white, such as it mass, inertia and aerodynamic properties.

The complete chassis model including suspension and tyre models is shown in Figure 3-15.

The chassis model in this state is usable, it can be given an initial velocity, and a number of steering inputs which enables its lateral response to be studied, it can also be combined with road models in order to investigate its ride characteristics. However due to rolling resistance, longitudinal components of lateral tyre forces and aerodynamic drag forces, the longitudinal velocity of the chassis reduces greatly during the duration of test manoeuvres. This change in vehicle speed would affect the responses of the vehicle and so needs to be reduced. In order to do this, the

chassis model can be combined with simple engine and drive-train models, which then in turn can be interfaced with a simple driver model/speed controller.

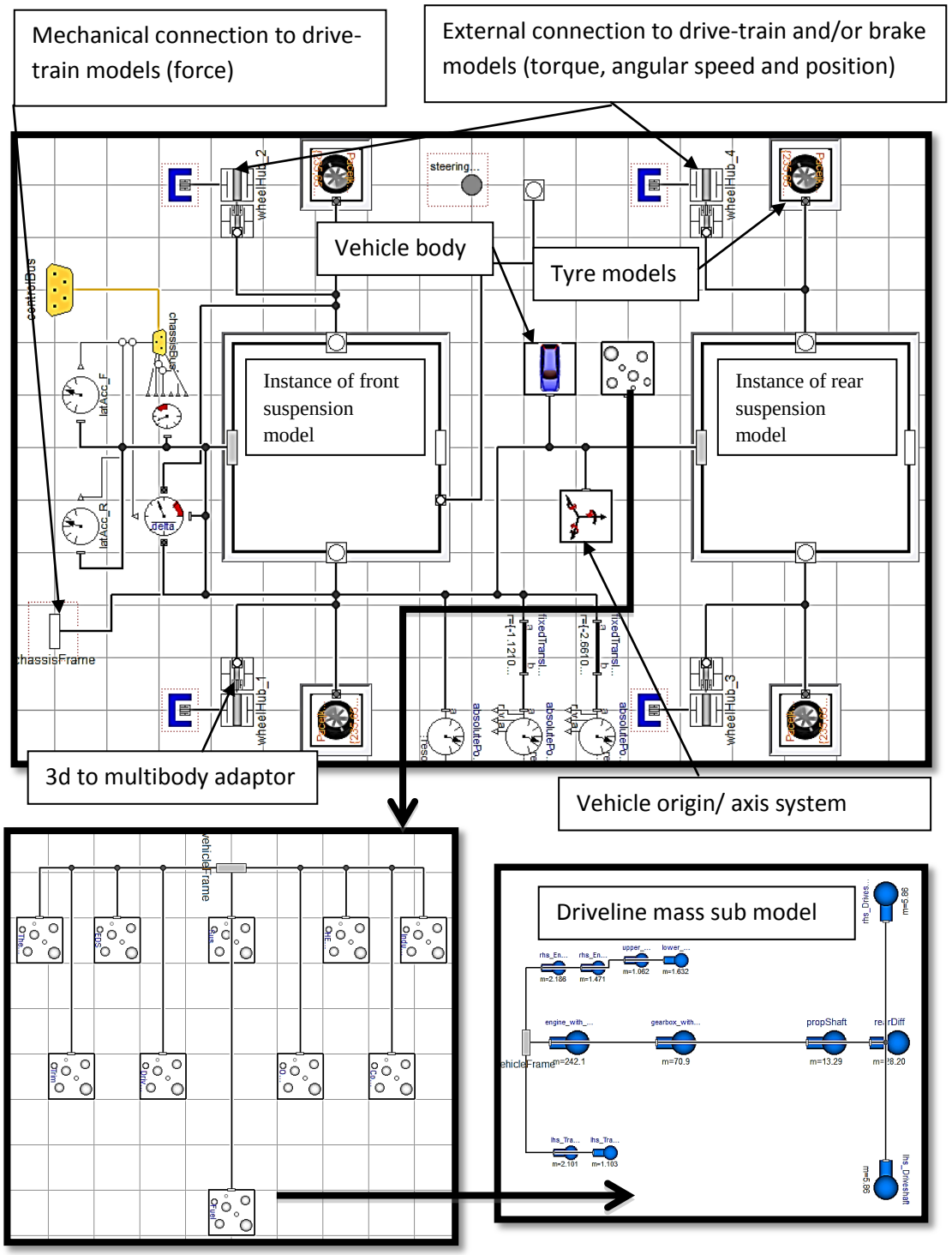

Figure 3-15 Chassis model components with detailed mass and inertia model

To ensure this section of the model is as accurate as possible when compared to the real vehicle, model based inertia tests were conducted. This consisted of using a model of an inertia rig, to which the vehicle could be attached and its roll, pitch and yaw inertia obtained. The rig consisted of a circular ground plane mounted on a revolute joint which allowed rotation about the z-axis. The vehicle was mounted to this ground plane so that its Cog was aligned with the rotation axis. A small torque was applied to the top of the revolute joint and the corresponding angular acceleration of the vehicle was measured. From the input torque and the resulting acceleration, the inertia of the vehicle can be calculated. The vehicle was mounted on its three different axes to obtain the roll, pitch and yaw moments of inertia. The test setup and inertia rig are shown in Figure 3-16.

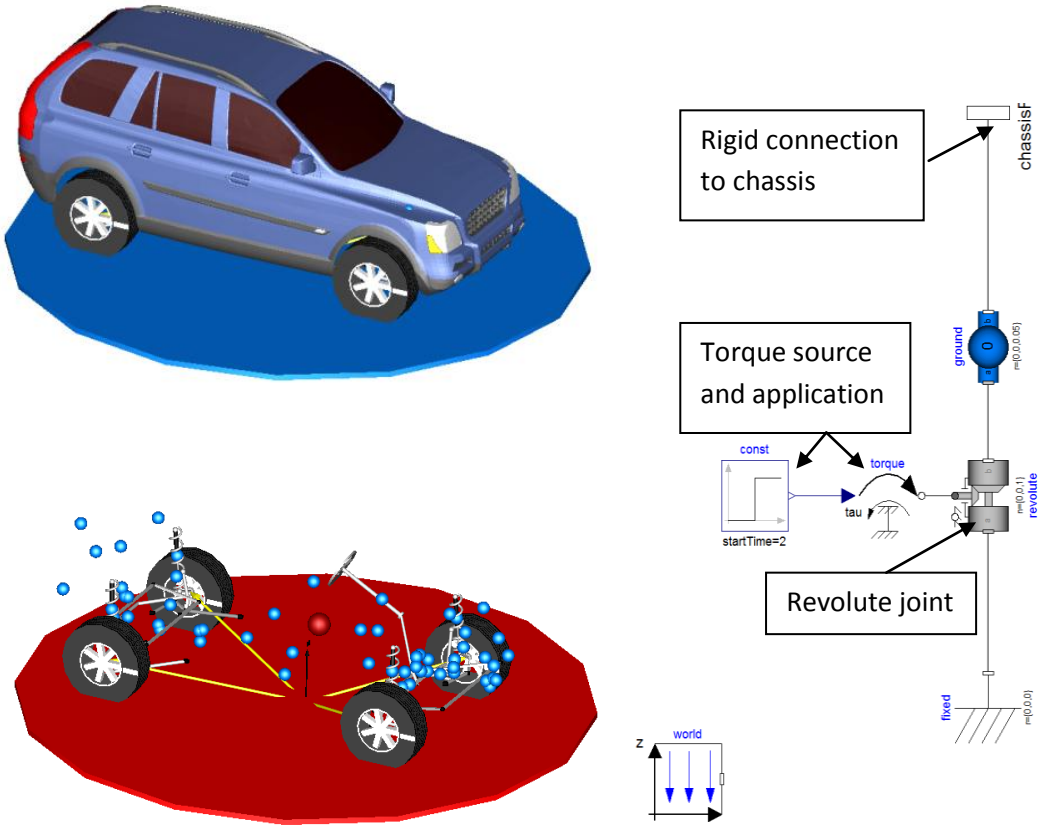

Figure 3-16 Inertia rig model (right) and test configuration (left)

The results from these model based tests are summarised in Table 3-3. The slight difference between the Dymola model presented here and the OEM's model will correspond to the level of detail used, the OEM's model lumped all mass and inertia properties within the body, where the Dymola model presented here, as previously discussed, uses a more component orientated method to include the individual properties of components that are of importance to this study.

Metric	Unit	Dymola Model	OEM Model
Vehicle Roll Inertia	Kg.m2	859.4	815.5
Vehicle Pitch Inertia	Kg.m2	3471.7	3365.0
Vehicle Yaw Inertia	Kg.m2	3776.5	3720.0

Table 3-3 Vehicle inertia properties comparison

3.6 Engine, Gearbox and Drive-train Models

The engine model employed is very simple, it follows the base engine class which is part of the vehicle interfaces library, it takes a throttle pedal position from the driver model as an input and turns this into a mass airflow via a linear lookup table over the entire pedal travel. This mass airflow is used as an input along with engine speed for the engine airflow/speed/torque map (obtained from the OEM), using this 3d map the engine torque at the given operating conditions is output. The complete engine model is shown in Figure 3-17.

The non-mechanical inputs and outputs for the engine model are grouped into busses, shown by the yellow connectors in the aforementioned figure. The mechanical output of the engine model which is torque and speed are connected to a multibody rotational flange which allows for connection to the gearbox model.

The Gearbox model is again another simple model, extending from the base transmission model of the vehicle interfaces library, which takes gear number as an input (from the driver model) and which is used to select the correct ratio via the use

of a lookup table, this is then applied to the torque input to give the output torque. The complete gearbox model is shown in Figure 3-18. The gearbox model takes its torque input from the engine model at the input multibody rotational flange, shown on the left side of Figure 3-18 and gives an output torque, again via a multibody rotational flange, shown on the right of the figure, to the drive-train model.

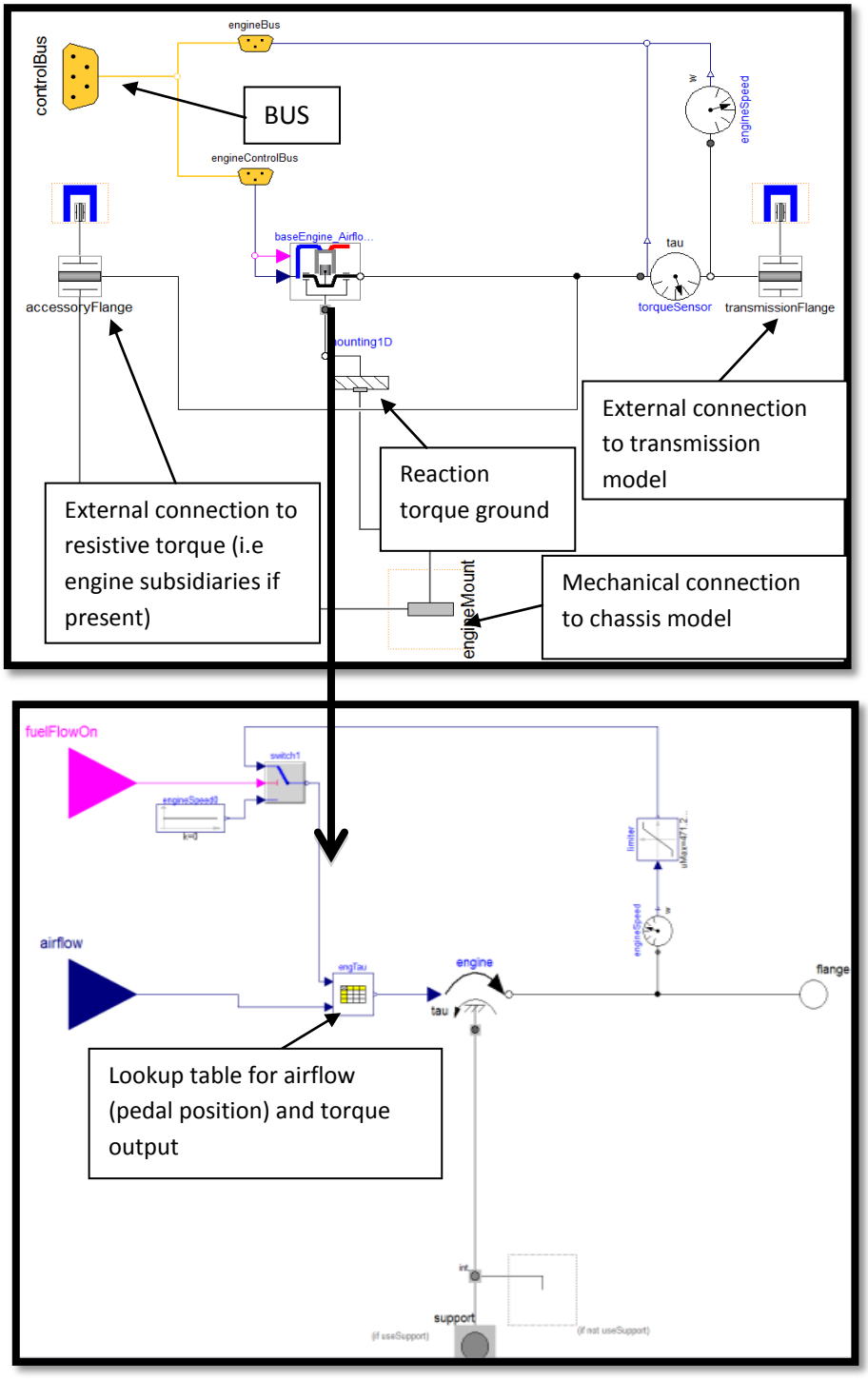

Figure 3-17 Engine model

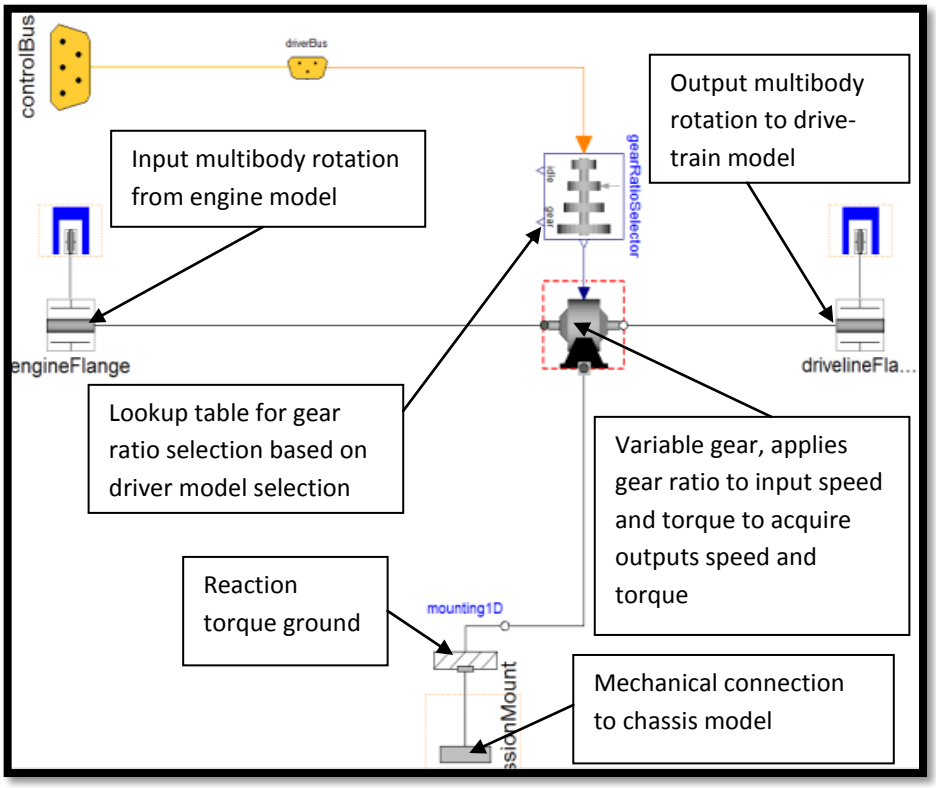

Figure 3-18 Gearbox model

The standard vehicle utilises a Haldex four wheel drive system. The philosophy behind this system is a mixture of an on demand four wheel drive system and a permanent system. The Haldex unit uses a combination of a hydraulically operated wet clutch and an electronically controlled centre differential to continually alter the front to rear torque split. Without knowing the intricacies of the control logic it would be impractical to try and accurately model the drive-train system and its accompanying control system. Due to this it was decided to utilise a simplified drive-train model. It is sensible to assume that in normal driving conditions up to just below limit handling the vehicle will be operating in front wheel drive mode, therefore a front wheel drive drive-train model, extending the base FWD drive-train model form the vehicle interfaces library, has been utilised.

The model consists of five multibody rotational flanges to enable connection to the chassis and gearbox models, the front two of which are connected to a simple differential model which contains an ideal differential gear to simply split the input torque between the two front wheels, and another ideal gear that allows the input of the differential drive ratio. The rear two flanges are connected to a torque source which applies a small negative torque to represent the rear wheels dragging which would be encountered in the real system when it is in 2WD mode. The fifth multibody rotational connection joins the drive-train to the gearbox model and is the torque and speed input from said model.

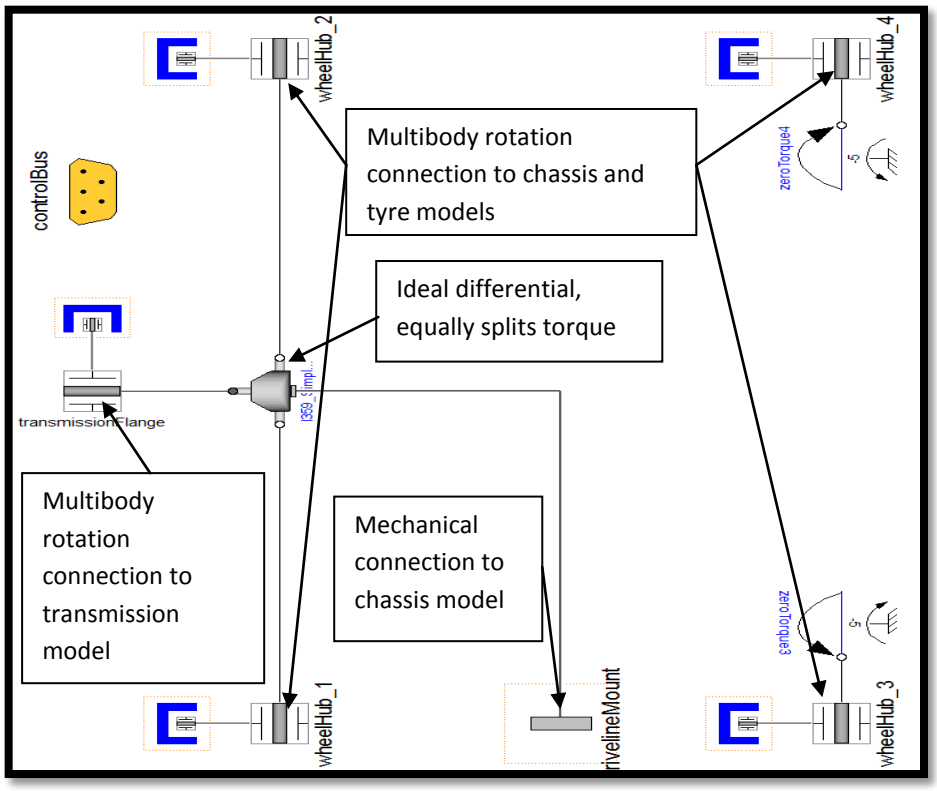

Figure 3-19 Drive-train model

The accuracy of the engine, drive-train and gearbox models are not of vital importance for this study. For the test manoeuvres carried out a speed profile will be given as an input and controlled via a PID controller using current vehicle speed as an input and outputting pedal position for the driver, the PID parameters used are

given in Appendix A. The engine, gearbox and drive-train models are just used as means of allowing the model to be driven in a realistic manner.

3.7 The Vehicle

The complete vehicle model is shown in Figure 3-20. As with the component models, it too is constructed in a fashion compatible with the vehicle interfaces library of Dymola, to aid in the creation, and fit with the philosophy of an easily adaptable, modular model.

The engine model is connected to the gearbox model via a multibody flange, which consists of a torque, rotational speed and rotational position. The gearbox is likewise connected to the drive-train. The drive-train connects to the chassis model using the same flanges, but here connections are between the four driveshafts and the hubs/uprights of the chassis model.

All non-mechanical inputs and outputs of the component models are added to a hierarchical bus network. As can be seen in each component model, there are two busses present, one carries signals in for use in the model and the other collects outputs for use at higher levels. This method allows a large number of outputs to be taken from individual component models and used at different levels of the overall model without the need for separate input and output connectors which can make the model untidy and cumbersome, it can also improve simulation speed.

This construction not only allows for the model to be easily interfaced with a number of driver models, but the modular construction allows individual component models to be easily replaced with higher fidelity models as and when needed for more diverse and in depth studies. One example of this could be to include a fully compliant drive-train model in order to investigate driveability.

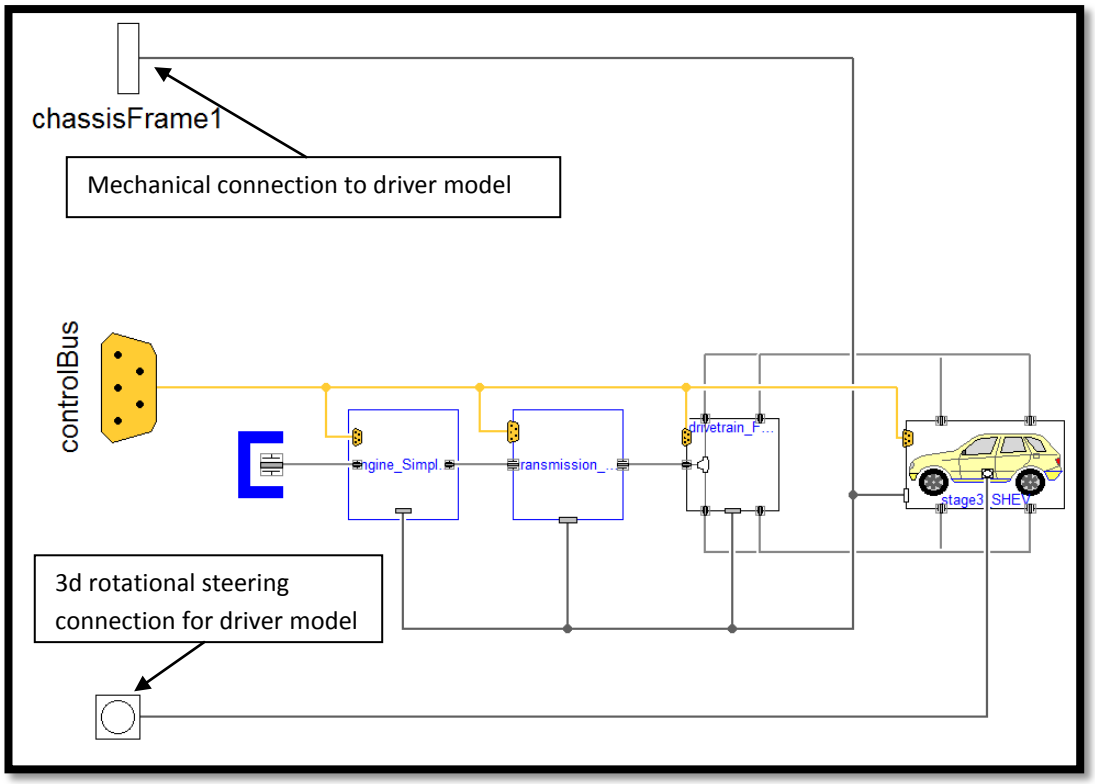

Figure 3-20 Complete vehicle model

3.8 Driver Model

In order to control the model, obtain desired speeds and apply specified steering procedures, it is necessary to utilise some sort of control model. Within the Modelon vehicle dynamics library there are a number of open and closed loop driver models. These range from very simple open loop models which use a series of time based lookup tables to define, steering, throttle, clutch and gear inputs, to much more complex closed loop models capable of performing path following based on queuing from road and environment models.

For the majority of the manoeuvres that will be utilised in this study a purely open loop model will suffice. A pre-defined open loop model is available in the aforementioned library, this consists of a number of inputs which allow the connection of any numerical source component from the Modelica or Modelon

libraries to define throttle, steering, clutch or gear number inputs. Alternatively if these values are to be constants then they can be hardcoded into the driver model interface.

The driver model utilised is shown in Figure 3-21, the blue input connections are numerical, they are connected to an adaptor which formats them as 1d rotational, for the steering wheel signal, and 1d translational for the pedal signals.

In order for this model to be utilised with the pre-discussed vehicle model, some formatting has to be conducted on the signals passed from the driver model to the vehicle model. This is done within the driver interface component shown in Figure 3-22. This extra formatting is required as all the inputs and outputs between subsystems within the model (with the exception of torque and speed signals between chassis and power-train components) are put on a BUS. As signals within Dymola are assigned real world values, such that an output from a rotational component will be defined as having a mechanical torque and speed, therefore this signal is known as a real world rotation. The signal BUS can only carry pure numerical data (integers, doubles, floats), meaning a numerical value with no information as to what the values relate to.

The driver interface converts 1d mechanical translations from pedal positions and gear shifter position to numerical values that can be carried on the BUS to the desired vehicle subsystems, these values are then converted back within the component models where they are utilised. These conversions are carried out using a number of sensors which either take the rotation or translation as an input, measure the value, and output a pure numerical measurement, or visa-versa.

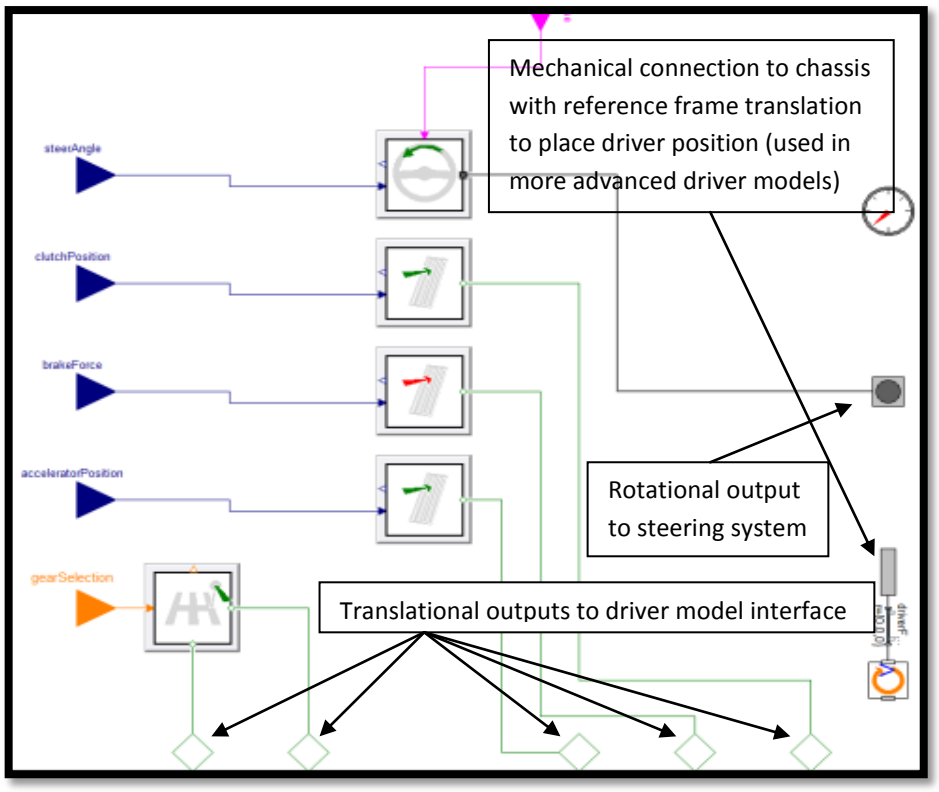

Figure 3-21 Driver model

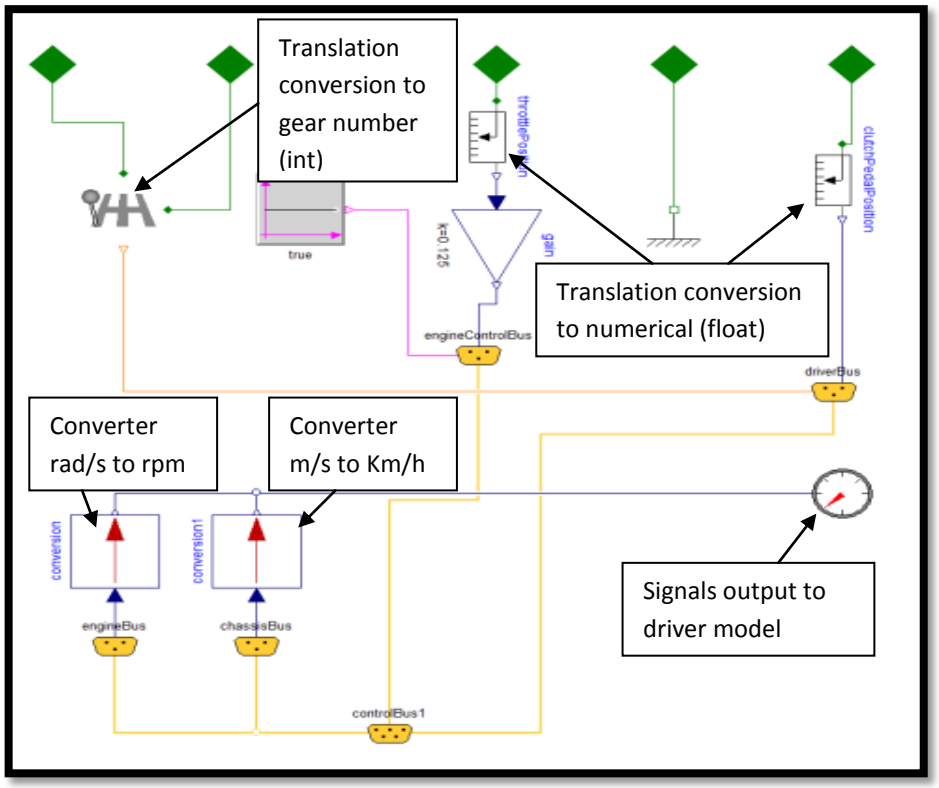

Figure 3-22 Driver model interface

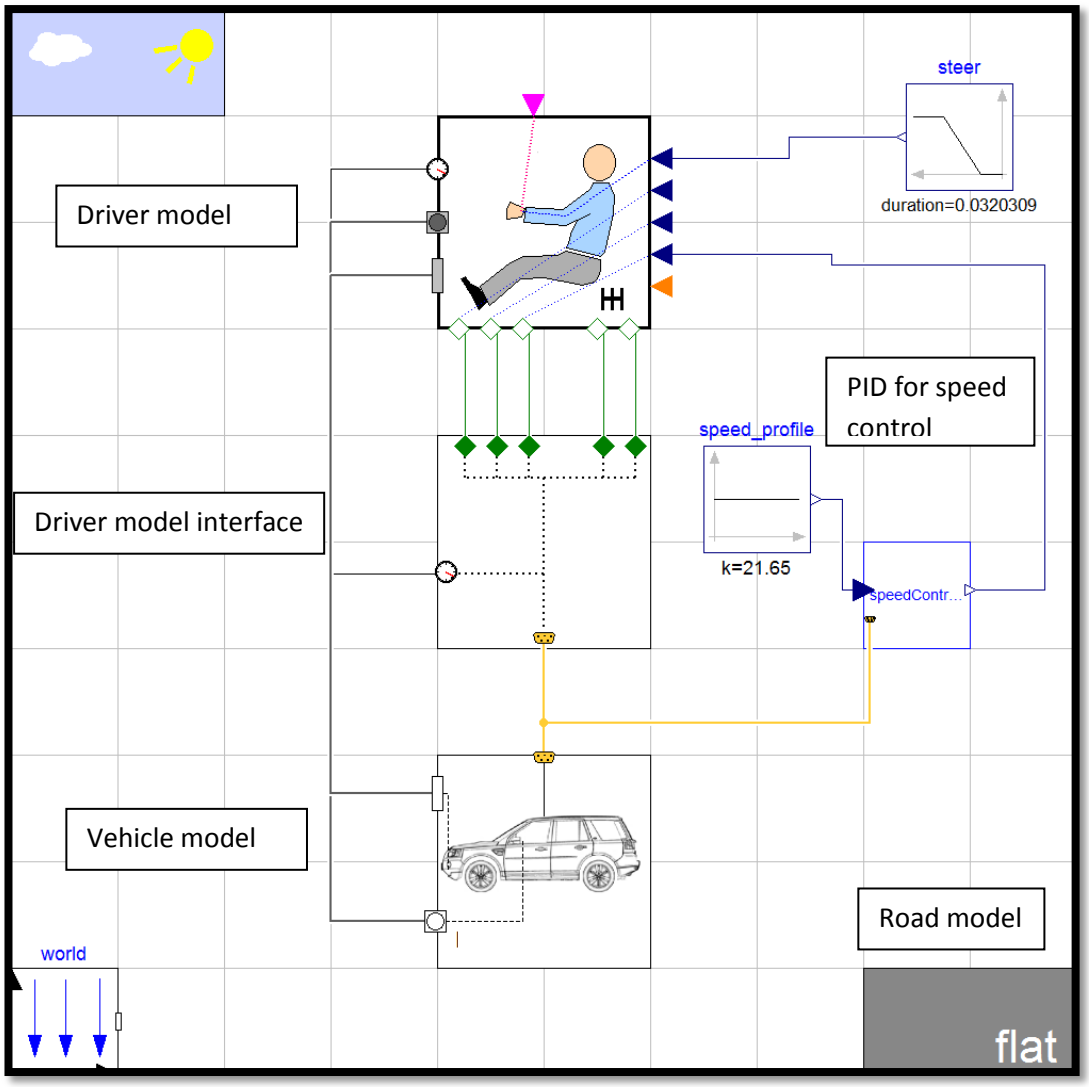

Figure 3-23 Complete model

3.9 Model Testing and Validation

In order for the model to be useful it must represent reality and/or the error in its outputs be known and quantifiable. In the field of vehicle dynamics, general practice is to compare model outputs to measured outputs from the real vehicle or its constituent parts.

One benefit of using the physical object orientated approach facilitated by Dymola is that a number of model based validation exercises can be conducted. Suspension models can be tested in the pre-defined corner and axle linkage rigs

included in the Modelon vehicle dynamics library. This allows kinematic, force, and compliance data to be obtained and compared against kinematic and compliance rig (K&C Rig) data obtained from real life tests. Such a process was discussed earlier where the suspension and chassis models were validated against data obtained from the OEM. Here validation will focus on the vehicle systems as a whole and compare top level outputs.

3.9.1 Vehicle Setup

In order to validate the vehicle model at a top level, outputs from the complete vehicle model need to be compared to measurements taken from the real vehicle. In order to obtain such measurements from the real vehicle it needs to be tested to obtain the required responses.

The vehicle under test here was not the exact vehicle modelled but a very similar platform belonging to the same family of vehicles. Both vehicles are 4wd, with 4 cylinder diesel engines, transversely mounted, the difference between the two relates to bodywork and some ergonomic optional extras, both are stated as having the same curb weight. The biggest difference between the vehicle model and the test vehicle are the tyres. The vehicle model uses a Michelin tyre model, the test vehicle has the same size and construction of tyre but they are manufactured by Continental. The Michelin tyre model had to be utilised with the vehicle model as it was the only tyre model available from the OEM, no other tyre data was available for use. Whilst the difference in tyres used from those modelled is likely to introduce discrepancies in the results, the data obtained from testing should be sufficient to indicate whether the model is capable of illustrating the basic trends of the vehicle's handling.

The small differences in vehicle specification were assumed to have very little or no effect on the model correlation, only the difference in the tyres used in testing

compared to those modelled were expected to have an influence. From experience it is also seen that due to differences in frictional coefficients between tyre and road in the model and in reality, the tyre model coefficients usually need altering to achieve model correlation, this was also the case here, the LMUY tyre coefficient was changed from unity to 0.7, giving a 30% reduction in peak lateral force generated by the tyre model. This value was found through consideration of the coefficient of friction between rubber and concrete and by trial and error in the modelling domain with comparison against test data, this value of LMUY is utilised for correlation in this section and the remainder of this study. It is likely that the LMUX coefficient will also need reducing a similar amount, however here this is left at unity as longitudinal dynamics are not within the main focus of this work.

To validate the vehicle model within the handling domain a number of lateral open loop tests were conducted, and using a data logger with sufficient sensors the vehicle responses were recorded. This real world data was then compared to the outputs given from the Dymola model that utilised the same inputs as the real vehicle. For instance the speed trace recorded from the vehicle was utilised as an input for the vehicle model, when this is combined with the corresponding steering trace, the outputs of the model should be comparable to those measured from the vehicle. The testing was carried out by the specifications of BSI 15037-1:1998, Road Vehicles – Vehicle dynamics test methods (BS150037-1:1998, 1998), and utilising manoeuvres and test techniques from BSI 7401:2011, Road Vehicles – Lateral Transient Response Test Methods – Open Loop Test Methods (BS7853:1996, 2011). From these industry standards it was decided that in order to validate the vehicle model, both its steady state and transient responses would need to be investigated. The vehicle's steady state behaviour can be summarised with its

understeer and roll gradients. Such metrics can be obtained from circular testing on a skid pan or comparison of steering and lateral acceleration and/or steering and roll angle for any steady state cornering manoeuvre. The vehicles transient responses can be illustrated through the use of ramp-to-step-steer and sinusoidal steer manoeuvres.

The minimum amount of data required from the vehicle during these tests, that would allow for sufficient validation is, lateral acceleration (at vehicle Cog), yaw rate, vehicle speed and steer angle, additionally it would also be valuable to know roll and pitch angles/rates and the drive-train operating mode (4WD or 2WD) although this is not crucial.

In order to obtain this data the vehicle was fitted with a data logger, with internal accelerometer and external gyro. The data logger also had the ability to connect to the vehicle's on board diagnostics (OBD) which enabled further information to be read from the vehicle CAN bus. Through this interface the vehicle's drive-train operating mode, yaw rate, lateral acceleration, steering angle and speed were also recorded. A complete list of recorded channels and logging rates is given in Appendix C with the test plan.

3.9.2 Instrumentation

The data logger used in this study was a Race Technology DL2, shown in Figure 3-25. This logger was utilised as it allowed direct connection to the vehicles on board diagnostic systems (OBD), this enabled the required signals to be logged directly from the vehicle CAN network, (the same signals that are utilised in the vehicle safety systems). The data logger itself has 16 extra 12v, 12 bit analogue inputs. However utilising the vehicles own sensing data also simplifies the logging task as the sensors are already mounted in the vehicle and pre calibrated. The CAN messages are able to be decoded by the data logger as it can be configured with the

CAN db file (obtained from the OEM). This file is simply loaded into the configuration software of the DL2 logger, as shown in Figure 3-24.

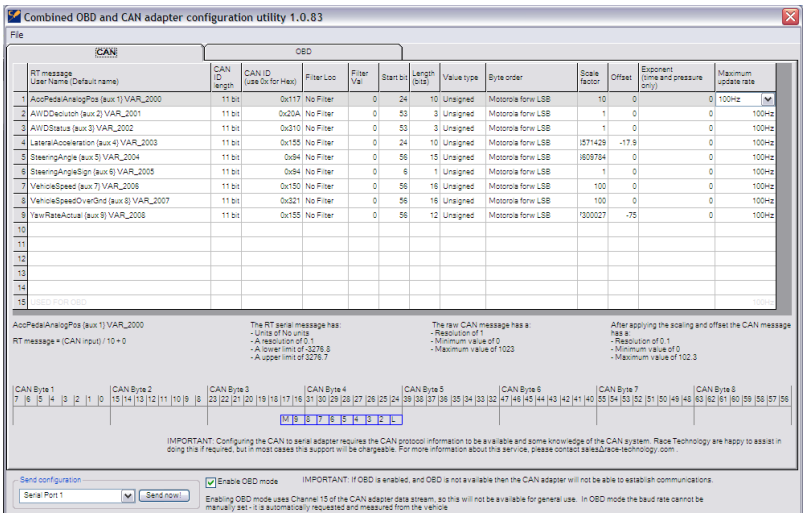

Figure 3-24 CAN Configuration

The data logger has a 12 bit analogue digital converter, prior to which is an electronic low pass RC filter, comprising of a 22 K ohm resistor and a 10 nf capacitor, this produces a cut off frequency of 723.4 Hz. The data is oversampled by the ADC at 10 KHz, after which in the processor an 8-point average is applied to the signal to smooth the data and store the signal at the user selected logging rate.

The RC filter mentioned previously attenuates the higher frequency content of the input signal by means of reducing the output voltage for higher frequencies, (due to capacitor's impedance decreasing with increasing frequency) as such at the cut off frequency the output voltage is 70.7% of the input.

As the data collected during testing is for use in the handling domain, where the maximum frequency of vehicle body motions of interest is under 20Hz (Segers, 2008), a logging frequency above 40Hz would prove sufficient for the signals of interest in this study, however due to higher frequencies that could be present due to noise in the signals, oversampling the signal ensures that these higher frequencies are accurately captured and do not present as aliases in lower frequencies. The

oversampling rate of the ADC is sufficiently high to ensure that it is at least twice the highest frequency content of the recorded signals, thus satisfying the Shannon-Nyquist theorem (Actel, 2007).

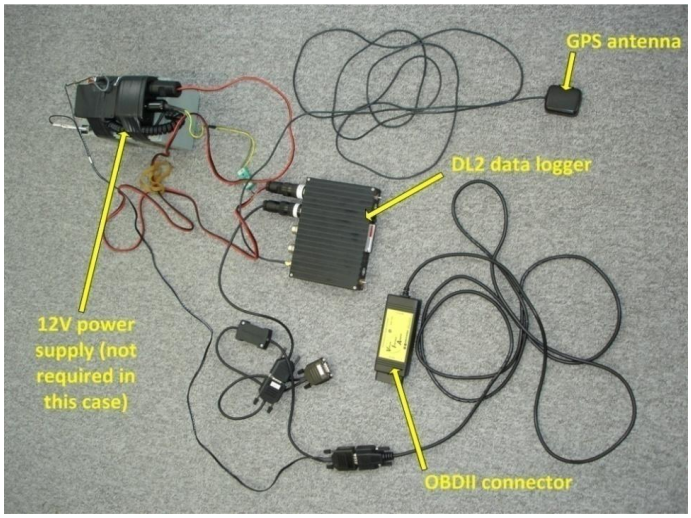

Figure 3-25 Data logging hardware

3.9.3 Instrumentation Installation

For the purpose of sensor verification the DL2 logger was mounted in between the driver and passenger seats on the centre console, this was as close to the vehicle Cog as possible without removing bits of trim. Whilst positioned accurately on the x and y axis of the vehicle, this position did mean that in the z-axis the logger was about 200mm higher than the Cog, which could explain some of the discrepancies observed in the two acceleration signals.

The gyro was fixed to the floor of the vehicle, behind the front seats on top of the tunnel. The wiring and powering of the Gyro is discussed and outlined in the sensor specification sheets given in appendix C.

The OBD2 connector plugged into the vehicle behind the glove box, in front of the passenger seat.

The data logger was powered from an inverter that was connected to the 12v power supply/lighter inside the vehicle.

Once the sensor verification had been conducted the data logger was moved from the centre console to the floor behind the passenger seat as it was a more convenient area where it did not interfere with the operation of the vehicle.

3.9.4 Sensor verification

From the data requirements previously mentioned it was deduced that, lateral acceleration, yaw rate, steer angle, and vehicle speed would need to be recorded, all of which are available from the CAN bus of the vehicle. Whilst these sensors are already calibrated as they are used for the vehicles control systems they were verified by comparison against external sensors. Steer angle, and vehicle speed being recorded in this method had previously been used in another study into driver habits and had been proved reliable, so here only lateral acceleration and yaw rate were checked.

Lateral acceleration data from the vehicle CAN was verified against an accelerometer within the DL2 data logger. The yaw rate from the CAN was verified against an external gyro connected to one of the DL2's analogue inputs. The technical specification for the data logger, internal accelerometer and externally connected gyro are given in Appendix C. The verification plots are also illustrated in said appendix and show good correlation between external sensors and the CAN signals from the vehicle. It is seen that whilst the two signals (external and CAN) are very similar, there are small discrepancies, most likely arising from differences in mounting location (accelerometer) and sensor type. It is also seen that the external sensors appear to have a larger noise content than the CAN signals. Due to this, and as it was thought that the CAN signals should be more reliable and accurate (due to

their use in the vehicles safety systems), they will be utilised for the main lateral acceleration and yaw rate signals throughout this study. The aforementioned gyro will be utilised to record vehicle roll and pitch motions.

3.9.5 Constant Radius Tests

Constant radius testing allows the steady state characteristics of the vehicle behaviour to be identified. The difference in the two vehicles steady state behaviour will prove important in later stages of this work as it enables test manoeuvres that are directly comparable between the two vehicles to be designed. Here however the steer and lateral acceleration data collected from vehicle testing is compared to the same outputs from the vehicle model. There are a number of ways of obtaining the steady state behaviour of a vehicle through testing; these are discussed in, Passenger Cars - Steady-state circular driving behaviour - Open loop test methods (BS4138:2004, 2004). The method used here consists of driving the vehicle on a fixed radius at discrete speeds (or levels of throttle position) and steer angles, the vehicle is held at each speed until steady state cornering is achieved, the speed is then increased and the process repeated, this is conducted until the vehicle reaches the limit of its handling, indicated by the tyres reaching their limit of adhesion with the road surface, and so the vehicles radius of turn no longer remains constant with the increases in speed, despite adjustments in steer angle being made. The test procedure carried out is given in Appendix C.

By creating a circular road model using the built in ‘road builder’ command within the Modelon vehicle dynamics library and utilising a driver model with closed loop steering it is possible to re-create the real world test in the modelling domain.

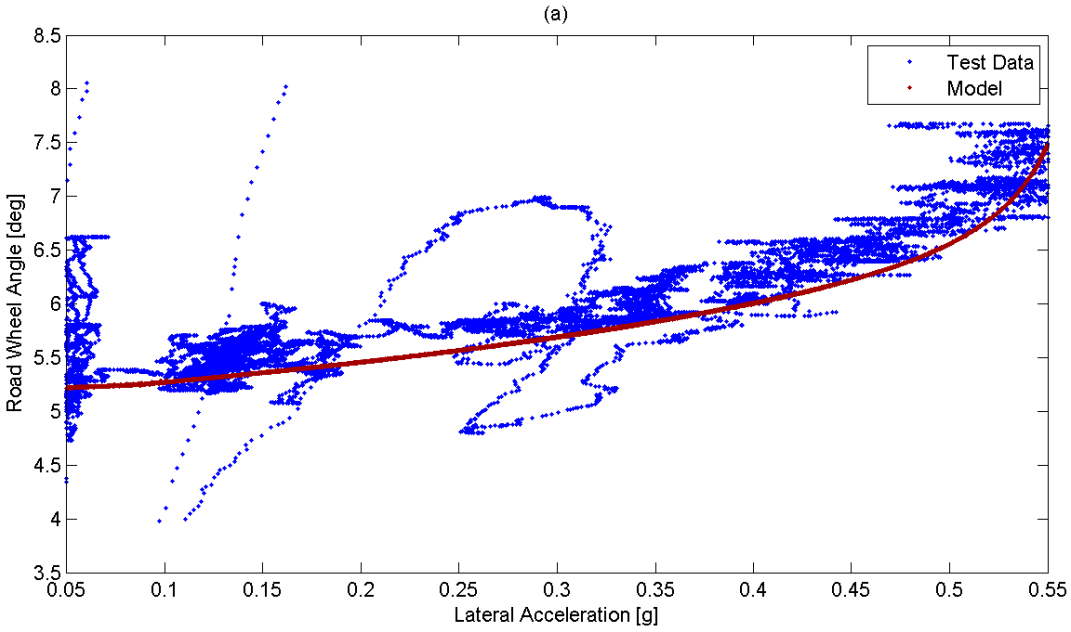

Figure 3-26 Steer angle and lateral acceleration for model and test vehicle

Throttle position inputs to the driver are left as open loop, allowing the input speed to be defined, the closed loop driver model when utilised with a road model is capable of performing route following, therefore with increasing levels of speed the driver model adjusts the steer angle to follow the road model.

Figure 3-26 shows the result of a 30m constant radius test and the equivalent output from the vehicle model. Here steer angle is plotted against lateral acceleration as it gives a convenient way of expressing the steady state handling of the vehicle. The gradient of the curve will give how many degrees of steer angle are required to achieve a given lateral acceleration (on the given radius of turn at a given speed) and is termed the understeer gradient. The results in Figure 3-26 show a good correlation between the model and test data, there is a slight constant offset in steer (y-axis), however this is due to the road wheel angle of the test data being calculated from the handwheel angle with a constant steering ratio, it looks as if the steering ratio used in the model of 14:1 is slightly smaller than that on the actual vehicle under test.

The gradients of each data set (understeer gradient) have been calculated by fitting the linear region of the data (0 – 0.15g) with a straight line, these gradients are shown in Table 3-4. It can be seen that the USG's of the two vehicles in the linear region match extremely well, the error is seen to be less than 1%, also the handling limit described by each curve shown in Figure 3-26 is very similar.

Test Data 30m		
Model	Test Data	% delta
1.51	1.52	-0.66

Table 3-4 SV and test vehicle undertsteer gradients in linear region

Due to some technical difficulties with the gyro utilised, it was not possible to obtain roll angle data thus making it impossible to compare roll gradients of the vehicle and model.

3.9.6 Ramp-to-Step Steer Tests

Ramp to step steer tests will be used at a later stage to make comparisons between the handling of the two vehicle models. Here the manoeuvre is used to compare vehicle responses to model responses for the purpose of model validation.

The ramp to step steer manoeuvre is conducted by travelling at a constant speed and giving a prescribed steer input over certain time period. The ramp to step steer was chosen over the traditional step steer due to the manoeuvres real life feasibility. Whilst in the modelling domain a pure step steer can be conducted, the actual manoeuvre carried out in real life is not representative of this, a driver can only apply steering so fast, and so the actual manoeuvre is more representative of a ramp. The method of conducting the ramp to step steer manoeuvre and a more detailed explanation of its choice over the conventional step steer is given in chapter 4.

Figure 3-27 and Figure 3-28 show the lateral acceleration and yaw rate responses of both the test vehicle and the model. The manoeuvres are conducted between 12

and 14 $\mathrm{m.s^{-1}}$ and target a lateral acceleration of 6 $\mathrm{m.s^{-2}}$. Results are shown for left and right hand tests respectively. It should be noted that the collected lateral acceleration data is quite noisy, this could be due to a number of reasons such as; sensor sensitivity, interference (electrical, mechanical vibration, noise or otherwise), or just environmental effects such as road surface roughness. Nevertheless the data shows good trends and is still useful for the purpose of validation.

It should be noted that whilst the steady state lateral acceleration is similar for both manoeuvres, the yaw rate differs slightly, this is due to the two tests being conducted at slightly different speeds, with slightly different steer angles being applied, this can be put down to human error whilst driving the test vehicle.

Firstly considering the lateral acceleration, it can be seen that there is good correlation between the test vehicle and the model. Steady state values correlate well suggesting that the understeer gradients of the model and test vehicle match, and that the steady state behaviour of the vehicle has been accurately captured by the model. The acceleration gain and overshoot also seem to match quite closely, with only slight differences which can be attributed to differences in the actual vehicle and tyre used, over those modelled, and/or differences in road surface frictional coefficient and surface roughness over those utilised in the model. The yaw rate responses again show good correlation between the model and test data. Once again steady state values are very close and yaw rate gains, peak, and overshoot values agree well, with maximum differences in the order of less than 10%.

3.9.7 Sinusoidal Steer Tests

Sinusoidal manoeuvres are also to be used at a later stage in order to study the transient responses of both vehicles. At this stage they are used to compare the lateral dynamics of the vehicle and the model for validation.

Figure 3-29 and Figure 3-30, like for the ramp-to-step steer manoeuvre illustrate the lateral acceleration and yaw rate responses for both the vehicle and the model. Again it can be said that the correlation between the two is very good. The response gains for both lateral acceleration and yaw rate match closely as do the peak values. The correlation shown here is better than that shown during the ramp-to-step steer manoeuvres shown in the previous section, one explanation for this could be due to the severity of the ramp to step steer test. The vehicle in question is equipped with a stability control system that will actively manipulate lateral acceleration and yaw rate via independently controlling wheel torques if these responses fall into certain regions, or if large handwheel rates are encountered. The severity of the handwheel input for the ramp-to-step steer test could trigger interaction from this stability control system, if this were to happen then the transient vehicle responses would differ from those suggested by the model.

3.9.8 Ride

The model is also to be used for ride analysis of the two vehicles. So ideally it also needs to be validated in this domain as well. As the model consists of compliant suspension and a fully rigid body with rigid component mountings it can only be used for analysis of ride resulting from suspension and suspension element deflections, the effects of vehicle components such as engine and driveline being compliantly mounted are not included. Combining this with the fact that it was not feasible to collect ride domain data for validating the model when the vehicle was tested (due to equipment and budget constraints) means that it was deemed acceptable to validate the model with the limited data supplied by the OEM.

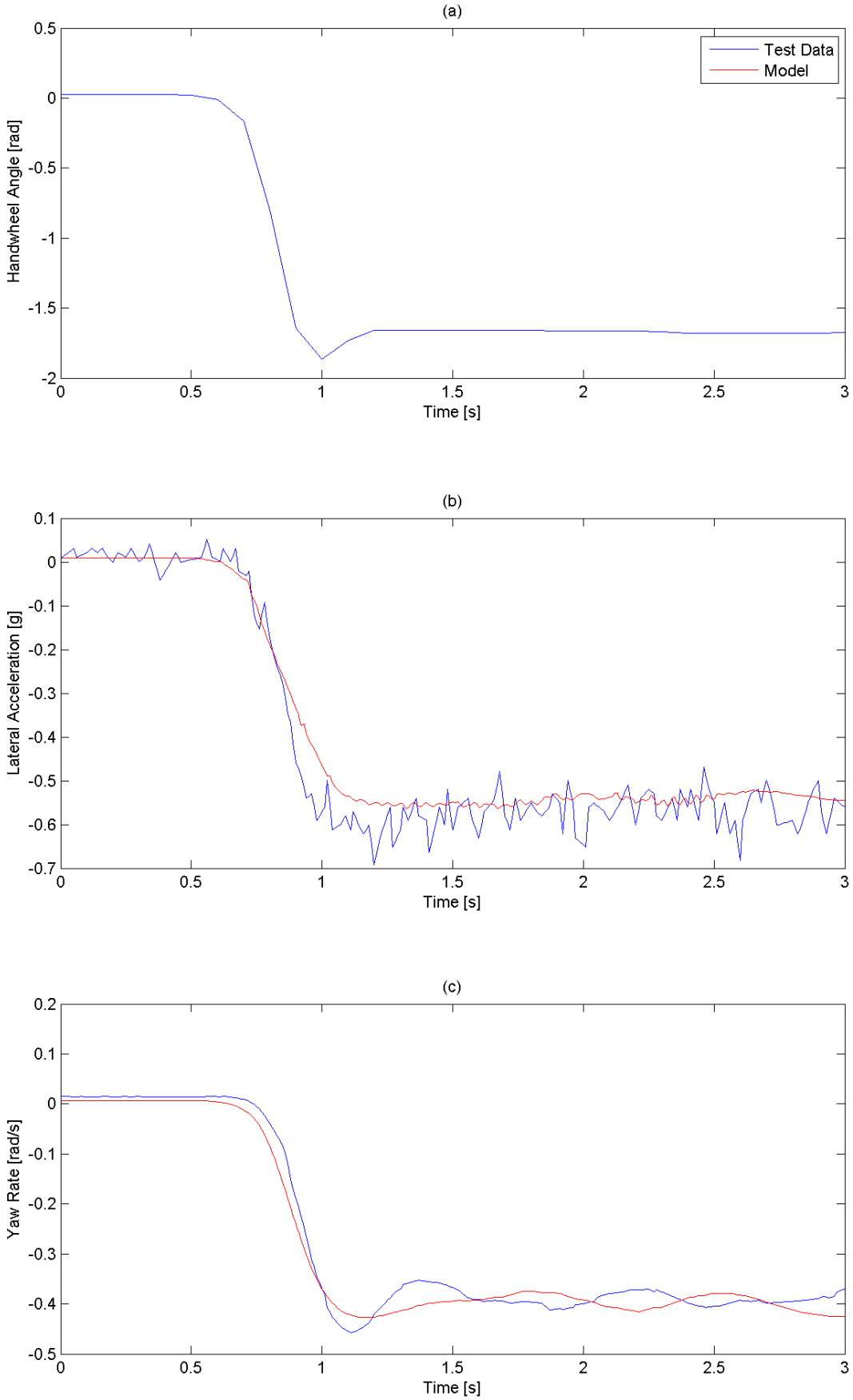

Figure 3-27 Lateral acceleration and yaw rate for test vehicle and model during ramp-to-step steer manoeuvre targeting 6 ms^{-2}

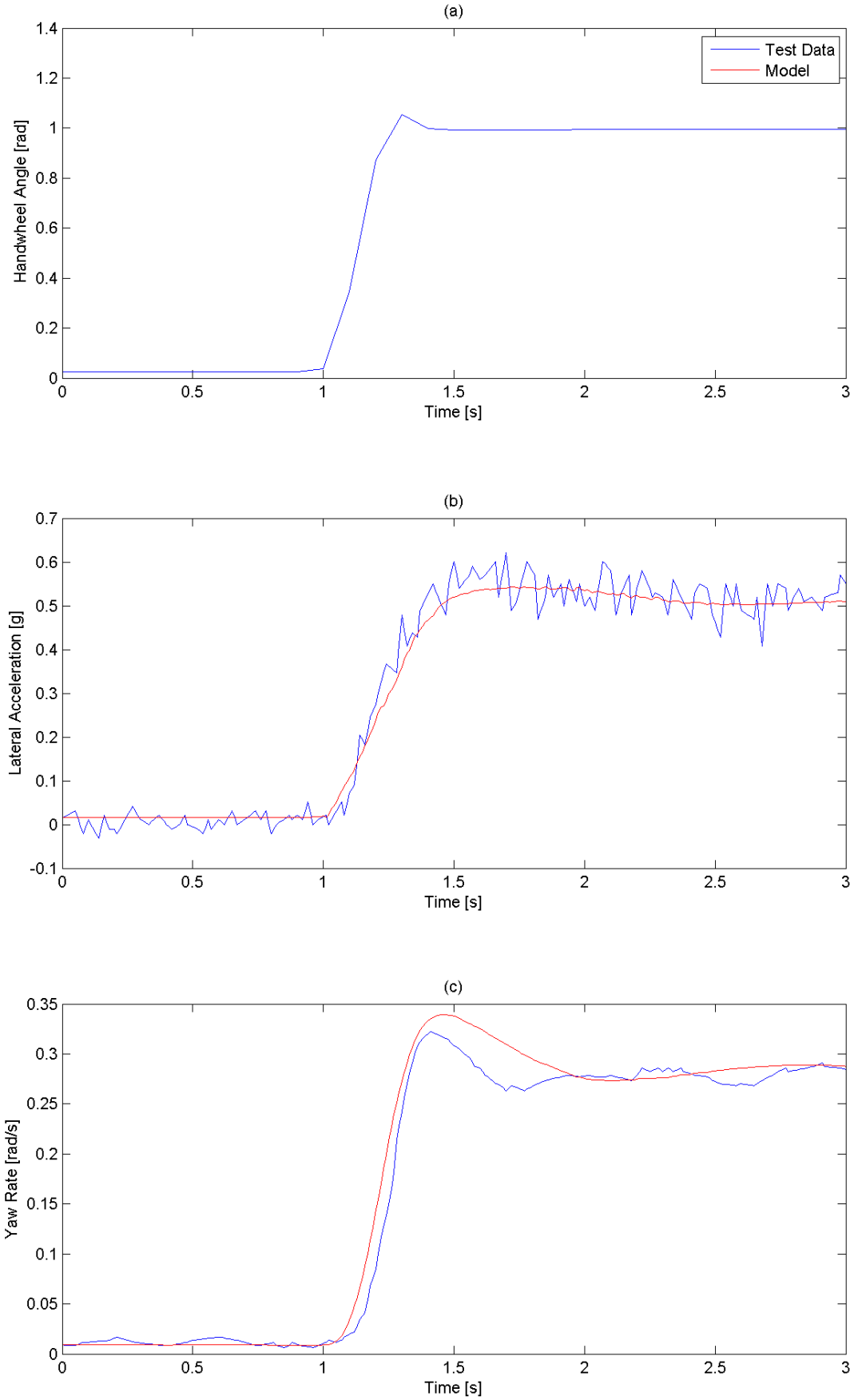

Figure 3-28 Lateral acceleration and yaw rate for test vehicle and model during ramp-to-step steer manoeuvre targeting 6 ms^{-2}

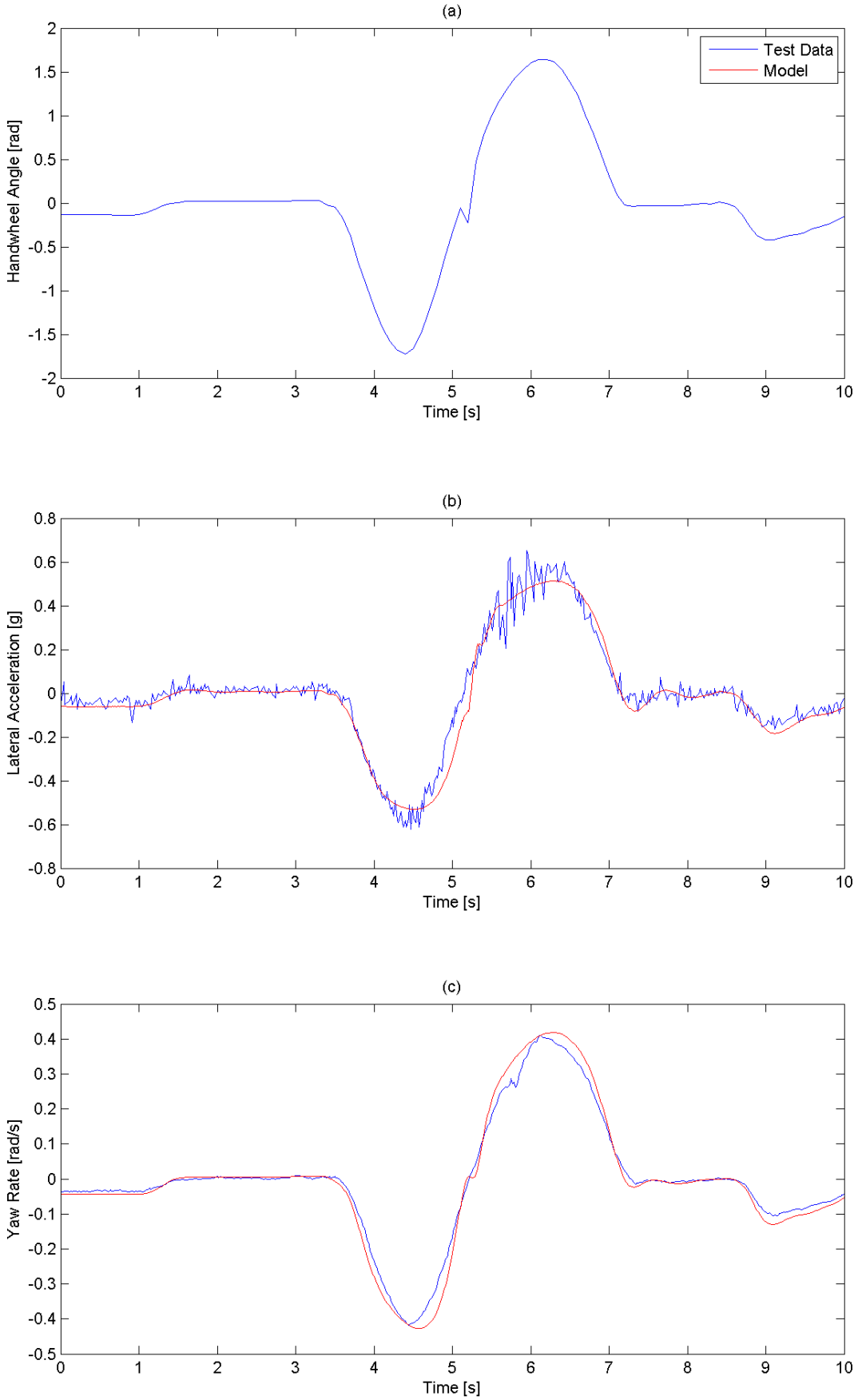

Figure 3-29 Lateral acceleration and yaw rate for test vehicle and model during sinusoidal steer manoeuvre

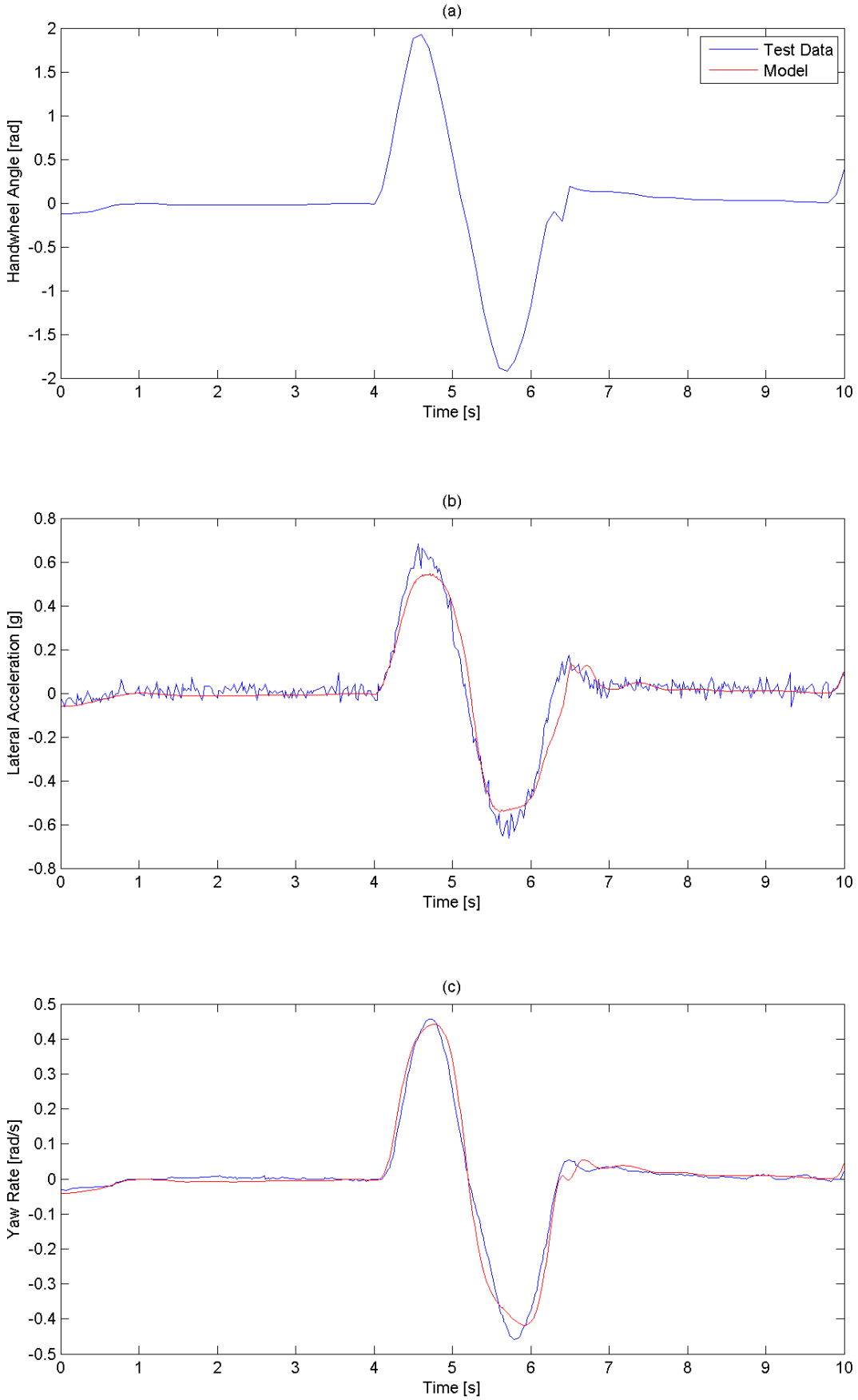

Figure 3-30 Lateral acceleration and yaw rate for test vehicle and model during sinusoidal steer manoeuvre

This data consisted of the kinematics data mentioned earlier and simple front and rear ride frequencies. These ride frequencies (obtained from the Dymola model) are shown in Figure 3-31.

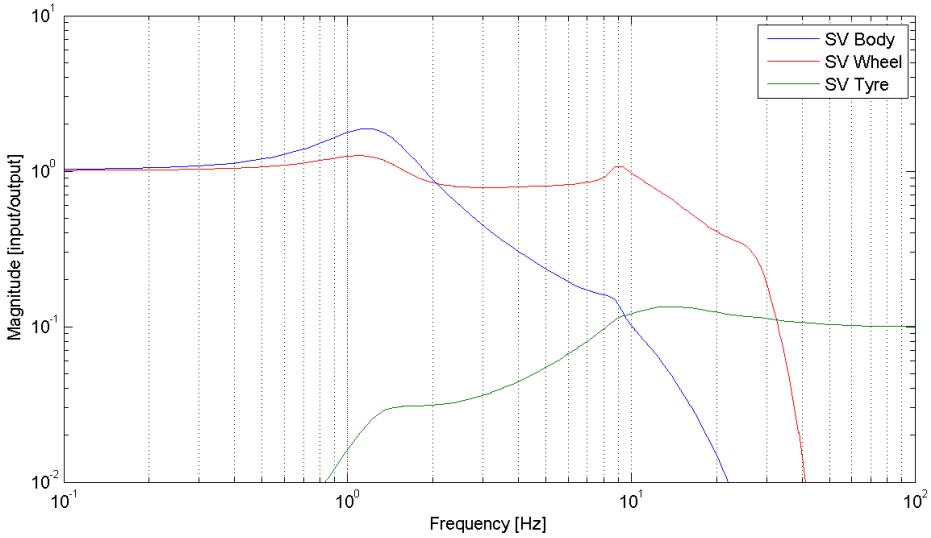

Figure 3-31 Frequency response of SV with front axle input

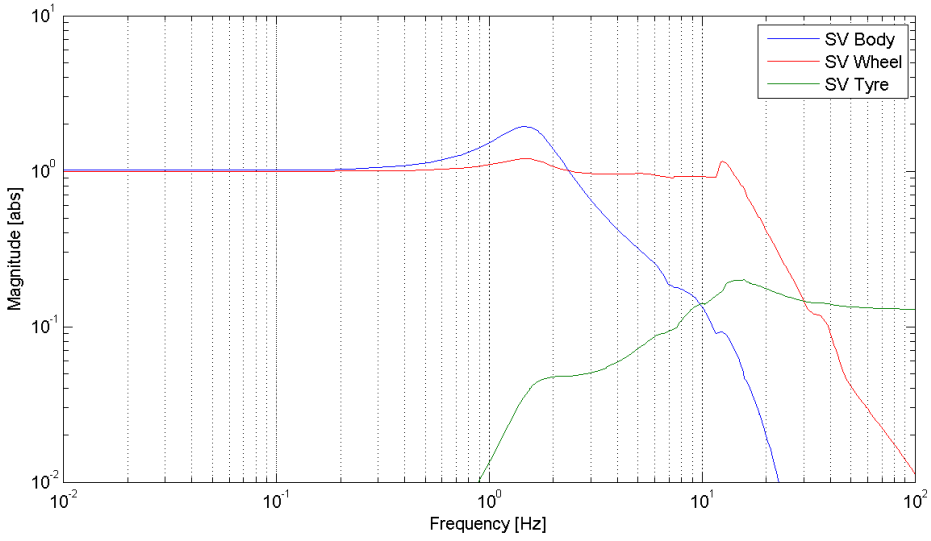

Figure 3-32 Frequency response of SV with rear axle input

Ride frequencies were obtained from the model by first linearising it and creating a state space model. The inputs to the model were displacements of the contact patch

at all four corners, the outputs, the displacement responses of the body (at the corresponding axle), wheel centre and tyre radius. Via Matlab the frequency response of the state space model was calculated separately for front and rear inputs. The two plots include the frequency responses for the sprung mass, un-sprung mass and tyre squash (rolling radius). Obviously the sprung mass response gives an insight into the body motion and ride quality, the response of the tyre radius quantifies the grip potential of the suspension and the un-sprung mass response will affect both the previous responses.

The results obtained from these simulations are shown in Figure 3-31 and Figure 3-32, which are compared to the OEM's model in Table 3-5. The results in the table show good agreement between the Dymola model and the OEM's vehicle model. The font ride frequencies agree exactly to 2 decimal places, the rear frequencies differ by less than 3%. Therefore it appears that the frequencies obtained by the Dymola model are acceptable. The fact that sprung mass natural frequencies from the Dymola model correlate with the values given by the OEM bodes well that the model can accurately represent body motions in the ride domain to a level acceptable for this study. Whilst the correlation of the models to real world data provides comfort that they represent reality, for this study it is not entirely necessary, the crux of this research focuses on the differences between two vehicles in the modelling domain, thusly rendering the absolute accuracy of the models not crucially important, as long as they at deemed accurate enough to show relative changes between the two vehicles.

	Unit	Dymola Model	OEM Model
Front frequency	Hz	1.23	1.23
Rear frequency	Hz	1.45	1.49

Table 3-5 Ride frequency comparison

3.10 The General Technology Vehicle (GTV)

In the previous sections the standard vehicle model has been constructed and validated. It is now appropriate to introduce the GTV, in terms of how it differs from the SV and the implementation of these differences in the modelling domain.

The GTV is an adaption of the SV into a range extended electric vehicle (REEV), it is in effect a SHEV. It uses a small internal combustion engine (a 3-cylinder fiat twin air engine) to run a generator that supplies electrical power to a battery pack, which then supplies power to an electric motor which drives the front wheels through a single speed gearbox. The EM consists of two, three phase DC, EM's sandwiched together; it is controlled by a bespoke ECU and power electronics. The battery pack is of lithium ion type and supplies power to the EM's via two DC-DC converters.

The layout of the vehicle is similar to the standard vehicle, the EM, gearbox, and ICE are in the existing engine bay. The only place available to package the large battery pack and DC-DC converters were in the luggage space at the rear of the vehicle, as a consequence of the size of the battery pack, the rear seats needed to be removed completely from the vehicle. Extra cooling was also implemented for the power electronics at the front of the vehicle. The GTV is only FWD, and all of the associated 4WD drive-train was removed. The arrangement can be seen in Figure 3-33.

As when discussing the model of the standard vehicle, each sub model will now be stepped through to discuss the changes made in more detail.

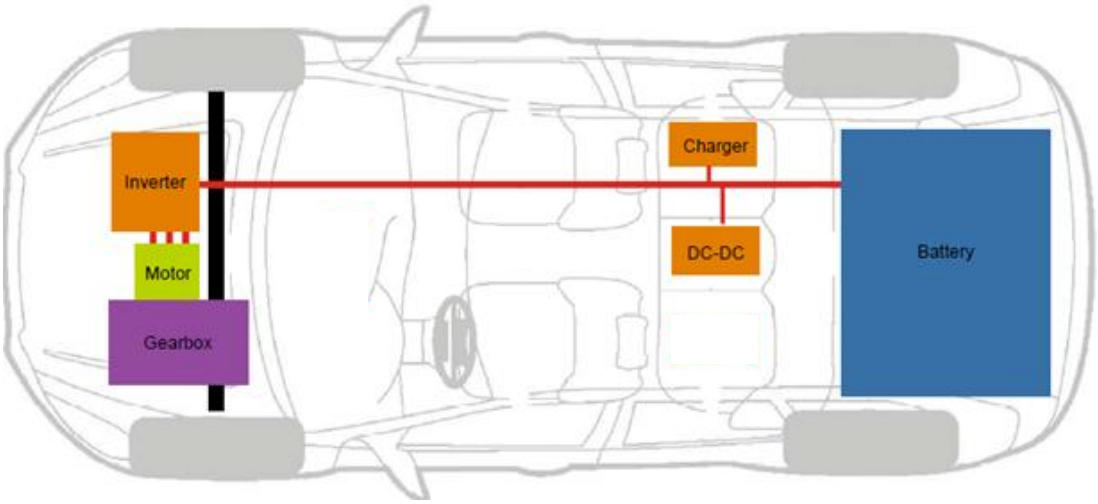

Figure 3-33 GTV Architecture

3.11 Suspension Linkages

As the GTV is an evolution of the SV the general architecture of the suspension remains the same. Only minor variations have been made for the purpose of packaging. The GTV has been equipped with a different steering rack, when this was fitted to the vehicle it clashed with the anti-roll bar arms, to overcome this, the ARB mounts to the subframe were moved 25mm downwards. This change was implemented in the form of two updates to the standard vehicle model, firstly the new steering rack had a different mass to the original and so the mass value for the steering rack was changed, secondly the geometric alteration to the ARB was included by simply altering its geometry, so any changes in wheel rate seen by this would be captured.

Perhaps the most significant change made to the suspension models relates to the force elements, namely the springs. As will be shown shortly there has been a not insignificant rearward shift in weight distribution. This change in total mass and its distribution will have two effects, firstly it will change the vehicles static ride heights at the front and rear, and secondly the ride frequencies of the vehicle will also

change. These two points in isolation could lead to fairly significant differences in the ride and handling of the two vehicles. The change in static ride heights mean that the front and rear roll centres will be in different positions relative to each other which will change the handling balance of the vehicle. The difference in ride frequency if large enough will have an effect on occupant comport and will also mean the level of damping provided would no longer be correct, this would lead to different levels of load variation seen at the tyre contact patch which would have a direct effect on both ride and handling. In order to avoid such changes and be able to make like for like comparisons between the two vehicles it was necessary to retune the ride heights and the ride frequencies of the GTV model to obtain the same values as the standard vehicle. This was carried out by stiffening the rear springs by 9.5%, once the stiffer springs were implemented the rear ride height was also brought back to its original value, this was checked via the rear damper lengths.

Figure 3-35 shows the rear ride frequencies of the two vehicle models. The data shown for the GTV is after the rear springs have been modified. It can be seen that the ride frequency of sprung mass on the rear axle of the GTV is identical to that of the standard vehicle, the magnitude of the response is larger at the natural frequency, this gives an early indication that due to the increase in mass and stiffer springs the rear axle now has too little damping. However above 2 Hz the body response of the GTV is seen to be smaller than that of the SV. The un-sprung mass natural frequency has remained unchanged, it can however be seen that the magnitude of the response is very slightly smaller on the GTV up to 10Hz, after this frequency the two responses are the same. The largest difference is seen in the response of the tyre, up to the natural frequency of the body response, circa 1.45 Hz, the response of the GTV's tyre radius is slightly larger, above this frequency the GTV's response is

considerably smaller than the SV's, this follows the same trend as the sprung mass response. So the increase in sprung mass and stiffness on the rear of the GTV looks to have created increased body and tyre responses below the sprung mass natural frequency, which will have negative effects on both ride quality and tyre grip capability, but conversely above this frequency body response and tyre responses have been reduced, indicating an improvement in ride quality and tyre grip capability.

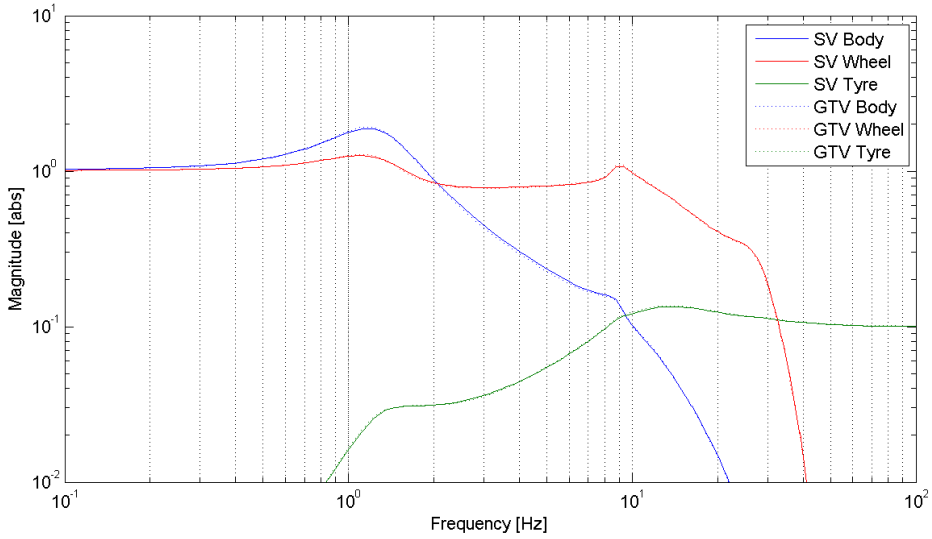

Figure 3-34 Standard vehicle and GTV front suspension components vertical frequency responses

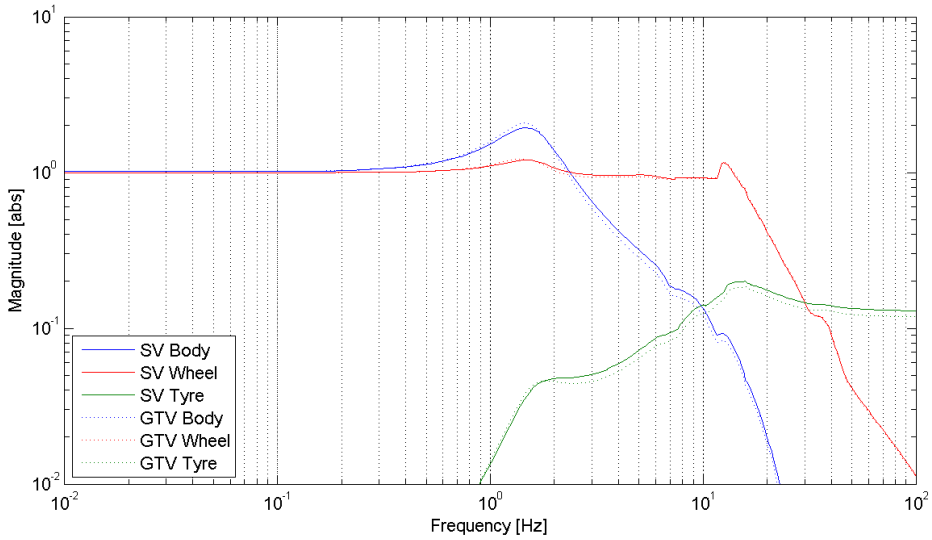

Figure 3-35 Standard vehicle and GTV rear suspension components vertical frequency responses

For completeness the frequency responses of the body, wheel and tyre displacements for the front of the two vehicles is also included in Figure 3-34. It can be seen that the same characteristics that were discussed for the rear responses are also present here, only to a much smaller extent.

3.12 Chassis Model

It was shown earlier how the mass properties of individual components were included into the mass sub model. This was to aid in the removal of components from the model, that were to be removed from the real vehicle. In order to implement these changes, masses of components that were completely removed, such as engine, gearbox etc, were simply deleted from the model. Components that were added in such as the electric motor, inverter, and battery pack were included as multi-body masses within the relevant mass sub model. An example of this is shown in Figure 3-36, the masses of the drive-train in the standard vehicle can be seen on the left and those of the GTV on the right.

The tyre models remain unchanged as the GTV will operate using the same tyres as the SV.

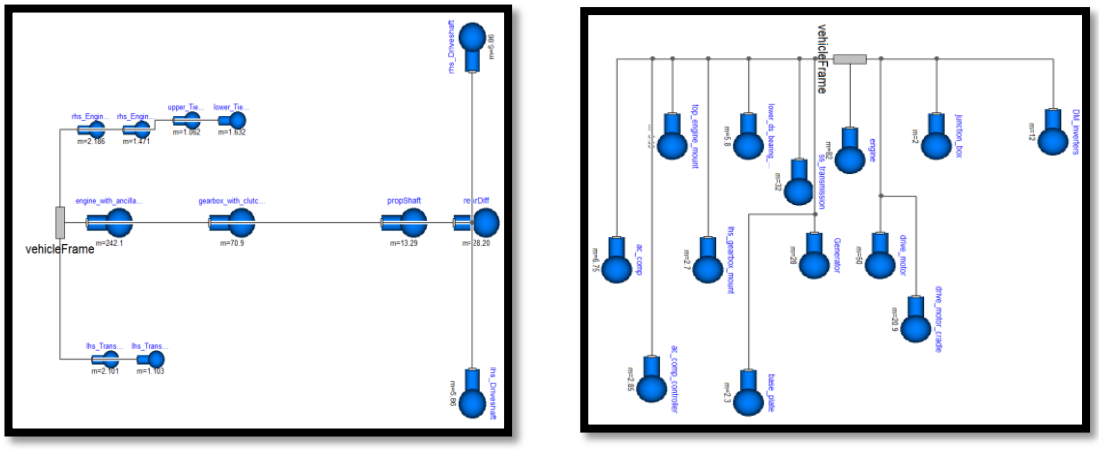

Figure 3-36 Drive-train components in standard vehicle and GTV

3.13 Engine and Drive-train

The GTV drive comes from an electric motor and drives the front wheels via a single speed gearbox. Whilst the characteristics of the electric motor are far different from that of the ICE that it replaced, no change has been made to the engine or drive-train models, the torque characteristics of the motor remain unchanged. The difference in the torque/speed characteristics of the two drive sources, without question will affect the performance of the vehicle, however this study is concerned with the ride and handling of the vehicle, not its drivability or outright straight line performance. As was mentioned when discussing the standard vehicle model, the engine and drive-train components are only used as a means to allow the front wheels to be driven during test manoeuvres. The difference in the two systems mass, inertia and architecture have been taken into account via the mass sub model within the chassis model.

3.14 Summary of changes

The majority of changes made to the vehicle ultimately result in changes to the vehicle mass and inertia properties. This is not surprising since there has been a large re-distribution of components throughout the entire vehicle. Table 3-8 shows a summary of the differences in the mass and inertia properties of the two vehicles. It can be seen that with the changes the vehicle has gone through its weight distribution has shifted rearwards quite significantly, this can be attributed largely to the removal of the engine and gearbox at the front of the vehicle and the addition of a large battery pack at the rear. The new, downsized ICE and EM have been installed in the engine bay which has to some extent mitigated this effect, but not entirely. The total mass of the car has increased by 74Kg and the Cog has moved further from the centreline of the vehicle along the y-axis. The roll inertia of the vehicle has reduced

although the pitch and yaw moments of inertia have both increased. As a consequence of the yaw inertia increasing the dynamic index has also increased by 2%.

The changes made to the suspension models were, the adjustment of the ARB attachment to the subframe to enable the new steering rack to be housed and the stiffening of the rear springs in order to obtain correct ride frequencies and ride heights. Both of these alterations have similar effects on the stiffness properties of the vehicle as a whole. Moving the ARB mounting has reduced the wheel rate in roll on the front axle, thusly lowering the front roll stiffness. Stiffening the springs on the rear axle has increased the wheel rate in heave (two wheel combined bump) and also increased the wheel rate in roll of that axle, this has the effect of increasing the roll stiffness of the rear axle. The softer roll stiffness of the front axle and the larger roll stiffness of the rear axle means that the roll stiffness distribution has migrated further rearwards. These changes can be seen in Table 3-9.

The two main changes mentioned here (weight distribution and stiffness characteristics) will have similar effect on the vehicle's handling. Both the rearwards shift in weight distribution, the reduction in front roll stiffness and increase in rear roll stiffness, will reduce the vehicles understeer gradient. In the previous chapter it was shown that the standard vehicle possessed an understeer characteristic in its understeer gradient, meaning as speed is increased to maintain a desired path more steer angel is required. With the changes made to the mass distribution and force elements, the GTV's undertseer gradient will have shifted towards oversteer. This is confirmed by the plots of road wheel angle against lateral acceleration (steer responses) for both the SV and the GTV shown in Figure 3-37. The three sub plots show the model outputs for both vehicles on 15, 60 and 240m radii, this covers a

speed range between 3 and 35 m/s. It can be seen across all speed and lateral acceleration ranges that the model of the GTV does exhibit a lower steering response than the SV, this shown by the smaller steer angle required to obtain the same level of lateral acceleration.

Dymola Model USG's in Linear range						
	Anti-clockwise			Clockwise		
Radius	SV	GTV	% delta	SV	GTV	% delta
15 m	0.52	0.33	36.54	0.51	0.43	15.69
60 m	1.34	1.24	7.46	1.32	1.26	4.55
240 m	1.19	1.08	9.24	1.18	1.10	6.78

Table 3-6 Understeer gradient comparison in linear regions

Figure 3-38 shows the gradients of the steering responses of Figure 3-37, the understeer gradients of the two vehicles. Whilst the two gradients are very close over all speed and lateral acceleration ranges, it can be seen that the GTV generally exhibits a lower understeer gradient than the standard vehicle. Table 3-6 compares the undertseer gradients of the two vehicle models at 0.15g (within the linear range). It can be seen that in this region there are considerable differences between the two vehicle models, the GTV exhibits a lower understeer gradient than the SV on all three radii (speed ranges). The differences between the two vehicles range from 4 – 37 %, consideration of this, and the difference illustrated previously between the SV model and test vehicle results in Table 3-4, where the error was shown to be less than 1%, proves that the differences observed between the two models are considerably larger than the scale of experimental errors. Furthermore, whilst the differences in the understeer gradients of the two vehicles outside of the linear range appear very small, the differences are still seen to be large enough to produce observable differences in the vehicles steady state responses shown in Figure 3-39. Whilst the understeer gradients of the two vehicles differ they still fall well within a normal

range of values shown with Table 3-7. The source gives a range of values taken from a test of 169 road passenger vehicles. The values stated are obtained from a constant speed circular test (at 62 mph) which is slightly different to the constant radius method used within this study, due to this it is likely that results will differ slightly, it has been shown that understeer gradient values found by the constant radius method are slightly smaller than those found by the constant radius method (Dixit, 2009). These differences arise due to the changing tractive force and aerodynamic forces during the constant radius test which are not present in the constant speed test (Milliken and Milliken, 1995). Despite this the range given in Table 3-7 gives an idea of the range of understeer gradients in road passenger vehicles, and shows the SV and GTV fall within this range, albeit at the lower end of the scale.

	Range of USG's		
	Min	Avg	Max
US Cars	0.7	4.4	8.2
Other	1.3	2.6	5.8

Table 3-7 Normal range of understeer gradients of road cars (Reid, 1984)

Observations made in this section allow the hypothesis, that whilst the differences in the understeer gradients of the two vehicle models are large enough to produce differences in the vehicles' steady state handling, which are of a large enough scale to be correctly captured by the vehicle models, the difference in the GTV's understeer gradient is not sufficiently large enough to place it outside of what can be considered a normal range.

		SV			GTV			delta		
		X	Y	Z	X	Y	Z	dX	dY	dZ
Cog Position	[m]	2.85421	-0.00206	0.71442	2.93075	-0.0076	0.7223	0.07654	-0.00554	0.00788
		Ixx	Iyy	Izz	Ixx	Iyy	Izz	dIxx	dIyy	dIzz
Moment of Inertia	[Kg.m2]	854.69	3425.04	3727.34	834.06	3660.65	3963.65	-20.63	235.61	236.31
Total Mass	[Kg]		2136			2209.75			73.75	
Weight Distribution	[%F/%R]		57/43			54/46			3% Rearwards	
Dynamic Index	[m/m]		1.00			1.02			2%	

Table 3-8 Mass and inertia metrics

		SV	GTV	% delta
Front Wheel Rate (Bump)	[N/m]	33800	33800	0.00
Front Wheel Rate (Roll)	[N/m]	74620	73900	-0.96
Rear Wheel Rate (Bump)	[N/m]	37760	40590	7.49
Rear Wheel Rate (Roll)	[N/m]	52.74	55.33	4.90
Front Roll Stiffness	[Nm/deg]	1667.30	1651.20	-0.97
Rear Roll Stiffness	[Nm/deg]	1176.95	1234.66	4.90
RSD	[%]	58.62	57.22	-1.40

Table 3-9 Stiffness metrics

So far the two vehicles static conditions and steady state handling have been discussed. By comparison of manoeuvres such as step steers or sinusoidal steers the changes in the vehicles transient handling characteristics can be seen. Figure 3-39 and Figure 3-40 show the lateral acceleration and yaw rate responses for both vehicle models. The former illustrates the responses during a 45 degree (handwheel angle) ramp-to-step steer manoeuvre, applied over 0.25 seconds at 15 $\mathrm{m.s^{-1}}$, and latter for a 0.5 Hz, 90 degree (handwheel angle) sinusoidal steer manoeuvre carried out at 15 $\mathrm{m.s^{-1}}$.

Inspection of the responses from the two models shows that whilst the differences are not huge, there are subtle deviations that should be noted. Firstly the peak values of both lateral acceleration and yaw rate are quite different, combining this with the differences in overshoot and damping properties could lead to a vehicle that feels very different from a driver/occupant perspective

It should also be noted that in these results the steady state lateral acceleration and yaw rates differ between the two vehicles, this again illustrates the differences in their understeer gradients. It is for this reason that manoeuvres used at a later stage of this study to directly compare the handling of the two vehicle models will be designed using the two different steering responses (from SV and GTV) to adjust the input steer angle for each vehicle in order to give an equivalent steady state response to allow direct comparison between the two vehicle models.

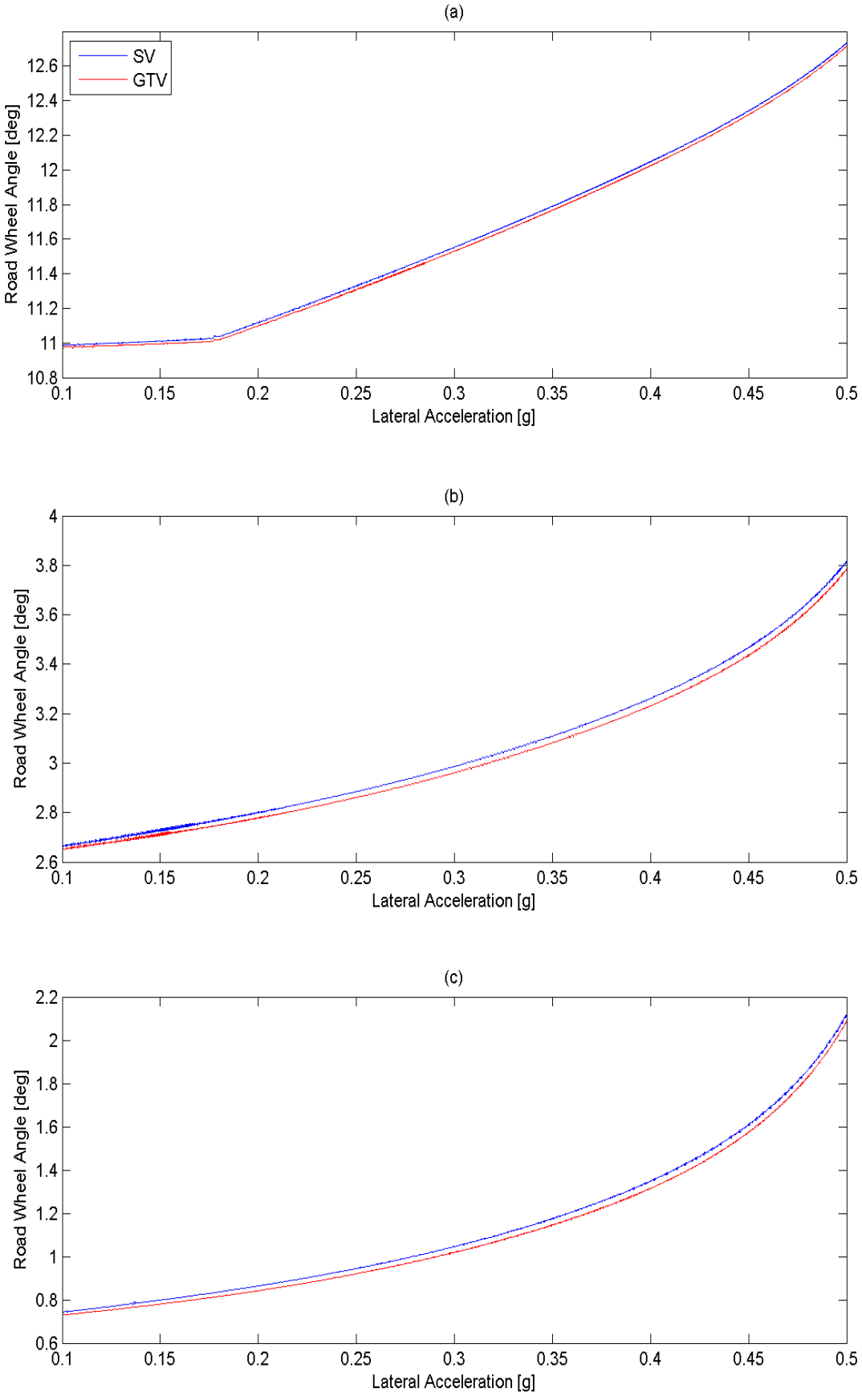

Figure 3-37 Steering response comparison on (a) 15, (b) 60 and (c) 240m radii

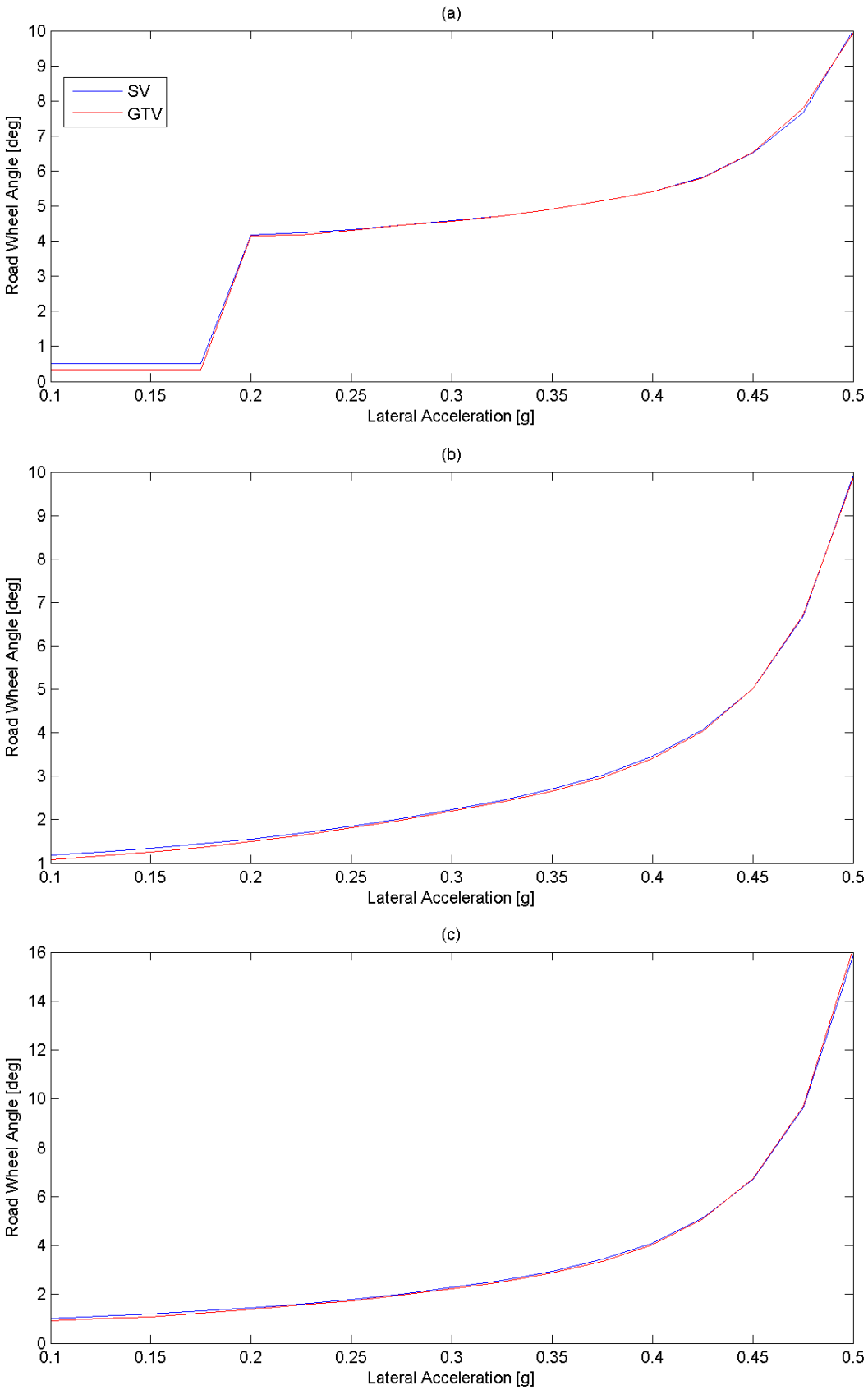

Figure 3-38 Understeer gradient comparison on 15, 60 and 240m radii

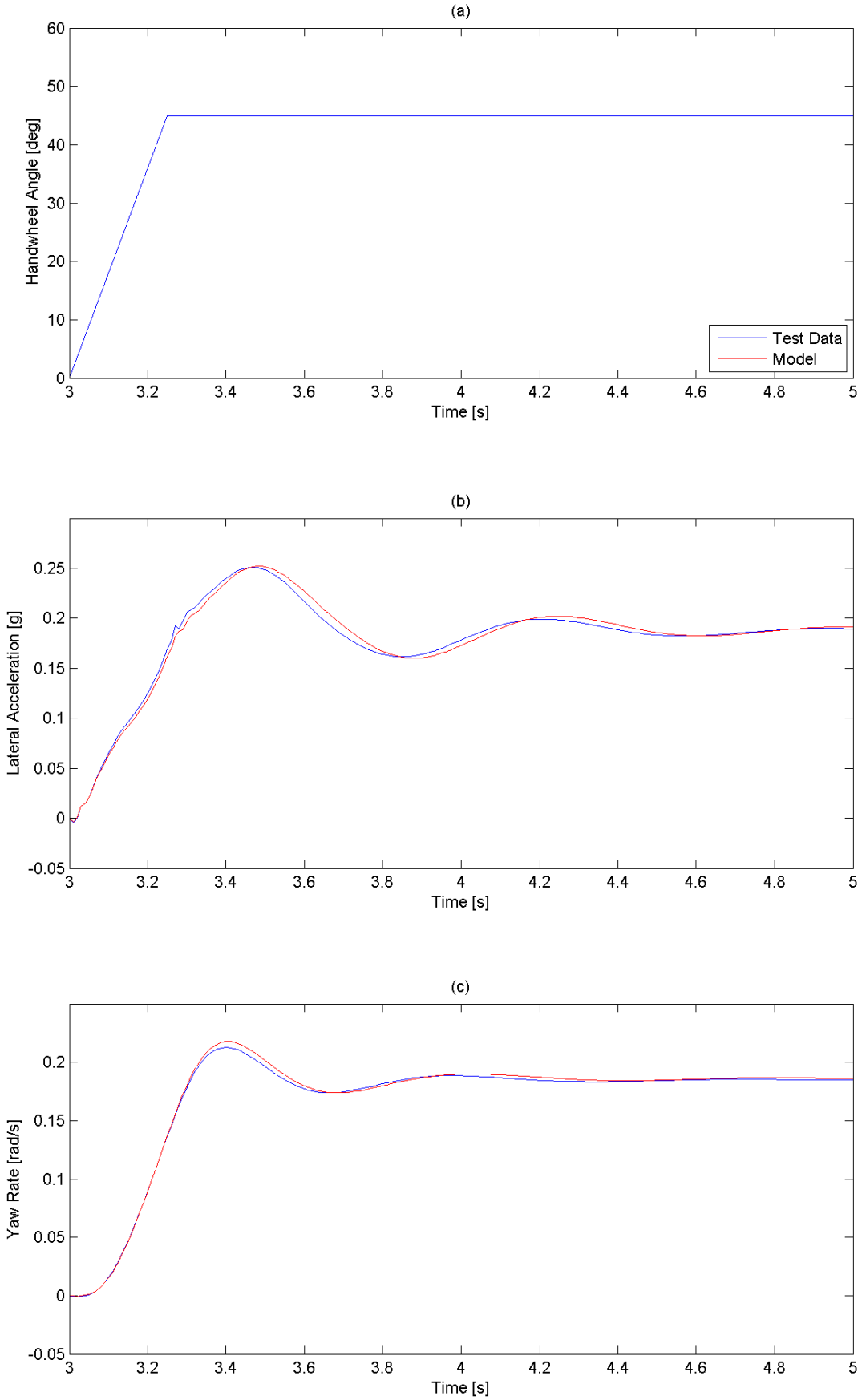

Figure 3-39 Lateral acceleration and yaw rate responses of both vehicle models during ramp-to-step steer manoeuvre at 15 m.s-1

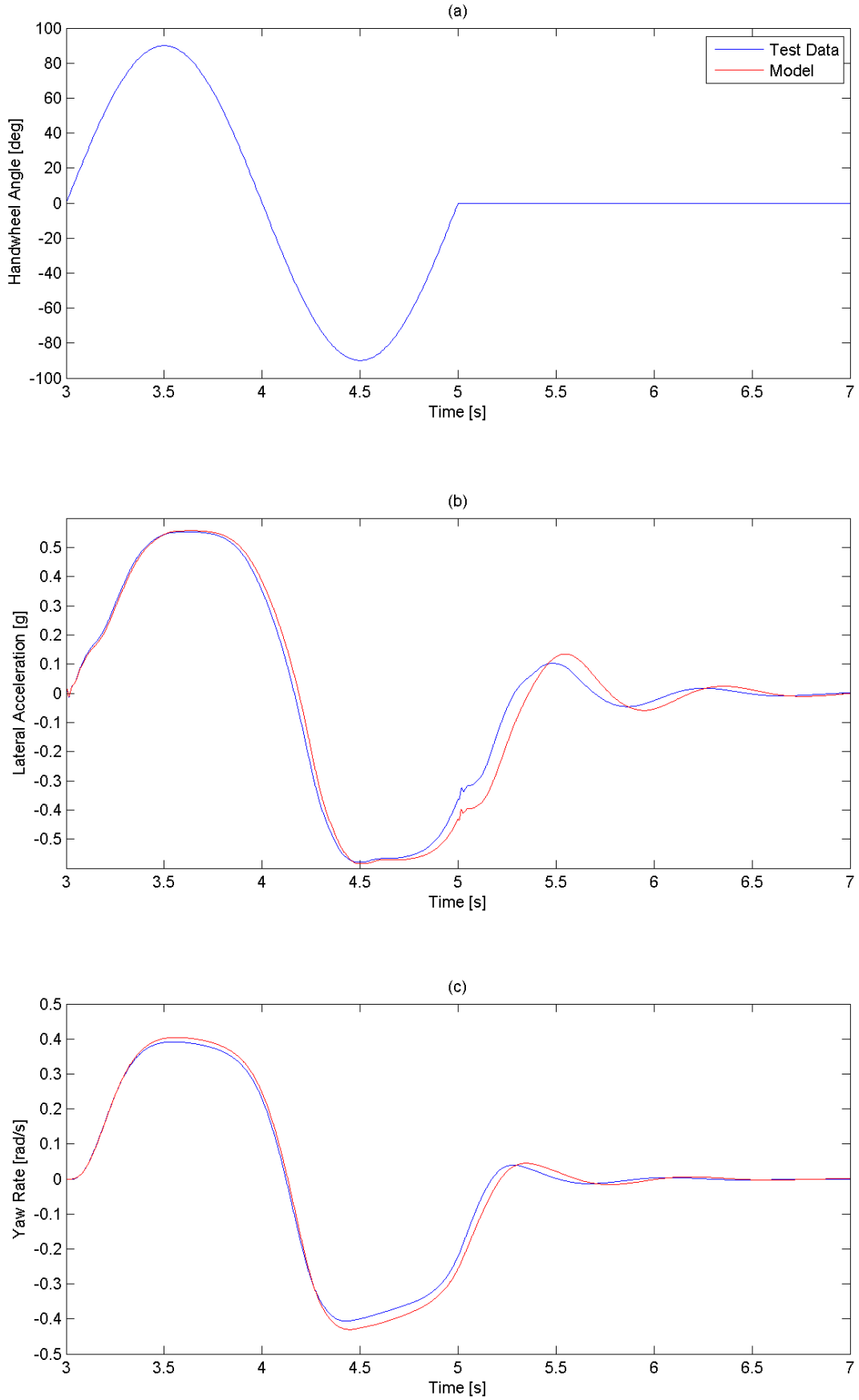

Figure 3-40 Lateral acceleration and yaw rate responses of both vehicle models during sinusoidal steer manoeuvre at 15 $\mathrm{m.s^{-1}}$

A brief summary of how the changes made alter the vehicles handling performance has been shown, this study will also focus on how ride comfort has been affected by the same changes. To give a similar, brief demonstration let us look at levels of occupant comfort inside the vehicle. Figure 3-41 shows the frequency weighted RMS vertical acceleration, for a seated person across the entire vehicle, (a) and (b) represent the standard vehicle and the GTV respectively. The x and y axes of the plots relate to the wheelbase and track width of the vehicle, the front axle lies at 0 on the x axis and the rear at -2.66. The vehicle centreline lies at 0 on the y axis of the plots. This specific plot is straight line running at 10 $\mathrm{m.s^{-1}}$ over an ISO grade C road. The levels of acceleration shown can be directly related to levels of comfort within the vehicle, this mapping is shown in Table 3-10. (Terminology for roads and data analysis used here is explained in detail in chapter 4). Looking at the aforementioned plots, initially it appears that both plots are quite similar, however closer inspection yields subtle differences. Firstly it can be seen that for the GTV (b) the higher comfort area situated around the Cog is smaller than that for the SV, not only has it reduced in size it has moved further rearwards within the vehicle. This clearly shows that now (in the GTV) occupants at the front of the vehicle will be subjected to slightly higher acceleration levels, i.e. lower comfort, whereas occupants at the rear will experience the opposite. Levels of comfort situated in this lower acceleration region, where it happens the occupants would normally be situated, fall within the 'a little uncomfortable' to 'fairly uncomfortable' bands, however as this region is slightly smaller, and shifted for the GTV it is possible that the occupants, especially those towards the front, will be subjected to higher levels of acceleration whilst sat inside the vehicle.

$m.s^{-2}$	Comfort Level
< 0.315	Not uncomfortable
0.315 - 0.63	A little uncomfortable
0.5 – 1	Fairly uncomfortable
0.8 - 1.6	Uncomfortable
1.25 - 2.5	Very uncomfortable
> 2	Extremely uncomfortable

Table 3-10 RMS acceleration comfort levels (BS2631-1:1997, 1997)

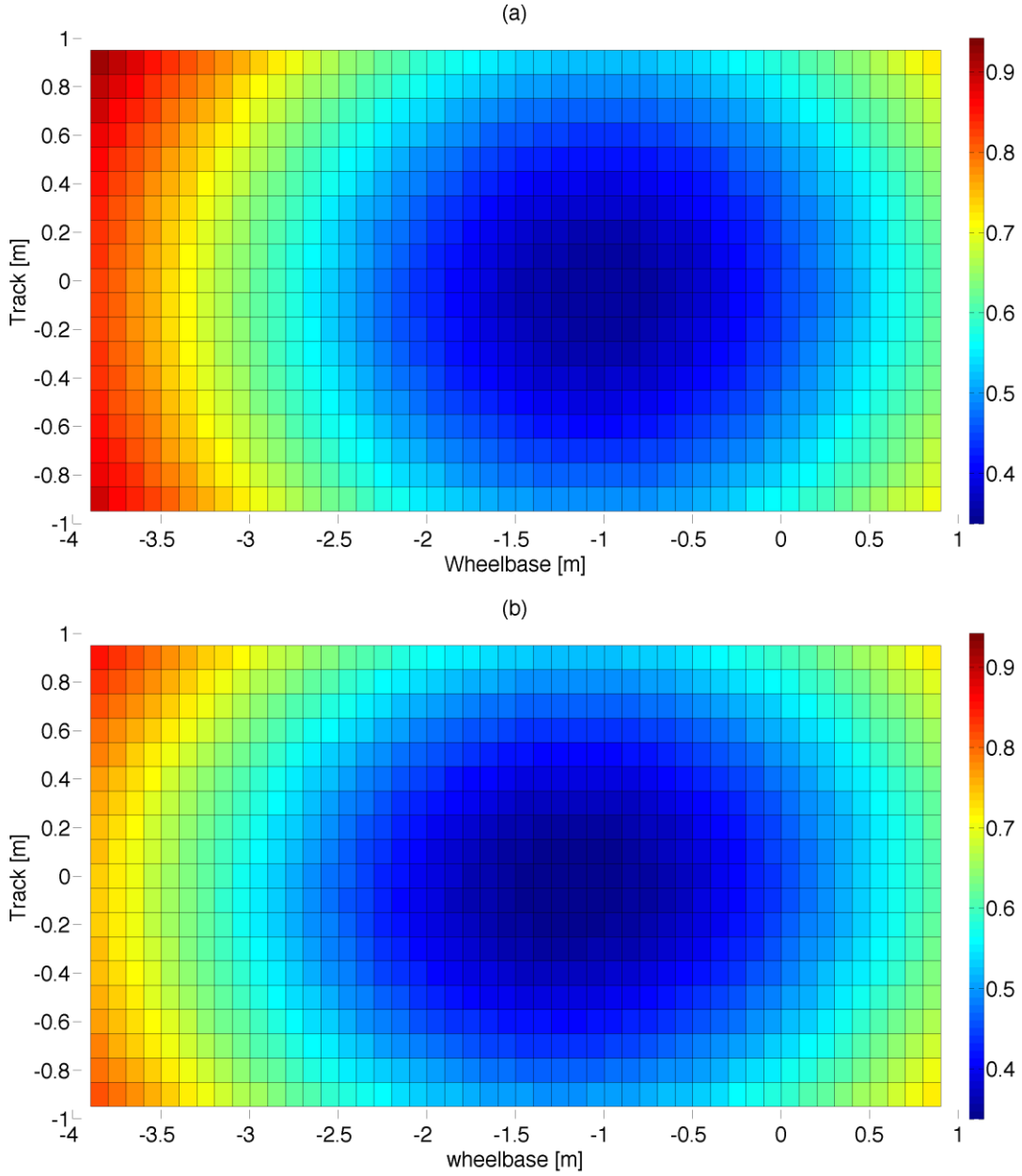

Figure 3-41 Frequency weighted RMS acceleration map of vehicle ISO road grade C, 10 $m.s^{-1}$

Figure 3-42 shows the frequency weighted RMS vertical accelerations but at specific points within the vehicle. As we are primarily interested in occupant comfort it seems apt to look at the positions where the occupants of the vehicle will be situated. Plots (a) – (d) show the frequency weighted acceleration levels at each of the occupant seats. It is clearly visible that the shift rearwards of what was identified previously as a higher comfort region has affected levels of comfort within the vehicle, it can be seen that occupants at the front of the GTV experience higher acceleration levels, whilst those at the rear experience lower. It is not until forward velocities of above 10m/s the difference between the vehicles becomes noticeable.

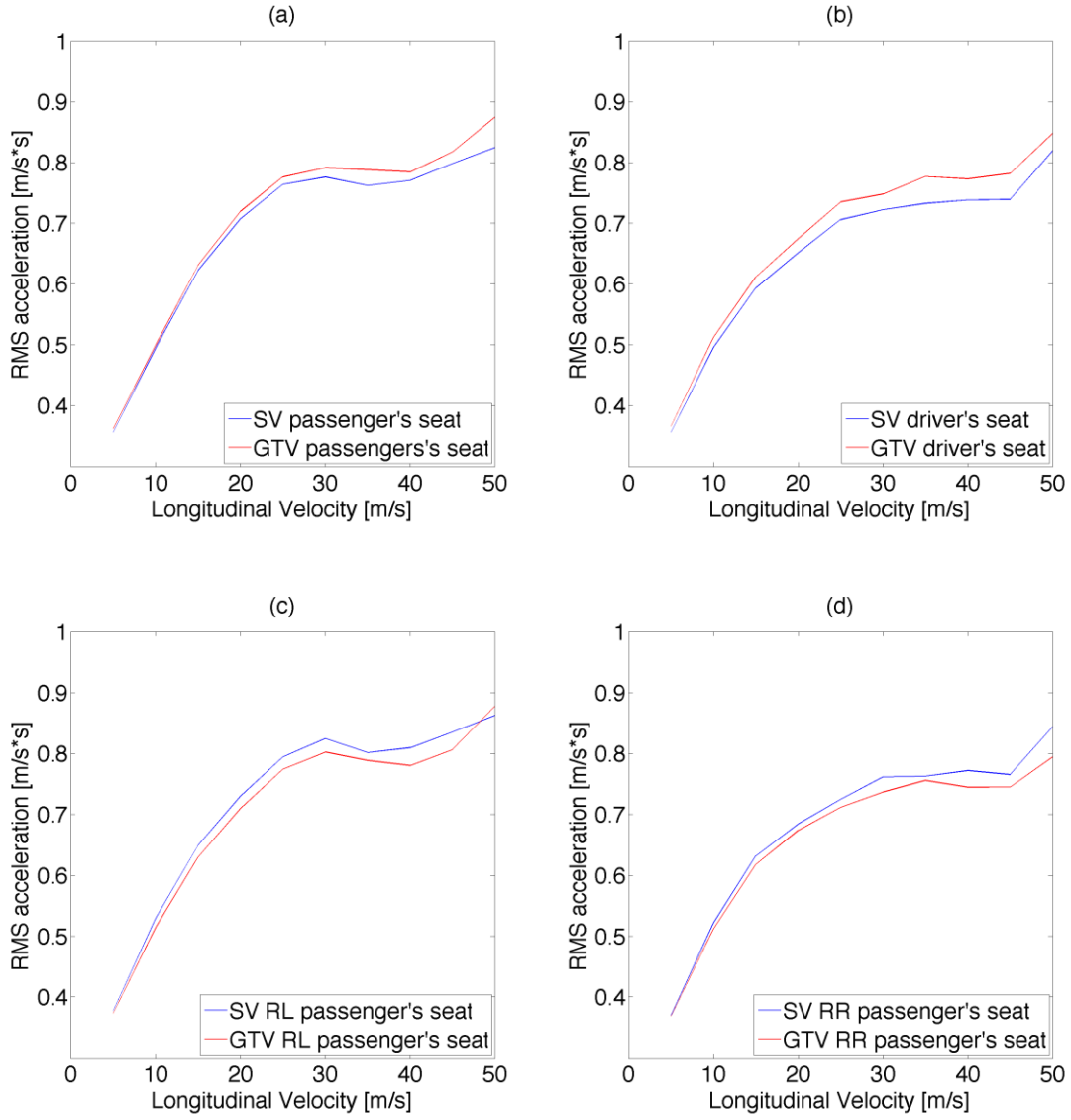

Figure 3-42 Frequency weighted RMS acceleration over speed range at occupant positions

The cause of the changes in the levels of vertical acceleration felt within the vehicle can be related to the mass and stiffness alterations made to the vehicle. The movement of the Cog, spring centre and pitch and bounce centres will affect the motion of the vehicle resulting from road load inputs, also the reduction of the roll inertia will increase roll acceleration seen from asymmetric road inputs, the vertical components of which will translate to vertical acceleration seen when looking at the RMS vertical accelerations previously shown, not to mention increased levels of head toss.

3.15 Conclusion

This chapter has given an overview and explanation of the SV and GTV with regard to the real vehicles and how such systems were modelled.

The model of the standard vehicle has been discussed at length with detailed illustrations showing the main components. It has been shown that the model was created in such a manner to allow easy integration of component models to create the full vehicle and thusly allow the vehicle model to be controlled by a number of driver models. It was shown how simplifications were made to keep the model complexity down, but at the same time how these were made in areas that would not influence the accuracy of the results obtained for this study.

To ensure that the model represents reality it was validated firstly against kinematic data and model based rig test data, and secondly against real world test data obtained from a similar vehicle under test conditions. The kinematic data showed good agreement between the Dymola model and the data given by the OEM. The data collected from the vehicle during testing also showed good correlation with the model outputs for the specific test manoeuvres used. In the ride domain, sprung mass natural frequencies were seen to correlate with the OEM's quoted values,

which illustrates the accuracy of the geometry, mass and stiffness data within the model. Further ride domain validation could be conducted against test data, although it was not required, or fully feasible within for this study. Whilst the accuracy of the model is important, for this study the main emphasis will be placed upon the difference between the two models, therefore the absolute accuracy of the models is not vital, the main concern is that they follow the correct trends and show the correct behaviour of the vehicles. Because of this it was deemed that that the correlation between the model and the real vehicle is of an acceptable level for the model to be used for the basis of this study.

After consideration of the SV, the GTV was introduced, the nature and extent of the changes that were made to the SV to create the GTV were explained and illustrations of how they were implemented in the modelling domain were presented. The changes shown here were implemented in the model simultaneously to real world vehicle development.

It can be said that the alterations made to the standard vehicle in order to create the GTV fall into one of two categories, the first being mass redistribution, the second being force element modifications. The second of these categories can be thought of as mainly an effect of the former.

Finally to close the loop the two vehicle models were directly compared by looking at their lateral acceleration and yaw rate responses to two open loop test manoeuvres, thusly illustrating differences in handling. Subtle differences in the vehicles handling were observed, but it was also shown that to make true like for like comparisons, test manoeuvres need to be designed using the steering responses (understeer gradients) of the respective vehicle to adjust steer inputs to obtain identical steady state lateral accelerations and yaw rates.

Ride comfort comparisons were displayed in the form of frequency weighted RMS vertical accelerations felt by the occupants, it was shown in this brief analysis that magnitude, and distribution of comfort within the GTV change due to the alterations made to the vehicle.

Later chapters will be concerned with much more detailed analysis and discussion of further results obtained from both models in order to quantify differences in the two vehicles' ride and handling characteristics.

Chapter 4 Vehicle Dynamics

4.1 Introduction

This chapter will introduce some vehicle dynamics principles of road vehicles that are of importance for this study. This will be done by applying simple vehicle dynamics models to the areas investigated within this work with the aim of not only introducing some basic vehicle dynamics but also highlighting, at the outset, where differences in the two vehicles' ride and handling are likely to arise from. Following this, specific test manoeuvres that have been utilised; initially during the validation of the standard vehicle model, and secondly to directly compare responses of both the standard and hybrid vehicle models, will be presented. The development of these test manoeuvres and the analysis that will be conducted on the results will be discussed at length to lay the foundation for the work that will presented in later sections.

4.2 Simple Vehicle Dynamics

4.2.1 Ride

A good place to start, and introduce the basics of vehicle ride that will be of importance for this study is with the simple two degree of freedom, pitch and bounce model. This model is discussed and analysed extensively by Olley at al (2002). It represents the car as a solid beam supported by two linear ride springs front and rear. It has only two degrees of freedom, pitch and bounce. Such a system is shown in Figure 4-1.

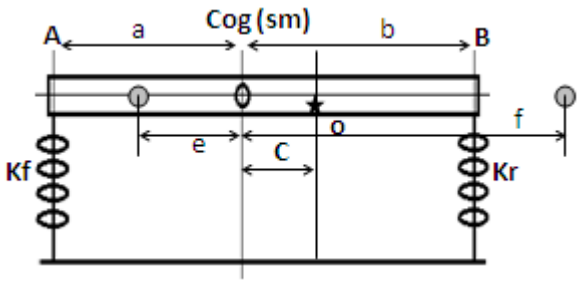

Figure 4-1 Two degree of freedom ride model

Investigation of this model in the aforementioned source yields some very interesting basic principles for ride comfort. It is shown that the distance C, of the spring centre O from the Cog is

$$C = \frac{K_f a - K_r b}{K_f + K_r} \tag{4.1}$$

The spring centre can be thought of as the point at which, if a vertical force where applied to the vehicle then the front and rear springs would compress equally (the vehicle would not pitch).

The spring centre O has a vertical linear rate and angular rate, the linear rate at O is

$$K_o = K_f + K_r \tag{4.2}$$

the angular rate about O is

$$Kt_o = K_f(a + c)^2 + K_r(b - c)^2 \tag{4.3}$$

Likewise there exists a linear and rotational rate about the Cog, given by

$$K_{cog} = \frac{K_f . K_r . l^2}{K_f a^2 - K_r b^2} \tag{4.4}$$

$$Kt_{cog} = K_f a^2 + K_r b^2 \tag{4.5}$$

The two equations of motion representing this system are shown in equations 4.6 and 4.7, evaluation and simplification of these equations of motion yields two natural frequencies, w_1 and w_2 for pitch and bounce respectively, furthermore two

oscillation centres are defined about which these natural frequencies act, these positions are defined from the cog as e and f.

It can be seen that the β term is present in both equations for pitch and bounce and so can be thought of as a coupling term between the two modes. Therefore when $\beta = 0$, it can be said that pitch and bounce modes are uncoupled, it also means the spring centre lies at the vehicle Cog. Such a condition was stated by Olley as giving poor ride as body motions are very irregular.

$$\ddot{Z} + \alpha Z + \beta\theta = 0 \tag{4.6}$$

$$\ddot{\theta} + \frac{\beta Z}{k^2} + \Upsilon\theta = 0 \tag{4.7}$$

Evaluation and simplification of these two equations of motions leads to the two previously mentioned natural frequencies for pitch and bounce, equations 4.8 and 4.9.

$$w_1^2 = \frac{\left(\alpha + \frac{\gamma}{k^2}\right) + \sqrt{\left(\alpha + \frac{\gamma}{k^2}\right)^2 - 4.\frac{\alpha.\gamma - \beta^2}{k^2}}}{2} \tag{4.8}$$

$$w_2^2 = \frac{\left(\alpha + \frac{\gamma}{k^2}\right) - \sqrt{\left(\alpha + \frac{\gamma}{k^2}\right)^2 - 4.\frac{\alpha.\gamma - \beta^2}{k^2}}}{2} \tag{4.9}$$

where

$$\alpha = \frac{K_f + K_r}{m} \tag{4.10}$$

$$\beta = \frac{K_f.a - K_r.b}{m} \tag{4.11}$$

$$\gamma = \frac{K_f.a^2 + K_r.b^2}{m} \tag{4.12}$$

The positions of the oscillation centres from the Cog are defined as

$$e = \frac{\beta}{(w_1^2 - \alpha)} \tag{4.13}$$

$$f = \frac{\beta}{(w_2^2 - \alpha)} \tag{4.14}$$

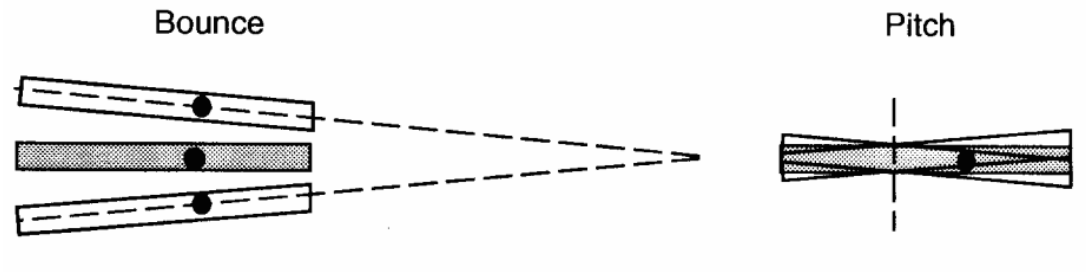

Figure 4-2 Pitch and bounce mode shapes

w_1 will be the highest frequency and w_2 the lowest, based on the above construction one oscillation centre will always be within the wheelbase, this will be the pitch centre, the other will always be outside, this is the bounce centre. The mode shapes of these two degree of freedom are shown in Figure 4-2. An input at or near one oscillation centre will start a rotation about the other, what is important for ride comfort is that that the oscillation centre for w_2 (the lower of the two frequencies) is started first, this ensures that when the vehicle is set oscillating by a road input the faster of the two oscillations effectively 'catches up' with the slower meaning that the pitch and bounce oscillations are in phase and the vehicle 'rides flat'. This is one of the fundamental criteria for Olley's flat ride, and is a fundamental reason why rear spring rates are higher than front spring rates. If the slowest oscillation is not started first, pitch and bounce frequencies can end up being out of phase, which will result in interference and uncomfortable ride. It is thought advantageous to aim for flatter ride, as bounce motions are thought of as 'less annoying' than pitch motions which tend to induce head jerk for occupants. Further criteria for good ride comfort outlined by Olley are that, the ratio of pitch/bounce frequency should be as close together as possible with a maximum ratio of 1.2, and

that rear springs should be at least 30% stiffer than the front (spring centre at least 6.5% of the wheelbase rearward of the Cog, but no more than 10%).

With regard to this study there are some important factors that should be noted. The mass, mass distribution and pitch inertia of the GTV are different to the SV, this results in the need for 're-tuning' of the spring rates in order to obtain the same static ride heights and ride frequencies as the SV. The mass distribution of the GTV will be more reward than the SV, meaning stiffer rear springs, this alone means that the spring centre will move rearwards. Looking at the equations presented in this section it can be seen that if spring centre and Cog are moved and/or the pitch inertia altered then the pitch and bounce frequencies will in turn be different and their oscillation centres will move. If the change in frequencies and movement of the oscillation centres is large enough then it could introduce much poorer levels of ride comfort than present in the SV. Furthermore, for this study it has to be assumed that the SV represents some form of optimum and so any deviations from its responses and characteristics have to be viewed as non-optimal.

A comparison of the pitch and bounce model for the SV and GTV is shown in Table 4-1. It can be seen that due to the stiffening of the rear springs of the GTV it is stiffer in both modes (pitch and bounce) about the spring centre and the Cog, however due to the GTV's increased mass and pitch inertia, its pitch and bounce frequencies are lower. Perhaps most interestingly, the pitch/bounce frequency ratio has decreased for the GTV, lowering the possibility of interference between the two oscillations, which could lead to high oscillation amplitudes, and meaning it now falls within the criteria mentioned by Olley, whereas the SV falls just outside. It is important to mention that in the GTV the spring centre has moved rearwards, (not so much in relation to the Cog as this has also moved, but considering its position from

the front axle shows the true extent of the change), this puts the oscillation centres much closer to the axles. The K^2/ab ratio has also increased and is approaching unity. It is interesting to note that this is a desirable condition for good ride, as long as Olley's other flat ride criterion are met Gillespie (2002). The coupling term β, is also larger for the GTV indicating that the pitch and bounce motions are more coupled, again another positive for good ride according to Olley. So in this guise it is possible that the GTV may exhibit more preferable ride qualities than the SV. However from the trends observed here it can be seen that any further stiffening of the rear springs, or an increase in the pitch inertia, could lead to the pitch and bounce centres reversing (as they will continue to migrate rearwards). Such a change would put the oscillation centre corresponding to the higher of the two frequencies inside the wheelbase and as such would be the oscillation that is started first from a road input, this would violate one of the main criteria for good ride comfort and could make achieving good ride in the GTV impossible.

Metric	Unit	SV	GTV	% delta
Vertical Rate at Cog $[K_{cog}]$	[N/m]	58181.38	61007.54	4.86
Angular Rate at Cog $[Kt_{cog}]$	[Nm/rad]	107647.40	112421.84	4.44
Spring Centre from Cog [C]	[m]	-0.20	-0.20	0.12
Spring Centre from front axle [C-a]	[m]	-1.36	-1.42	4.42
Vertical rate at Spring Centre (O)	[N/m]	59500.00	62400.00	4.87
Angular Rate at Spring Centre (O)	[Nm/rad]	115041.62	120195.72	4.48
Pitch Frequency [W1]	[rad/s]	6.12	5.84	-4.60
Bounce Frequency [W2]	[rad/s]	5.05	4.98	-1.36
Pitch Centre from Cog [e]	[m]	-0.59	-0.98	66.33
Bounce Centre from Cog [f]	[m]	2.43	1.69	-30.53
Pitch Centre from front axle [e-a]	[m]	-1.75	-2.20	25.78
Bounce Centre from front axle [f-a]	[m]	1.27	0.47	-63.07
Pitch/Bounce Ratio [W1/W2]	-	1.21	1.17	-3.28
K2/ab	-	0.82	0.94	14.45

Table 4-1Pitch and Bounce Model Metrics

It must be noted that this is a very simplified linear model, it consists of only two degrees of freedom and therefore no interaction/contribution of wheel or roll modes are present and there is no damping included. Whilst limited it gives a simplified insight into where changes may arise from between the two vehicles in this study, and further more brings to light some trends that may be observed when investigating the more detailed full vehicle model in later sections. In summary, as the GTV has been shown to possess a larger K^2/ab ratio, and pitch and bounce oscillation centres closer to the axles, with frequencies that are more closely matched along with more coupled pitch and bounce modes, due to its larger β component, it might be expected that the GTV will achieve flatter ride over uneven road surfaces, this will be seen in the pitch responses of the vehicle, i.e. the GTV will pitch less than the SV for the same input. It should also manifest itself within the body motions as less vertical acceleration at the extremities of the vehicle body. However there could also be an increase in vertical acceleration seen on the vehicle body due to increased bounce mode motion. These hypotheses will be revisited when analysing the ride results in the coming chapters.

4.2.2 Handling

To understand how changes in vehicle architecture affect the overall lateral dynamics of the vehicle, it is useful to consider the basic principles of vehicle dynamics. Utilising a simple vehicle model, such as the Bicycle model the basic principles of vehicle dynamics can be introduced, these basic principles can then be used to answer questions pertaining to why changes in vehicle architecture lead to changes in a vehicle's dynamic characteristics.

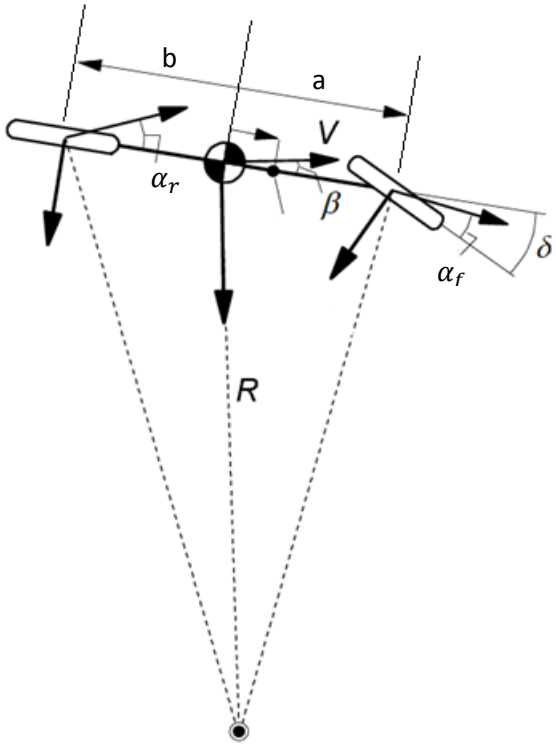

Figure 4-3 Bicycle model

Figure 4-3 shows a representation of a simple vehicle. Its track has been compressed to form a single track, it therefore does not include any weight transfer effects, it is void of any suspension, and it has tyres with a linear cornering stiffness which are connected via a completely rigid chassis. This is one of the simplest vehicle models used for vehicle dynamics, due to its single track it is called the "Bicycle" model. It is a two degree of freedom model, lateral velocity and yaw angle (V_y and ψ), longitudinal velocity V_x (usually constant) and steer angle δ are used as inputs. When the vehicle is in a steady state turn, as shown in the previous figure, it has a tangential velocity to the turn radius V_x this acts at an angle β (body slip angle) to the body, in practice the body slip angle is very small and it can be assumed that $V_x = v$ (the component of velocity along the vehicle longitudinal axis). It also has a lateral velocity V_y which acts towards the turn centre perpendicular to

V_x. The vehicle yaws about the turn centre and so has a yaw angle ψ. The force produced to enable the vehicle to corner comes solely from the tyres cornering stiffness and is equal and opposite to the centrifugal force acting at the vehicle Cog perpendicular to V_x. Its motion can be described by two equations, one for forces and one for moments. These have been developed time and again in numerous texts (Milliken and Milliken, 1995, Olley et al., 2002, Gillespie, 1992, Wong, 2001). It is possible to express these equations in a derivative form to illustrate how the forces and moments are influenced by changes in the body slip angle β, yaw rate r, and steer angle δ. As such the two equations can be written as

$$ma_y = \frac{\partial y}{\partial \beta}\beta + \frac{\partial y}{\partial r}r - \frac{\partial y}{\partial \delta}\delta \tag{4.15}$$

$$I_{zz}\alpha = \frac{\partial N}{\partial \beta}\beta + \frac{\partial N}{\partial r}r - \frac{\partial N}{\partial \delta}\delta \tag{4.16}$$

where

$$\frac{\partial y}{\partial \beta} = C_f + C_r, \qquad \frac{\partial y}{\partial r} = {}^{1}\!/_{V}\,(C_f.a - C_r.b), \qquad \frac{\partial y}{\partial \delta} = -C_f$$

$$\frac{\partial N}{\partial \beta} = (C_f.a - C_r.b), \quad \frac{\partial N}{\partial r} = {}^{1}\!/_{V}\,(C_f.a^2 - C_r.b^2), \qquad \frac{\partial N}{\partial \delta} = -C_f.a$$

Whilst these partial derivatives represent a very simplified linear vehicle they can be used to pinpoint areas where handling differences may arise between the two vehicles under investigation in this study.

The $\frac{\partial y}{\partial \beta}$ term is simply the sum of front and rear cornering stiffness and so relates to the rate at which the lateral force for the whole vehicle will be built with respect to

body slip angle. Relating this to the problem at hand, if, and it is quite likely, that the cornering stiffness's of the tyres are affected when the standard vehicle undergoes changes it will result in different rates of lateral tyre force generation between the two vehicles, which will directly affect response times. Inversely this term also shows that if body slip angles are different between the two vehicles then they will generate different levels of lateral force.

The $\frac{\partial y}{\partial r}$ term is a measure of the forces resulting directly from the yaw rate, it is related to the lateral tyre forces that comprise the yaw moment, Milliken terms this derivative the lateral force/yaw coupling derivative. Again it can be seen that any change in mass distribution and/or cornering stiffness will effect this term.

The final force derivative, $\frac{\partial y}{\partial \delta}$ is the lateral force generated directly by the steer angle at the front wheels, steer angles of the two vehicles in this study will be different, for reasons that will be discussed shortly, also it has already been mentioned that cornering stiffness's are likely to be effected by the changes the SV will undergo and so again there will be differences in the lateral force generated by the two vehicles.

Moving onto the moment derivatives, the first of these, $\frac{\partial N}{\partial \beta}$, which Milliken terms the static directional stability derivative, is a measure of the moment produced about the Cog arising from body slip angle, it follows that if $-C_r.b$ is larger than $C_f.a$ then the moment is stabilising, the vehicle is always trying to straighten itself, this effectively means that the vehicle is understeer. Both vehicles in this study have understeer characteristics but both possess different weight distributions and cornering stiffness's and so this term will vary in magnitude for the different

vehicles, showing they intrinsically posses different levels of understeer, thus have different steering responses and thus respond to steer inputs at different rates.

$\frac{\partial N}{\partial r}$ is the yaw damping derivative, it can be seen that due to changes that have taken place to the vehicles' mass distributions, this term will be different, and so will result in different yaw responses.

Finally $\frac{\partial N}{\partial \delta}$ illustrates the change in moment due to steering, it can be thought of as the control moment, and again it can be seen that it is dependent on the weight distribution and front cornering stiffness. Again as changes have been made to both of these parameters, this term will differ between the two vehicles and so different yaw responses will likely be obtained from steering inputs.

In summary, consideration of the partial derivatives outlined in this section can give clues as to how and why the two vehicles' handling will differ, however they are derived from a simple linear model, and the parameters within them are co-dependent, so whilst they provide a useful insight, the non-linear multi-body models produced within this study will provide a more representative view of the handling differences that will present themselves due to the changes that have been made to the SV when producing the GTV.

Further analysis of the bicycle model yields an expression for the understeer gradient of the simple 2DOF model, in terms of the aforementioned derivatives this is expressed as

$$\text{USG} = W\left[\frac{N_\beta}{Y_\delta N_\beta - N_\delta Y_\beta}\right]\frac{180}{\pi} \tag{4.17}$$

Using this equation with parameters shown in Table 4-2 the understeer gradient can be calculated for the two vehicles in question in this study, this is shown in Table 4-3.

Parameter	Unit	SV	GTV
a (front axle to Cog)	[m]	1.16	1.22
b (rear axle to Cog)	[m]	1.5	1.44
V (forward Velocity)	[m/s]	7.214	7.214
Mf (Mass Front)	[Kg]	1196	1193.27
Mr (Mass Rear)	[Kg]	940	1016.49
Cf (front tyres cornering stiffness)	[N/rad]	-175800	-172800
Cr (rear tyres cornering stiffness)	[N/rad]	-156400	-159600

Table 4-2 SV and GTV Parameters in linear region

	Unit	SV	GTV	% delta
Bicycle Model	[deg/g]	0.51	0.32	37.3
Dymola Model (in linear region of tyre)	[deg/g]	0.52	0.33	36.5

Table 4-3 Bicycle model and Dymola model understeer gradients in linear region

In the majority of conditions, understeer gradients calculated by the bicycle model are not comparable to those obtained from the Dymola models, or the actual vehicle under test. Calculating the understeer gradient from the bicycle model, as has been done in this section, only accounts for weight distribution and tyre cornering stiffness effects on the resulting gradient, there are however more numerous factors effecting the overall understeer gradient of an actual vehicle, these can be summarised as; tyre cornering stiffness, load transfer, lateral force compliance steer, roll steer, steering compliance, aligning torque, and camber thrust all of which effect the understeer gradient, and it is found that the contribution of the tyre cornering stiffness is relatively small compared to the other factors (Dixit, 2009). However, comparable numbers can be obtained from the Dymola model if the tyre model remains within the linear region, and if lateral forces remain low enough as not to introduce the effects of suspension compliances, and lateral load transfer. Within section 3.14, understeer gradients were obtained from the Dymola model, one of the simulations conducted fits into the criteria previously outlined. In

Figure 3-38 (a), between 0.1 and 0.17g, the vehicle is operating at a very low speed within the linear region of the tyre, and as such understeer gradients shown here correlate well with those obtained from the bicycle model, the two sets of figures are summarised in Table 4-3.

There are some important speeds related to the understeer gradient of the vehicle, the first of these which was proposed by General Motors as a way for expressing the understeer of a car, is termed the Characteristic Speed (Milliken and Milliken, 1995). The characteristic speed is defined as the speed at which and understeer vehicle's steering angle is twice the Ackermann angle, this can be defined as;

$$2\left(\frac{57.3l}{R}\right) = \left(\frac{57.3.l}{R}\right) + USG.a_y \tag{4.18}$$

As $a_y = \frac{V^2}{R}$

$$V_{char} = \sqrt{\frac{57.3.l}{USG}} \tag{4.19}$$

	Unit	SV	GTV
V_{char}	[m/s]	17.34	21.77

Table 4-4 Characteristic Speeds for SV and GTV in linear region

As the two vehicles in this study have the same wheelbase, the GTV has a higher characteristic speed than the SV due to its lower USG, this is important as it has been shown by Milliken (1995) and Olley (2002), that the yaw rate response reaches a maximum at a vehicles characteristic speed, meaning that the GTV will exhibit its peak yaw rate at a higher speed than the SV. This is something that will be drawn upon when analysing the handling results. The Characteristic speeds for SV and GTV, calculated using the USG from the bicycle model are shown in Table 4-4.

Similarly to the characteristic speed for the understeer vehicle, the oversteer vehicle also has an important speed, termed the Critical Speed. The critical speed is

the speed at which responses of the oversteer car become divergent, small inputs to steering result in very large lateral accelerations and yaw rates. Looking back to the derivatives of the bicycle model derived earlier, the critical speed can be explained as the speed at which the under/oversteer derivative N_β is equal to the yaw damping moment N_r, as speed increases the yaw damping will decrease, and will no longer balance the under/oversteer moment, leading to divergent responses. As the vehicles under investigation here do not possess an oversteer characteristic the critical speed will not be of use in further analysis. However it is interesting to note that the characteristic speed for an understeer vehicle, the speed where peak yaw rate responses are observed, is equal to the critical speed of an oversteer vehicle, where the yaw rate responses approach infinity (Milliken and Milliken, 1995). The critical speed can thusly be defined as;

$$V_{crit} = \sqrt{\frac{-57.3.l}{USG}} \tag{4.20}$$

There is one more interesting speed that will prove useful in upcoming analysis of the handling results, this is the Tangent Speed. The tangent speed is defined as the speed at which the vehicle will operate with no body slip angle. When a vehicle travels at low speed on a constant radius the rear wheels will track a smaller radius than the front (nose out attitude), as lateral acceleration and slip angles increase there will become a point where both front and rear axles will track the same radius, body slip angle at the Cog will be zero, above this speed the rear axle will track a wider radius than the front (nose in attitude). Tangent speed can also be defined as (Milliken and Milliken, 1995);

$$V_t = \sqrt{-\frac{l.b.C_r}{m.a}} \tag{4.21}$$

Tangent speeds for the SV and GTV (in the linear region) are shown in Table 4-5. As the tangent speed dictates at what speed the vehicle changes form a nose out to a nose in attitude in cornering, it has an effect of the magnitude of tyre slip angles, which can prove useful in later sections when analysing the handling characteristics of the two vehicles.

	Unit	SV	GTV
$V_{tangent}$	[m/s]	15.8	15.1

Table 4-5 Tangent speeds for SV and GTV in linear region

4.3 Test Manoeuvres and Data Analysis

Later in this work a comparison of the two vehicles in both ride and handling domains will be conducted. For ride this will be conducted by exciting the model with a series of rough road inputs. For handling the testing will form two parts, one looking at steady state responses, the other at transient responses.

In order to ensure accuracy in all the manoeuvres they need to be designed carefully to ensure the vehicle operating conditions are analogous to the vehicles' real world use. Also as will be shown in this section it is important that the manoeuvres are not designed in such a way as to unfairly weight the response of one vehicle over the other.

4.3.1 Steady State Handling Manoeuvres

As the steady state handling responses will be utilised to design the transient manoeuvres, it is appropriate that these are addressed first.

There are a number of ways to investigate a vehicle's steady state handling, these are discussed thoroughly in BS4138:2004 (2004). The method that will be utilised for this study, due to its ease of implementation in both the real world and simulation domains, will be the constant radius method. This method employs a predefined

fixed radius, which the vehicle must follow at discrete longitudinal velocities. Recording of longitudinal velocity, lateral acceleration and steer angle from such tests yields the information that is required for this study. Whilst the methods discussed in the standard are sufficient for specifying the manoeuvre procedure and data requirements they are lacking in their exploration of the validity of the results. In the aforementioned source both longitudinal velocity and lateral acceleration are coupled. This is of course unavoidable, however it is not noted that the steer responses (understeer gradients) will differ depending on velocity. If we consider a vehicle travelling on a constant radius trajectory at constant speed it will achieve some nominal lateral acceleration, if we consider the same vehicle now travelling on a radius twice the size of the first, it is clear that now to obtain the same level of lateral acceleration it will have to travel $\times\sqrt{2}$ faster and its steer angle will be considerably different. To be able to fully characterise the steady state handling of a vehicle, its longitudinal velocity needs to be accounted for. Also for this study, as the steering responses obtained from the constant radii tests are to be used to design the transient manoeuvres, the inclusion of the vehicle velocity becomes even more crucial.

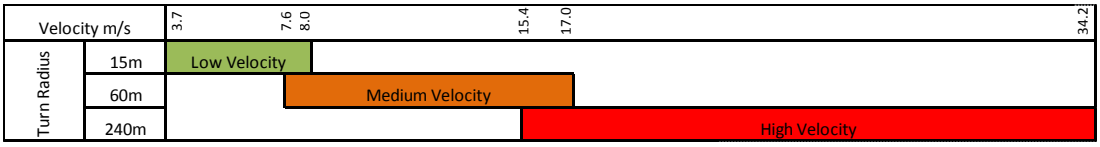

Figure 4-4 Constant radii test range

For handling manoeuvres the usable speed range of the vehicle can be considered 0 – 35 $m.s^{-1}$. The maximum lateral acceleration of the vehicle in question for this study was thought to be circa ±5 ms^{-2}, it was decided that test range would be between 3 and 35 $m.s^{-1}$, at lateral accelerations between ±0.5 and ±5 $m.s^{-2}$. To

cover this speed and lateral acceleration range it was found that three separate constant radii tests would be required, on 15, 60 and 240m radii. The exact breakdown of the speed range can be seen in Figure 4-4. This in effect gives six areas where the vehicles handling can be investigated, low, medium and high speed, and as the lateral acceleration range for these speed ranges is repeated, they can be further subdivided into low and high lateral accelerations.

If both vehicles under investigation in this study are simulated carrying out the previously mentioned constant radii tests, their steering angles and lateral accelerations can be compared to illustrate the differences in their steady state handling. Namely steering angle can be plotted against lateral acceleration to illustrate how the steering response changes with increasing lateral acceleration/longitudinal velocity. This is generally termed the steering response, of which the gradient is referred to as the understeer gradient. The different types of steering responses are shown in Figure 4-5.

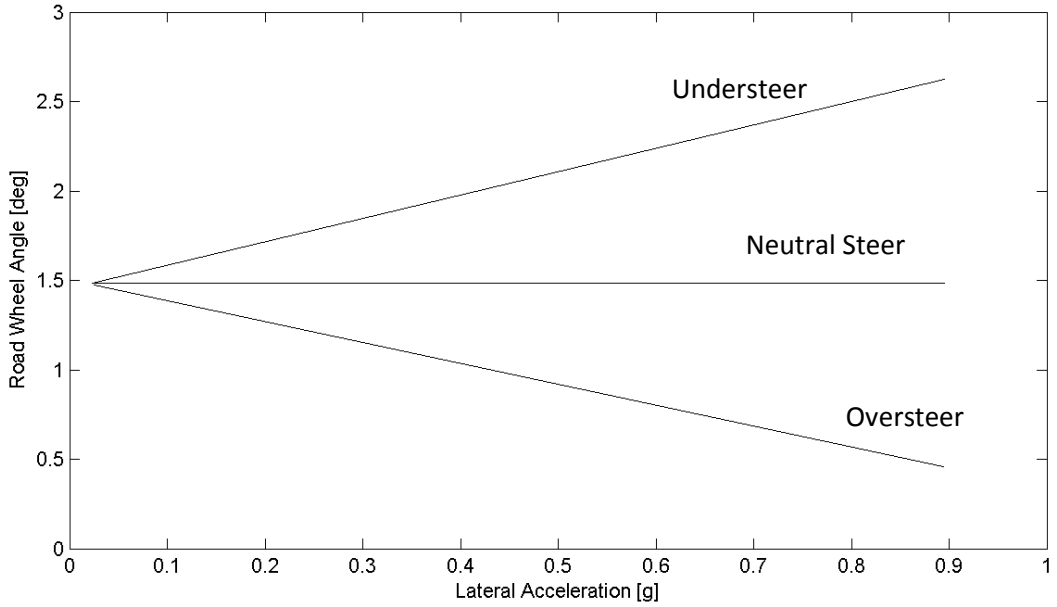

Figure 4-5 Steady state steering responses example

For steady state handling, if a vehicle under increasing lateral acceleration/longitudinal velocity requires an increase in steering angle to maintain its path then it is said to understeer, as with no change in steering it would 'understeer' the desired path. If the vehicle requires no change in steer angle it is neutral steer, and finally if the vehicle requires a decrease in steer angle it is oversteer, as it would 'oversteer' the desired path with no change in steering angle.

The results from these simulations can be also used to obtain a velocity and steer angle to target any level of lateral acceleration encompassed by the test manoeuvres, furthermore the same levels of lateral acceleration can be targeted at differing longitudinal velocities, and vice-versa. This method is used to specify the transient manoeuvres. For instance, the test range has been set as 3 – 35 $m.s^{-1}$ at discrete levels of lateral acceleration, ranging from 0.1 to 0.5 g, in 0.05 g increments, knowing this and utilising the constant radii test results, steer angles and velocities can be obtained for each targeted lateral acceleration in the low, medium and high speed ranges. This can be done for both vehicles, so despite their different steering responses and understeer gradients, equivalent steer angles will be used to ensure both obtain/target the same steady state response during their individual test manoeuvres, this will allow response metrics to be directly compared.

4.3.2 Transient Handling Manoeuvres

A number of transient manoeuvres for road vehicles are discussed in BS7853:1996 (2011). For this study a variant of the step steer manoeuvre; the ramp to step steer, and sinusoidal steer will be utilised.

The ramp to step steer manoeuvre was chosen over the step steer as it is more representative of a real world event. In reality an average driver has been found capable of applying extremely fast, handwheel rates between 800 and 1900 deg. s^{-1},

however this is affected by steering geometry and damping within the system. (Forkenbrock and Elsasser, 2005). It is very likely that this value will change significantly vehicle to vehicle. In applying very high steering rates, second order effects of the steering systems are introduced into the vehicle responses. Also due to the extreme handwheel rate, large front tyre slip angles are built and the tyres are put into a post limit condition at the very outset of the manoeuvre, this has the effect of producing very irregular top level vehicle responses. In order to obtain sensible and comparable vehicle responses it was found that a handwheel rate no larger than 400 $\mathrm{deg.\,s^{-1}}$should be used, this provides a fast enough input to be able to look at the transient open loop responses of the vehicles, but isn't so large as to introduce the added complexities just mentioned. Whilst this application rate is reasonably fast it is still far more representant of a ramp than a step. The steering application rate of 400 $\mathrm{deg.\,s^{-1}}$ will be the value utilised throughout this study.

Input rate and naming aside, the ramp to step steer was chosen as it is a good way of investigating the transient responses of the vehicles. The sinusoidal steer is also useful for investigating the transient responses of the vehicles in the same way as the ramp to step steer manoeuvre, but it is especially useful for looking at the transient to transient responses, i.e. the transition from one transient during the initial part of the manoeuvre to the transient in the opposite direction during the second part of the manoeuvre. Vehicle responses will be investigated by comparison of response times, peak values, overshoot values and phasing, these will be fully described later in this section.

As previously discussed the transient manoeuvre inputs are derived from the constant radii test, Table 4-6 shows a test matrix for the ramp to step steer and sinusoidal steer manoeuvres, the steering input rate for the ramp to step steer

manoeuvres as mentioned is 400 deg. s^{-1} and 0.5 Hz for the sinusoidal steer manoeuvres.

	Longitudinal Velocity $[m.s^{-1}]$	Steer Angle (handwheel) [rad]		Targeted Lateral Acceleration [g]
		SV	GTV	
Low Speed	-	-	-	0.050
	3.693	2.839	2.836	0.100
	4.529	2.844	2.841	0.150
	5.266	2.878	2.872	0.200
	5.795	2.927	2.921	0.250
	6.308	2.983	2.978	0.300
	6.774	3.045	3.040	0.350
	7.214	3.113	3.105	0.400
	7.606	3.188	3.182	0.450
	7.995	3.288	3.283	0.500
	8.378	3.518	3.516	0.550
Medium Speed	5.413	0.672	0.671	0.050
	7.639	0.689	0.685	0.100
	9.340	0.705	0.700	0.150
	10.810	0.723	0.718	0.200
	12.020	0.745	0.739	0.250
	13.170	0.772	0.765	0.300
	14.190	0.803	0.797	0.350
	15.180	0.843	0.835	0.400
	16.060	0.896	0.887	0.450
	16.960	0.985	0.978	0.500
	17.800	1.278	1.276	0.550
High Speed	-	-	-	0.050
	15.360	0.190	0.188	0.100
	18.780	0.206	0.202	0.150
	21.650	0.224	0.218	0.200
	24.230	0.245	0.238	0.250
	26.530	0.270	0.263	0.300
	28.640	0.304	0.296	0.350
	30.660	0.348	0.340	0.400
	32.500	0.417	0.407	0.450
	34.230	0.546	0.540	0.500
	-	-	-	0.550

Table 4-6 Transient manoeuvre test matrix

A limited number of the transient manoeuvres descried in this section have been carried out in the real world using the standard vehicle in order to validate the standard vehicle model, all the tests were carried out as closely as possible in accordance with BS150037-1:1998 (1998), the exact test plan for this testing can be found in appendix C.

For testing in the modelling domain the comprehensive range of manoeuvres listed in Table 4-6 were used, at this point it is appropriate to illustrate the data that is collected from the models and how it is used to objectively compare the two vehicles, as was conducted for the steady state manoeuvres.

The vehicle models can be simulated using the inputs provided. As the basis of this study is to identify differences in the two vehicles' ride and handling characteristics, the analysis will have two main parts, firstly the differences between them will be identified by investigation of vehicle level outputs, namely, lateral accelerations and yaw rates, these results will be treated, in ways that will be discussed in detail shortly. Following this and based on the outcomes of this first analysis, a more in depth investigation will be conducted into the reasons behind the differences discovered, by looking at lower level responses.

This section will only concentrate on the treatment of the initial data, as the secondary investigation just mentioned can take many forms depending on the trends in the data obtained during the first part of the analysis.

Let us first consider the ramp to step steer manoeuvre. The steer input and corresponding lateral acceleration and yaw rate responses are shown in Figure 4-6, along with the response metrics of interest. For both lateral acceleration and yaw rate, peak values, overshoot, response times and phasing will be calculated. The

peak value is exactly that, the largest value seen in the response. The overshoot is the percentage difference between the peak value and the steady state value.

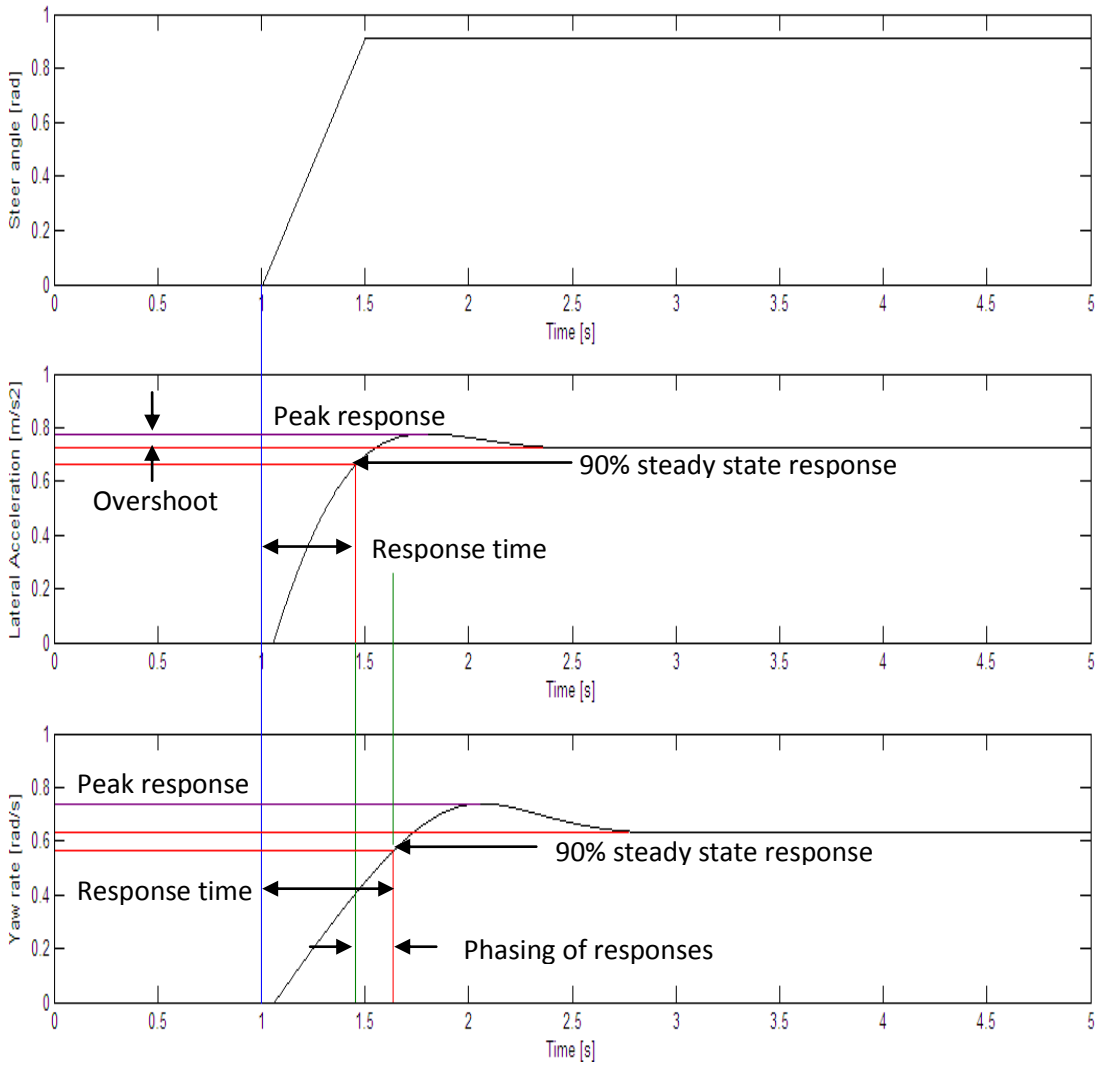

Figure 4-6 Ramp to step steer response metrics

The response time is the time taken from the initial steering input, to the point where the response reaches 90% of its steady state value. And finally the phasing of the two responses is the time between one reaching 90% of its steady state value and the other doing the same.

Figure 4-7 illustrates the response metrics that are used for the sinusoidal steer manoeuvres. Again the peak responses are recorded, this done for both the first and the second peaks. As there is effectively no steady state region to this manoeuvre the

response times used are those from the initiation of steering, to the peak of the response, again for both first and second peaks. The phasing of lateral acceleration and yaw rate here is calculated as the time difference between the peak values, again for both first and second peaks.

These metrics can be calculated directly from the model output files, and then plotted against lateral acceleration for each speed range. By doing this for both vehicles, trends in handling and also areas where the two vehicles' handling differs is easy to recognise.

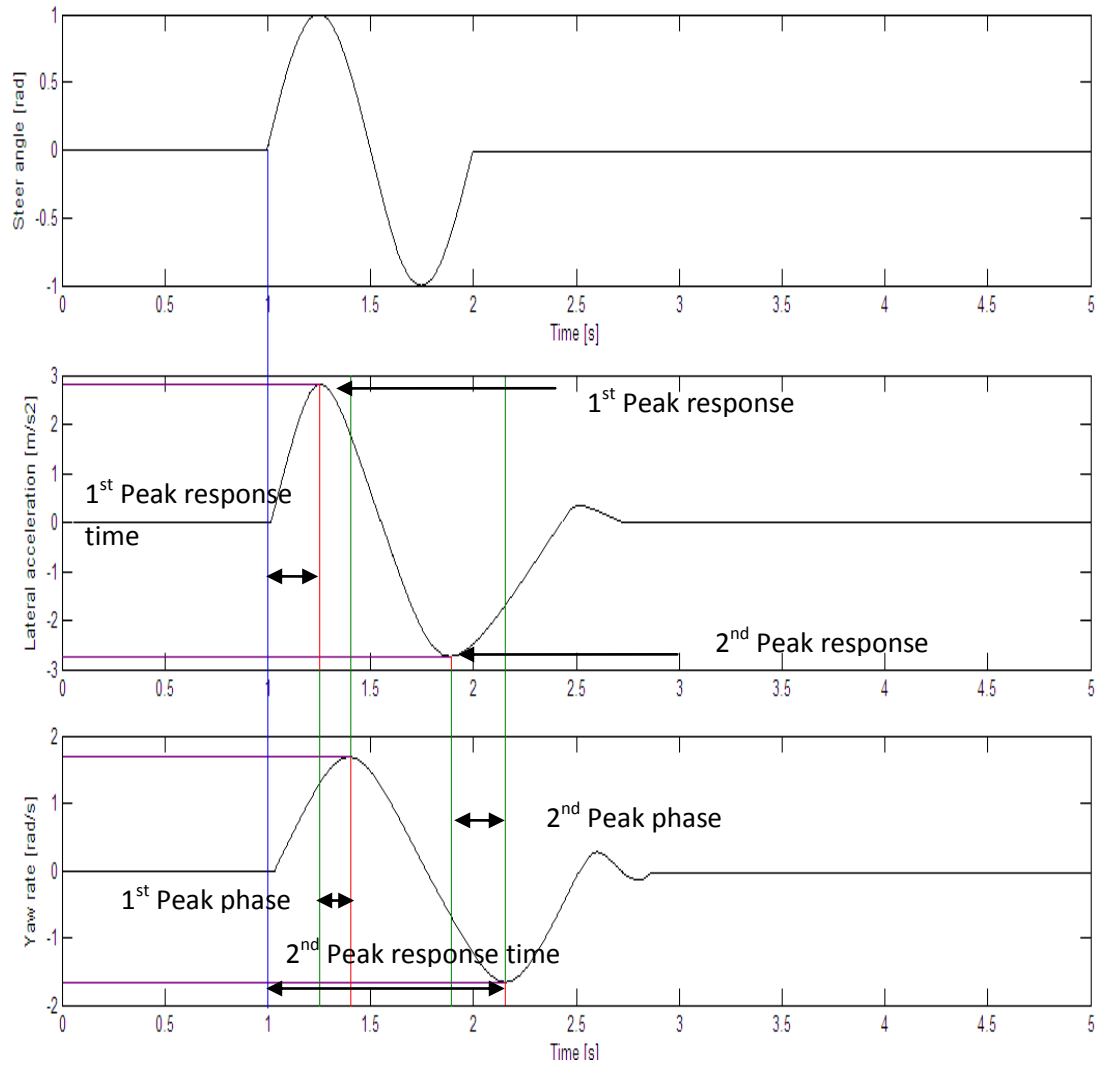

Figure 4-7 Sinusoidal steer response metrics

The derivation and investigation of these responses across the three speed ranges forms the first part of the analysis carried out for this study. Investigation of the trends obtained from this initial analysis by interrogating the vehicle responses at a vehicle and component level will form the second part of the analysis.

One vehicle metric that it is hypothesised will play a significant role in determining the transient responses of the vehicles, is the position of the centre of percussion/inertial conjugate. The centre of percussion can be defined as follows, "The location at which no translation occurs when a free body with finite mass and inertia properties is loaded in a direction that does not pass through its centre of gravity. No translation occurs at this point during load application, whether or not the load is percussive." (Blundell and Harty, 2004). The position of the centre of percussion on the vehicle in plan view (x-y plane) can be found by considering the vehicle at the initiation of steering angle application, as is shown in Figure 4-8.

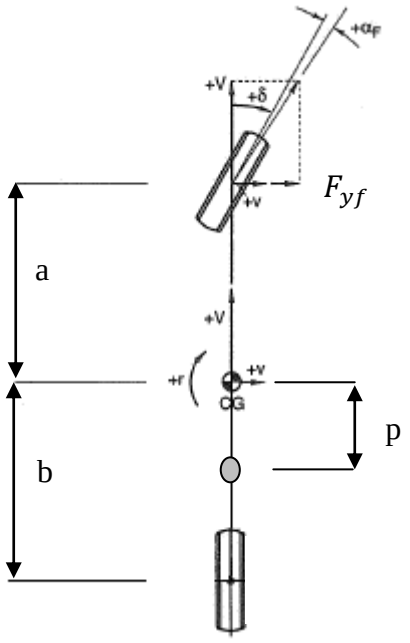

Figure 4-8 Vehicle and instant of turn in

The forces and moments acting on the vehicle at this point are

$$F_{yf} \,.\, a = \, I_{zz} \,.\, \dot{r} \tag{4.22}$$

$$F_{yf} = m \, .\alpha y \tag{4.23}$$

so

$$\frac{F_{yf} \, .\, a}{I_{zz}} = \, \dot{r} \tag{4.24}$$

At the centre of percussion (Point p)

$$\dot{r} . p = \, \alpha y \tag{4.25}$$

Inclusion of the centre of percussion into the moment term gives

$$\frac{F_{yf} \, .\, a}{I_{zz}} \,.p = \, \alpha y \tag{4.26}$$

Solve for p

$$\frac{F_{yf} \, .\, a}{I_{zz}} . p = \frac{F_{yf}}{m} \tag{4.27}$$

As $I_{zz} = m. k^2$

$$\frac{a}{K^2} \,.p \, = 1$$

Or

$$\frac{K^2}{a} = p \tag{4.28}$$

It is useful to divide this by b, this way the position of the centre of percussion is viewed as a ratio in terms of its position from the rear axle. In doing this we get; when p = b (centre of percussion on the rear axle)

$$\frac{K^2}{a \,.\, b} = 1 \tag{4.29}$$

The position of the centre of percussion with relation to the rear axle has been termed the dynamic index (DI), defined as

$$DI = \frac{K^2}{a\,.\,b} \tag{4.30}$$

From this derivation it should be noted that;

DI < 1 – Centre of percussion in-front of rear axle

DI = 1 – Centre of percussion on the rear axle

DI > 1 – Centre of percussion behind rear axle

The effects of the position of the centre of percussion on vehicle handling have been found to be quite significant (Bobier et al., 2008, Olley et al., 2002). These effects can be summarised by consideration of two distinct DI values, first of all consider a DI larger than 1, the centre of percussion is behind the rear axle, so during the initial transient phase the vehicle will begin to yaw about this point, as this is behind the rear axle, the rear tyres are shifted into the turn thus building slip angle and force in the incorrect direction to negotiate the corner. Now let us consider a DI smaller than 1, the centre of percussion is now in front of the rear axle, and so in the same cornering situation just mentioned, as the vehicle begins to yaw, it will do so about the centre of percussion, as this is now ahead of the rear axle, the rear tyres are shifted out of the turn, thus building slip angle and force in the correct direction for cornering. As can be imagined with a DI behind the rear axle and the initial tyre force being generated in the incorrect direction to negotiate the corner, the lateral force build up is delayed, however, this can lead to a large yaw moment being produced during this initial transient phase due to the opposition of front and rear tyre forces. When the DI is in front of the rear axle the lateral force build up is

expedited, the respective yaw moment produced however is not as large in this scenario as front and rear tyre forces act in the same direction.

There is much conjecture about optimum values of DI, some say for optimum handling it should be as low as possible (Olley et al., 2002), others, where significant testing has been carried out believe that values are heavily dependent on driver skill, high performance competition vehicles with highly skilled drivers can have low DI values (0.6 – 0.85), low DI values require extremely fast driver reactions and it has been found that too low values of DI can create a vehicle that reacts too fast for even the most skilled drivers. For road vehicles it is thought that optimum values lie between 0.9 and less than 1 (Blundell and Harty, 2004). Such values should allow fast enough lateral responses of the vehicle but not so fast as to be out of the realms of control for the average road user.

As the position of the centre of percussion is dependent on the radius of gyration of the vehicle, it is clear that if the mass and inertia properties are changed as they are when a vehicle undergoes hybridisation (as in this study), by the addition and removal of components, then the DI will be altered. It has been shown that a change in DI of 0.01 can be perceived by average drivers, so even small changes in mass and inertia properties can have significant effects on vehicle handling and driver perception. The DI values of the vehicles under investigation in this study are shown in Table 4-7.

	SV	GTV	% delta
DI	1.00	1.02	2.00

Table 4-7 DI Values

4.3.3 Ride Domain Simulations

In order to conduct the ride domain analysis of the two vehicles a source of measurable and known vertical disturbance is required. There are two possible options for this, the first is to use a 4 or 7-post rig model, this is effectively 4 actuators under each wheel of the model and an optional 3 actuators attached at some point to the vehicle body which are used to apply aerodynamic forces as well as body pitch and roll angles. As aerodynamic forces produced by the vehicles under investigation here are very small and as the ride analysis would take the form of straight line driving, there is no need for a 7-post rig model, and a 4-post would suffice. The inputs into the four actuators would comprise of white noise to replicate a random road unevenness profile, this input would have to be scaled in order to give required values of PSD. The downsides of using a 4-post rig model are that it requires significant time to create the sets of graded white noise inputs which are required for each test speed, also as the vehicle model is effectively stationary during the test procedure velocity dependant effects, such as damping, within the tyre model are lost. The second option is to model sections of uneven roads which the vehicle model can be simulated driving over. This is made easier by the road builder functions within the Modelica vehicle dynamics library, which will take an unevenness profile (displacement) and create a road model from it. This can be carried out with a number of different unevenness profiles to create different levels of road roughness. Usage of this second method will capture all velocity dependant characteristics within the tyre model as the vehicle is in motion, also only one set of road models needs to be created for each roughness grade as the vehicle speed can be changed independently.

The second method just described has been implemented for this study, and will be further explained in the following section.

4.3.4 Road Modelling

To build a road model that will aid in studying the ride domain characteristics of the vehicles under question, knowledge of the physical height deviation of the road surface under each wheel of the vehicle must be obtained. The physical and statistical properties of road surfaces have been studied and documented within literature and can be generally thought of as obeying the hypothesis of isotropy (Robson, 1978, Dodds and Robson, 1973, Heath, 1988). Isotropy implies that all straight tracks on the surface can be described by the same spectral characteristics, regardless of their position or orientation. Under this assumption the two parallel wheel tracks along the road surface will have equal spectral densities, however, whilst there spectra are equal, the actual elevation they describe can be different, such differences between the left and right wheel tracks impart a roll disturbance on the vehicle, this roll disturbance isn't represented in the spectra of the wheel tracks, and for this reason it is also important to define the coherence between the two tracks (Bogsjö, 2009). The coherence function shows the level of correlation between each track as a function of frequency. It has been shown that the coherence between left and right wheel tracks is exponentially decreasing (Bogsjö, 2009, Bogsjö, 2007). For example, low frequency/high wavelength disturbances in the road, such as hills, bridges even speed bumps, the left and right tracks will be highly correlated in terms of their vertical displacement, the coherence function will be near one. For higher frequency/shorter wavelength disturbances, such as variations in surface texture, the two wheel tracks are less correlated and the coherence function will approach zero.

For this study the method proposed by Cebon and Newland (1983) has been utilised, this method uses the desired PSD of the road profile as an input and computes the inverse Fourier transform with a set of randomly generated phase angles to obtain a 2d unevenness profile of the road ${Z_r}^l$ as shown by equation 4.31

$$ {Z_r}^l = \sum_{k=0}^{N-1} \sqrt{S_k}\ e^{i[\theta_k + \frac{2\pi k_r}{N}]}\ \ k\ and\ r = 0,1,2\ \ldots, (N-1) \tag{4.31} $$

Where

$S_k = \dfrac{2\pi}{N\Delta}\, S(\gamma_k)$

$S(\gamma_k) =\ desired\ spectral\ density$

$\Delta = delta\ distance\ between\ road\ nodes$

$\theta_k = a\ set\ of\ randon\ phase\ angles, uniformly\ distributed\ bwteen\ 0\ and\ 2\pi$

The desired spectral density can be obtained from the guidelines given in (BS7853:1996, 1996) on the fitting of measured road PSD's as is utilised by Tyan et al (2004). Here the desired spectral density is represented as

$$ S(\gamma_k) =\ \varphi(n_0)\left(\frac{n}{n_0}\right)^{-w} \tag{4.32} $$

Where

$n = \dfrac{\Omega}{2\pi} = desired\ spatial\ frequency\ (cycles/m)$

$\varphi(n_0) = degree\ of\ road\ roughness\ at\ n_0$

$n_0 = 0.1\ cycles/m$

$w\ is\ \ the\ waviness\ number, for\ the\ majority\ of\ roads = 2$

The degree of road roughness given by the aforementioned British Standard is shown in Table 4-8, for this study the geometric mean values were utilised.

	degree of road roughness $\varphi(n_0)$ $(10^{-6}m^2/(cycle/m)$, where $n_0 = 0.1\ cycles/m$		
Road Class	Lower Limit	Geometric Mean	Upper Limit
A (very good)	-	16	32
B (good)	32	64	128
C (Average)	128	256	512
D (poor)	512	1024	2048
E (very poor)	2048	4096	8192

Table 4-8 Road roughness values classified by British Standard

The second road profile is created by summing two separate profiles Y_r and X_r, the first of these is created using the same phase angles as were used previously, and so is correlated with this first track, the second uses newly generated phase angles (still between 0 and 2π) ϕ_k. The correlated unevenness profiles is generated by

$$Y_r = \sum_{k=0}^{N-1} n_{12k}\sqrt{S_k}\ e^{i[\theta_k + \frac{2\pi k_r}{N}]}\ \ k\ and\ r = 0,1,2\ldots,(N-1) \tag{4.33}$$

And the uncorrelated unevenness profile by

$$X_r = \sum_{k=0}^{N-1} \sqrt{1 - {n^2}_{12k}}\sqrt{S_k}\ e^{i[\phi_k + \frac{2\pi k_r}{N}]}\ \ k\ and\ r = 0,1,2\ldots,(N-1) \tag{4.34}$$

The second track is now given by

$${Z_r}^r = Y_r + X_r \quad r = 0,1,2\ldots,(N-1) \tag{4.35}$$

In these equations$n_{12k} = \frac{S_{12k}}{S_k}$, is the coherence function between the two tracks, where S_{12k} is the cross-spectral density of the two tracks. As these profiles have been assumed to follow the hypothesis of isotropy the coherence function can be calculated from the desired PSD (equal for both tracks) and the track width of the vehicle (Bogsjö, 2009), however it has been shown that the coherence function is not sensitive to changes in the spectral density of road profiles (Robson, 1978) and

so can be represented more simply via an exponential model (Bogsjö, 2007, Hongbin et al., 2011).

$$n_{12k} = e^{-b\,\gamma_k} \tag{4.36}$$

Where b is the track width of the vehicle, and as previously γ_k is the spatial frequency range.

Example results obtained from this method of road surface modelling are shown in Figure 4-9 to Figure 4-11.

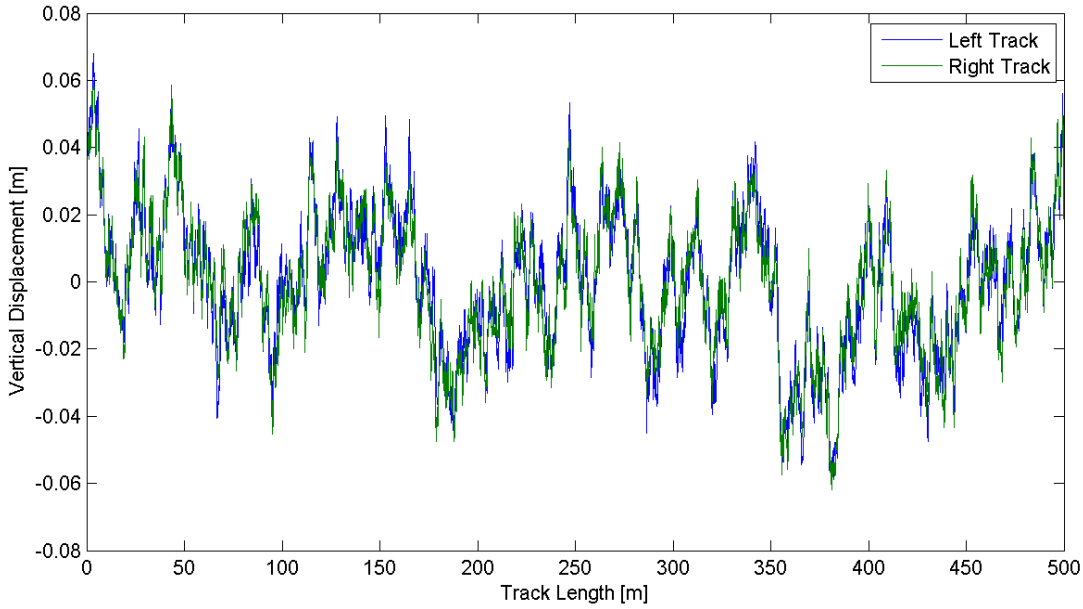

Figure 4-9 Example of modelled grade C road displacement profile

Using the method outlined in this section a number of road models were created, these models are displayed in Figure 4-12 along with the grading defined by the British Standard, where the coloured lines represent the road models created for this study.

Simulation of the two vehicle models driving over these rough road models provides a means of investigating the ride comfort, however due to large amounts of data that are created a defined way of viewing and analysing the results is needed.

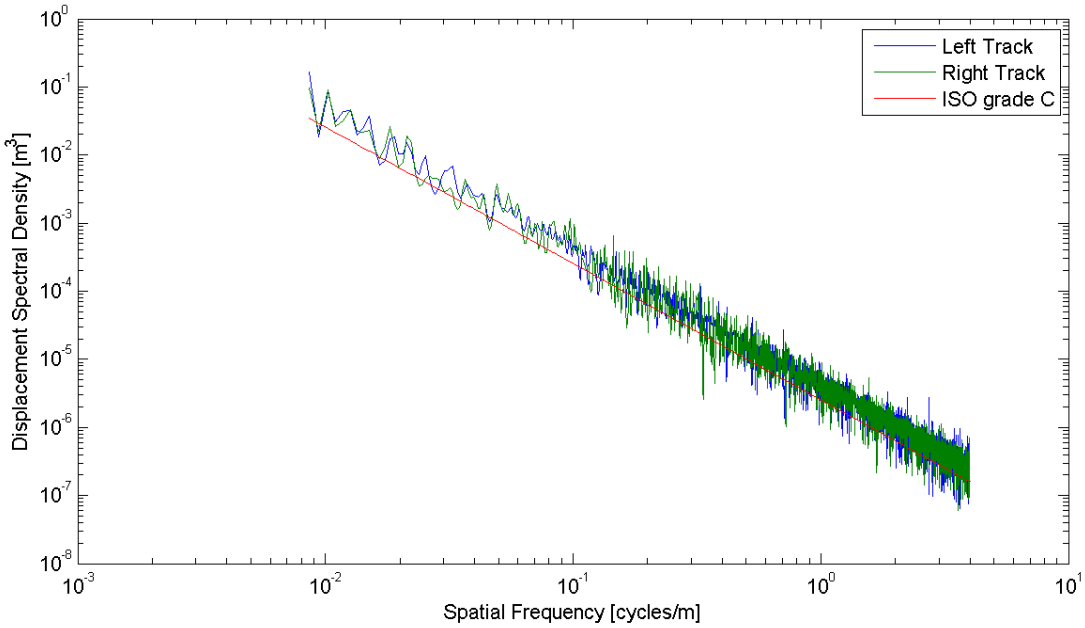

Figure 4-10 PSD of modelled road tracks

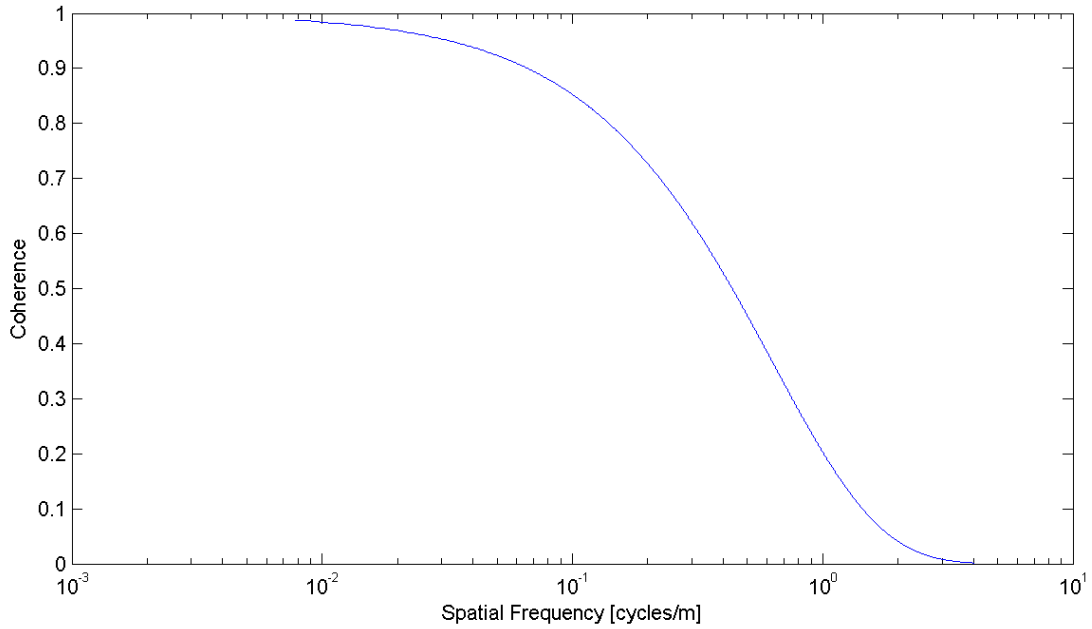

Figure 4-11 Coherence function between left and right tracks

Within the ride domain portion of this study, occupant comfort is of primary importance. Occupant comfort is a function of the vehicle body motion, which itself is a function of the loads received through the tyres from the road.

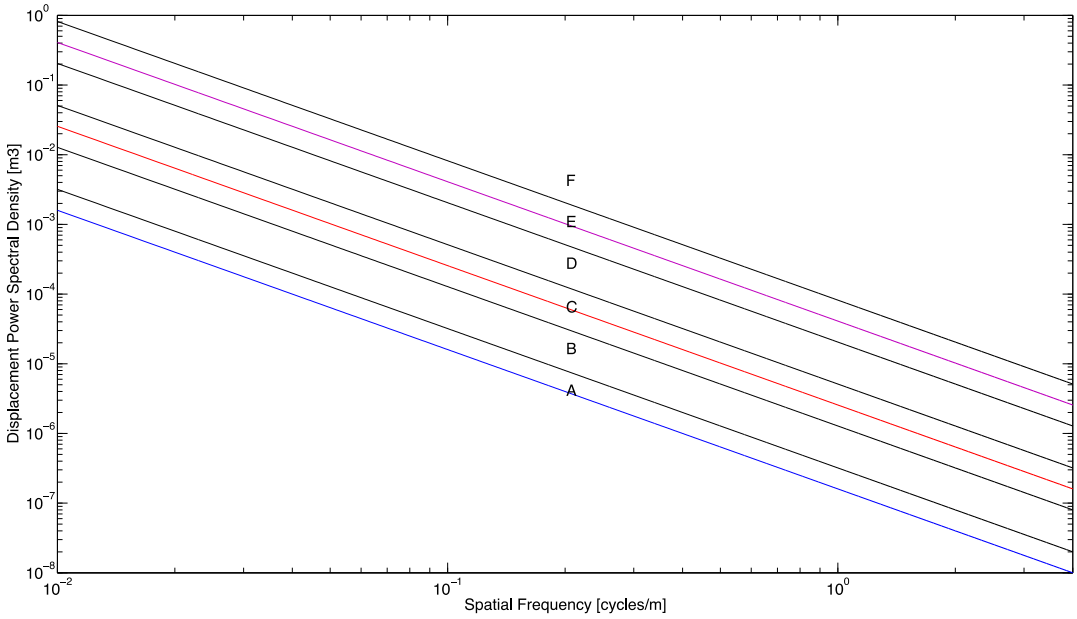

Figure 4-12 Modelled road roughness profiles and British Standard ratings

From this it can be said that the ride analysis should focus on two main areas, the first being tyre forces, more specifically contact patch normal forces. The second area being occupant comfort arising from vehicle body (sprung mass) motion. The first of these areas can be investigated through statistical analysis of the forces generated. However the second, body motion, is more convoluted. How can body motions be related to occupant comfort? What motions and frequencies are occupants more susceptible to?

BS2631-1:1997 (1997) details specific accelerations that a seated human is most susceptible to, how to treat such acceleration data and even sets subjective comfort limits based on the objective data. Following the previous reference, vertical accelerations within the vehicle at the height of the base of the seat supporting the occupants are recorded (using a matrix of 980 accelerometers), as suggested this data is weighted in the frequency domain as to give a higher weighting to frequencies which a seated human will feel more discomfort towards. The weighting filter is detailed in the standard and illustrated in Figure 4-13. Further to applying this filter,

the RMS of the weighted acceleration is calculated, this forms the data that will be used for the analysis of occupant comfort as it can be directly related to the comfort levels given in the standard.

When investigating the contact patch loads, again due to the large amount of data that will be generated and the randomness of it, (arising from the rough road inputs) it is most beneficial to conduct a statistical analysis of the data. This will take the form of investigation of the standard deviations of the contact patch loads, this way, as in the handling section, results can be reduced to a single metric for each speed to allow easy identification of trends and differences between the two models. Also analysis of the standard deviations of contact patch loading will give important information regarding the forces being passed to the vehicle body through the springs and dampers.

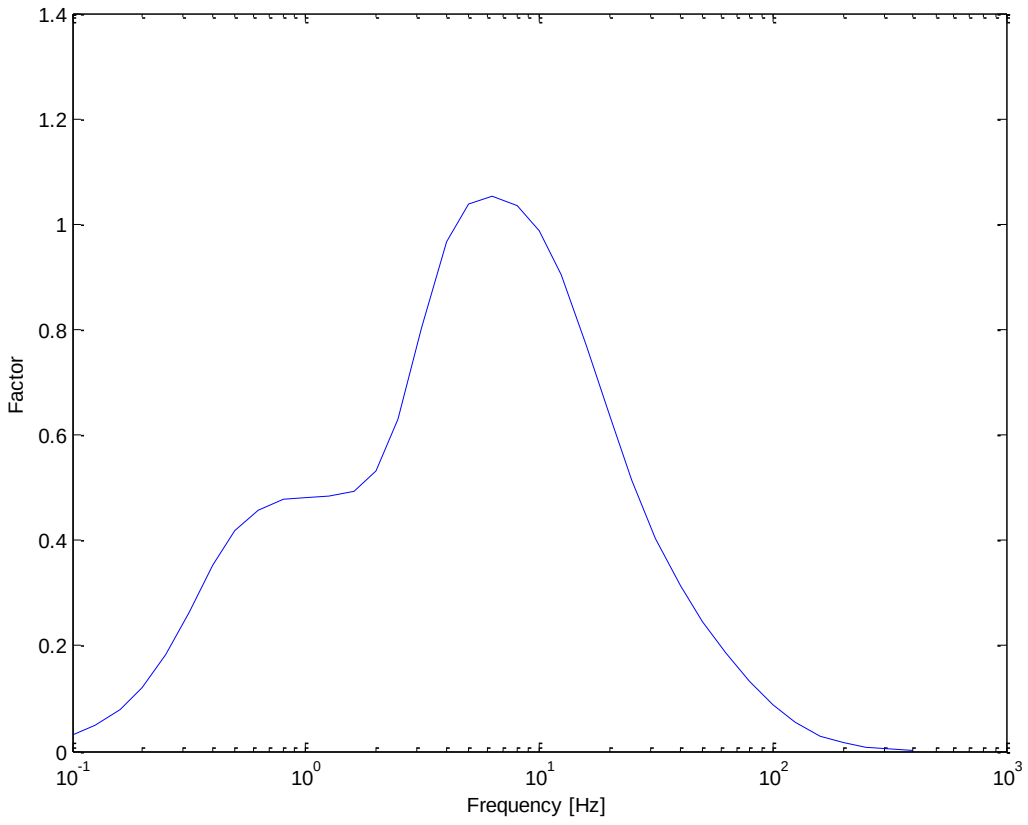

Figure 4-13 Vertical acceleration weighting filter

4.4 Conclusion

This chapter has introduced some basic vehicle dynamics principles and data analyses that are of importance for this study.

Using the simple models that were introduced it was shown how component and vehicle level changes that are made to the vehicles within this study can affect both ride and handling. These models were very simplified and whilst they provide an idea of how the changes made to the vehicles in this study may affect their ride and handling characteristics, the mutibody models constructed especially for this study will prove much more useful in identifying exactly what differences will occur and where they arise from.

Specific industry standard ride and handling manoeuvres that will be used in order to compare the two vehicles in this study were discussed in detail. For handling it was shown how the transient manoeuvres were designed from the results of the steady state manoeuvres, in order to produce results that are easily and fairly comparable between vehicles. For the ride domain simulations it was shown how occupant comfort levels can be linked to objective data, and most importantly how this data will be obtained from the vehicle models. The treatment and presentation of results was also illustrated, so that when results are presented the reader will understand and follow the methods being used.

Chapter 5 Result and Analysis – Ride Comfort

5.1 Introduction

This chapter will present and analyse results obtained from the different ride domain case studies utilised within this work.

Results will be discussed at a vehicle and component level in terms of responses resulting from uneven road inputs. This will form the objective portion of the results, however using industry standard rating systems for human comfort, these vehicle responses will be subjectively linked to occupant comfort. This means that it will be possible to definitively answer, not only whether one vehicle will be perceived as having better ride comfort than the other, but also where the differences arise from and how they may be mitigated.

5.2 Rough Road Ride Comfort

Ride comfort is of vital importance in a hybrid vehicle as it is in any vehicle. Alterations that have been made to the vehicle under investigation here, as discussed in previous chapters, have been shown to have significant effects on the vehicle's mass and mass distribution, as a result it is likely that the vehicle's ride characteristics will have been effected.

As shown in the previous chapter, a number of 3-dimensional road models with varying power spectral densities were created. These roads are classified via an ISO rating system based on their power spectral density. The two roads used here consist of ISO grades A and C. A can be thought of as equivalent to a British motorway, a road that is well maintained and generally in good condition. The ISO road grade C

can be thought of as an older road that has not been as well maintained, something that might be equivalent to a British B/C road. Both vehicle models are simulated running over a section of this road at varying longitudinal velocities. These velocities range from 5 $\mathrm{m.s^{-1}}$ to 50 $\mathrm{m.s^{-1}}$ and cover the entire usable range of the vehicle.

As was discussed in chapter 4, when carrying out an investigation in the ride domain, for passenger vehicles, two main areas should be considered. The first ultimately dictates the second, but should be considered separately due to its effect on the vehicle in the handling domain. This of course is contact patch load variation. The second and perhaps more general point is occupant comfort and is investigated through vertical acceleration levels inside the vehicle. It seems sensible to start this investigation where all the forces originate, the contact patch.

5.2.1 Contact Patch Load Variation

A large portion of vehicle dynamics can be considered as the management of contact patch load variation. Distribution and magnitude of load variation at the tyre contact patch directly affects a vehicle's ride and handling. The variation in contact patch load from road inputs has two effects, the first will impact on occupant comfort, generally speaking large variations in contact pact load will produce large variations in vertical body acceleration and thus offer lower levels of comfort. The second will impact on handling, again inputs from the road will cause variations in contact patch load which will affect lateral and longitudinal slip, affecting the forces generated and thus affecting the lateral and longitudinal dynamics of the vehicle. It has been widely shown that minimization of contact patch load variation is beneficial for both ride and handling of road vehicles.

Through the use of the two vehicle models constructed for this study, we can directly investigate the forces generated at the contact patch of both the SV and the GTV.

Looking directly at the contact patch loads doesn't yield much useful information, as can be seen in Figure 5-1 the data is noisy and hard to decipher. For completeness the frequency content of the contact patch loads shown, is given in Figure 5-2, in the form of power spectral densities. It can be seen that the two main peaks in the PSD's correspond to the sprung mass (large peak between 1-2Hz), and the un-sprung mass (smaller peak around 10 Hz). The integral of the power spectral densities is equal to the square of the RMS' of the contact patch loads, which could be used to further investigate said responses, however for this it will be more beneficial to study the standard deviations of the contact patch loads, as these will yield the variance in the loading about the mean, not about 0 as with the RMS values. The standard deviation of the contact patch loads and mean values for the SV and GTV when running on both ISO road grades A and C are shown in Table 5-1 to Table 5-3, (grade A) and Table 5-5 to Table 5-7, (Grade C). This data is plotted against speed for both vehicles and road grades in Figure 5-3 and Figure 5-4. Within the tables of the mean CP loads, the standard uncertainty (standard deviation of the average) is also given so results can be quoted to 95% confidence. The standard uncertainty is defined as, $\pm\frac{\sigma}{\sqrt{n}}$, where σ is the standard deviation and n is the number of sample points obtained from the simulation result (here 1000). To give a confidence interval of 95% this becomes; $\pm\frac{1.96\sigma}{\sqrt{n}}$.

If we begin by considering the contact patch loads of the two vehicles when driving on the grade A road, the first thing to notice is the similarity of the standard deviations in all four contact patch loads. At speeds below 30 $\mathrm{m.s^{-1}}$ there is almost

no noticeable difference in the variation of contact patch load between the two vehicles. The variations in front contact patch load begin to deviate slightly between the two vehicles at speeds above 30 $\mathrm{m.s^{-1}}$ however it is apparent that the difference is not very large. The rear contact patch load variation does show a slightly larger difference between the two vehicles over the entire speed range, those for the GTV being slightly higher. Whilst this difference is fairly constant from 5 – 30 m/s, after this it does steadily increase.

Differences between the two vehicles are much the same when observing the result of the rougher of the two road variants, the grade C road. The same trends observed for the loading on the grade A road are also present here. Whilst again there is little or no difference in the variance of the contact patch load until above 30 m/s, after this speed it can be seen that the standard deviation of the GTV's contact patch loads increase quite dramatically. For both road roughness variations at higher speeds the differences are significant, the GTV shows standard deviations 10-18% higher than the SV. It is interesting to note that differences between the two vehicles are largest on the smoother of the two road models. Such an anomaly could be explained by the amount of damping. On a smoother road, levels of low speed damping are more influential on body motions than high speed damping, due to smaller, less harsh road inputs allowing the dampers to operate within the low speed region. Hence if levels of low speed damping are now incorrect on the GTV due to its altered mass and inertia properties, but the high speed damping characteristics aren't so drastically miss-matched, then it is conceivable that ride characteristics could be worse on a smoother road.

It should be noted that for both road grades the difference in the mean contact patch loads remain fairly constant and reflect the changes made to the weight

distribution. The mean contact patch loads at the front have reduced by 1-3% for the GTV, and the rear, have increased by 7-10%.

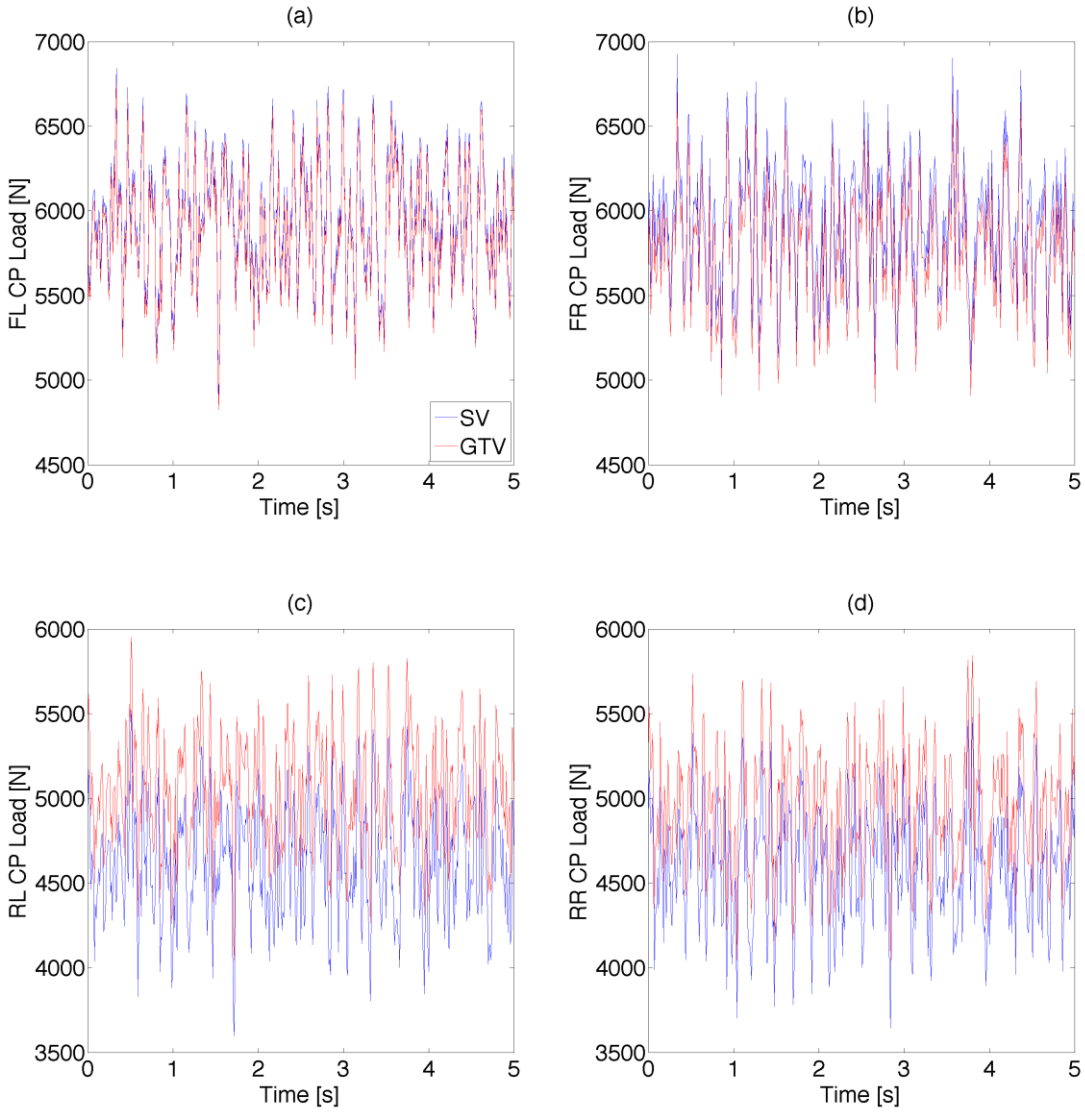

Figure 5-1 Raw contact patch loads at 15 m. s^{-1} on grade C road

The figures shown within this section highlight some asymmetry between contact patch load variation on the left and right hand side of the vehicles. This is seen in the responses of both vehicles, although it is slightly more pronounced for the GTV, where we see an asymmetry of up to 7-8% of the standard deviation, front and rear, compared to only 2-3% for the SV.

	Standard Deviation in CP load [N]							
	SV				GTV			
Speed $m.s^{-1}$	FL	FR	RL	RR	FL	FR	RL	RR
5.0	40.5	40.1	39.3	38.9	40.3	40.0	38.7	38.9
10.0	62.8	65.0	64.3	64.1	62.9	65.1	64.4	64.9
15.0	77.7	80.3	79.0	80.5	77.6	80.4	78.8	80.8
20.0	92.1	95.3	92.7	96.8	92.0	95.5	92.7	96.3
25.0	104.6	105.9	106.1	110.2	104.5	105.9	107.0	110.4
30.0	114.9	114.9	119.6	120.6	115.6	115.1	121.4	120.3
35.0	125.6	125.9	132.9	129.8	125.7	127.3	135.7	131.9
40.0	134.7	137.5	139.8	140.4	137.8	135.8	146.7	142.1
45.0	150.6	156.5	157.3	162.0	172.5	165.9	184.1	175.9
50.0	173.3	162.5	191.3	179.5	204.0	175.9	226.1	198.8

Table 5-1 Contact patch load standard deviation, grade A road

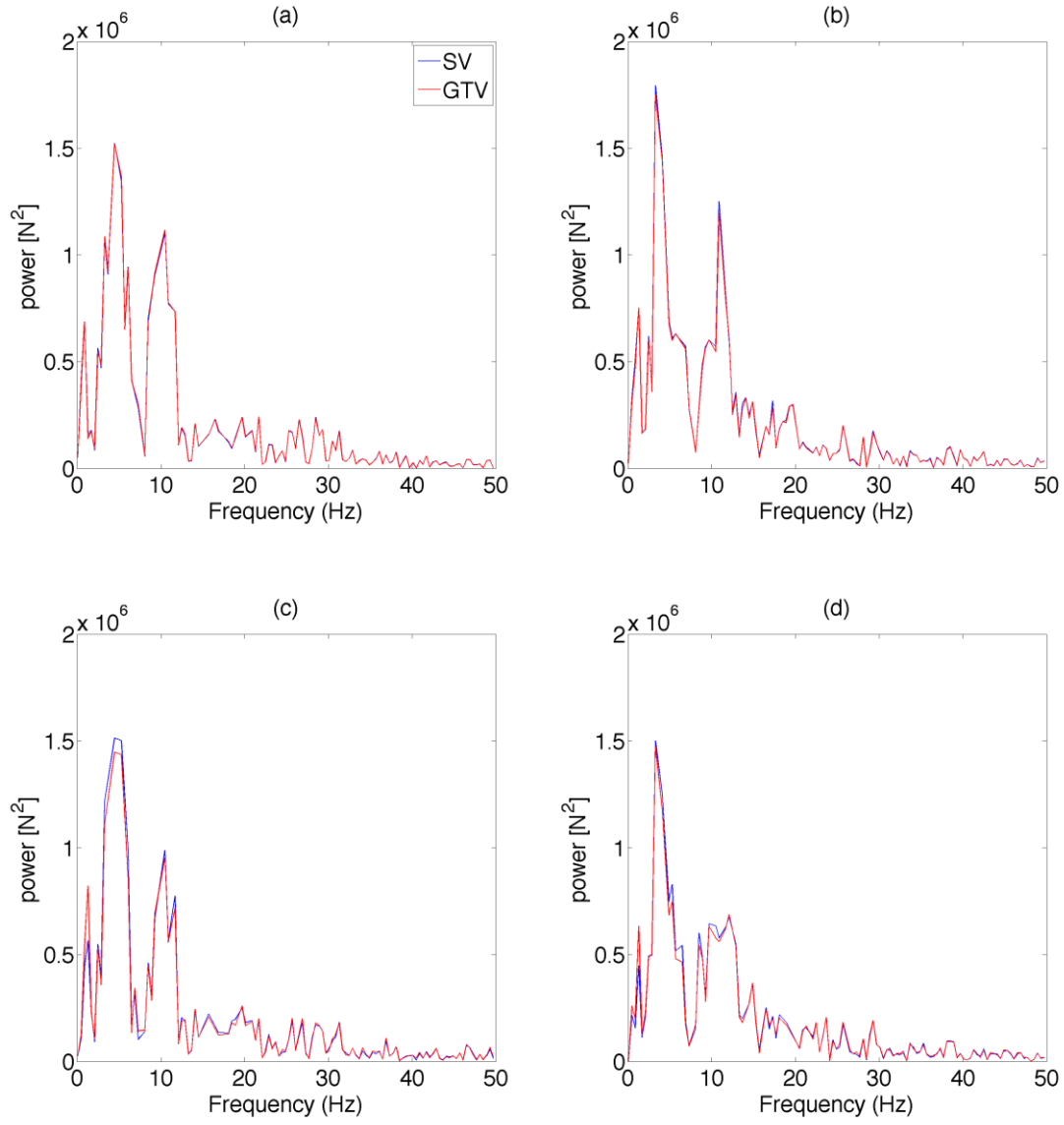

Figure 5-2 Grade C at 15m/s contact patch load PSD's

Speed $m.s^{-1}$	Mean CP Loads [N]							
	FL		FR		RL		RR	
5.0	5990.9	±2.5	5953.4	±2.5	4586.7	±2.4	4561.1	±2.4
10.0	5980.6	±3.9	5941.6	±4.0	4598.4	±4.0	4572.4	±4.0
15.0	5960.5	±4.8	5922.9	±5.0	4617.4	±4.9	4592.0	±5.0
20.0	5934.0	±5.7	5896.5	±5.9	4643.4	±5.7	4616.9	±6.0
25.0	5901.3	±6.5	5863.4	±6.6	4678.1	±6.6	4651.9	±6.8
30.0	5861.3	±7.1	5822.8	±7.1	4717.4	±7.4	4690.7	±7.5
35.0	5815.6	±7.8	5778.1	±7.8	4766.1	±8.2	4740.6	±8.0
40.0	5762.5	±8.3	5724.2	±8.5	4822.0	±8.7	4792.8	±8.7
45.0	5704.7	±9.3	5662.9	±9.7	4884.8	±9.7	4854.5	±10.0
50.0	5634.9	±10.7	5598.0	±10.1	4957.1	±11.9	4926.2	±11.1

Table 5-2 Mean contact patch loads for SV with 95% confidence interval, grade A road

Speed $m.s^{-1}$	Mean CP Loads [N]							
	FL		FR		RL		RR	
5.0	5932.7	±2.5	5802.6	±2.5	5012.2	±2.4	4920.7	±2.4
10.0	5922.8	±3.9	5790.8	±4.0	5024.6	±4.0	4931.6	±4.0
15.0	5902.6	±4.8	5772.1	±5.0	5043.9	±4.9	4951.6	±5.0
20.0	5876.1	±5.7	5745.9	±5.9	5069.4	±5.7	4976.2	±6.0
25.0	5843.3	±6.5	5712.5	±6.6	5105.3	±6.6	5011.3	±6.8
30.0	5803.0	±7.2	5672.5	±7.1	5144.2	±7.5	5050.1	±7.5
35.0	5758.2	±7.8	5627.1	±7.9	5194.0	±8.4	5098.7	±8.2
40.0	5704.2	±8.5	5574.2	±8.4	5249.5	±9.1	5152.1	±8.8
45.0	5641.7	±10.7	5518.0	±10.3	5309.7	±11.4	5219.7	±10.9
50.0	5565.5	±12.6	5457.5	±10.9	5369.3	±14.0	5306.2	±12.3

Table 5-3 Mean contact patch loads for GTV with 95% confidence interval, grade A road

Speed $m.s^{-1}$	% difference in standard deviation				% difference in mean CP load			
	FL	FR	RL	RR	FL	FR	RL	RR
5.0	0.50	0.38	1.51	0.24	0.97	2.53	-9.28	-7.88
10.0	-0.14	-0.18	-0.24	-1.18	0.97	2.54	-9.27	-7.85
15.0	0.12	-0.13	0.28	-0.35	0.97	2.55	-9.24	-7.83
20.0	0.14	-0.16	0.04	0.49	0.98	2.55	-9.17	-7.78
25.0	0.08	-0.05	-0.88	-0.19	0.98	2.57	-9.13	-7.72
30.0	-0.55	-0.13	-1.47	0.21	0.99	2.58	-9.05	-7.66
35.0	-0.10	-1.09	-2.09	-1.65	0.99	2.61	-8.98	-7.55
40.0	-2.31	1.28	-5.00	-1.17	1.01	2.62	-8.87	-7.50
45.0	-14.54	-6.01	-17.03	-8.59	1.10	2.56	-8.70	-7.52
50.0	-17.73	-8.21	-18.19	-10.77	1.23	2.51	-8.32	-7.71

Table 5-4 Percentage difference in standard deviations and mean CP loads, grade A road

This is likely to be linked to the Cog of the GTV moving further from the centre line, this will of course load one side of the vehicle more significantly than the other, thusly affecting the contact patch loads. It is also apparent that larger levels of asymmetry are present in the contact patch loads on the grade A road over the grade C road.

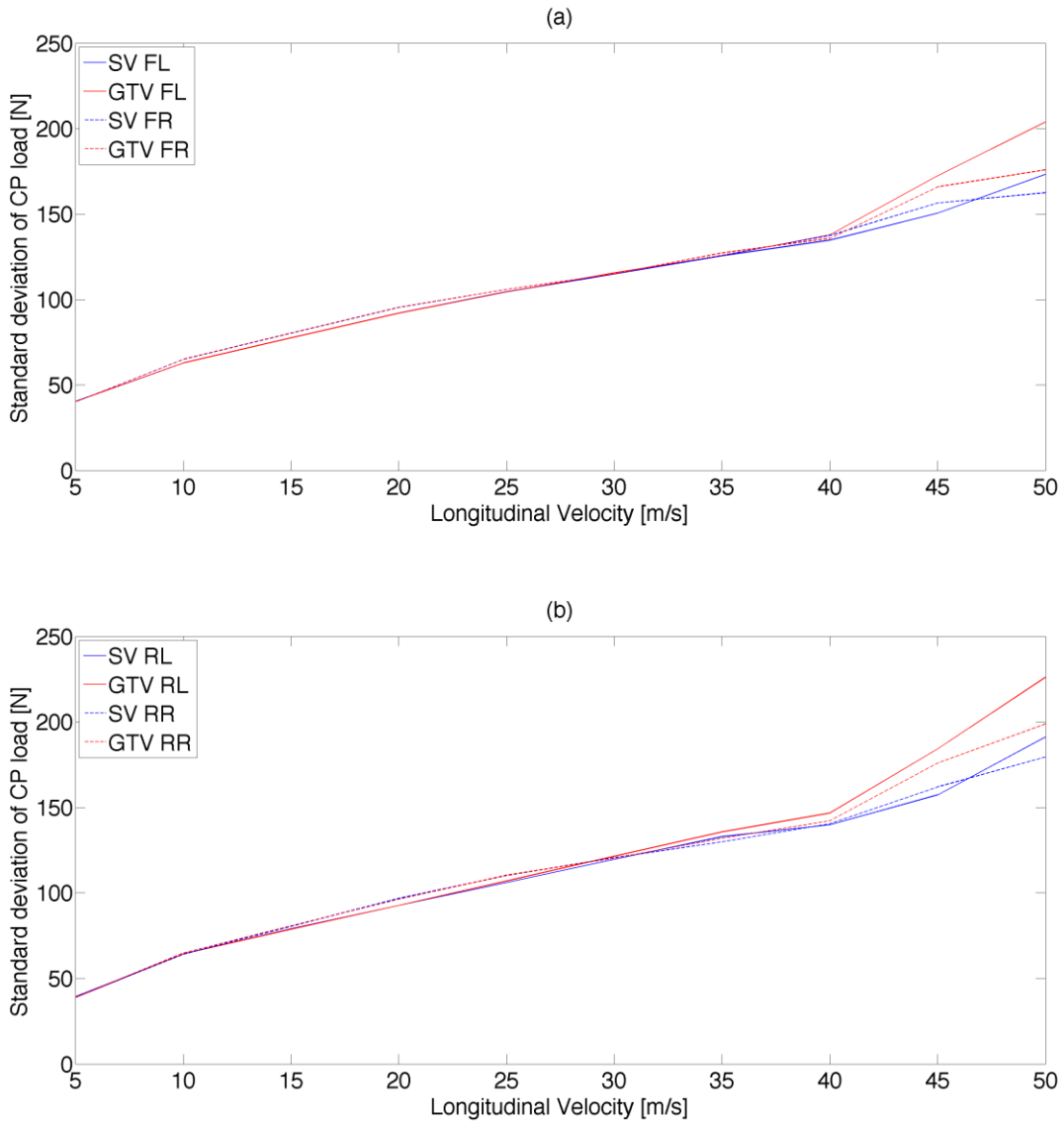

Figure 5-3 Contact patch load standard deviations on grade A road

Speed $m.s^{-1}$	Standard Deviation in CP load [N]							
	SV				GTV			
	FL	FR	RL	RR	FL	FR	RL	RR
5.0	193.6	182.3	184.1	177.8	193.9	182.3	187.7	182.9
10.0	276.7	269.0	272.1	263.7	276.3	268.1	269.3	261.4
15.0	346.5	343.3	329.8	328.8	346.2	339.8	327.7	325.8
20.0	417.9	404.8	397.9	396.3	416.3	400.6	397.8	394.1
25.0	475.4	461.9	446.3	441.9	472.9	456.6	447.3	440.7
30.0	507.4	500.8	493.5	492.8	505.2	495.2	498.9	493.6
35.0	546.8	531.6	527.4	496.1	542.0	527.3	531.2	499.4
40.0	593.4	568.5	571.5	539.5	584.9	568.4	577.5	547.0
45.0	651.5	608.7	637.0	601.9	670.9	623.4	685.3	626.0
50.0	751.6	797.0	761.7	812.9	814.0	785.7	865.8	836.7

Table 5-5 Contact patch load standard deviations, grade C

Speed $m.s^{-1}$	Mean CP Loads [N]							
	FL		FR		RL		RR	
5.0	5989.5	±12.0	5951.9	±11.3	4589.9	±11.4	4563.1	±11.0
10.0	5986.6	±17.2	5942.8	±16.7	4601.2	±16.9	4577.6	±16.3
15.0	5961.2	±21.5	5919.2	±21.3	4620.9	±20.4	4593.8	±20.4
20.0	5934.1	±25.9	5899.4	±25.1	4644.9	±24.7	4621.0	±24.6
25.0	5905.5	±29.5	5868.6	±28.6	4676.2	±27.7	4653.0	±27.4
30.0	5865.7	±31.4	5823.5	±31.0	4717.0	±30.6	4684.8	±30.5
35.0	5820.1	±33.9	5782.8	±32.9	4767.9	±32.7	4749.7	±30.7
40.0	5770.2	±36.8	5732.8	±35.2	4821.0	±35.4	4801.0	±33.4
45.0	5713.2	±40.4	5651.8	±37.7	4896.0	±39.5	4850.5	±37.3
50.0	5627.8	±46.6	5611.1	±49.4	4938.1	±47.2	4945.5	±50.4

Table 5-6 Mean contact patch loads for SV, with 95% confidence interval, grade C

Speed $m.s^{-1}$	Mean CP Loads [N]							
	FL		FR		RL		RR	
5.0	5931.9	±12.0	5801.6	±11.3	5015.5	±11.6	4921.8	±11.3
10.0	5929.4	±17.1	5792.7	±16.6	5027.1	±16.7	4936.6	±16.2
15.0	5903.7	±21.5	5768.7	±21.1	5047.4	±20.3	4953.4	±20.2
20.0	5875.9	±25.8	5748.6	±24.8	5070.9	±24.7	4979.5	±24.4
25.0	5847.1	±29.3	5717.5	±28.3	5103.0	±27.7	5013.2	±27.3
30.0	5807.5	±31.3	5672.8	±30.7	5143.6	±30.9	5044.0	±30.6
35.0	5761.9	±33.6	5631.6	±32.7	5194.0	±32.9	5109.6	±31.0
40.0	5710.2	±36.3	5582.9	±35.2	5249.0	±35.8	5162.0	±33.9
45.0	5656.7	±41.6	5500.1	±38.6	5330.0	±42.5	5207.6	±38.8
50.0	5604.8	±50.5	5424.4	±48.7	5404.6	±53.7	5273.1	±51.9

Table 5-7 Mean contact patch loads for GTV, with 95% confidence interval, grade C

Speed $m.s^{-1}$	% difference in standard deviation				% difference in mean CP load			
	FL	FR	RL	RR	FL	FR	RL	RR
5.0	-0.18	-0.01	-1.94	-2.87	0.96	2.52	-9.27	-7.86
10.0	0.15	0.35	1.03	0.86	0.96	2.53	-9.26	-7.84
15.0	0.07	1.02	0.64	0.91	0.96	2.54	-9.23	-7.83
20.0	0.38	1.02	0.02	0.56	0.98	2.56	-9.17	-7.76
25.0	0.53	1.14	-0.22	0.28	0.99	2.58	-9.13	-7.74
30.0	0.43	1.12	-1.10	-0.16	0.99	2.59	-9.04	-7.67
35.0	0.88	0.82	-0.72	-0.66	1.00	2.61	-8.94	-7.58
40.0	1.44	0.01	-1.05	-1.39	1.04	2.62	-8.88	-7.52
45.0	-2.98	-2.42	-7.58	-4.00	0.99	2.68	-8.86	-7.36
50.0	-8.30	1.41	-13.66	-2.92	0.41	3.33	-9.45	-6.62

Table 5-8 Percentage difference in standard deviations and mean CP loads, grade C

As mentioned previously this seems unusual, as it would be expected that any differences between the two vehicles would be more pronounced on rougher roads, where inputs are larger. It would be easy to put this down to asymmetries in the road, however let us consider the key differences in the conditions of operation of the vehicles on the smoother road compared to the rougher road. When the road is smoother, inputs from it, to the vehicle are smaller, and so isolation from road inputs are less of an issue and the control of the body motion is more crucial, similarly to a pure handling event. With this in mind it again brings us back to the topic of damping, and the levels of damping being un-matched with the GTV's new mass properties. Damping will be discussed in more detail in following sections as it is crucial not only for control of contact path load but also road isolation and occupant comfort.

Let us know consider body motions arising from the road inputs that have caused the contact patch load variations we have been discussing. Body pitch motion is a factor largely considered to drive occupants perception of ride comfort as it defines levels of 'head toss' felt by said occupants.

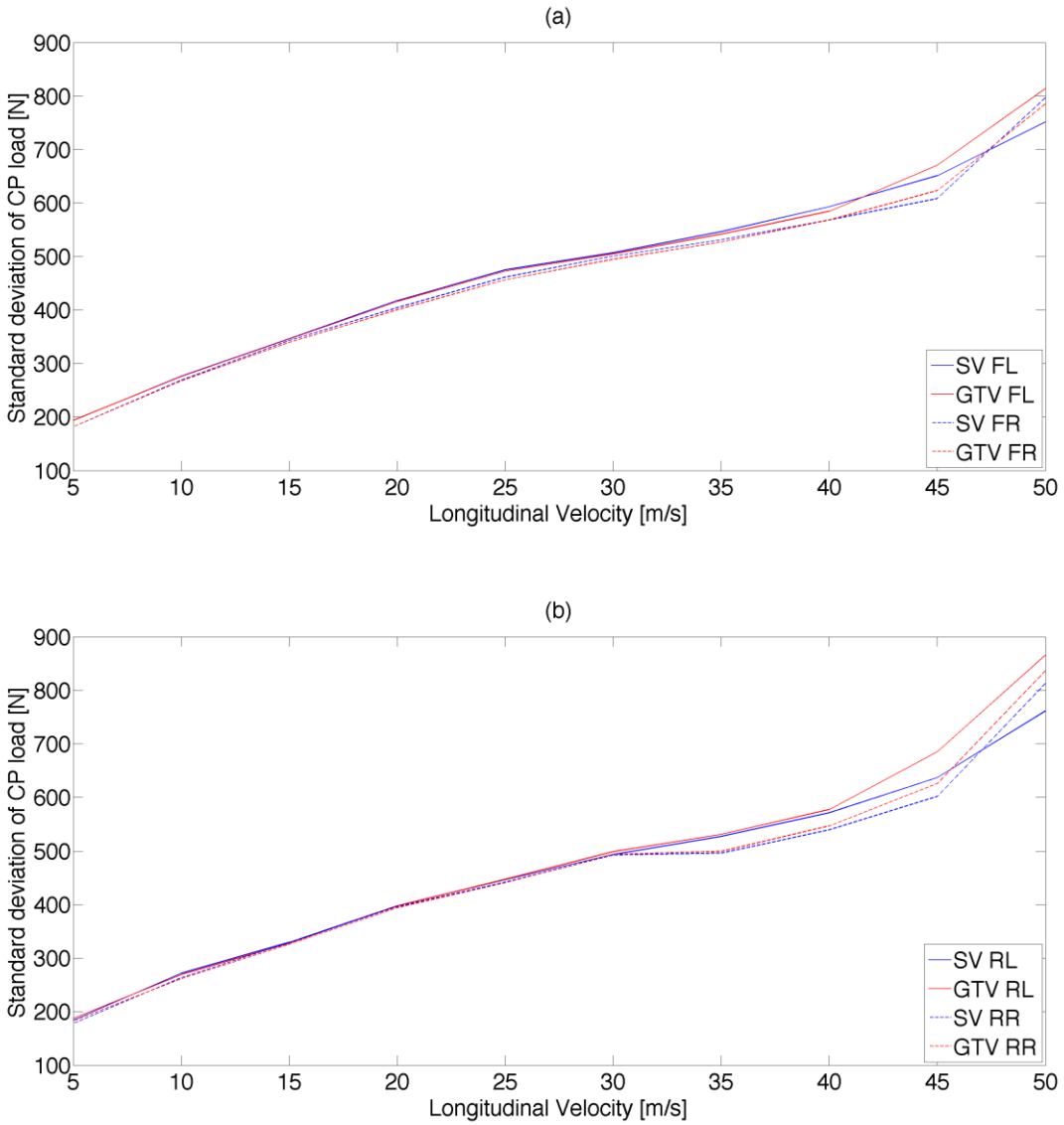

Figure 5-4 Contact patch load standard deviations on grade C road

As with the contact patch loads, pitch data will again be expressed as standard deviations for each speed, as this yields far more useful information than the raw data, shown in Figure 5-6. Although before moving away from the raw data, it can be seen that the pitch angles of the two vehicles, shown in Figure 5-6 (a) are different to begin with due to increased rear tyre squash, a result of the higher and differently distributed mass of the GTV.

The basic shape of the pitch angle responses shown in Figure 5-7 (a) can be attributed to wheelbase filtering. Wheelbase filtering is an effect of the front and

rear axles seeing the same road input but delayed in time, the time delay is equal to the wheelbase divided by the forward velocity. At certain velocities inputs at the front and rear axle occur at such time differences that they can effectively filter the pitch and bounce modes of the vehicle (Gillespie, 1992, Milliken and Milliken, 1995, Olley et al., 2002). For example, if

$$V_{long} = 20 \text{ m.s}^{-1}$$

$$L = 2.661 \text{ m}$$

$$F_{hz} = 1.25$$

$$R_{hz} = 1.5$$

Where V_{long} is longitudinal velocity, L is wheelbase and F/R_{hz} are the front and rear ride frequencies, then,

$$d_t = \frac{L}{V_{long}} = 0.13305 \tag{5.1}$$

$$P_f = \frac{1}{F_{hz}} = 0.8 \tag{5.2}$$

$$P_f - d_t = 0.667 = \frac{1}{R_{hz}} = P_r \tag{5.3}$$

Where d_t is the time difference between front and rear inputs, and $P_{f/r}$ are the front and rear periods. This simple calculation shows that at 20 m.s^{-1}, here the rear oscillation will be started by the road input at the exact time that it's period is equal to the remaining period of the front oscillation, thus confirming that at this speed after one period the front and rear oscillations will be in phase (ride flat).

Similarly there can be wavelengths in the road and vehicle velocities that will correspond to filtering the bounce motion and the vehicle will exhibit more of the pure pitch mode. Generally wavelengths in the road equal to the wheelbase or integer divisions thereof, as well as very long wavelengths tend to induce pure bounce motions in the body response, wavelengths equal to double wheelbase or odd

integer divisions of double the wheelbase will induce more of a pure pitch motion. For vehicles that follow Olley's good ride criteria it is seen that pitch responses are most prominent at lower vehicle speeds, and at higher speeds pitch responses reduce.

This can also be investigated another way, via the frequency response of the vehicle body to road inputs. Figure 5-5 shows the frequency response of the pitch (a) and bounce (b) modes of the vehicle body at forward velocities of 10, 20 and 30 m/s. In terms of the pitch mode, it is easiest to see the effect of wheelbase filtering in the 10 m/s response at just below 4 Hz, this corresponds to a wavelength in the road input equal to the wheelbase. Such minima are present in the 20 and 30 m/s responses at circa 7.5 and 11.3 Hz respectively, they are however not as visible due to the smaller magnitude of response at these frequencies. The 20 and 30 m/s responses also show minimisation of the pitch mode at circa 1.25 and 1.4 Hz, which respectively, corresponds to wavelengths equal to 1/6 and 1/8 the wheelbase.

The bounce mode responses are perhaps clearer than the pitch mode, Figure 5-5 (a) clearly shows distinct minima in the responses at circa 2, 3.8 and 5.6 Hz corresponding to wavelengths equal to twice the wheelbase.

The magnitude of the responses show us that the pitch natural frequency for the SV is circa 1.7 Hz, for the GTV it is circa 1.6, these frequencies correspond to those that were calculated in chapter 4 when studying the pitch and bounce model, however, here all the suspension elements, stiffnesses, damping and accompanying geometry are taken into account. However similarly to the values given in chapter 4, the GTV also shows here a reduction in pitch frequency of about 5-6%. The bounce frequencies are more closely matched at circa 1.2 Hz for both SV and GTV, again as was shown with the simplified pitch and bounce model.

Comparing the two vehicles in these figures illustrates that generally, in the pitch mode the GTV shows larger responses at frequencies below the natural frequency, between this point and 8Hz it can be said the response of the GTV is very slightly smaller, above 8 Hz both vehicles' responses are similar. The bounce mode responses show that the GTV always exhibits larger responses than the SV, with the exception of below the natural frequency at 10 m/s, where the GTV's response is marginally smaller. One thing is clear from both plots, the GTV possesses less wheelbase filtering effect than the SV, it can be seen that at each of the minima (null points) in both pitch and bounce response the GTV shows a considerably larger response that the SV (less of a null point). Again, recalling the pitch and bounce model parameters, it was shown that the GTV exhibited more coupling between pitch and bounce modes, it is for this reason the GTV sees less wheelbase filtering. These figures again confirm that generally the GTV will exhibit larger pitch and bounce responses than the SV.

What has been shown here can be linked to the standard deviations of the pitch responses shown in Figure 5-7 (a), firstly note how the pitch responses for both vehicles decrease with forward velocity, secondly due to increased pitch and bounce coupling the GTV clearly shows higher standard deviation in pitch response at all forward velocities above 10 m/s.

In terms of pitch rate, it is seen that there is very little difference between the two vehicles. It was shown previously that the pitch frequency of the GTV was slightly lower than that of the SV, this could offer some explanation to why the pitch angle responses of the GTV are larger, but the pitch rate responses are more or less the same.

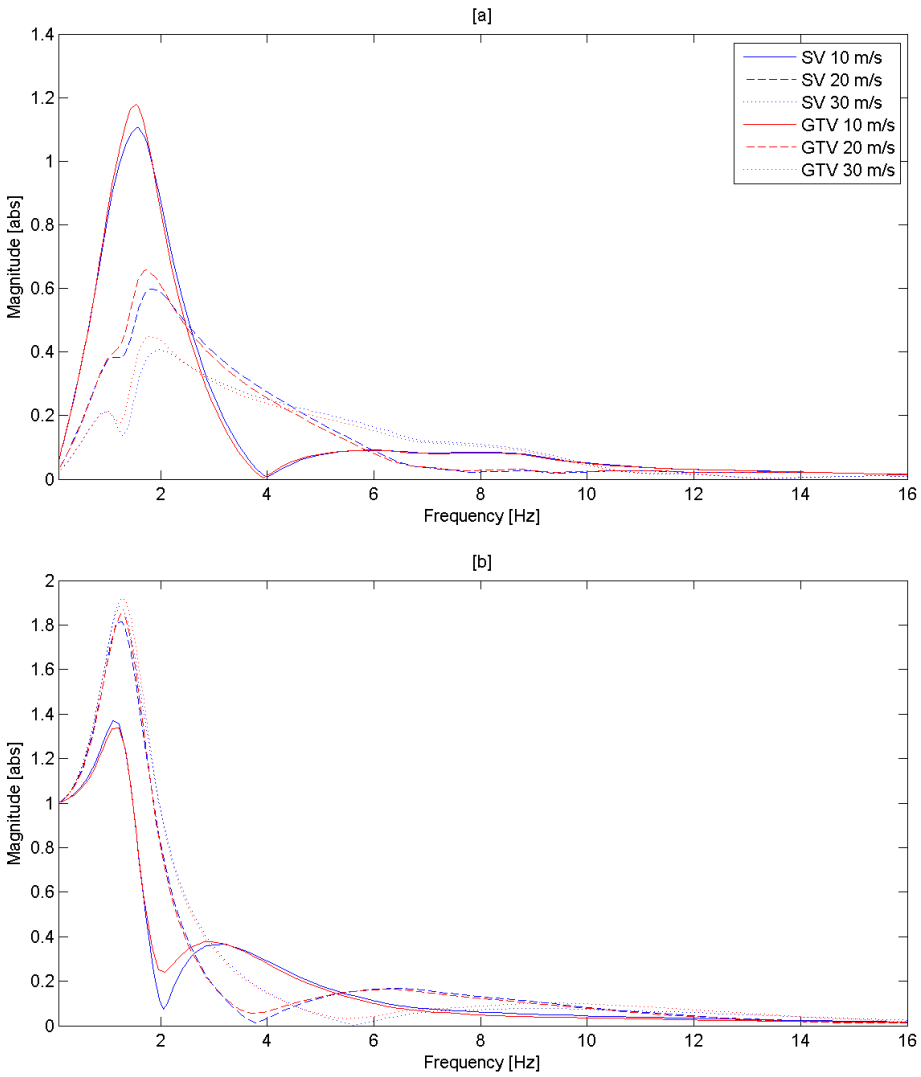

Figure 5-5 Pitch and bounce mode frequency responses

Whilst the pitch angles and pitch velocities are related to the stiffness and damping properties of the vehicles', the pitch accelerations give clues regarding the inertia properties. In chapter 3 it was shown that the pitch inertia of the GTV had increased quite substantially, for this reason the GTV exhibits the lowest deviations in pitch accelerations of the two vehicles, as shown in Figure 5-7 (c). The pitch response and its derivatives illustrate well how the variation in contact patch load affects body motions in the ride domain.

Whilst looking at the variation in contact patch load gives an insight into the difference in forces being transferred to the body, which ultimately will dictate the

body motions which the occupants will perceive, it does not tell the whole story. As was mentioned, the moments of inertia of the vehicle body have changed in the GTV when it has undergone its updates. The GTV possesses a pitch inertia which is 7% higher and a roll inertia which is 2.5% lower than the SV. It was also shown when discussing the two degree of freedom pitch and bounce model in chapter 4 that the GTV has a higher rotational stiffness in the pitch plane, owing to the increased stiffness of the rear springs, a further effect of stiffening the rear springs on the GTV is that the spring centre has moved further rearward. Taking into account the increase in pitch inertia, the aforementioned rotational stiffness, and geometric movement of spring centre and Cog, means that whilst the GTV does generally exhibit larger variations in contact patch load, and has been shown to exhibit larger pitch and bounce responses than the SV, these may not be translated into higher levels of discomfort for the occupants. This has already been illustrated by looking at the pitch angle and its derivatives, where larger deviations in angles were seen but smaller accelerations. It also needs to be noted that whilst pitch motions will play a large role on occupant comfort, especially at the extremities of the vehicle, bounce and roll motions will also have a part to play, and the complete vehicle motion is a complex mixture of them all. On top of this due to the change in mass properties, the levels of damping will also likely be incorrect for the GTV, and will play a large role in the overall effect on the vehicle's ride comfort. By looking at motions of the vehicle body as a whole, all changes that have taken place with the vehicle will be incorporated into the results. This will be investigated in the following section where we will look at levels of vertical acceleration inside the vehicle in terms of occupant comfort.

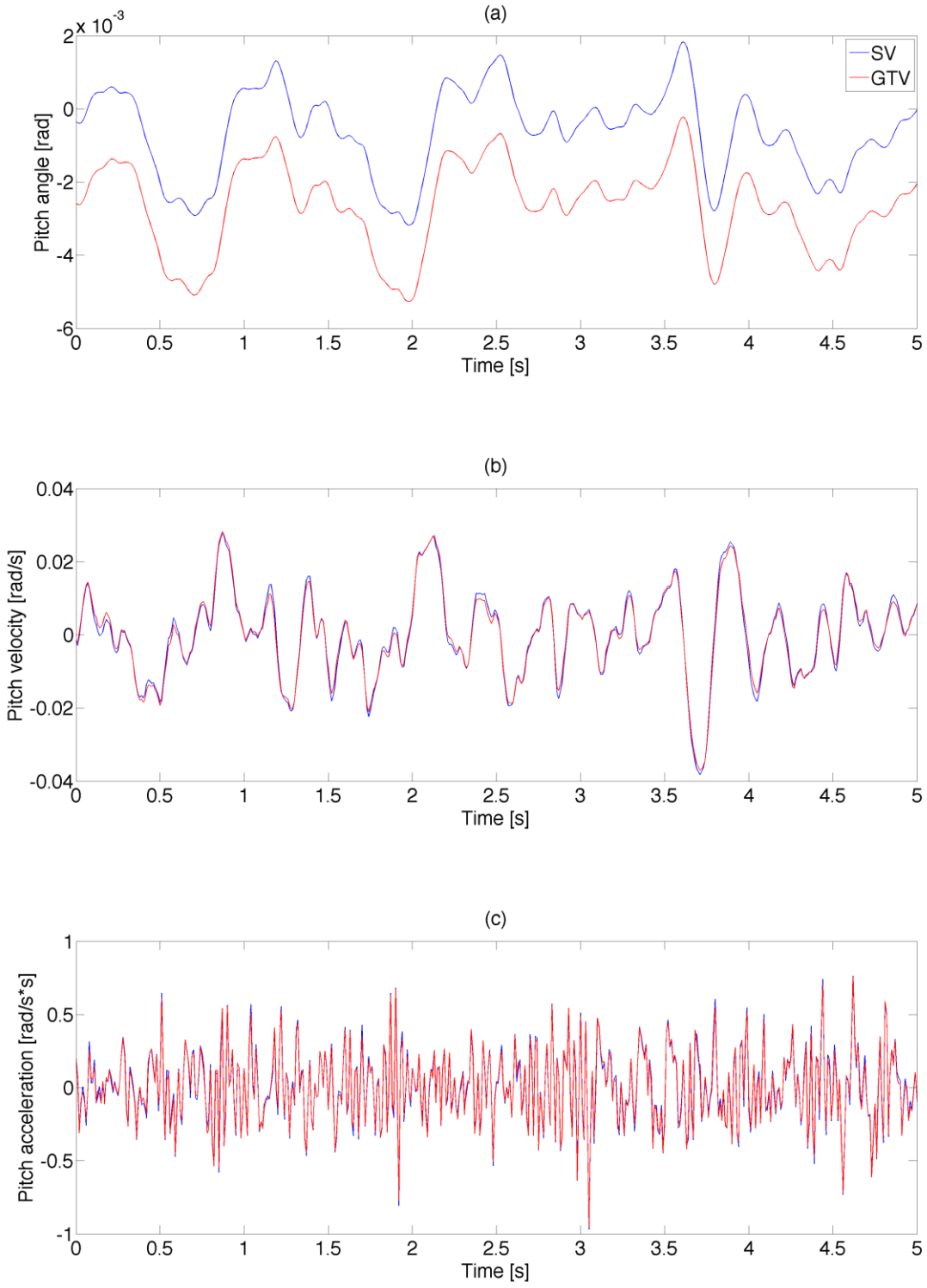

Figure 5-6 Pitch response comparison on grade C road at 15 m. s^{-1}

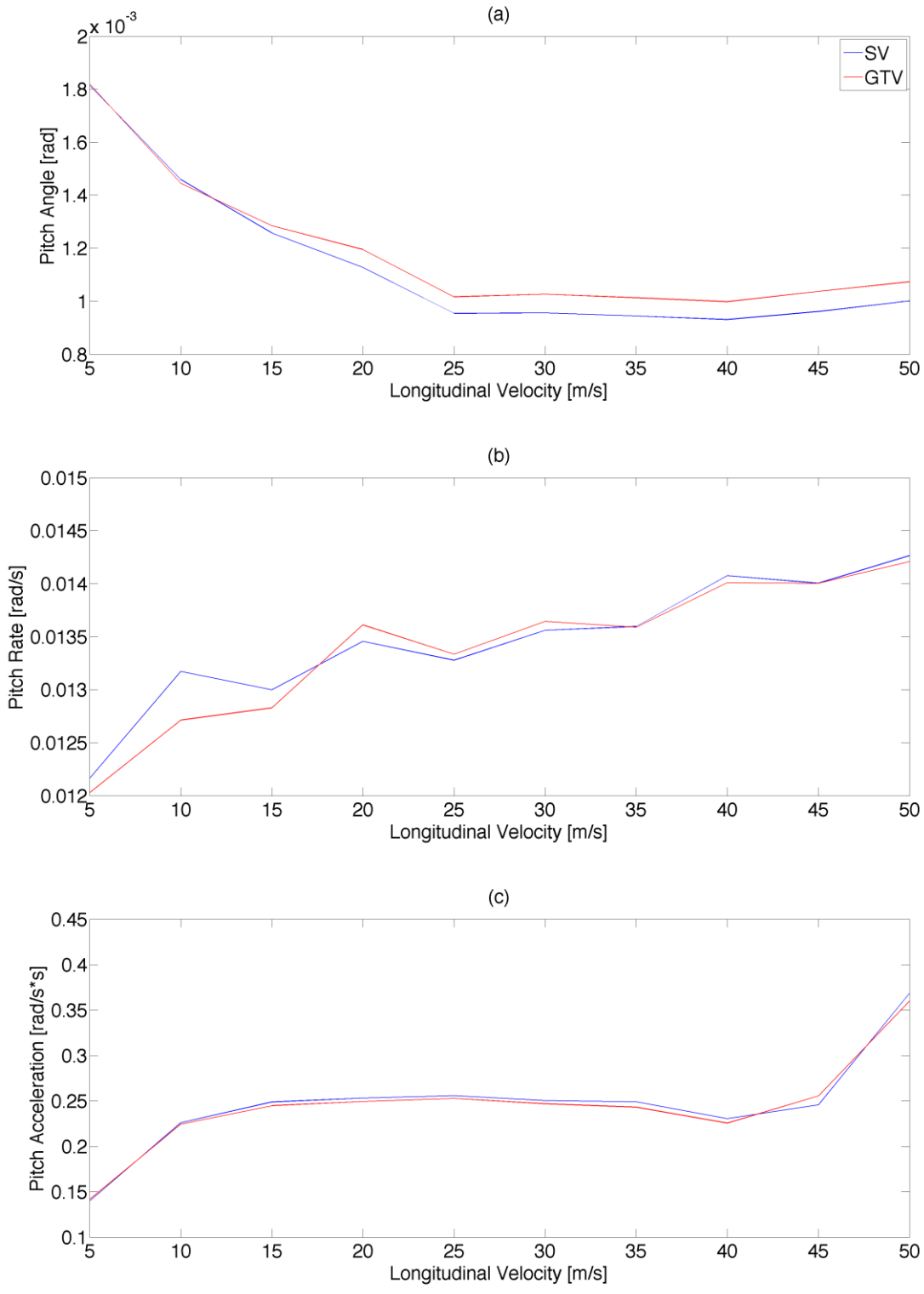

Figure 5-7 Standard deviation of pitch responses on grade C road

5.2.2 Occupant Comfort

The previous section investigated the difference in contact patch load variation between the two vehicles. It was shown that at low speeds there was little difference between them, however as speed increased it was the GTV that exhibited larger variations in contact patch load, especially on the smoother of the two road models. This trait was linked to the differences in mass distribution and front and rear heave stiffness's affecting the vehicles' pitch motions, and possibly damping. Here the impact of these effects on occupant comfort will be illustrated.

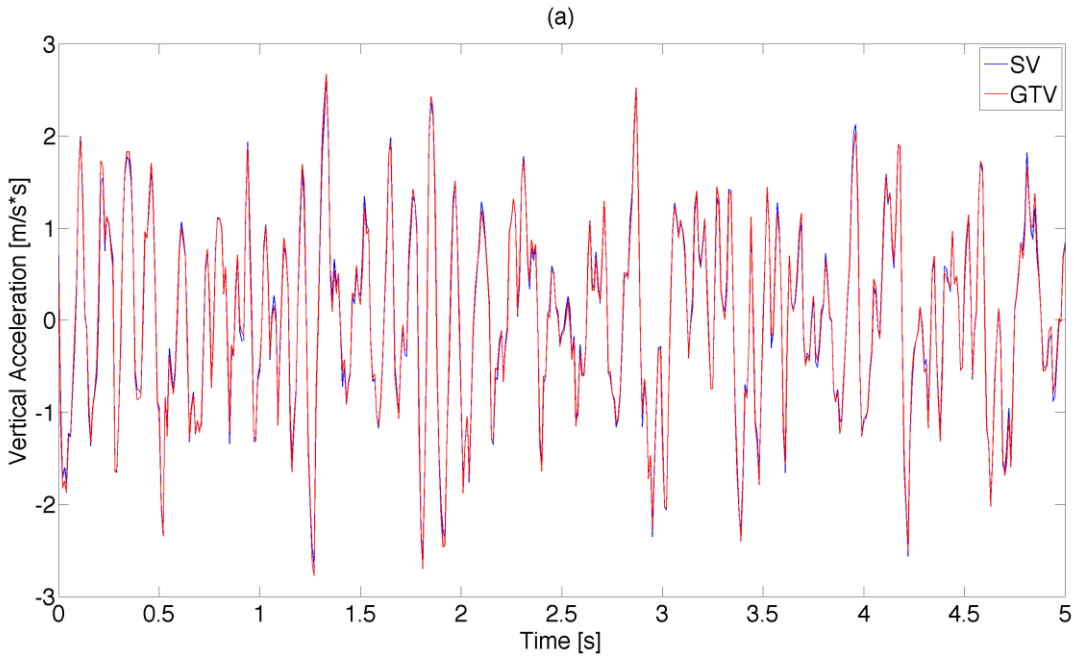

Figure 5-8 Raw acceleration data on grade C road at 10 m. s^{-1}

As first described in chapter 4, the results presented here are treated with a frequency weighting which gives emphasis to acceleration frequencies to which a seated human is more susceptible to discomfort. This treated data is then used to obtain the vertical RMS accelerations presented in this chapter. This makes the data much easier to analyse as it again gives a single metric that can be investigated over the vehicle speed range. Once again to illustrate this, some un-processed data for a

point on the front left of both of the vehicles (one of the 980 points that makes up the contour plot shown in Figure 5-11) is shown in Figure 5-8.

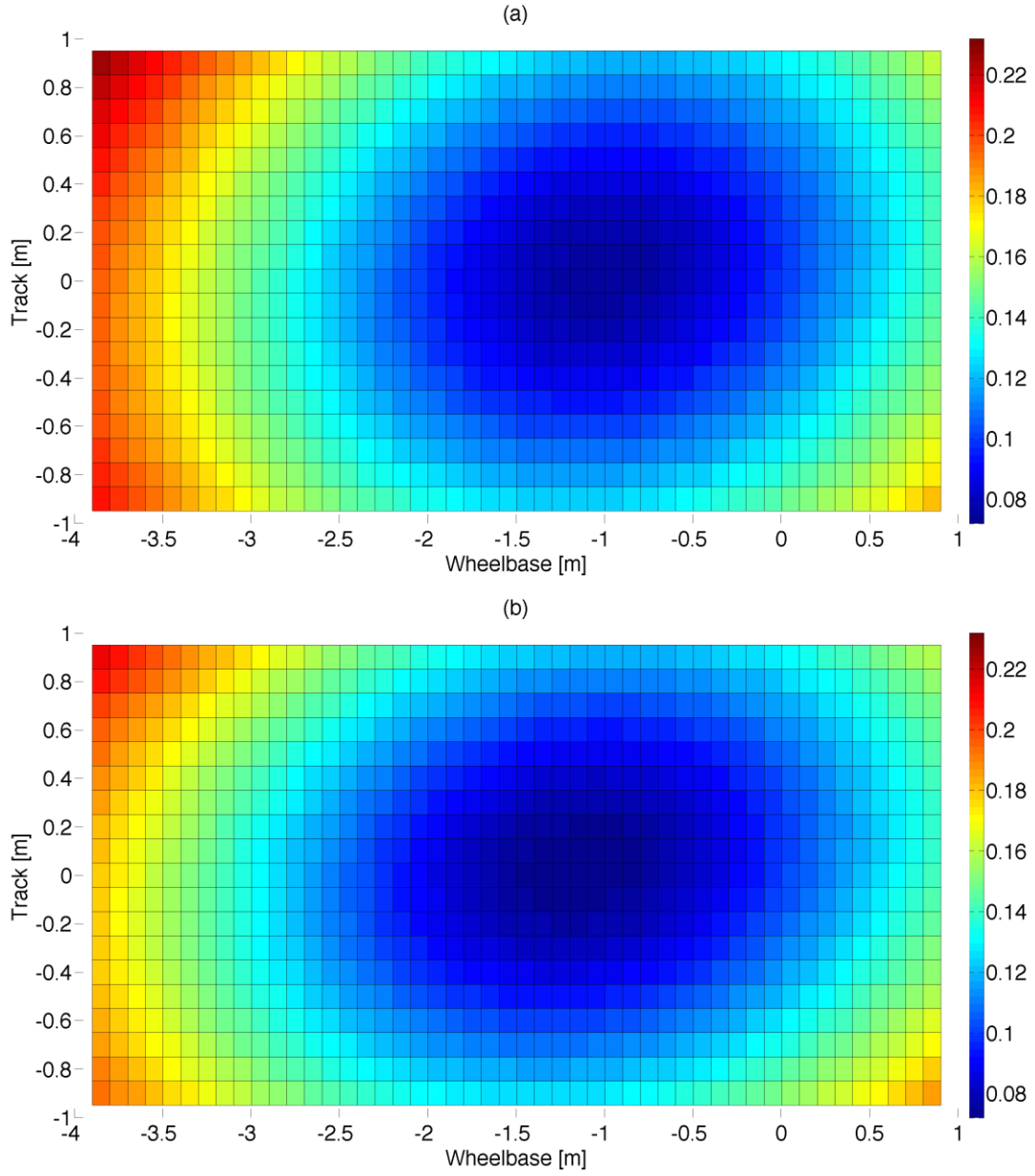

Figure 5-9 Frequency weighted RMS vertical acceleration for vehicle topology, road A at 10 $\mathrm{m.s^{-1}}$

Figure 5-9 and Figure 5-10 show the frequency weighted RMS vertical acceleration for a seated person in both the SV (a) and GTV (b) on the grade A road at 10 and 35 $\mathrm{m.s^{-1}}$ respectively. Both figures generally show that GTV and the SV exhibit very similar levels of acceleration, however for the GTV it can be seen that the low acceleration region in the centre is more centralised (in the fore-aft plane) in

the vehicle, this low acceleration region is centralised around the Cog and spring centre and so explains why it is further rearwards in the GTV.

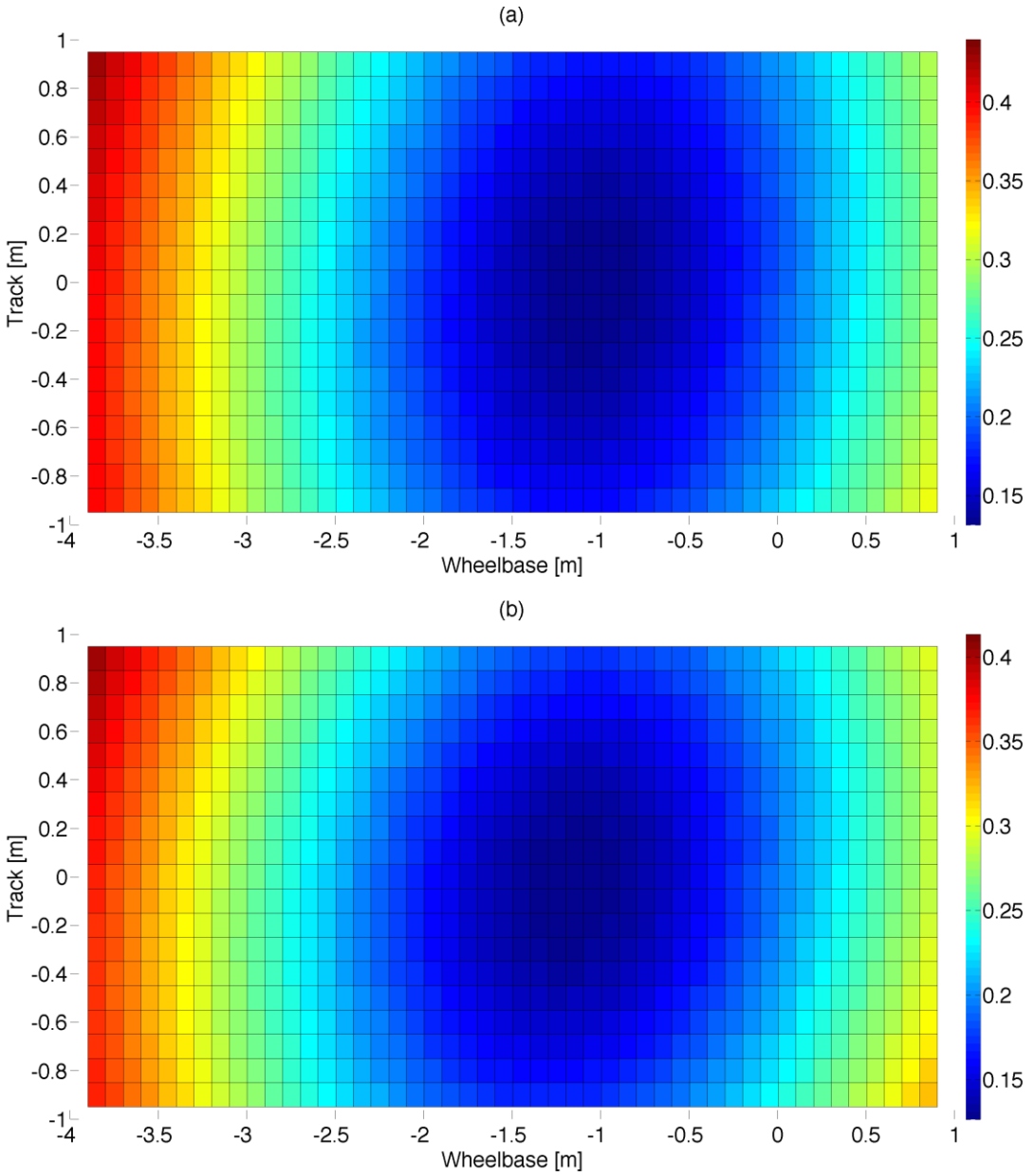

Figure 5-10 Frequency weighted RMS vertical acceleration for vehicle topology, road A at 35 $\mathrm{m.s^{-1}}$

The levels of acceleration at the extremities of the vehicles are higher in the SV, this can especially be seen at the rear, at either corner. The asymmetry that was highlighted in the standard deviations of the contact patch loads is also present here and is especially apparent at higher speeds. Figure 5-11 and Figure 5-12 show the

same data but for the two vehicles travelling over the grade C road. As would be expected the acceleration levels are higher for the rougher road. It is again the GTV that generally has the more centralised low acceleration/higher comfort region. As there is less asymmetry in the results it is visible that the GTV does seem to have higher levels of acceleration measured along the edges of the wheelbase. This is most likely due to the GTV's increased pitch inertia and reduced roll inertia. It has been shown that whilst the GTV had larger pitch angle deviations than the SV, its lower pitch mode frequency and larger pitch inertia lead it to having very similar pitch rate deviations and lower pitch acceleration deviations, as such the vertical acceleration levels at the front and rear extremities of the vehicle are lower. On the other hand the roll inertia of the GTV has been reduced, leading to higher levels of vertical acceleration along lateral extremities of the vehicle. It is also important to note that within the centre of the vehicle, around the Cog and spring centre, the GTV does actually show slightly higher levels of acceleration, this will be due to the GTV exhibiting larger bounce responses than the SV, as was shown in the previous section of this chapter when looking at the pitch and bounce modes in the frequency domain.

The results presented in the Figure 5-9, Figure 5-10, Figure 5-11 and Figure 5-12 are very good for giving an overview of the levels of occupant comfort over the entire vehicle topology, and how the changes to the vehicle have effected its body motions, they have been included at the two specific speeds to provide the reader with a general overview. However, here we are concerned with the comfort levels felt by the occupants and so further results will concentrate on the acceleration/comfort levels felt specifically at, the driver's seat, front passenger seat and the two rear passenger seats, as shown in Figure 5-13 and Figure 5-14.

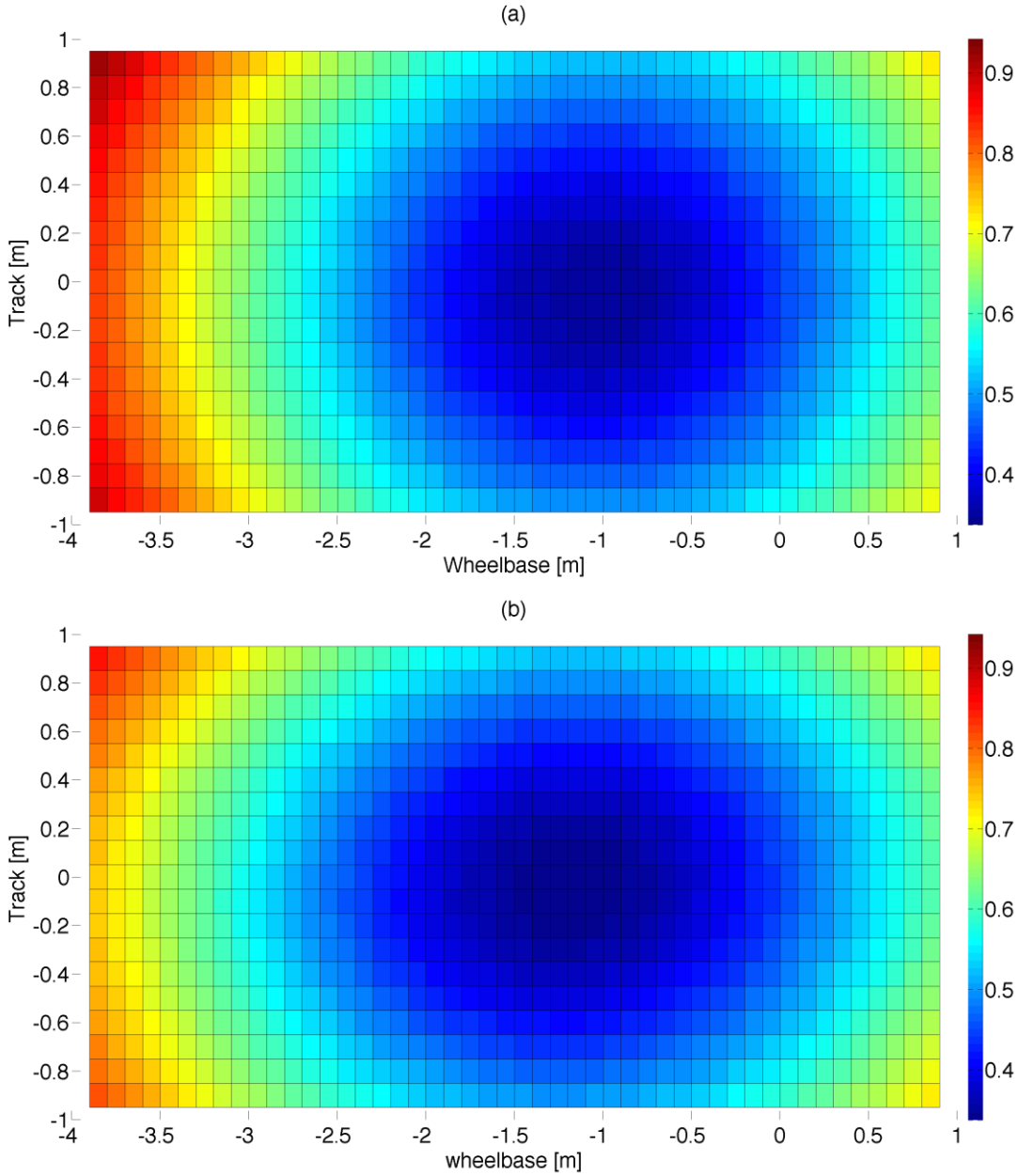

Figure 5-11 Frequency weighted RMS vertical acceleration for vehicle topology, road C at 10 $\mathrm{m.s^{-1}}$

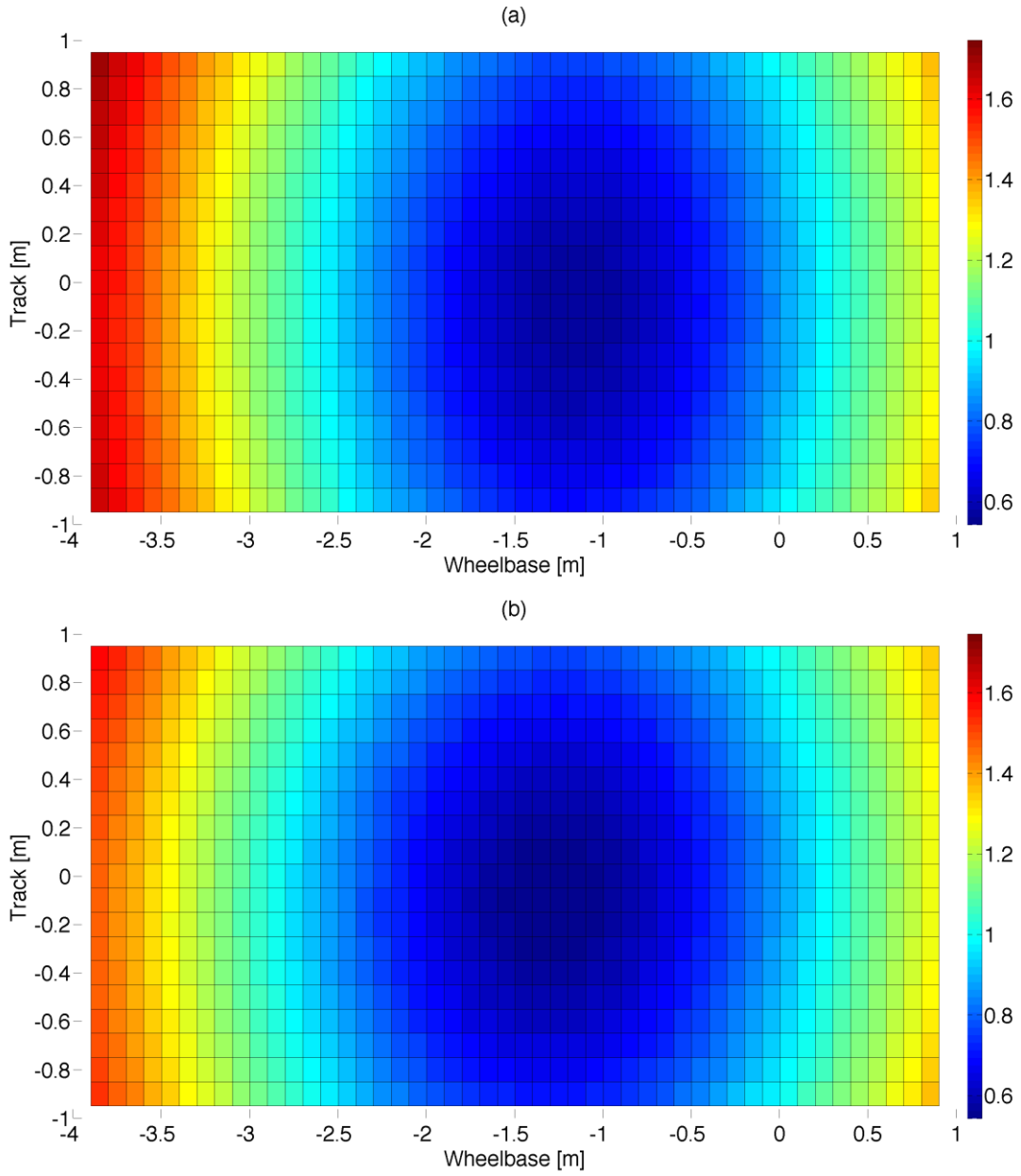

Figure 5-12 Frequency weighted RMS vertical acceleration for vehicle topology, road C at 35 $\mathrm{m.s^{-1}}$

One of the most interesting aspects that is noticeable when looking at the RMS accelerations at the occupant positions, is that for both road roughness variations, the GTV shows lower levels of comfort for the front occupants but higher levels for the rear. This is however consistent with what was seen in the topology plots, the lower acceleration/higher comfort region has migrated rearwards with the Cog and spring centre, thusly exposing occupants seated toward the front of the vehicle to higher

vertical accelerations resulting from pitching and bouncing modes, whereas occupants seated at the rear of the vehicle now have the benefit of being seated nearer the Cog and spring centre, in a lower acceleration/higher comfort region.

The general trends of the plots show that at low speeds there is very little difference between SV and GTV, as speed increases the comfort levels on the two vehicles diverge, and maximum differences are seen between 25 – 40 m/s. It can be seen by referencing Table 5-9, which illustrates how these acceleration levels relate to comfort, according to BS2631-1:1997 (1997), that the levels of acceleration on the grade A road all fall under "not uncomfortable", for the grade C road acceleration levels, once the vehicle speed is above 10 m/s, fall within "fairly uncomfortable".

The specific shapes of Figure 5-13 and Figure 5-14, which show turning points for both vehicles around the 25 – 40 m/s region, can again be explained by the effects previously shown in Figure 5-5, where by the pitch responses of the vehicle decrease with increasing forward velocity, however the opposite is true for the bounce response, up until 30-40 m/s the reduction in the pitch response is large enough to reduce the overall acceleration levels inside the vehicle, despite the increasing bounce response, above 40 m/s this is no longer true and an increase in vertical acceleration is seen due to this.

It appears that one of the main drivers for the changes we see in occupant comfort is the rearwards shift in Cog and spring centre of the GTV. Whilst it was shown that the GTV does in fact have larger pitch responses than the SV, the pitch centre, cog and spring centre have all moved rearwards, thusly effecting the perceived vertical accelerations of the occupants arising from the pitch motion of the vehicle.

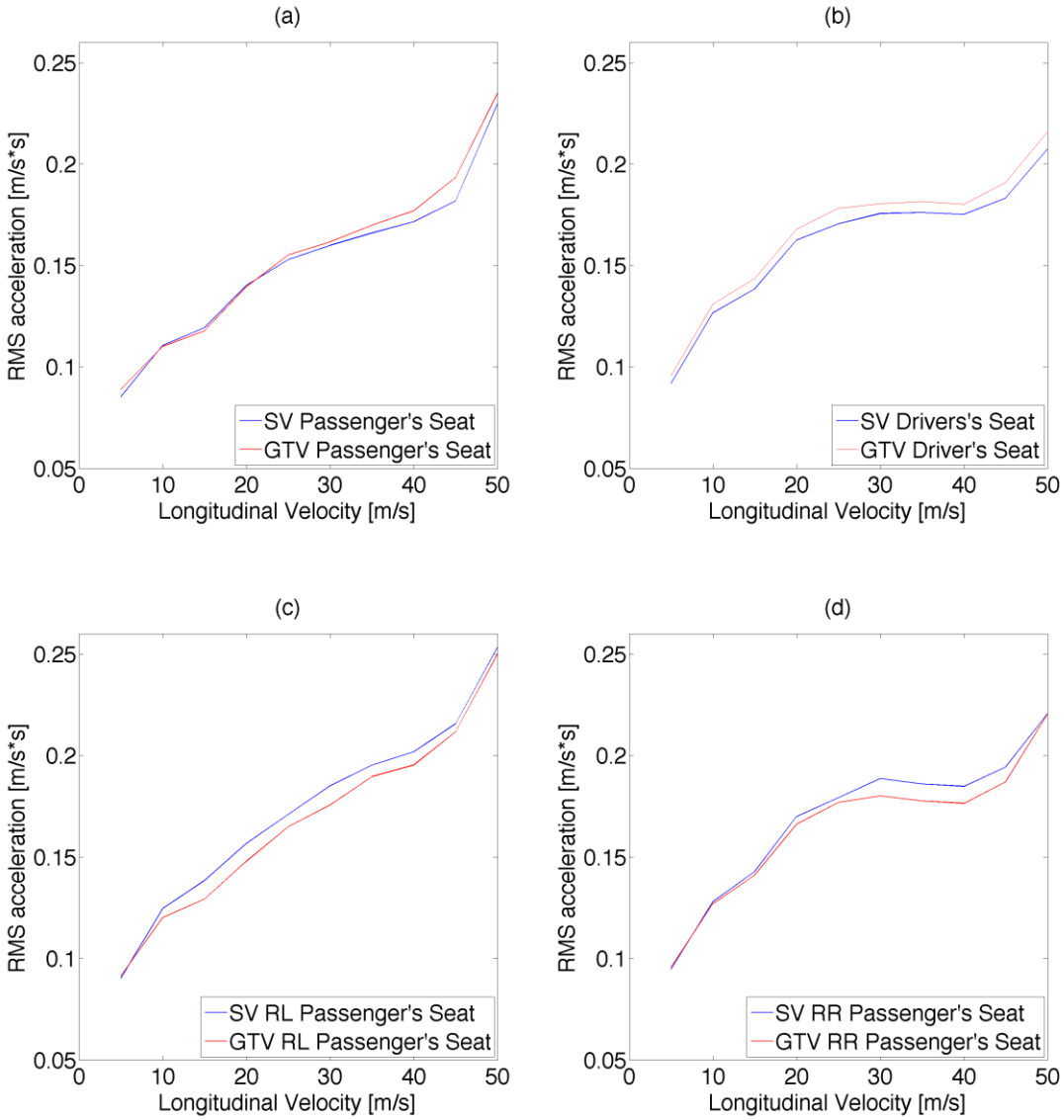

Figure 5-13 RMS acceleration at occupant positions, grade A road

m/s²	Comfort Level
< 0.315	Not uncomfortable
0.315 - 0.63	A little uncomfortable
0.5 – 1	Fairly uncomfortable
0.8 - 1.6	Uncomfortable
1.25 - 2.5	Very uncomfortable
> 2	Extremely uncomfortable

Table 5-9 RMS acceleration comfort levels (BS2631-1:1997, 1997)

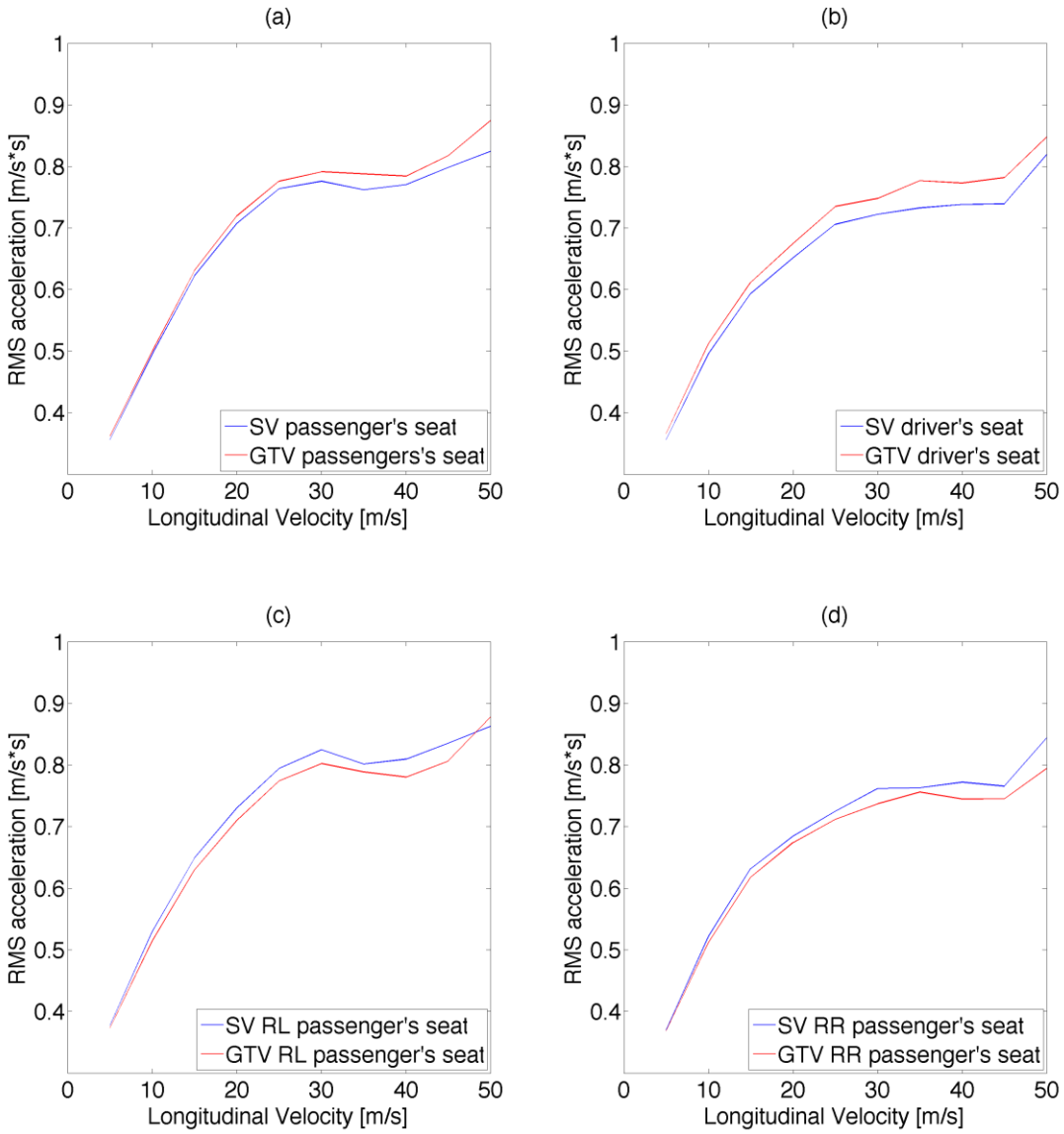

Figure 5-14 RMS acceleration at occupant positions, grade C road

On both grades of road the occupants seated at the front of the GTV will feel higher levels of discomfort than those seated at the back, when compared to the SV. Peak differences seen between the vehicles are 0.015 $\mathrm{m.s^{-2}}$ front and rear on the grade A road, and 0.08 $\mathrm{m.s^{-2}}$ front and 0.04 $\mathrm{m.s^{-2}}$ rear, on the grade C road. At first this may seem insignificant however if we consider BS2631-1:1997 (1997) it is stated that whilst there is a large variation in individuals ability to perceive vibration, most people can detect weighted accelerations as low as 0.015 to 0.02 $\mathrm{m.s^{-2}}$, and a

fit and healthy person can even detect changes in acceleration as low as 0.01 $\mathrm{m.s^{-2}}$. With this in mind it is clear that there will be a perceivable difference in comfort levels between the vehicles on both grades of road.

As when discussing the contact patch loads, and perhaps to a greater extent here, a good deal of asymmetry can be seen in the acceleration data on the grade A road. Figure 5-13 shows that the occupants on the left hand side of the vehicle are subjected to larger acceleration levels than those on the right. The difference between the left and right hand side of the vehicle is between 0.02 – 0.03 $\mathrm{m.s^{-2}}$. Whilst this is apparent for both vehicles, it is more pronounced for the GTV. The GTV sees asymmetries between left and right occupant positions up to 70% larger than the SV. The asymmetry has a number of causes, the first being that the Cog of the GTV has moved further from the centreline of the vehicle (to the right), it was shown in the topology plots that the lower acceleration/higher comfort region was centred around the Cog, so as this will have moved very slightly right in the GTV, the occupants on the left side of the vehicle will be exposed to slightly higher levels of vertical acceleration and vice-versa. The Cog of the SV was already very slightly off the centreline of the vehicle, hence there is asymmetry in the SV results, but the further movement of the Cog in the GTV has exacerbated this trait in the vehicle. Secondly as a result of this cog movement, there is a likely discrepancy in the damping requirements, one side of vehicle is more loaded, one is less, and if the movement of the Cog was large enough then it could have compromised the dampers performance in their current setup. However one question relating to these levels of asymmetry still remains, why is it that this characteristic is only visible on the smoother of the two roads? Again as proposed previously, a possible explanation comes from the levels damping, and to explain this it is useful to look at the

histograms of the damper velocities, which are shown in Figure 5-15 and Figure 5-16, and the associated statistics shown in Table 5-10 and Table 5-11. It can be seen that when both vehicles are on the grade A road that all four dampers spend much more time in the low speed regions. The low speed damping, between ±0.025 $\mathrm{m.s^{-1}}$, is concerned with the control of the body, (the sprung mass motion on the springs) (Segers, 2008). It can be seen that on the smooth road the damping of both vehicles is roughly 15 % in high speed and 85 % in low speed. If we now consider the rough (grade C) road, we can see that the situation has almost exactly reversed, the dampers now spend 25 % of their time in low speed regions and 75 % of their time in high speed regions. This signifies that on the rough road, the road inputs are dominating the damping requirements, and on the smoother road it is the body motion that dominates the damping requirements.

When looking at the damper velocity histograms there are a few important points, firstly, well tuned dampers should produce histograms that represent a normal distribution, a symmetrical bell curve means that the damper is spending equal amounts of time in bump and rebound. For example if the histogram has large peaks in the low speed region it would indicate too little low speed damping, this can be rectified by increasing the low speed damping or reducing the high speed damping. If the damper histogram is very flat, the low speed damping can be reduced or the high speed damping increased.

Considering Figure 5-15 and Table 5-10 presented here for the vehicles on the smoother of the two road variations, we can see that whilst both histograms for the SV and GTV are not ideal (not symmetrical), we are using the SV as a baseline, so comparisons will be made to this. It can be seen that there is little difference between the amount of time both vehicles' damper's are spending in high and low

speed regions, however when looking at differences between bump and rebound, it's a different story. Here we can see quite significant differences between the two vehicles, but noticeably, only in the low speed region. At the front of the vehicle the left corner spends more time in low speed rebound and less time in low speed bump than the SV, the statistics of the right front are still well matched between the two vehicles. At the rear, the left corner is spending more time in low speed bump and less time in low speed rebound than on the SV, likewise is the right corner. Such differences between the two vehicles indicate that the GTV requires less low speed bump damping on the front left and more at both left and right rear corners. Generally this shows too much low speed bump damping at the front of the GTV and an insufficient amount at the rear. This is consistent with the mass distribution changes that have occurred to the GTV. Mass has been shifted rearwards, reducing load on the front axle and increasing it on the rear, meaning that the front will now have too much damping for the reduced body mass, and the rear too little for the increased mass. So in comparison to the SV the front sprung mass is overdamped on the GTV and the rear underdamped (this is of course in relation to the two vehicles, not whether the system is under or overdamped in relation to critical damping). This is a valid and important point which will need addressing with all hybrid vehicles which are constructed from existing conventionally powered vehicles, as it not only effects ride comfort but also handling. However we began looking at the damper velocities in order to explain the asymmetry in ride comfort of the GTV on the grade A road. To investigate this we should consider the differences between the two vehicles on the left and right hand sides. Again using the statistics in Table 5-10 as an example, we can see that the right hand side of the GTV generally spends more time in low speed bump and less time in low speed rebound than the SV, the left

hand side of the GTV shows a greater proportion of the time spent in low speed rebound. Whilst the SV also shows asymmetries in its damping, the magnitude is larger for the GTV. The largest differences between the two vehicles are seen at the rear, this is as expected as this is where the majority of mass has been added to the GTV. The fact that the dampers on the right hand side of the GTV are spending more time in low speed bump signifies that there is a lack of low speed bump damping on this side of the vehicle. This ties in with the Cog moving further from the centre line of the vehicle, to the right. The left hand side of the GTV is likewise lacking low speed rebound damping. As the Cog of the GTV has shifted rearwards and to the right, it is the right rear that will be the most unsuited to its new conditions in the GTV. The asymmetries in the damping discussed here are predominantly present in the low speed damping, if we consider Figure 5-16 and the statistics in Table 5-11 which are for the rougher (grade C) road, as was previously mentioned the damping is now dominated by the high speed region and so the poorly matched low speed damping for the GTV has less of an effect on the overall ride of the vehicle. Interestingly the results obtained from the grade C road show that there are large discrepancies between the time spent in high speed bump and rebound by the individual dampers (asymmetric histograms), however this is true for both vehicles, and the difference between the two vehicles is actually much smaller than on the grade A road. So whilst perhaps both vehicles could benefit from damper adjustments, the alterations that have been made to the GTV in this study have not compromised its ride characteristics on rougher roads as much as they have on smoother roads, in comparison to the SV. As previously mentioned the characteristics of the high and low speed damping are different as the low speed damping is controlling the body motions whereas the high speed damping is

isolating the road inputs, the way the high speed damping isolates the body from road inputs is primarily done by controlling the un-sprung mass (Milliken and Milliken, 1995), as this has remained unchanged, its damping requirements have similarly remained unchanged and ride on the rougher roads is much the same between the two vehicles. And so it can be said that the addition and redistribution of mass in the GTV has mainly affected the low speed damping requirements and thusly affected its ride characteristics on smoother roads.

If we consider what has been discussed here it can be said that to bring the GTV damper histograms back in line with the SV's it would be necessary to make alterations mentioned in Table 5-12, this data is derived from the statistics shown for both vehicles on both grades of road.

In a more general sense of hybrid vehicles that are converted to hybrids from conventionally powered vehicles, it will be necessary to address their damping requirements which will be different due to their atypical mass distribution, as shown here the main differences are likely to be between front and rear, and to a lesser extent cross car if the Cog moves off the centreline, then, as here, the need for asymmetrical damping will arise. It has also been shown that as the sprung mass is increased the low speed damping becomes more important, and incorrect levels of low speed damping will affect handling and the ride comfort levels on smoother roads. On rougher roads it was shown levels of low speed damping become less important, but high speed damping will need adjusting to suite new mass properties to properly isolate road inputs, if un-sprung masses are altered.

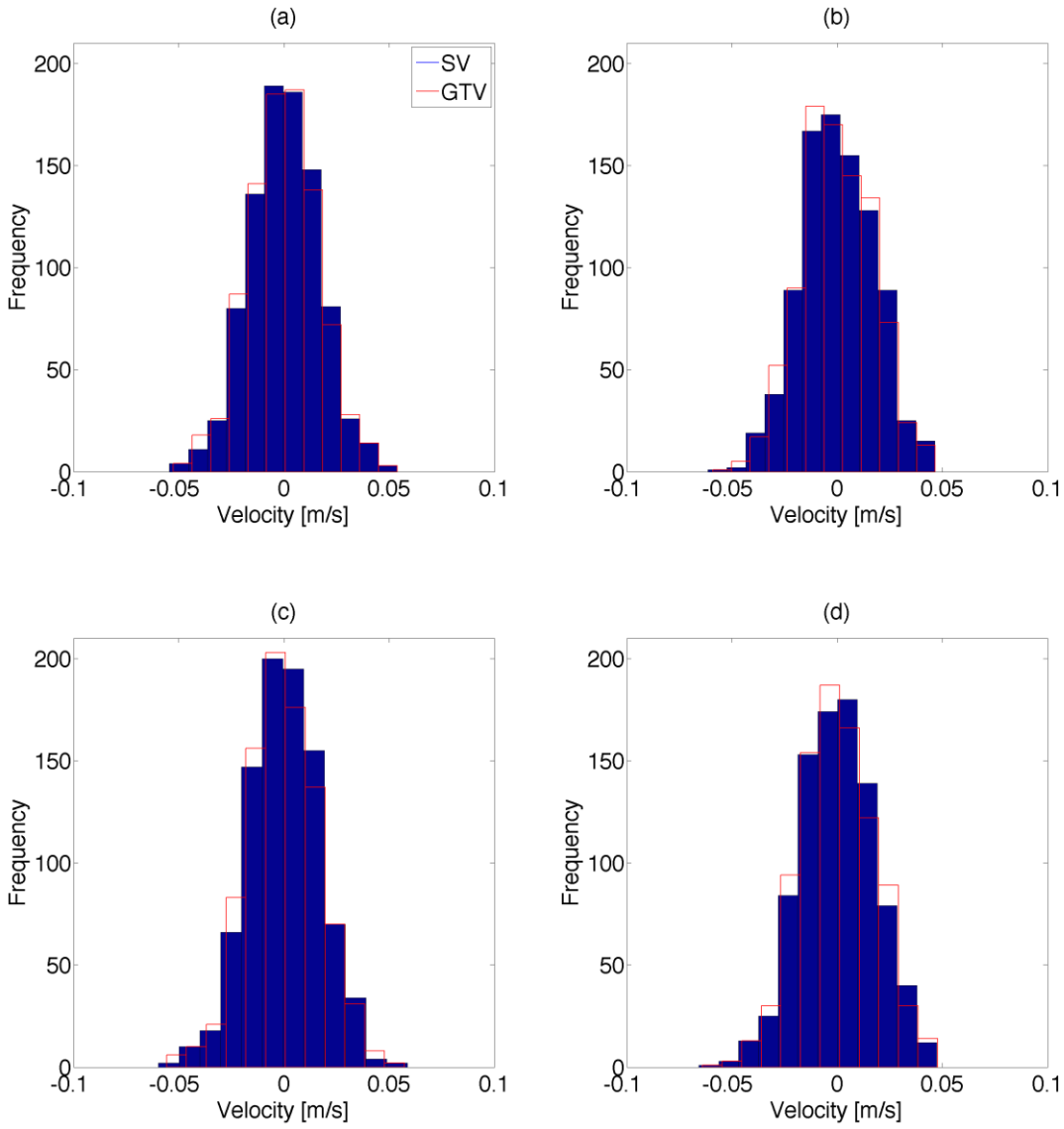

Figure 5-15 Damper velocity histograms, grade A road at 20 m. s^{-1}

	GTV				SV			
	Bump %	Rebound %	Bump-Rebound %	Total %	Bump %	Rebound %	Bump-Rebound %	Total %
LF HS	5.9	6.3	-0.4	12.2	5.8	6.5	-0.8	12.3
LF LS	43.6	44.2	-0.6	87.8	44.5	43.2	1.3	87.7
RF HS	7.0	6.3	0.7	13.3	6.9	6.5	0.3	13.4
RF LS	44.5	41.5	3.0	86.0	44.6	41.6	3.0	86.3
LR HS	6.2	6.8	-0.6	13.0	6.5	7.0	-0.4	13.5
LR LS	44.7	42.3	2.4	87.0	44.0	42.5	1.4	86.5
RR HS	7.1	7.4	-0.3	14.5	7.2	8.0	-0.8	15.2
RR LS	44.4	41.1	3.3	85.5	42.6	42.2	0.4	84.8

Table 5-10 Damper velocity statistics, grade A road at 20 m/s

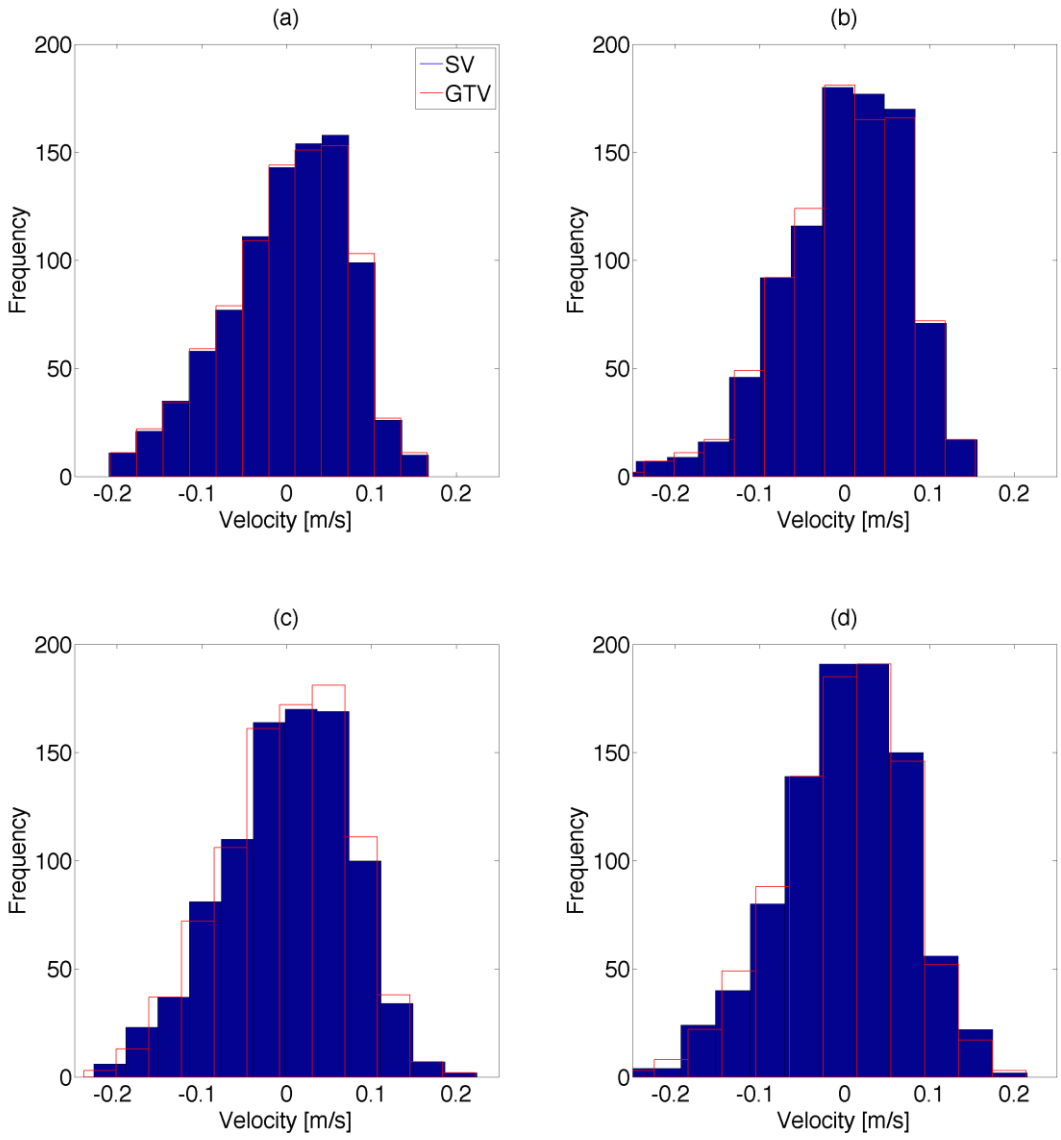

Figure 5-16 Damper velocity histograms, grade C road at 20 m. s^{-1}

	GTV				SV			
	Bump %	Rebound %	Bump-Rebound %	Total %	Bump %	Rebound %	Bump-Rebound %	Total %
LF HS	33.9	42.0	-8.1	75.9	34.1	42.3	-8.2	76.4
LF LS	12.6	11.5	1.1	24.1	12.4	11.2	1.2	23.6
RF HS	32.9	42.0	-9.1	74.9	32.6	42.3	-9.7	74.9
RF LS	13.7	13.1	0.7	26.8	13.6	13.2	0.4	26.8
LR HS	33.4	41.3	-7.9	74.8	34.2	40.6	-6.4	74.9
LR LS	13.8	11.4	2.4	25.2	13.4	11.7	1.7	25.1
RR HS	34.4	39.0	-4.5	73.4	35.2	39.3	-4.1	74.5
RR LS	12.1	14.5	-2.4	26.6	11.8	13.6	-1.8	25.5

Table 5-11 Damper velocity statistics, grade C road at 20 m. s^{-1}

	LF		RF		LR		RR	
	LS	HS	LS	HS	LS	HS	LS	HS
Bump	Reduce	-	Reduce	-	Increase	Reduce	Increase	Reduce
Rebound	Increase	-	-	-	-	Reduce	Reduce	-

Table 5-12 Needed damper adjustments

Table 5-12 shows that generally levels of high speed damping are too large at the rear of the GTV, and the requirements for low speed damping follow the changes in the mass distribution. By reducing the low speed damping at the front and increasing it at the rear body motions should be better controlled.

5.3 Conclusion

Investigation of the GTV's ride comfort has been carried out by looking at a few key vehicle responses. From the results presented here it is possible to quantify the changes made to occupant comfort both subjectively in terms of comfort and objectively in terms of actual vehicle operating conditions.

It was shown that due to acceleration levels inside the vehicle increasing for the front occupants and decreasing for the rear occupants, overall changes in comfort are a little mixed, however occupants at the front of the vehicle could feel higher levels of discomfort in the GTV, while those at the rear could feel improved comfort levels. The changes in occupant comfort arise from differing vertical acceleration levels of the vehicle body, which were linked to changes in mass distribution, inertia, stiffness properties and then consequently incorrect levels of damping.

Low acceleration/higher comfort regions within the vehicle tracked the movement of the Cog and spring centre due to mass re-distribution, this means in the GTV the highest comfort region was further rearwards and slightly to the right of the same region in the SV. Consequently this also means that if occupants now sit

further from the Cog, such as the passenger in the front left seat, they will experience lower comfort levels. It was also shown that due to the GTV's increased pitch inertia, pitch accelerations are lower and so linear acceleration levels at the extremities of the vehicle are reduced in comparison to the SV. In contrast the GTV's roll inertia is reduced and so levels of acceleration along the left and right edges are increased. Whilst the reduced pitch acceleration of the GTV yields lower acceleration levels at the extremities of the vehicle, it was shown to possess larger pitch angle and bounce responses, this can be attributed to a higher degree of coupling between pitch and bounce modes primarily due to the stiffer rear springs on the GTV. Also as a result of its increased bounce mode response, vertical acceleration levels around the centre of the vehicle increased. Due to this it was shown that contact patch load variation in the GTV was larger than that in the SV, especially on rough roads and at high vehicle speeds. This larger variation in contact patch load will also have ramifications on vehicle handling as it will directly affect the magnitude of longitudinal and lateral tyre forces generated.

In terms of damping, it was shown that the reduced mass on the front axle has led to too much low speed damping at the front, the increased mass on the rear axle in combination with stiffer springs requires an increase in low speed damping at the rear. Due to the Cog in the GTV moving further from the centreline, it was also confirmed that there is a slight requirement for asymmetric damping. It was shown that ride comfort can become quite asymmetric without this, even a result of the small off centre movement of the Cog shown here. The effects of the incorrect levels of damping present on the GTV manifest themselves mainly in the ride comfort on smoother roads, (it would also be present in handling scenarios) due to the low speed damping primarily controlling body motions. On rough roads as the

damping requirements shift to be more dominated by the high speed regions the inadequacies of the low speed damping are not so prominent. Whilst the mean tyre loads of the GTV were shown to increase at the rear and decrease very slightly at the front, (following the weight distribution change), which is of course an unavoidable effect, the variation of the loading can be managed with correct levels of damping, this would lead to a smaller force variation being transmitted to the vehicle body and thus reduced acceleration levels and higher comfort, it could also reduce the pitch responses of the GTV, which would also increase occupant comfort (Sharp, 2002).

One problem that could be encountered with the need to alter low speed damping is that the un-sprung mass has remained unchanged, and so its damping requirements have also remained unchanged. Therefore if damping levels are changed too much for optimization of the control of the sprung mass then the un-sprung mass will be under/overdamped, which in itself will cause serious problems for vehicle ride and handling. Furthermore whilst it has been shown there is a requirement for the damping to be adjusted, it may not be the whole solution. It was seen when investigating the vehicles' pitch responses that the GTV does exhibit lower pitch accelerations due to its increased pitch inertia, thus increasing comfort very slightly at the extremities of the vehicle body. Despite lower pitch accelerations, it was shown that pitch angles and larger for the GTV. It may be the case that there is a need for extra pitch mode control of the vehicle body with atypical mass and inertia characteristics. Systems for exactly this have started to appear in motorsport over the last two years, in Formula 1, Lotus utilities a Front-Rear InterConnected (FRIC) system, similar systems are being used and pursued by most teams on the F1 grid (Nowlan, 2013). Such systems work by hydraulically connecting the front and rear suspensions via a third spring damper unit, when the vehicle pitches, fluid is

displaced at one end, and used to control the ride height at the other, as such, the system can be used to reduce pitch motions and control ride heights under rough road inputs and braking.

Whilst it was shown here that pitch accelerations were lower for the GTV, it is conceivable that with some vehicle architectures they could increase, in such cases, whilst body position and velocity are controlled by the springs and dampers, there could be a need to separately control body accelerations, such control can be achieved through the use of inerters. This would mean that position, velocity and acceleration of the vehicle body could be controlled and tuned separately, thusly allowing for better ride height control through stiffer springs to cope with increased sprung mass, increased low speed damping to control this, and inerters to separately tune body/wheel accelerations (Papageorgiou and Smith, 2006).

Results here have highlighted areas that need attention for this specific study, however, they are all carry over, and will need to be given consideration for new hybrid vehicles in the future, especially those that will be designed around existing conventional vehicle platforms. This has been shown to be mainly a result of the different (slightly atypical) mass distribution that can arise due to the introduction of components that are specific to hybrid vehicles.

Results and analysis from this chapter will be tied in with results from the following chapter, which concentrates on the handling domain, and finally overall conclusions will be drawn.

Chapter 6 Result and Analysis: Handling

6.1 Introduction

This chapter will outline and analyse results obtained from both vehicle models during the handling domain case studies used within this work. As within the previous chapter vehicle level responses will be presented and compared between the two vehicles, the differences in the two vehicles' handling will be analysed and linked to component level changes that have been made when creating the GTV. Finally conclusions will be drawn to outline how the GTV's handling differs from the SV.

6.1.1 Steering Response

As with vehicle ride, vehicle handling will also be affected by the changes made to the SV when creating the GTV.

When it comes to vehicle handling, the main factors that a driver and other occupants will notice are lateral acceleration yaw and roll responses. Lateral acceleration and yaw rate play a large role in how the driver will perceive the handling of the vehicle, if these responses are of incorrect magnitude, too oscillatory, too fast/not fast enough then it can leave the driver with a multitude of unwanted feelings with regard to the vehicles handling. It is for this reason that these are the main response that will be the focal point of this chapter.

Chapter 4 introduced steering responses and the understeer gradient. It is important to consider the steer responses at the outset of the handling analysis as vehicles with different responses (different understeer gradients) will have different

steady state responses to the same steering input. As the vehicles in question hear have different mass properties and roll stiffness distributions their steering responses vary. To be able to compare directly the transient responses of both vehicles it is necessary that they both achieve the same steady state response for a given test manoeuvre, this in effect means that the two vehicles by virtue of their different understeer gradients require different steering inputs to obtain the same level of steady state lateral acceleration and yaw rate. By comparing the steering responses of both vehicles the difference in steering angle required between each vehicle can be calculated.

The vehicles' steering responses can be obtained from the Dymola models in the same manner that it is obtained from a vehicle during real world testing, through constant radius tests, such tests were previously described in chapter 4. Data obtained for steered angle and lateral acceleration will vary greatly depending on the speed of the vehicle. For example, consider a vehicle travelling at 5 $\mathrm{m.s^{-1}}$ with a fixed steer angle of 2 degrees (road wheel angle) and achieving a lateral acceleration of 0.2g, this vehicle, at this point has an understeer gradient of 10 degrees/g. Considering the same vehicle now travelling at 10 $\mathrm{m.s^{-1}}$ with the same steered angle, its lateral acceleration will now have increased, assuming linearly with speed it would now be 0.4g, this would mean the vehicle now has an understeer gradient of 5 degrees/g. For this study, in order to be able to obtain correct steering angles for both vehicles over a range of speeds, it was necessary to obtain the vehicles' steering responses over such a range. Said responses for both vehicles were obtained on 15, 60 and 240m radii at increasing speeds. The vehicles' speed range during the 15m test, ranged from circa 3 $\mathrm{m.s^{-1}}$ to circa 8 $\mathrm{m.s^{-1}}$, during the 60m radius test the speed range is circa 7 $\mathrm{m.s^{-1}}$ to 18 $\mathrm{m.s^{-1}}$ and for the 240m radius test it is circa 15

$m.s^{-1}$ to 35 $m.s^{-1}$. These ranges are shown in Figure 6-1. Within these test ranges it means that the vehicles' handling can be investigated in six key areas, low, medium and high speed at low and high lateral acceleration. Steered angle and lateral acceleration achieved from the three constant radius tests are shown in Figure 6-2.

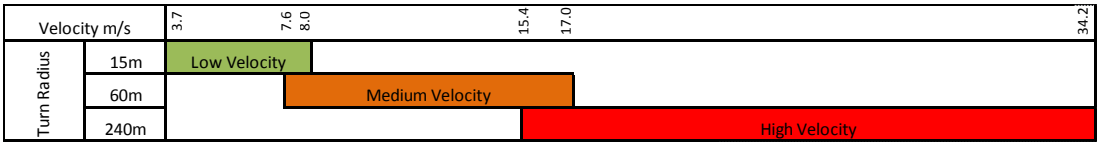

Figure 6-1 Velocity ranges for vehicle tests

Figure 6-2 shows the steered angle and lateral acceleration for both vehicles. Whilst differences are subtle, they are significant in effecting the handwheel angle. It can be seen from these plots that the GTV consistently requires a lower steered angle of the road wheels to obtain the same steady state lateral acceleration response as the SV, meaning it has a lower understeer gradient.

The fact that the GTV has a lower understeer gradient is no surprise, in chapter 4, it was shown that due to the large re-distribution of mass in the vehicle (mainly towards the rear), a stiffer spring rate was required at the rear axle to obtain the same ride frequency as the conventional vehicle. These two factors; increased mass on the rear axle, and stiffer spring rates at the rear, both lead to increased loading of the rear tyres, both statically and dynamically. Higher dynamic loadings result from the increase in rear roll stiffness, which causes a larger amount of weight transfer at the rear, and as a result less at the front. This extra shift in weight transfer means that the loads on the rear tyres are less balanced (left to right) and so their cornering capability is reduced. This lower cornering capability leads to the reduction seen in the required steering angle of the vehicle, as its handling balance has moved towards oversteer.

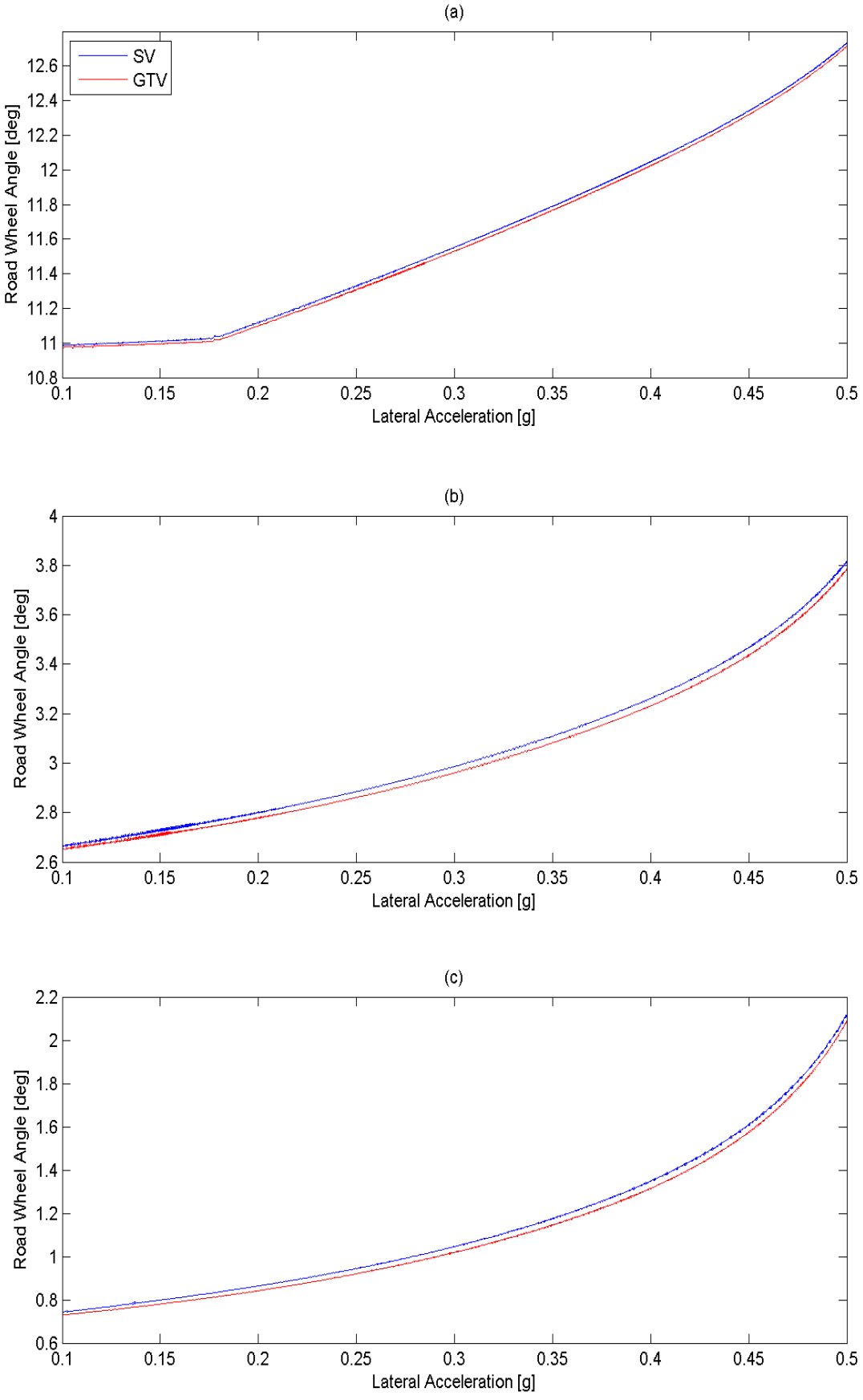

Figure 6-2 Steering response for constant radius tests on (a) 15, (b) 60 and (c) 240m radii

Figure 6-2 (a), (b) and (c) give the ability to obtain the steering angle required for both vehicles to obtain a desired level of steady state lateral acceleration. This was carried out when constructing the handling manoeuvres to be used for this study, a number of steady state lateral accelerations were chosen and then the required steering angles for both vehicles obtained. This allows direct comparison of the two vehicles' responses as they will both obtain the same level of steady state lateral acceleration and yaw rate during the test manoeuvres. This method is also much more analogous to the vehicles' real world use, over applying the same steering angle to both, as when a vehicle is being driven, the driver will apply a steering angle until they sense the correct yaw rate and lateral acceleration has been obtained which allows them to negotiate the corner at the speed at which they are travelling. In a vehicle with a lower understeer gradient the driver will apply less steering angle as the vehicle will require a smaller steering input to obtain the same steady state yaw rate and lateral acceleration to negotiate that same corner.

6.2 Ramp to step steer results

Ramp to step steer manoeuvres were carried out to target discrete levels of lateral acceleration within different regions of vehicle handling, as described in the previous section. From the three constant radius tests that were conducted steer angles and speeds were selected for ramp to step steer tests in order to obtain steady state lateral acceleration ranging from 0.1g to 0.5g in 0.05g increments. This covers the full range of vehicle handling. Manoeuvres were carried out in both a clockwise and anti-clockwise direction.

From the results a number of metrics useful for characterising the handling responses of a vehicle were calculated. These metrics are presented for all ramp to step steer manoeuvres, plotted against lateral acceleration.

6.2.1 Ramp to Step Steer Metrics

Figure 6-3 shows peak lateral accelerations obtained by both vehicles over the range of ramp to step steer manoeuvres. Breaking the vehicle responses down into regions, it can be said that in low speed (a), low and high g regions the SV achieves greater peak lateral accelerations than the GTV. The same is true for medium speed low lateral g. Within the medium speed high lateral g region it is the GTV that achieves greater peak lateral accelerations. And within the high speed region again it is the GTV that achieves the largest peak lateral accelerations. The transition from the SV having a higher peak lateral acceleration to the GTV, occurs circa 13 $\mathrm{m.s^{-1}}$. It should also be noted that the difference between the two vehicles is largest at low speed, as speed increases this difference diminishes.

Figure 6-4 illustrates overshoot of the peak lateral acceleration from steady state for both vehicles, the same observations that were made for the peak lateral acceleration values in Figure 6-3 are also present here. This is of course expected as the tests have been setup so both vehicles achieve the same steady state responses, therefore amounts by which they overshoot this steady state response will follow the same trend as their peak responses. The SV exhibits higher overshoot values and thus a more oscillatory response in the low speed range across all steady state lateral accelerations, although above 0.4g the difference is less than 1%. Within the medium speed, low lateral acceleration range, the SV is again more oscillatory than the GTV, as seen with the peak lateral acceleration values there is a transition at 0.3g (13 $\mathrm{m.s^{-1}}$) after which the GTV exhibits more oscillatory lateral acceleration responses. The GTV remains more oscillatory throughout the high speed range. The highest levels of overshoot are seen in the low lateral acceleration range of all speed regions and it can be seen that as lateral acceleration increases the overshoot values

decrease. In the low speed, low lateral acceleration range there is an 8% difference in the overshoot values of the two vehicles, within the medium speed range this difference reduces to 5% and within the high speed range the difference decreases further to just 2%. It can therefore be said that the difference in the lateral acceleration overshoot of the two vehicles decreases as speed increases.

Figure 6-5 shows lateral acceleration response times, this is the time taken from the initial steering input, for the vehicles' lateral acceleration responses to reach 90% of their steady state value. It can be seen that the GTV yields slower responses in almost all conditions. Differences between the two vehicle responses are slightly smaller in low lateral acceleration regions and it can be seen at 0.2g in the medium speed region the response times of the two vehicles are identical. Across all speeds in high lateral acceleration regions the difference between the two vehicles' response times are fairly constant, between 2% and 4%, with the exception of at 0.5g in the high speed range where results are almost identical.

Figure 6-6 shows peak yaw rate responses for both vehicles. Within the low speed region (a), peak yaw rates of the two vehicles are very similar, at low lateral accelerations the GTV achieves 1% higher peak yaw rates than the SV, at 0.35g there is a transition so that at high lateral accelerations the SV exhibits higher peak yaw rates. When operating within the medium speed range, the GTV achieves 2% higher peak yaw rates across all lateral accelerations. The GTV also yields higher peak yaw rates across the high speed range (c), generally responses are very similar however larger differences are observed at 0.5g.

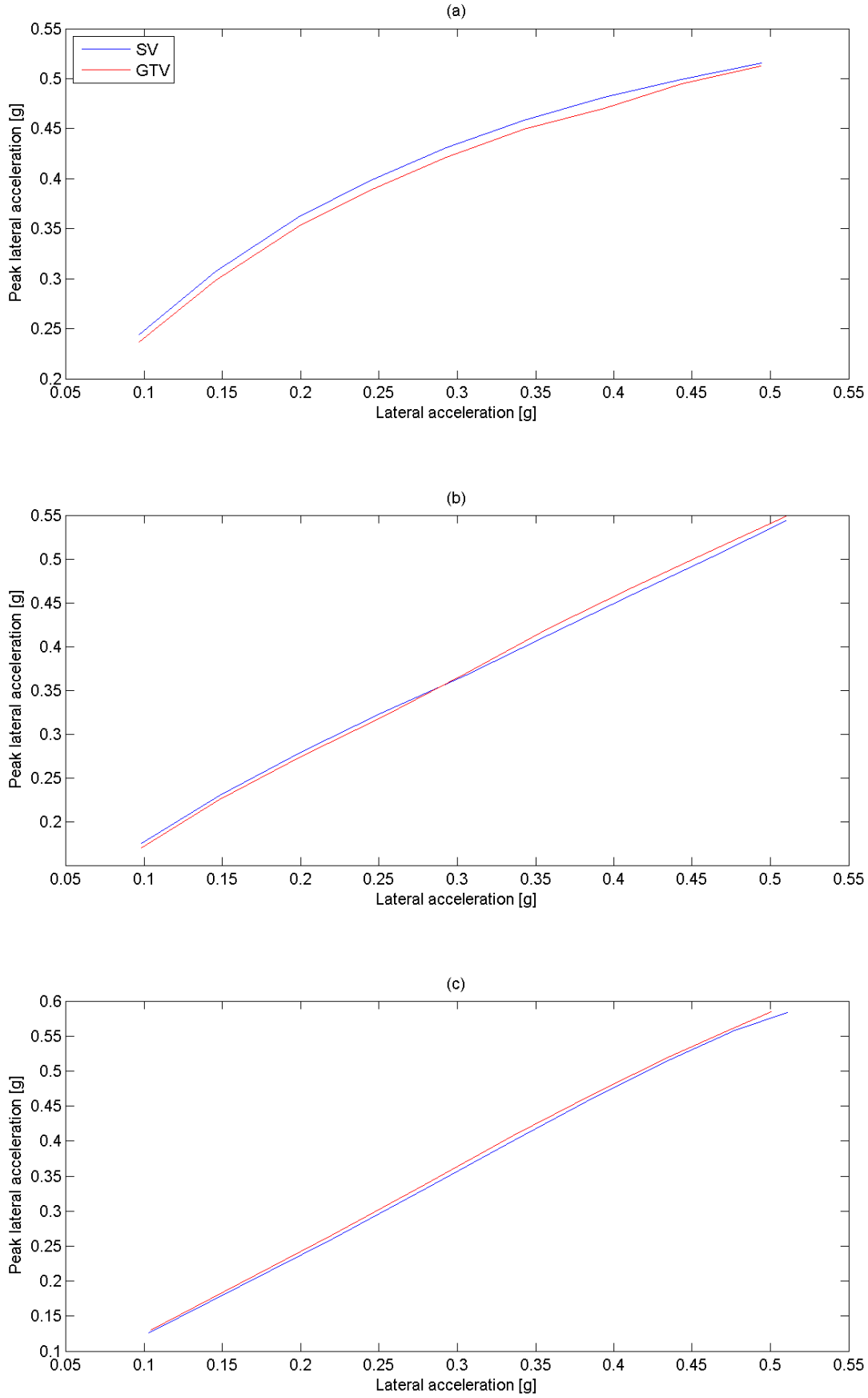

Figure 6-3 Peak lateral acceleration responses for (a) low, (b) medium and (c) high speed

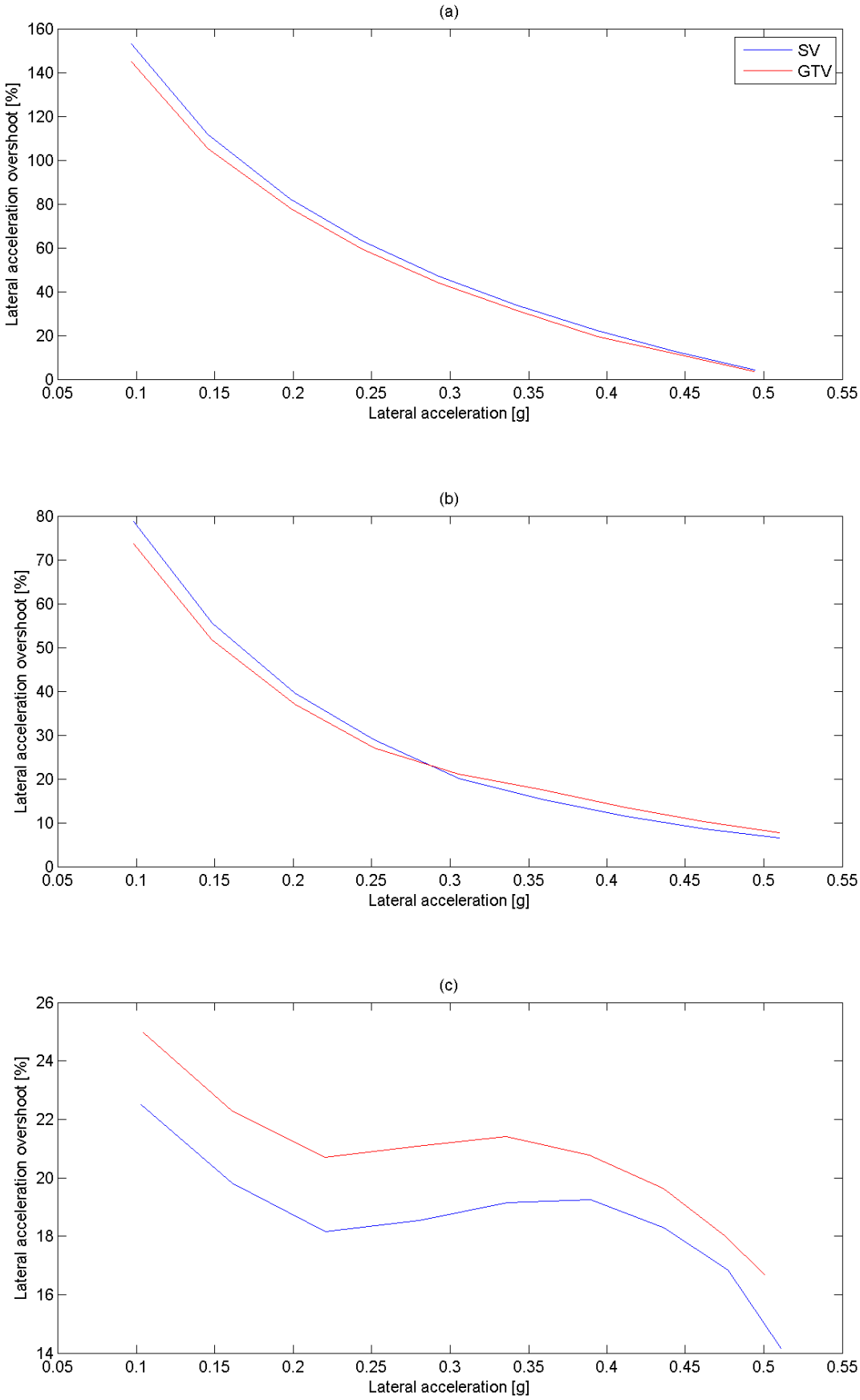

Figure 6-4 Lateral acceleration overshoot responses for (a) low, (b) medium and (c) high speed

Figure 6-7 shows yaw rate overshoot, for both vehicles. Again as with the lateral acceleration responses, and as you would expect the trends are the same as those observed in the peak yaw rate responses. Here it is shown that generally the GTV is more oscillatory, it is only within the low speed high lateral acceleration region (above 0.35g) that the SV shows a higher yaw rate overshoot. The largest difference between the two vehicle responses can be observed in medium speed range with differences of between 2-3%, large differences can also be seen in the mid lateral acceleration range of the high speed region, differences in the two vehicles' responses here are up to 2.5%.

Figure 6-8 shows yaw rate response times for both vehicles, as with the lateral acceleration response times this is the time taken from the initial steering input to the time when the yaw rate response reaches 90% of its steady state value. Within the low speed region (a) it is shown that the GTV responds faster in yaw than the SV across all lateral accelerations. The difference between the response times of the two vehicles increases steadily from 1% in the low lateral acceleration region, to 3% in the high lateral acceleration region. At medium speed, low lateral acceleration, (up to 0.15g) response times for both vehicles are identical, between 0.15 and 0.35g the GTV responds about 2% slower, from 0.35g onwards responses are again identical. In the high speed region the GTV's yaw rate responses are slower than the SV, and the difference between the two remains fairly constant over the entire lateral acceleration range. The largest differences in the two vehicles responses are seen in the high speed region, here differences in the responses times are in the order of 2-4%. From this it can be said that at low speeds, where yaw rates are larger, the GTV responds faster than the SV. As speed increases responses become similar, until within high speed regions the GTV responds slower than the SV.

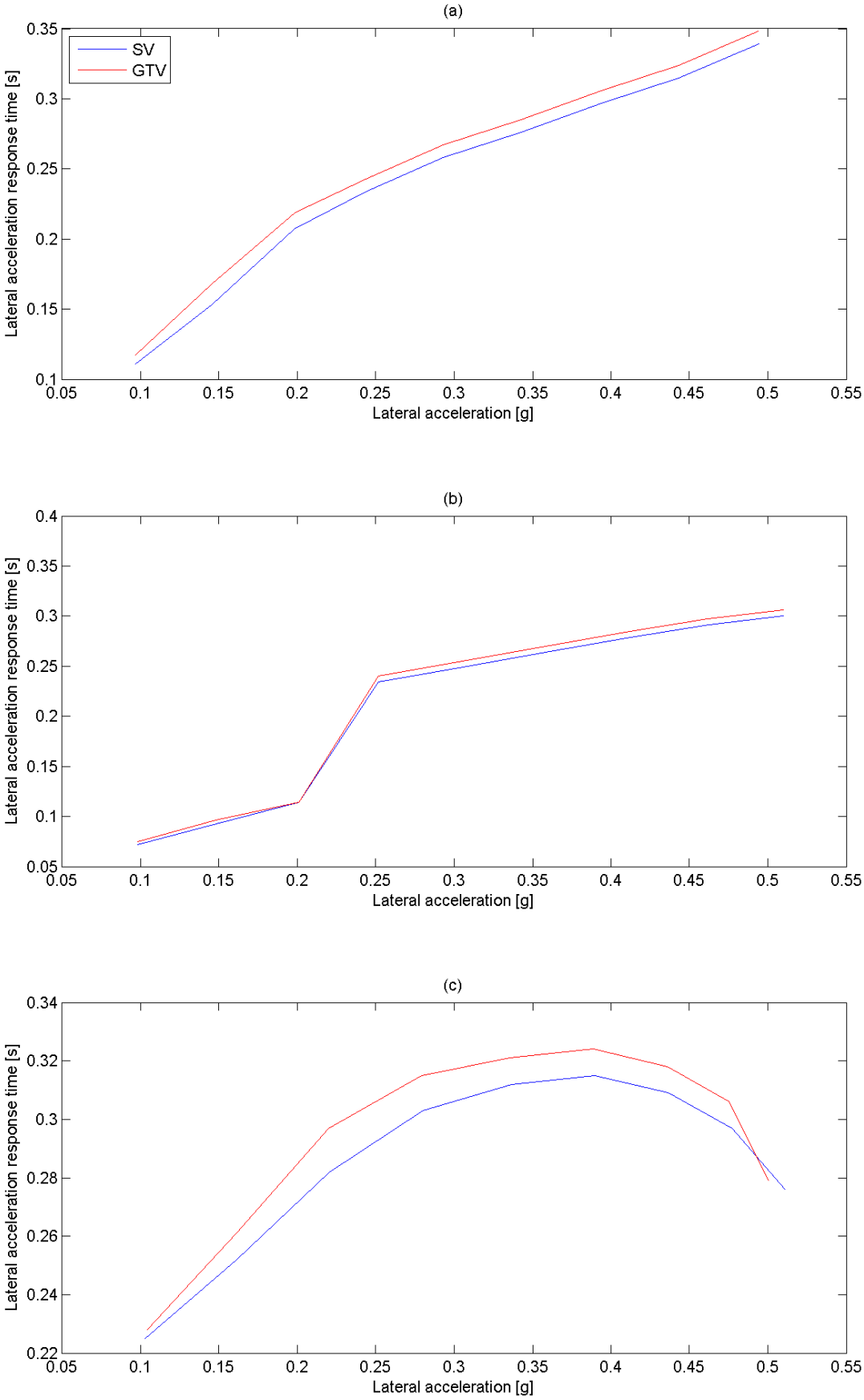

Figure 6-5 Lateral acceleration response time responses for (a) low, (b) medium and (c) high speed

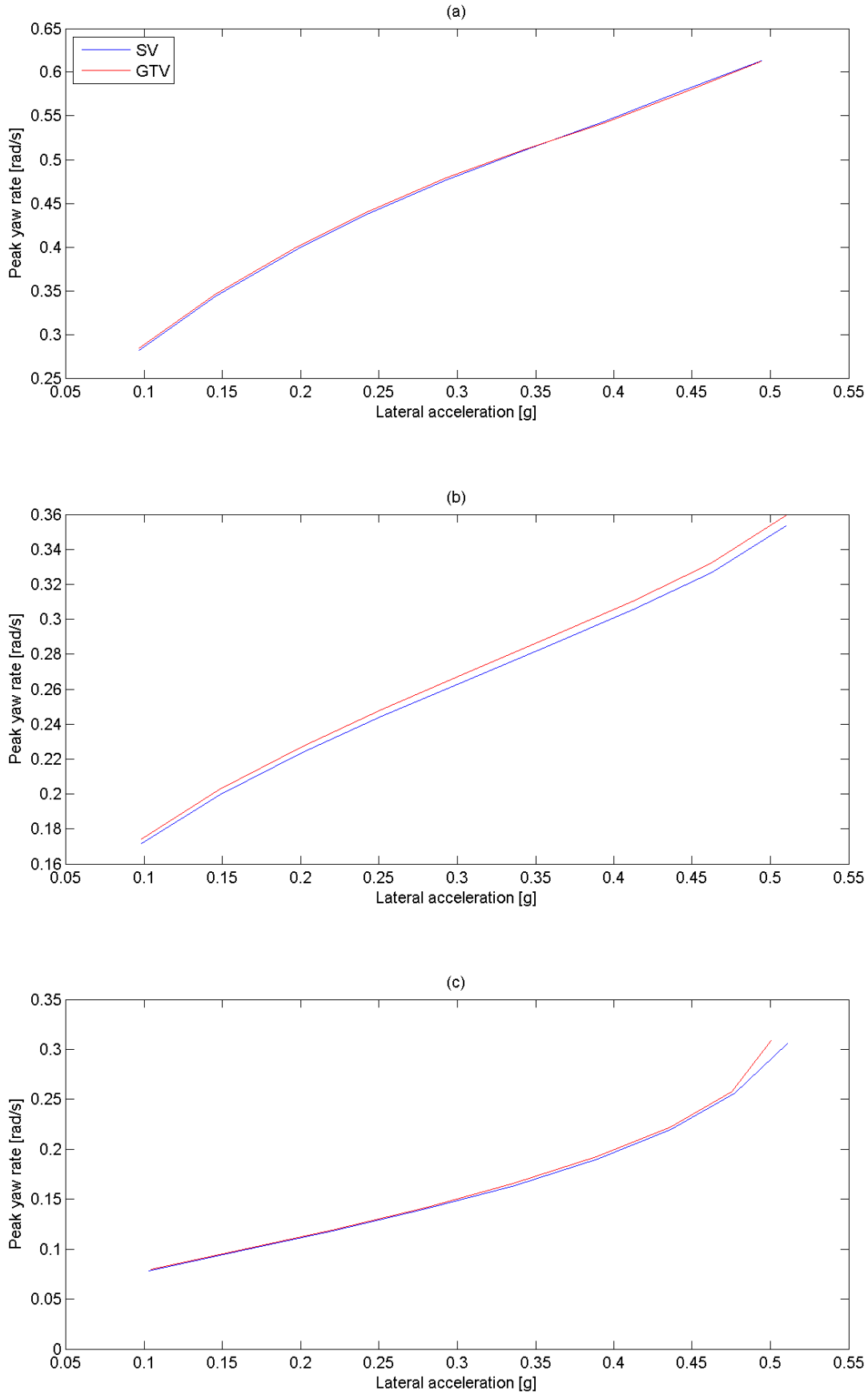

Figure 6-6 Peak yaw rate responses for (a) low, (b) medium and (c) high speed

As the speed increases the yaw rate responses become smaller, as the steer angle is reducing (due to the radii of turns being used), so initial results suggest that for large yaw rates the GTV responds faster, and for smaller yaw rates it is the SV that responds faster.

Figure 6-9 shows the phasing between the time when the lateral acceleration response reaches 90% of its steady state and when the yaw rate does the same. Within the low speed region (a) the GTV exhibits less of a phase difference between the two responses across all lateral accelerations, this is due to the lateral acceleration response of the GTV being slower than that of the SV and the yaw rate response being faster within these operating conditions. In the medium speed region (b) there is a very small difference in the phasing of the two vehicles' responses. It should be noted that above 0.2g the phasing becomes negative, this indicates that the yaw rate responses of both vehicles is faster than the lateral acceleration response. In the low lateral acceleration region the phasing of the two vehicles is generally the same. In the high lateral acceleration region, when the phasing becomes negative it is shown that the GTV exhibits a greater phase difference although now it is the yaw rate that is occurring before the lateral acceleration. The high speed region (c) again also shows negative phasing of lateral acceleration and yaw rate, here at low lateral acceleration, the phase differences of the two vehicles is very similar, but as lateral acceleration increases so does the difference between both sets or responses. In this high speed range the GTV shows a larger phase difference than the SV across all lateral acceleration regions (the only exception to this trend, as with other responses illustrated is at 0.5g, where results are very similar), again with the yaw rate response occurring before that of the lateral acceleration.

The largest phase differences are seen in the low speed region at both extremes of the lateral acceleration range. It is also within the low speed region that the biggest difference between the two vehicles can be observed. Phase differences are smallest in the medium speed region, in the middle of the lateral acceleration range the yaw rate and lateral acceleration responses occur almost simultaneously. It should be noted that whilst lateral acceleration responses across the differing speed ranges are constant, the yaw rate responses are reducing, this is one of the main reasons that the yaw rate response times reduce much more substantially than the lateral acceleration response times, and it is for this reason that phasing of the two responses changes sign in the medium speed range.

The phasing of the lateral acceleration and yaw rate give important information regarding attitude of the vehicle body. As lateral acceleration relates to the rate in which the vehicle begins to travel laterally, and the yaw rate the rate in which the vehicle re-orientates itself, the phase difference indicates the magnitude and sign of the body slip angle. If the yaw rate occurs before the lateral acceleration then the body slip angle will be negative (front of vehicle angled towards the turn centre) and vice-versa. In the way it is calculated here a negative phase relates to yaw rate before lateral acceleration, and so a negative body slip angle. This is important for driver queuing, vehicle manufacturers will aim for the vehicles yaw rate response to occur quicker than the lateral acceleration response at higher speeds as it will prompt the driver to stop applying steering which is useful for avoiding high speed limit conditions.

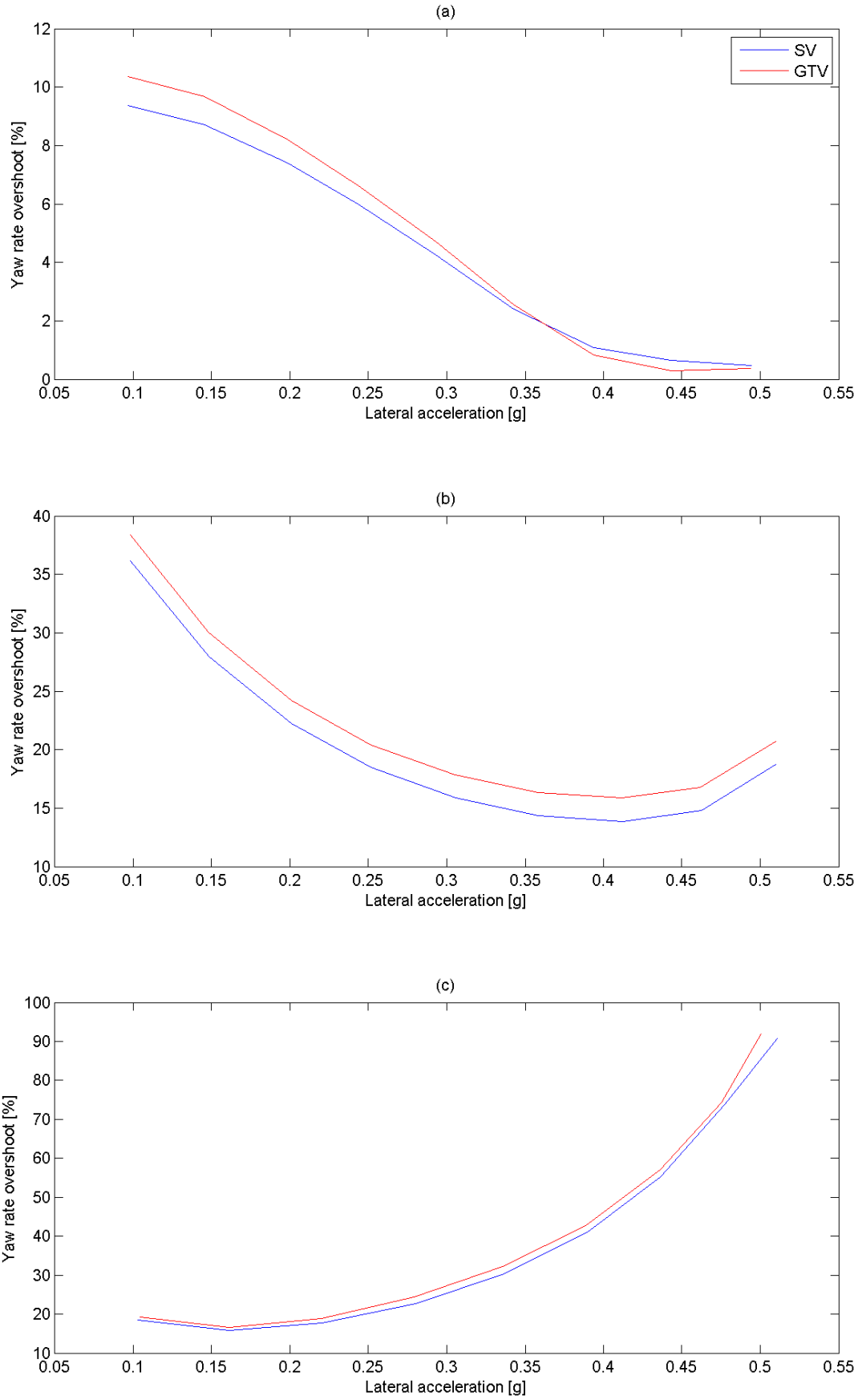

Figure 6-7 Yaw rate overshoot responses for (a) low, (b) medium and (c) high speed

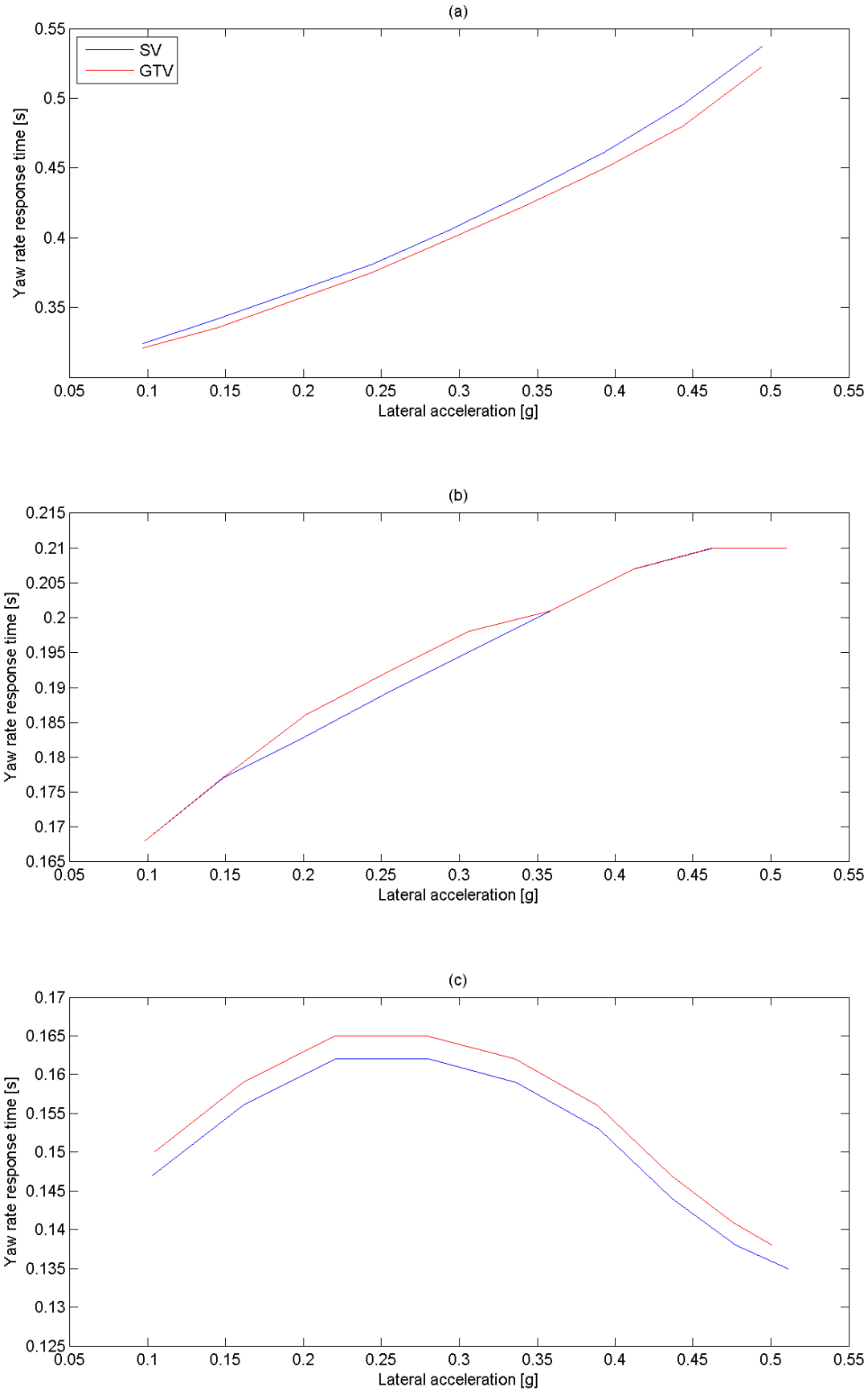

Figure 6-8 Yaw rate response time responses for (a) low, (b) medium and (c) high speed

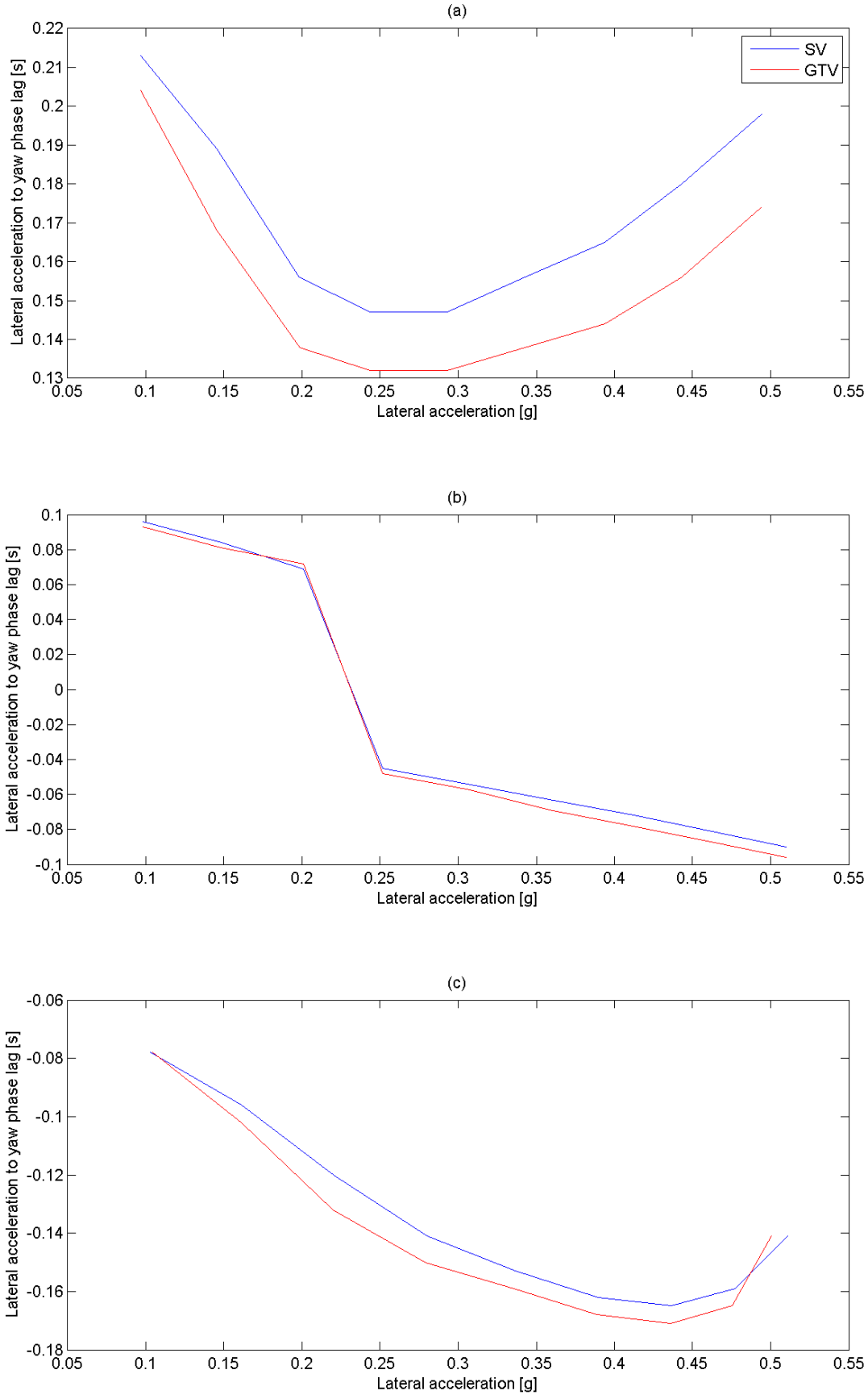

Figure 6-9 Phasing of lateral acceleration and yaw rate for (a) low, (b) medium and (c) high speed

	Low Lateral g	High Lateral g
Low Speed	**Lateral Acceleration** - GTV yields smaller peak values and is less oscillatory **Lateral Acceleration Response Time** - GTV responds slower **Yaw Rate** - GTV Yields higher peak values and is more oscillatory **Yaw Rate Response Time** - GTV responds faster **Phasing of Lateral Acceleration and Yaw Rate** - GTV shows less phase difference, lateral acceleration before yaw	**Lateral Acceleration** - GTV yields smaller peak values and is less oscillatory **Lateral Acceleration Response Time** - GTV responds slower **Yaw Rate** - GTV Yields smaller peak values and is less oscillatory **Yaw Rate Response Time** - GTV responds faster **Phasing of Lateral Acceleration and Yaw Rate** - GTV shows less phase difference, lateral acceleration before yaw
Medium Speed	**Lateral Acceleration** - GTV yields smaller peak values and is less oscillatory **Lateral Acceleration Response Time** - GTV responds slower **Yaw Rate** - GTV Yields higher peak values and is more oscillatory **Yaw Rate Response Time** – up to 0.15g identical, from 0.15 - 0.35 GTV responds slower **Phasing of Lateral Acceleration and Yaw Rate** – Responses very similar, 0.25g onwards GTV has larger phase difference, above 0.2g yaw before lateral acceleration	**Lateral Acceleration** - GTV yields higher peak values and is more oscillatory **Lateral Acceleration Response Time** - GTV responds slower **Yaw Rate** - GTV Yields higher peak values and is more oscillatory **Yaw Rate Response Time** - GTV responds slower **Phasing of Lateral Acceleration and Yaw Rate** – GTV has larger phase difference, yaw before lateral acceleration
High Speed	**Lateral Acceleration** - GTV yields higher peak values and is more oscillatory **Lateral Acceleration Response Time** - GTV responds slower **Yaw Rate** - GTV Yields higher peak values and is more oscillatory **Yaw Rate Response Time** - GTV responds slower **Phasing of Lateral Acceleration and Yaw Rate** – GTV has larger phase difference, yaw before lateral acceleration	**Lateral Acceleration** - GTV yields higher peak values and is more oscillatory **Lateral Acceleration Response Time** - GTV responds slower **Yaw Rate** - GTV Yields higher peak values and is more oscillatory **Yaw Rate Response Time** - GTV responds slower **Phasing of Lateral Acceleration and Yaw Rate** – GTV has larger phase difference, yaw before lateral acceleration

Table 6-1 Summary of ramp-to-step steer metrics

These results can be summarised to give a clearer picture for the overall vehicle behaviour in the six regions, this is shown in Table 6-1. These trends can be further investigated by interrogating the vehicle responses directly.

In this section metrics describing peak response, overshoot and response times were presented and summarised. In the following sections points made in this summary are investigated further by looking directly at outputs from the vehicle models. This will be carried out at steady state lateral accelerations of 0.2g and 0.4g. These two specific points have been chosen for no other reason other than they represent the low and high lateral acceleration regions.

Figure 6-10 to Figure 6-13 show the lateral acceleration and yaw rate responses for both vehicles during ramp-to-step steer manoeuvres targeting 0.2g and 0.4g steady state lateral accelerations which correspond to low and high g respectively. The three plots show the responses at three longitudinal velocities which give rise to the vehicles travelling on a 15m (a), 60m (b) and 240m (c) steady state radii, or low, medium and high speed regions. The three longitudinal velocities are; 5.27, 10.81 and 21.65 $\mathrm{m.s^{-1}}$ for the low lateral acceleration regions and 7.21, 15.18 and 30.66 $\mathrm{m.s^{-1}}$ for the high lateral acceleration regions.

6.2.2 Lateral Acceleration Response Times

The trends from the metrics described in Table 6-1 state that, in the low lateral acceleration range the GTV's lateral acceleration response was slower than that of the SV. To investigate this lets consider Newton's second law, from this we know that the force acting on a body is equal to its mass multiplied by its resulting acceleration. Therefore it seems logical to look at the lateral forces acting upon the two vehicles, for this we can look at the lateral tyre forces.

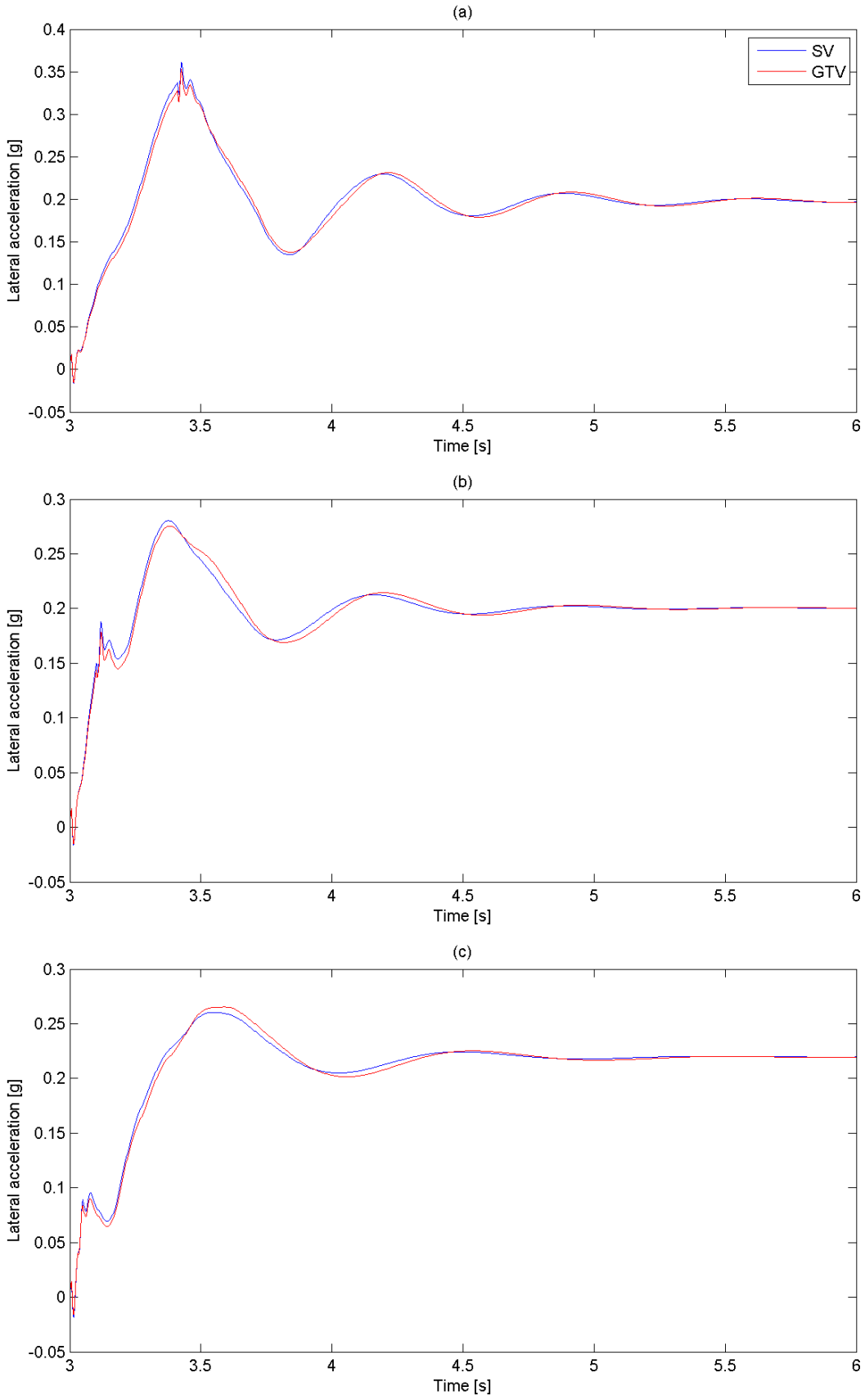

Figure 6-10 Lateral acceleration responses for 0.2g target ramp to step steer at (a) low, (b) medium and (c) high speed

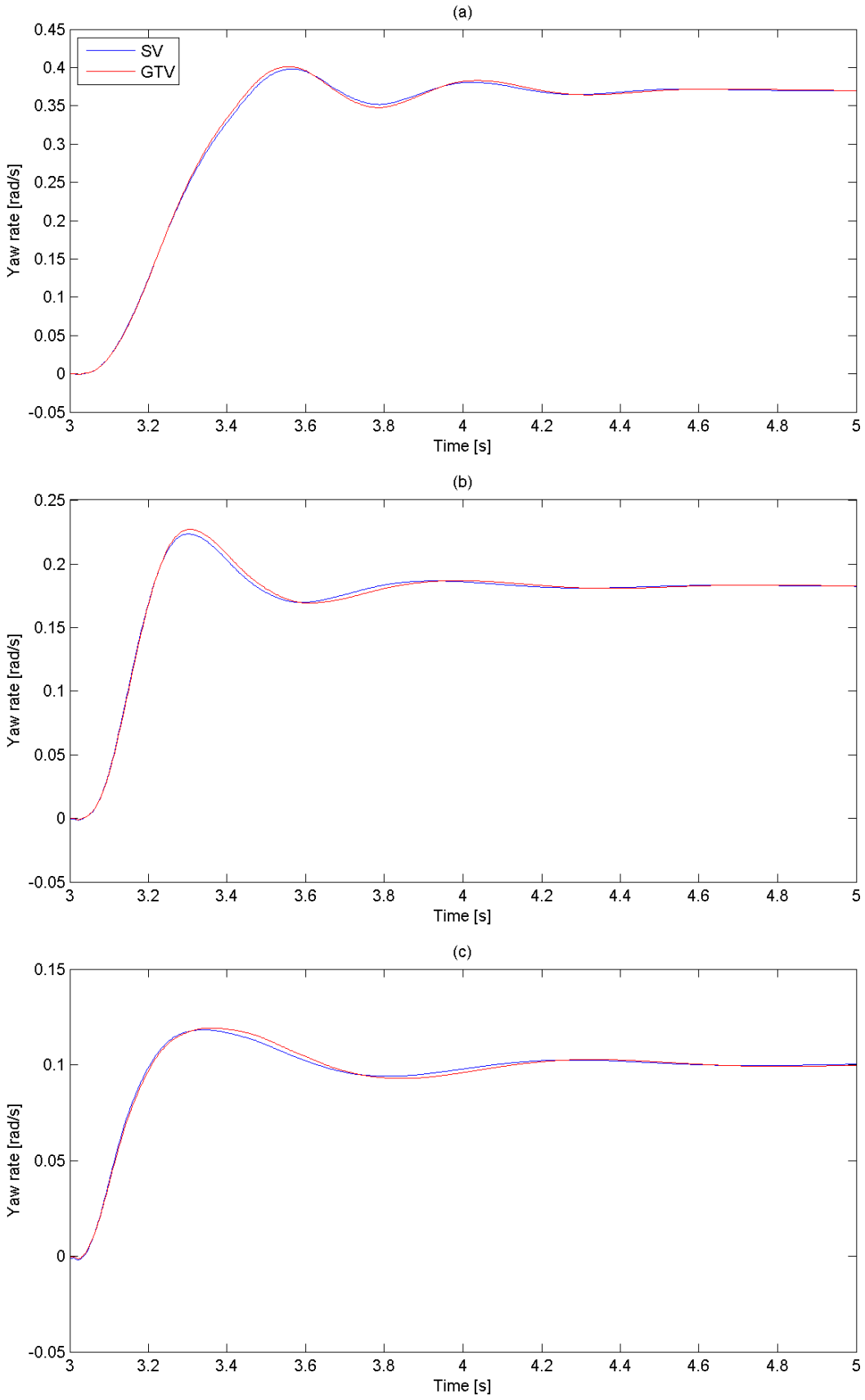

Figure 6-11 Yaw rate responses for 0.2g target ramp to step steer at (a) low, (b) medium and (c) high speed

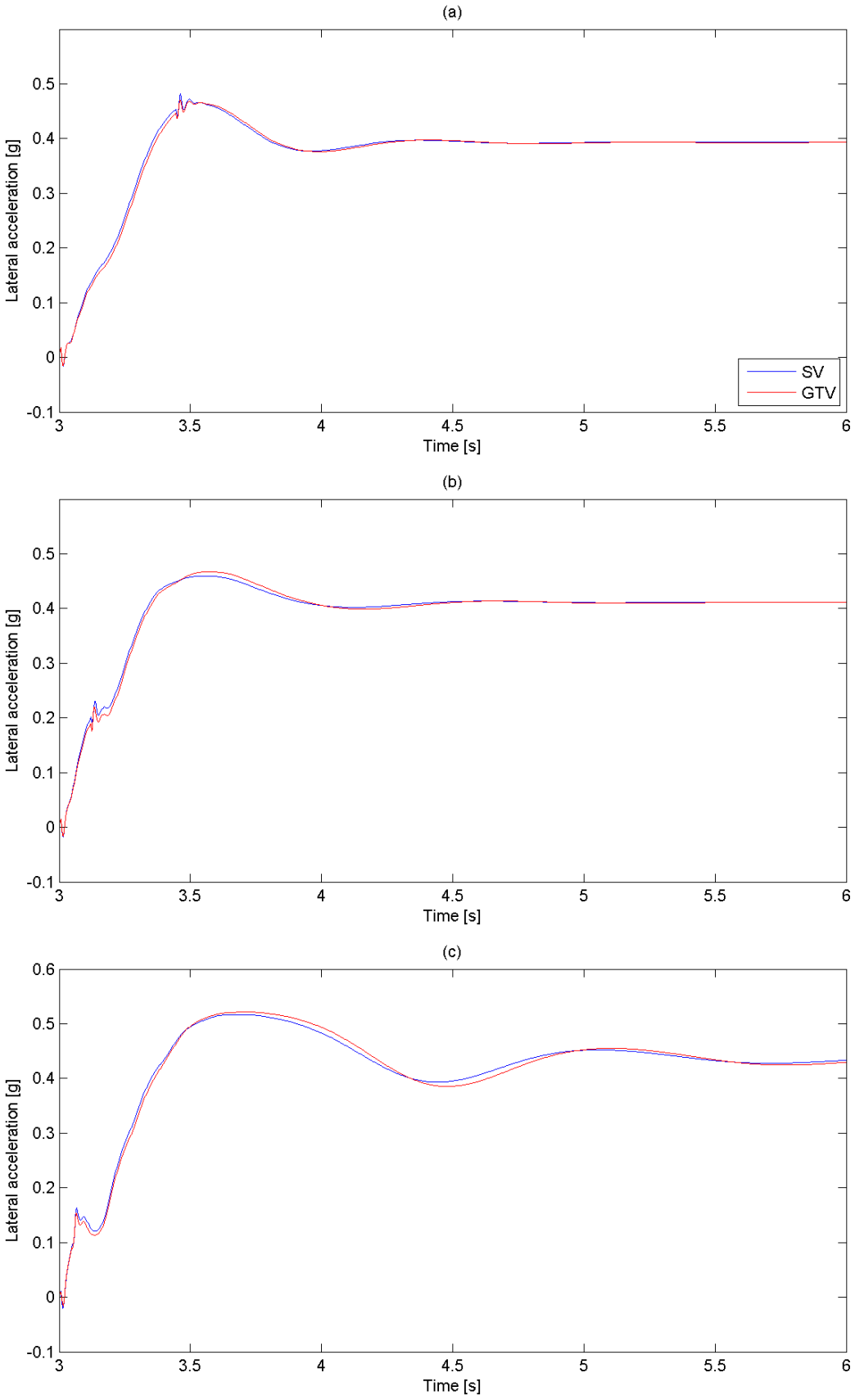

Figure 6-12 Lateral acceleration responses for 0.4g target ramp to step steer at (a) low, (b) medium and (c) high speed

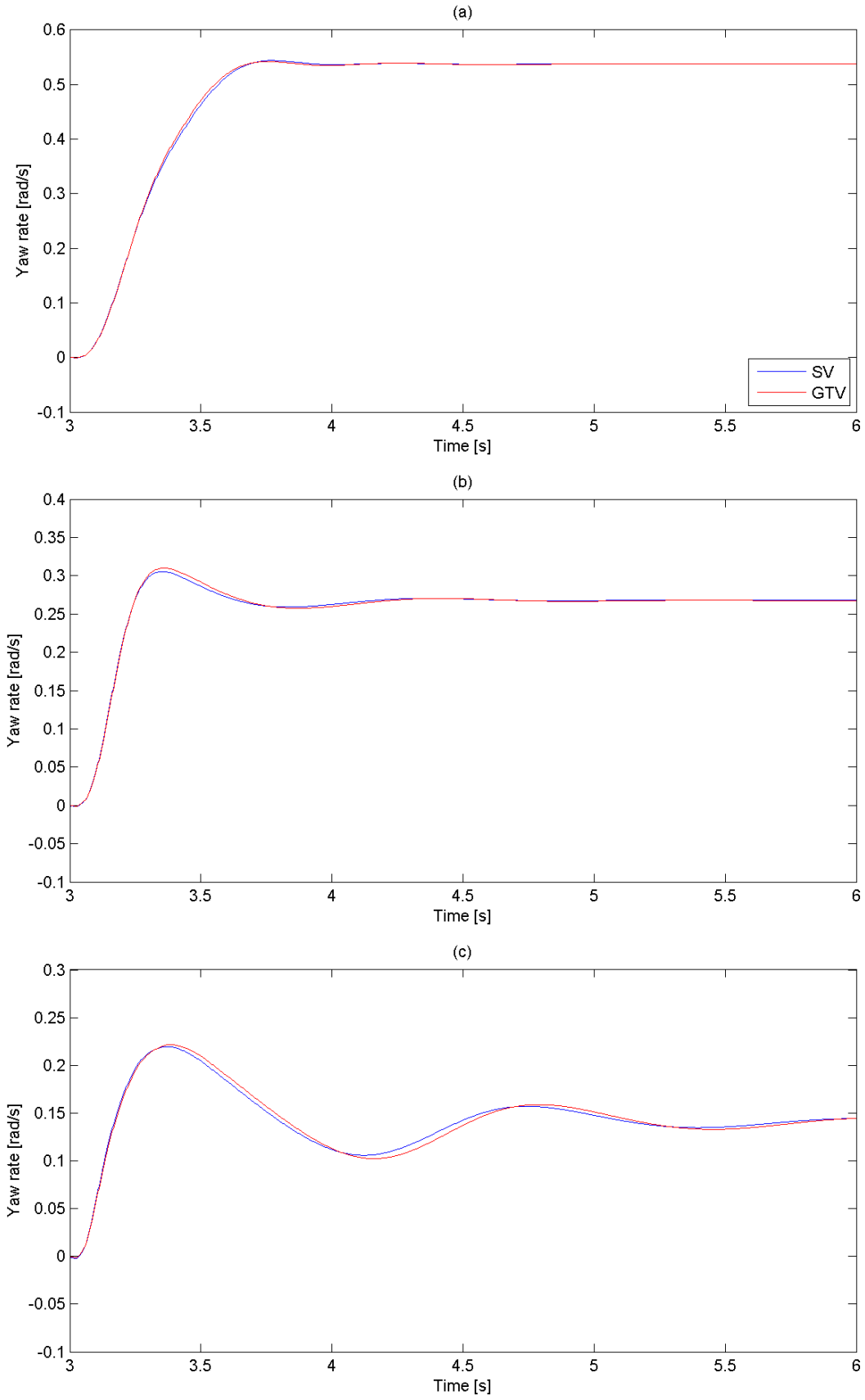

Figure 6-13 Yaw rate responses for 0.4g target ramp to step steer at (a) low, (b) medium and (c) high speed

Figure 6-14 shows just this, the total lateral tyre forces produced by both vehicles. The first point to notice is that within the region from the initial steering input (3 seconds) to the time when the response reaches 90% of steady state, it can be seen that the two vehicle responses exhibit very similar rates of change, and if any difference, it is the GTV that shows a slightly slower total lateral force response. To relate this to the lateral acceleration response time of the vehicles the mass of each vehicle must be considered. The mass of the SV is 2136 Kg and the GTV slightly heavier at 2209.75 Kg, combining this with the slightly slower lateral force response of the GTV it is clear that the GTV will respond slower. A second point to make in this area is that the GTV has a higher dynamic index (DI) than the SV, this explains the difference in the rate of change of lateral force generation of the two vehicles, despite them having very similar steering inputs. A larger DI expresses that the centre of percussion (CoP) is further behind the rear axle, therefore the inertial effects at the point of steering angle application lead to the rear tyre slip angle being generated in the incorrect direction to negotiate the corner, this leads to a delay in rear tyre force generation in the correct direction, and so the total lateral force generation is delayed, this can be seen in Figure 6-16. Before continuing it should also be noted that the steady state region of the lateral acceleration responses shows that the steady state values of both vehicles are the same, circa 0.2g, the same region of the total lateral force responses shows a significant difference between the SV and the GTV, this again illustrates, that the GTV due to its greater mass needs to obtain a larger lateral force to obtain the same level of lateral acceleration as the SV.

The above explanation can also be related to the tangent speed of the two vehicles. As was shown in chapter 4 the GTV has a lower tangent speed than the

SV, referring to work conducted by Olley (2002) it was shown that the higher the tangent speed of the vehicle the quicker the lateral acceleration response time.

The high lateral acceleration regions show the same trend in lateral acceleration response times and can be explained by the same mechanisms discussed for the low lateral acceleration regions.

6.2.3 Lateral Acceleration Responses

Within the low lateral acceleration range it was stated the GTV exhibits smaller, less oscillatory lateral acceleration responses than the SV at low and medium speeds, however at high speeds the opposite occurs. This can be clearly seen in Figure 6-10, and is confirmed when looking at the total lateral forces in Figure 6-14. The tyre forces in the low and medium speed ranges (a) and (b) respectively, show very similar peak values, and referring to the previously discussed mass differences it makes sense that the GTV would achieve a smaller peak lateral acceleration. However in the high speed range the lateral tyre force peak for the GTV is considerably larger than that of the SV. To investigate this it is useful to consider the derivatives of the Bicycle model mentioned earlier in Chapter 4. Whilst this is a very simplified linear model and direct comparisons can't be made, it is useful to illustrate vehicle responses. In chapter 4 it was stated that there are six derivatives for the forces and moments acting on the body of the simple vehicle. As discussed, the side force due to body slip angle term, Y_β, shows the increase in lateral force incurred due to body slip angle. Figure 6-15 shows the body slip angle responses (at the Cog) of both vehicles, it should be noted that at low and medium speeds (a) and (b) respectively, the body slip angle of the SV is larger than that of the GTV and is positive. In the high speed region it can be seen that the body slip angle is now negative, and in magnitude, said angle of the GTV is larger. Consideration of the Y_β

derivative shows that for positive body slip angles a negative cornering force is produced; conversely for negative body slip angles a cornering force complimentary to cornering will be produced. This explains why within the low and medium speed ranges, when the body slip angle is positive, the SV yields larger peak lateral accelerations, yet at higher speeds, when the body slip angle is negative, the opposite is true. To illustrate this let us consider the vehicle operating conditions. Steer angles and yaw rates are very similar between the two vehicles so the effects of these terms can be neglected for the purpose of this analysis, as can the N_β term, as moments produced by this derivative are very small. This leaves us with the Y_β derivative. As previously mentioned when the slip angle is positive the lateral force induced subtracts from the total cornering force, although in low and medium speeds the GTV has a smaller body slip angle than the SV, the two are sufficiently similar (only 8% - 15% different at low and medium speeds) so there is no real advantage gained by the GTV, in terms of the force induced by the Y_β derivative (bearing in mind that the GTV's, mass is also larger). However in the high speed region where the body slip angle is negative, (so the force generated from this angle now adds to the total cornering force) and larger for the GTV (some 25% larger), the GTV now has the ability to create a sufficiently higher lateral force and corresponding peak lateral acceleration than the SV.

Table 6-1 shows that in the high lateral acceleration region the GTV yields smaller lateral acceleration responses in the low speed range, however in the medium and high speed ranges its responses are larger than that of the SV. As discussed with the low lateral acceleration range, it is the body slip angle that accounts for this. Figure 6-19 (a) shows in the low speed, high g region both vehicles operate with a positive body slip angle. In the medium speed range the SV still operates with a

positive body slip angle, although that of the GTV is now negative. This negative body slip angle now creates a lateral force that is complimentary to cornering and so the GTV is able to achieve a greater peak lateral acceleration. The same is true in the high speed, high g region, although here both vehicles have negative body slip angles, the GTV's is larger (in magnitude) and so again it is able to achieve greater peak lateral accelerations.

The change in direction of the body slip angels of the vehicles at different speeds illustrates the different tangent speeds of the two vehicles. Due to its more rearward mass distribution, the GTV has a lower tangent speed than the SV. This was shown in the previous section to be the reason why the SV has faster lateral acceleration responses.

6.2.4 Yaw Rate Response Times

Table 6-1 shows that within the low speed, low lateral acceleration range the GTV responded faster in yaw than the SV. However at higher speeds it is the SV that responds faster. The same trend is seen in the high lateral acceleration regions.

There are a number of factors that are contributing to the yaw rate response time of both vehicles; yaw inertia, mass and wheelbase of the vehicles, longitudinal velocity and corner radius all play a part. Let us start by considering the vehicle properties. The GTV has larger yaw inertia, this alone suggests that it should respond slower in yaw than the SV. A secondary effect of this higher yaw inertia is a higher dynamic index. The effect of this manifests itself in the generation of rear slip angle at the instant of turn in. At the instant of steering angle application the vehicle will begin to yaw about the CoP, with this point behind the rear axle the rear slip angle will initially be generated in the incorrect direction for cornering.

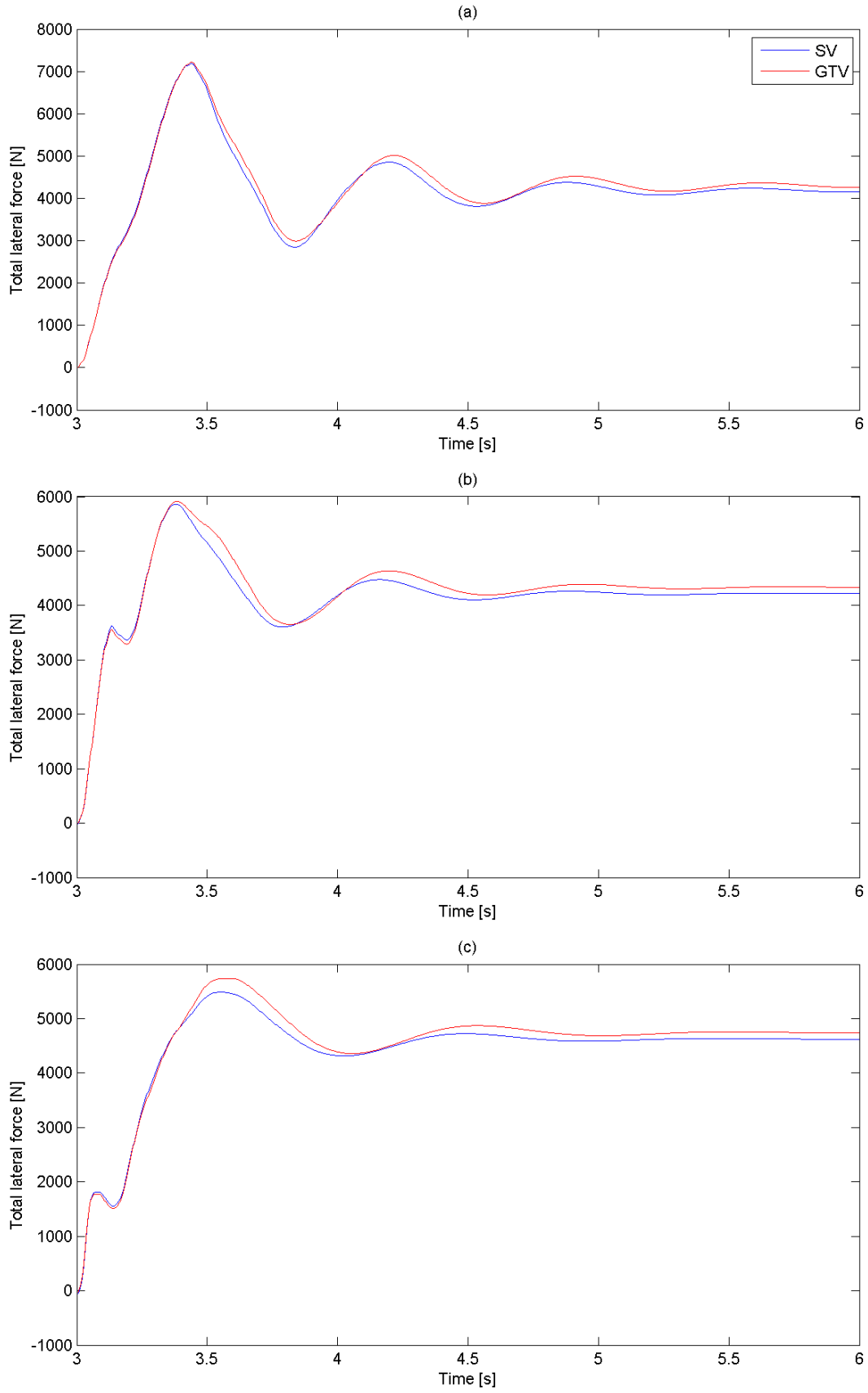

Figure 6-14 Total lateral tyre force responses for 0.2g target ramp to step steer at (a) low, (b) medium and (c) high speed

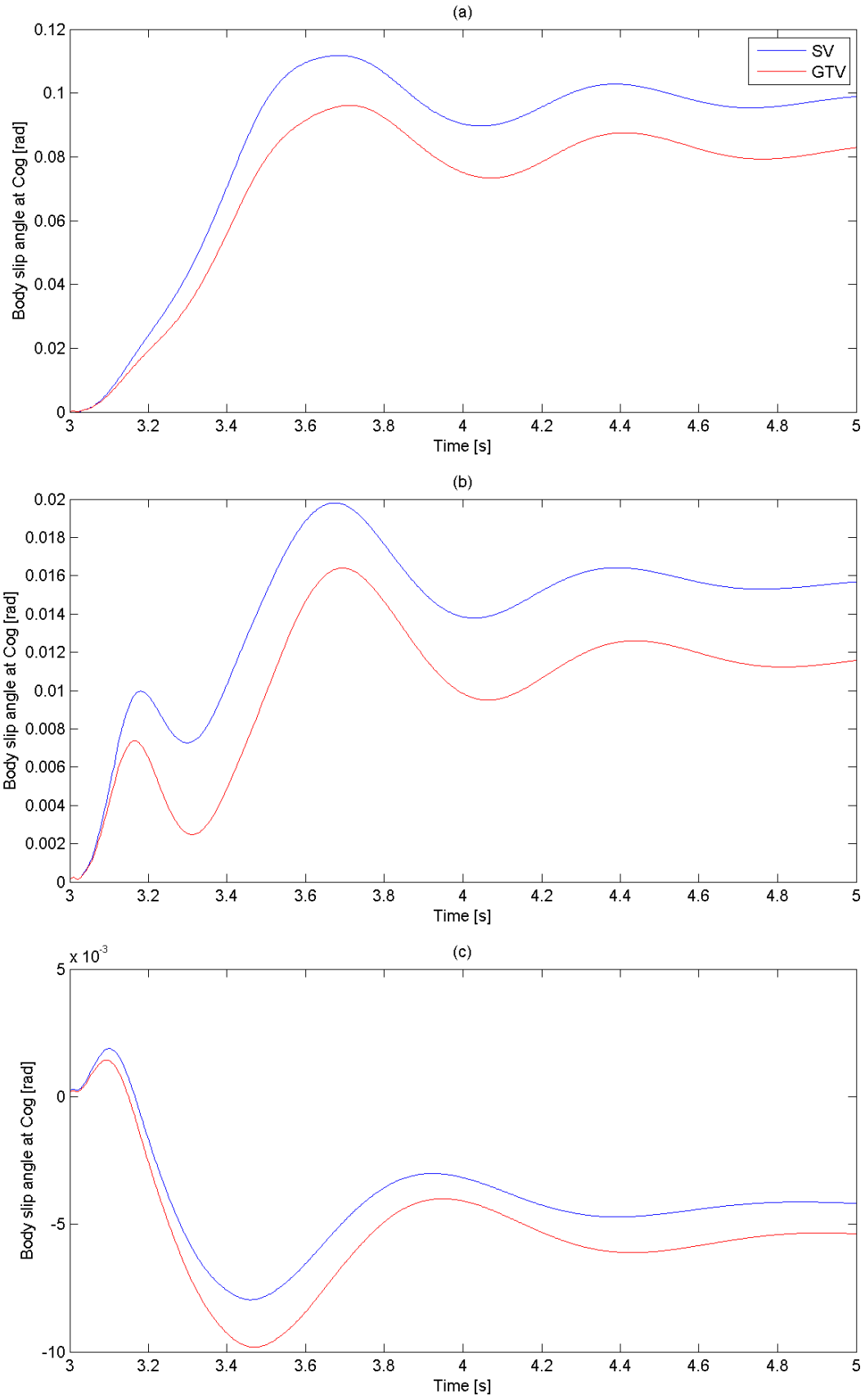

Figure 6-15 Difference in body slip angle response for 0.2g target ramp to step steer at (a) low, (b) medium and (c) high speed

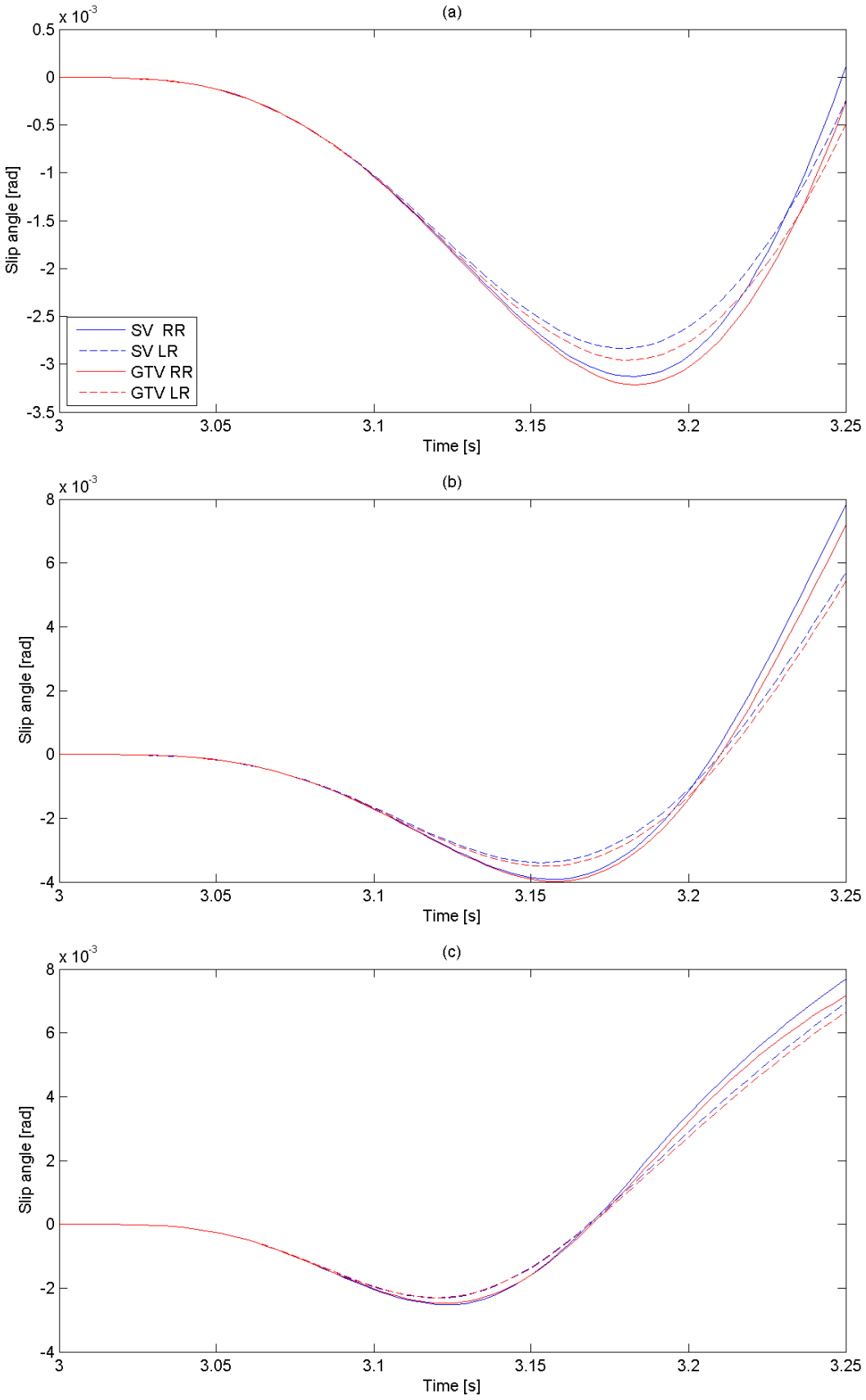

Figure 6-16 Difference in rear tyre slip angle response for 0.2g target ramp to step steer at (a) low, (b) medium and (c) high speed

For the GTV as this point is further rearwards this effect will be larger than for the SV. Considering the low lateral acceleration manoeuvres and responses, it has been shown that in the low speed region, where the effective turn radius is small and so the yaw rate is large, the GTV responds faster, in the medium speed range the response time for the GTV is slower, although here results are a little mixed and it can be said response times for both vehicles are very similar. Within the high speed region where turn radius is now much larger and the yaw rate much lower, the GTV responds slower than the SV. Clearly with the GTV responding faster in the low speed region the effect of the yaw inertia and the DI are not the only factors at play.

It was previously shown that the body slip angle at the Cog of both vehicles changes with speed and effective radius due to steer angle changes. At low speeds with a small effective radius when the steer angle is large, the body slip angle at the Cog is positive, in the medium speed range it is still positive but smaller and in the high speed range on a large radius, with small steer angle it is negative. These body slip angles combined with the DI effects are what are dictating the response times of the vehicles.

To illustrate what is occurring we shall go through the mechanism of the vehicles initial turn in, in detail. As previously mentioned both vehicles have DI's larger than one, hence at the time when the initial steering angle is applied both vehicles begin to yaw about the CoP, which is behind the rear axle. This generates slip angles at the rear tyres in the incorrect direction to negotiate the corner, at this point the rear tyres will generate a lateral force out of the turn. The first effect of this, is that, this yaw in about the CoP creates a positive body slip angle. Simultaneously, due to the direction of tyre forces a very large yaw moment is created about the Cog, this can be seen in Figure 6-17 and Figure 6-18 which shows the yaw moments and

corresponding yaw accelerations for each vehicle. If these two figures are compared to Figure 6-16 which shows the rear tyre slip angles it can be seen that the peak yaw moments and yaw accelerations align with the minimum values of the rear tyre slip angles, as this is when there is the biggest difference between front and rear slip and so also front and rear cornering force. As this yaw moment about the Cog builds the vehicle will transition from yawing about the CoP to yawing about the Cog, as this happens the rear tyre slip angles will be generated in the correct direction for cornering and the vehicle will then begin to yaw about the turn centre with a body slip angle. It has already been shown that in the low speed region the vehicle operates with a large positive body slip angle, so the effect of the initial yaw about the CoP means that this is generated in the correct direction and so when the transition from yawing about the CoP to the Cog to the turn centre occurs no change in body slip angle is needed as it continues to build in the positive direction. Furthermore as the CoP is further behind the rear axle for the GTV this effect is larger, meaning the GTV will generate a larger yaw moment and hence obtain a larger yaw acceleration than the SV. In the medium speed range the same effects take place, however within this region, due to the steer angle and rear slip angles the body slip angle has reduced. Now the initial yaw about the CoP creates a larger positive body slip than required, due to this during the transition from yaw about the CoP to about the turn centre, there exists an oscillation in body slip, see Figure 6-15. As the GTV has a higher yaw inertia than the SV any changes in its body slip angle will take longer, it is this that slows the response of the GTV and so the SV responds faster, in this medium speed low g region.

A similar effect occurs in the high speed region, except here it is more pronounced as the vehicles operate in this region with a negative body slip angle.

Again due to the yaw about the CoP a positive body slip angle and large yaw moment are produced, during the yaw transition phase now a complete reversal in body slip must take place and so again due to its larger yaw inertia the GTV transitions slower and so responds slower in yaw than the SV.

The slower responses of the GTV at higher speeds can also be attributed to the faster generation of tyre slip angles at these speeds and a reduction in the yaw damping. It was mentioned how the inertial effects create large yaw moments due to the negative rear tyre slip angle, as speed increases these slip angles will be generated faster, also yaw damping will reduce, meaning that the vehicle will respond faster to these perturbations in rear slip not allowing their full effect to take place. This is illustrated in Figure 6-18 which shows the yaw acceleration of the two vehicles, notice that in the low speed region the extra rearwards offset of the CoP on the GTV leads to a larger yaw moment and hence larger yaw acceleration, enabling it, despite its larger yaw inertia to respond faster. As the speed increases, these inertial effects become less influential as they cannot develop the rear slip angle to the full extent to which they could at lower speeds, as the transition phase begins earlier. Due to this the GTV does not generate as large yaw moments and corresponding yaw accelerations as it did at lower speeds, combining this with its larger yaw inertia contributes to its slower response at higher speeds. This can also be witnessed in Figure 6-16 which shows that as speed increases the magnitude of the negative slip angle induced becomes much smaller and more equal between the two vehicles.

As previously mentioned a similar trend in yaw rate response time is observed in the high lateral acceleration regions, although here the GTV only responds faster in the low speed region. The same mechanisms mentioned above are also responsible

for the responses here. The only difference is that the body slip angle becomes smaller and eventually negative sooner, as the tangent speed is reached sooner in this speed region, this was mentioned when discussing the lateral acceleration responses and is shown in Figure 6-19.

These results suggest that below the vehicles tangent speed it is possible for the GTV to respond faster in yaw, however, closer to, or above this speed the GTV will respond slower due to body attitude changes taking longer because of its higher yaw inertia.

6.2.5 Yaw Rate Response's

Within the low lateral g range the GTV exhibits larger and more oscillatory yaw rate responses across low, medium and high speed ranges.

There are two main contributors to the GTV achieving larger yaw rates in the low lateral acceleration range. The first and primary reason relates to the production of the yaw moment. When discussing the yaw rate response times it was shown that due to the vehicle inertial properties, during the initial transient part of the manoeuvre the GTV was able to create a much larger yaw moment. If we look at the timing of the peak of this yaw moment and the timing of the yaw rate responses in the low lateral acceleration region, it can be said that the two occur very closely together. The effect of these two responses occurring closely to each other is that the yaw rate will be larger than if they didn't coincide. As the yaw moment produced by the GTV is larger than that produced by the SV its corresponding yaw rate is larger.

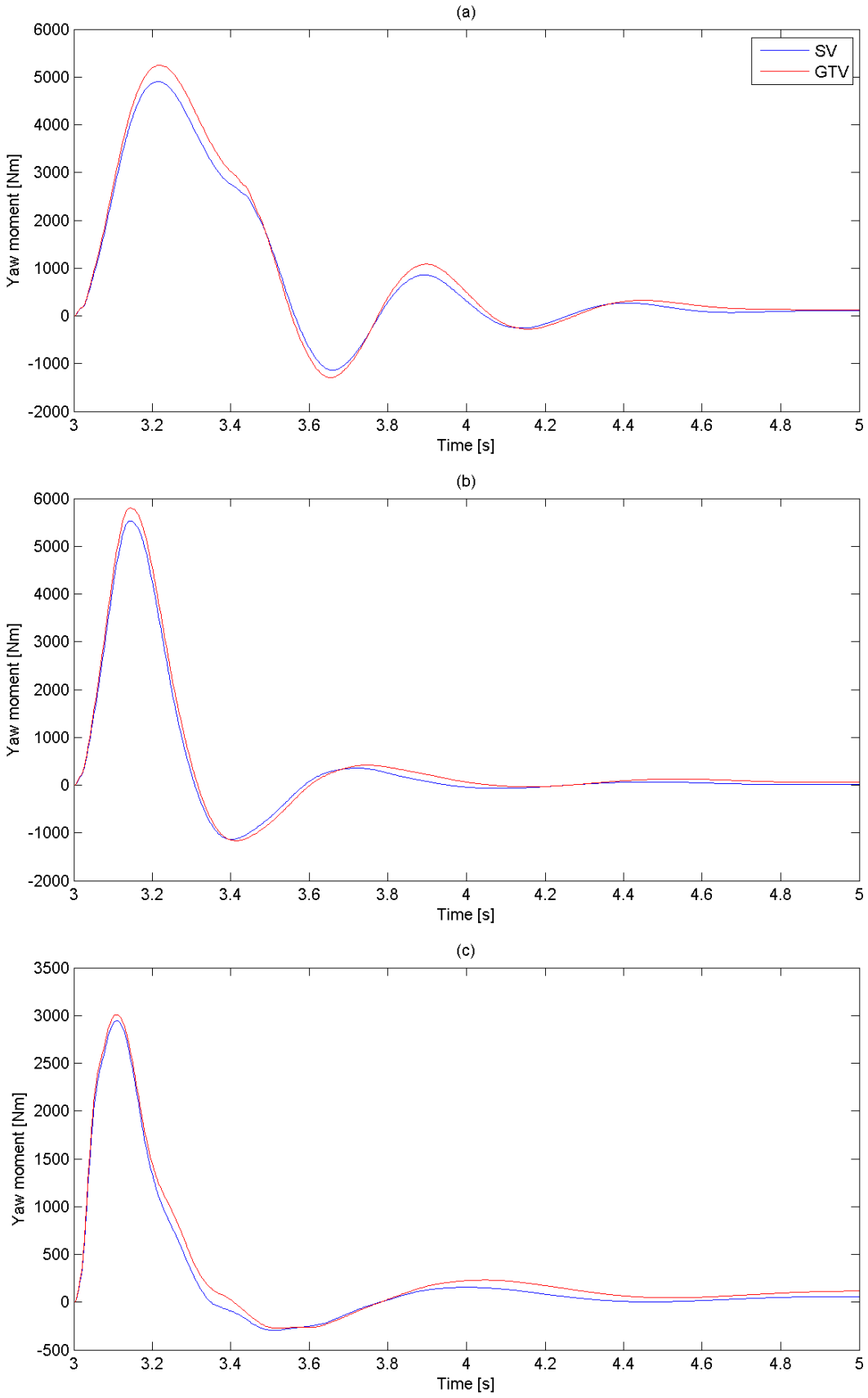

Figure 6-17 Difference in yaw moment responses for 0.2g target ramp to step steer at (a) low, (b) medium and (c) high speed

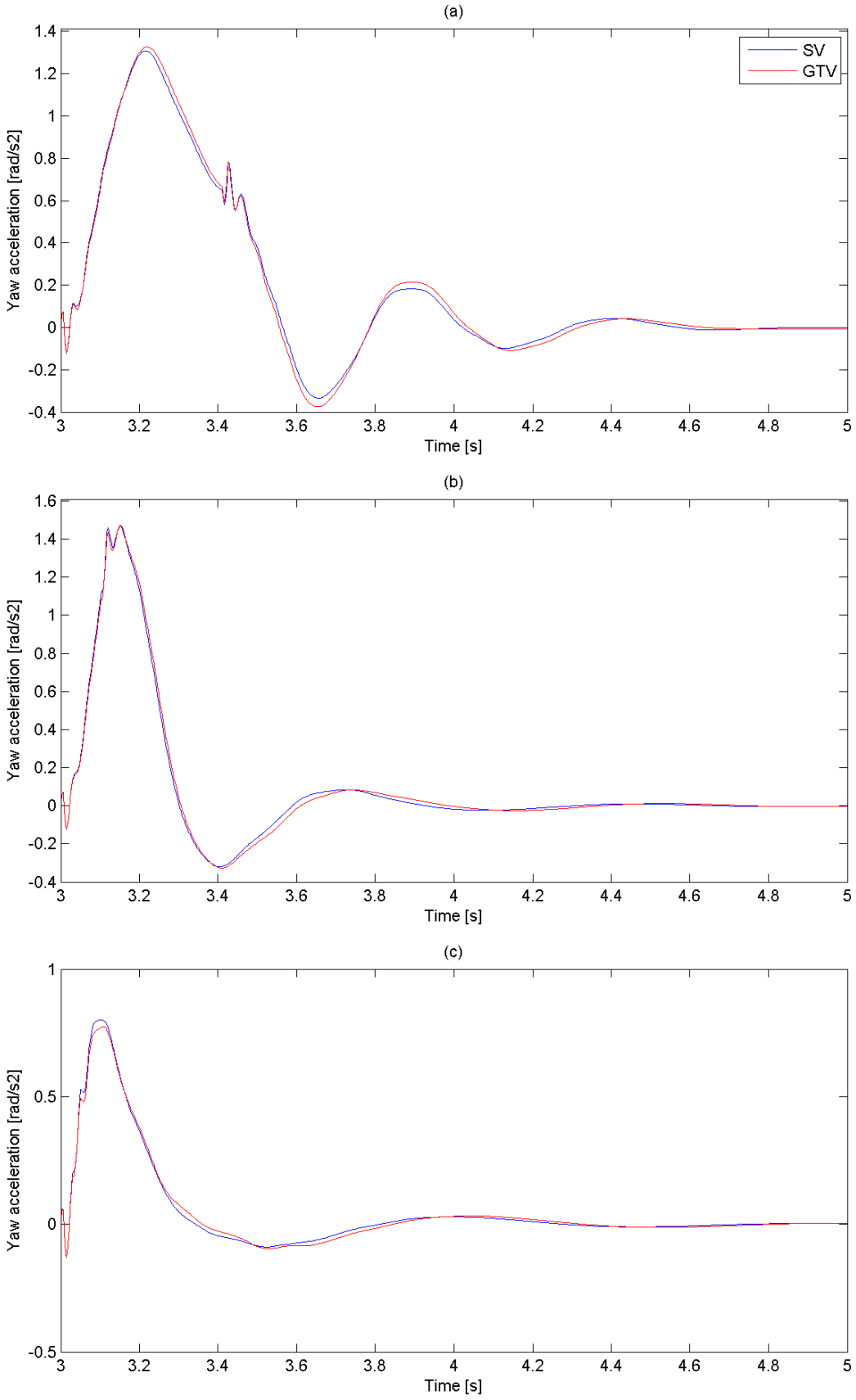

Figure 6-18 Difference in yaw acceleration responses for 0.2g target ramp to step steer at (a) low, (b) medium and (c) high speed

The second contributor to the GTV achieving a larger more oscillatory yaw rate than the SV in this region is due to its more centralised weight distribution, this in itself has two effects, the first of which is that the yaw moment produced by the front tyres will be increased, this can be seen in Figure 6-40 as the difference in the steady state yaw moments. It is also one of the derivatives of the bicycle model (N_δ) mentioned in chapter 4 and simply is a measure of the size of the yaw moment produced by the steered angle. The other effect of having a more centralised weight distribution is that the yaw damping is reduced, this can be shown by the N_r derivative of the bicycle model.

So with its capability to produce a larger yaw moment due to its inertial properties and weight distribution, combined with its reduced yaw damping, it is easy to see why in this low lateral acceleration region the GTV obtains larger more oscillatory yaw rate responses.

Moving on to the high lateral acceleration regions, it was shown, that despite what has been mentioned for the low lateral acceleration regions, yaw rate responses of the GTV here are smaller at low speed. In the medium and high speeds again responses for the GTV are larger.

Firstly let us consider the difference in manoeuvre between low and high lateral acceleration regions. As the lateral acceleration increases, so must the speed (fixed radius), as the speed increases the steady state yaw rate must also increase, to be able to negotiate the same radius corner. This means that in the high lateral acceleration regions the resulting yaw rates will be larger than in the low lateral acceleration regions. It has also been shown that generally the yaw rate response times increase as the lateral g increases. If we re-visit the first reason given for the yaw rate response being larger in the low lateral acceleration regions, it was shown that the

large yaw moment produced by the vehicles' inertial effects during the transient part of the manoeuvre coincided closely with the peak yaw rates. Here, in the high lateral acceleration region, this is no longer the case, especially at low speed. Consider Figure 6-13 and Figure 6-20, which show the yaw rate responses and the yaw moments in the high lateral acceleration regions. Notice now the large peak in yaw moment occurs considerably before the peak in yaw rate, this is especially apparent in the low speed range where the yaw rate response time is longest. This means that in this low speed range the GTV is not receiving as much of a benefit from its larger yaw moment in terms of its peak yaw rate response, purely as the yaw rate is larger and so takes longer to build. This effect is most pronounced in the low speed region, it can be seen that at about 3.5 seconds, near where the yaw rate peaks, the yaw moments of both vehicles have diminished and are more equal for both GTV and SV. The yaw rate responses in the low speed region are largest and so this is where the yaw rate response times are longest, as the speed increases the yaw rates become smaller and so do the response times, meaning that in the medium and high speed regions the yaw rate response more closely coincides with the large peak in yaw moment caused by the inertial effects, meaning that the GTV, in these regions does see the benefit of its larger peak yaw moment, and so achieves larger peak yaw rates than the SV.

These results suggest that for manoeuvres with large yaw rates, or more sedate manoeuvres where yaw rate response times are longer the GTV will exhibit smaller peak yaw rates than the SV, however for manoeuvres with smaller yaw rates or more severe manoeuvres indicating quicker yaw rate responses the GTV will exhibit larger peak yaw rates, which are more oscillatory.

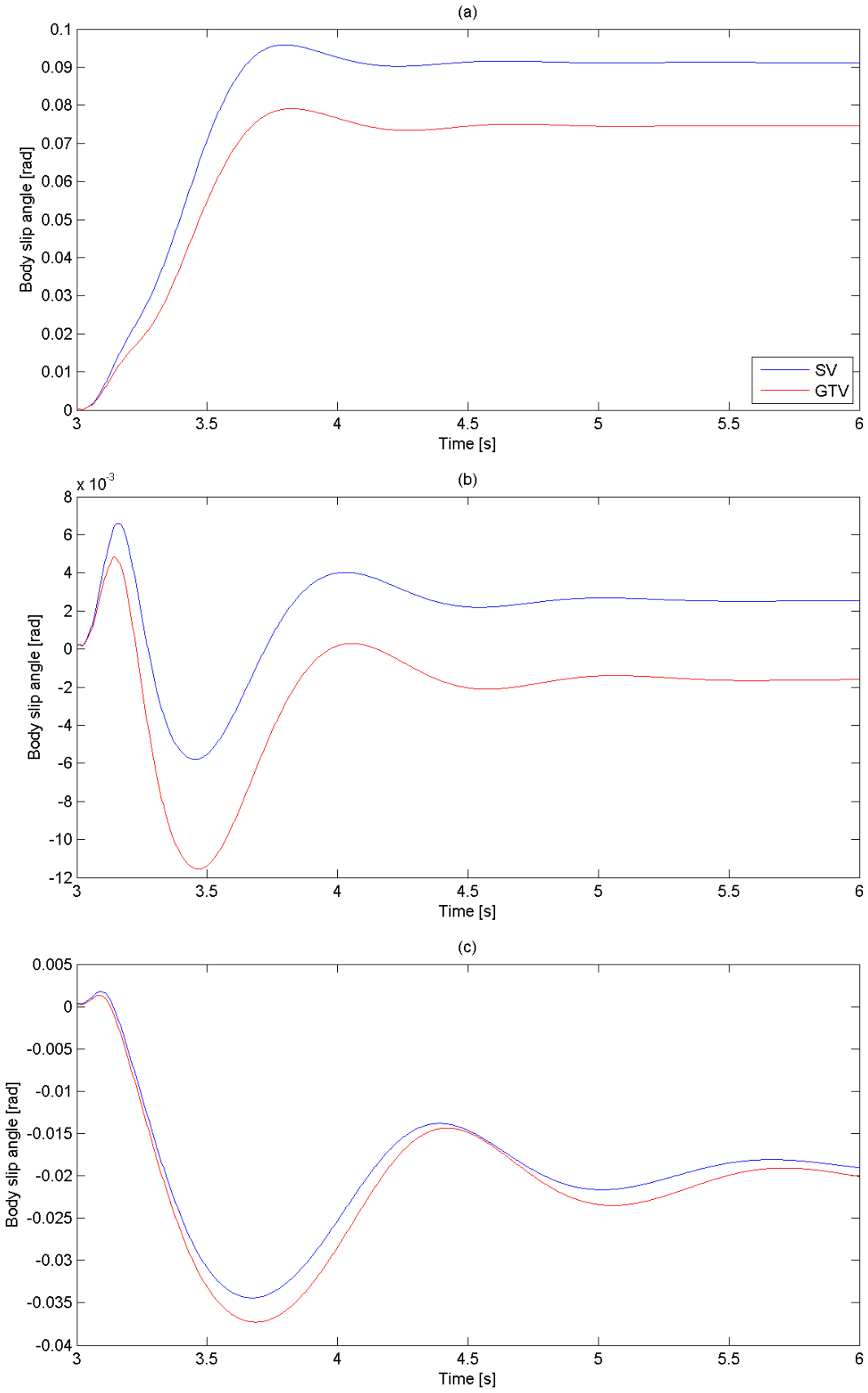

Figure 6-19 Difference in body slip angle response for 0.4g target ramp to step steer at (a) low, (b) medium and (c) high speed

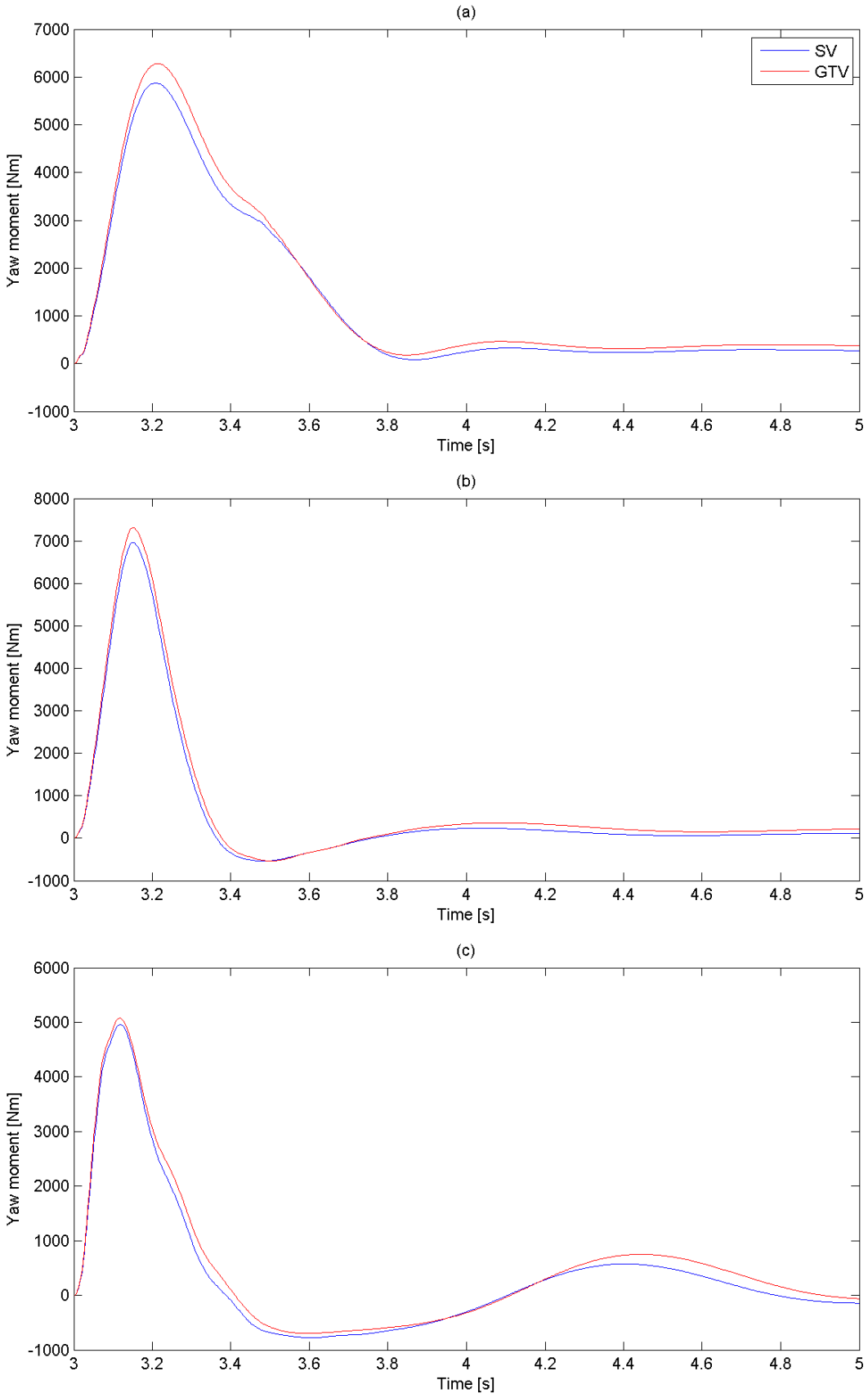

Figure 6-20 Difference in yaw moment response for 0.4g target ramp to step steer at (a) low, (b) medium and (c) high speed

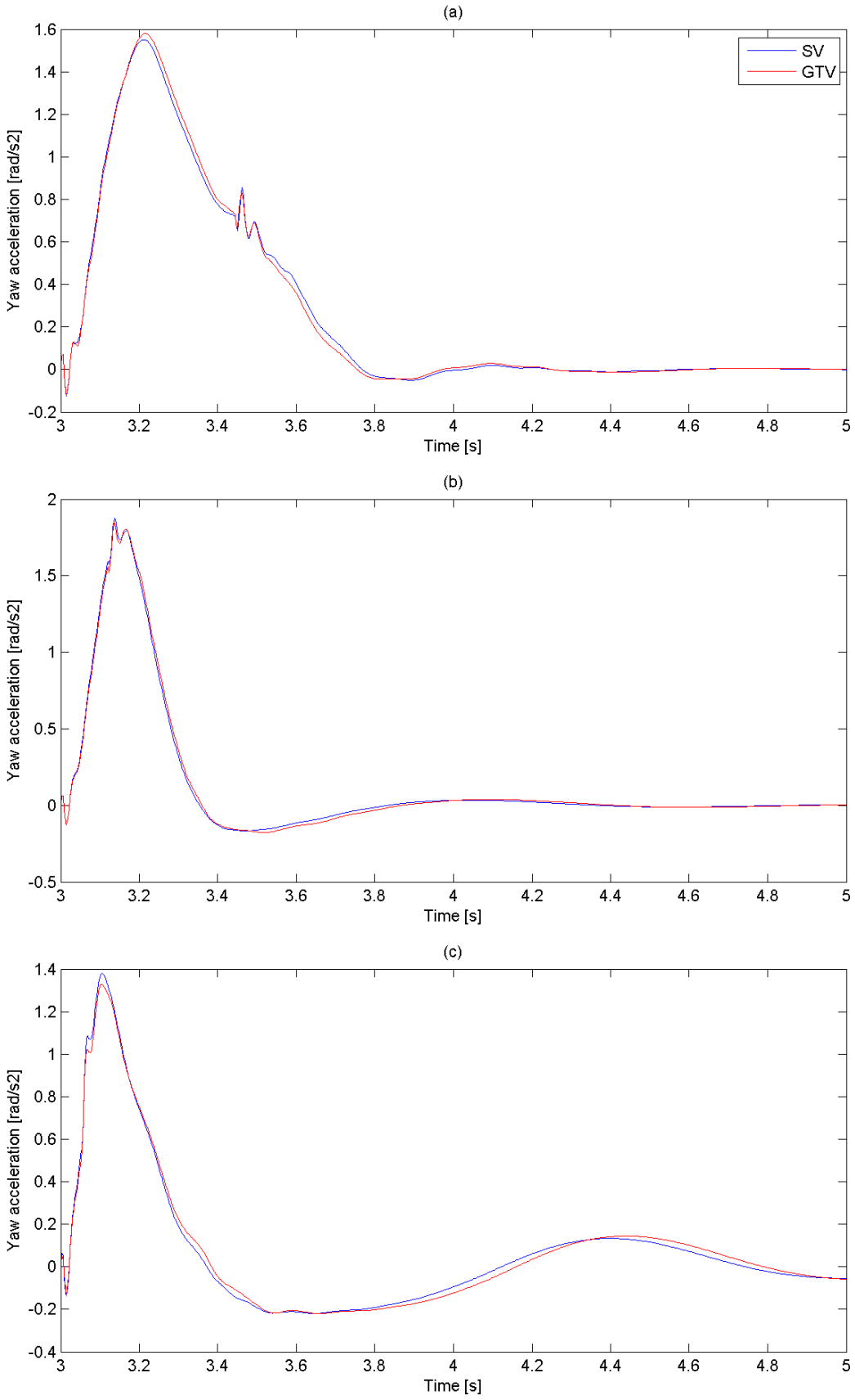

Figure 6-21 Difference in yaw acceleration response for 0.4g target ramp to step steer at (a) low, (b) medium and (c) high speed

Such effects could be dangerous as generally yaw rates are smaller at higher speed and larger at lower speeds, the aforementioned effects could result in the GTV producing higher peak yaw rates at high speed and lower peak yaw rates at low speed (when compared to the SV), resulting in a vehicle that could feel less responsive at low speed an too responsive or unstable at high speed.

6.3 Sinusoidal Steer Results

Sinusoidal steer manoeuvres as described in chapter 4 were performed with both vehicles. Steering angles and longitudinal velocities derived from the constant radius tests, as used for the ramp to step steer manoeuvres, were again used here. Although the sinusoidal steer manoeuvre has no steady state region, these steer angles and velocities allow certain values of steady state lateral acceleration to be targeted, allowing manoeuvres to be categorised in the same six regions as the ramp to step steer manoeuvres. Simulations were carried out with a 0.5 Hz steering input frequency and in both a clockwise (right initial turn) and anti-clockwise (left initial turn) direction.

As with the ramp to step steer manoeuvres certain metrics were calculated from the vehicle responses in order to quantify handling differences, these metrics will be presented in the following sections, and the trends that they identify investigated further.

6.3.1 Sinusoidal Steer Metrics

Figure 6-22 and Figure 6-23 show the first and second peak lateral accelerations for the sinusoidal steer manoeuvre, the first and second peaks relate to the left and right turn respectively. Looking at Figure 6-22 it can be seen that in the low speed range (a) that the peak responses of the GTV are smaller than those of the SV across the majority of the lateral acceleration range. As lateral acceleration increases the peak

responses become more similar until at limit handling they are more or less identical. The figure also shows that both vehicles exhibit a more oscillatory response in the low speed low lateral acceleration range, the overshoot of the response diminishes as lateral acceleration increases, this occurs for the SV more so than for the GTV. Figure 6-22 (b) which shows the medium speed range illustrates very linear peak lateral acceleration responses across the entire lateral acceleration range. Here between 0.1g and 0.25g the peak responses of the two vehicles are very similar, as we move into the high lateral acceleration range it is the GTV that exhibits the greater peak lateral acceleration responses. In (c), the high speed region, the GTV yields higher peak lateral acceleration responses across the whole of the lateral acceleration range. In the low lateral acceleration region the responses of both vehicles are very similar but as lateral acceleration increases, so does the difference between the two vehicles' responses.

Figure 6-23 again shows peak lateral acceleration responses but for the second peak. Trends here are much the same as what has just been discussed with regard to Figure 6-22. Although it can be seen in (a) that the responses for both vehicles are much less oscillatory, overshoot in the low lateral acceleration range has reduced and continues to decrease as lateral acceleration increases, so much so that in the low speed, high lateral acceleration region there is in fact no overshoot at all as the peak responses do not reach the targeted steady state responses. The medium speed responses in (b) are very similar to the first peak responses only opposite in sign. The high speed region (c) also shows similar responses to those seen for the first peaks, it should however be noted that the responses are more similar to each other, there is less of a difference between the two vehicles. One main difference between

the first and second peak responses in the high speed, high lateral acceleration range is that the responses of both vehicles are more oscillatory.

At low speed in both low and high lateral acceleration regions, the first peak response is larger than the second, at medium speed the same is true until 0.45g, where after the second peak is larger than the first. In the high speed region the second peaks are larger than the first from 0.25g onwards. This clearly shows that as speed is increasing the overall response is becoming more oscillatory as the second peak is becoming larger than the first. This effect is slightly more pronounced for the GTV, meaning the difference between the GTV's first and second peak lateral accelerations is greater than those of the SV.

Figure 6-24 and Figure 6-25 show the first and second peak lateral acceleration response times. This is the time taken from the initial steering input to the time when the lateral acceleration reaches its first and second peaks respectively. In Figure 6-24 it can be seen that the GTV responds slower across all speed and lateral acceleration ranges. In the low speed region (a) the difference between the two vehicles steadily grows as lateral acceleration increases, in the medium speed range (b) the opposite is true and in the high speed range (c) the difference between the two vehicles is fairly constant over the entire lateral acceleration range. It should be noted that as a whole the response times increase as speed increases.

Figure 6-25 shows the response times for the second lateral acceleration peaks. Here the situation is not as clear as it was when discussing the first peak response times. For the second peak response times, in the low speed region, the GTV again has slower responses, but now only until 0.3g, at 0.35g the responses of the two vehicles are identical and from there onwards the GTV responds faster.

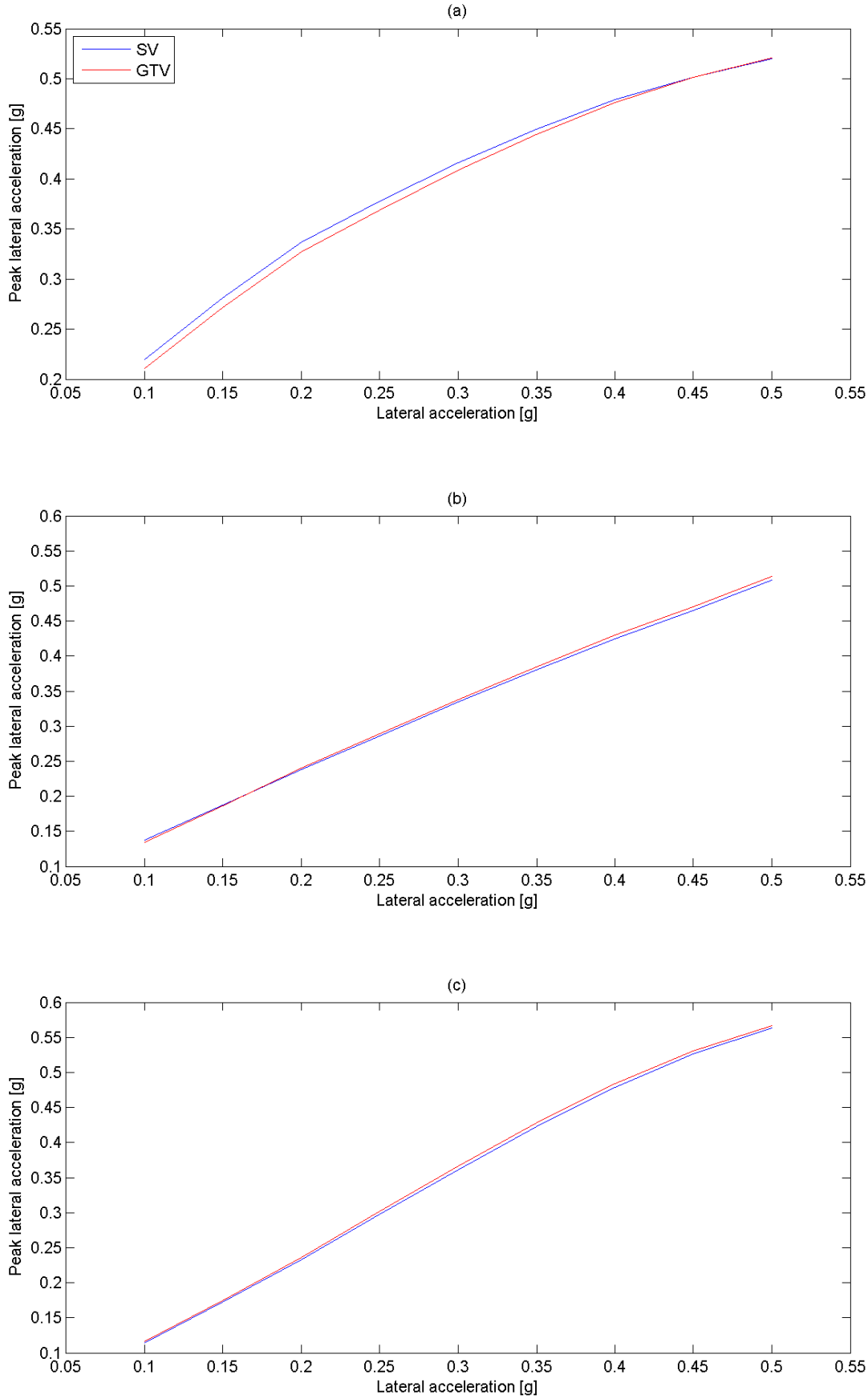

Figure 6-22 First peak lateral acceleration for (a) low, (b) medium and (c) high speed

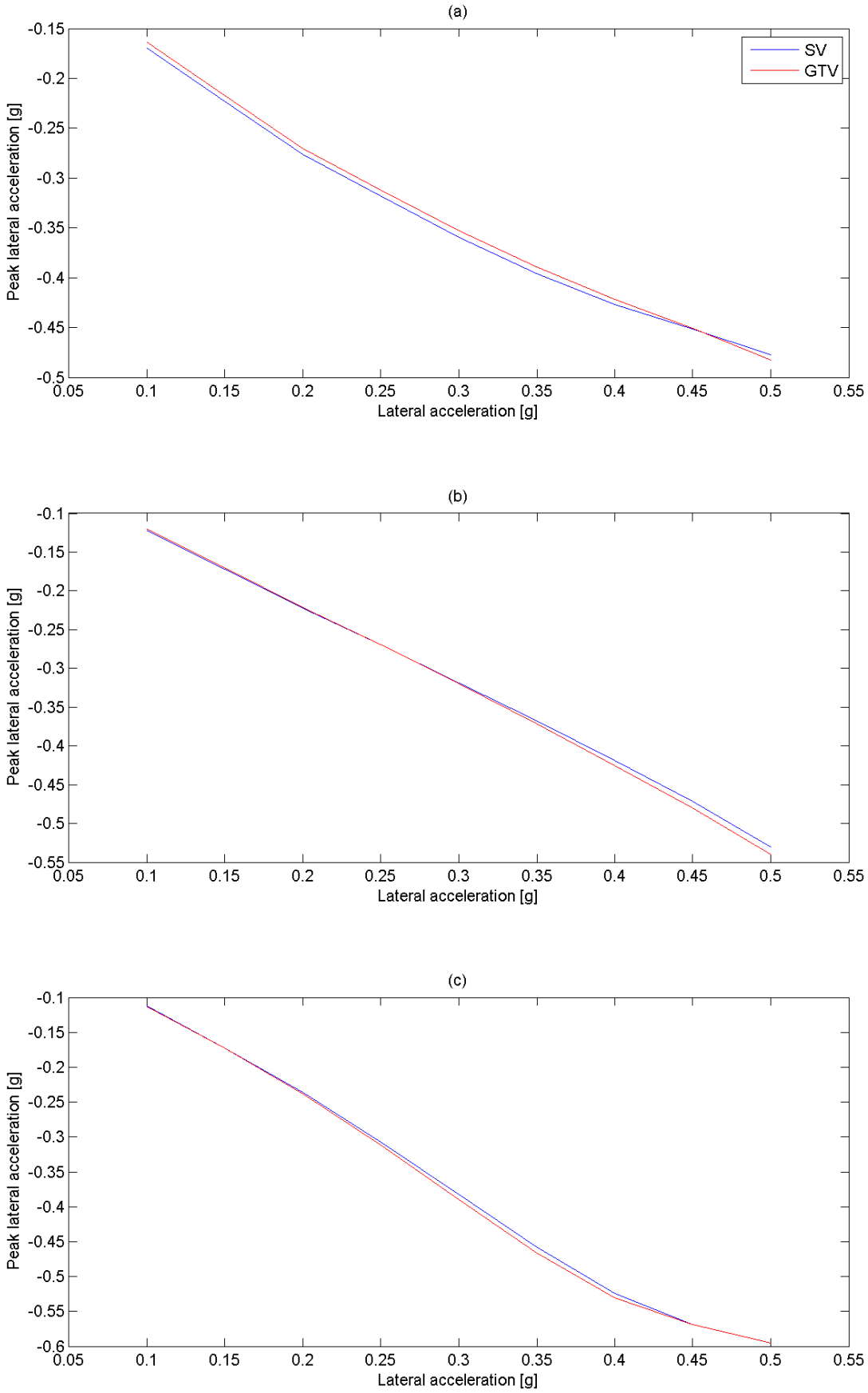

Figure 6-23 Second peak lateral acceleration for (a) low, (b) medium and (c) high speed

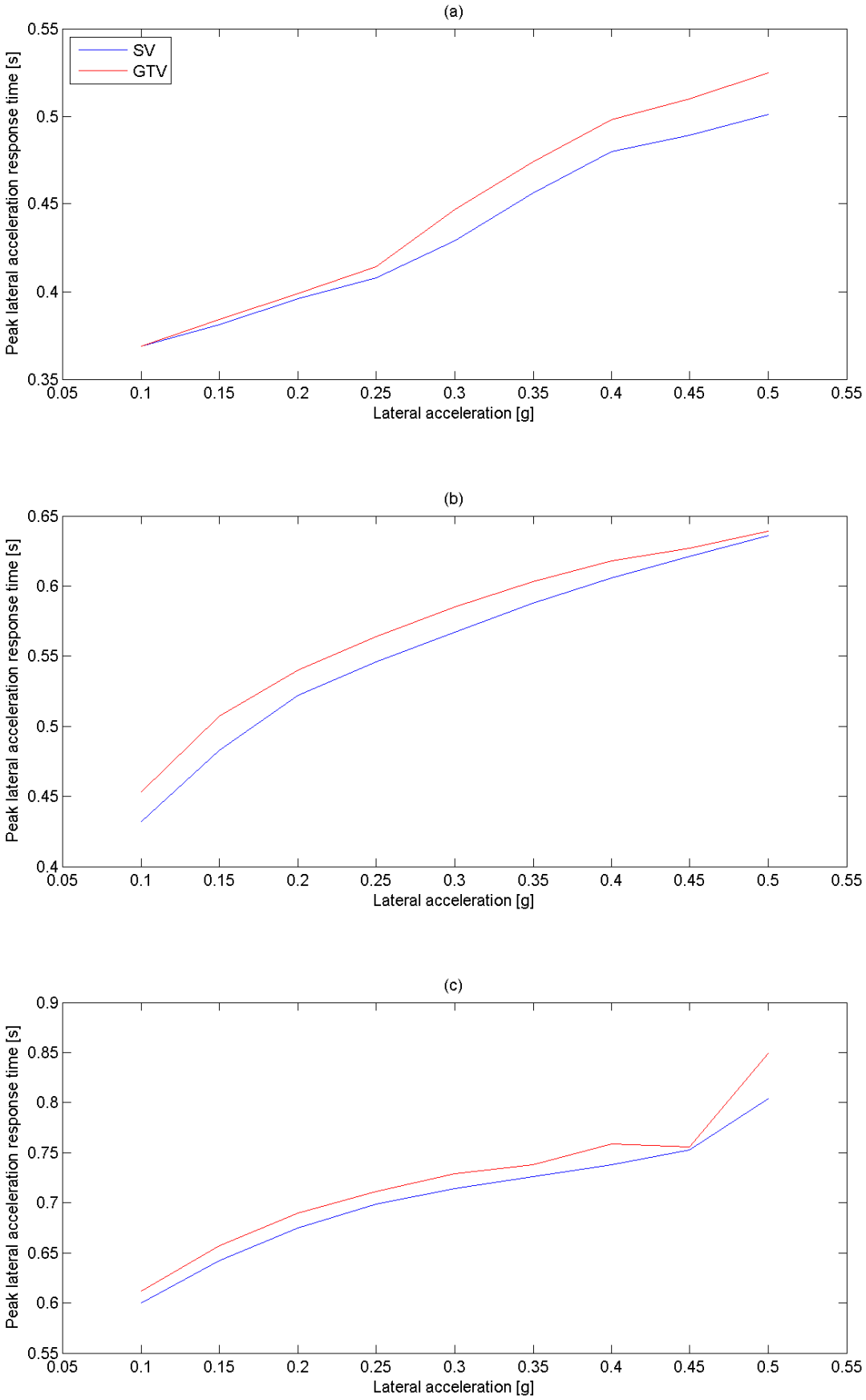

Figure 6-24 First peak lateral acceleration response time for (a) low, (b) medium and (c) high speed

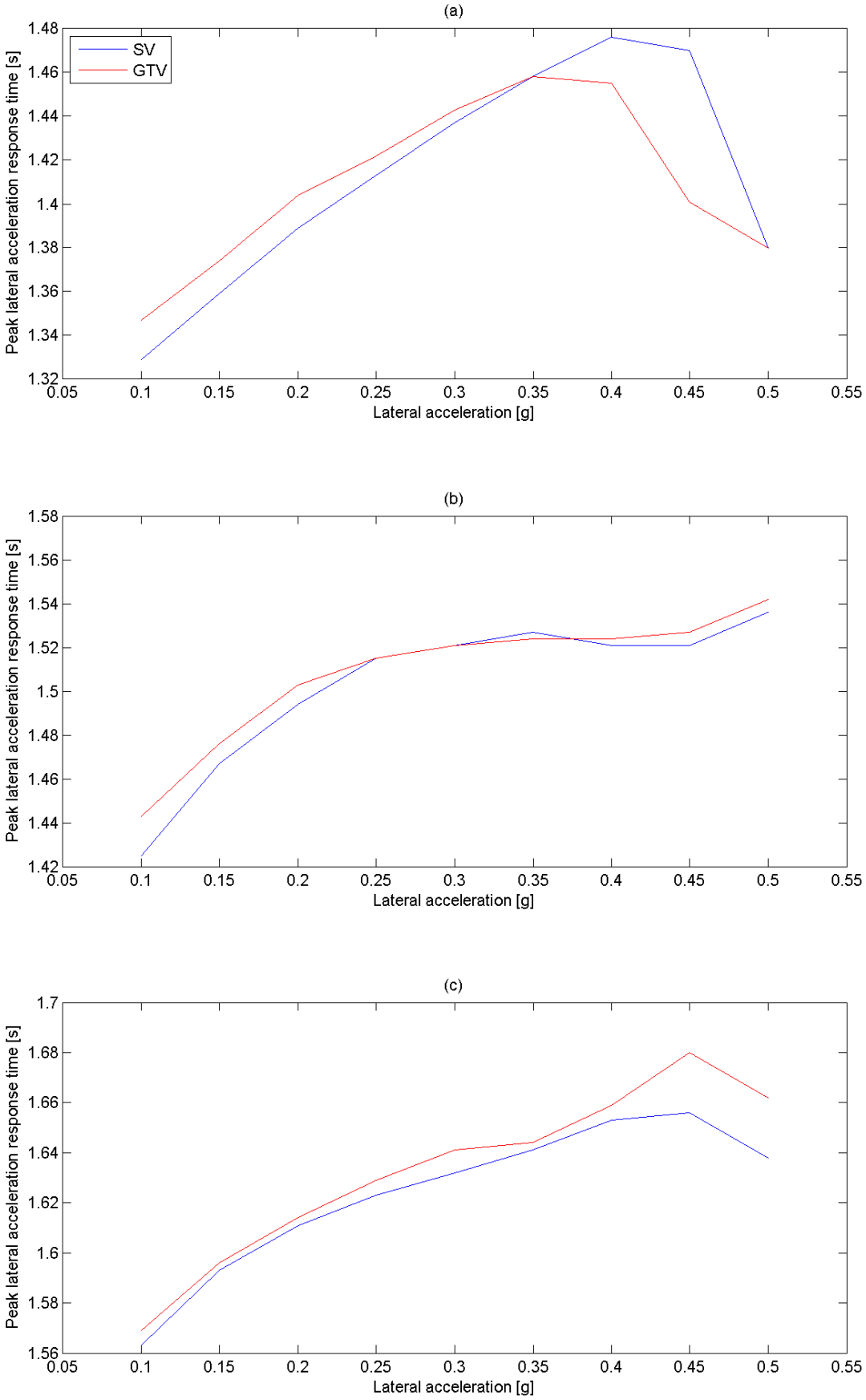

Figure 6-25 Second peak lateral acceleration response time for (a) low, (b) medium and (c) high speed

In the medium speed range it can be said that in general the GTV responds slower than the SV, although between 0.25g and 0.35g responses of the two vehicles are very similar. Finally in the high speed range, it is the SV that responds faster over the entire lateral acceleration range. Again for the second peak lateral accelerations as with the first peaks the quickest response times are seen in the low speed range and the longest in the high speed range.

Figure 6-26 and Figure 6-27 show the phase differences between peak lateral acceleration and yaw rate responses for the first and second peak responses respectively. As in the ramp to step steer section a negative phase difference relates to yaw rate reaching its peak value before lateral acceleration. Looking at Figure 6-26 within the low speed range (a), it seen that the GTV exhibits smaller phase lags between lateral acceleration and yaw, with lateral acceleration occurring before yaw rate for both vehicles across the entire lateral acceleration range. This indicates that both vehicles in this low speed range, during the first phase of the sinusoidal steer operate with positive body slip angles. The phasing increases as lateral acceleration increases, this is due to the yaw rate response time increasing at a greater rate than the lateral acceleration response time as the targeted lateral acceleration increases, this happens to greater extent for the SV.

The medium speed range shown in (b) shows that in the low lateral acceleration region the GTV again exhibits a smaller phase lag than the SV, however as the vehicles cross from low to high lateral acceleration, the phase becomes negative, indicating that yaw rate is now occurring before lateral acceleration (again indicating transition from below to above the tangent speed), this shows the transition from positive to negative body slip angle at the Cog, this happens at a lower lateral acceleration (and longitudinal velocity) for the GTV than it does for the SV due to

the more reward position of its Cog. In the medium speed, high lateral acceleration range the phasing of lateral acceleration and yaw is still larger in magnitude for the GTV. The phasing becomes negative as the lateral acceleration increases due to the lateral acceleration response slowing at a greater rate with increasing targeted lateral acceleration than the yaw rate response. The difference between the two vehicles also diminishes as lateral acceleration increases. This is opposite to what is occurring in the low speed range.

In the high speed range shown in (c), the phasing is negative for both vehicles over the entire lateral acceleration range. The GTV exhibits a larger phase difference than the SV over the majority of the lateral acceleration range and the magnitude of the phase lag increases with lateral acceleration, similarly to the medium speed range. It can be seen that the variation in phase lag over the lateral acceleration range is much greater here than it is in any of the other speed ranges.

As the GTV exhibits less of a phase lag in both the low and medium speed ranges it indicates that its body slip angle is less than that of the SV. In the high speed range the GTV has a larger negative phase lag indicating that its body slip angle is likewise negative and larger than that of the SV.

Figure 6-27 shows the phasing of the second peak lateral accelerations and yaw rates. In the low speed low lateral acceleration range shown in (a) the GTV exhibits smaller phase lags than the SV. From 0.3g onwards as we move into the high lateral acceleration range it is now the SV that exhibits smaller phase lags between the two responses. The crossing indicates that the GTV has moved from having a smaller to a larger body slip angle than the SV.

Within the medium speed range a similar trend is shown to the corresponding range from phase differences of the first peak responses, although here it is much

more non-linear. The GTV yields a slightly smaller positive phase difference over the majority of the lateral acceleration range, although between 0.4 and 0.45g the phase difference becomes negative, (again indication the transition from a positive to a negative body slip angle at the Cog) now the GTV exhibits a larger negative phase difference.

The high speed region (c) shows that both vehicles exhibit negative phase differences. In the low lateral acceleration range it is the GTV that has a larger phase difference than the SV. Just before 0.35g the phase differences of both vehicles become very similar and stay so across the rest of the lateral acceleration range.

Figure 6-28 and Figure 6-29 show the first and second peak yaw rates during the sinusoidal steer manoeuvres for both vehicles. The first of these shows that the GTV exhibits larger peak yaw rates than the SV across all speeds and lateral accelerations during this first phase of the sinusoidal steer. In the low speed range the difference between the two vehicles is largest at low lateral accelerations, where the GTV's response is 1.8% larger, this difference diminishes to less than 0.5% at high lateral accelerations. In the medium speed range the difference between the two vehicles remains fairly constant, only varying between 1.4 and 1.9% over the entire range. Again in the high speed range the vehicles' responses are very similar, here, the largest differences are also seen at low levels of targeted lateral acceleration.

Figure 6-29 shows that the yaw rate responses of the second peaks are even more closely matched than the first ones. The low and medium speed ranges show very similar trends. In these two ranges the responses of the two vehicles are almost identical at low values of lateral acceleration. The two vehicle responses become slightly more diverse as the targeted steady state lateral acceleration increases, and

show their most considerable difference at limit handling. For the majority of both test ranges it is the SV that exhibits slightly larger peak yaw rate values, the only exception to this being above 0.45g in the medium speed range where the GTV yields a larger response.

The high speed region shown in (c) shows the largest differences in the vehicle responses. At low lateral accelerations the two vehicles again show almost identical responses, as the targeted lateral acceleration increases the difference between the two vehicles' responses also increases, here it is the GTV that once again yields the largest responses.

Making a comparison between the first and second peak yaw rate responses shows that in the low and high speed regions the peak yaw rate responses of the second peak are larger for both vehicles than those of the first, indicating a more oscillatory response. This however isn't the case for the medium speed range, where the second peak responses are actually slightly smaller than the first.

Figure 6-30 shows the first peak yaw rate response times, as for the lateral acceleration responses, this is the time taken from the initial steering input to when the response reaches its peak value. Response times in the low speed range are fairly linear, it can be seen that in this speed region the GTV responds faster than the SV across all lateral acceleration ranges. In the medium speed range the story is much the same, the GTV responds faster across the entire targeted lateral acceleration range. However here the difference between the two vehicles is smaller than it was in the low speed range. The high speed range shown in (c) illustrates that the GTV now responds slower than the SV over the whole lateral acceleration range. In this high speed region the response times of the two vehicles are most similar in the low

lateral acceleration range, the difference between the two increases as the lateral acceleration increases.

Figure 6-31 again shows peak yaw rate response times, but now for the second peak of the sinusoidal steer manoeuvre. In the low speed range, shown in (a), it can be seen in the low lateral acceleration region the GTV responds faster than the SV. From 0.3g onwards, the high lateral acceleration region, it is the SV that responds faster. The differences in responses in both the low and high lateral acceleration regions, of this low speed range are very small, generally less than 0.5%. The medium speed range shown in (b) is a little clearer as the GTV responds faster across both low and high lateral acceleration ranges. However, once again the differences in the two vehicle responses are very small, up until 0.35g the two vary by less than 1%, towards the limit of handling where the response times decrease quite dramatically the difference becomes larger. The high speed region shown in (c) yields a similar trend to that shown in low speed region. In the low lateral acceleration range the GTV responds faster than the SV, in the high lateral acceleration range, above 0.3g the SV now responds faster. However as has been the case throughout these second peak yaw rate response times, the difference between the two vehicle responses is very small, in the low lateral acceleration range differences are again less than 1%, this only increase to about 2.5% at the limit of handing where the biggest difference is observed.

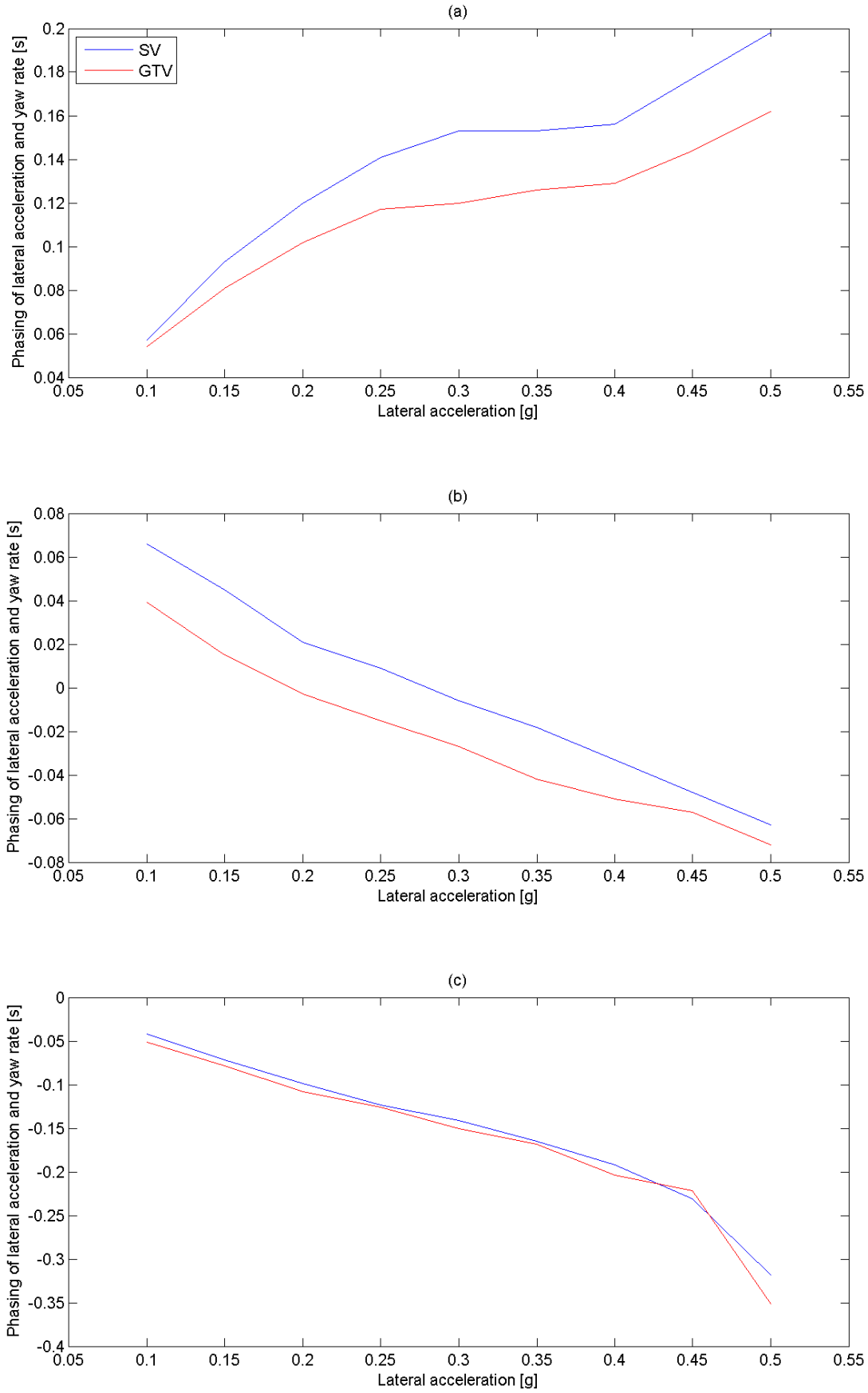

Figure 6-26 Phasing of first peak lateral acceleration and yaw rate responses for (a) low, (b) medium and (c) high speed

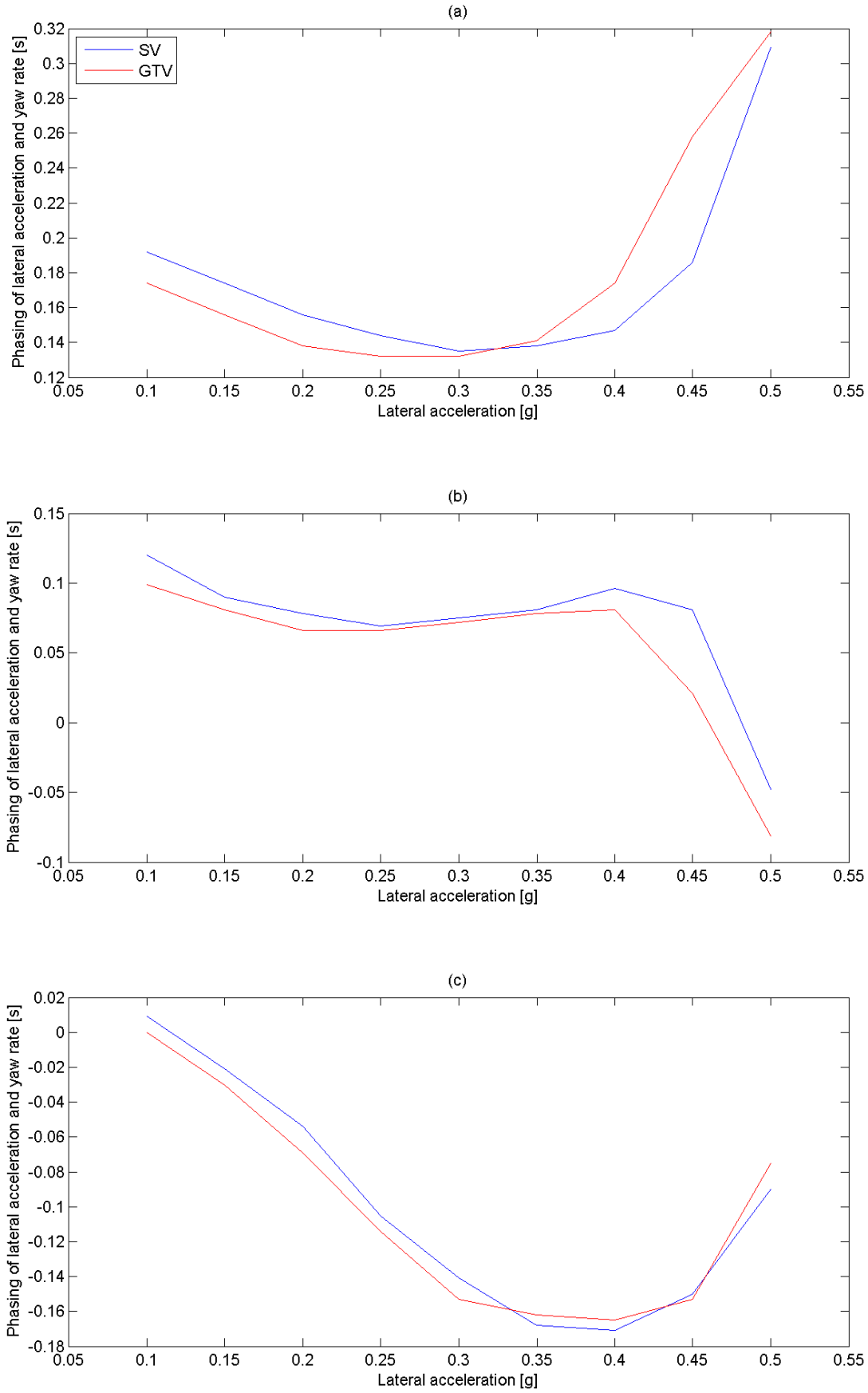

Figure 6-27 Phasing of second peak lateral acceleration and yaw rate responses for (a) low, (b) medium and (c) high speed

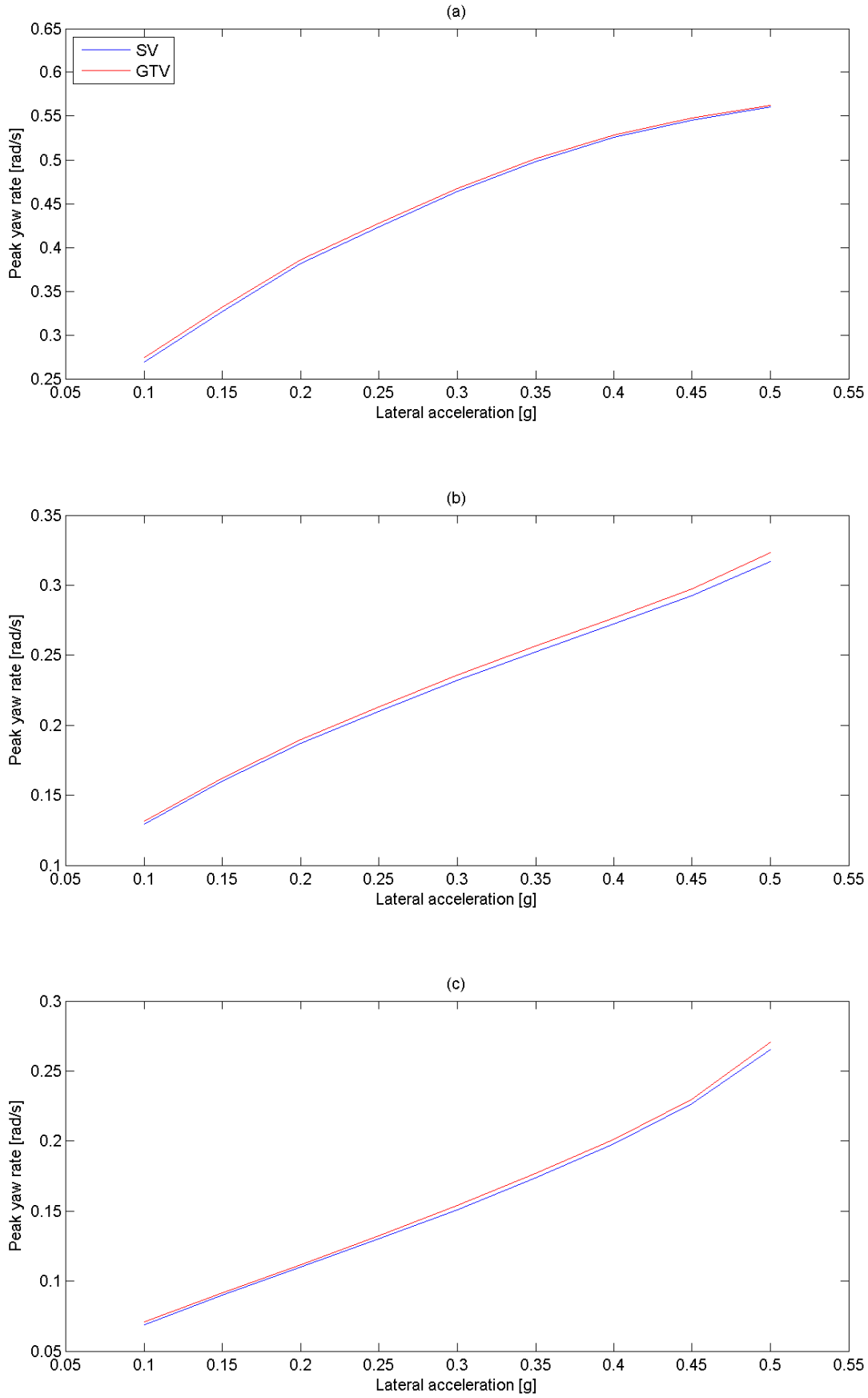

Figure 6-28 First peak yaw rate response for (a) low, (b) medium and (c) high speed

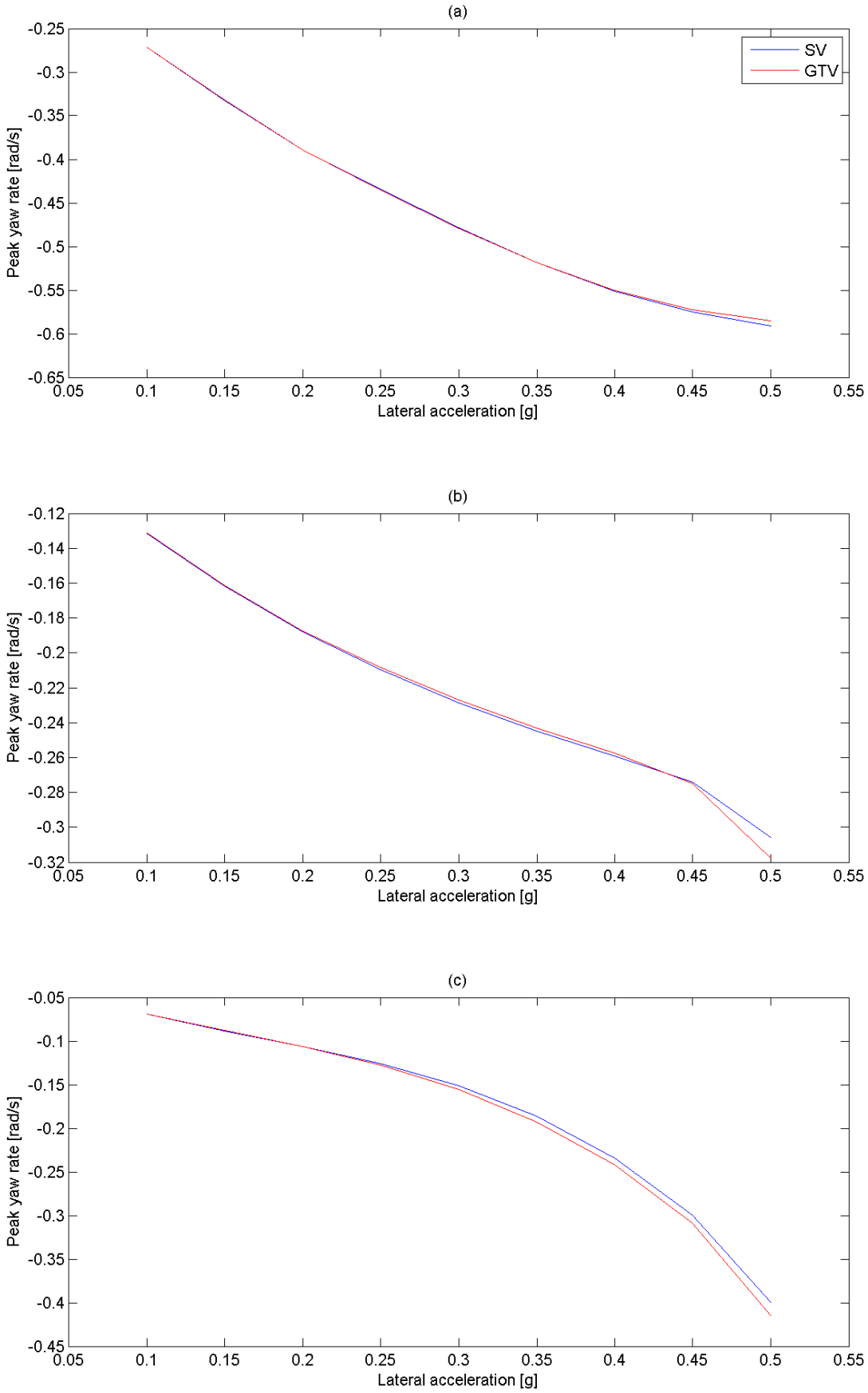

Figure 6-29 Second peak yaw rate response for (a) low, (b) medium and (c) high speed

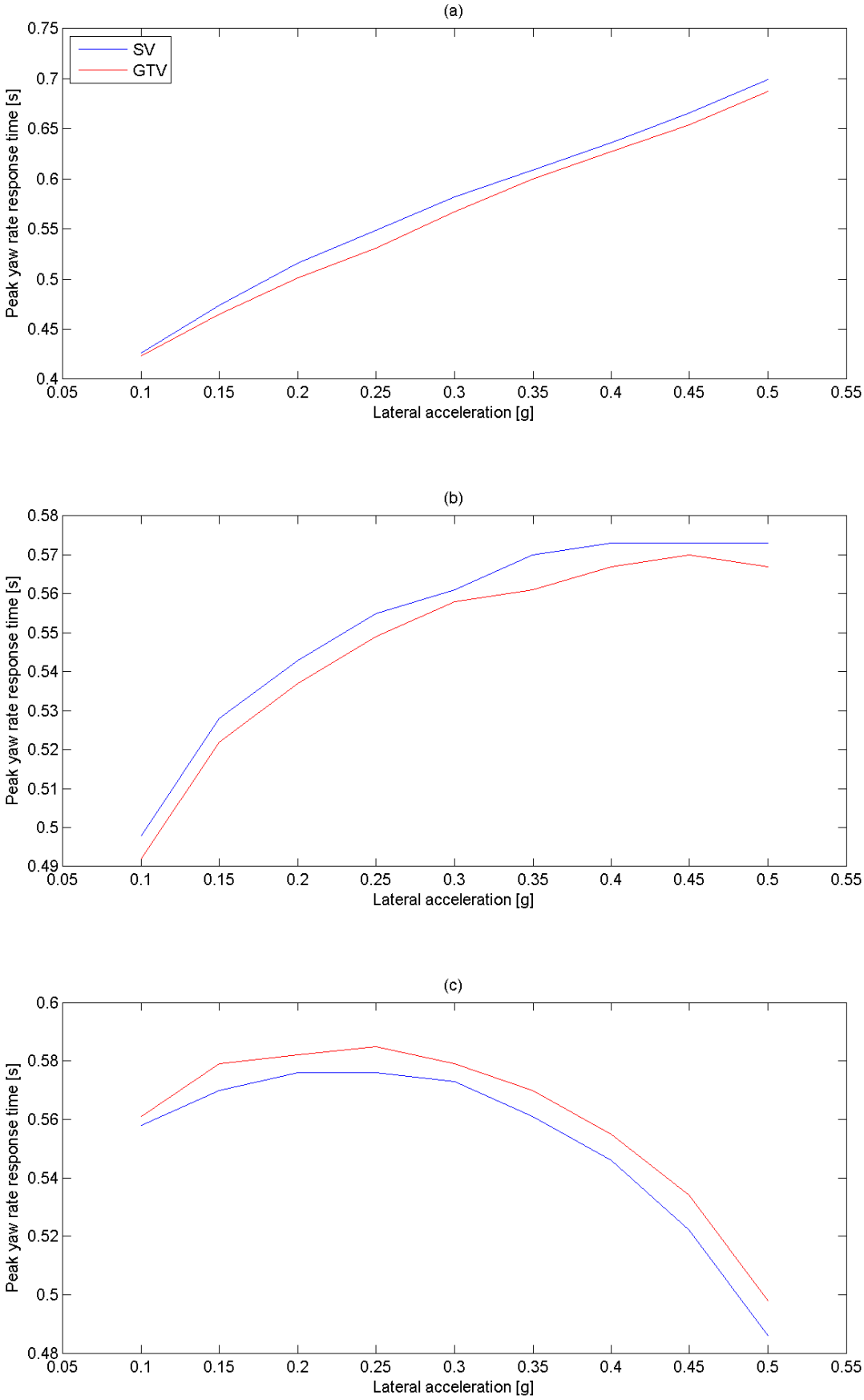

Figure 6-30 First peak yaw rate response times for (a) low, (b) medium and (c) high speed

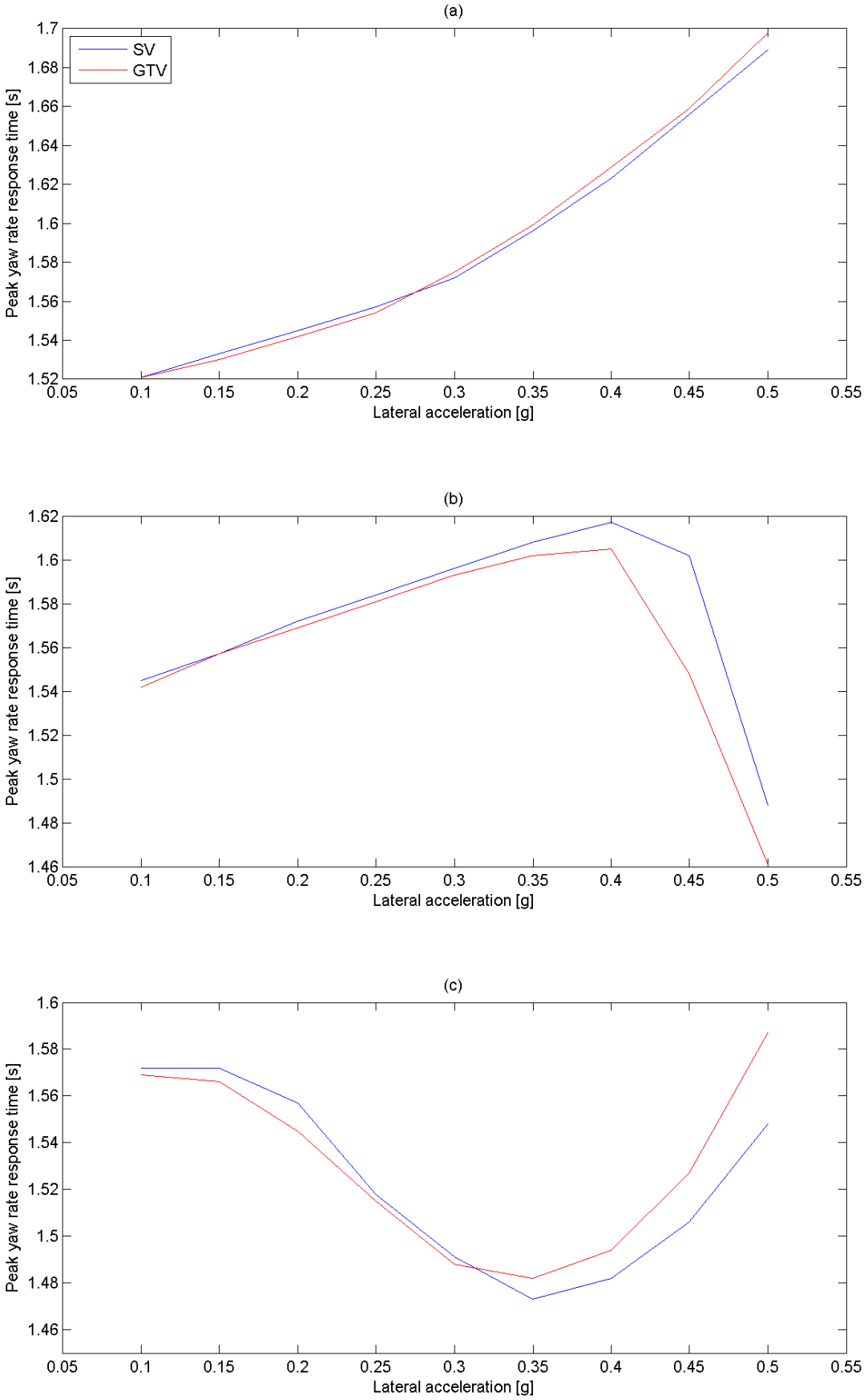

Figure 6-31 Second peak yaw rate response times for (a) low, (b) medium and (c) high speed

	Low Lateral g	High Lateral g
Low Speed	**Lateral Acceleration(1)** - GTV yields smaller peak values **Lateral Acceleration Response Time(1)** - GTV responds slower **Yaw Rate(1)** - GTV yields larger peak values **Yaw Rate Response Time(1)** - GTV responds faster **Phasing of Lateral acceleration and Yaw(1)** - GTV exhibits smaller positive phase **Lateral Acceleration(2)** - GTV yields smaller peak values **Lateral Acceleration Response Time(2)** - GTV responds slower **Yaw Rate(2)** - Equal **Yaw Rate Response Time(2)** - GTV responds faster **Phasing of Lateral acceleration and Yaw(2)** - GTV exhibits smaller positive phase	**Lateral Acceleration(1)** - GTV yields smaller peak values **Lateral Acceleration Response Time(1)** - GTV responds slower **Yaw Rate(1)** - GTV yields larger peak values **Yaw Rate Response Time(1)** - GTV responds faster **Phasing of Lateral acceleration and Yaw(1)** -GTV exhibits smaller positive phase **Lateral Acceleration(2)** - GTV yields smaller peak values **Lateral Acceleration Response Time(2)** - from 0.35g onwards GTV responds faster **Yaw Rate(2)** - Very similar, GTV larger smaller at limit handling **Yaw Rate Response Time(2)** - GTV responds slower **Phasing of Lateral acceleration and Yaw(2)** - GTV exhibits larger positive phase
Medium Speed	**Lateral Acceleration(1)** - GTV yields smaller peak value until 0.15-0.2g then larger **Lateral Acceleration Response Time(1)** - GTV responds slower **Yaw Rate(1)** - GTV yields larger peak values **Yaw Rate Response Time(1)** - GTV responds faster **Phasing of Lateral acceleration and Yaw(1)** - GTV exhibits smaller positive phase until 0.2g, 0.2g onwards GTV exhibits larger negative phase **Lateral Acceleration(2)** - GTV yields smaller peak value **Lateral Acceleration Response Time(2)** - GTV responds slower until 0.25g, 0.25g onwards responses are the same **Yaw Rate(2)** - GTV yields smaller peak values **Yaw Rate Response Time(2)** - GTV responds faster **Phasing of Lateral acceleration and Yaw(2)** - GTV exhibits smaller positive phase	**Lateral Acceleration(1)** - GTV yields larger peak **Lateral Acceleration Response Time(1)** - GTV responds slower **Yaw Rate(1)** - GTV yields larger peak values **Yaw Rate Response Time(1)** - GTV responds faster **Phasing of Lateral acceleration and Yaw(1)** - GTV exhibits larger negative phase **Lateral Acceleration(2)** - GTV yields larger peak **Lateral Acceleration Response Time(2)** - 0.3g - 0.35g responses are very similar, 0.35g onwards GTV responds slower **Yaw Rate(2)** - GTV yields smaller peak values although larger at limit handling **Yaw Rate Response Time(2)** - GTV responds faster **Phasing of Lateral acceleration and Yaw(2)** - GTV exhibits smaller positive phase until 0.4g, 0.45g onwards GTV exhibits larger negative phase

	Low Lateral g	High Lateral g
High Speed	**Lateral Acceleration(1)** - GTV yields larger peak values **Lateral Acceleration Response Time(1)** - GTV responds slower **Yaw Rate(1)** - GTV yields larger peak values **Yaw Rate Response Time(1)** - GTV responds slower **Phasing of Lateral acceleration and Yaw(1)** - GTV exhibits larger negative phase **Lateral Acceleration(2)** - GTV yields larger peak values **Lateral Acceleration Response Time(2)** - GTV responds slower **Yaw Rate(2)** - GTV yields larger peak values **Yaw Rate Response Time(2)** - GTV responds faster **Phasing of Lateral acceleration and Yaw(2)** - GTV exhibits larger negative phase	**Lateral Acceleration(1)** - GTV yields larger peak values **Lateral Acceleration Response Time(1)** - GTV responds slower **Yaw Rate(1)** - GTV yields larger peak values **Yaw Rate Response Time(1)** - GTV responds slower **Phasing of Lateral acceleration and Yaw(1)** - GTV exhibits larger negative phase **Lateral Acceleration(2)** - GTV yields larger peak values **Lateral Acceleration Response Time(2)** - GTV responds slower **Yaw Rate(2)** - GTV yields larger peak values **Yaw Rate Response Time(2)** - GTV responds slower **Phasing of Lateral acceleration and Yaw(2)** - Mixed but very similar

Table 6-2 Summary of sinusoidal steer metrics

In this section metrics illustrating key factors in the vehicles' lateral responses have been presented and summarised, in the following sections these summaries will be expanded upon by investigating the direct outputs of the vehicle models. This will be carried out for 0.2g and 0.4g targeted lateral accelerations to cover both the low and high lateral acceleration regions. Lateral acceleration and yaw rate responses for these manoeuvres are shown in Figure 6-32, Figure 6-33, Figure 6-34 and Figure 6-35.

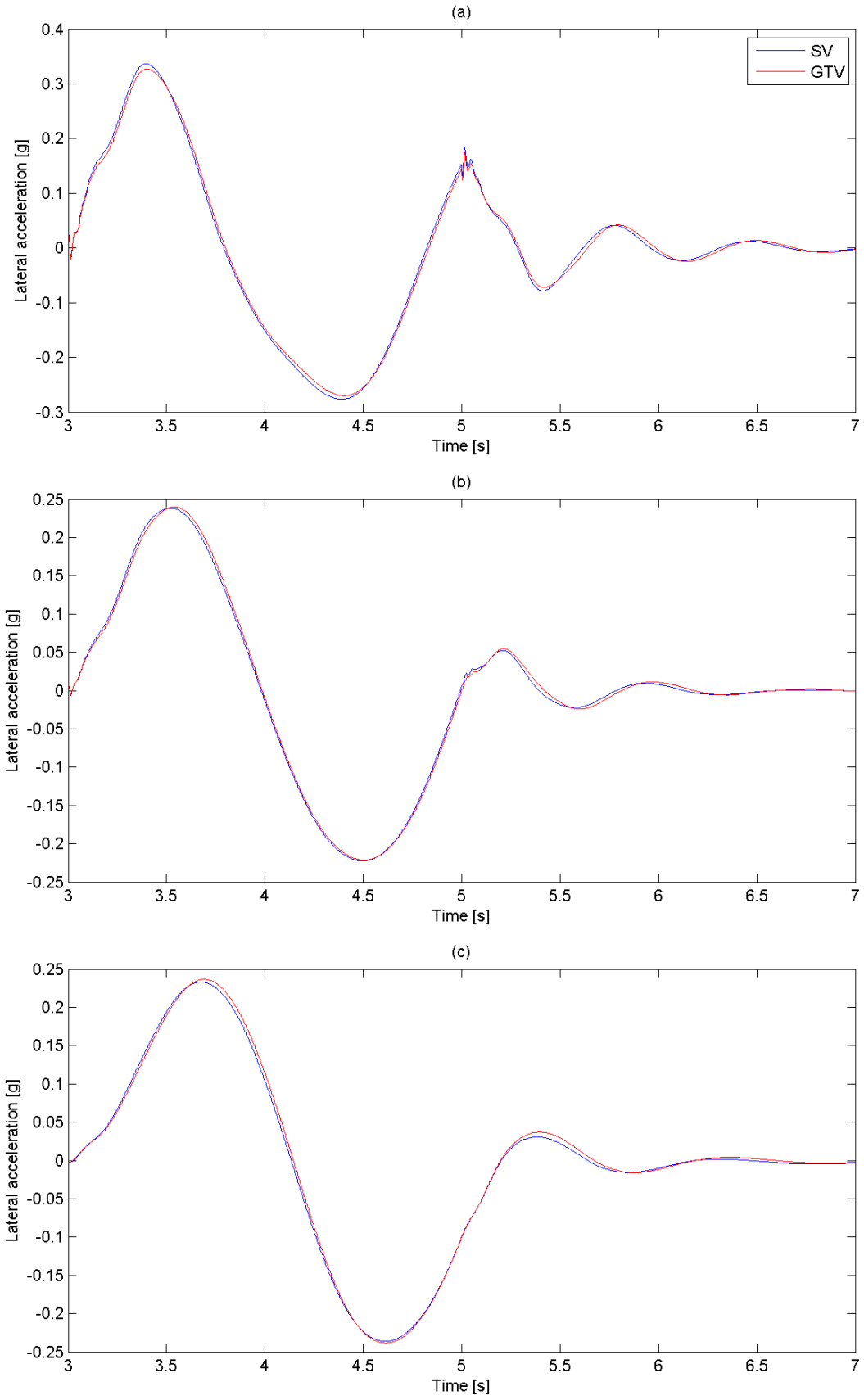

Figure 6-32 Lateral acceleration responses for 0.2g target sinusoidal steer at (a) low, (b) medium and (c) high speed

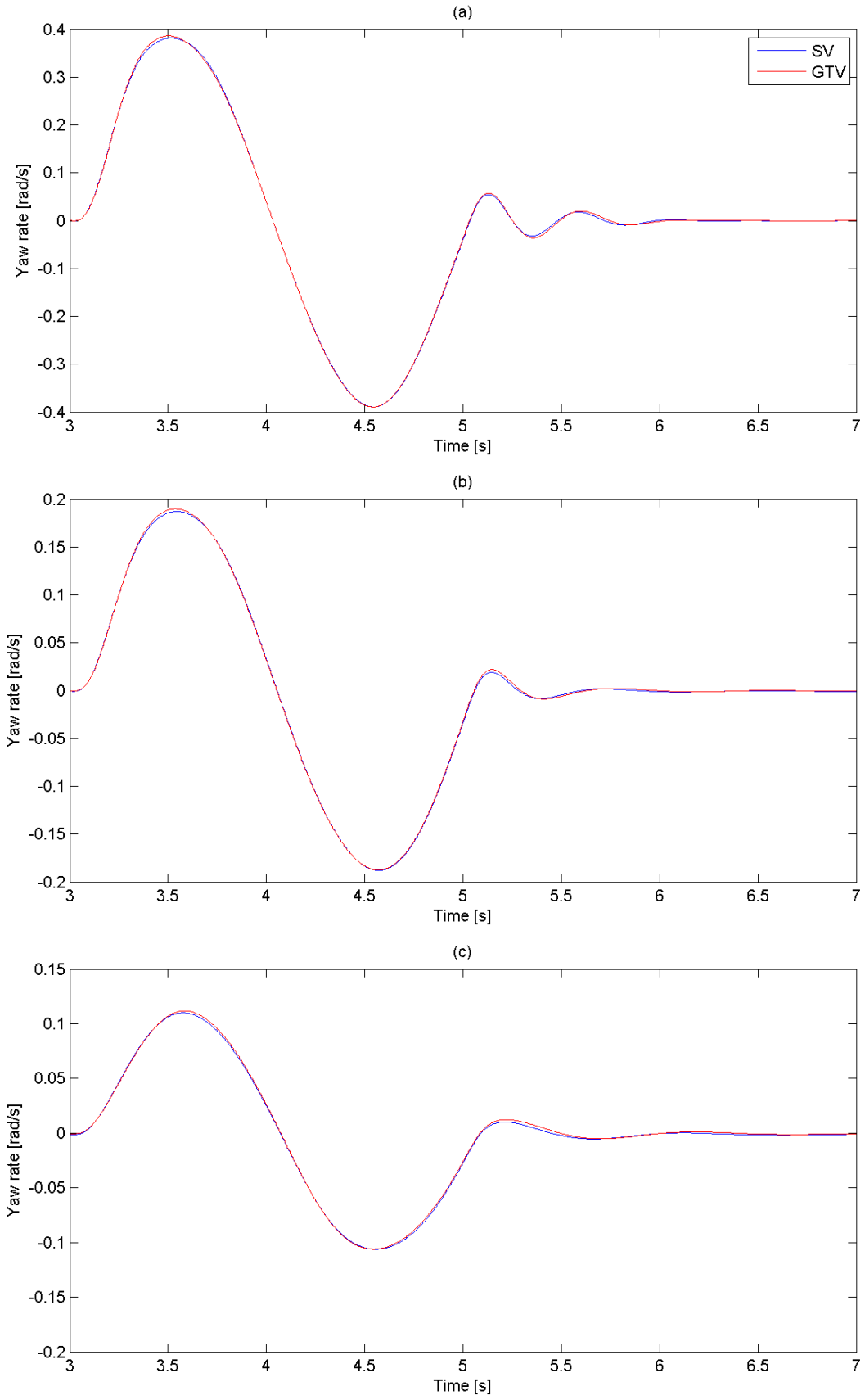

Figure 6-33 Yaw rate responses for 0.2g target sinusoidal steer at (a) low, (b) medium and (c) high speed

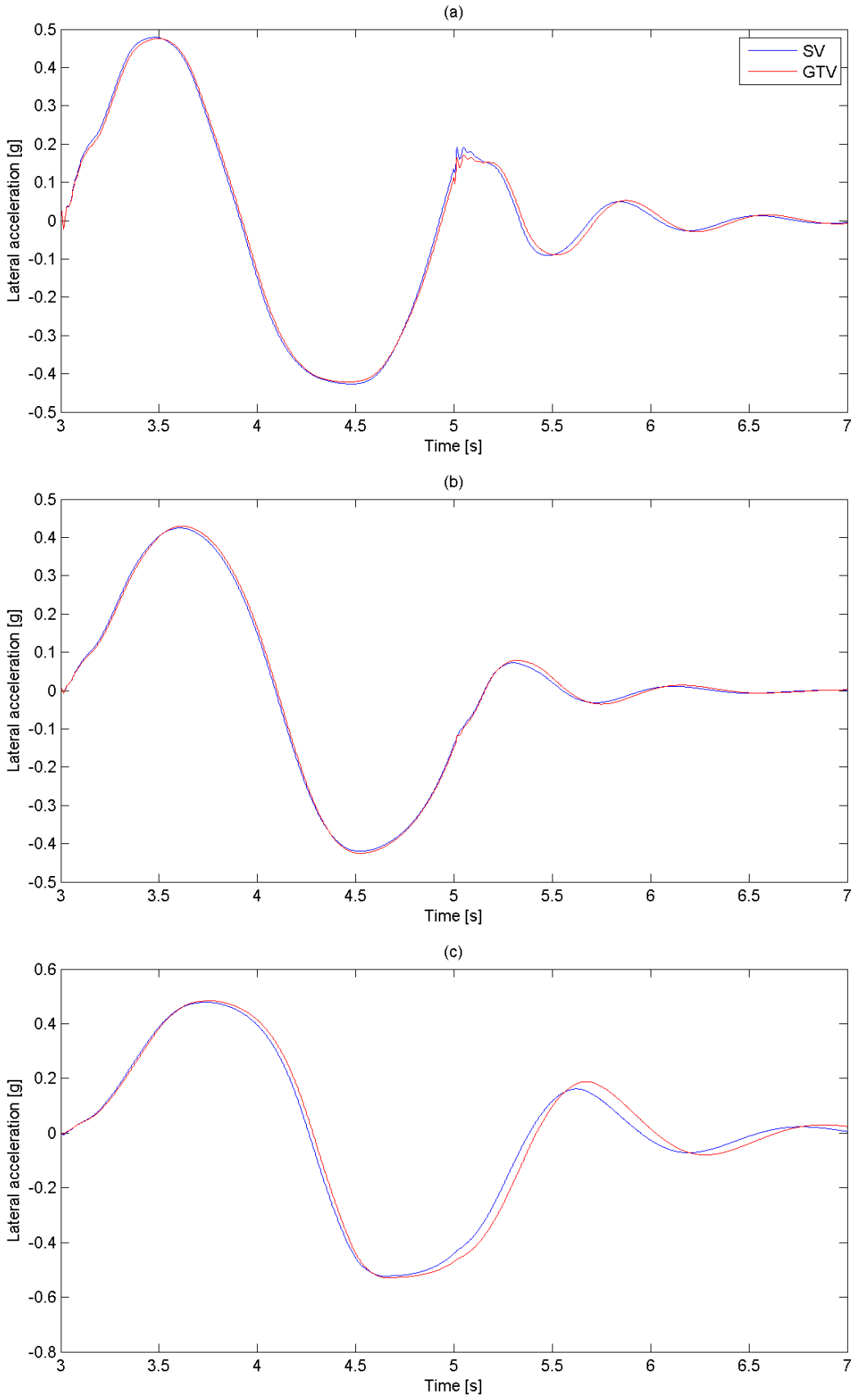

Figure 6-34 Lateral acceleration responses for 0.4g target sinusoidal steer at (a) low, (b) medium and (c) high speed

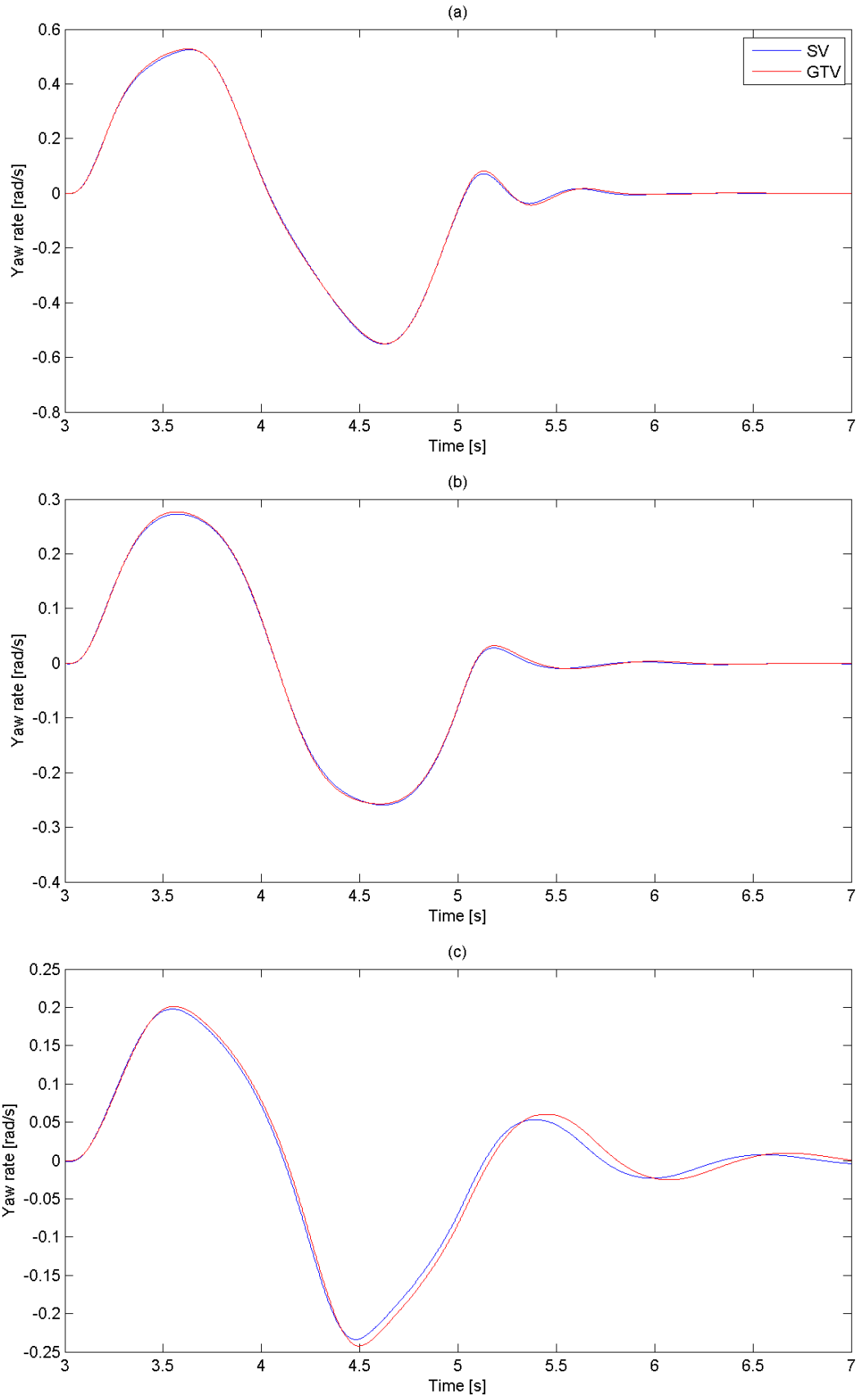

Figure 6-35 Yaw rate responses for 0.4g target sinusoidal steer at (a) low, (b) medium and (c) high speed

6.3.2 Peak Lateral Acceleration responses

Table 6-2 shows that for both the first and second peaks, in the low lateral acceleration range, the GTV at low and medium speeds yields smaller peak lateral acceleration responses than the SV. In the high speed range, for both first and second peaks the GTV now yields larger lateral acceleration peak values. In the high lateral acceleration range a similar trend is seen, but now the GTV changes from yielding a smaller response to a larger response than the SV in the medium speed range.

As was previously discussed in the ramp-to-step steer section when discussing the peak lateral acceleration responses, the body slip angle plays a large role in dictating the magnitude of said responses. The body slip angles of both vehicles, for these manoeuvres are shown in Figure 6-36 and Figure 6-37 for low and high lateral acceleration respectively.

Before beginning a more in depth discussion it should be noted that previously when investigating the ramp to step steer results, as the vehicle was only travelling in one direction during the manoeuvre, the body slip angle was discussed as positive or negative relating to whether or not it produced a non-complimentary or complimentary effect to cornering, during a sign steer manoeuvre as the vehicle travels in both directions, both positive and negative slip angles will be present to start with. Because of this the body slip angle will now only be described as complimentary or non-complimentary to cornering, depending on whether its effects create a larger or smaller slip angle at the rear tyres (nose in or nose out attitude). In terms of the definition used when discussing ramp to step steers, it can be said that a complimentary body slip angle is negative during a left hand turn and positive during a right hand turn.

Looking at the body slip angles of the vehicles for both the low and high lateral acceleration manoeuvres shown in Figure 6-36 and Figure 6-37 it is seen that the body slip angle at the Cog swaps from being non-complimentary to complimentary to cornering at the same points as where the GTV goes from exhibiting a smaller peak lateral acceleration than the SV to exhibiting a larger peak value. As was discussed in section 6.2.3 this is due to the cornering force created by the body slip angle and whether or not this is in a direction which is complimentary to cornering. As was shown in the aforementioned section this reversal in body slip angle happens between 11 and 13 m/s. Below this speed the body slip angles of both vehicles are non-complimentary to cornering, although the body slip angle of the SV is larger, due to the more centralised Cog of the GTV the lateral force induced by the angle is larger for the latter and so it is unable to achieve a peak lateral acceleration value comparable to that of the SV. From 0.2g onwards in the medium speed range (11 – 13 m/s), due to the slip angles at the front and rear tyres, the body slip angles have reversed and are now complimentary to cornering. Again the GTV receives a higher lateral force from the body slip angle, which is now also larger than that exhibited by the SV and so is able to achieve a higher peak lateral acceleration than the SV.

6.3.3 Lateral Acceleration Response Times

Table 6-2 shows that the GTV yields slower lateral acceleration responses in all of the speed and lateral acceleration regions. The lateral acceleration response times are dictated by the magnitude and the rate at which lateral tyre force is generated. As with the analysis carried out in the ramp-to-step steer section, looking at the lateral tyre force response is a good place to start, this is shown in Figure 6-38 and Figure 6-39.

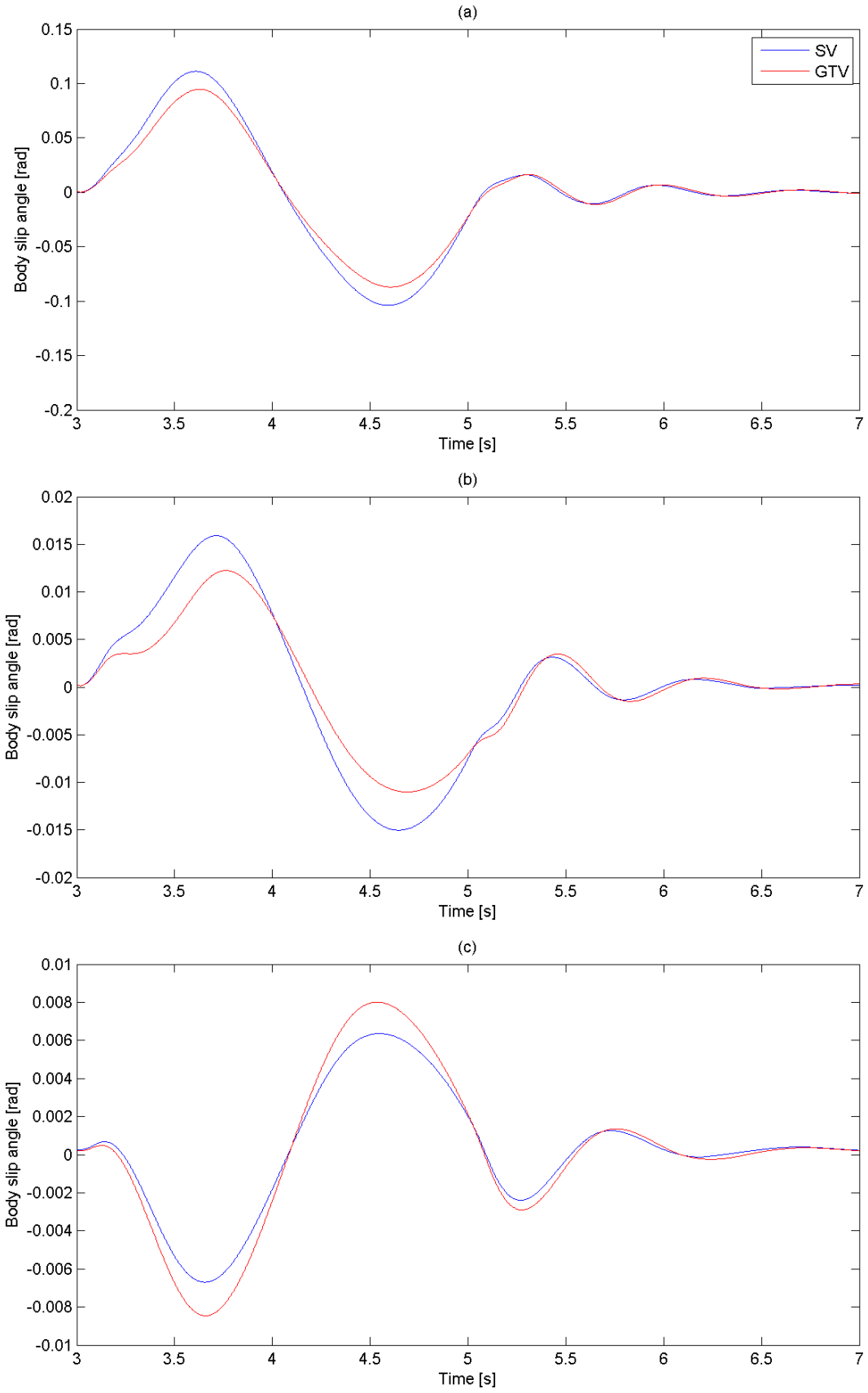

Figure 6-36 Difference in body slip angle at Cog responses for 0.2g target sinusoidal steer at (a) low, (b) medium and (c) high speed

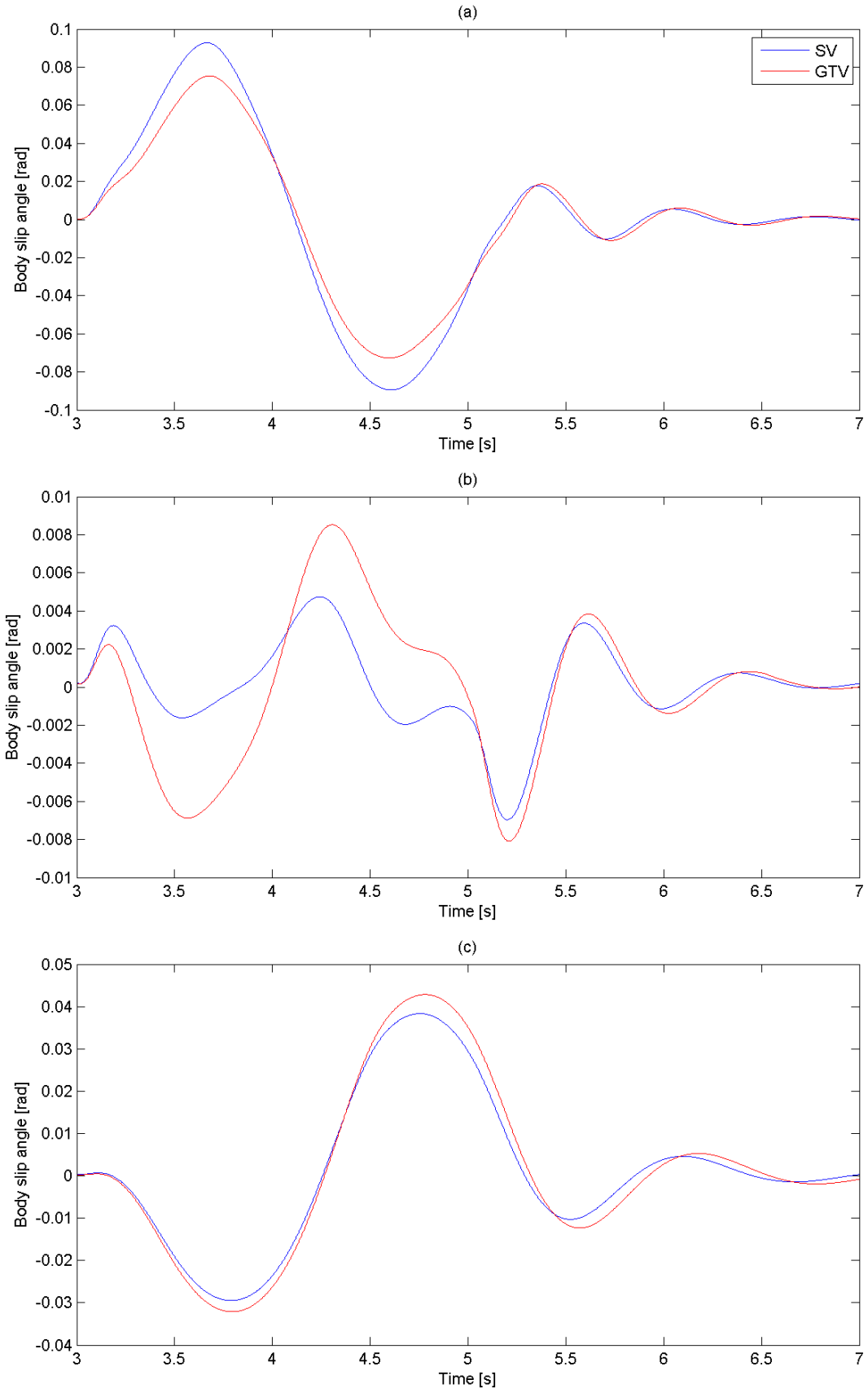

Figure 6-37 Difference in body slip angle at Cog responses for 0.4g target sinusoidal steer at (a) low, (b) medium and (c) high speed

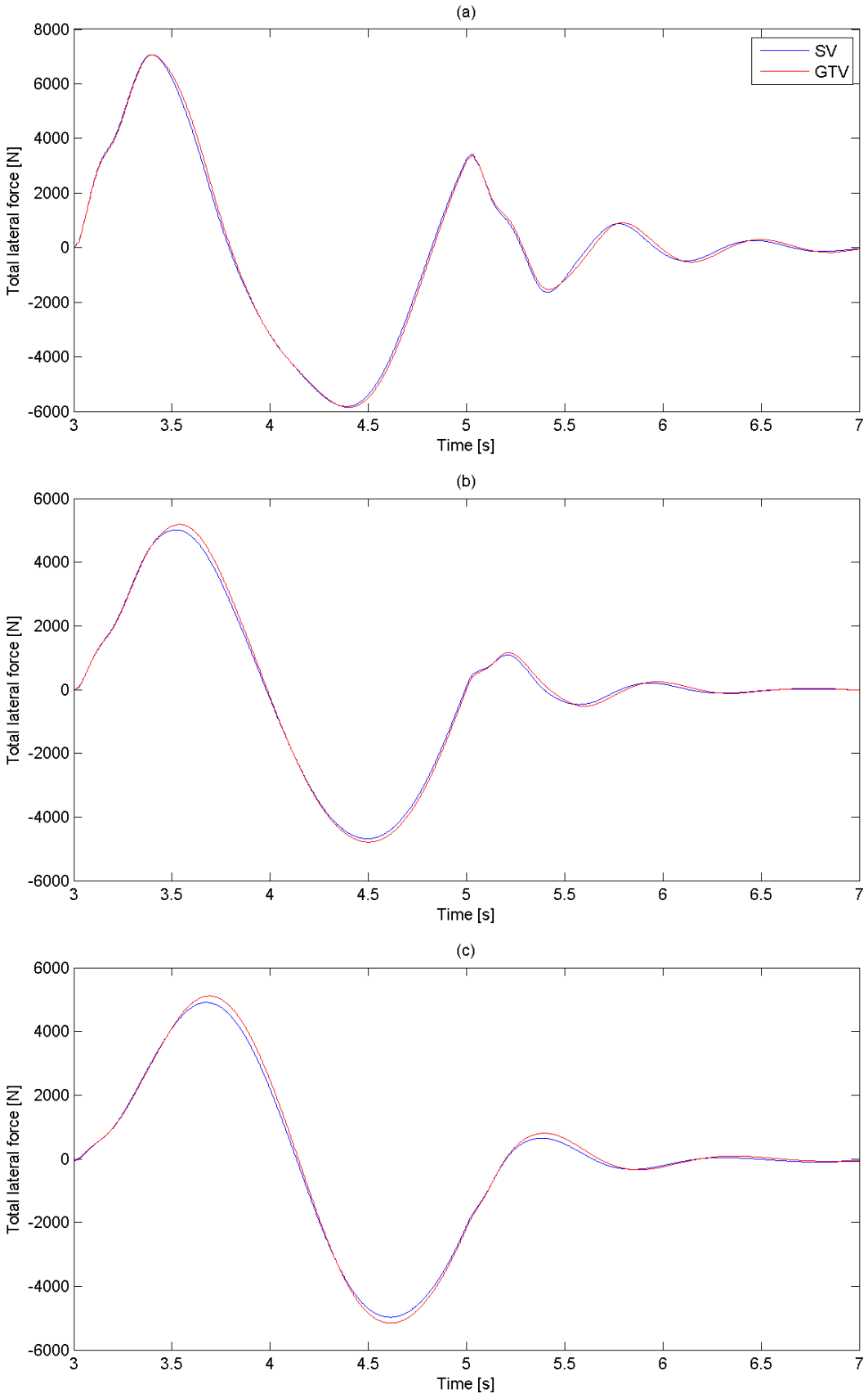

Figure 6-38 Difference in lateral force responses for 0.2g target sinusoidal steer at (a) low, (b) medium and (c) high speed

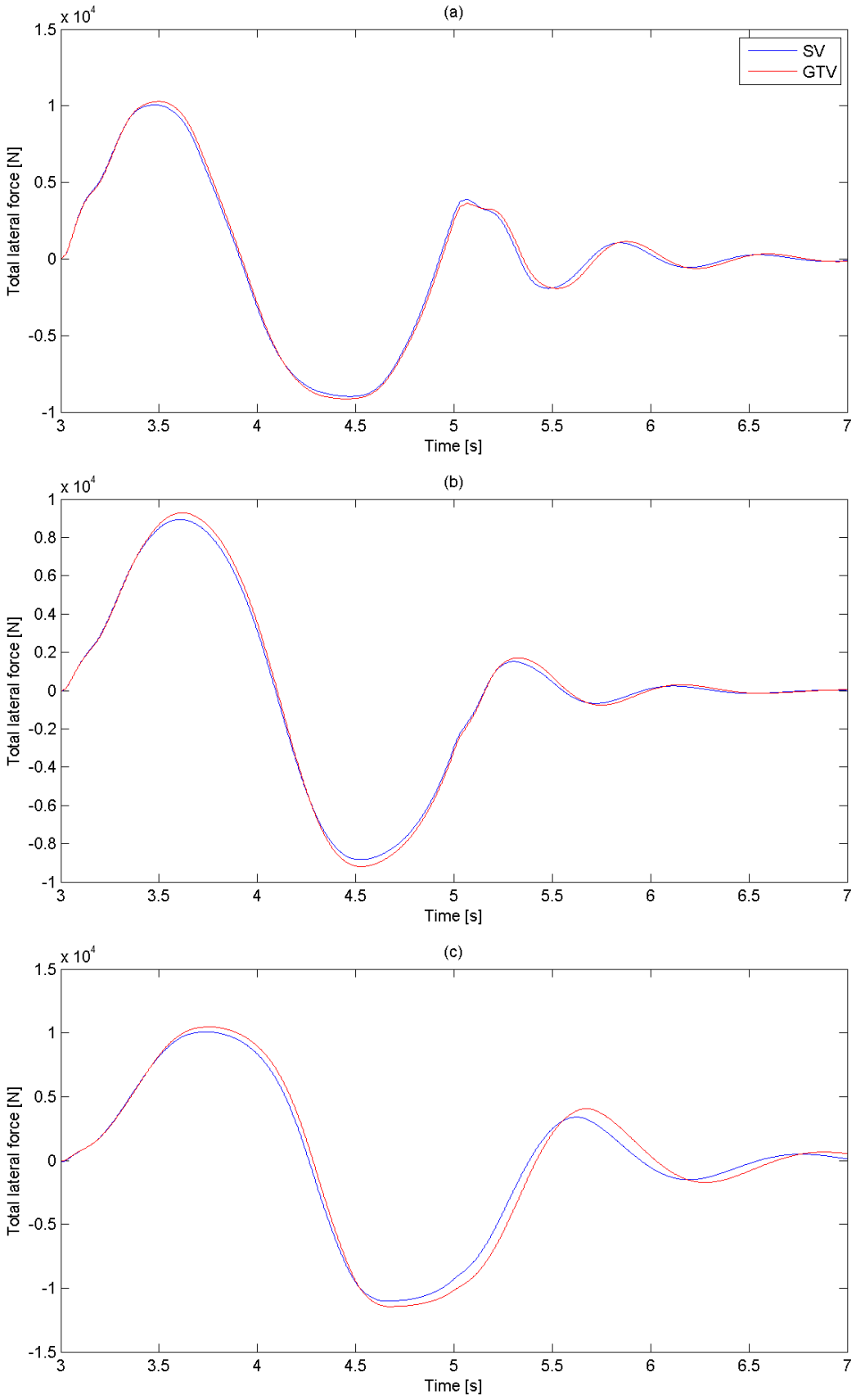

Figure 6-39 Difference in lateral force responses for 0.4g target sinusoidal steer at (a) low, (b) medium and (c) high speed

It can be seen that overall for both the low and high lateral acceleration ranges the GTV generates lateral tyre force at a slightly lower rate than the SV, the peak in lateral tyre force for the GTV can clearly be seen to be later than for the SV, this is due to its higher DI, and so the inertial effects are delaying the tyre force generation further for the GTV. Even if the lateral tyre forces of both vehicles are developed at the same rate the GTV would still respond slower as it has a larger mass and needs a proportionally larger tyre force to obtain the same level of lateral acceleration as the SV. As was discussed for the ramp to step steer manoeuvres, it has been shown that a vehicle with a higher tangent speed will have faster lateral acceleration responses (other factors equal), here this is the SV.

6.3.4 Yaw Rate Response Times

Table 6-2 shows that for the first peak yaw rates in the low and medium speed ranges, at both low and high lateral accelerations, the GTV has the quickest yaw rate responses. In the high speed range it is the SV that responds faster than the GTV in both the low and high lateral acceleration regions. This is illustrated by looking at Figure 6-40 and Figure 6-41 which show the yaw moments and yaw accelerations of the two vehicles for the 0.2g sinusoidal steer manoeuvre. For now if we just consider the first peak of the manoeuvre, it is shown that the GTV always produces a larger peak yaw moment than the SV. Figure 6-40 also shows that the highest yaw moment is produced in the low speed region, and the lowest in the high speed region. Looking at the respective peak yaw moments in each of the three speed regions it can be seen that for the GTV it reduces to a greater extent with speed than for the SV. The effect of this can be seen in Figure 6-41 which shows the corresponding yaw accelerations for the two vehicles, notice that in the low and medium speed regions the GTV has larger peak yaw accelerations, however in the high speed

region this is no longer the case. So it is the greater reduction in yaw moment of the GTV, combined with its larger yaw inertia that restricts its yaw acceleration and so ultimately leads to it responding slower than the SV in the high speed region. The same trends are shown for the high lateral acceleration region where 0.4g is targeted, the yaw moments and yaw accelerations for this are shown in Figure 6-42 and Figure 6-43.

This greater loss in yaw moment with increasing speed for the GTV can be attributed to two main factors. Firstly as was discussed when commenting on the ramp to step steer manoeuvres, as the speed of the vehicle increases there is less time available for the inertial effects to develop slip angles at the rear. This being the reason why the GTV is able to obtain larger yaw moments and hence quicker response times, means that as the effect of the inertial properties reduces, the GTV will begin to respond slower. Secondly, the steering application for these manoeuvres is applied at 0.5Hz. Remember in section 6.1.1 , it was shown that GTV has a lower understeer gradient and hence requires a smaller steering angles to obtain the same steady state lateral acceleration as the SV. As the steering inputs for the GTV are smaller and applied at the same frequency as those of the SV, they are in effect applied at a lower rate. Keeping this in mind, it should also be pointed out that the difference in the two steering angles required for the GTV and SV are largest at high speeds, accounting for the magnitude of the input and the frequency at which it is applied, the difference in the two application rates in the low speed range is circa 0.1%, however in the high speed range the difference is circa 2.7%. At high speed the slower application of the GTV's steering input will also have the effect of reducing the inertial effects on rear slip angle generation during the transient phase, once again meaning that the GTV will not be able to develop a large enough yaw

moment and resulting acceleration to respond faster than the SV as it did in the lower speed regions. The rear slip angles in Figure 6-44 show the reduction in the aforementioned inertial effects. The low speed region shown in (a) shows large negative overshoot in the rear slip angle for both vehicles, but noticeably more for the GTV, it is at this point that the GTV generates its larger yaw moment which gives it, its larger yaw acceleration. Moving from the low speed region to the high speed region it can be seen that these negative slip angles are reducing in magnitude and hence the tyre force that is creating the large yaw moments is also reducing. It can be seen that this effect diminishes more for the GTV than for the SV, this is due to the steering input rate being slower for the former, as previously mentioned.

The generation of body slip angle will also have an effect on the yaw rate response times, as was discussed for the yaw rate response times of the ramp to step steer manoeuvres in section 6.2.4 . It was previously shown that the magnitude and direction of the body slip angles change from the low to high speed manoeuvres. In the low speed region the yaw about the CoP due to the inertial effects means that the body slip angle is built in the required direction, in the medium speed range the same is true, although here, due to the small body slip angle required, especially for the GTV it is generated too quickly, and so when the vehicle is transitioning from initial corner entry towards steady state, there will be a small oscillation in body slip angle, as seen most predominantly for the GTV in this region, in both Figure 6-36 and Figure 6-37. In the high speed region the same is true, but now a full reversal in body slip angle is required as it is initially built in the incorrect direction. These oscillations and changes in the direction of body slip angle require a change in poise of the vehicle body, as the yaw inertia of the GTV is larger it will require a larger

force from the tyres to do so, and therefore be slower to respond, this therefore also adds to the yaw rate response time of the GTV.

Table 6-2 showed that the response times of the second yaw rate peaks followed different trends from the first ones which have been discussed. To begin to explain this, let us remember that the slip angles produced at the rear tyres due to the vehicles' inertial properties have a reduced effect as speed increases, due to the limited time they have to develop. Also as we increment through the speed regions the steer angles become smaller, again this will limit the effect of the vehicles' inertial properties. Further to this, as was previously mentioned, the steering inputs are supplied at different rates, which become more different as speed increases (GTV has smaller steering inputs compared to SV and so lower application rate). At the outset of this second phase of the sinusoidal steer manoeuvre the vehicle already has a slip angle at the rear which is generated in the same direction as the inertial effects would generate it during the start of the second transient phase, these rear slip angles are however much larger than those that could be generated by the inertial effects, this means that inertial properties of both vehicles wont influence this second transient in the way they did the first. A large yaw moment will be produced regardless, for both vehicles due to the direction and magnitude of the rear slip angles induced by the first part of the manoeuvre. Due to this the yaw acceleration and response time (in this second phase) is primarily governed by the magnitude of the rear slip angle generated in the first part of the manoeuvre, along with the force generated by the steer angle at the front. Therefore looking at the low speed range across all lateral acceleration regions it makes sense that the responses are very similar, the steer angles and application rates are very similar, the GTV will have a slightly larger rear slip angle, meaning that it will produce a larger yaw moment,

however due to its larger yaw inertia it does not realise a quicker response, and response times of both vehicles are very similar. The medium speed range is a little more convoluted in the higher lateral acceleration region. Again in the low lateral acceleration region results are very similar for the same reasons mentioned previously. In the high lateral acceleration region it should be pointed out that the GTV is operating with a larger body slip angle which is complimentary to cornering/rear slip angle generation. The SV has a higher tangent speed meaning its body slip angle migrates from non-complimentary to complimentary at a higher speed, so in the higher lateral acceleration region of this medium speed range the GTV has significantly larger rear slip angles than the SV during the first part of the manoeuvre enabling it to create a larger yaw moment and yaw acceleration during this second transient which in turn makes it respond faster than the SV. In the high speed region, the similarities have returned as both vehicles now possess body slip angles which are complimentary to the rear tyre slip angles, and although this is larger for the GTV, here in the high lateral acceleration region the difference in the steered angle and application rate is greatest, meaning that for the GTV the front axle is contributing less to the yaw moment generation, therefore results that are similar in the low lateral acceleration region become more diverse as lateral acceleration increases, with the GTV responding slower.

In summary, at low and medium speeds the GTV will responds faster in yaw for the first steering input, as its CoP is further rearwards leading to slip angles being generated at the rear tyres that create large yaw moments about the Cog. In high speed regions the inertial effects have less time to develop slip angles at the rear tyres and so have less of an effect, leading to the SV responding faster in yaw. Also

in this high speed region the GTV's steering inputs are smaller and applied at a lower rate than the SV's, which will also contribute to its slower response times.

During the second phase of these sinusoidal steer manoeuvres or any prolonged transient event, the GTV and SV will respond very similarly in terms of yaw rate response times, as the inertial effects that were responsible for generating rear slip angles and hence large yaw moments during the initial transient have little or no effect due to larger slip angles already being present at the rear tyres. It was shown that larger differences between the two vehicles' yaw rate response times will be present due to their differing tangent speeds, in the medium speed range the GTV will switch body slip angles at a lower speed than the SV, when this is the case the GTV has the ability to create larger rear slip angles during the initial part of the manoeuvre and so can create larger yaw moments and corresponding yaw accelerations during the second transient.

6.3.5 Peak Yaw Rate Responses

Peak yaw rate responses for the first peaks of the sinusoidal steer manoeuvres where shown to be larger for the GTV in both the low and high lateral acceleration regions at all speeds.

As was first mentioned in section 6.2.5 when discussing peak yaw rate responses during step steer manoeuvres, the GTV has a more centralised weight distribution, this has two main effects when considering the yaw rate responses. The first of which is that the yaw moment induced by the front tyres due to the steering angle increases, and thus increases the yaw rate response. The second effect, as discussed in detail in chapter 4, is that the yaw damping has reduced, this will of course lead the vehicle towards a larger, more oscillatory yaw rate response. Combining these two effects with the fact that the GTV has a larger DI and so during the initial

transient condition the inertial effects can create a greater yaw moment, it is clear why a greater peak yaw rate can be achieved by the GTV.

The second peak yaw rate of the manoeuvres are almost identical between the two vehicles, the low lateral acceleration ranges show almost no difference in responses at all speeds. In the low and medium speeds the only observable differences are seen at the limit of handling. In the high speed region there is a slightly bigger difference in the high lateral acceleration region which shows the GTV again exhibiting a larger peak yaw rate response.

Inertial effects do not play as large a role during the second phase of the sinusoidal steer manoeuvre. Again, as the steering angle changes the vehicle will begin to yaw about the CoP, although now slip angles are already present at the rear tyres and are larger than would be generated by the inertial effects. Because of this the difference in the yaw moment produced by the GTV and SV now only relies on the difference in rear slip angle obtained during the first phase of the manoeuvre and the difference in front lateral force due to steered angle. The difference in rear slip angle and the corresponding lateral force due to the initial part of the manoeuvre are very small, the slip angles will only vary mainly by the difference in body slip angle. The difference in steer angle is also very small, at low and medium speeds, as previously mentioned the difference is of the order of less than 1% which is negligible, and hence in these regions we see negligible differences in the peak yaw rate responses. As speed increases it was shown that the difference in the steer angle of the two vehicles also increases (due to their understeer gradients), in the high speed range this difference increases to just under 3%. So in the low speed region, the steered angle is very slightly less for the GTV but the rear slip angles are sufficiently larger due to its weight distribution and body slip angle so that it can

achieve a large enough yaw moment to allow it to yield the same peak yaw rate as the SV. In the medium speed range, again responses are extremely similar, with GTV exhibiting a larger response at the limit of handling. As discussed in the previous section, this is due to the GTV being able to generate larger rear slip angles in the initial part of the manoeuvre due to it being above its tangent speed and so its body slip angle complimenting rear slip angle generation, meantime the SV is still much closer to its tangent speed and hence has a body slip angel near zero. In the high speed range the steering inputs for the GTV are considerably less than those of the SV, although the rear slip angles are now also considerably larger due to its much larger body slip angle, which is complementary to rear slip angle generation during the first part of the manoeuvre, therefore this results in larger yaw moments for the GTV which allow it to achieve greater peak yaw rates.

These results suggest that whilst for an initial input the GTV will always yield a larger yaw rate response than the SV, it is not until above its tangent speed it will do so for a secondary input. This is due to the inertial effects that enabled the GTV to create a larger yaw moment than the SV during the initial transient, having little or no effect on the second transient due to larger slip angles already present at the rear tyres. However once above its tangent speed the GTV has a larger body slip angle than the SV, which is complimentary to rear slip angle generation, and so during the first phase of the sinusoidal steer it generates larger rear slip angles, which in turn, during the second transient phase create larger yaw moments than the SV leading to larger yaw rate responses.

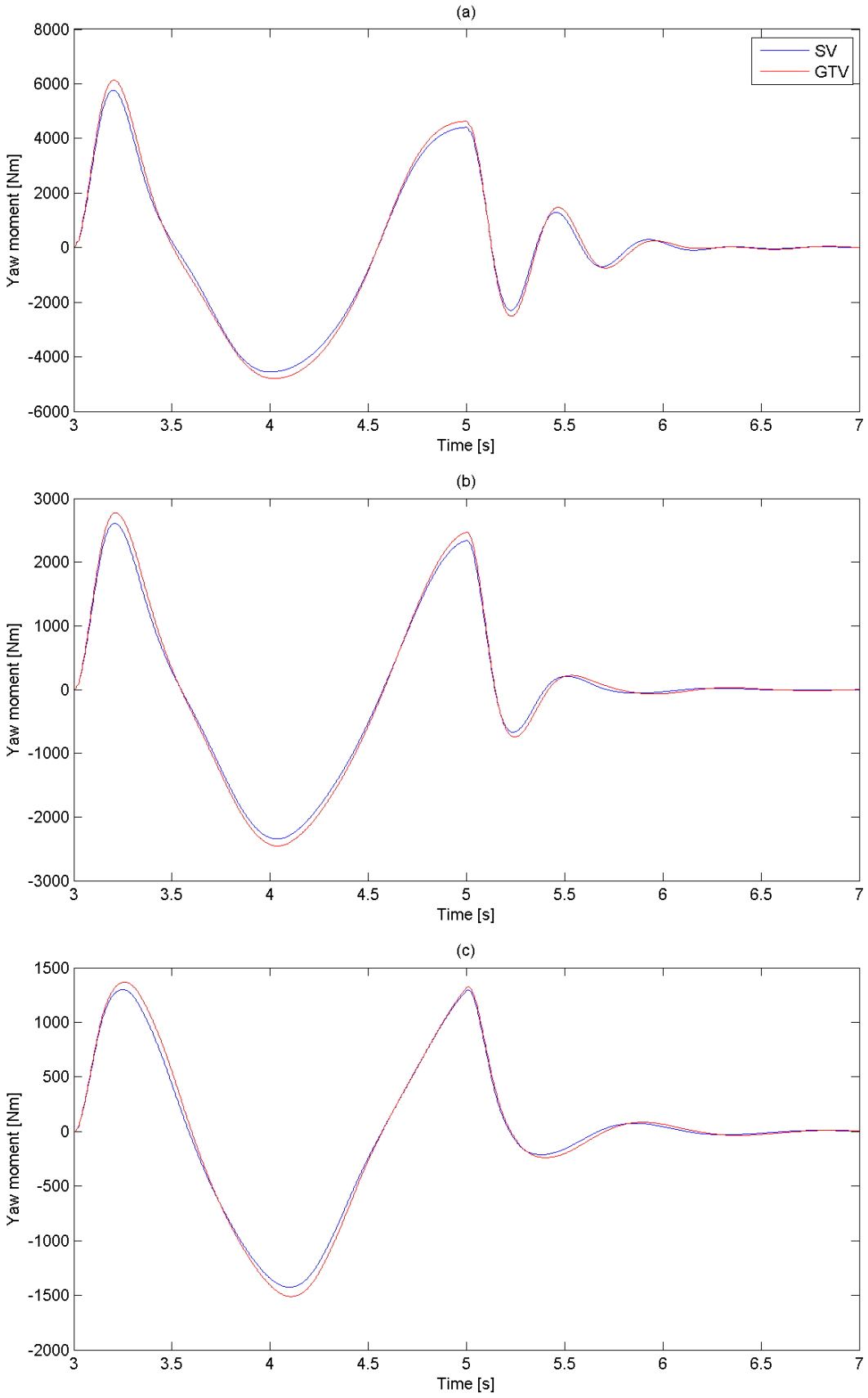

Figure 6-40 Difference in yaw moment responses for 0.2g target sinusoidal steer at (a) low, (b) medium and (c) high speed

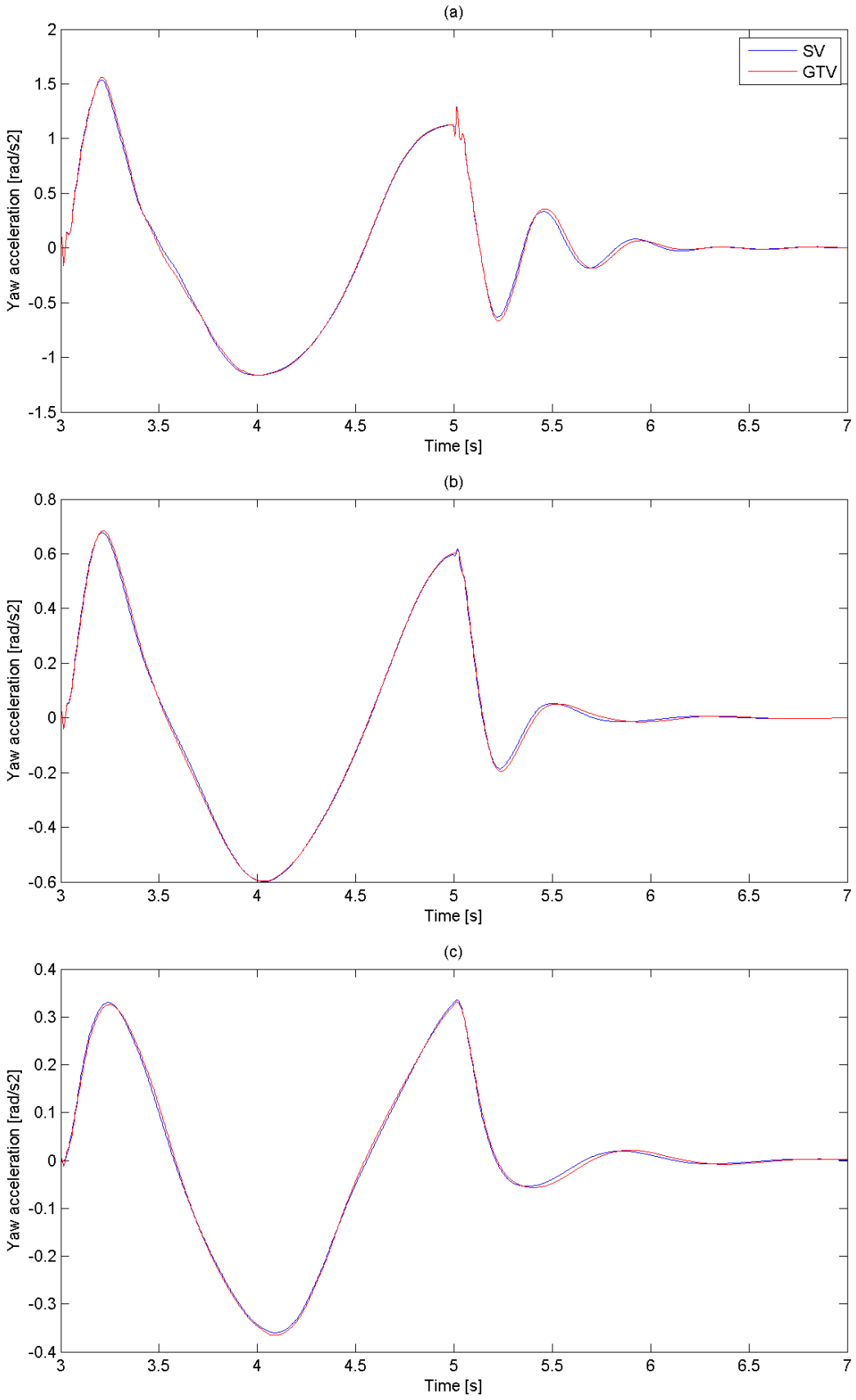

Figure 6-41 Difference in yaw acceleration responses for 0.2g target sinusoidal steer at (a) low, (b) medium and (c) high speed

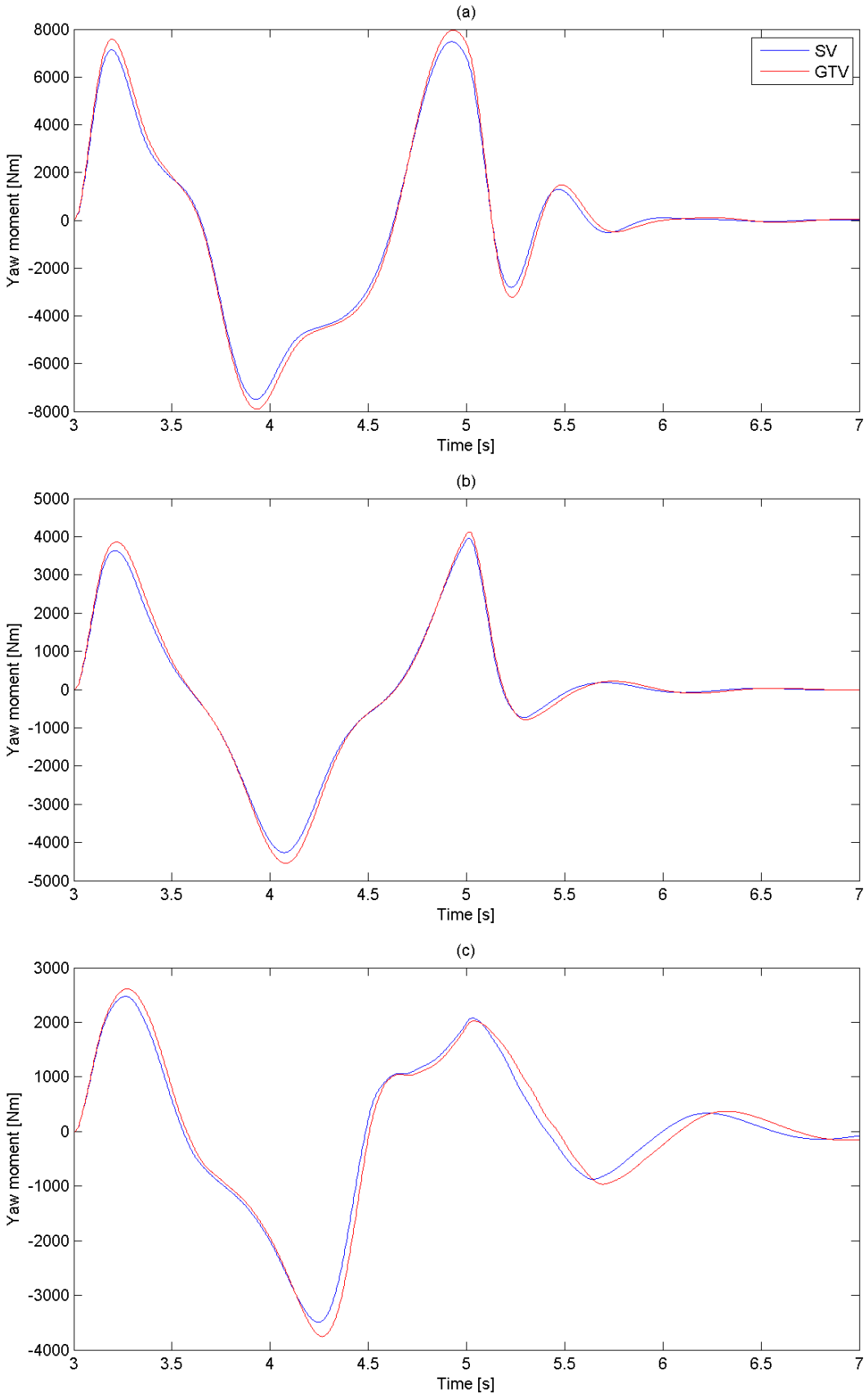

Figure 6-42 Difference in yaw moment responses for 0.4g target sinusoidal steer at (a) low, (b) medium and (c) high speed

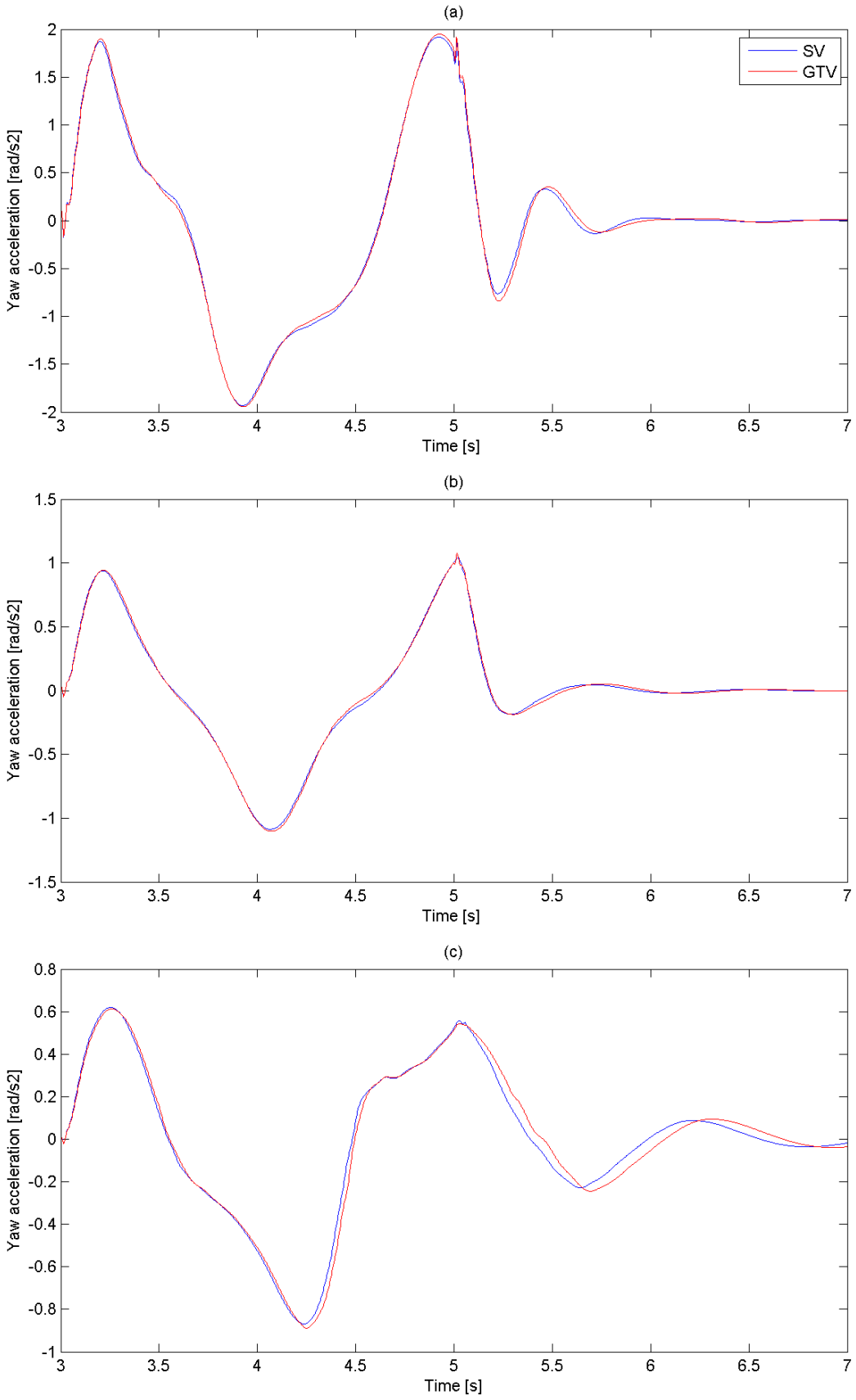

Figure 6-43 Difference in yaw acceleration responses for 0.4g target sinusoidal steer at (a) low, (b) medium and (c) high speed

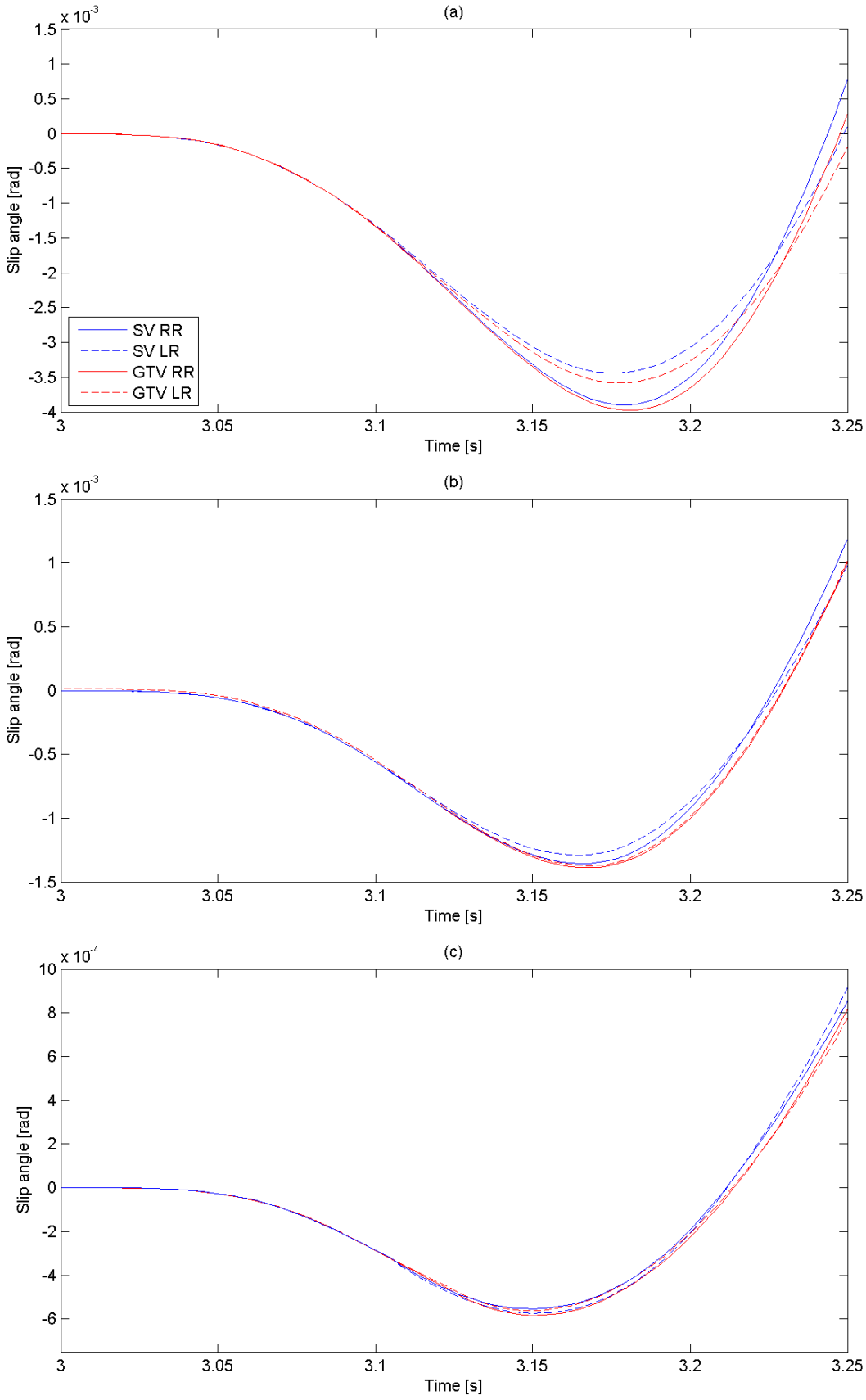

Figure 6-44 Difference in rear slip angle responses for 0.2g target sinusoidal steer at (a) low, (b) medium and (c) high speed

6.4 Conclusion

This chapter has used three standardised manoeuvres to illustrate the differences in the steady state and transient handling of the two vehicles. Steady state differences were illustrated by comparison of the steering responses of the two vehicles. These responses were then used to obtain steering angles and speeds for the ramp to step steer and sinusoidal steer manoeuvres. Ramp to step steer manoeuvres have been used to illustrate the steady state to transient responses of the vehicles, and sinusoidal steer manoeuvres to illustrate the same for initial entry, but then also a transient to transient condition.

The constant radius tests provided the steering responses of the two vehicles, it came as no surprise that due to the GTV having a higher roll stiffness at the rear, due to its stiffer ride springs, utilised to obtain the same ride frequencies and static ride heights as the SV, combined with its more rearward weight distribution, its understeer gradient was lower than that of the SV. This was shown to be the case over the slow, medium and high speed ranges. As the speed and lateral acceleration increased the differences between the two vehicles becomes larger. In practice, for the driver, this means that in all operating conditions smaller steer angles are needed to negotiate the same corner when operating the GTV. Bigger differences will be noticed as the speed increases. While both vehicles still posses understeer tendencies (require more steer to negotiate the same radius as speed increases), the GTV has moved closer to neutral steer.

In terms of the vehicles transient responses, it was shown that the inertial properties and mass distribution of the vehicles play a significant role. Due to the changes that have been made to the SV in creating the GTV it possesses a further rearward weight distribution, higher mass and higher yaw inertia than the SV. The

GTV's higher mass and its more rearward distribution have a number of effects on the vehicle handling properties. The first of these is that due to the increased mass on the rear tyres, larger slip angles will be produced at the rear for the GTV for any given cornering manoeuvre, this leads to the tangent speed of the vehicle being reduced. The GTV will move from operating with a 'nose in' attitude to a 'nose out' attitude at a lower speed than the SV because of this. Secondly the more centralised mass distribution of the GTV also leads to reduced yaw damping. And thirdly as the GTV possesses less of an understeer characteristic than the SV, its characteristic speed is lower. Finally considering the inertial properties of the vehicle, it was shown that due to the more centralised weight distribution of the GTV and its increased yaw inertia, its DI had increased. The differences in the handling responses of the two vehicles can be explained by the secondary effects of the changes in mass and inertia properties outlined above. It has been shown that due to the increased mass, larger DI and reduced understeer characteristic, the GTV will always yield slower lateral acceleration responses than the SV. In terms of the magnitude of the GTV's lateral acceleration responses, below its tangent speed it is unable to obtain the same levels of peak lateral acceleration as the SV (for the given steering inputs), however above its tangent speed, due to its body slip angle no longer inhibiting slip angle generation it is able to create larger slip angles and hence larger lateral acceleration responses. In terms of the two vehicles' yaw responses, the GTV's increased DI means that it has the ability to create a larger yaw moment during the initial transient phase, combining this with its reduced yaw damping leads it to create larger yaw rate responses than the SV. Its yaw rate response times are governed by the same effects as just mentioned however the vehicle speed also plays a large role. The inertial effects can develop more fully at lower speeds or when the

responses are larger, so at lower speeds and manoeuvres with larger yaw rates the GTV will respond faster, however at higher speed or manoeuvres with smaller yaw rates, its yaw rate responses will be slower than the SV.

Clearly from the differences in magnitude of the lateral acceleration and yaw rate responses, the former being smaller at low speeds and larger at high speeds, and the latter always being larger for the GTV, the driver will receive different queues from the vehicle. The larger yaw rate responses but smaller lateral acceleration responses (at lower speeds) could lead to the driver feeling they have used too much steering angle in entry to the corner, as the vehicle will re-orientate its self (yaw) to a larger extent than it will accelerate laterally, such a feeling could prompt the driver to continually adjust steering angle whilst negotiating the corner (in much same way that body roll is known to make drivers over estimate the required steer angle). At higher speeds when the both yaw rate and lateral acceleration responses are larger for the GTV, the vehicle could feel much more sensitive to steering inputs (in terms of response magnitude). Similar effects will be felt with regard to the response times in the low speed region where lateral acceleration responses are slower but yaw rate responses faster, in the higher speed regions both lateral acceleration and yaw rate responses are slower which could give the impression to the driver that the vehicle is lethargic and slow to respond to steering inputs. The fact that in the high speed region responses of the GTV are larger but response times slower could be very dangerous, slower response times could prompt the driver to utilise larger steer angles, which in turn would lead to much larger responses when the vehicle does react.

When studying the transient to transient handling of the two vehicles during the sinusoidal steer manoeuvres it was shown that the inertial effects do not have the

same effect on the vehicles' handling, due to already present large slip angles generated by the first part of the manoeuvre, as a result the secondary transient responses of the vehicles are somewhat normalised. Trends in lateral acceleration responses and response times remain similar to those previously discussed, only the differences between the vehicles are reduced. However yaw rate responses and yaw rate response times are different, as they are primarily governed by the generation of the yaw moments, which, in the first transient are heavily influenced by the inertial effects, as previously mentioned such inertial effects are much less influential during the second transient. It was shown that the slip angles already possessed by the vehicle from the first phase of the manoeuvre govern the yaw responses of the second phase. Once again the lower tangent speed of the GTV plays a significant role. It was shown that below the GTV's tangent speed its yaw rates were lower, and yaw rate response times were longer than those of the SV, however above its tangent speed, now, due to its larger slip angles (during the first phase) its second peak yaw rates are larger and its response times quicker than those of the SV. This once again could cause driver confidence or stability issues, if at higher speeds its responses are significantly larger and faster than at lower speeds in such transient conditions.

The above comparisons are relative and it is difficult to make absolute remarks on the GTV's handling, however it is fair to assume that the standard vehicle represents some form of satisfactory/optimal handling and so the aforementioned deviations from this can be viewed as sub optimal (for the average driver). Furthermore it has been shown that larger differences in handling between low and high speed are observed with the GTV, this clearly is not optimal as it will lead to the vehicle feeling very different depending on the speed range.

Results summarised, and remarks made here will be utilised along with the ride domain results and analysis to draw conclusions on the findings of this study in the wider context of future hybrid electric vehicles.

Chapter 7 Conclusion

This thesis was aimed at investigating and understanding the effects of hybrid propulsion and associated systems on vehicle dynamics. This has been investigated by means of multibody modelling of the vehicles in question, real world validation of said models, and following this a comprehensive ride and handling comparison with detailed data analysis of model outputs.

Chapters 1 and 2 outlined the initial scope of this work and gave rise to the motivation.

The modelling and model validation of the two multibody models created in Dymola was discussed at length in chapter 3. The model structure was initially discussed with respect to the standard vehicle model, following this, the changes made to the standard vehicle, to create the GTV were introduced, their inclusion in the modelling domain to create the GTV model were also discussed at length. This modelling chapter showed, that through the use of physical multibody modelling, as facilitated by Dymola, changes in the modelling domain can be made in the same way, and simultaneously to, changes made to the real vehicle, not only this but all models represent physical systems and so have inherent physical meaning. One feature of the models that does this point justice is the inclusion of detailed mass models, this, as well as allowing for the simultaneous model and real vehicle updating also meant that the models could be fully parameterised with component level data, meaning that no timely and costly rig testing of the real vehicle was necessary to obtain vehicle level parameters. Further to this, important features of the model, such as its modular construction for ease of adaption to other vehicle

platforms were illustrated. The theme of physical modelling carried through into the model validation, where model based test rigs were utilised to validate component models before their assembly into the full vehicle model. Full vehicle model validation was then carried out against test data obtained from the real vehicle on a proving ground. Testing of the standard vehicle proved very useful and correlation between the model and real world data was very strong which provided confidence in the accuracy of the models used in this work.

Chapter 4 gave further justification to this study as it introduced some illustration of why alterations made to the vehicles in this study may lead to changes in their ride and handling characteristics. This was done through the introduction of two very simple vehicle models, through which it looked separately at ride and handling. These simple models also proved useful when discussing the results of the two multibody models, as differences in the top level vehicle responses could be explained by consideration of the analysis of the simple models. Also within this section of the thesis, the design and selection of test manoeuvres was presented. First of all it was shown how simple steady state handling manoeuvres would be conducted in order to obtain the different steering responses in different steady state conditions. These steering responses were then utilised to obtain equivalent steering inputs for both vehicles to allow them to obtain/target the same steady state responses during the transient manoeuvres.

Comparison of the vehicle models began in chapter 5 with the simulation and analysis of both vehicle models in the ride domain. Due to the nature of the results obtained from these simulations, a large part of the analysis took on a statistical form. To summarise the findings, it was found that at higher speeds, due to more coupling in pitch and bounce modes the GTV exhibited larger levels of contact patch

load variation and as such greater levels of occupant discomfort at the front of the vehicle but very slightly increased comfort at the rear due to the shift in Cog and spring centre. It was also found that there was a level of asymmetry in the contact patch load variation and ride comfort of the GTV that was only noticeable on the smoother variant of the two roads used. The rearwards migration of the Cog and the stiffer rear suspension springs of the GTV were found to be the reason for the larger contact patch load variation and decreased occupant comfort at the front of the vehicle. The asymmetry seen in the GTV was attributed to inadequacies in the low speed damping that arose due to the altered mass distribution. This effect only presented itself during simulations with the smoother of the two roads, as in such situations the dampers were spending a much higher percentage of their time in low speed regions. It is the low speed damping that controls the motions of the sprung mass, and so any changes to the sprung mass properties will require changes to the low speed damping. Similar effects were not seen on the rougher roads as here inputs are more severe so the high speed damping is most frequent, as this is tuned primarily for isolation of road inputs and control of the un-sprung mass, changes to sprung mass will not have such a large impact on these damping requirements. The requirement for low speed damping was shown to follow the migration of the Cog, in this case it is the right rear that requires the largest addition.

Chapter 6 was concerned with the handling domain results and analysis. The two vehicles' handling was investigated in two main areas, steady state and transient. The two vehicles' steady state handling was compared through constant radius manoeuvres, from this their steering responses could be directly compared. Due to the stiffening of the rear suspension springs and the rewards movement of the Cog, the GTV possessed a lower steering response than the SV, stating that it had less of

an understeer characteristic. Outside of the linear region, differences between the two vehicles were largest at higher speeds.

The transient handling analysis could be further subdivided into two parts; initial transient responses, and, transient to transient responses (pure transient handling), these were investigated using ramp to step steer and sinusoidal steer manoeuvres respectively. By carrying out said manoeuvres over the entire vehicle speed and lateral acceleration range, response metrics could be plotted over these same ranges, allowing for easy identification of differences in the two vehicles' handling characteristics. Once these differences had been identified they were investigated further by interrogation of vehicle and component level responses.

It was shown that due to the mass and inertia properties of the GTV differing from the SV, its handling had changed quite significantly. The GTV was shown to exhibit slower lateral acceleration responses across all test ranges, the difference in magnitude of lateral acceleration responses between vehicles is speed dependant, below the GTV's tangent speed its lateral acceleration responses are smaller than those of the SV, and above this speed they are larger. The GTV was shown to always exhibit larger yaw rates than the SV, however its yaw rate response times are also shown to have a higher speed dependency than the SV's, at lower speeds it's responses are faster than the SV's yet at higher speeds they are slower.

During the sinusoidal steer manoeuvres, where focus was on purely transient handling, trends in lateral acceleration were seen to be the same as those observed when investigating the ramp to step steers, only the differences between vehicles was smaller. Yaw rates and the associated response times were quite different, now below the GTV's tangent speed its yaw rate responses were smaller and slower than the SV's, above this speed it exhibited larger and faster responses than the SV.

All the trends found in the handling results are heavily linked to the changes in mass and mass distribution. Due to the more rearward mass distribution of the GTV it obtains larger rear slip angles and so different body slip angles than the SV, facilitating its lower tangent speed. Due to its higher mass and yaw inertia the GTV's DI has increased, this influences the total lateral force generation and slows the GTV's lateral acceleration responses. However at the same time, the GTV also owes to this its ability to create much larger yaw moments and so larger yaw rate responses. It has been shown that the effect of the inertial properties is largest at low speeds when slip angles have longer to develop. It has also been shown that they are less effective during pure transient handling as in such conditions, responses are governed by the larger slip angles already present within the tyre, this explained the normalisation of the lateral acceleration responses between the two vehicles, and the trends in yaw rate seen in the pure transient conditions.

7.1 Conclusion in a Wider Context

During the literature review a number of hybrid electric vehicles were introduced, it seems important, that whilst this study focussed on one type of series hybrid vehicle, that the results obtained can be applied to other versions of hybrid architecture. The vehicles that were introduced at the beginning of this study in the literature review will again be discussed here as a means of applying the results of this research to a wider context.

Before continuing to discuss how the findings from this study can be applied to such vehicle configurations, it will be worthwhile re-introducing some of the main vehicle metrics from both the ride and handling domains that were shown to effect vehicle responses. However in this context we shall consider how such metrics change with vehicle configuration.

From the handling domain these metrics are the DI and USG. Figure 7-1 shows DI plotted against USG, this data was obtained from the Dymola model of the GTV, the DI and USG were altered by moving the position of the battery pack along the x axis, spring rates at the front and rear were altered in order to keep ride heights and ride frequencies the same. USG's are taken at 0.15g on a 60m radius. The figure shows that from the far left of the x-axis, moving to the right, the mass distribution shifts forwards, the DI reaches a minimum where the yaw inertia is a minimum.

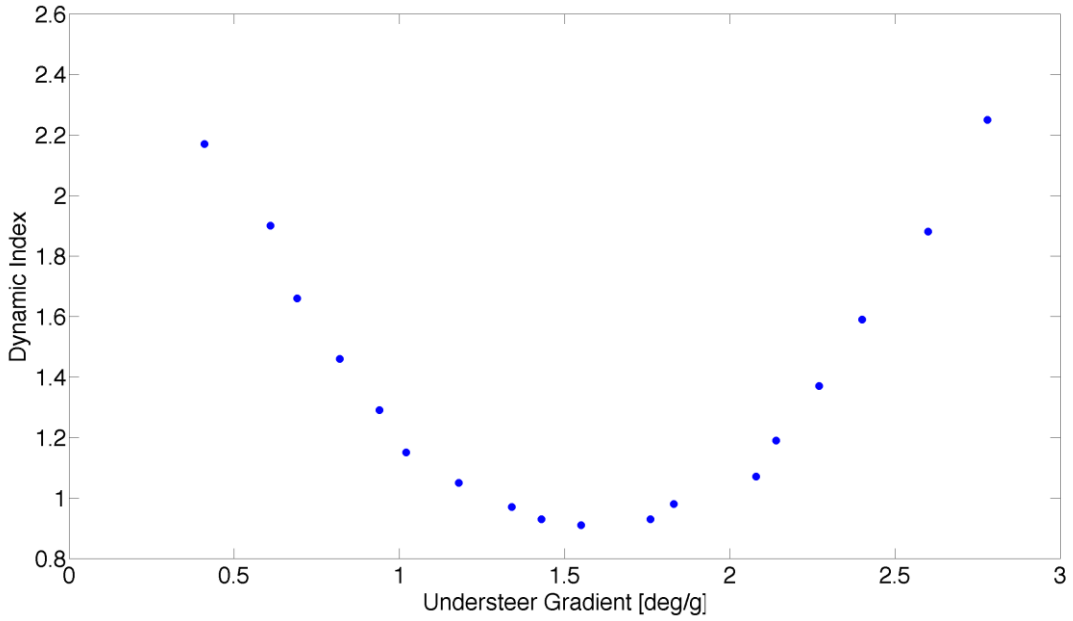

Figure 7-1 DI and USG

This figure shows the general behaviour of the USG and DI with changing mass distribution, it should be noted though that values from it should not be quoted as absolute, it is quite specific to the vehicles within this study, with their ride frequencies, wheelbase and mass properties. The translation of the curve along the x-axis can be effected by roll stiffness distribution, and the steepness by the separation of the front and rear stiffness's. It can however be used to show how such vehicle metrics respond to vehicle parameter changes, if the axes are considered non

dimensional. The shape of the curve will always follow a second order quadratic, only the scaling will change with vehicle parameters.

In the ride domain, basic metrics that helped with analysis were obtained from the 2dof pitch and bounce model. Figure 7-2 shows the movement of the oscillation centres (e and f) for the same vehicle parameters that were used to obtain the DI and USG data in Figure 7-1. As the geometric relationship between the spring centre and the Cog is held constant, the position of the spring centre from the front axle is used as the independent x-axis. The region bounded by the vertical lines (between the a spring centre of -1.05 and -1.45m from the front axle) indicates acceptable oscillation centre locations as defined by Olley's criteria for good ride, that is that the lower of the two frequencies (pitch or bounce) is started first by an input from the road (oscillation centre e inside wheelbase).

Beginning at the left hand side of the x-axis represents a vehicle with a very rearward mass distribution, and as such, ride springs that are stiffer at the rear than the front, moving along the axis to the right represents the Cog moving forwards in the vehicle (facilitated here by battery pack location), the maxima of both curves represents the point where the pitch inertia is at its lowest and as such the $\frac{k^2}{a.b}$ ratio also reaches its minimum. As with Figure 7-1 this data is quite specific to vehicles on this study, however the relationship shown can be applied to other similar vehicles, as a means of showing the effect of certain vehicle parameters in the ride domain.

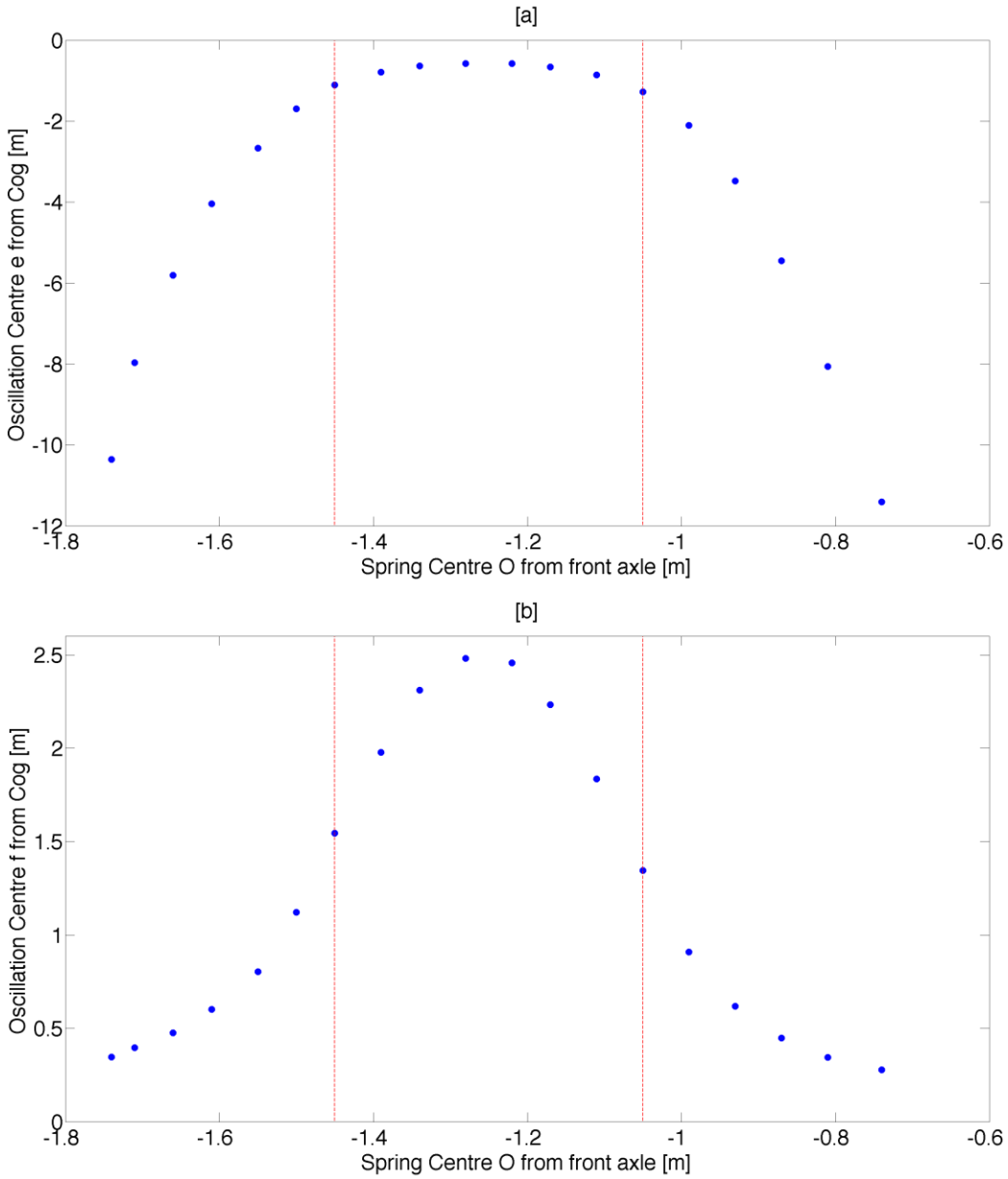

Figure 7-2 Oscillation centres from pitch and bounce model

7.1.1 Series Hybrid Electric Vehicles

SHEV's employ a downsized ICE coupled with a generator unit to create power to drive a separate motor generator unit, which in turn drives the wheels. As there is no need to have a mechanical connection between the wheels and the ICE/generator unit, it can be packaged freely within the vehicle, however, space within passenger road vehicles is quite limited, therefore based on current architectures, and what can be considered possible, it is foreseen that the ICE and generator can be either located

at the front or rear of the vehicle. As for the battery pack it can be surmised, from a packaging perspective, that it must then be placed at the opposite end of the vehicle than the ICE/generator unit, or distributed along the centre of the vehicle in the floor such as in the Mercedes AMG Coupe Electric drive and the GM autonomy concept. As for the drive motor, this can in theory be placed at the front or rear, even multiple drive motors could be used to drive the front and rear axles, even individual corners independently, such setups are hypothesised in literature due to the ease at which drive forces can be used to manipulate vehicle dynamics. With the placement of these main power-train components in mind, we can use the information that has been presented in this research, and create hypotheses regarding the parameters that the previously mentioned vehicle layouts could possess.

A SHEV architecture with downsized ICE/generator and the front and battery pack at the rear represents the vehicle that was investigated within the main body of this work, and so will not be discussed again here.

A SHEV with a downsized ICE/generator in the rear, with battery pack at the front can be considered opposite to the layout that was studied within this research. Such vehicles would possess a considerable forward weight distribution, especially as a portion of, or even all of the battery pack could be in front of the front axle, as such there would be a need to significantly stiffen the front springs and soften the rears, also the yaw and pitch moments of inertia are likely going to be quite high.

The third possible configuration for the SHEV is with the battery pack located along the floor of the vehicle, and with ICE/generator at front or rear, it is envisioned that such a vehicle would possess a very central weight distribution, low Cog position and low yaw and pitch moments of inertia.

7.1.2 Parallel Hybrid Electric Vehicles

PHEV's power-trains are more complex than SHEV's, they can drive the vehicle via EM, ICE or a mixture of the two, as such they have mechanical connections between both ICE and EM and the wheels. This means that packaging isn't quite so free as for the SHEV, although in passenger road vehicles there isn't the amount of free space required to take full advantage of the SHEV architecture, so layout differences seen between PHEV's and SHEV's will not be so large. One advantage of the PHEV is that it doesn't need a separate generator unit like the SHEV, it does however still require a gearbox as the ICE is used to drive the wheels. The PHEV power-train still consists of an ICE (with gearbox) an EM and a battery pack.

As discussed in chapter 2 there are two distinct ways in which a PHEV can be implemented, the first being to downsize the ICE and supplement it with an EM, the second is termed a power hybrid where by the ICE is not downsized and the EM is used for extra performance. The first of these, from a packaging perspective can be viewed as the same as a SHEV, the downsized ICE and EM are likely to be of similar mass and dimensions to the ICE/generator and EM within a SHEV, and as such similar packaging options are available. As it is assumed that, as in this study, the battery pack is by far heaviest single component, it would again be sensible to assume that the ICE and EM would be placed at the opposite end of the vehicle to the battery pack, or at either end with the battery pack in the centre, resulting in a similar vehicle layout, in terms of mass properties to the SHEV's discussed in the previous section.

The power hybrid variant of a PHEV on the other hand will have a considerably heavier ICE (as it is not downsized), this leads to a hypothesis that the ICE with gearbox and EM will balance the weight of the battery pack if mounted at opposite

ends of the vehicle. The resulting vehicle would likely possess a very central weight distribution, it will have a larger mass than the SHEV's previously discussed, and very large yaw and pitch moments of inertia.

It can also be assumed that PHEV layouts with a battery pack in the centre along the floor of the vehicle would have a weight distribution governed by the positioning of the ICE and EM. So a PHEV with ICE and EM at the front and battery pack in the centre would have a forward weight distribution and vice-versa. Both of which would have lower yaw and pitch moments of inertia than the architectures with the battery pack at the longitudinal extremities. Such variants would require spring rates that would allow for carrying the extra mass at the given end of the vehicle.

7.1.3 Series Parallel Hybrid Electric Vehicles

The SPHEV has the most complex power-train architecture of the vehicles discussed so far, as it can be run as either a series or a parallel vehicle, it consists of an ICE with a generator, a gearbox with planetary gear system and an EM. It can be assumed that with the added complexity and components from both series and parallel architectures, this power-train will have the highest mass.

As with the PHEV, it is likely that that mass of the ICE, gearbox and generator will be somewhere equal to the mass of the battery pack, once again meaning if they are located at opposite ends of the vehicle, the resulting vehicle will have a very centralised mass distribution, with high yaw and pitch movements of inertia. Similarly the front and rear engine concepts, with battery pack in the centre also hold true for the SPHEV, and similar suspension stiffness's will be required.

7.1.4 Other HEV Variants

Within the literature review a number of other HEV's were discussed, such as micro hybrids, mild hybrids and fuel-cell electric vehicles.

It is thought that micro and mild HEV architectures will not have very much effect on a vehicles ride and handling prosperities, as they can be considered conventionally powered vehicles with the addition of larger starter motors, or have an EM in place of the ICE flywheel, to facilitate engine stop/start, limited low speed driving in electric only mode or power boost. Power-train architectures are the same as for a conventionally powered vehicle, with very minimal mass addition.

Fuel cell electric vehicles on the other hand would most likely fit within SHEV, with the hydrogen fuel cell replacing the ICE as the energy source, the layouts discussed in the SHEV section would still be true for a fuel cell electric vehicle.

7.1.5 HEV architecture summary

In the previous sections the different variants of HEV have been discussed in terms of the possible packaging option available within the limited space of a passenger road vehicle. It was shown that whilst power-train architectures can differ considerably, possible packaging options are quite limited. Due to this, from what has been discussed, it can be said that for SHEV's, PHEV's, SPHEV's and FCHEV's the packaging of the power-train and resulting vehicle configuration can be split into three main groups; forward, central and rear mass distribution.

These three configurations can now be discussed in more detail, in terms of what such a layout means for the resulting vehicles ride and handling characteristics, all the while, the types of HEV layout refers to will be kept mind.

7.1.6 Hybrid Architectures with Forward Mass Distribution

From previous sections, it was decided that a SHEV or downsized PHEV with a downsized ICE, generator and EM located at the rear, with the battery pack located at the front of the vehicle, and both power PHEV's and SPHEV's with ICE and EM at the front and battery pack in the centre could exhibit such a mass distribution.

Such a configuration dictates that the required front suspension stiffness be higher than the rear to carry the load on the front axle, it is also assumed that yaw and pitch moments of inertia could be quite large, especially for the SHEV, those for the PHEV and SPHEV could be slightly less due to the battery pack location.

In the handling domain, both the more forward mass distribution and the stiffening of the front springs dictate an increase in USG. Having a large mass such as the battery pack, at the front of the vehicle, possibly in front of the front wheels (for the SHEV) will also greatly increase the yaw inertia of the vehicle. Based on data from this research, assuming that resulting vehicle masses of vehicles discussed here are similar to the vehicles in this study, it can be assumed such configurations could be placed in Figure 7-1 with a DI above 1.1, and a USG around 2 deg/g. Clearly such values of DI are extremely large and far from an optimal value of between 0.9 and 1 as discussed chapter 4. The USG's are larger than that of the vehicles in question in this study, and whilst it can be considered not outside of a normal range, shown in chapter 3, it can be said it is also quite large. The magnitude of the DI means that such vehicles would exhibit very slow lateral acceleration responses, but on the other hand could exhibit fast yaw rate responses. The larger USG, has obvious effects on the steady state handling of the vehicle and also makes it likely that such vehicles, due to a low characteristic speed will achieve peak yaw rates at low speeds, something that when combined with what has been discussed about the effect of the DI on yaw rate response could be quite dangerous.

Whilst the DI is somewhat fixed by the mass and inertia properties of the vehicle, the USG can be altered with the use of front and rear ant-roll bars. The roll stiffness distribution of the vehicle could be tuned so that the USG would be considerably lower, however this is not as ideal as it first seems. Drastically tuning the USG with

the use of ARB's will only effect the handling of the vehicle once outside the linear range of the tyre, this would lead to a sharp transition from the USG in the linear region of handling to the USG in the non-linear range, something that could feel very strange from a driver's perspective.

Considering these hypothetical vehicles in the ride domain, again making use of the data that was used to derive Figure 7-1 and Figure 7-2, the spring centre would likely lie somewhere over 1 meter behind the front axle. Such positioning shows that the positions of the spring centres could be outside a range deemed acceptable by Olley's ride criteria. It can be seen that the oscillation centre e, might fall outside of the wheelbase and thusly be a bounce centre, leaving oscillation centre f inside the wheelbase as the pitch centre, this means that road inputs will excite oscillations around e, which happens to be the higher of the two frequencies, therefore making it impossible to achieve flat ride.

Such configurations would also mean that the higher comfort region for occupants, that was shown to track the movement of the Cog and spring centre, would be placed very close to the front axle, most likely in front of any occupants of the vehicle, and so all occupants, especially those at the rear would be subjected to lower levels of comfort arising from pitch and bounce motions of the vehicle body.

Clearly such vehicles would also need much increased low speed damping at the front to account for extra mass and stiffer springs on the front of the vehicle.

7.1.7 Hybrid Architectures with Central Mass Distribution

It has been stated that a centralised mass distribution would be obtained in SHEV's and PHEV's (with downsized ICE's) with batteries mounted centrally along the floor of the vehicle and the ICE and EM's located at either end. A power PHEV or a SPHEV can also have centralised mass distributions if the ICE, gearbox and EM's

are placed at one end, and the battery pack at the opposite end of the vehicle. Whilst the mass distribution of these vehicles can be considered similar, there would be a large difference in the inertia properties between the SHEV, downsized PHEV and the power PHEV and SPHEV. The former have the batteries centralised in the vehicle thusly reducing yaw and pitch moments of inertia, the latter two have both ICE and battery pack located at opposite extremities, thusly creating large yaw and pitch moments of inertia.

A mass distribution of 50/50 dictates that the DI will be at its minimum value for a given yaw inertia, mass and wheelbase. Considering Figure 7-1 this puts both vehicles at the minima of the curve, however as the SHEV and downsized PHEV would possess a lower yaw inertia that the power PHEV and the SPHEV this minima will be at a lower DI. Such a configuration is good, so long as the mass, wheel base and yaw inertia don't dictate a DI that is below 0.9, in this situation a vehicle that has very fast transient lateral acceleration responses could be produced, meaning the vehicle could respond too fast for an average driver, possibly creating dangerous situations. Whilst it is likely that the SHEV and downsized PHEV could have a DI as low as 0.9, that of the power PHEV and SPHEV will be much larger, perhaps over 1.1. As for the USG, as the mass distribution is 50/50, and as it is preferable in the ride domain to have a higher ride frequency at the rear, it is conceivable that the USG could be slightly oversteer. Such configurations could have DI and USG characteristics as defined in Figure 7-3. Again the USG's of these vehicles could be tuned with the roll stiffness distributions by adjusting ARB rates, this could however produce vehicles that have an understeer characteristic in the non-linear region of handling and an oversteer characteristic in the liner region.

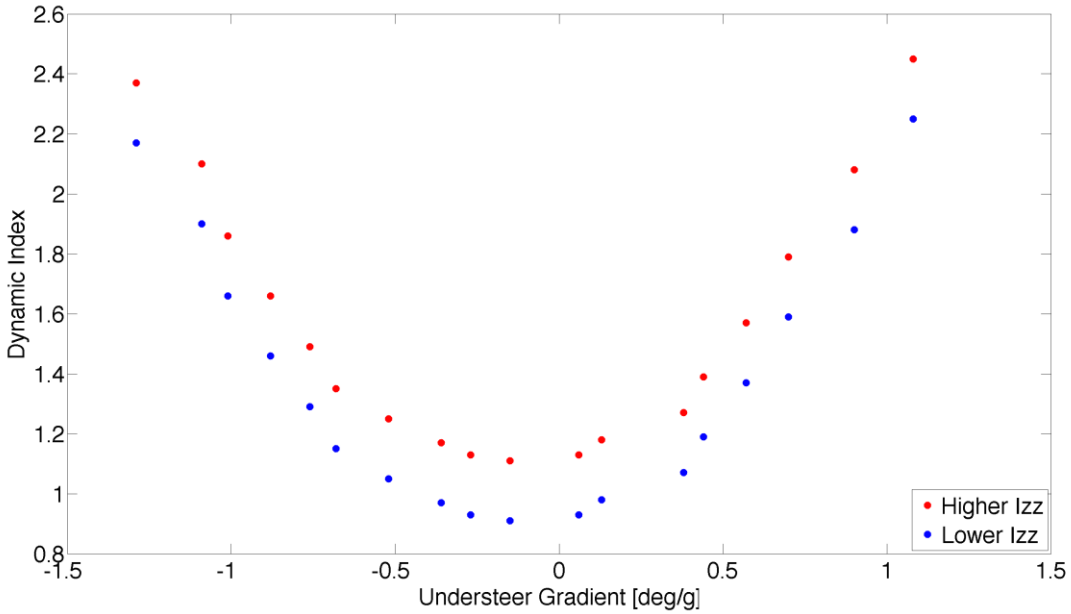

Figure 7-3 Example of DI and USG relationship with low USG

Once again turning our attention to the ride domain, the vehicles here with their centralised weight distribution, if setup to possess a rear ride frequency higher than the front would also dictate that the spring centre would be placed just rearwards of the Cog, thusly for the SHEV and downsized PHEV, which have lower pitch inertias, it is likely the oscillations centres e and f would fall within the optimum region, somewhere near the maxima on both a and b of Figure 7-2, meaning oscillation centre e would fall within the wheelbase and hence be a pitch centre, causing inputs from the road to start oscillations about f, the lower of the two frequencies first, again satisfying one of Olley's criteria for good ride. However in the case of the power PHEV and the SPHEV, which have been assumed to have quite large pitch moments of inertia, as a result of which, both natural frequencies are lower, and as such the resulting oscillation centres can fall outside of the desired region (however it could be very close to the boundary of being acceptable), oscillation centre e would be behind the rear axle and for reasons previously mentioned this violates criteria for good ride. Unfortunately methods to mitigate

this, i.e. bring the oscillation centre e back within the wheelbase, would worsen the oversteer characteristic in the handling domain, as it facilitates a further separation in front and rear stiffness's.

As both vehicles have a spring centre and Cog near the centre of the vehicle, it is likely that the higher comfort region within the vehicle is situated around the occupants, thusly improving ride comfort.

7.1.8 Hybrid Architectures with Rearward Mass Distribution

Finally let us consider hybrid vehicle architectures that can have a rearwards mass distribution. It was assumed that a SHEV or downsized PHEV with downsized ICE, generator and EM located at the front with battery pack located at the rear (a more extreme version of the vehicles in this study), a PHEV and a SPHEV with centralised battery pack and rear mounted ICE, generator and EM's, would possess a significant rearwards weight distribution, the power PHEV and SPHEV even more so than the SHEV or downsized PHEV.

With a significant rearwards mass distribution, rear stiffness's would need to be significantly higher than the front, yaw a pitch moments of inertia could be considered similar to forward mass distribution scenarios, and lower than the power PHEV and SPHEV with centralised mass distributions. Such a stiffness and mass distribution would almost certainly dictate an oversteer characteristic in terms of the USG of such vehicles. As yaw moments of inertia could be similar to the forward mass distribution scenario, it makes sense to assume the DI would be of the same magnitude, possibly as large as 1.1. This clearly shows DI and USG values that can be considered anything but as desired. The negative, (oversteer), USG would make such a vehicle unstable and dangerous, re-visiting what has been mentioned previously with tuning of roll stiffness distribution to effect the USG again could fix

the problem in the non-linear range of handling but not the linear range. The high DI will give the vehicle slow lateral acceleration responses, but faster yaw rate responses. Overall it can be considered preferable to have a high DI over a low DI coupled with a low USG, but such metrics are a long way from optimal.

In the ride domain the spring centre and Cog will be significantly rearwards, meaning, the higher comfort region will be also, as in this study subjecting occupants at the front of the vehicle to higher levels of discomfort. It is likely that the positions of the oscillation centres will fall just outside the desired region in Figure 7-2, to the left. Again meaning it is possible that the oscillation centre e could fall outside the wheelbase, leading to poor ride quality.

As in this study, and as was mentioned for the forward mass distribution layout, significantly more low speed damping would be required on the rear than the front due to the higher mass and stiffness on the that axle.

7.1.9 Summary of Hypothetical Vehicle Layouts

From the discussion of possible, perhaps extreme, vehicle layouts for the main hybrid architectures discussed in the last few sections, it is apparent that certain trends are present.

SHEV's with ICE, generator and EM located at the rear and battery pack at the front, along with PHEV and SPHEV with front mounted ICE etc. and mid battery pack location, result in vehicles with high USG's and DI's, the probability of oscillation centres falling in a location where good ride could be achieved is low, and the higher comfort region within the vehicle would be located quite far forwards in the vehicle.

SHEV's and downsized PHEV with central batteries and ICE etc. at either end, along with power PHEV and SPHEV with batteries and ICE/motors at opposite

ends, produce vehicles with possible oversteer characteristics, negative USG's, and lower DI's for vehicles with low yaw and pitch moments of inertia, but higher DI's for vehicles with high yaw and pitch moments of inertia. For the vehicles with lower yaw and pitch inertias, it is foreseen that good ride could be achieved, as the mass properties dictate good locations of the oscillation centres. In terms of the vehicles with higher inertias, it is possible that good ride could also be obtained, although oscillation centres could fall just outside of the desired region. Having said this for both high and low yaw and pitch inertia variants, the higher comfort (lower vertical acceleration) region inside the vehicle is likely to surround the occupants, thusly improving ride comfort within such vehicles.

Finally, a SHEV or downsized PHEV with ICE etc. mounted at the front of the vehicle with battery pack at the rear, or a power PHEV and SPHEV with centralised battery pack and ICE etc. at the rear, can be thought to tend towards vehicles with steady state oversteer characteristics, and larger DI's. Oscillation centres again are likely to fall outside of what is desired for good ride, and the higher comfort region within the vehicle will be shifted considerably towards the rear.

Figure 7-4 and Figure 7-5 show regions where the discussed vehicle configurations lie with regard to their DI, USG and oscillation centres. From this discussion it is possible to draw conclusions on which type of layout should be targeted for each specific hybrid architecture discussed.

SHEV's with a battery pack at the rear and downsized ICE and generator at the front could, in its extreme, perhaps with drive motor also at the rear, lead to a vehicle which is dangerous due to it having a steady state oversteer characteristic, it's DI will likely be higher also giving issues with transient responses. It could be difficult to achieve good ride due to unfavourable oscillation centre positions, again

especially in extreme cases. However such a configuration, if not at the extreme, as was shown in the main body of this research can lead to a vehicle with satisfactory ride and handling characteristics, careful placement of ICE, motors and batteries will be required to ensure the weight distribution does not shift too far rearwards.

The opposite configuration to this, a SHEV with battery located at the front and ICE at the rear, can be seen as a safe option. It will have high USG and DI. Whilst a high DI can lead to fast transient yaw rate response, it will exhibit slower transient lateral acceleration responses, coupled with a high USG could produce a vehicle that fells 'lethargic' and 'unresponsive' but would not produce any dangerous situations. Such a configuration could be beneficial for larger, slower vehicles, but would not be a good configuration for higher performance vehicles. In an extreme forward weight distribution configuration it could prove difficult to achieve good ride characteristics, as with its opposite layout, however again with careful battery pack and ICE packaging it could be possible to minimize such a forward weight distribution and perhaps achieve satisfactory ride characteristics.

The SHEV with a mid battery pack location, and ICE etc. located at either end, could be a good option. However it has the possibility to produce a vehicle with steady state oversteer characteristics and a low DI, which would not be good combination. However if weight distribution can be kept just outside of the 50/50, preferably towards the front with some careful packaging, or if rear cornering stiffness can be reduced by careful tyre sizing and construction, then a vehicle with a modest USG and fairly optimal DI could be produced. The ride domain situation is also positive, its lower pitch inertia and centred mass distribution should mean that it is fairly easy to create a vehicle with fundamentally sound ride characteristics, which

should make achieving good ride much easier. Higher occupant comfort would also be present as the occupants would be seated around the Cog and spring centre.

These three vehicle configurations give rise to the same conclusions for the downsized PHEV.

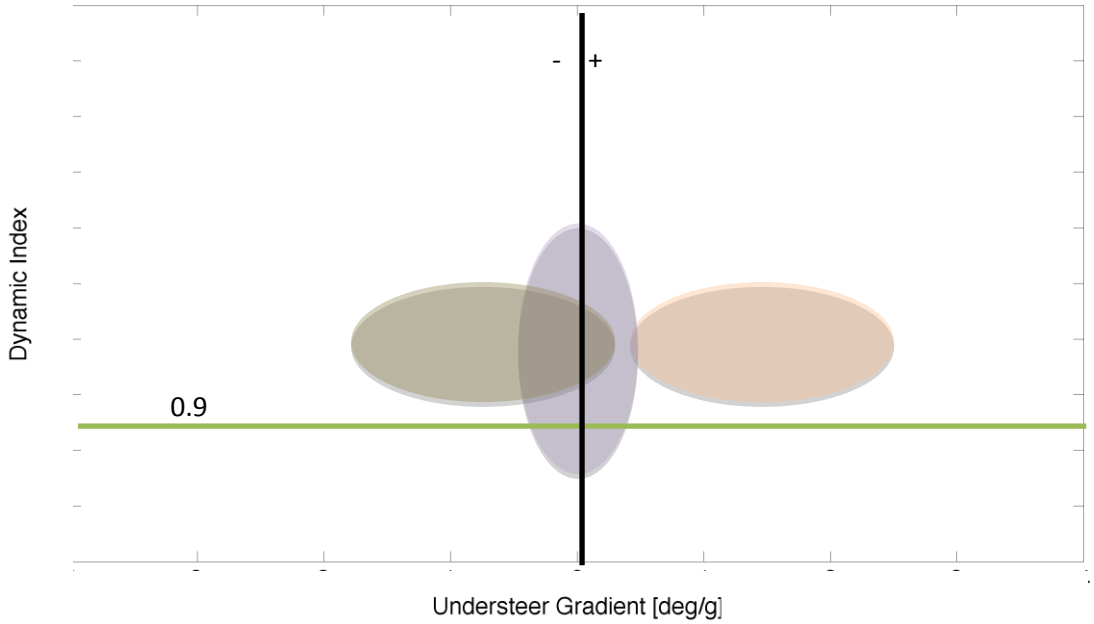

Figure 7-4 General DI and USG regions

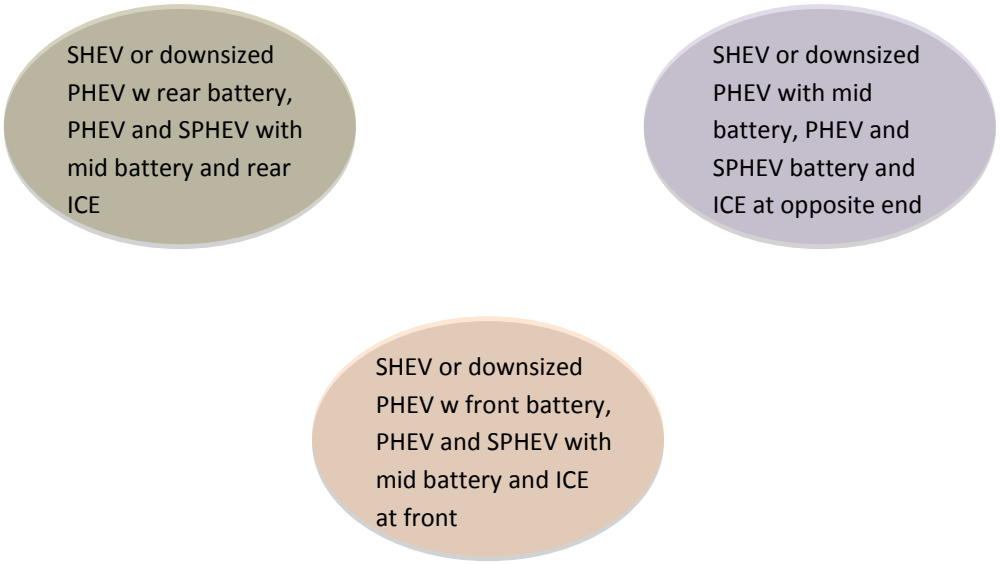

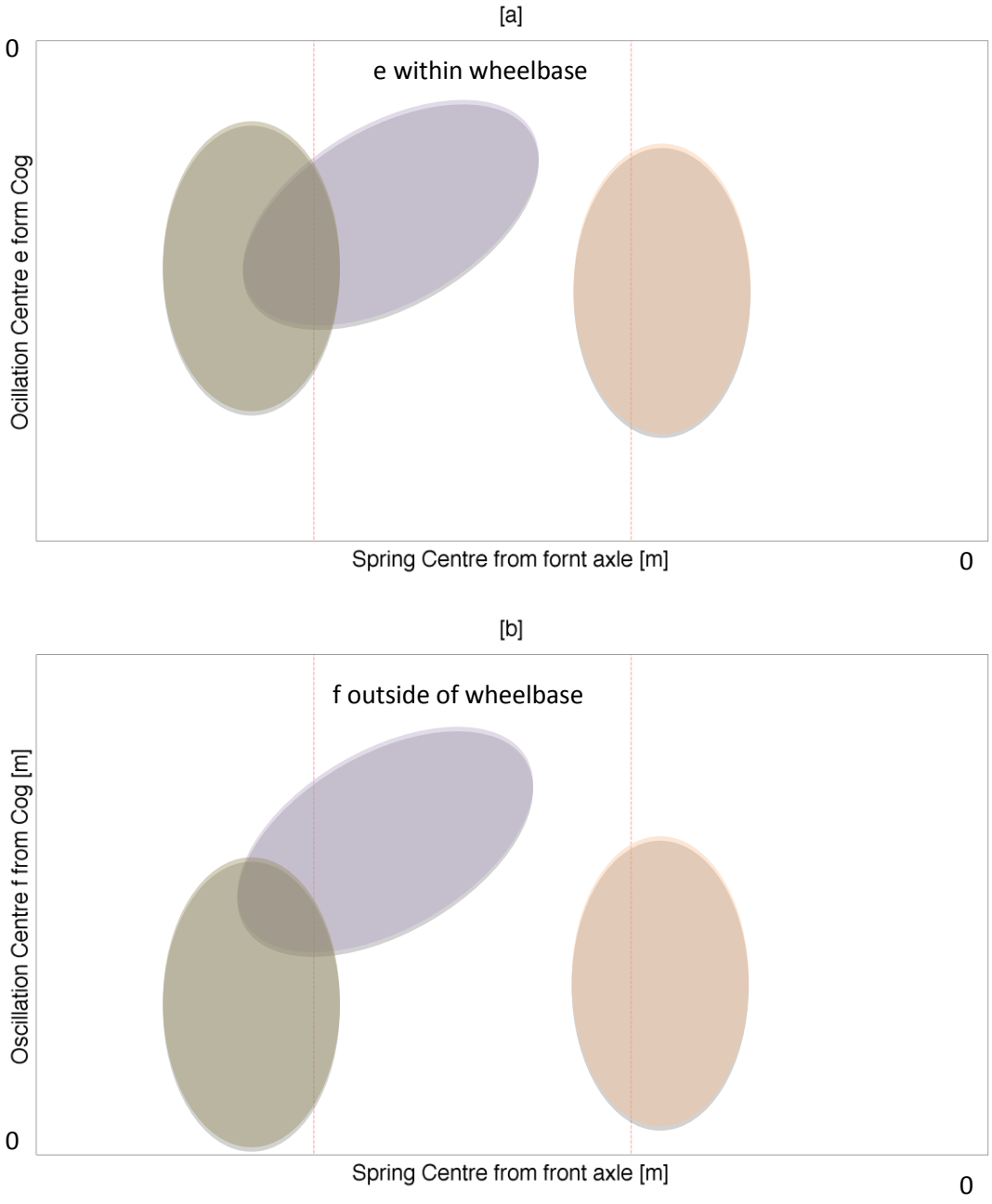

Figure 7-5 Oscillation Centre regions

In terms of the power PHEV and SPEV, the mid battery and rear ICE location could lead to a vehicle with steady state oversteer characteristics. It will have a moderate to high DI. Good ride characteristics again could be difficult to achieve, due to a rearward spring centre. However as with other vehicles mentioned, with careful packaging, and/or tyre sizing and construction, if a not too rearward weight

and stiffness distribution could be achieved then it would be possible to obtain satisfactory ride and handling characteristics.

Power PHEV's and SPHEV with mid battery location and ICE etc. at the front, again represent a safe option in terms of handling, such a layout would produce vehicle with large USG's and moderate to high DI's. It could be possible to obtain good ride, but at their extreme, considerably stiffer front suspension would be needed than rear, possibly making it difficult to locate oscillation centres in an area that could lead to fundamentally good ride characteristics. Again as this is a safe option it could be well suited to larger vehicles, it would however lead to vehicles that could feel 'unresponsive' in terms of their handling, something not well suited to sportier applications.

Finally the power PHEV and SPHEV with battery and ICE at opposite ends, would lead to a vehicle with a high DI due to large moments of inertia, however due to a centralised weight distribution it could have quite a low or even negative USG. Such a vehicle's larger pitch moment of inertia would also make it difficult to achieve good ride at a fundamental level. One plus of such layouts is that again as the Cog and spring centre are central, occupants would be seated in a higher comfort region within the vehicle. Generally however it is foreseen that this layout would not produce a vehicle with satisfactory ride or handling characteristics.

Whilst these last few sections have given an insight into what can be expected with certain architectures, actual vehicle parameters will be very specific to the vehicle in question, and mass and inertia properties will vary. However these sections present a likely trend, and as such can be used to assume general ride and handling characteristics about such vehicle. It has been shown that mass and inertia properties play a large role in governing whether a vehicle can have good or bad ride

and handling, it should however be noted that careful packaging and consideration of resulting suspension stiffness's (via tyre cornering stiffness) can be used to tune vehicles that have been said to be just outside what is considered acceptable to get them to exhibit satisfactory ride and handling characteristics.

From this section a first guess at an acceptable layout for a certain future hybrid architecture can be made, in general extreme weight distributions should be avoided with any, and aiming for a weight distribution near 50/50 with not excessive moments of inertia is seen to be positive for all hybrid architectures discussed.

Mass and inertia parameters in future hybrid vehicles look set to become more influential on ride and handling, as a result, such parameters need more in depth consideration in terms of their effects on vehicle ride and handling at the outset of design. Whilst mass and inertia properties are extremely influential on vehicle ride and handling, they are not easy to tune downstream of the design stage due to packaging requirements.

Whilst focussing on the benefits of new technologies, older fundamentals should not be overlooked, the philosophy of the hybrid vehicle, that the sum of the technologies should be of greater value than their constituent parts, should always be kept in mind and applied to all areas of the vehicle, including ride and handling.

7.2 Contribution

This thesis has resulted in an improved understanding of how the inclusion of hybrid drive-trains and their associated components influence a vehicles ride and handling characteristics. It is important to note that this study has not included the effects of any control systems whose use may be made possible by the inclusion of hybrid drive. Further to this the realms of this study are based within the sub-limit to limit

handling, no work on post limit handing has been conducted. The contributions that have been made by this study are as follows;

1. The effects on ride and handling, of creating a REEV (SHEV) from an existing front engine conventionally powered vehicle have been investigated. This has lead to a greater understanding of what mechanisms contribute to changing the vehicles ride and handling characteristics. Such information is valuable for vehicle designers and manufactures of future hybrid vehicles.
2. The position of the centre of percussion (DI ratio) has been shown to be an extremely useful metric in determining the effects of the different inertial properties encountered from the inclusion of hybrid drive-trains on vehicle transient handling. Consideration of this metric may be useful for vehicle designers at the outset of hybrid vehicle design to ensure correct inertial properties are obtained at that point, as downstream tuning of such vehicle parameters is extremely difficult.
3. A new form of vehicle benchmarking/data analysis in the handling domain has been introduced. This utilised input parameter sweeps in the modelling domain to obtain vehicle responses over the vehicles entire operational range. Visualisation of response metrics over this range allows for easy identification of trends and patterns in responses, which could prove useful for future vehicle model benchmarking and comparative studies.
4. Research of open loop test methods for obtaining steady state vehicle characteristics showed that currently speed ranges are not accounted for directly in vehicles steering responses. This work presented the need to conduct multiple test manoeuvres on increasing constant radii in order to obtain steering responses over the vehicles planned speed range to somewhat

decouple lateral acceleration and longitudinal velocity as each have their own effect on the steering response of the vehicle.

5. Main findings from this research have been generalised, and applied to current hybrid vehicle architectures, as a means of showing what factors should be accounted for, and which packaging options are preferable for ride and handling when considering a new hybrid vehicle.

7.3 Future Work

The research accomplished within this study has made a large step in investigating how hybrid drive-trains and technologies affect vehicle ride and handling, however there is considerably more scope to this problem. Whilst this study has looked at vertical and lateral vehicle dynamics there is the need to assess vehicle longitudinal dynamics. The introduction of electric motors into vehicle drive-trains is likely to affect vehicle driveability, also braking dynamics are likely to change significantly with the introduction of regenerative braking, such effects could be investigated using similar methods as have been utilised in this study. Other benefits of electric motors in vehicle drive-trains, through their fast response times and high torque deliveries, include possibilities for further active control systems, such systems could be used to greatly manipulate vehicle ride and handling and need further in depth investigation, in combination with the passive/pure vehicle dynamics effects investigated here.

It was also mentioned when discussing the ride domain results that technologies such as hydraulically interconnected suspensions and inerters may prove beneficial for the ride and handling of future hybrid vehicles, this is clearly an area of investigation that should be pursued.

Finally the vehicle model developed in this study has been done so in such a way that it is capable of forming the basis of future work to be carried out in vehicle ride and handling. It can easily be extended to include extra degrees of freedom, such as compliant drive-trains for the aforementioned study of driveability and longitudinal vehicle dynamics. It can easily be interfaced with control models to assess the advantages achievable by active control of hybrid drive-trains. Furthermore its modular construction lends it to being easily adaptable to form other variants of hybrid vehicles. It is envisaged that hybrid vehicles will become more popular and it is certain that technologies within such vehicles will continue to develop, this model can form the basis of future models that can be used to investigate all of the above within one modular adaptable model.

References

ACEA 2004. ACEA's CO2 Commitment. Brussels: European Automobile Manufacturers Association.

Actel 2007. Improving ADC Results Through Oversampling and Post-Processing of Data. *available at http://www.actel.com/documents/Improve_ADC_WP.pdf*, accessed 16/10/13.

Akhgari, A., Sangtarash, F., Esfahanian, M. & Amiri, M. (2008). Modeling and Optimizing Handling Parameters of a Series Hybrid Electric City Bus Using Adams/Car. *In:* SAE International Power-trains, Fuels and Lubricants Congress, June 23-25 Shanghai, China. SAE International, Paper No 2008-01-1560.

Aliexpress. 2010. *IDG-500 Breakout Board Specification* [Online]. Available: http://www.aliexpress.com/store/product/For-Arduino-Gyro-Breakout-Board-IDG500-Dual-500-D-s-Integrated-X-and-Y-axis-Gyros/214862_671252907.html, accessed 05/01/2010.

Amjad, S., Neelakrishnan, S. & Rudramoorthy, R. (2010). Review of design considerations and technological challenges for successful development and deployment of plug-in hybrid electric vehicles. *Renewable and Sustainable Energy Reviews*, Vol 14, Pages 1104 - 1110.

Amjada, S., Neelakrishnana, S. & Rudramoorthy, R. (2010). Review of design considerations and technological challenges for successful development and deployment of plug-in hybrid electric vehicles. *Renewable and Sustainable Energy Reviews*.

Andreasson, J. (2007). *On Generic Road Vehicle Motion Modelling and Control.* Ph.D. Thesis, KTH Vetenskap Och Konst.

Assadian, F. & Hancock, M. (2006). Impact of regenerative braking on vehicle stability. *In:* Hybrid Vehicle Conference, The Institution of Engineering and Technology, Coventry, UK. Pages 173 - 184.

Automotive Intelligence. 2003. *General Motor Autonomy Concept* [Online]. Available: http://www.autointell.com/nao_companies/general_motors/gm-autonomy/gm-autonomy-02.htm accessed 06/06/2013.

Bayindir, K., Gözüküçük, M. & Teke, A. (2011). A comprehensive overview of hybrid electric vehicle: Power-train configurations, power-train control techniques and electronic control units. *Energy Conservation and Management*, 52, 1305 - 1313.

Beiker, S. A. & Vachenauer, R. C. (2009). The Impact of Hybrid-Electric Power-trains on Chassis Systems and Vehicle Dynamics. *SAE International,* Paper No 2009-01-0442.

Blundell, M. & Harty, D. (2004). *The Multibody Systems Approach to Vehicle Dynamics*, Elsevier Butterworth-Heinemann.

Bobier, C. G., Laws, S. M. & Gerdes, C. J. (2008). *Transient Response of Alternative Vehicle Configurations: A Theoretical and Experimental Study on Effects of Atypical Moments of Inertia.* American Automotive Control Conference, June 11 - 13 Seattle, Washington, USA. Pages 230 - 235.

Bogsjö, K. (2007). Evaluation of Stochastic Models of Parellel Road Tracks. *Journal of Probabilistic Engineering Mechanics,* 22, 362 - 370.

Bogsjö, K. (2009). Coherence of road roughness in left and right wheel-path. *Vehicle System Dynamics: International Journal of Vehicle Mechanics and Mobility,* 46, 599 - 609.

Brown, P., Jackson, N., Sykes, L., Wheals, J. & Wiseman, M. (2002). *A Hybrid and Fuel Cell Vehicle Future?* Future Car Congress, June 2 -5 2002 Arlington, Virginia.

Browne, A. L. & Arambages, A. (1981). Modelling the Thermal State of Tyres for Power Loss Calculations. *SAE technical paper series*, Paper No 810163.

BS2631-1:1997 1997. Mechanical Vibration and Shock - Evaluation of human exposure to whole-body vibration, Part 1: General Requirments. BSI.

BS4138:2004 2004. Passenger Cars - Steady-state circular driving behaviour - Open loop test methods.

BS7853:1996 1996. Mechanical Vibration - Road Surface Profiles - Reporting of Measured Data.

BS7853:1996 2011. Road Vehicles - Lateral transient response test methods - Open loop test methods. BSI.

BS150037-1:1998 1998. Road Vehicles - Vehicle dynamics test methods - Part 1: General conditions for passenger cars.: BSI.

BSISO 2011. Road Vehicles - Lateral transient response test methods - Open loop test methods. BSI.

Burke, A. (2007). Batteries and Ultracapacitors for Electric, Hybrid, and Fuel Cell Vehicles. *Proceedings of the IEEE,* Vol 95, Issue 4, Pages 806 - 820.

Cebon, D. & Newland, D. E. (1983). Artificial Generation of Road Surface Topography by the Inverse F.F.T. Method. *Vehicle Systems Dynamics*, 12, 160 - 165.

Chan, C., Bouscayrol, A. & Chen, K. (2010). Electric, Hybrid, and Fuel-Cell Vehicles: Architectures and Modeling. *IEEE Transactions on Vehicular Technology,* Vol 59, Issue 2, Pages 589 - 598.

Chan, C. C. (2007). The State of the Art of Electric, Hybrid, and Fuel Cell Vehicles. *Proceedings of the IEEE,* Vol 95, Issue 4, 704 - 718.

Chau, K. & Chan, C. (2007). Emerging Energy-Efficient Technologies for Hybrid Electric Vehicles. *Proceedings of the IEEE,* Vol 95, Issue 4, Pages 821 - 835.

Chau, K. T. & Wong, Y. S. (2002). Overview of Power Management in Hybrid Electric Vehicles. *Energy Conversion and Management,* Vol 43, Issue 15, 1953 - 1968.

Chen, K., Bouscayrol, A., Berthon, A., Delarue, P., Hissel, D. & Trigui, R. (2009). *Global Modelling of Different Vehicles*. IEEE Vehicular Technology Magazine. IEEE.

Chu, T. (2001). *Eigenstructure Analysis of Automobile Steering Dynamics with Application to Robust Four-Wheel-Steering Control.* Ph.D. Thesis, University of Warwick.

Crolla, D., Ren, Q., ElDemerdash, S. & Yu, F. (2008). *Controller design for hybrid vehicles – state of the art review.* IEEE Vehicle Power and Propulsion Conference, Harbin. Pages 1 - 6.

Dixit, N., R,. (2009). *Evaluation of Vehicle Understeer Gradient Definitions.* MSc, Ohio State University.

Dodds, C. & Robson, J. (1973). THE DESCRIPTION OF ROAD SURFACE ROUGHNESS. *Journal of Sound and Vibration*.

Dorfi, H. R., Keum, B. B. & Wheeler, R. L. (2005). Vibration Models of Radial Tires: Application to Rolling and Non-Rolling Events. *SAE Technical Paper 2005-01-2526*.

Dugoff, H., Fancher, P. & Segel, L. (1970). An Analysis of Tire Traction Properties and Their Influence on Vehicle Dynamic Performance. *SAE Technical Paper 700377*.

ECCC. 2012. *Road transport: Reducing CO2 emissions from vehicles* [Online]. Available: http://ec.europa.eu/clima/policies/transport/vehicles/index_en.htm accessed 22/06/2013.

Emadi, A. (2005). *Handbook of automotive power electronics and motor drives,* Taylor & Francis.

Emadi, A. & Wirasingha, S. (2011). Classification and Review of Control Strategies for Plug-In Hybrid Electric Vehicles. *IEEE Transactions on Vehicular Technology,* Vol 60, Issue 1, Pages 111 - 122.

Emadi, A., Yoong, M. & Rajashekara, K. (2008). Power Electronics and Motor Drives in Electric, Hybrid Electric, and Plug-In Hybrid Electric Vehicles. *IEEE Transactions on Industrial Electronics,* Vol 55, Issue 6, Pages 2237 - 2245

Farahani, A., Palmer, T. & Zhang, Y. (1998). A Finite Element Tire Model and Vibration Analysis: A New Approach. *Tire Science and Technology,* Vol 26, Issue 3, 149-172.

Forkenbrock, G. & Elsasser, D. 2005. An Assessment of Human Driver Steering Capability. Washington: National Highway Traffic Safety Administration.

Fredriksson, J., Andreasson, J. & Laine, L. (2004). *Wheel Force Distribution for Improved Handling in a Hybrid Electric Vehicle using Nonlinear Control.* IEEE Conference on Decision and Control, Vol 4, Pages 4081 - 4086.

Gallaghera, K. & Muehleggerb, E. (2011). Giving green to get green? Incentives and consumer adoption of hybrid vehicle technology. *Journal of Environmental Economics and Management,* Vol 61, Issue 1, Pages 1 - 15.

Gao, Y., Chu, L. & Ehsani, M. (2007). *Design and Control Principles of Hybrid Braking System for EV, 1EV and FCV.* IEEE Vehicle Power and Propulsion Conference, Pages 384 - 391.

Gao, Y. & Ehsani, M. (1999). Investigation of the Effectiveness of Regenerative Braking for EV and HEV. *SAE Paper No. 1999-01-2910.*

Gao, Y. & Ehsani, M. (2001). Electronic Braking System of EV And HEV—Integration of Regenerative Braking, Automatic Braking Force Control and ABS. *SAE Paper 2001-01-2478.*

Gao, Y., Ehsani, M. & Miller, J. (2005). Hybrid Electric Vehicle: Overview and State of the Art. *Proceedings of the IEEE International Symposium on Industrial Electronics,* Vol 1, Pages 307 - 316.

Genta, G. (2006). *Motor Vehicle Dynamics Modelling and Simulation,* London, World Scientific Publishing.

Gillespie, T. D. (1992). *Fundamentals of Vehicle Dynamics,* Warrendale, PA, SAE.

Gipser, M. 2008. *F-Tire Status and Outlook* [Online]. Esslingen University of Applied Sciences, accessed 08/01/2009.

Goryca, J. 2010. Force and Moment Plots from Pacejka 2002 Magic Formula Tire Model Coefficients. U.S. Army Tank-automotive and Armaments Research, Development and Engineering Center.

Hall, W., Mottram, J. & Jones, R. P. (2004a). Finite element simulation of a rolling automobile tyre to understand its transient macroscopic behaviour. *Proceedings of the Institution of Mechanical Engineers, Part D: Journal of Automobile Engineering*, Vol 218, 1393-1408.

Hall, W., Mottram, J. & Jones, R. P. (2004b). Tire modelling methodology with the explicit finite element code LS-DYNA. *Tire Science and Technology*, Vol 32, Pages 236-261.

Hamedi, B., Català, A., Cañellas, S. & Elahimehr, A. (2007). A New Hybrid (Bi-Fuel) Vehicle Suspension Development. *SAE Technical Paper 2007-01-0861*.

Han, J., Park, Y. & Park, Y.-S. (2011). *Adaptive regenerative braking control in severe cornering for guaranteeing the vehicle stability of fuel cell hybrid electric vehicle* Vehicle Power and Propulsion Conference, Chicago, IL. Pages 1 - 5.

Heath, A. N. (1988). Evaluation of the Isotropic Road Roughness Assumption. *Vehicle Systems Dynamics*, Supplement 1, 157 - 160.

Hermance, D. & Shinichi, A. (2006). *Hybrid Vehicles: Lessons Learned and Future Prospects.* Convergence, October 16 - 18 2006 Detroit, Michigan.

Hongbin, R., Sizhong, C. & Zhicheng, W. (2011). *Model of Excitation of random Road Profile in Time Domain for a Vehicle with Four Wheel.* International Conference on Mechatronic Science, Electrical Engineering and Computer Science,

Hung, Y., Wu, C., Lo, S., Chen, B., Wu, E. & Chen, P. (2010). *Development of a hardware in-the-loop platform for plug-in hybrid electric vehicles.* International Symposium on Computer Communication Control and Automation (3CA), Tainan. Vol 1, Pages 45 - 48.

HybridVehicleOrg. 2005. *The First Hybrid Vehicle by Dr Ferdinand Porsche* [Online]. Available: http://www.hybrid-vehicle.org/hybrid-vehicle-porsche.html accessed 30/11/2009.

InvenSense 2008. IDG-500 Gyro Data Sheet, available at https://www.sparkfun.com/datasheets/Components/SMD/Datasheet_IDG500.pdf, accessed 22/10/2013.

Jeuland, N. & Ubrich, E. 2007. Perspectives for post-Euro 4 standards for passenger and light commercial vehicles (Euro 5, Euro 5+, Euro 6). Paris: IPF.

Kirsch, D. (2000). *THE ELECTRIC VEHICLE AND THE BURDEN OF HISTORY*, Rutgers University Press.

Li, Y., Zeng, Q., Wang, C. & Wang, L. (2009). *Research on Control Strategy for Regenerative Braking of a Plug-in Hybrid Electric City Public Bus.* Second International Conference on Intelligent Computation Technology and Automation, Vol 1, Pages 842 - 845.

Liu, Q., Kaiser, G., Boonto, S., Werner, H., Holzmann, F., Chretien, B. & Korte, M. (2011). *Two-Degree-of-Freedom LPV Control for a through-the-Road Hybrid Electric Vehicle via Torque Vectoring.* IEEE Conference on Decision and Control and European Control Conference, Orlando, FL. Pages 1274 - 1279.

Lo, E. (2009). *Review on the Configurations of Hybrid Electric Vehicles.* 3rd International Conference on Power Electronics Systems and Applications, Hong Kong. Pages 1 - 4.

Maggetto, G. & Van Mierlo, J. (2000). Electrical and Electric Hybrid Vehicle Technology: A Survey. *In:* Electric Hybrid and Fuel Cell Vehicles, IEE Seminar. IEE, 1 - 11.

Milliken, W. F. & Milliken, D. L. (1995). *Race Car Vehicle Dynamics,* Warrendale, PA, SAE.

Mitchell, W. & Schmitt, P. (2007). Autonomous and Modular Electric Vehicle Drive, Brake, Steer, and Suspend Unit. *IPCOM*.

Nowlan, D. (2013). *The Beautiful Simplicity of FRIC*. Racecar Engineering. Chelsea Magazine Company. Vol 23. Pages 73 - 77.

Olley, M., Milliken, W. F. & Milliken, D. L. (2002). *Chassis Design, Principles and Analysis,* Warrendale, PA, SAE.

Pacejka, H. B. (2002). *Tyre and Vehicle Dynamics*, Oxford, Elsevier Science.

Pacejka, H. B. & Bakker, E. (1991). The Magic Formula Tyre Model. *Vehicle Systems Dynamics,* Vol 21, Pages 1-18.

Papageorgiou, C. & Smith, M. (2006). Positive Real Synthesis Using Matrix Inequalities for Mechanical Networks: Application to Vehicle Suspension. *IEEE TRANSACTIONS ON CONTROL SYSTEMS TECHNOLOGY*, Vol 14, Issue 3, Pages 423 - 435.

Pauwelussen, J. & Schmeitz, A. (2001). *An Efficient Dynamic Ride and Handling Model for Arbitrary Road Uneveness,* Warrendale PA, SAE.

Perry, T. 2004. *GENERAL MOTORS ON THE HY-WIRE* [Online]. Available: http://spectrum.ieee.org/green-tech/advanced-cars/loser-general-motors-on-the-hywire accessed 06/06/2013.

Pusca, R., Ait-Amirat, Y., Berthon, A. & Kauffmann, J. (2004). *Fuzzy-logic-based control applied to a hybrid electric vehicle with four separate wheel drives.* IEE Control Theory Applications, Vol 151, Pages 73 - 81.

RaceTechnology. (2009). DL2 Technical Specification. *http://www.race-technology.com/wiki/index.php/DL2/TechSpecification* accessed 15/10/2013.

Rajashekara, K. (1994). History of Electric Vehicles in General Motors. *IEEE Transactions on ndustry Applications,* Vol 30, Issue 4, Pages 897 - 904.

Reid, M., Leffert, P., Cobb, W. (1984). Typical Vehicle Parameters for Dynamics Studies Revised for the 1980's. *SAE International*.

Robson, J. D. (1978). The Role of the Parkhilovskii Model in Road Description. *Vehicle Systems Dynamics,* 7, 153 - 162.

Segers, J. (2008). *Analysis Techniques for Racecar Data Acquisition,* Warrendale, PA., SAE.

Shah, R. M. R. A. (2013). *DEVELOPMENT OF A 4WD VEHICLE POWER-TRAIN SYSTEM MODEL FOR DRIVEABILITY INVESTIGATION.* Ph.D. Thesis, University of Warwick.

Shang, M., Chu, L., Guo, J., Fang, Y. & Zhou, F. (2010). *Braking Force Dynamic Coordinated Control for Hybrid Electric Vehicles* 2nd International Conference on Advanced Computer Control (ICACC), Shenyang. Vol 4, Pages 411 - 416.

Sharp, R. S. (2002). Wheelbase filtering and automobile suspension tuning for minimising motions in pitch. *Journal of Automobile Engineering,* 216, pp.933-946.

Sung, O. (2005). *Evaluation of motor characteristics for hybrid electric vehicles using the hardware-in-the-loop concept.* IEEE transactions on Vehicular Technology, Vol 54, Pages 817 - 824.

Supplier Business LTD. (2008). Hybrid Vehicles and Components Report 2008. Available: http://www.supplierbusiness.com/uploadedpdfs/hybrid_sample.pdf accessed 24/11/2009.

Svendenius, J. (2007). *Tire Modeling and Friction Estimation.* Ph.D. Thesis, Lund University.

Tyan, F., Hong, Y., Tu, S. & Jeng, W. (2004). Generation of Random Road Profiles. *CSME,* Pages 1373 - 1378.

Waltermann, P. (1996). Modelling and Control of the Longitudinal and Lateral Dynamics of a Series Hybrid Vehicle. *In:* IEEE International Conference on Control Applications, Dearborn, MI. Pages 191 - 198.

Wei, D., Fuwu, Y. & Du, C. (2010). *Power-train Control Strategies Overview for Hybrid Electric Vehicles.* Asia-Pacific Power and Energy Engineering Conference (APPEEC), Chengdu. Pages 1 - 5.

Wong, Y. J. (2001). *Theory of Ground Vehicles*, John Wiley and Sons.

Yim, S., Choi, J. & Yi, K. (2012). *Coordinated Control of Hybrid 4WD Vehicles for Enhanced Maneuverability and Lateral Stability.* IEEE Transactions on Vehicular Technology, Vol 61, Pages 1946 - 1950.

Yoong, M., Gan, Y., Gan, G., Leong, C., Phuan, Z., Cheah, B. & Chew, K. (2010). *Studies of Regenerative Braking in Electric Vehicle.* IEEE Conference on Sustainable Utilization and Development in Engineering and Technology, Kuala Lumpur. Pages 40 - 45,

Yu, Z. & Jing, L. (2011). *An Experiment Study of Diesel Engine with Variable Injection Timing and EGR Rate Strategies for Realization of Euro IV Emission Standard.* World Automation Congress, Puerto Vallarta, Mexico. Pages 1 - 4.

Zegelaar, P. W. A. (1998). *The Dynamic Response fo Tyres to Brake Torque Variations and Road Uneveness*, Delft, The Netherlands, Delft University of Technology.

Zhong, H., Guoqiang, A., Qiang, J., Yang, L. & Zhuo, B. (2006). *The Development of A Real-Time Hardware-in-the-Loop Test Bench for Hybrid Electric Vehicles Based on Multi-Thread Technology.* IEEE International Conference on Vehicular Electronics and Safety, Beijing. Pages 470 - 475.

Aliexpress. 2010. *IDG-500 Breakout Board Specification* [Online]. Available: http://www.aliexpress.com/store/product/For-Arduino-Gyro-Breakout-Board-IDG500-Dual-500-D-s-Integrated-X-and-Y-axis-Gyros/214862_671252907.html accessed 05/01/2010.

InvenSense 2008. IDG-500 Gyro Data Sheet, available at https://www.sparkfun.com/datasheets/Components/SMD/Datasheet_IDG500.pdf, accessed 22/10/2013.

RaceTechnology. (2009). DL2 Technical Specification. *http://www.race-technology.com/wiki/index.php/DL2/TechSpecification* accessed 15/10/2013.

Appendix A Standard Vehicle Model Data

A.1 Suspension Geometry

All coordinate are from origin used in Dymola model, where (0,0,0) lies on the vehicle centreline, front wheel centreline at wheel centre height. Forwards (x), leftwards (y), upwards (z) are positive.

FRONT GEOMETRY[mm] McPherson Strut							
		LEFT			RIGHT		
	Point Number	X	Y	Z	X	Y	Z
lca_front	1	-13.87	405.34	-93.62	-13.87	-405.34	-93.62
lca_rear	2	-279.43	405.34	-81.5	-279.43	-405.34	-81.5
lower_ball_joint	3	12.5	769.86	-135.44	12.5	-769.86	-135.44
top_mount	4	-32.4	591.87	645	-32.4	-591.87	645
wheel_center	5	0	798	0	0	-798	0
contact_patch	6	0.55	801.56	-345.4	0.55	-801.56	-345.4
spindle_align	7	0	698	-1.05	0	-698	-1.05
tierod_outer	8	-141.78	735.27	-55.97	-141.78	-735.27	-55.97
tierod_inner	9	-177.39	380	-26	-177.39	-380	-26
spring_seat_upper	10	-31.52	596.79	626.8	-31.52	-596.79	626.8
spring_seat_lower	11	-20.11	660.32	391.87	-20.11	-660.32	391.87
strut_knuckle	12	-5.95	646.6	100.21	-5.95	-646.6	100.21
bumper_lower	13	-23.89	609.48	469.71	-23.89	-609.48	469.71
bumper_upper	14	-30.64	595.52	608.68	-30.64	-595.52	608.68
subframe_front	15	432.61	548	155.75	432.61	-548	155.75
subframe_rear	16	-447.39	361	-82.25	-447.39	-361	-82.25
damper_body_upper	17	-32.4	591.87	645	-32.4	-591.87	645
damer_body_lower	18	-7.25	643.32	127.18	-7.25	-643.32	127.18
subframe_mid_1	19	1707.61	0	-365	1707.61	0	-365
subframe_mid_2	20	1707.61	0	-365	1707.61	0	-365
droplink_external	21	-52.48	574.31	339.22	-52.48	-574.31	339.22
droplink_to_ARB_arm	22	-65.92	547.12	-6.96	-65.92	-547.12	-6.96
ARB_at_subframe	23	-277.39	310	-29.5	-277.39	-310	-29.5

Table A-1 Front suspension geometry

REAR GEOMETRY [mm] Quadralink with Strut		LEFT			RIGHT		
	Point	X	Y	Z	X	Y	Z
upper_strut_mount_pivot	24	-2720.49	601.57	647.4	-2720.49	-601.57	647.4
strut_mount_knuckle	25	-2684.01	639.81	62.38	-2684.01	-639.81	62.38
front_quad_to_frame	26	-2514.81	321.56	6.36	-2514.81	-321.56	6.36
rear_quad_to_frame	27	-2776.87	309.58	-28.39	-2776.87	-309.58	-28.39
front_quad_to_spindle	28	-2557.14	734.56	-44.85	-2557.14	-734.56	-44.85
rear_quad_to_spindle	29	-2776.41	729	-83.35	-2776.41	-729	-83.35
strut_seat_lower	30	-2647.56	707.22	-138.67	-2647.56	-707.22	-138.67
tension_strut_to_body	31	-2036.39	513.6	23.6	-2036.39	-513.6	23.6
wheel_center	32	-2661.09	796.67	3.97	-2661.09	-796.67	3.97
contact_patch	33	-2660.53	806.96	-349.6	-2660.53	-806.96	-349.6
spindle_align	34	-2661.09	696.73	0.49	-2661.09	-696.73	0.49
spring_seat_upper	35	-2719.56	602.53	632.61	-2719.56	-602.53	632.61
spring_seat_lower	36	-2704.86	635.96	381.46	-2704.86	-635.96	381.46
subframe_front	37	-2429.39	500	77.8	-2429.39	-500	77.8
subframe_rear	38	-2856.09	479.7	152.4	-2856.09	-479.7	152.4
bumper_lower	39	-2710.48	612.06	486.89	-2710.48	-612.06	486.89
bumper_upper	40	-2719.62	602.48	633.44	-2719.62	-602.48	633.44
spring_seat_upper2	41	-2721.79	600.2	668.2	-2721.79	-600.2	668.2
spring_seat_lower2	42	-2688.89	634.7	140.3	-2688.89	-634.7	140.3
subframe_mid_1	43	1707.61	0	-365	1707.61	0	-365
subframe_mid_2	44	1707.61	0	-365	1707.61	0	-365
droplink_external	45	-2630.38	587.57	281.72	-2630.38	-587.57	281.72
droplink_to_ARB_arm	46	-2583.66	592.99	57.6	-2583.66	-592.99	57.6
ARB_at_subframe	47	-2922.64	317.2	21.43	-2922.64	-317.2	21.43

Table A-2 Rear suspension geometry

A.2 Suspension Springs

Linear main spring data	Front	Rear
Rate [N/mm]	29	30.5
Free length [mm]	414.868	358.781
Coils	5	5

Table A-3 Suspension coil spring data

A.3 Anti Roll Bars

Linear main spring data		
	Front	Rear
Rate [N.m/rad]	2226.2	2175.7

Table A-4 Anti-roll bar spring data

A.4 Dampers

Rear damper force/velocity spline		
Velocity [m/s]	Force [N] (front)	Force [N] (rear)
-0.79	-983.5	-906
-0.52	-787.5	-726
-0.39	-691	-630.5
-0.26	-592	-538.5
-0.13	-446	-369
-0.052	-159	-141
-0.025	-89.5	-89
0	0	0
0.025	102	90
0.052	239	195.5
0.13	858	603
0.26	1182	826
0.39	1356.5	994.5
0.52	1518	1171.5
0.79	1859	1575.5

Table A-5 Front and rear damper force velocity data

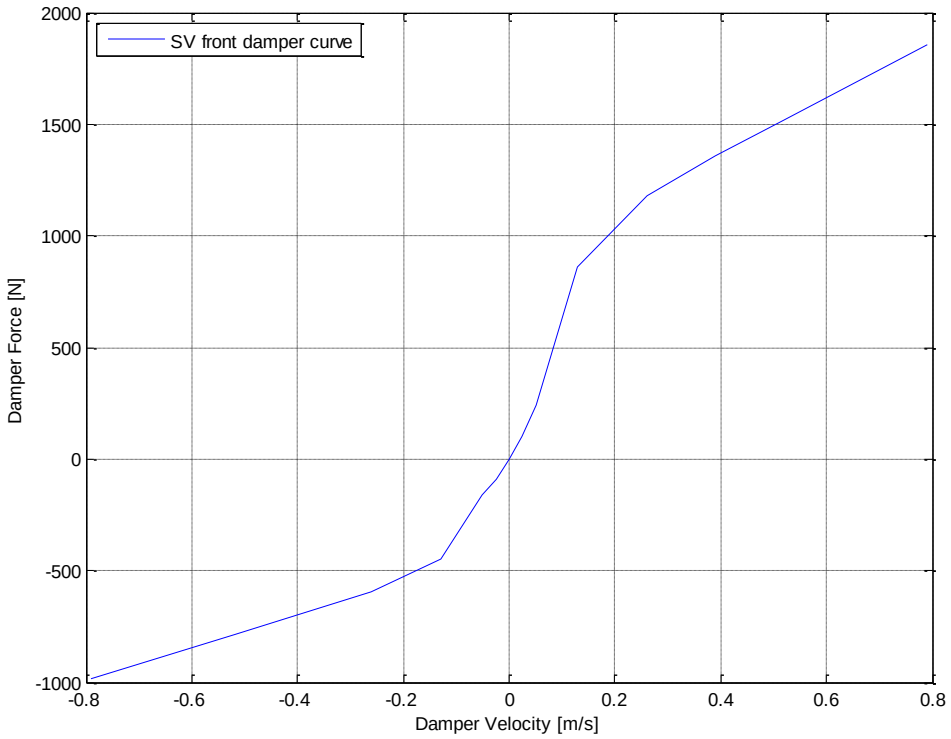

Figure A-1 Front damper force/velocity

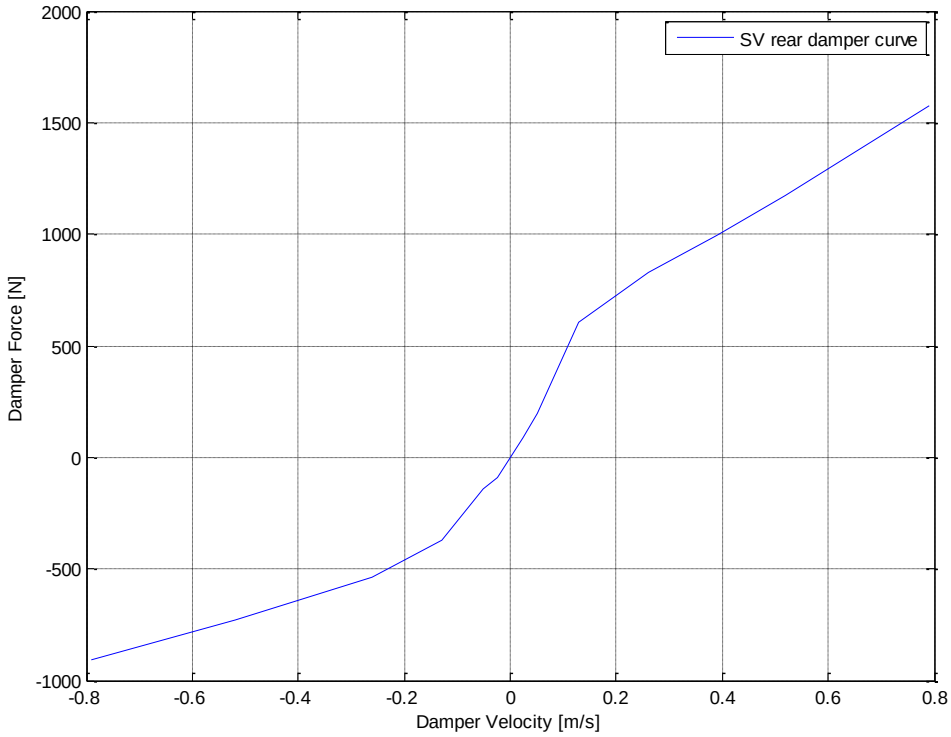

Figure A-2 Rear damper force/velocity

A.5 Bump Rubbers

Front bump rubber force/displacement spline	
Compression [mm]	Force [N]
0	0
1	14.19
2	27.11
3	38.82
4	48.14
5	57.11
6	68.81
7	82.44
8	98.05
9	115.16
10	132.68
11	150.84
12	169.84
13	186.97
14	202.95
15	217.17
16	229.2
17	239.1
18	247.68
19	255.89
20	263.75
21	271.9
22	280.28
23	288.89
24	297.75
25	306.86
26	316.23
27	325.9
28	336.01
29	347.02
30	358.58
31	370.27
32	382.8
33	396.22
34	409.42
35	423.81
36	439.82
37	455.47
38	472.44

Note: front bump rubbers are implemented in series with main spring, with 121.26 mm (calculated from strut and spring geometry) of main spring compression before bump rubber engagement.

39	490.64
40	509.96
41	530.94
42	552.54
43	576.35
44	601.49
45	628.34
46	657.26
47	688.15
48	720.82
49	757.05
50	796.11
51	837.06
52	882.6
53	932.51
54	986.79
55	1047.39
56	1114.18
57	1187.82
58	1270.61
59	1362.95
60	1468.32
61	1587.55
62	1724.87
63	1884.59
64	2070.45
65	2287.89
66	2542.94
67	2844.94
68	3208.23
69	3648.72
70	4189.93
71	4867.03
72	5726.84
73	6849.14
74	8360.85
75	10482.5
76	13654.6
77	18855.6

Table A-6 Front bump rubber data

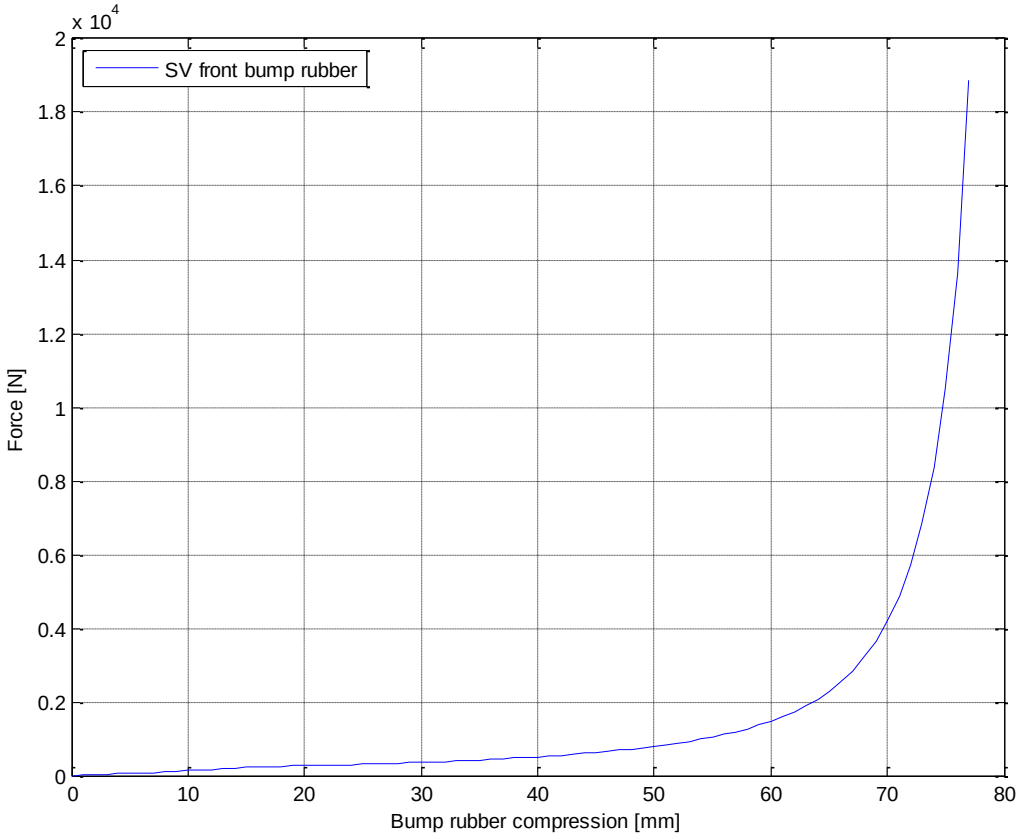

Figure A-3 Front bump rubber data

Rear bump rubber force/displacement spline	
Compression [mm]	Force [N]
0	0
1	17.74
2	32.84
3	46.34
4	59.14
5	71.54
6	83.75
7	96.56
8	110.26
9	125.24
10	141.34
11	159.35
12	178.74
13	196.65
14	212.73

Note: rear bump rubbers are implemented in series with main spring, with 156.98 mm (calculated from strut and spring geometry) of main spring compression before bump rubber engagement.

15	231.16
16	252.24
17	275.16
18	299.84
19	328.02
20	355.96
21	382.72
22	411.79
23	439.05
24	466
25	488.72
26	509.55
27	529.72
28	549.69
29	570.05
30	591.21
31	615.47
32	637.9
33	661.76
34	689.24
35	714.89
36	741.7
37	770.23
38	800.17
39	831.23
40	864.96
41	899.12
42	939.19
43	980.05
44	1028.17
45	1075.31
46	1125.44
47	1183.2
48	1245.04
49	1311.05
50	1384.5
51	1466.58
52	1556.18
53	1655.45
54	1768.3
55	1892.31
56	2048.76
57	2226.05

58	2424.8
59	2654.1
60	2922.81
61	3244.71
62	3626.29
63	4082.41
64	4640.88
65	5335.99
66	6207.1
67	7370.22
68	8976.56
69	11272.6
70	14758
71	20326

Table A-7 Rear bump rubber data

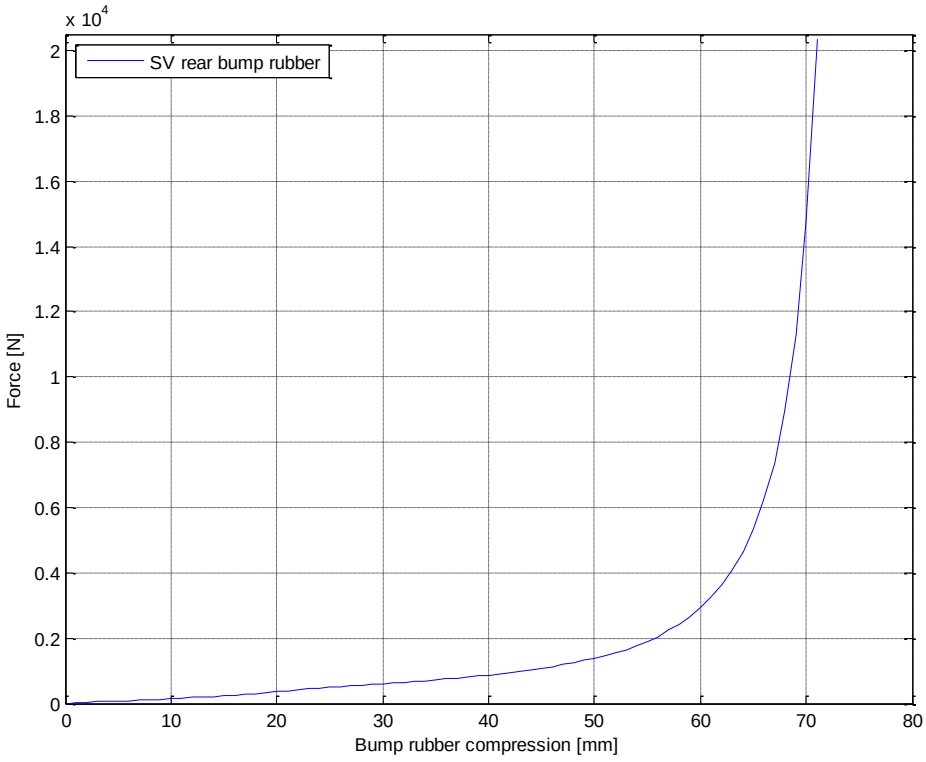

Figure A-4 Rear bump rubber data

A.6 Bushes

A.6.1 Point 1 front lower control arm to subframe

Translation					
front lca at subframe					
DAMPING X [N.s/mm]		DAMPING X [N.s/mm]		DAMPING X [N.s/mm]	
21		13		1.5	
STIFFNESS X		STIFFNESS Y		STIFFNESS Z	
Comp [mm]	Force [N]	Comp [mm]	Force [N]	Comp [mm]	Force [N]
-0.6374	-9855	-1.0257	-8668.6	-5.1166	-7035
-0.6284	-9636	-1.0182	-8571.2	-5.0371	-6753.6
-0.6093	-9198	-0.9871	-8181.6	-4.8418	-6190.8
-0.5887	-8760	-0.9562	-7792	-4.5999	-5628
-0.5667	-8322	-0.9217	-7402.4	-4.3133	-5065.2
-0.5462	-7884	-0.886	-7012.8	-3.974	-4502.4
-0.5218	-7446	-0.8468	-6623.2	-3.5906	-3939.6
-0.4974	-7008	-0.8065	-6233.6	-3.1591	-3376.8
-0.4729	-6570	-0.7642	-5844	-2.6946	-2814
-0.4461	-6132	-0.7207	-5454.4	-2.2006	-2251.2
-0.4182	-5694	-0.6766	-5064.8	-1.6842	-1688.4
-0.3927	-5256	-0.6313	-4675.2	-1.1392	-1125.6
-0.3632	-4818	-0.5833	-4285.6	-0.7196	-703.5
-0.3329	-4380	-0.5346	-3896	-0.3606	-351.8
-0.3024	-3942	-0.4857	-3506.4	0	0
-0.2714	-3504	-0.4346	-3116.8	0.3606	351.8
-0.2393	-3066	-0.3812	-2727.2	0.7196	703.5
-0.2067	-2628	-0.3279	-2337.6	1.1392	1125.6
-0.1726	-2190	-0.2746	-1948	1.6842	1688.4
-0.1386	-1752	-0.2195	-1558.4	2.2006	2251.2
-0.1039	-1314	-0.1646	-1168.8	2.6946	2814
-0.0704	-876	-0.1105	-779.2	3.1591	3376.8
-0.0445	-547.5	-0.0691	-487	3.5906	3939.6
-0.0226	-273.8	-0.0356	-243.5	3.974	4502.4
0	0	0	0	4.3133	5065.2
0.0226	273.8	0.0356	243.5	4.5999	5628
0.0445	547.5	0.0691	487	4.8418	6190.8
0.0704	876	0.1105	779.2	5.0371	6753.6
0.1039	1314	0.1646	1168.8	5.1166	7035
0.1386	1752	0.2195	1558.4		
0.1726	2190	0.2746	1948		
0.2067	2628	0.3279	2337.6		
0.2393	3066	0.3812	2727.2		
0.2714	3504	0.4346	3116.8		
0.3024	3942	0.4857	3506.4		
0.3329	4380	0.5346	3896		

0.3632	4818	0.5833	4285.6
0.3927	5256	0.6313	4675.2
0.4182	5694	0.6766	5064.8
0.4461	6132	0.7207	5454.4
0.4729	6570	0.7642	5844
0.4974	7008	0.8065	6233.6
0.5218	7446	0.8468	6623.2
0.5462	7884	0.886	7012.8
0.5667	8322	0.9217	7402.4
0.5887	8760	0.9562	7792
0.6093	9198	0.9871	8181.6
0.6284	9636	1.0182	8571.2
0.6374	9855	1.0257	8668.6

Table A-8 Lower control arm front to subframe bush translational stiffness and damping

Rotation		
Front lca at subframe		
DAMPING rX [N.mm.s/deg]	DAMPING rY [N.mm.s/deg]	DAMPING rZ [N.mm.s/deg]
7.44	5.04	7.32
STIFFNESS rX [N.mm/deg]	STIFFNESS rY [N.mm/deg]	STIFFNESS rZ [N.mm/deg]
7440	5040	7320

Table A-9 Lower control arm front to subframe bush rotational stiffness and damping

XP (LHS)	1721.48	395.34	271.38
YP (LHS)	1239.600	-17214.800	17214.800

Table A-10 Lower control arm front to subframe bush x and y axis projections for orientation (LHS)

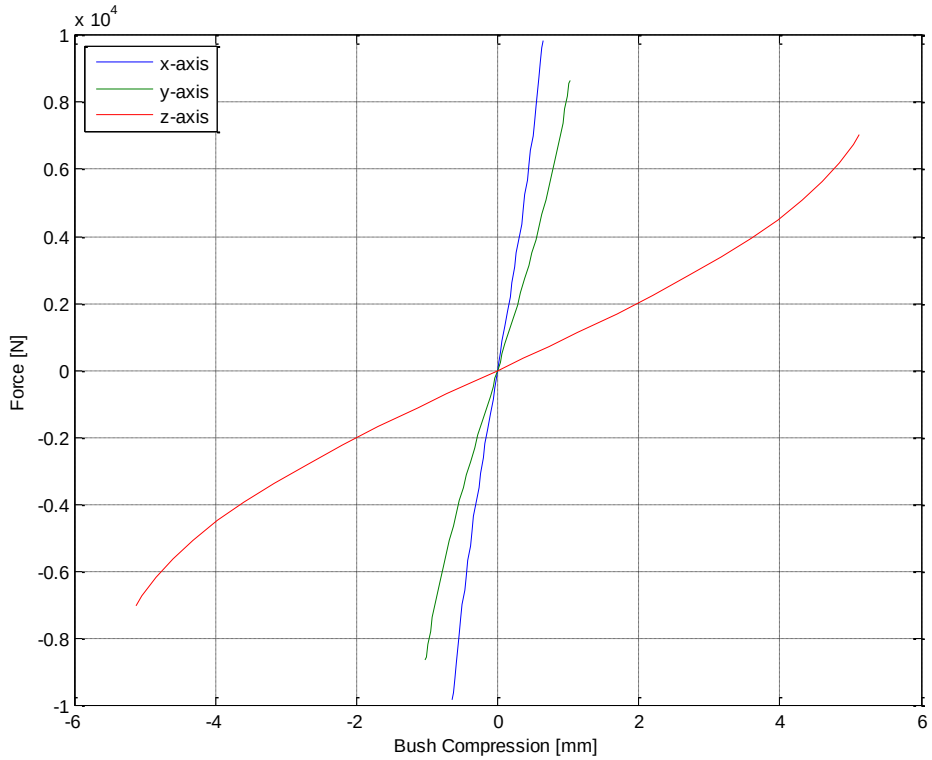

Figure A-5 Lower control arm front to subframe translational bush stiffness

A.6.2 Point 2 rear lower control arm to subframe

Translation					
rear lca at subframe					
DAMPING X [N.s/mm]		DAMPING X [N.s/mm]		DAMPING X [N.s/mm]	
0.5		0.406		0.942	
STIFFNESS X		STIFFNESS Y		STIFFNESS Z	
Comp [mm]	Force [N]	Comp [mm]	Force [N]	Comp [mm]	Force [N]
-6.87	-8398	-3.69	-4950	-8.06	-4950
-6.84	-7904	-3.62	-4800	-8.03	-4800
-6.81	-7410	-3.53	-4600	-7.99	-4600
-6.78	-6916	-3.44	-4400	-7.94	-4400
-6.75	-6422	-3.34	-4200	-7.88	-4200
-6.7	-5928	-3.24	-4000	-7.8	-4000
-6.65	-5434	-3.13	-3800	-7.7	-3800
-6.58	-4940	-3.01	-3600	-7.57	-3600
-6.47	-4446	-2.9	-3400	-7.41	-3400
-6.29	-3952	-2.77	-3200	-7.2	-3200
-5.98	-3458	-2.65	-3000	-6.95	-3000
-5.55	-2964	-2.52	-2800	-6.65	-2800

-5.01	-2470	-2.38	-2600	-6.31	-2600
-4.34	-1976	-2.24	-2400	-5.93	-2400
-3.53	-1482	-2.09	-2200	-5.52	-2200
-2.5	-988	-1.93	-2000	-5.07	-2000
-1.28	-494	-1.77	-1800	-4.61	-1800
0	0	-1.6	-1600	-4.11	-1600
1.28	494	-1.42	-1400	-3.6	-1400
2.5	988	-1.24	-1200	-3.08	-1200
3.53	1482	-1.04	-1000	-2.55	-1000
4.34	1976	-0.84	-800	-2.02	-800
5.01	2470	-0.53	-500	-1.23	-500
5.55	2964	0	0	0	0
5.98	3458	0.53	500	1.23	500
6.29	3952	0.84	800	2.02	800
6.47	4446	1.04	1000	2.55	1000
6.58	4940	1.24	1200	3.08	1200
6.65	5434	1.42	1400	3.6	1400
6.7	5928	1.6	1600	4.11	1600
6.75	6422	1.77	1800	4.61	1800
6.78	6916	1.93	2000	5.07	2000
6.81	7410	2.09	2200	5.52	2200
6.84	7904	2.24	2400	5.93	2400
6.87	8398	2.38	2600	6.31	2600
		2.52	2800	6.65	2800
		2.65	3000	6.95	3000
		2.77	3200	7.2	3200
		2.9	3400	7.41	3400
		3.01	3600	7.57	3600
		3.13	3800	7.7	3800
		3.24	4000	7.8	4000
		3.34	4200	7.88	4200
		3.44	4400	7.94	4400
		3.53	4600	7.99	4600
		3.62	4800	8.03	4800
		3.69	4950	8.06	4950

Table A-11 Lower control arm rear to subframe bush translational stiffness and damping

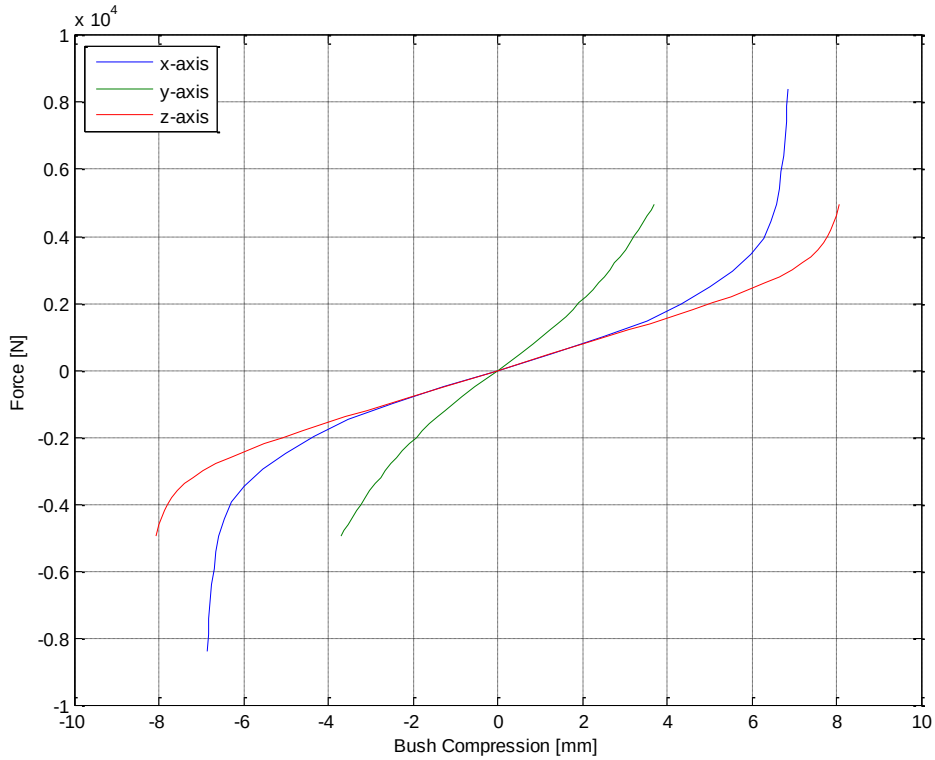

Figure A-6 Lower control arm rear to subframe translational bush stiffness

Rotation					
rear lca at subframe					
DAMPING rX [N.mm.s/deg]		DAMPING rY [N.mm.s/deg]		DAMPING rZ [N.mm.s/deg]	
2.23402		3.24631		2.47837	
STIFFNESS rX		STIFFNESS rY		STIFFNESS rZ	
Rotation [deg]	Torque [N.mm]	Rotation [deg]	Torque [N.mm]	Rotation [deg]	Torque [N.mm]
-13.5	-30800	-13.5	-47300	-17	-43800
-13	-29700	-13	-45300	-15	-37800
-12	-27100	-12	-41100	-13	-32600
-11	-24700	-11	-37200	-10	-25000
-10	-22400	-10	-33400	-8	-20000
-9	-20100	-9	-29800	-7	-17600
-8	-17900	-8	-26200	-6	-15100
-7	-15700	-7	-22800	-5	-12600
-6	-13500	-6	-19400	-4	-10200
-5	-11300	-5	-16200	-3	-7600
-4	-9000	-4	-12900	-2	-5000
-3	-6800	-3	-9700	-1	-2400
-2	-4500	-2	-6500	0	0
-1	-2200	-1	-3200	1	2400

0	0	0	0	2	5000
1	2200	1	3200	3	7600
2	4500	2	6500	4	10200
3	6800	3	9700	5	12600
4	9000	4	12900	6	15100
5	11300	5	16200	7	17600
6	13500	6	19400	8	20000
7	15700	7	22800	10	25000
8	17900	8	26200	13	32600
9	20100	9	29800	15	37800
10	22400	10	33400	17	43800
11	24700	11	37200		
12	27100	12	41100		
13	29700	13	45300		
13.5	30800	13.5	47300		

Table A-12 Lower control arm rear to subframe bush rotational stiffness and damping

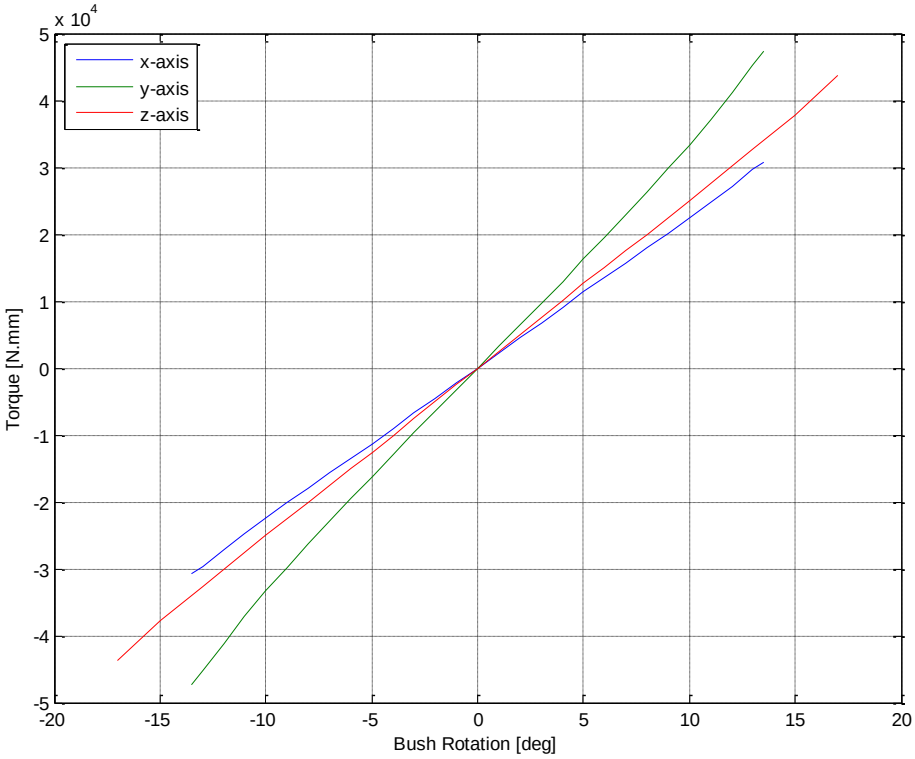

Figure A-7 Lower control arm rear to subframe rotational bush stiffness

XP	1695.21	769.86	229.56
YP	115874.8	-64863.1	-638162

Table A-13 Lower control arm rear to subframe bush x and y axis projections for orientation (LHS)

A.6.3 Point 3 lower ball joint

Translation		
lca at upright		
DAMPING X [N.s/mm]	DAMPING X [N.s/mm]	DAMPING X [N.s/mm]
47.6986	9.52257	111.591
STIFFNESS X [N/mm]	STIFFNESS Y [N/mm]	STIFFNESS Z [N/mm]
4774.45	19591.6	11249.3

Table A-14 Lower ball joint bush translational stiffness and damping

Rotation		
lca at upright		
DAMPING rX [N.mm.s/deg]	DAMPING rY [N.mm.s/deg]	DAMPING rZ [N.mm.s/deg]
0.3333	0.3333	0.3333
STIFFNESS rX [N.mm/deg]	STIFFNESS rY [N.mm/deg]	STIFFNESS rZ [N.mm/deg]
1.00E-08	1.00E-08	1.00E-08

Table A-15 Lower ball joint bush rotational stiffness and damping

XP	1987.04	405.34	283.5
YP	-4912.72	-51203.3	107642.1

Table A-16 Lower ball joint bush x and y axis projections for orientation (LHS)

A.6.4 Point 8 tie-rod outer

Translation		
tie rod at spindle		
DAMPING X [N.s/mm]	DAMPING X [N.s/mm]	DAMPING X [N.s/mm]
81.8644	77.1765	71.1459
STIFFNESS X [N/mm]	STIFFNESS Y [N/mm]	STIFFNESS Z [N/mm]
8186.44	7717.65	7114.59

Table A-17 Tie-rod outer bush translational stiffness and damping

Rotation		
tie rod at spindle		
DAMPING rX [N.mm.s/deg]	DAMPING rY [N.mm.s/deg]	DAMPING rZ [N.mm.s/deg]
1	1	1
STIFFNESS rX [N.mm/deg]	STIFFNESS rY [N.mm/deg]	STIFFNESS rZ [N.mm/deg]
0.00	0.00	0.00

Table A-18 Tie-rod outer bush rotational stiffness and damping

XP	1949.39	735.27	309.03
YP	131847.2	-78380.1	-645216

Table A-19 Tie-rod outer bush x and y axis projections for orientation (LHS)

A.6.5 Point 15 subframe to chassis front

Translation				
Subframe front				
DAMPING X [N.s/mm]		DAMPING X [N.s/mm]		DAMPING X [N.s/mm]
2.95371		5.92545		0.965683
STIFFNESS X		STIFFNESS Y		STIFFNESS Z [N/mm]
Comp [mm]	Force [N]	Comp [mm]	Force [N]	737.808
-3.44226	-11889	-5.15258	-8964	
-3.36186	-11228.5	-4.89133	-8466	
-3.27466	-10568	-4.62329	-7968	
-3.18335	-9907.5	-4.35405	-7470	
-3.08315	-9247	-4.0801	-6972	
-2.97405	-8586.5	-3.80046	-6474	
-2.85374	-7926	-3.51892	-5976	
-2.72494	-7265.5	-3.23467	-5478	
-2.57993	-6605	-2.94733	-4980	
-2.42203	-5944.5	-2.65839	-4482	
-2.24413	-5284	-2.36764	-3984	
-2.04472	-4623.5	-2.0739	-3486	
-1.82412	-3963	-1.77976	-2988	
-1.57132	-3302.5	-1.48292	-2490	
-1.28271	-2642	-1.18817	-1992	
-0.96661	-1981.5	-0.88883	-1494	
-0.63371	-1321	-0.59509	-996	
-0.3107	-660.5	-0.29544	-498	
0	0	0	0	
0.310703	660.5	0.295443	498	

0.633707	1321	0.595086	996
0.96661	1981.5	0.888829	1494
1.28271	2642	1.18817	1992
1.57132	3302.5	1.48292	2490
1.82412	3963	1.77976	2988
2.04472	4623.5	2.0739	3486
2.24413	5284	2.36764	3984
2.42203	5944.5	2.65839	4482
2.57993	6605	2.94733	4980
2.72494	7265.5	3.23467	5478
2.85374	7926	3.51892	5976
2.97405	8586.5	3.80046	6474
3.08315	9247	4.0801	6972
3.18335	9907.5	4.35405	7470
3.27466	10568	4.62329	7968
3.36186	11228.5	4.89133	8466
3.44226	11889	5.15258	8964

Table A-20 Subframe to chassis front bush translational stiffness and damping

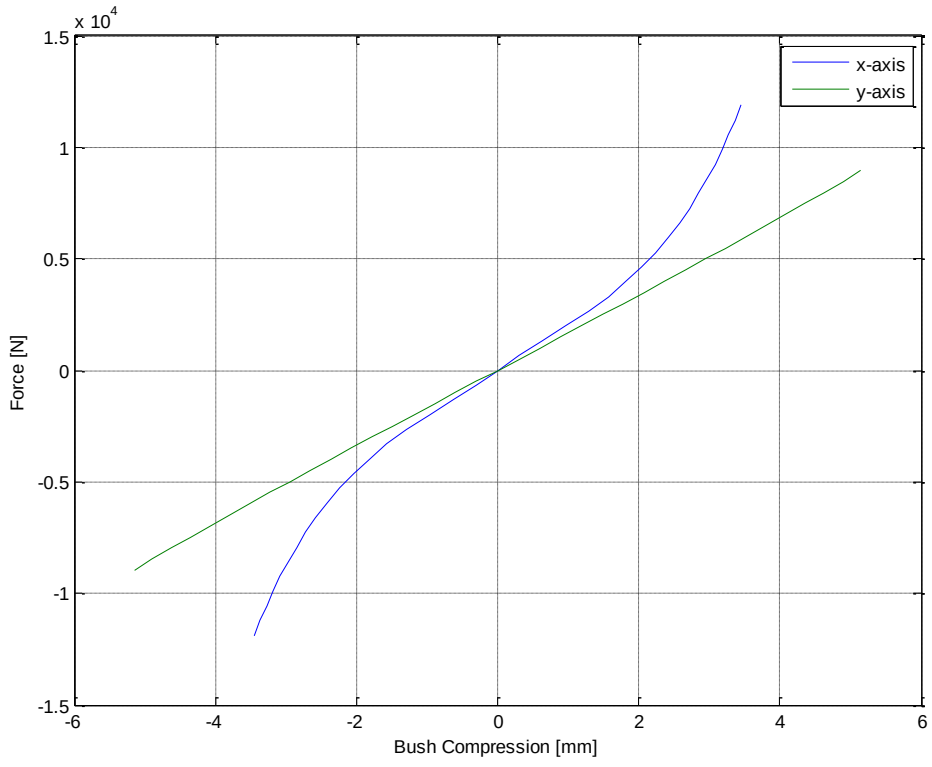

Figure A-8 Subframe to chassis front translational bush stiffness

Rotation		
Subframe front		
DAMPING rX [N.mm.s/deg]	DAMPING rY [N.mm.s/deg]	DAMPING rZ [N.mm.s/deg]
0.777778	0.777778	0.777778
STIFFNESS rX [N.mm/deg]	STIFFNESS rY [N.mm/deg]	STIFFNESS rZ [N.mm/deg]
3500	3500	3500

Table A-21 Subframe to chassis front bush rotational stiffness and damping

XP	1	0	0
YP	0	1	0

Table A-22 Subframe to chassis front bush x and y axis projections for orientation (LHS)

A.6.6 Point 16 subframe to chassis rear

Translation					
Subframe rear					
DAMPING X [N.s/mm]		DAMPING X [N.s/mm]		DAMPING X [N.s/mm]	
2.78377		4.87876		2.96443	
STIFFNESS X		STIFFNESS Y		STIFFNESS Z	
Comp [mm]	Force [N]	Comp [mm]	Force [N]	Comp [mm]	Force [N]
-3.78804	-16407	-1.99824	-8757	-2.6628	-5385.1
-3.72626	-15495.5	-1.93136	-8270.5	-2.58462	-5055.4
-3.66018	-14584	-1.85718	-7784	-2.48553	-4725.7
-3.5885	-13672.5	-1.7788	-7297.5	-2.38324	-4396
-3.50902	-12761	-1.69402	-6811	-2.27005	-4066.3
-3.42234	-11849.5	-1.60214	-6324.5	-2.12126	-3736.6
-3.32506	-10938	-1.51026	-5838	-1.97308	-3406.9
-3.21538	-10026.5	-1.41088	-5351.5	-1.79199	-3077.2
-3.094	-9115	-1.3057	-4865	-1.6176	-2747.5
-2.95362	-8203.5	-1.19652	-4378.5	-1.43341	-2417.8
-2.79594	-7292	-1.08214	-3892	-1.24432	-2088.1
-2.61566	-6380.5	-0.96426	-3405.5	-1.05224	-1758.4
-2.40788	-5469	-0.83748	-2919	-0.86065	-1428.7
-2.1587	-4557.5	-0.7111	-2432.5	-0.66736	-1099
-1.85332	-3646	-0.57792	-1946	-0.46937	-769.3
-1.46784	-2734.5	-0.44024	-1459.5	-0.33638	-549.5
-1.01416	-1823	-0.29706	-973	-0.16909	-274.8
-0.51178	-911.5	-0.15088	-486.5	0	0
0	0	0	0	0.169092	274.8
0.51178	911.5	0.15088	486.5	0.33638	549.5

1.01416	1823	0.29706	973	0.469372	769.3
1.46784	2734.5	0.44024	1459.5	0.66736	1099
1.85332	3646	0.57792	1946	0.860648	1428.7
2.1587	4557.5	0.7111	2432.5	1.05224	1758.4
2.40788	5469	0.83748	2919	1.24432	2088.1
2.61566	6380.5	0.964259	3405.5	1.43341	2417.8
2.79594	7292	1.08214	3892	1.6176	2747.5
2.95362	8203.5	1.19652	4378.5	1.79199	3077.2
3.094	9115	1.3057	4865	1.97308	3406.9
3.21538	10026.5	1.41088	5351.5	2.12126	3736.6
3.32506	10938	1.51026	5838	2.27005	4066.3
3.42234	11849.5	1.60214	6324.5	2.38324	4396
3.50902	12761	1.69402	6811	2.48553	4725.7
3.5885	13672.5	1.7788	7297.5	2.58462	5055.4
3.66018	14584	1.85718	7784	2.6628	5385.1
3.72626	15495.5	1.93136	8270.5		
3.78804	16407	1.99824	8757		

Table A-23 Subframe to chassis rear bush translational stiffness and damping

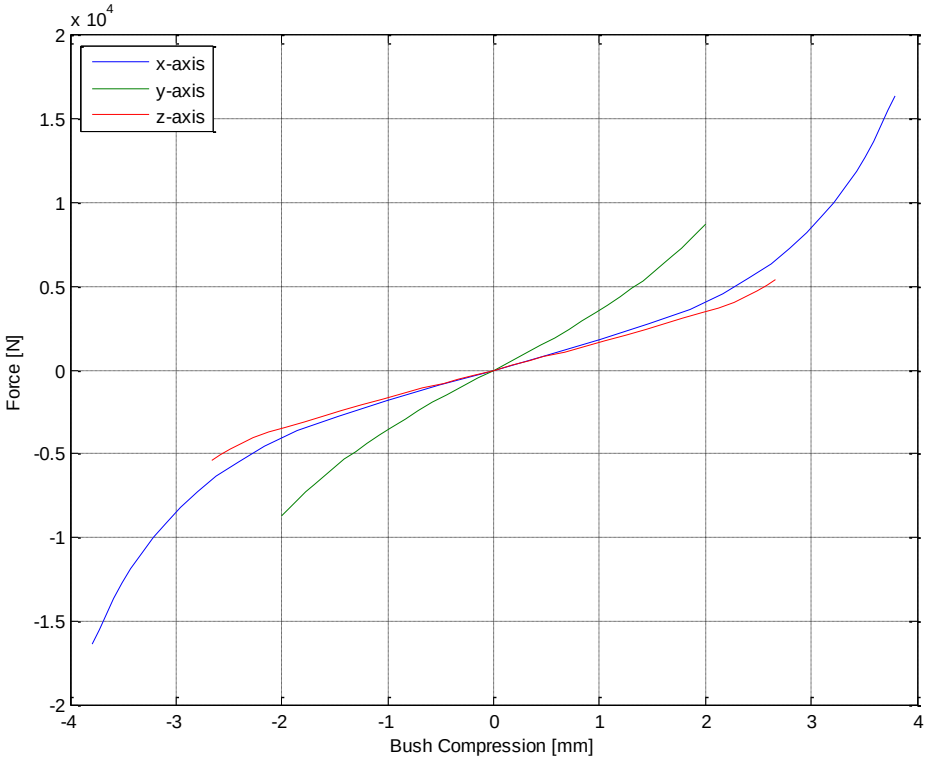

Figure A-9 Subframe to chassis rear translational bush stiffness

Rotation		
Subframe rear		
DAMPING rX [N.mm.s/deg]	DAMPING rY [N.mm.s/deg]	DAMPING rZ [N.mm.s/deg]
0.777778	0.777778	0.777778
STIFFNESS rX [N.mm/deg]	STIFFNESS rY [N.mm/deg]	STIFFNESS rZ [N.mm/deg]
3500	3500	3500

Table A-24 Subframe to chassis rear bush rotational stiffness and damping

XP	1	0	0
YP	0	1	0

Table A-25 Subframe to chassis rear bush x and y axis projections for orientation (LHS)

A.6.7 Point 26 front quad to subframe

Translation				
front quad at subframe				
DAMPING X N.s/mm		DAMPING X [N.s/mm]		DAMPING X [N.s/mm]
8.35536		13.3851		0.342861
STIFFNESS X		STIFFNESS Y		STIFFNESS Z [N/mm]
Comp [mm]	Force [N]	Comp [mm]	Force [N]	324.74
-1.57016	-15720	-4.54121	-26955	
-1.51882	-14672	-4.29179	-25158	
-1.45747	-13624	-4.03238	-23361	
-1.39613	-12576	-3.77297	-21564	
-1.32479	-11528	-3.50355	-19767	
-1.25344	-10480	-3.23414	-17970	
-1.1721	-9432	-2.95473	-16173	
-1.08075	-8384	-2.66531	-14376	
-0.97941	-7336	-2.3659	-12579	
-0.85807	-6288	-2.04648	-10782	
-0.73672	-5240	-1.72707	-8985	
-0.59538	-4192	-1.38766	-7188	
-0.45403	-3144	-1.04824	-5391	
-0.30269	-2096	-0.69883	-3594	
-0.15134	-1048	-0.34941	-1797	
-0.08067	-524	-0.17971	-898.5	
0	0	0	0	
0.080672	524	0.179707	898.5	
0.151344	1048	0.349414	1797	
0.302688	2096	0.698828	3594	

0.454033	3144	1.04824	5391
0.595377	4192	1.38766	7188
0.736721	5240	1.72707	8985
0.858065	6288	2.04648	10782
0.979409	7336	2.3659	12579
1.08075	8384	2.66531	14376
1.1721	9432	2.95473	16173
1.25344	10480	3.23414	17970
1.32479	11528	3.50355	19767
1.39613	12576	3.77297	21564
1.45747	13624	4.03238	23361
1.51882	14672	4.29179	25158
1.57016	15720	4.54121	26955

Table A-26 Front quad link to subframe bush translational stiffness and damping

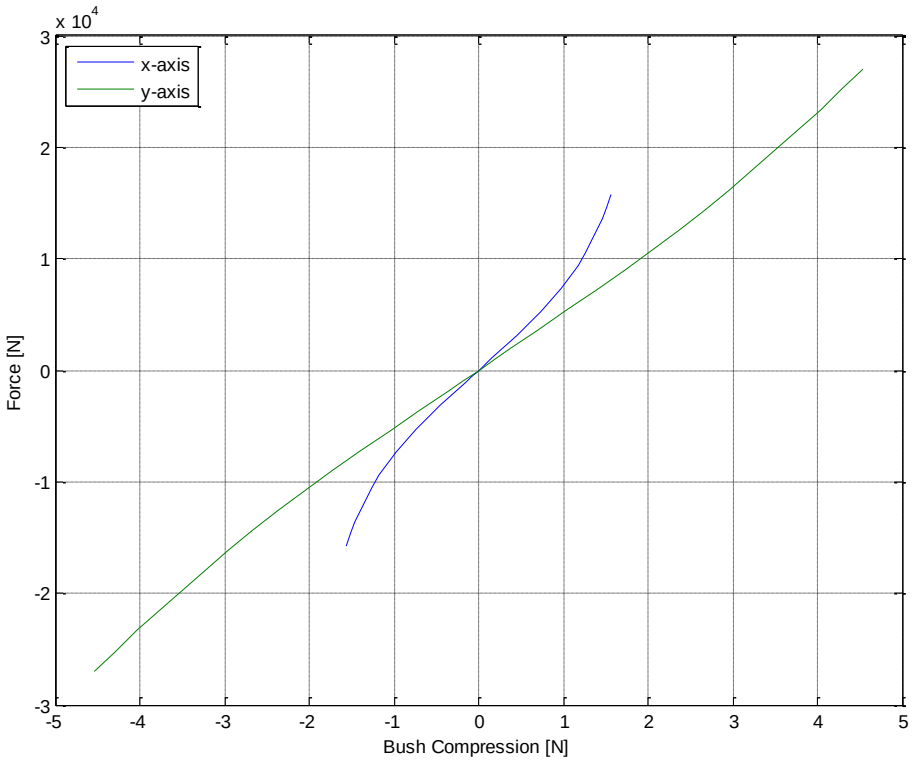

Figure A-10 Front quad link to subframe bush translational bush stiffness

Rotation		
front quad at subframe		
DAMPING rX [N.mm.s/deg]	DAMPING rY [N.mm.s/deg]	DAMPING rZ [N.mm.s/deg]
0.8	0.8	0.642857
STIFFNESS rX [N.mm/deg]	STIFFNESS rY [N.mm/deg]	STIFFNESS rZ [N.mm/deg]
4000	4000	1800

Table A-27 Front quad link to subframe bush rotational stiffness and damping

XP	4264.75	734.56	320.15
YP	171920.3	-257483	-1699394

Table A-28 Front quad link to subframe bush x and y axis projections for orientation (LHS)

A.6.8 Point 27 rear quad link to subframe

Translation				
rear quad at frame				
DAMPING X N.s/mm		DAMPING X [N.s/mm]		DAMPING X [N.s/mm]
123.22		12.486		4.17026
STIFFNESS X		STIFFNESS Y		STIFFNESS Z [N/mm]
Comp [mm]	Force [N]	Comp [mm]	Force [N]	417.026
-0.90776	-12570	-1.93833	-14940	
-0.85518	-11732	-1.83464	-13944	
-0.80059	-10894	-1.72595	-12948	
-0.75001	-10056	-1.61626	-11952	
-0.69442	-9218	-1.50057	-10956	
-0.63984	-8380	-1.37788	-9960	
-0.57926	-7542	-1.2542	-8964	
-0.52067	-6704	-1.12351	-7968	
-0.46109	-5866	-0.98982	-6972	
-0.3975	-5028	-0.85113	-5976	
-0.33392	-4190	-0.71144	-4980	
-0.26834	-3352	-0.56975	-3984	
-0.20075	-2514	-0.42807	-2988	
-0.13617	-1676	-0.28438	-1992	
-0.06758	-838	-0.14269	-996	
-0.03479	-419	-0.07234	-498	
0	0	0	0	
0.034792	419	0.072344	498	
0.067584	838	0.142688	996	
0.136168	1676	0.284377	1992	

0.200752	2514	0.428065	2988
0.268336	3352	0.569754	3984
0.33392	4190	0.711442	4980
0.397504	5028	0.851131	5976
0.461088	5866	0.989819	6972
0.520671	6704	1.12351	7968
0.579255	7542	1.2542	8964
0.639839	8380	1.37788	9960
0.694423	9218	1.50057	10956
0.750007	10056	1.61626	11952
0.800591	10894	1.72595	12948
0.855175	11732	1.83464	13944
0.907759	12570	1.93833	14940

Table A-29 Rear quad link to subframe bush translational stiffness and damping

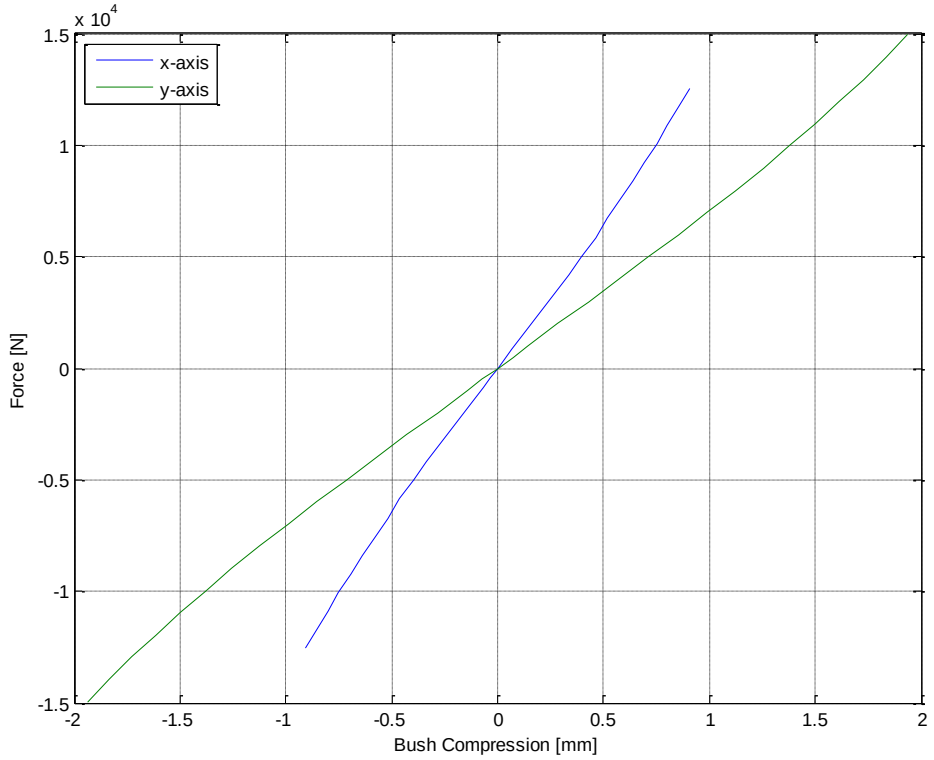

Figure A-11 Rear quad link to subframe bush translational bush stiffness

Rotation					
rear quad at subframe					
DAMPING rX [N.mm.s/deg]		DAMPING rY [N.mm.s/deg]		DAMPING rZ [N.mm.s/deg]	
0.908257		0.920128		0.603175	
STIFFNESS rX		STIFFNESS rY		STIFFNESS rZ	
Rotation [deg]	Torque [N.mm]	Rotation [deg]	Torque [N.mm]	Rotation [deg]	Torque [N.mm]
-7.00001	-102910	-7.00001	-106065	-14	-21167.1
-6.50001	-86864.2	-6.50001	-91145	-13	-19189.2
-6.00001	-74303.7	-6.00001	-79459.3	-12	-17594.4
-5.50001	-63898.6	-5.50001	-69461.1	-11	-15963.8
-5.00001	-55084.5	-5.00001	-60627.3	-10	-14572.1
-4.5	-47419.5	-4.50001	-52695.1	-9	-13207.2
-4	-40520.8	-4	-45437.8	-8	-11834.8
-3.5	-34227.5	-3.5	-38781.7	-7	-10438.2
-3	-28408.8	-3	-32394.1	-6	-9076.9
-2.5	-22942	-2.5	-26256	-5	-7601.8
-2	-17754.7	-2	-20377.2	-4	-6105.6
-1.5	-12825.7	-1.5	-14692.7	-3	-4563.3
-1	-8118.2	-1	-9163.6	-2	-3016.4
-0.5	-3703.8	-0.5	-4085.7	-1	-1487.7
0	0	0	0	0	0
0.5	3703.8	0.5	4085.7	1	1487.7
1	8118.2	1	9163.6	2	3016.4
1.5	12825.7	1.5	14692.7	3	4563.3
2	17754.7	2	20377.2	4	6105.6
2.5	22942	2.5	26256	5	7601.8
3	28408.8	3	32394.1	6	9076.9
3.5	34227.5	3.5	38781.7	7	10438.2
4	40520.8	4	45437.8	8	11834.8
4.5	47419.5	4.50001	52695.1	9	13207.2
5.00001	55084.5	5.00001	60627.3	10	14572.1
5.50001	63898.6	5.50001	69461.1	11	15963.8
6.00001	74303.7	6.00001	79459.3	12	17594.4
6.50001	86864.2	6.50001	91145	13	19189.2
7.00001	102910	7.00001	106065	14	21167.1

Table A-30 Rear quad link to subframe bush rotational stiffness and damping

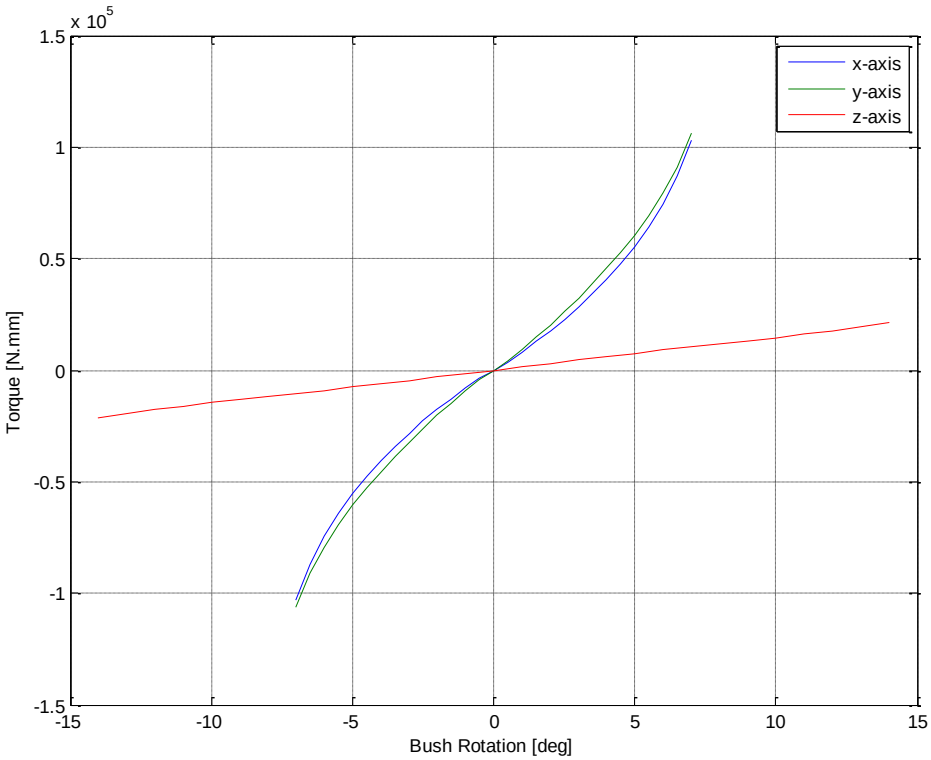

Figure A-12 Rear quad link to subframe bush rotational bush stiffness

XP	4484.02	729	281.65
YP	155383.196	-221338	-1900891

Table A-31 Rear quad link to subframe bush x and y axis projections for orientation (LHS)

A.6.9 Point 28 front quad link at upright

Translation				
front quad at upright				
DAMPING X [N.s/mm]		DAMPING X [N.s/mm]		DAMPING X [N.s/mm]
11.3569		0.862512		0.186978
STIFFNESS X		STIFFNESS Y		STIFFNESS Z [N/mm]
Comp [mm]	Force [N]	Comp [mm]	Force [N]	229.796
-1.82801	-15300	-1.98128	-15015	
-1.73987	-14280	-1.92452	-14014	
-1.64774	-13260	-1.85777	-13013	
-1.55261	-12240	-1.79102	-12012	
-1.45247	-11220	-1.70427	-11011	
-1.34534	-10200	-1.60752	-10010	

-1.22821	-9180	-1.49077	-9009
-1.10207	-8160	-1.35401	-8008
-0.97094	-7140	-1.20726	-7007
-0.8308	-6120	-1.04051	-6006
-0.69267	-5100	-0.86376	-5005
-0.55354	-4080	-0.68701	-4004
-0.4164	-3060	-0.51026	-3003
-0.27927	-2040	-0.3435	-2002
-0.14013	-1020	-0.16675	-1001
-0.07007	-510	-0.08338	-500.5
0	0	0	0
0.070067	510	0.083376	500.5
0.140134	1020	0.166752	1001
0.279268	2040	0.343504	2002
0.416402	3060	0.510255	3003
0.553536	4080	0.687007	4004
0.69267	5100	0.863759	5005
0.830804	6120	1.04051	6006
0.970937	7140	1.20726	7007
1.10207	8160	1.35401	8008
1.22821	9180	1.49077	9009
1.34534	10200	1.60752	10010
1.45247	11220	1.70427	11011
1.55261	12240	1.79102	12012
1.64774	13260	1.85777	13013
1.73987	14280	1.92452	14014
1.82801	15300	1.98128	15015

Table A-32 Front quad link to upright bush translational stiffness and damping

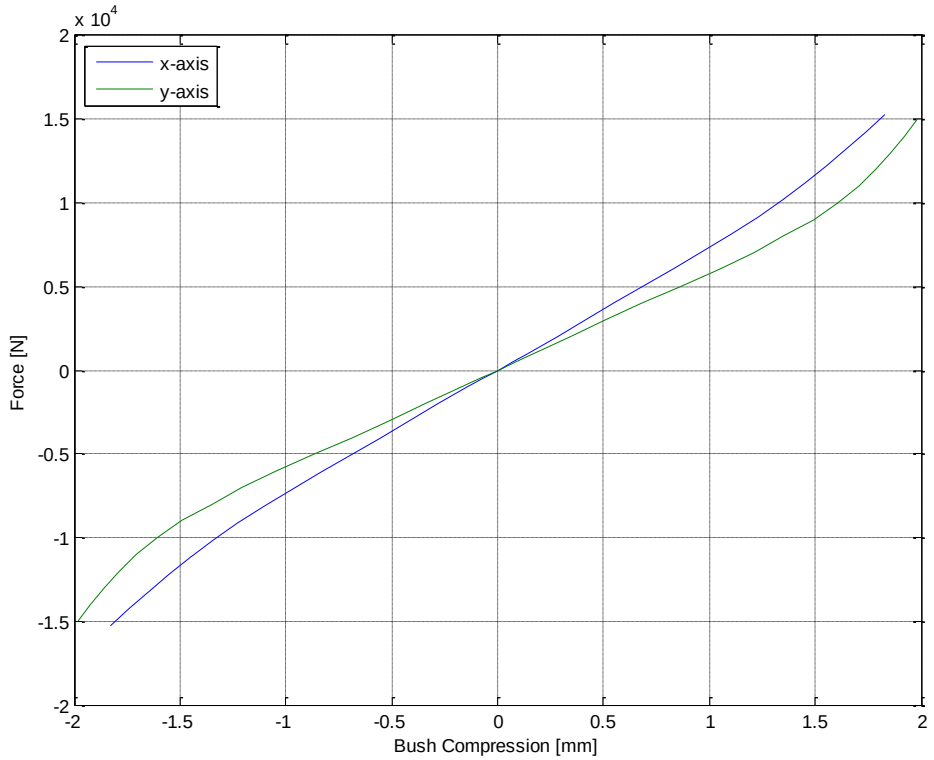

Figure A-13 Front quad link to upright bush translational bush stiffness

Rotation		
front quad at upright		
DAMPING rX [N.mm.s/deg]	DAMPING rY [N.mm.s/deg]	DAMPING rZ [N.mm.s/deg]
7.29948	7.29953	2.49992
STIFFNESS rX [N.mm/deg]	STIFFNESS rY [N.mm/deg]	STIFFNESS rZ [N.mm/deg]
7294.75	7295.32	2499.19

Table A-33 Front quad link to upright bush rotational stiffness and damping

XP	4222.42	-321.56	371.36
YP	168673.1	205445.3	-1739944

Table A-34 Front quad link to upright bush x and y axis projections for orientation (LHS)

A.6.10 Point 29 rear quad link at upright

Translation				
rear quad at upright				
DAMPING X [N.s/mm]		DAMPING X [N.s/mm]		DAMPING X [N.s/mm]
174.613		0.931267		0.824225
STIFFNESS X		STIFFNESS Y		STIFFNESS Z [N/mm]
Comp [mm]	Force [N]	Comp [mm]	Force [N]	468.909
-0.90389	-12570	-0.99951	-14940	
-0.85157	-11732	-0.95841	-13944	
-0.79724	-10894	-0.91231	-12948	
-0.74692	-10056	-0.86521	-11952	
-0.69159	-9218	-0.81211	-10956	
-0.63726	-8380	-0.75201	-9960	
-0.57694	-7542	-0.69091	-8964	
-0.51861	-6704	-0.62281	-7968	
-0.45928	-5866	-0.55171	-6972	
-0.39596	-5028	-0.47561	-5976	
-0.33263	-4190	-0.39851	-4980	
-0.26731	-3352	-0.3194	-3984	
-0.19998	-2514	-0.2403	-2988	
-0.13565	-1676	-0.1592	-1992	
-0.06733	-838	-0.0801	-996	
-0.03466	-419	-0.04105	-498	
0	0	0	0	
0.034663	419	0.041051	498	
0.067326	838	0.080101	996	
0.135652	1676	0.159202	1992	
0.199979	2514	0.240303	2988	
0.267305	3352	0.319404	3984	
0.332631	4190	0.398505	4980	
0.395957	5028	0.475606	5976	
0.459283	5866	0.551707	6972	
0.51861	6704	0.622808	7968	
0.576936	7542	0.690909	8964	
0.637262	8380	0.75201	9960	
0.691588	9218	0.81211	10956	
0.746915	10056	0.865211	11952	
0.797241	10894	0.912312	12948	
0.851567	11732	0.958413	13944	
0.903893	12570	0.999514	14940	

Table A-35 Rear quad link to upright bush translational stiffness and damping

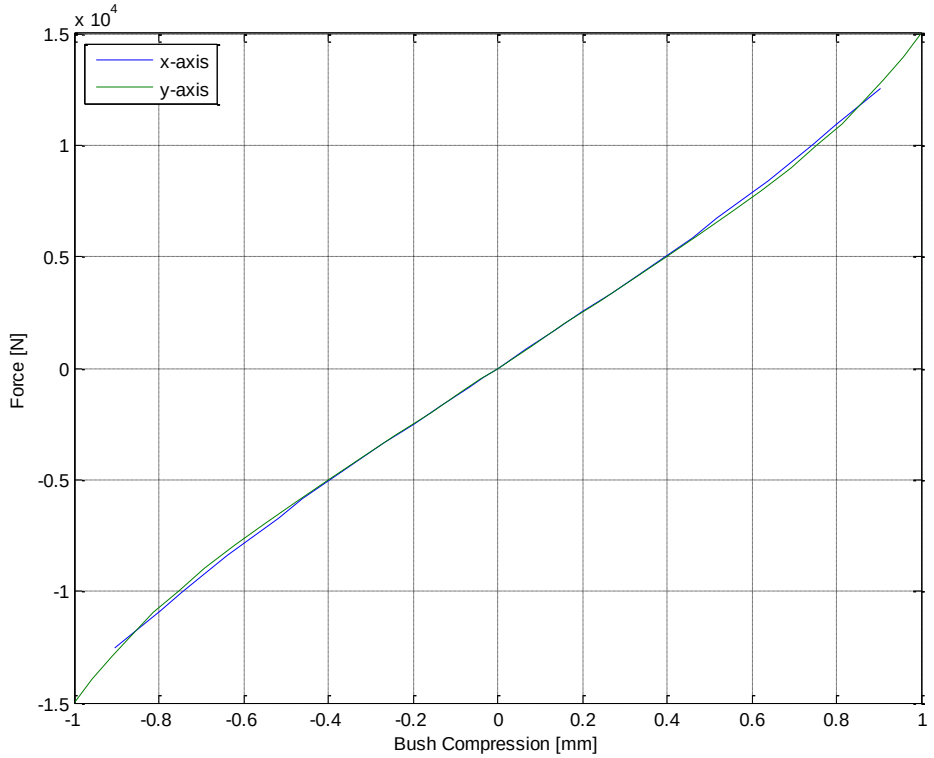

Figure A-14 Rear quad link to upright bush translational bush stiffness

Rotation					
rear quad at upright					
DAMPING rX [N.mm.s/deg]		DAMPING rY [N.mm.s/deg]		DAMPING rZ [N.mm.s/deg]	
0.475962		0.479201		0.376238	
STIFFNESS rX		STIFFNESS rY		STIFFNESS rZ	
Rotation [deg]	Torque [N.mm]	Rotation [deg]	Torque [N.mm]	Rotation [deg]	Torque [N.mm]
-7.00002	-102910	-7.00002	-106065	-14	-21167.1
-6.50002	-86864.2	-6.50002	-91145	-13	-19189.2
-6.00001	-74303.7	-6.00002	-79459.3	-12	-17594.4
-5.50001	-63898.6	-5.50001	-69461.1	-11	-15963.8
-5.00001	-55084.5	-5.00001	-60627.3	-10	-14572.1
-4.50001	-47419.5	-4.50001	-52695.1	-9	-13207.2
-4.00001	-40520.8	-4.00001	-45437.8	-8	-11834.8
-3.50001	-34227.5	-3.50001	-38781.7	-7	-10438.2
-3.00001	-28408.8	-3.00001	-32394.1	-6	-9076.9
-2.5	-22942	-2.50001	-26256	-5	-7601.8
-2	-17754.7	-2	-20377.2	-4	-6105.6
-1.5	-12825.7	-1.5	-14692.7	-3	-4563.3
-1	-8118.2	-1	-9163.6	-2	-3016.4
-0.5	-3703.8	-0.5	-4085.7	-1	-1487.7
0	0	0	0	0	0

0.500001	3703.8	0.500001	4085.7	1	1487.7
1	8118.2	1	9163.6	2	3016.4
1.5	12825.7	1.5	14692.7	3	4563.3
2	17754.7	2	20377.2	4	6105.6
2.5	22942	2.50001	26256	5	7601.8
3.00001	28408.8	3.00001	32394.1	6	9076.9
3.50001	34227.5	3.50001	38781.7	7	10438.2
4.00001	40520.8	4.00001	45437.8	8	11834.8
4.50001	47419.5	4.50001	52695.1	9	13207.2
5.00001	55084.5	5.00001	60627.3	10	14572.1
5.50001	63898.6	5.50001	69461.1	11	15963.8
6.00001	74303.7	6.00002	79459.3	12	17594.4
6.50002	86864.2	6.50002	91145	13	19189.2
7.00002	102910	7.00002	106065	14	21167.1

Table A-36 Rear quad link to upright bush rotational stiffness and damping

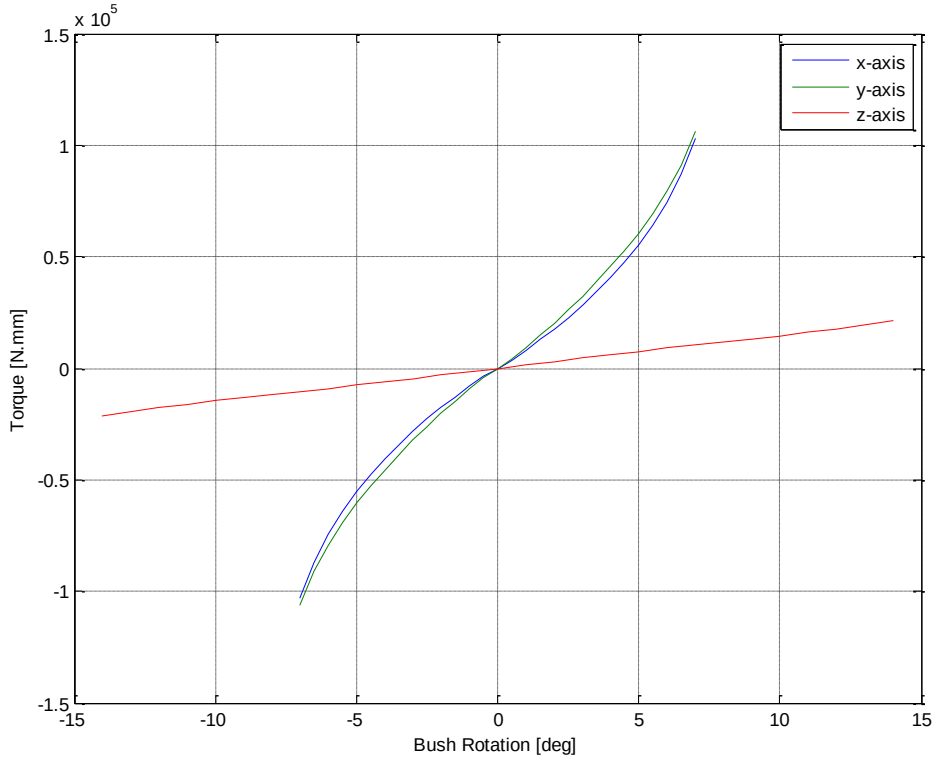

Figure A-15 Rear quad link to upright bush rotational bush stiffness

XP	4484.48	-309.58	336.61
YP	159298.618	272643.959	-1871502.188

Table A-37 Rear quad link to upright bush x and y axis projections for orientation (LHS)

A.6.11 Point 30 Longitudinal link to upright

Translation					
long link at upright					
DAMPING X [N.s/mm]		DAMPING X [N.s/mm]		DAMPING X [N.s/mm]	
0.896255		0.762134		0.159551	
STIFFNESS X		STIFFNESS Y		STIFFNESS Z	
Comp [mm]	Force [N]	Comp [mm]	Force [N]	Comp [mm]	Force [N]
-1.94435	-3012	-1.15687	-4384	-7.0872	-1435.6
-1.9168	-2811.2	-1.11859	-4164.8	-6.81477	-1342.6
-1.88255	-2610.4	-1.08071	-3945.6	-6.48251	-1246.7
-1.8442	-2409.6	-1.04053	-3726.4	-6.11585	-1150.8
-1.80535	-2208.8	-0.99356	-3507.2	-5.70688	-1054.9
-1.7604	-2008	-0.94338	-3288	-5.26512	-959
-1.70615	-1807.2	-0.8942	-3068.8	-4.78446	-863.1
-1.6401	-1606.4	-0.83942	-2849.6	-4.2816	-767.2
-1.52165	-1405.6	-0.78144	-2630.4	-3.75233	-671.3
-1.3442	-1204.8	-0.72606	-2411.2	-3.22047	-575.4
-1.13955	-1004	-0.66519	-2192	-2.67291	-479.5
-0.9228	-803.2	-0.60011	-1972.8	-2.12625	-383.6
-0.69875	-602.4	-0.53523	-1753.6	-1.58899	-287.7
-0.58273	-502	-0.47165	-1534.4	-1.03902	-191.8
-0.23135	-200.8	-0.40717	-1315.2	-0.51386	-95.9
0	0	-0.33869	-1096	0	0
0.23135	200.8	-0.27071	-876.8	0.513862	95.9
0.582726	502	-0.17005	-548	1.03902	191.8
0.698751	602.4	-0.13546	-438.4	1.58899	287.7
0.922801	803.2	-0.06778	-219.2	2.12625	383.6
1.13955	1004	0	0	2.67291	479.5
1.3442	1204.8	0.067779	219.2	3.22047	575.4
1.52165	1405.6	0.135457	438.4	3.75233	671.3
1.6401	1606.4	0.170046	548	4.2816	767.2
1.70615	1807.2	0.270714	876.8	4.78446	863.1
1.7604	2008	0.338692	1096	5.26512	959
1.80535	2208.8	0.407171	1315.2	5.70688	1054.9
1.8442	2409.6	0.471649	1534.4	6.11585	1150.8
1.88255	2610.4	0.535228	1753.6	6.48251	1246.7
1.9168	2811.2	0.600106	1972.8	6.81477	1342.6
1.94435	3012	0.665185	2192	7.0872	1435.6
		0.726063	2411.2		
		0.781442	2630.4		
		0.83942	2849.6		
		0.894199	3068.8		
		0.943377	3288		

0.993556	3507.2
1.04053	3726.4
1.08071	3945.6
1.11859	4164.8
1.15687	4384

Table A-38 Longitudinal link to upright bush translational stiffness and damping

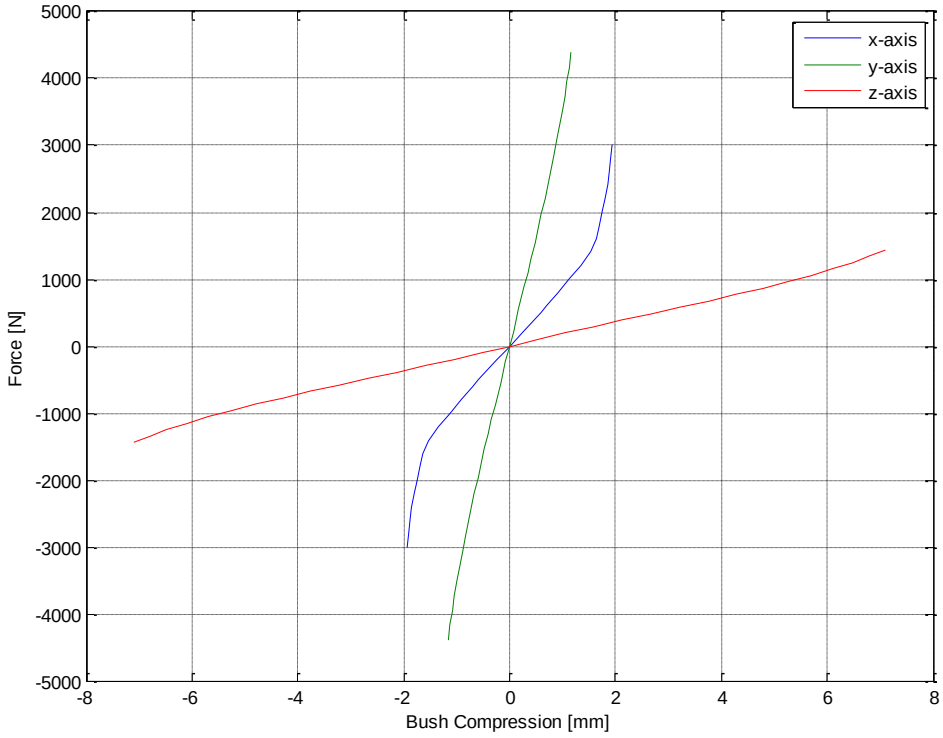

Figure A-16 Longitudinal link to upright bush translational bush stiffness

Rotation		
long link at upright		
DAMPING rX [N.mm.s/deg]	DAMPING rY [N.mm.s/deg]	DAMPING rZ [N.mm.s/deg]
0.352941	0.34375	0.432432
STIFFNESS rX [N.mm/deg]	STIFFNESS rY [N.mm/deg]	STIFFNESS rZ [N.mm/deg]
1200	1100	3200

Table A-39 Longitudinal link to upright bush rotational stiffness and damping

XP	3743.97	507.28	387.19
YP	-168185.027	835676.3096	531413.0458

Table A-40 Longitudinal link to upright bush x and y axis projections for orientation (LHS)

A.6.12 Point 31 Longitudinal link to chassis

Translation					
long link at chassis					
DAMPING X [N.s/mm]		DAMPING X [N.s/mm]		DAMPING X [N.s/mm]	
0.658957		0.577485		0.114891	
STIFFNESS X		STIFFNESS Y		STIFFNESS Z	
Comp [mm]	Force [N]	Comp [mm]	Force [N]	Comp [mm]	Force [N]
-5.26878	-5315	-6.96506	-6908.3	-13.4878	-1731.4
-5.20648	-5102.4	-6.92566	-6759.2	-13.0355	-1626.8
-5.13648	-4889.8	-6.80991	-6361.6	-12.4098	-1510.6
-5.05838	-4677.2	-6.67865	-5964	-11.6922	-1394.4
-4.97698	-4464.6	-6.52969	-5566.4	-10.8782	-1278.2
-4.88988	-4252	-6.35734	-5168.8	-9.97912	-1162
-4.79388	-4039.4	-6.17008	-4771.2	-9.02041	-1045.8
-4.69139	-3826.8	-5.95492	-4373.6	-8.0007	-929.6
-4.58269	-3614.2	-5.71197	-3976	-6.95388	-813.4
-4.46179	-3401.6	-5.42831	-3578.4	-5.88367	-697.2
-4.33309	-3189	-5.09815	-3180.8	-4.82796	-581
-4.19669	-2976.4	-4.7049	-2783.2	-3.78555	-464.8
-4.04089	-2763.8	-4.23514	-2385.6	-2.78634	-348.6
-3.87029	-2551.2	-3.67128	-1988	-1.82312	-232.4
-3.67929	-2338.6	-3.00653	-1590.4	-0.89391	-116.2
-3.47059	-2126	-2.27357	-1192.8	0	0
-3.22359	-1913.4	-1.51061	-795.2	0.893912	116.2
-2.94249	-1700.8	-0.94672	-497	1.82312	232.4
-2.62499	-1488.2	0	0	2.78634	348.6
-2.2591	-1275.6	0.946721	497	3.78555	464.8
-1.8638	-1063	1.51061	795.2	4.82796	581
-1.4532	-850.4	2.27357	1192.8	5.88367	697.2
-0.86825	-531.5	3.00653	1590.4	6.95388	813.4
0	0	3.67128	1988	8.0007	929.6
0.868248	531.5	4.23514	2385.6	9.02041	1045.8
1.4532	850.4	4.7049	2783.2	9.97912	1162
1.8638	1063	5.09815	3180.8	10.8782	1278.2
2.2591	1275.6	5.42831	3578.4	11.6922	1394.4
2.62499	1488.2	5.71197	3976	12.4098	1510.6
2.94249	1700.8	5.95492	4373.6	13.0355	1626.8
3.22359	1913.4	6.17008	4771.2	13.4878	1731.4
3.47059	2126	6.35734	5168.8		
3.67929	2338.6	6.52969	5566.4		
3.87029	2551.2	6.67865	5964		
4.04089	2763.8	6.80991	6361.6		
4.19669	2976.4	6.92566	6759.2		

4.33309	3189	6.96506	6908.3
4.46179	3401.6		
4.58269	3614.2		
4.69139	3826.8		
4.79388	4039.4		
4.88988	4252		
4.97698	4464.6		
5.05838	4677.2		
5.13648	4889.8		
5.20648	5102.4		
5.26878	5315		

Table A-41 Longitudinal link to chassis bush translational stiffness and damping

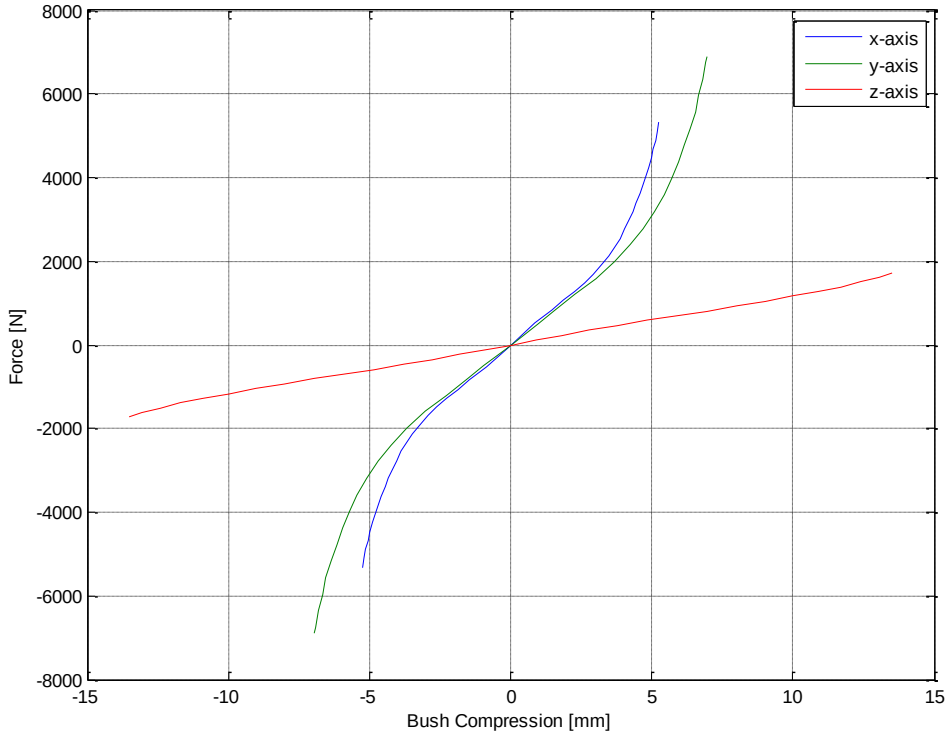

Figure A-17 Longitudinal link to chassis bush translational bush stiffness

Rotation		
long link at chassis		
DAMPING rX [N.mm.s/deg]	DAMPING rY [N.mm.s/deg]	DAMPING rZ [N.mm.s/deg]
0.730912	0.34375	0.544787
STIFFNESS rX [N.mm/deg]	STIFFNESS rY [N.mm/deg]	STIFFNESS rZ [N.mm/deg]
2716	700	1197

Table A-42 Longitudinal link to chassis bush rotational stiffness and damping

XP	4355.17	707.22	226.33
YP	153315.048	-847418.617	-302221.110

Table A-43 Longitudinal link to chassis bush x and y axis projections for orientation (LHS)

A.6.13 Point 37 subframe to chassis front

TRANSLATION					
subframe at frame		subframe at frame		subframe at frame	
DAMPING X [N.s/mm]		DAMPING X [N.s/mm]		DAMPING X [N.s/mm]	
0.459535		2.25346		0.348418	
STIFFNESS X		STIFFNESS Y		STIFFNESS Z	
Comp [mm]	Force [N]	Comp [mm]	Force [N]	Comp [mm]	Force [N]
-4.80333	-2522.4	-1.25247	-2497.5	-5.35462	-2569.7
-4.70602	-2431.2	-1.2071	-2397.6	-5.30347	-2476.8
-4.45426	-2228.6	-1.11446	-2197.8	-5.18069	-2270.4
-4.1526	-2026	-1.01572	-1998	-5.02761	-2064
-3.80754	-1823.4	-0.91818	-1798.2	-4.84003	-1857.6
-3.42188	-1620.8	-0.81733	-1598.4	-4.59425	-1651.2
-3.00492	-1418.2	-0.71589	-1398.6	-4.28187	-1444.8
-2.57276	-1215.6	-0.61425	-1198.8	-3.87529	-1238.4
-2.1258	-1013	-0.50891	-999	-3.357	-1032
-1.67824	-810.4	-0.40797	-799.2	-2.72682	-825.6
-1.03035	-506.5	-0.25696	-499.5	-1.67865	-516
-0.50638	-253.3	-0.12803	-249.8	-0.82858	-258
0	0	0	0	0	0
0.506376	253.3	0.128032	249.8	0.806376	258
1.03035	506.5	0.256955	499.5	1.59035	516
1.67824	810.4	0.407967	799.2	2.46052	825.6
2.1258	1013	0.508909	999	2.9394	1032
2.57276	1215.6	0.614251	1198.8	3.32939	1238.4
3.00492	1418.2	0.715893	1398.6	3.63567	1444.8
3.42188	1620.8	0.817334	1598.4	3.88005	1651.2
3.80754	1823.4	0.918176	1798.2	4.07893	1857.6
4.1526	2026	1.01572	1998	4.24361	2064
4.45426	2228.6	1.11446	2197.8	4.37949	2270.4
4.70602	2431.2	1.2071	2397.6	4.49777	2476.8
4.80333	2522.4	1.25247	2497.5	4.54522	2569.7

Table A-44 Subframe to chassis front bush translational stiffness and damping

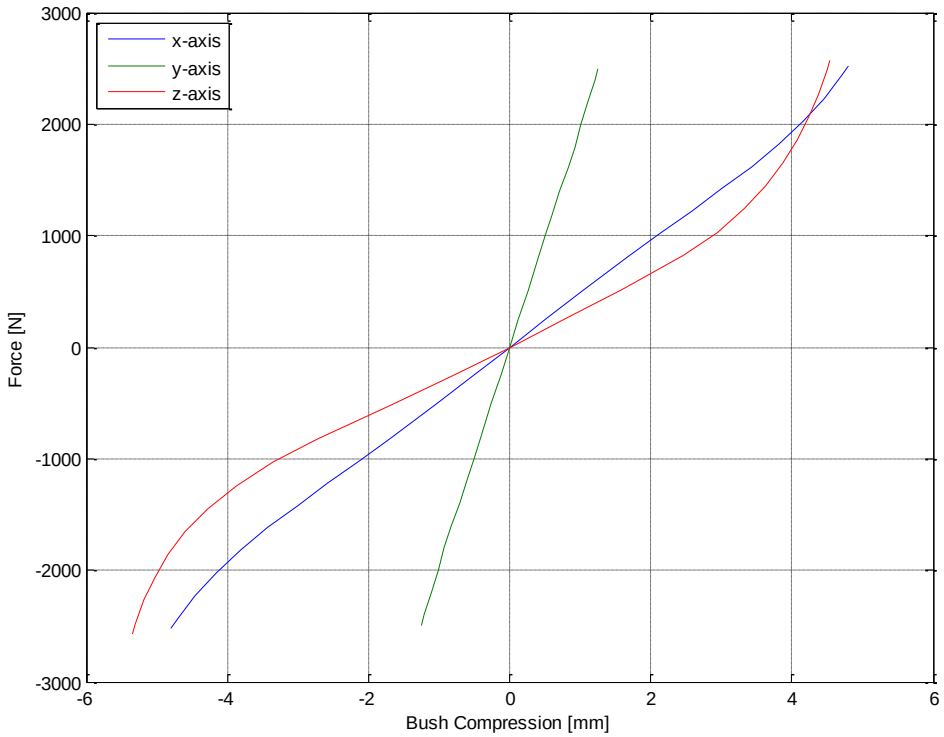

Figure A-18 Subframe to chassis front bush translational bush stiffness

Rotation		
subframe at frame		
DAMPING rX [N.mm.s/deg]	DAMPING rY [N.mm.s/deg]	DAMPING rZ [N.mm.s/deg]
0.77778	0.77778	0.77778
STIFFNESS rX [N.mm/deg]	STIFFNESS rY [N.mm/deg]	STIFFNESS rZ [N.mm/deg]
3500	3500	3500

Table A-45 Subframe to chassis front bush rotational stiffness and damping

XP	1	0	0
YP	0	1	0

Table A-46 Subframe to chassis front bush x and y axis projections for orientation (LHS)

A.6.14 Point 38 subframe to chassis rear

Translation					
subframe at frame rear					
DAMPING X [N.s/mm]		DAMPING X [N.s/mm]		DAMPING X [N.s/mm]	
3.71768		8.52833		1.44516	
STIFFNESS X		STIFFNESS Y		STIFFNESS Z	
Comp [mm]	Force [N]	Comp [mm]	Force [N]	Comp [mm]	Force [N]
-2.69933	-8950	-2.50554	-8352	-3.1242	-2675.4
-2.65231	-8500	-2.39477	-7888	-3.01777	-2511.6
-2.59077	-8000	-2.2788	-7424	-2.89043	-2347.8
-2.52354	-7500	-2.16014	-6960	-2.75989	-2184
-2.449	-7000	-2.03657	-6496	-2.61845	-2020.2
-2.36137	-6500	-1.9079	-6032	-2.44142	-1856.4
-2.26813	-6000	-1.77653	-5568	-2.26498	-1692.6
-2.1596	-5500	-1.64416	-5104	-2.05564	-1528.8
-2.04026	-5000	-1.50439	-4640	-1.85301	-1365
-1.90572	-4500	-1.36212	-4176	-1.64057	-1201.2
-1.75229	-4000	-1.21835	-3712	-1.42323	-1037.4
-1.57885	-3500	-1.06998	-3248	-1.2029	-873.6
-1.38382	-3000	-0.92161	-2784	-0.98306	-709.8
-1.16818	-2500	-0.77015	-2320	-0.76152	-546
-0.94174	-2000	-0.61848	-1856	-0.53529	-382.2
-0.70961	-1500	-0.46371	-1392	-0.38346	-273
-0.47247	-1000	-0.30874	-928	-0.19263	-136.5
-0.23844	-500	-0.15247	-464	0	0
0	0	0	0	0.192631	136.5
0.238436	500	0.152469	464	0.383461	273
0.472472	1000	0.308738	928	0.535286	382.2
0.709608	1500	0.463707	1392	0.761523	546
0.941744	2000	0.618476	1856	0.98306	709.8
1.16818	2500	0.770145	2320	1.2029	873.6
1.38382	3000	0.921614	2784	1.42323	1037.4
1.57885	3500	1.06998	3248	1.64057	1201.2
1.75229	4000	1.21835	3712	1.85301	1365
1.90572	4500	1.36212	4176	2.05564	1528.8
2.04026	5000	1.50439	4640	2.26498	1692.6
2.1596	5500	1.64416	5104	2.44142	1856.4
2.26813	6000	1.77653	5568	2.61845	2020.2
2.36137	6500	1.9079	6032	2.75989	2184
2.449	7000	2.03657	6496	2.89043	2347.8
2.52354	7500	2.16014	6960	3.01777	2511.6
2.59077	8000	2.2788	7424	3.1242	2675.4
2.65231	8500	2.39477	7888		

2.69933	8950	2.50554	8352

Table A-47 Subframe to chassis rear bush translational stiffness and damping

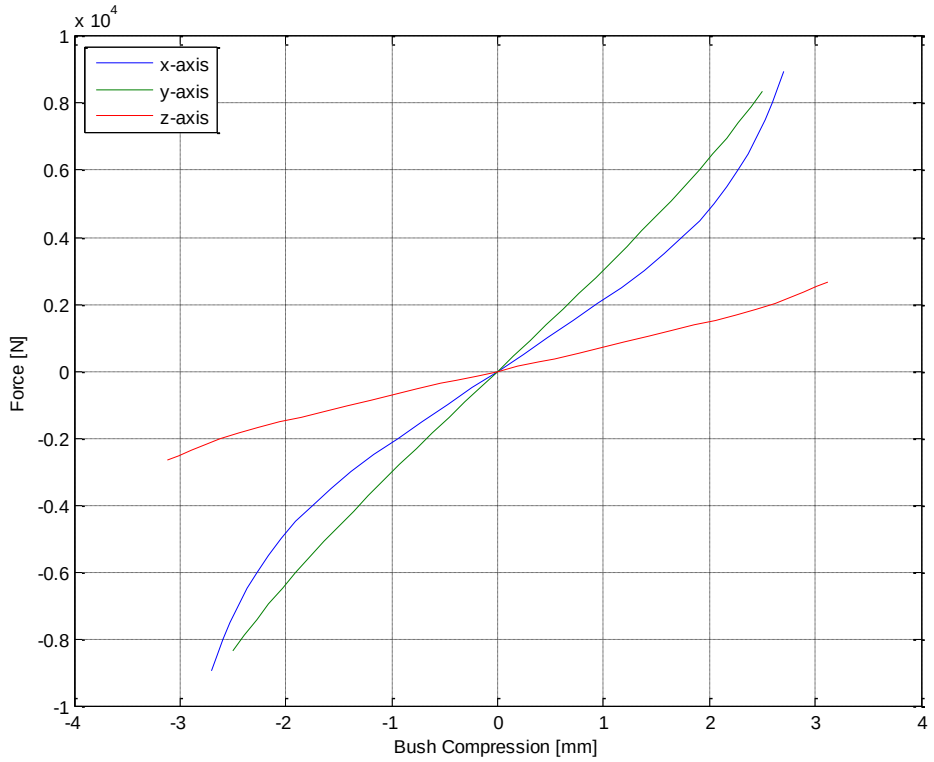

Figure A-19 Subframe to chassis rear bush translational bush stiffness

Rotation		
subframe at frame		
DAMPING rX [N.mm.s/deg]	DAMPING rY [N.mm.s/deg]	DAMPING rZ [N.mm.s/deg]
0.77778	0.77778	0.77778
STIFFNESS rX [N.mm/deg]	STIFFNESS rY [N.mm/deg]	STIFFNESS rZ [N.mm/deg]
3500	3500	3500

Table A-48 Subframe to chassis rear bush rotational stiffness and damping

XP	1	0	0
YP	0	1	0

Table A-49 Subframe to chassis rear bush x and y axis projections for orientation (LHS)

A.7 Standard Vehicle Mass and Inertia Data

Front Suspension								
			Cog [mm]			Moments of Inertia [Kg.m2]		
L/R	Part	Mass [Kg]	X	Y	Z	Ix	Iy	Iz
na	Front Subframe	30.2	96.7	-3.9	-69.4	3.4	3.1	6.3
na	Anti-Roll Bar	3.9	-222.7	0.0	-11.6	0.5	0.0	0.5
R	Wishbone assembly							
R	Lower Arm RH	4.5	-131.6	-475.6	-100.6	0.1	0.1	0.1
R	Bush - Lower Arm RH	0.2	-7.4	-404.0	-91.0	0.0	0.0	0.0
R	Bush - Lower Arm RH	1.5	-282.4	-348.0	-88.0	0.0	0.0	0.0
R	Ball Joint RH	0.6	10.6	-760.0	-125.0	0.0	0.0	0.0
R	Strut assembly							
R	Shock Absorber RH	4.0	-21.4	-620.0	360.0	0.1	0.1	0.0
R	Spring RH	1.9	-29.4	-615.0	511.0	0.0	0.0	0.0
R	Top Mtg RH	0.4	-32.4	-590.0	645.0	0.0	0.0	0.0
R	Top Mount Brg RH.	0.4	-32.4	-590.0	675.0	0.0	0.0	0.0
R	Upright assembly							
R	Knuckle RH	4.7	-4.4	-768.0	36.0	0.0	0.0	0.0
R	Hub + Brg. RH	2.9	1.0	-830.0	0.0	0.0	0.0	0.0
L	Wishbone assembly							
L	Lower Arm LH	4.5	-131.6	475.6	-100.6	0.1	0.1	0.1
L	Bush - Lower Arm LH	0.2	-7.4	404.0	-91.0	0.0	0.0	0.0
L	Bush - Lower Arm LH	1.5	-282.4	348.0	-88.0	0.0	0.0	0.0
L	Ball Joint LH	0.6	10.6	760.0	-125.0	0.0	0.0	0.0
L	Strut assembly							
L	Shock Absorber LH	4.0	-21.4	620.0	360.0	0.1	0.1	0.0
L	Spring LH	1.9	-29.4	615.0	511.0	0.0	0.0	0.0
L	Top Mtg LH	0.4	-32.4	590.0	645.0	0.0	0.0	0.0
L	Top Mount Brg. LH	0.4	-32.4	590.0	675.0	0.0	0.0	0.0
L	Upright assembly							
L	Knuckle LH	4.7	-4.4	768.0	36.0	0.0	0.0	0.0
L	Hub + Brg LH.	2.9	1.0	830.0	0.0	0.0	0.0	0.0
	Wheels and tyres							
R	19" Tyre F-RH	15.9	-0.4	-796.0	0.0	1.0	1.6	1.0
L	19" Tyre F-LH	15.9	-0.4	796.0	0.0	1.0	1.6	1.0
R	Alloy Wheel (19") F-Rh	13.5	-0.4	-810.0	0.0	0.3	0.4	0.3
L	Alloy Wheel (19") F-Lh	13.5	-0.4	810.0	0.0	0.3	0.4	0.3

Table A-50 Standard vehicle front suspension mass and inertia data

Rear Suspension								
			Cog [mm]			Moments of Inertia [Kg.m2]		
L/R	Part	Mass [Kg]	X	Y	Z	Ix	Iy	Iz
na	Subframe (+brkts & fxgs)	18.7	-2688.4	-1.0	79.0	1.69	0.55	2.15
na	Anti roll bar	5.4	-2855.4	0.0	42.0	0.86	0.06	0.92
R	Front transverse link RH	0.9	-2533.4	-525.0	-18.0	0.03	0.00	0.03
R	Strut and Spring Assembly RH	10.5	-2706.4	-623.1	400.2	0.31	0.31	0.01
R	Rear transverse link RH	1.5	-2777.4	-520.0	-56.0	0.03	0.00	0.03
R	Longitudinal link - RH	2.3	-2293.4	-594.0	-44.0	0.00	0.09	0.09
R	Upright assembly							
R	Knuckle RH	7.4	-2666.4	-732.0	16.0	0.06	0.06	0.03
R	Wheel bearing RH	0.8	-2661.1	-795.0	5.0	0.00	0.00	0.00
R	Driveflange RH	1.8	-2661.1	-827.0	5.0	0.00	0.00	0.00
L	Front transverse link LH	0.9	-2533.4	525.0	-18.0	0.03	0.00	0.03
L	Longitudinal link LH	2.3	-2293.4	594.0	-44.0	0.00	0.09	0.09
L	Strut and Spring Assembly LH	10.5	-2706.4	623.1	400.2	0.31	0.31	0.01
L	Rear transverse link LH	1.5	-2777.4	520.0	-56.0	0.03	0.00	0.03
L	Upright assembly							
L	Knuckle LH	7.4	-2666.4	732.0	16.0	0.06	0.06	0.03
L	Wheel bearing LH	0.8	-2661.1	795.0	5.0	0.00	0.00	0.00
L	Driveflange LH	1.8	-2661.1	827.0	5.0	0.00	0.00	0.00
	Wheels and tyres							
R	19" Tyre R-RH	15.9	-2661.4	-794.0	4.0	0.95	1.57	0.95
L	19" Tyre R-LH	15.9	-2661.4	794.0	4.0	0.95	1.57	0.95
R	Alloy Wheel (19") R-Rh	13.5	-2661.4	-810.0	4.0	0.27	0.41	0.27
L	Alloy Wheel (19") R-Lh	13.5	-2661.4	810.0	4.0	0.27	0.41	0.27

Table A-51 Standard vehicle rear suspension mass and inertia data

Chassis Mountings								
			Cog [mm]			Moments of Inertia [Kg.m2]		
L/R	Part	Mass [Kg]	X	Y	Z	Ix	Iy	Iz
R	RHS Eng Mtg Brkt	1.5	238.6	-457.0	543.0	0.01	0.00	0.01
R	RHS Eng Mount	2.2	207.6	-530.0	456.0	0.01	0.01	0.01
L	LHS Trans. Mtg Brkt	1.1	142.6	418.0	282.0	0.00	0.00	0.00
L	LHS Trans Mount	2.1	139.6	453.0	406.0	0.00	0.01	0.01
na	Upper Tie Rod Link	0.7	247.6	-514.0	588.0	0.00	0.01	0.01
na	UTR BIW Brkt	0.3	39.6	-501.0	609.0	0.00	0.00	0.00
na	Lower Tie Rod Link	0.5	-23.4	-304.0	24.7	0.00	0.00	0.00
na	LTR Large Bush	0.6	-74.4	-304.0	-46.0	0.00	0.00	0.00
na	LTR Small Bush	0.5	37.6	-304.0	12.0	0.00	0.00	0.00

Table A-52 Standard vehicle chassis mountings mass and inertia data

Engine (inc gearbox clutch etc) and driveline								
			Cog [mm]			Moments of Inertia [Kg.m2]		
L/R	Part	Mass [Kg]	X	Y	Z	Ix	Iy	Iz
na	Power Unit, clutch + flywheel	242.1	159.1	-50.6	222.2	27.80	11.46	24.08
na	Gearbox	70.9	121.6	292.0	89.0	0.83	1.03	0.76
	Exhaust Assembly							
na	Hot End Assy	9.1	-247.4	85.0	94.0	0.04	0.18	0.20
na	Cold End Assy	28.0	-2543.4	-7.0	-2.0	2.49	18.39	20.66
	Driveline Parts							
na	RDU + Coupling	28.2	-2561.4	-3.0	37.0	0.11	0.55	0.58
na	Propshaft	13.3	-1267.4	-24.0	85.0	0.02	4.44	4.44
na	Rear drive shaft RH	5.9	-2673.4	-446.0	17.0	0.24	0.01	0.24
na	Rear drive shaft LH	5.9	-2673.4	446.0	17.0	0.24	0.01	0.24
	Air Intake Assembly							
na	Dirty air intake ducting - plastic	0.4	127.6	820.0	485.0	0.01	0.03	0.03
na	Air filt,DAD assy+Resonator	2.0	399.6	575.0	362.0	0.14	0.11	0.07
na	Clean Air Duct	1.5	477.6	160.0	367.0	0.05	0.03	0.02

Table A-53 Standard vehicle engine, driveline and subsidiaries mass and inertia data

Cooling								
			Cog [mm]			Moments of Inertia [Kg.m2]		
L/R	Part	Mass [Kg]	X	Y	Z	Ix	Iy	Iz
na	Transmission Oil cooler	0.7	585.6	390.0	318.0	0.00	0.00	0.00
na	Transmission Oil cooler Hose Set	0.3	482.6	325.0	225.0	0.00	0.00	0.00
na	Radiator SI6P	22.0	637.6	0.0	271.0	0.32	0.10	0.24
na	Electric Fan Assy	4.0	580.6	-16.0	241.0	0.22	0.08	0.15
na	Condenser	2.9	673.6	-20.0	273.0	0.18	0.07	0.11
na	Rad Brackets & Mounts	2.4	609.1	0.4	189.5	0.24	0.12	0.12
na	Expansion Tank	0.6	215.6	-643.0	545.0	0.00	0.01	0.00
na	Exp Tank Cap	0.1	197.6	-603.0	615.0	0.00	0.00	0.00
na	Coolant Hose Set SI6-A	1.8	307.6	-85.0	408.0	0.05	0.11	0.13
na	Coolant (3 kg. Inc. in P.U.)	4.0	383.6	-257.0	420.0	0.50	0.26	0.61

Table A-54 Standard vehicle cooling system mass and inertia data

HEVAC								
			Cog [mm]			Moments of Inertia [Kg.m2]		
L/R	Part	Mass [Kg]	X	Y	Z	Ix	Iy	Iz
na	Aircon. Pipe Set	3.1	225.4	-439.2	422.3	0.02	0.07	0.07
na	Body Air Outlets/ Ducts	0.3	-3177.4	0.0	582.0	0.09	0.00	0.09
na	Comp (inc. in Engine) 6.31kg	0.0	1707.6	0.0	-365.0	0.00	0.00	0.00
na	Stop start coolant pump	0.4	-503.4	-94.0	188.0	0.00	0.00	0.00
na	Refridgerant	0.8	-612.4	-47.0	460.0	0.00	0.00	0.00
na	Heater A/C & Blower Unit	10.0	-466.3	-13.9	472.0	0.20	0.30	0.30

Table A-55 Standard vehicle heating and AC system mass and inertia data

Steering								
			Cog [mm]			Moments of Inertia [Kg.m2]		
L/R	Part	Mass [Kg]	X	Y	Z	Ix	Iy	Iz
na	Steering rack - LH/RH	10.5	-184.4	58.0	0.0	1.07	0.04	1.05
na	Steering column - LH/RH	4.0	-622.4	373.0	575.0	0.02	0.06	0.05

Table A-56 Standard vehicle steering system mass and inertia data

EDS								
			Cog [mm]			Moments of Inertia [Kg.m2]		
L/R	Part	Mass [Kg]	X	Y	Z	Ix	Iy	Iz
na	Battery H7	24.0	13.6	400.0	572.0	0.10	0.21	0.19

Table A-57 Standard vehicle battery mass and inertia data

Fuel System								
			Cog [mm]			Moments of Inertia [Kg.m2]		
L/R	Part	Mass [Kg]	X	Y	Z	Ix	Iy	Iz
na	Fuel Tank Assy	11.8	-2144.4	7.0	83.0	1.15	0.56	1.37
na	Tank Cradle	8.9	-2162.4	-4.0	-29.0	0.92	0.29	1.15
na	Fuel Filler Assy (inc. Cap)	1.4	-2743.4	-506.0	264.0	0.06	0.08	0.05
na	Petrol UF lines	1.8	-1225.4	-248.0	-21.0	0.00	0.26	0.26
na	Charcoal can	2.3	-2984.4	801.0	619.0	0.01	0.01	0.01

Table A-58 Standard vehicle fuel system mass and inertia data

Trim								
			Cog [mm]			Moments of Inertia [Kg.m2]		
L/R	Part	Mass [Kg]	X	Y	Z	Ix	Iy	Iz
na	Fuel Filler	0.4	-2927.4	-851.0	650.0	0.00	0.00	0.00
na	Tailgate Trim	3.4	-3327.4	0.0	811.0	0.32	0.08	0.25
na	Rear Seat Complete	39.4	-2405.4	3.0	525.0	6.23	3.21	6.15
na	Space saver spare tyre	6.3	-2921.4	0.0	287.0	0.27	0.27	0.50
na	Space saver spare wheel	8.9	-2921.4	0.0	312.0	0.20	0.20	0.31
na	Jack & Jack Retention	2.3	-2862.4	0.0	229.0	0.06	0.06	0.01
na	Spare Wheel Retention	0.2	-2952.4	0.0	419.0	0.00	0.00	0.00
na	Toolkit	0.5	-3201.4	-570.0	455.0	0.00	0.00	0.00
na	Rear Carpet	8.0	-1718.4	-4.0	109.0	1.87	1.50	3.36
na	Wrench	0.5	-2888.4	0.0	229.0	0.00	0.00	0.00

Table A-59 Standard vehicle trim mass and inertia data

Body								
			Cog [mm]			Moments of Inertia [Kg.m2]		
L/R	Part	Mass [Kg]	X	Y	Z	Ix	Iy	Iz
na	Body	1063.6	-1342.7	-12.6	476.7	539.00	1635.00	1841.00
R	Driver	75.0	-1279.4	374.0	587.0	4.73	10.12	8.07
L	Passenger	75.0	-1279.4	-374.0	587.0	4.73	10.12	8.07

Table A-60 Standard vehicle body mass and inertia data

Complete standard vehicle						
Mass	Cog x [mm]	Cog y [mm]	Cog z [mm]	Ix [Kg.m2]	Iy [Kg.m2]	Iz [Kg.m2]
2150.00	1158.34	2.05	351.6	859.40	3471.69	3776.50

Table A-61 Complete standard vehicle mass and inertia data

A.8 Tyre model

The tyre model utilised in this study is of MF05 type, and is described by equations for the three orthogonal forces and moments as described in the paper by Goryca (2010), the plotting method also outlined in this paper has been utilised to illustrate

the lateral and longitudinal tyre forces of the model as shown in Figure A-20 and Figure A-21.

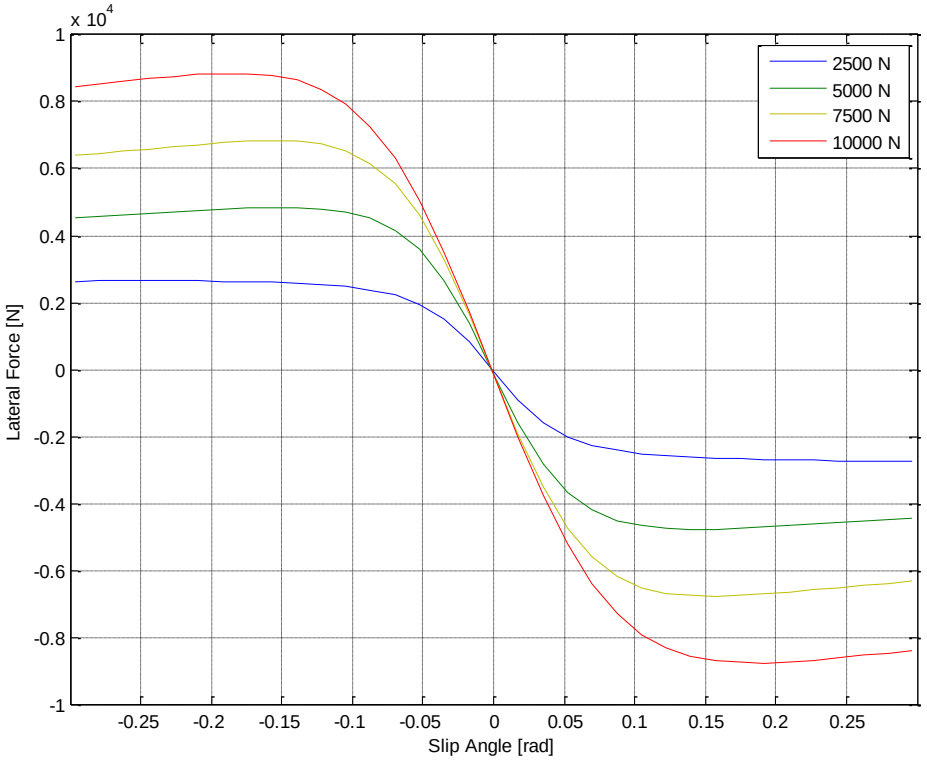

Figure A-20 Lateral tyre force characteristics

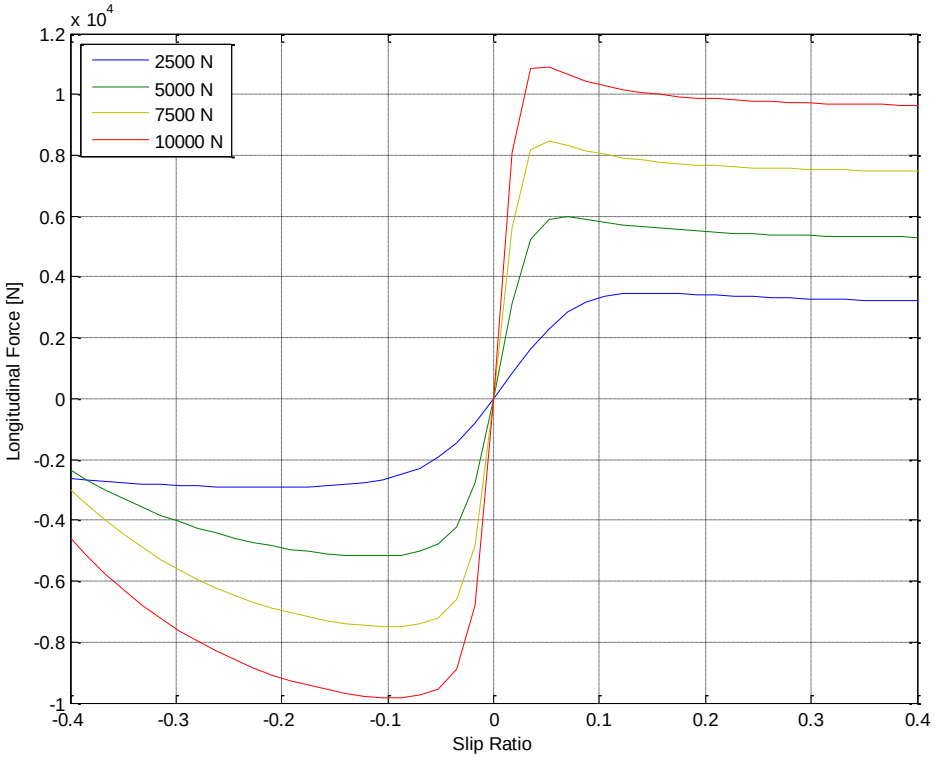

Figure A-21 Longitudinal tyre force characteristics

A.8.1 Tyre data file (.tir format)

$----------MDI_HEADER
[MDI_HEADER]
FILE_TYPE = 'tir'
FILE_VERSION = 2
FILE_FORMAT = 'ASCII'
(COMMENTS)
[redacted]
'Nom. Section width (m) 0.235'
'Nom. aspect ratio (-) 65'
'Infl. pressure (Pa) 220000'
'Rim radius (m) 0.2159'
'Measurement ID' J5I3K170 NEUF'
'Test speed (m/s) 22.2'
'Road surface Safety walk'
'Road condition Dry'
[redacted]
'Matricule 0908FKW73700'
[redacted]
'TED Xpur = 4.1538'
'TEG Xpur = 4.1307'
'TED Xcouple = 9.1287'
'TEG Xcouple = 9.1269'
'TED Ypur = 0.16'
'TEG Ypur = 0.16'

[redacted] – Tyre make/model and identifiers removed

```
'TED Ycouple          = 6.4368'
'TEG Ycouple          = 6.434'
'TED Mzpur            = 1.39'
'TEG Mzpur            = 1.39'
'TED Mzcouple          = 60.9561'
'TEG Mzcouple          = 56.8953'
'TED Mx               = 0.44'
'TEG Mx               = 0.53'
'TED My               = 72.2102'
'TEG My               = 71.1391'
$----------------------------------------------------------------------units
[UNITS]
LENGTH                = 'meter'
FORCE                 = 'newton'
ANGLE                 = 'degree'
MASS                  = 'Kg'
TIME                  = 'second'
$----------------------------------------------------------------------model
[MODEL]
PROPERTY_FILE_FORMAT    = 'MF_05'
USE_MODE              = 14            $typarr(  1)      $Tyre use switch
FITTYP                = 5             $typarr(  2)      $Magic Formula Version number
MFSAFE1               = -528          $typarr(  3)
MFSAFE2               = 0             $typarr(  4)
MFSAFE3               = 0             $typarr(  5)
VXLOW                 = 1             $typarr(  29)
LONGVL                = 22.2          $typarr(  6)      $Measurement speed
$---------------------------------------------------------------------dimension
[DIMENSION]
UNLOADED_RADIUS       = 0.369         $typarr(  7)      $Free tyre radius
WIDTH                 = 0.235         $typarr(  8)      $Nominal section width of the tyre
RIM_RADIUS            = 0.2159        $typarr(  9)      $Nominal rim radius
RIM_WIDTH             = 0.1905        $typarr(  10)     $Rim width
$-----------------------------------------------------------------------shape
[SHAPE]
{radial width}

1.0                   0
1.0                   0.2
1.0                   0.4
1.0                   0.5
1.0                   0.6
1.0                   0.7
1.0                   0.8
1.0                   0.85
1.0                   0.9
0.9                   1
$---------------------------------------------------------------------vertical
[VERTICAL]
VERTICAL_STIFFNESS    = 263916.5176     $typarr(  15)     $Tyre vertical stiffness
VERTICAL_DAMPING      = 500             $typarr(  16)     $Tyre vertical damping
BREFF                 = 3               $typarr(  11)     $Low load stiffness e.r.r.
DREFF                 = 0.19258         $typarr(  12)     $Peak value of e.r.r.
FREFF                 = 0.052698        $typarr(  13)     $High load stiffness e.r.r.
FNOMIN                = 5297.4          $typarr(  14)     $Nominal wheel load
$-------------------------------------------------------------long_slip_range
[LONG_SLIP_RANGE]
```

```
KPUMIN              = -0.402813       $typarr(  23)      $Minimum valid wheel slip
KPUMAX              = 0.473345        $typarr(  24)      $Maximum valid wheel slip
$----------------------------------------------------------------slip_angle_range
[SLIP_ANGLE_RANGE]
ALPMIN              = -17.5           $typarr(  25)      $Minimum valid slip angle
ALPMAX              = 17.5            $typarr(  26)      $Maximum valid slip angle
$-------------------------------------------------------inclination_slip_range
[INCLINATION_ANGLE_RANGE]
CAMMIN              = -5.5            $typarr(  27)      $Minimum valid camber angle
CAMMAX              = 5.5             $typarr(  28)      $Maximum valid camber angle
$-------------------------------------------------------vertical_force_range
[VERTICAL_FORCE_RANGE]
FZMIN               = 480.67          $typarr(  21)      $Minimum allowed wheel load
FZMAX               = 11679.34        $typarr(  22)      $Maximum allowed wheel load
$-----------------------------------------------------------------------scaling
[SCALING_COEFFICIENTS]
LFZO                = 1               $typarr(  31)      $Scale factor of nominal (rated) load
LCX                 = 1               $typarr(  32)      $Scale factor of Fx shape factor
LMUX                = 1               $typarr(  33)      $Scale factor of Fx peak friction coefficient
LEX                 = 1               $typarr(  34)      $Scale factor of Fx curvature factor
LKX                 = 1               $typarr(  35)      $Scale factor of Fx slip stiffness
LHX                 = 1               $typarr(  36)      $Scale factor of Fx horizontal shift
LVX                 = 1               $typarr(  37)      $Scale factor of Fx vertical shift
LGAX                = 1               $typarr(  58)      $Scale factor of camber for Fx
LCY                 = 1               $typarr(  38)      $Scale factor of Fy shape factor
LMUY                = 0.7             $typarr(  39)      $Scale factor of Fy peak friction coefficient
LEY                 = 1               $typarr(  40)      $Scale factor of Fy curvature factor
LKY                 = 1               $typarr(  41)      $Scale factor of Fy cornering stiffness
LHY                 = 1               $typarr(  42)      $Scale factor of Fy horizontal shift
LVY                 = 1               $typarr(  43)      $Scale factor of Fy vertical shift
LGAY                = 1               $typarr(  44)      $Scale factor of camber for Fy
LTR                 = 1               $typarr(  45)      $Scale factor of Peak of pneumatic trail
LRES                = 1               $typarr(  46)      $Scale factor for offset of residual torque
LGAZ                = 1               $typarr(  47)      $Scale factor of camber for Mz
LXAL                = 1               $typarr(  48)      $Scale factor of alpha influence on Fx
LYKA                = 1               $typarr(  49)      $Scale factor of alpha influence on Fx
LVYKA               = 1               $typarr(  50)      $Scale factor of kappa induced Fy
LS                  = 1               $typarr(  51)      $Scale factor of Moment arm of Fx
LSGKP               = 1               $typarr(  52)      $Scale factor of Relaxation length of Fx
LSGAL               = 1               $typarr(  53)      $Scale factor of Relaxation length of Fy
LGYR                = 1               $typarr(  54)      $Scale factor of gyroscopic torque
LMX                 = 1               $typarr(  55)      $Scale factor of overturning couple
LVMX                = 1               $typarr(  57)      $Scale factor of Mx vertical shift
LMY                 = 1               $typarr(  56)      $Scale factor of rolling resistance torque
$-----------------------------------------------------------------longitudinal
[LONGITUDINAL_COEFFICIENTS]
PCX1                = 1.34217         $typarr(  61)      $Shape factor Cfx for longitudinal force
PDX1                = 1.182941948     $typarr(  62)      $Longitudinal friction Mux at Fznom
PDX2                = -0.181268403    $typarr(  63)      $Variation of friction Mux with load
PDX3                = 0               $typarr(  60)      $Variation of friction Mux with camber
PEX1                = -0.264834325    $typarr(  64)      $Longitudinal curvature Efx at Fznom
PEX2                = 0.021703478     $typarr(  65)      $Variation of curvature Efx with load
PEX3                = 0.006707003     $typarr(  66)      $Variation of curvature Efx with load    squared
PEX4                = -5.31894        $typarr(  67)      $Factor in curvature Efx while driving
PKX1                = 38.21202914     $typarr(  68)      $Longitudinal slip stiffness Kfx/Fz at Fznom
PKX2                = -0.001652799    $typarr(  69)      $Variation of slip stiffness Kfx/Fz with load
PKX3                = 0.635594009     $typarr(  70)      $Exponent in slip stiffness Kfx/Fz with load
```

```
PHX1              = 0            $typarr(  71)     $Horizontal shift Shx at Fznom
PHX2              = 0            $typarr(  72)     $Variation of shift Shx with load
PVX1              = 0            $typarr(  73)     $Vertical shift Svx/Fz at Fznom
PVX2              = 0            $typarr(  74)     $Variation of shift Svx/Fz with load
RBX1              = 24           $typarr(  75)     $Slope factor for combined slip Fx reduction
RBX2              = 19.4924      $typarr(  76)     $Variation of slope Fx reduction with kappa
RCX1              = 1.046        $typarr(  77)     $Shape factor for combined slip Fx reduction
REX1              = 0            $typarr(  82)     $Curvature factor of combined Fx
REX2              = 0            $typarr(  83)     $Curvature factor of combined Fx with load
RHX1              = 0.00286862   $typarr(  78)     $Shift factor for combined slip Fx reduction
PTX1              = 1.385730163  $typarr(  79)     $Relaxation length SigKap0/Fz at Fznom
PTX2              = -5.99375E-05 $typarr(  80)     $Variation of SigKap0/Fz with load
PTX3              = -0.635594009 $typarr(  81)     $Variation of SigKap0/Fz with exponent of load
$-----------------------------------------------------------------------overturning
[OVERTURNING_COEFFICIENTS]
QSX1              = 0.0013874    $typarr(  86)
QSX2              = 0.56084      $typarr(  87)
QSX3              = 0.042436     $typarr(  88)
$-----------------------------------------------------------------------lateral
[LATERAL_COEFFICIENTS]
PCY1              = 1.4872       $typarr(  91)     $Shape factor Cfy for lateral forces
PDY1              = 0.95243      $typarr(  92)     $Lateral friction Muy
PDY2              = -0.15155     $typarr(  93)     $Variation of friction Muy with load
PDY3              = -0.7369      $typarr(  94)     $Variation of friction Muy with squared camber
PEY1              = -0.015952    $typarr(  95)     $Lateral curvature Efy at Fznom
PEY2              = -0.94021     $typarr(  96)     $Variation of curvature Efy with load
PEY3              = 0.071813     $typarr(  97)     $Zero order camber dependency of curvature Efy
PEY4              = -11.8164     $typarr(  98)     $Variation of curvature Efy with camber
PKY1              = -20.5177     $typarr(  99)     $Maximum value of stiffness Kfy/Fznom
PKY2              = 1.8255       $typarr(  100)    $Load at which Kfy reaches maximum value
PKY3              = 1.236        $typarr(  101)    $Variation of Kfy/Fznom with camber
PHY1              = 0.0017688    $typarr(  102)    $Horizontal shift Shy at Fznom
PHY2              = 0.00003891   $typarr(  103)    $Variation of shift Shy with load
PHY3              = 0.052745     $typarr(  104)    $Variation of shift Shy with camber
PVY1              = 0.0053659    $typarr(  105)    $Vertical shift in Svy/Fz at Fznom
PVY2              = -0.0029696   $typarr(  106)    $Variation of shift Svy/Fz with load
PVY3              = -0.20399     $typarr(  107)    $Variation of shift Svy/Fz with camber
PVY4              = -0.12704     $typarr(  108)    $Variation of shift Svy/Fz with camber and load
RBY1              = 15.5999      $typarr(  109)    $Slope factor for combined Fy reduction
RBY2              = 12.7794      $typarr(  110)    $Variation of slope Fy reduction with alpha
RBY3              = -0.0059063   $typarr(  111)    $Shift term for alpha in slope Fy reduction
RCY1              = 1.01227      $typarr(  112)    $Shape factor for combined Fy reduction
REY1              = 0            $typarr(  122)    $Curvature factor of combined Fy
REY2              = 0            $typarr(  123)    $Curvature factor of combined Fy with load
RHY1              = -0.00331613  $typarr(  113)    $Shift factor for combined Fy reduction
RHY2              = 0            $typarr(  124)    $Shift factor for combined Fy reduction with load
RVY1              = 0.226192     $typarr(  114)    $Kappa induced side force Svyk/Muy*Fz at Fznom
RVY2              = 0.220492066  $typarr(  115)    $Variation of Svyk/Muy*Fz with load
RVY3              = 7.95736      $typarr(  116)    $Variation of Svyk/Muy*Fz with camber
RVY4              = 72.3874      $typarr(  117)    $Variation of Svyk/Muy*Fz with alpha
RVY5              = 0.0517276    $typarr(  118)    $Variation of Svyk/Muy*Fz with kappa
RVY6              = 0            $typarr(  119)    $Variation of Svyk/Muy*Fz with atan(kappa)
PTY1              = 1.6094       $typarr(  120)    $Peak value of relaxation length SigAlp0/R0
PTY2              = 1.8255       $typarr(  121)    $Value of Fz/Fznom where SigAlp0 is extreme
$-------------------------------------------------------------rolling
[ROLLING_COEFFICIENTS]
QSY1              = 0.01         $typarr(  126)    $Rolling resistance torque coefficient
```

```
QSY2             = 0          $typarr(  127)    $Rolling resistance torque depending on Fx
QSY3             = 0          $typarr(  128)    $Rolling resistance torque depending on speed
QSY4             = 0          $typarr(  129)    $Rolling resistance torque depending on speed ^4
$-----------------------------------------------------------------------aligning
[ALIGNING_COEFFICIENTS]
QBZ1             = -12.0384       $typarr(  131)    $Trail slope factor for trail Bpt at Fznom
QBZ2             = -3.6771        $typarr(  132)    $Variation of slope Bpt with load
QBZ3             = 1.556          $typarr(  133)    $Variation of slope Bpt with load squared
QBZ4             = -0.054154      $typarr(  134)    $Variation of slope Bpt with camber
QBZ5             = 1.9626         $typarr(  135)    $Variation of slope Bpt with absolute camber
QBZ9             = -0.00022365    $typarr(  136)    $Slope factor Br of residual torque Mzr
QBZ10            = 0              $typarr(  130)    $Slope factor Br of residual torque Mzr
QCZ1             = 1.2042         $typarr(  137)    $Shape factor Cpt for pneumatic trail
QDZ1             = 0.12426        $typarr(  138)    $Peak trail Dpt"
QDZ2             = 0.0043466      $typarr(  139)    $Variation of peak Dpt" with load
QDZ3             = -0.50619       $typarr(  140)    $Variation of peak Dpt" with camber
QDZ4             = 20.6657        $typarr(  141)    $Variation of peak Dpt" with camber squared
QDZ6             = -0.0048371     $typarr(  142)    $Peak residual torque Dmr"
QDZ7             = 0.0057361      $typarr(  143)    $Variation of peak factor Dmr" with load
QDZ8             = -0.25752       $typarr(  144)    $Variation of peak factor Dmr" with camber
QDZ9             = -0.041413      $typarr(  145)    $Variation of peak factor Dmr" with camber and
load
QEZ1             = -1.0188        $typarr(  146)    $Trail curvature Ept at Fznom
QEZ2             = 1.7001         $typarr(  147)    $Variation of curvature Ept with load
QEZ3             = -0.82832       $typarr(  148)    $Variation of curvature Ept with load squared
QEZ4             = -0.29747       $typarr(  149)    $Variation of curvature Ept with sign of Alpha-t
QEZ5             = 45.4329        $typarr(  150)    $Variation of Ept with camber and sign Alpha-t
QHZ1             = 0.0035151      $typarr(  151)    $Trail horizontal shift Sht at Fznom
QHZ2             = 0.0020731      $typarr(  152)    $Variation of shift Sht with load
QHZ3             = 0.10627        $typarr(  153)    $Variation of shift Sht with camber
QHZ4             = 0.093382       $typarr(  154)    $Variation of shift Sht with camber and load
SSZ1             = -0.004320807   $typarr(  155)    $Nominal value of s/R0: effect of Fx on Mz
SSZ2             = 0.030102702    $typarr(  156)    $Variation of distance s/R0 with Fy/Fznom
SSZ3             = 1.590807306    $typarr(  157)    $Variation of distance s/R0 with camber
SSZ4             = -0.758224815   $typarr(  158)    $Variation of distance s/R0 with load and
camber
QTZ1             = 0          $typarr(  159)    $Gyration torque constant
MBELT            = 0          $typarr(  160)    $Belt mass of the wheel
```

A.9 PID Parameters for speed controller

K = 0.5

Nd = 500

Ti = 10

Td = 0.01

As used in full vehicle model for step and sinusoidal steer maneovres to keep desired speed.

Appendix B General Technology Vehicle Model Data

To save duplicating data already given for the standard vehicle, only the alterations that have been made to the GTV model will be given here, meaning parameters that are not mentioned in this section are identical to those given in appendix A.

B.1 GTV Suspension Geometry

ARB mount on subframe raised 25mm to allow new steering rack to be housed

FRONT GEOMETRY[mm] McPherson Strut							
		LEFT			RIGHT		
	Point Number	X	Y	Z	X	Y	Z
ARB_at_subframe	23	-277.39	310	-4.5	-277.39	-310	-4.5

Table B-1 Alterations to GTV front suspension geometry

B.2 Suspension Springs

Linear main spring data		
	Front	Rear
Rate [N/mm]	29	33.4
Free length [mm]	414.868	358.781
Coils	5	5

Table B-2 Suspension coil spring data

B.3 Mass and Inertia Data

Chassis Mountings								
			Cog [mm]			Moments of Inertia [Kg.mm2]		
L/R	Part	Mass [Kg]	X	Y	Z	Ix	Iy	Iz
R	RHS Eng Mtg Brkt	0	Removed					
R	RHS Eng Mount	0	Removed					
L	LHS Trans. Mtg Brkt	0	Removed					
L	LHS Trans Mount	0	Removed					
n/a	Upper Tie Rod Link	0	Removed					
n/a	UTR BIW Brkt	0	Removed					
n/a	Lower Tie Rod Link	0	Removed					
n/a	LTR Large Bush	0	Removed					
n/a	LTR Small Bush	0	Removed					

Table B-3 Changes to GTV chassis mounting mass and inertia data

Engine (inc gearbox clutch etc) and driveline								
			Cog [mm]			Moments of Inertia [Kg.mm2]		
L/R	Part	Mass	X	Y	Z	Ix	Iy	Iz
n/a	Power Unit, clutch + flywheel	0	Removed					
n/a	Gearbox	0	Removed					
n/a	Exhaust Assembly							
n/a	Hot End Assy	0	Removed					
n/a	Cold End Assy	0	Removed					
n/a	Driveline Parts							
n/a	RDU + Coupling	0	Removed					
n/a	Propshaft	0	Removed					
n/a	Rear drive shaft RH	0	Removed					
n/a	Rear drive shaft LH	0	Removed					

Table B-4 Changes to GTV engine and driveline mass and inertia data

Cooling								
			Cog [mm]			Moments of Inertia [Kg.mm2]		
L/R	Part	Mass [Kg]	X	Y	Z	Ix	Iy	Iz
n/a	Charge Air Cooler DW12-MA	0	Removed					
n/a	Expansion Tank	0	Removed					
n/a	Exp Tank Cap	0	Removed					

Table B-5 Changes made to GTV cooling system mass and inertia data

Steering								
			Cog [mm]			Moments of Inertia [Kg.mm2]		
L/R	Part	Mass [Kg]	X	Y	Z	Ix	Iy	Iz
n/a	Steering rack - LH/RH(NEW EVOQUE)	14.50	-184.44	58.00	0.00	1.48	0.06	1.45
n/a	Steering column - LH/RH	3.95	-622.44	373.00	575.00	0.02	0.06	0.05

Table B-6 Changes to GTV steering system mass and inertia data

Fuel System								
			Cog [mm]			Moments of Inertia [Kg.mm2]		
L/R	Part	Mass [Kg]	X	Y	Z	Ix	Iy	Iz
n/a	Fuel Tank Assy	0	Removed					
n/a	Tank Cradle	0	Removed					
n/a	Fuel Filler Assy	0	Removed					

Table B-7 Changes made to GTV fuel systems mass and inertia data

Trim								
			Cog [mm]			Moments of Inertia [Kg.mm2]		
L/R	Part	Mass [Kg]	X	Y	Z	Ix	Iy	Iz
n/a	Tailgate Trim	0	Removed					
n/a	Rear Seat Complete	0	Removed					
n/a	Space saver spare tyre	0	Removed					
n/a	Space saver spare wheel	0	Removed					
n/a	Jack & Jack Retention	0	Removed					
n/a	Spare Wheel Retention	0	Removed					
n/a	Toolkit	0	Removed					
n/a	Rear Carpet	0	Removed					
n/a	Wrench	0	Removed					

Table B-8 Changes made to GTV trim mass and inertia data

Ricardo Additions Front								
			Cog [mm]			Moments of Inertia [Kg.mm2]		
L/R	Part	Mass [Kg]	X	Y	Z	Ix	Iy	Iz
n/a	Fiat Twin Air Engine	82.00	261.95	-154.56	85.85	2.34	2.32	1.24
n/a	Mounting cradle, loom, hoses and bracketry	70.90	121.56	292.00	89.00	0.83	1.03	0.76
n/a	Single Speed Transmission	32.00	23.18	312.87	35.83	0.85	1.29	0.67
n/a	Generator	28.00	261.95	29.38	85.65	0.64	0.64	0.50
n/a	Electric Drive Motor	50.00	41.21	35.03	166.04	0.45	0.29	0.45
n/a	Motor Cradel	20.90	112.50	107.81	132.85	0.55	0.93	0.86
n/a	AC Comp	6.75	323.48	271.47	140.13	0.03	0.03	0.02
n/a	AC Comp CNTRLR	2.85	253.13	59.00	-110.87	0.03	0.06	0.08
n/a	Junction Box	2.00	-77.81	-323.99	328.05	0.02	0.02	0.01
n/a	Top Engine Mount	3.95	261.11	-365.79	403.21	0.02	0.03	0.02
n/a	Lower ds Bearing Mount	5.80	124.68	-236.13	155.57	0.04	0.04	0.01
n/a	Base Plate	2.30	279.11	-166.72	25.31	0.01	0.01	0.03
n/a	LHS Gearbox Mount	2.70	82.58	382.45	202.26	0.01	0.04	0.03
n/a	DM Inverters	12.00	261.11	-365.79	485.00	0.05	0.11	0.14

Table B-9 Additions to front of GTV model mass and inertia data

Ricardo Additions Rear								
			Cog [mm]			Moments of Inertia [Kg.mm2]		
L/R	Part	Mass [Kg]	X	Y	Z	Ix	Iy	Iz
n/a	Battery Pack	240.00	-2630.28	0.03	372.01	17.70	11.60	26.87
n/a	Brackets	21.32	-2423.59	0.51	348.96	2.75	1.88	4.55
n/a	DC-DC left	3.45	-2661.14	300.00	335.00	0.14	0.02	0.01
n/a	DC-DC centre	3.45	-2661.14	0.00	335.00	0.14	0.01	0.01
n/a	DC-DC right	3.45	-2661.14	-300.00	335.00	0.14	0.01	0.01
n/a	r-cube	2.00	-2961.14	-600.00	635.00	0.02	0.01	0.02
n/a	Junction Box	3.00	-2861.14	200.00	285.00	0.02	0.01	0.02
n/a	Charger	6.20	-3161.14	-200.00	285.00	0.03	0.04	0.03
n/a	Fuel Tank	6.60	-1646.44	154.00	148.75	0.01	0.02	0.02
n/a	Fuel	15.00	-1646.44	154.00	148.75	0.03	0.04	0.04

Table B-10 Additions to rear of GTV model mass and inertia data

Appendix C Vehicle Testing and Model Validation

C.1 Vehicle Instrumentation

C.1.1 DL2 Specification

Memory	Compact flash type I, FAT16 PC format, 128MB to 2GB.
GPS	Logs position, altitude, speed, heading, position accuracy, speed accuracy, heading accuracy. Tracks of all satellites in view.
5Hz	Logs all data at 5Hz (every 200ms). Typical error (CEP) 3m, under good conditions this is reduced to about 1m.
GPS antenna	Magnetic base, 3.3v active antenna with SMA connector
Analogue Inputs	Either 8 or 16 external inputs (optional), all 12 bit resolution, with a maximum input of 12v and resolution of about 3mV. All inputs are protected to twice maximum input voltage. Input impedance >100k.
Frequency Inputs	4 external frequency inputs with a maximum input frequency >2kHz. Suitable for wheel, shaft, or engine speeds, may require additional sensors.
Lap Beacon Input	Ground momentarily to indicate track beacon.
Start Sample Input/Output	Input requires grounding to start sampling and again to stop sampling. Open collector output with a maximum current of 50mA
External Power Supply Requirements	12v nominal input, (between 10v and 15v). Current consumption of about 180mA including GPS, dependant on compact flash card size.
+5v Reference Out	Maximum current draw 100mA, tolerance 1%.
Ignition In Signal	(High Level) Triggered by fast voltage transients. Can be connected directly to the low tension side of the ignition coil, or coupled to a high-tension lead.
Ignition In Signal (Low Level)	Requires a triggering voltage of 4V. Suitable for connection directly to most ECU tacho outputs. Maximum input frequency >300Hz.
Case Construction	CNC aluminium, black anodised. Front cover high impact polycarbonate. Sealed using ‘o’ rings.

Connector Type	4 x Binder 423 Series 12-Way Male Bulkhead Connectors (09-0131-68-12)
Main Processor	High performance 40MHz RISC with embedded flash program memory
GPS Serial Port	User configurable for baud rate (1 or 5Hz) and messages. Factory set at 4800 baud and outputting NMEA messages of $GPRMC and $GPGGA.
DL2 Serial Port	Serial output to drive our dashboard or video overlay products. Serial input used for inputting RS232 data for storage during a run, from an ECU, OBDII adapter or any other compatible device.
Accelerometers	2 axis, precision digital output. Guaranteed 2g minimum full scale on both axes.

Table C-1 DL2 technical specification (RaceTechnology, 2009).

Figure C-1 RaceTechnology DL2 data logger (RaceTechnology, 2009).

C.2 DL2 Connections

Binder 09-0131-68-12

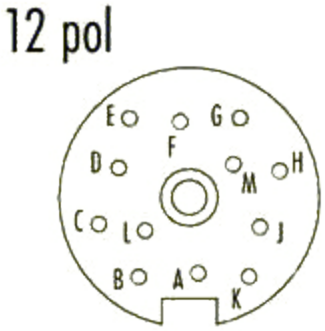

Figure C-2 DL2 data logger connections (RaceTechnology, 2009)

Connector	Pin №		Description	Range
Conn-1 Binder 423 Series Male Bulkhead (09-0131-68-12)	1	A	Digital/Frequency I/P#1	0v (low), 5-12v (High)
	2	B	Low V RPM I/P	0v (low), 5-12v (High)
	3	C	Status O/P (Low while Logging)	30mA shared with Conn-2 Pin11
	4	D	RPM Gnd	Gnd
	5	E	High RPM I/P	Special
	6	F	Trigger I/P (Gnd to Toggle Logging)	Active Low
	7	G	Power In	9-15v
	8	H	Digital/Frequency I/P#3	0v (low), 5-12v (High)
	9	J	Digital/Frequency I/P#4	0v (low), 5-12v (High)
	10	K	Digital/Frequency I/P#2	0v (low), 5-12v (High)
	11	L	Lap Beacon I/P (Gnd to indicate beacon)	Gnd to Toggle Logging
	12	M	GND	Gnd
Conn-2 Binder 423 Series Male Bulkhead (09-0131-68-12)	1	A	DL2 Serial Comms receive	RS-232 Rx (Male d-type pin 2)
	2	B	Charger Supply (Optional) I/P	12v
	3	C	Trigger I/P (Gnd to Toggle Logging)	Active Low
	4	D	Gnd	Gnd
	5	E	CAN High	Not Implemented
	6	F	CAN Low	Not Implemented
	7	G	Power In	9-15v
	8	H	GPS Serial Comms receive	RS-232 RX
	9	J	GPS Serial Comms transmit	RS-232 TX
	10	K	DL2 Serial Comms transmit	RS-232 Tx (Male d-type pin 3)
	11	L	Status O/P (Low while Logging)	30mA shared with Conn-1 Pin3
	12	M	Lap Beacon I/P (Gnd to indicate beacon)	Gnd to Toggle Logging
Conn-3 Binder 423 Series Male Bulkhead (09-0131-68-12)	1	A	Analogue I/P	0-12v
	2	B	GND	Gnd
	3	C	Analogue I/P#12	0-12v
	4	D	Analogue I/P#11	0-12v
	5	E	Analogue I/P#10	0-12v
	6	F	Analogue I/P#9	0-12v

	7	G	Power In	9-15v
	8	H	5v Auxilliary	Max 100mA shared with Conn-4 Pin 8
	9	J	Analogue I/P#16	0-12V
	10	K	Analogue I/P#15	0-12V
	11	L	Analogue I/P#13	0-12V
	12	M	Gnd	Gnd
Conn-4 Binder 423 Series Male Bulkhead (09-0131-68-12)	1	A	Analogue I/P#6	0-12v
	2	B	GND	Gnd
	3	C	Analogue I/P#4	0-12v
	4	D	Analogue I/P#2	0-12v
	5	E	Analogue I/P#3	0-12v
	6	F	Analogue I/P#1	0-12v
	7	G	Power In	9-15v
	8	H	5v Auxilliary	Max 100mA shared with Conn-3 Pin 8
	9	J	Analogue I/P#8	0-12V
	10	K	Analogue I/P#7	0-12V
	11	L	Analogue I/P#5	0-12V
	12	M	Gnd	Gnd

Table C-2 DL2 connection pins (RaceTechnology, 2009).

C.3 DL2 internal accelerometer

The DL2 data logger has an in built dual axis, 2g accelerometer, the sensor is pre calibrated. The accelerometer is mounted on a fully floating, damped platform within the logger to isolate it further from noise (RaceTechnology, 2009).

C.4 External Gyro Specification

InvenSense

Integrated Dual-Axis Gyro

IDG-500

FEATURES

- Integrated X- and Y-axis gyros on a single chip
- Two separate outputs per axis for standard and high sensitivity:
  - X-/Y-Out Pins: 500°/s full scale range, 2.0mV/°/s sensitivity
  - X/Y4.5Out Pins: 110°/s full scale range, 9.1mV/°/s sensitivity
- Integrated amplifiers and low-pass filters
- Auto-Zero function
- On-chip temperature sensor
- High vibration rejection over a wide frequency range
- High cross-axis isolation by proprietary MEMS design
- 3V single-supply operation
- Hermetically sealed for temp and humidity resistance
- 10,000 g shock tolerant
- Smallest dual axis gyro package at 4 x 5 x 1.2mm
- RoHS and Green Compliant

APPLICATIONS

- General Motion Sensing
- Vehicle Motion Analysis
- Platform Stabilization
- Inertial Measurement Units

GENERAL DESCRIPTION

The IDG-500 is an integrated dual-axis angular rate sensor (gyroscope). It uses InvenSense's proprietary and patented MEMS technology with vertically driven, vibrating masses to make a functionally complete, low-cost, dual-axis angular rate sensor. All required electronics are integrated onto a single chip with the sensor.

The IDG-500 gyro uses two sensor elements with novel vibrating dual-mass bulk silicon configurations that sense the rate of rotation about the X- and Y-axis (in-plane sensing). This results in a unique, integrated dual-axis gyro with guaranteed-by-design vibration rejection and high cross-axis isolation. It is specifically designed for demanding consumer applications requiring low cost, small size and high performance.

The IDG-500 gyro includes the integrated electronics necessary for application-ready functionality. It incorporates X- and Y-axis low-pass filters and an EEPROM for on-chip factory calibration of the sensor. Factory trimmed scale factors eliminate the need for external active components and end-user calibration. This product is lead-free and Green Compliant.

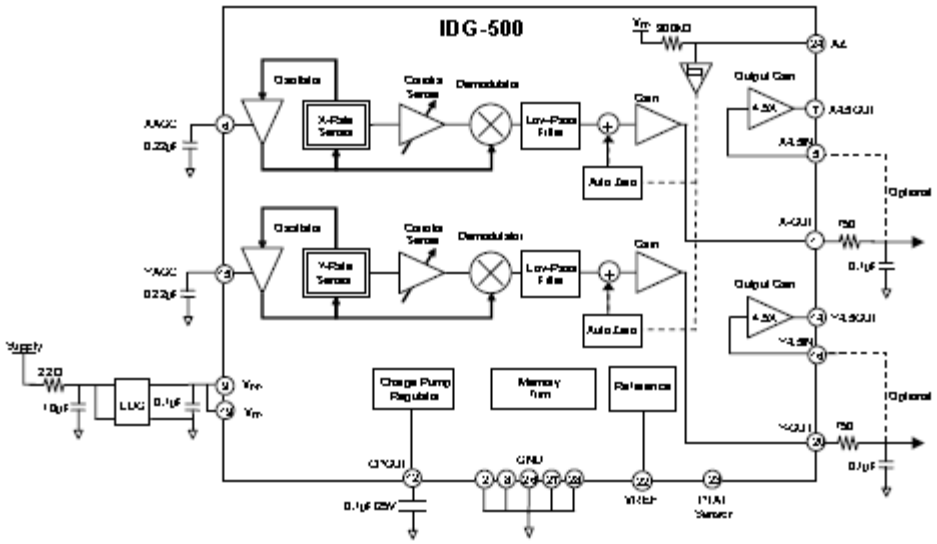

InvenSense

IDG-500

SPECIFICATIONS

All parameters specified are @ VDD = 3.0 V and Ta = 25°C. External LPF @ 2kHz. All specifications apply to both axes.

PARAMETER	CONDITIONS		MIN	TYP	MAX	UNITS
SENSITIVITY						
Full-Scale Range	At X-OUT and Y-OUT			±500		°/s
	At X4.5Out and Y4.5Out			±110		°/s
Sensitivity	At X-OUT and Y-OUT			2.0		mV/°/s
	At X4.5Out and Y4.5Out			9.1		mV/°/s
Initial Calibration Tolerance	At X-OUT and Y-OUT			±5		%
Over Specified Temperature	At X-OUT and Y-OUT			±10		%
Nonlinearity	At X-OUT and Y-OUT, Best Fit Straight Line			<1		% of FS
Cross-axis Sensitivity				±1		%
REFERENCE						
Voltage (VREF)				1.35		V
Tolerance				±50		mV
Load Drive				100		µA
Capacitive Load Drive	Load directly connected to VREF			100		pF
Power Supply Rejection	VDD= 2.7 V to 3.3V			1		mV/V
Over Specified Temperature				±5		mV
ZERO-RATE OUTPUT						
Static Output (Bias)	Factory Set			1.35		V
Initial Calibration Tolerance	Relative to VREF	With Auto Zero		±20		mV
		Without Auto Zero		±250		
Over Specified Temperature	Relative to VREF	Without Auto Zero		±50		mV
Power Supply Sensitivity	@ 50 Hz			10		°/sec/V
FREQUENCY RESPONSE						
High Frequency Cutoff	Internal LPF -90°			140		Hz
LPF Phase Delay	10Hz			-4.5		°
MECHANICAL FREQUENCIES						
X-Axis Resonant Frequency			20	24	28	kHz
Y-Axis Resonant Frequency			23	27	31	kHz
Frequency Separation	X and Y Gyroscopes			3		kHz
NOISE PERFORMANCE						
Total RMS Noise	Bandwidth 1 Hz to 1kHz, At X-OUT and Y-OUT			0.8		mV rms
OUTPUT DRIVE CAPABILITY						
Output Voltage Swing	Load = 100kΩ to $V_{dd}/2$		0.05		Vdd-0.05	V
Capacitive Load Drive				100		pF
Output Impedance				100		Ω
POWER ON-TIME						
Zero-rate Output	Settling to ±3°/s			50	200	ms
AUTO ZERO CONTROL						
Auto Zero Logic High	Rising Input			1.9		V
Auto Zero Logic Low	Falling Input			0.9		V
Auto Zero Pulse Duration			2		1500	µsec
Offset Settle Time After Auto Zero				7		msec

InvenSense

IDG-500

PARAMETER	CONDITIONS	MIN	TYP	MAX	UNITS
POWER SUPPLY (VDD) Operating Voltage Range Quiescent Supply Current Over Specified Temperature		2.7	3.0 7 ±2	3.3	V mA mA
TEMPERATURE SENSOR Sensitivity Offset Output Impedance	Range -20 to +85°C		4 1.25 12		mV/°C V kΩ
TEMPERATURE RANGE Specified Temperature Range		-20		+85	°C

RECOMMENDED OPERATING CONDITIONS

Parameter	Min	Typical	Max	Unit
Power Supply Voltage (VDD)	2.7	3.0	3.3	V
Power Supply Voltage (VDD) Rise Time (10% - 90%)			20	ms

ABSOLUTE MAXIMUM RATINGS

Stress above those listed as "Absolute Maximum Ratings" may cause permanent damage to the device. This is a stress rating only and functional operation of the device under these conditions is not implied. Exposure to absolute maximum rating conditions for extended periods may affect device reliability.

Parameter	Rating
Power Supply Voltage (VDD)	-0.3V to +6.0V
Acceleration (Any Axis, unpowered)	10,000g for 0.3ms
Operating Temperature Range	-40 to +105°C
Storage Temperature Range	-40 to +125°C

InvenSense

IDG-500

PIN DESCRIPTION

Number	Pin	Description
2, 8, 26, 27, 28	GND	Ground
9, 19	VDD	Positive supply voltage
1	X-OUT	Rate output for rotation about the X-axis
5	X4.5IN	X-axis input to the 4.5X amplifier
6	XAGC	Amplitude control capacitor connection
7	X4.5OUT	X-axis output of the 4.5X amplifier
12	CPOUT	Charge pump capacitor connection
14	Y4.5OUT	Y-axis output of the 4.5X amplifier
15	YAGC	Amplitude control capacitor connection
16	Y4.5IN	Y-axis input to the 4.5X amplifier
20	Y-OUT	Rate output for rotation about the Y-axis
22	VREF	Precision reference output
23	PTATS	Temperature Sensor Output
24	AZ	X & Y Auto Zero control pin
10, 11, 13, 21, 25	RESV	Reserved. Do not connect.
3, 4, 17, 18	NC	Not internally connected. May be used for PCB trace routing.

PIN CONNECTION (TOP VIEW)

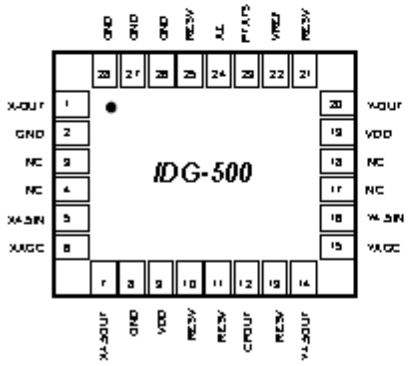

28-pin, 4mm x 5mm x 1.2mm
QFN Package

RATE SENSITIVE AXIS

This is a dual-axis rate sensing device. It produces a positive output voltage for rotation about the X- or Y-axis, as shown in the figure below.

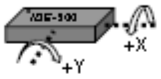

InvenSense

IDG-500

DESIGN NOTES

1. Overview

The IDG-500 gyro is a dual-axis gyroscope consisting of two independent vibratory MEMS gyroscopes. One detects rotation about the X-axis; the other detects rotation about the Y-axis. Each structure is fabricated using InvenSense's proprietary bulk silicon technology. The structures are covered and hermetically sealed at the wafer-level. The cover shields the gyro from EMI.

The gyroscope's proof-masses are electrostatically oscillated at resonance. An internal automatic gain control circuit precisely sets the oscillation of the proof masses. When the sensor is rotated about the X- or Y-axis, the Coriolis effect causes a vibration that can be detected by a capacitive pickoff. The resulting signal is amplified, demodulated, and filtered to produce an analog voltage that is proportional to the angular rate.

2. Amplitude Control

The scale factor of the gyroscope depends on the amplitude of the mechanical motion and the trim setting of the internal programmable gain stages. The oscillation circuit precisely controls the amplitude to maintain constant sensitivity over the temperature range. The capacitors (0.22µF, ±10%) connected to Pin 6 (XAGC) and Pin 15 (YAGC) are compensation capacitors for the amplitude control loops.

3. Internal Low-Pass Filter

After the demodulation stage, there is a low-pass filter that limits noise and high frequency artifacts from the demodulator before final amplification. The typical filter characteristics are shown below.

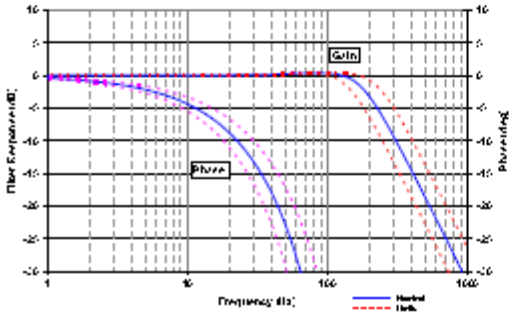

4. External Low-Pass Filter

To further attenuate high-frequency noise, an optional external low-pass filter may be used.

5. Gyro Outputs

The IDG-500 gyro has two X-outputs and two Y-outputs, with scale factors and full-scale sensitivities as summarized below.

Axis	Gyro Output	Sensitivity (mV/°/s)	Full-Scale Range (±°/s)
X	X-OUT	2	500
	X4.5OUT	9.1	110
Y	Y-OUT	2	500
	Y4.5OUT	9.1	100

Having two sensitivities and two full-scale ranges per output allows the end user to have one output that can be used for faster motions (over a full scale range of ±500°/sec), and second output that can be used for slower motions (over a full scale range of ±110°/sec). Thus a lower-resolution analog-to-digital converter (ADC) may be used to digitize the motion, with the gain of 4.5 in the _4.5OUT output effectively giving the user additional two-plus bits of resolution.

The IDG-500 gyro outputs are independent of supply voltage (i.e. they are not ratiometric).

Gyro rotation rate is calculated as:

(Gyro Output Voltage – Gyro Zero-Rate Out)/Sensitivity

where the Zero-Rate Output (ZRO) is nominally VREF. There is a temperature dependence to ZRO, and an initial accuracy to ZRO.

6. Auto Zero

Auto Zero (AZ) is a function that is used to maximize the gyro's dynamic range when using the _4.5OUT outputs.

AZ works by keeping the gyro's Zero-Rate Output (ZRO) close to VREF, and thus allows the user to achieve a wider usable signal range, without using external analog high pass filters.

When activated, the Auto Zero circuit internally nulls the ZRO to VREF. The typical usage of Auto Zero is in conditions where:

1. The gyro's motion is known, such as when:
   a. The gyro is stationary

b. Other sensors can report angular rotation rate

2. The DC value of the gyro output is not important, but only the AC value is. In this case, a digital ac filter may be used to extract the gyro data, which provides a higher-quality output than is possible with an analog R-C filter.

The Auto Zero function is initiated on the rising edge of the AZ pin. The Auto Zero settling time is typically 7ms. This time includes the time required for nulling the ZRO and for the settling of the internal low pass filter (LPF). If the external LPF bandwidth is less than 200Hz, the Auto Zero settling time will be longer than specified.

The AZ pulse width should meet the specified minimum time requirement of 2µs to start the Auto Zero function, and should be shorter than the maximum specified time of 1500µs. The Auto Zero pulse should occur after the start-up period to cancel any initial calibration error.

7. Temperature Sensor

A built-in Proportional-To-Absolute-Temperature (PTAT) sensor provides temperature information on Pin 23 (PTATS). The temperature sensor output signal is analog, and has a bias of approximately 1.25V at room temperature, and increases at a rate of 4mV/°C. The output impedance is nominally 12kΩ and is therefore not designed to drive low impedance loads. If necessary, the output can be externally buffered with a low offset-drift buffer, and optionally a low-pass filter to minimize noise.

8. High Impedance Nodes

XAGC (pin 6) and YAGC (pin 15) pins are high impedance (>1Mohm) nodes. Any coating, glue or epoxy on these pins or on the capacitors connected to these pins, will affect part performance and should be avoided.

9. Proper Interface Cleaning

Proper cleaning of PCB solder pads prior to assembly is recommended. PCB surface contaminants at XAGC (pin 6) or YAGC (pin 15) device interfaces may affect part performance.

10. Power Supply Filtering

NOTE: Power supply Voltage (VDD) rise time (10% - 90%) must be less than 20 ms, at VDD (pins 9 and 19), for proper device operation.

The IDG-500 gyro should be isolated from system power supply noise by a combination of an RC filter that attenuates high frequency noise and a Low Drop Out Power supply regulator (LDO) that attenuates low frequency noise. The figure below shows a typical configuration.

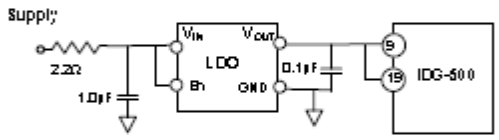

The low-pass RC filter should be chosen such that it provides significant attenuation of system noise at high frequencies. The LDO should be a low noise regulator (<100µV/rtHz) that exhibits good noise rejection at low frequencies.

Gyro data from (InvenSense, 2008).

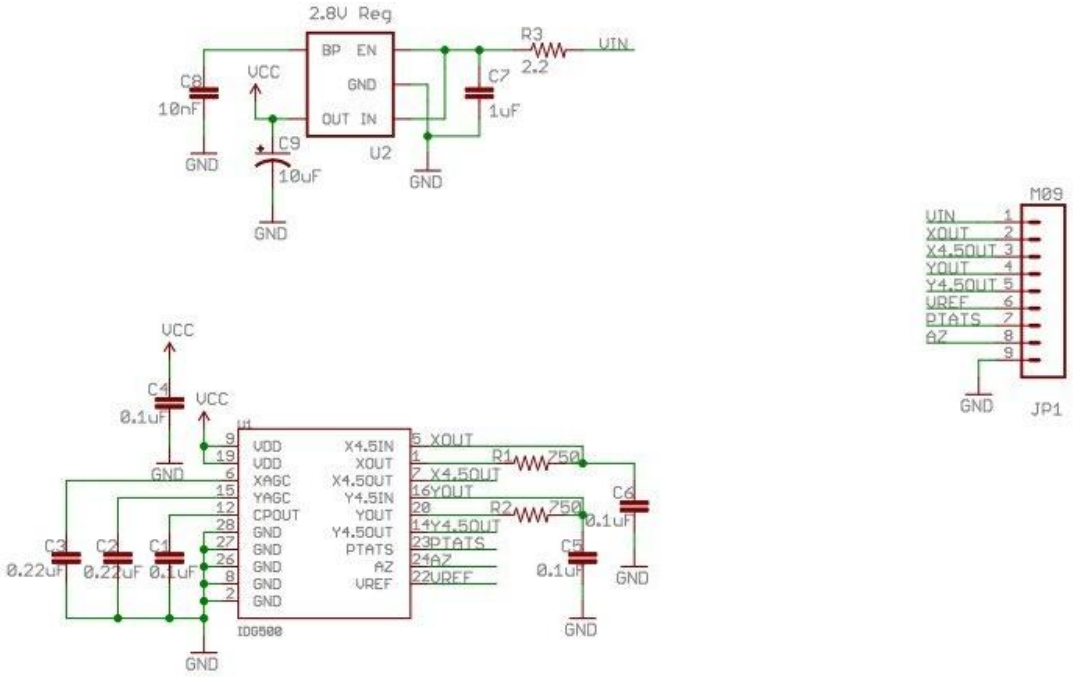

Figure C-3 IDG-500 breakout board wiring (Aliexpress, 2010)

C.5 External Gyro Loom and Calibration

The breakout board that the external gyro was mounted on met the requirements of the sensor data sheet and included input voltage isolation, input voltage regulation and RC filters on the signals creating low pass filters of 21.2 KHz, as shown in Figure C-8. As the breakout board had a voltage regulator that accepted an input between 3V and 7V, the sensor could be directly connected too the voltage supply form the DL2 logger without the need of an extra potential divider. The sensor on breakout board and loom are shown in Figure C-4 and Figure C-5.

A calibration factor of (81.48 x Vsig – 110) x 4.55 was used to calibrate both signal voltages of the gyro. This was calculated by assuming a linear response between -500 deg/s and 500 deg/s. It can be seen that for this work x and y outputs have sensitivity of 9.1mV.deg/s, if the higher resolution signals were to be used (2mV.deg/s) the calibration factor would be (81.48 x Vsig – 110).

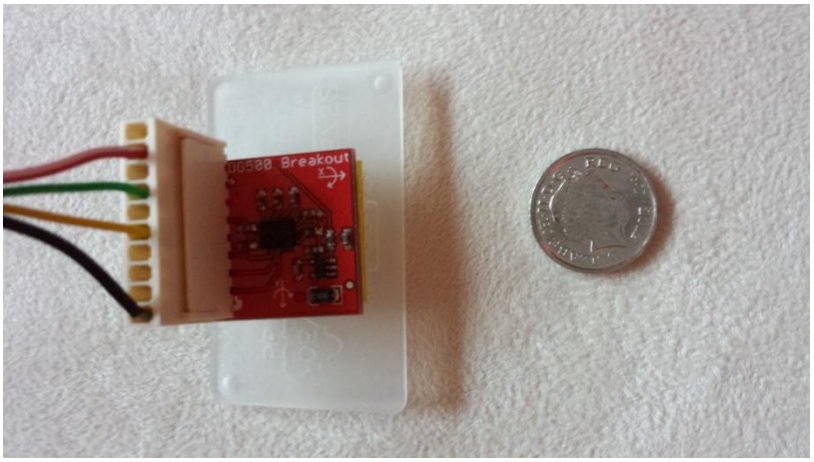

Figure C-4 Gyro on breakout board

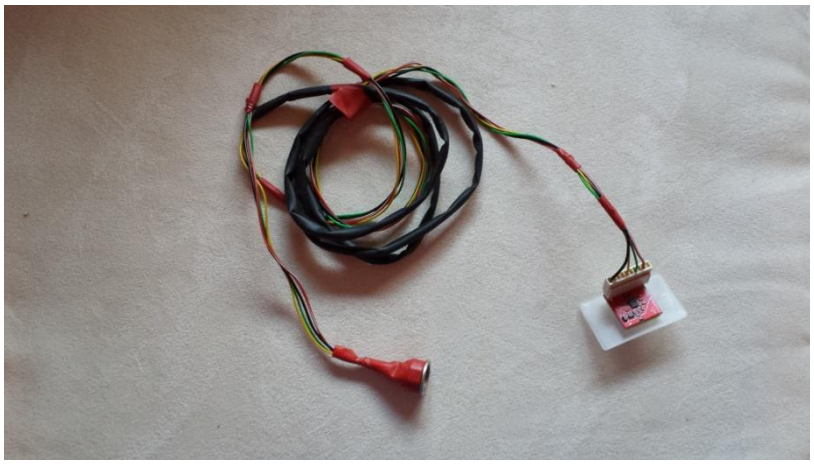

Figure C-5 Gyro and loom

Sensor	Range	Accuracy	Logging rate
Accelerometer (DL2 internal)	+- 2g	Unknown	100 Hz
Gyro (external)	+- 110 deg/s	+-0.366 deg/s	100 Hz
Steering angle CAN	0 -1440 deg	+-0.0440 deg	100 Hz
Steer angle sign	Logical 0-1	-	100 Hz
Vehicle speed CAN	0 – 320 m/s	+-0.01 m/s	100 Hz
AWD mode CAN	Logical 0 -1	-	100 Hz
Yaw Rate CAN	+-75 deg/s	+-0.0366 deg/s	100 Hz
Lateral Acceleration CAN	+-17.9 m/s	+-0.035 m/s	100 Hz

Table C-3 Sensor specifications and logging rates

C.6 Sensor verification

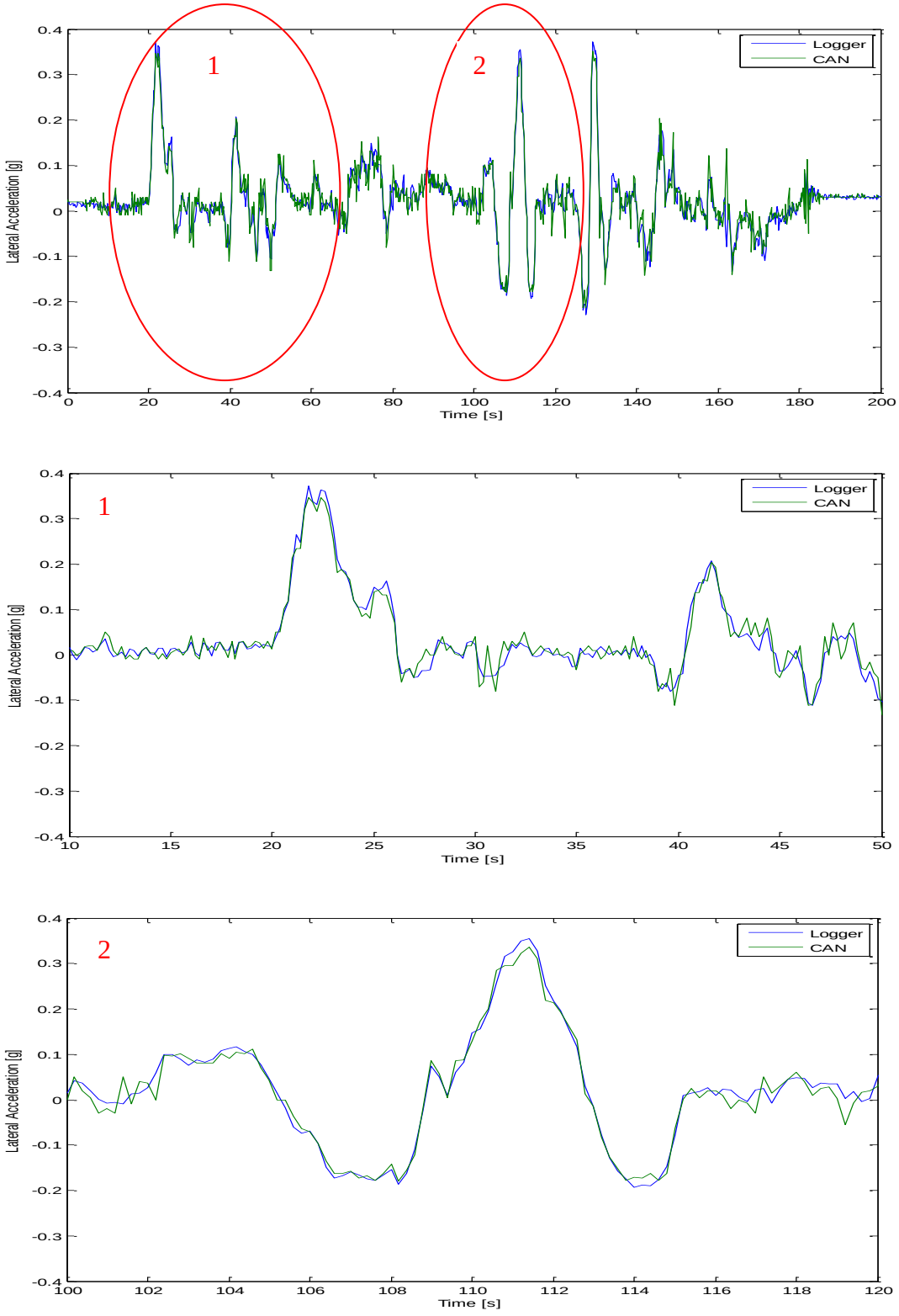

Figure C-6 DL2 accelerometer comparison with CAN acceleration signal

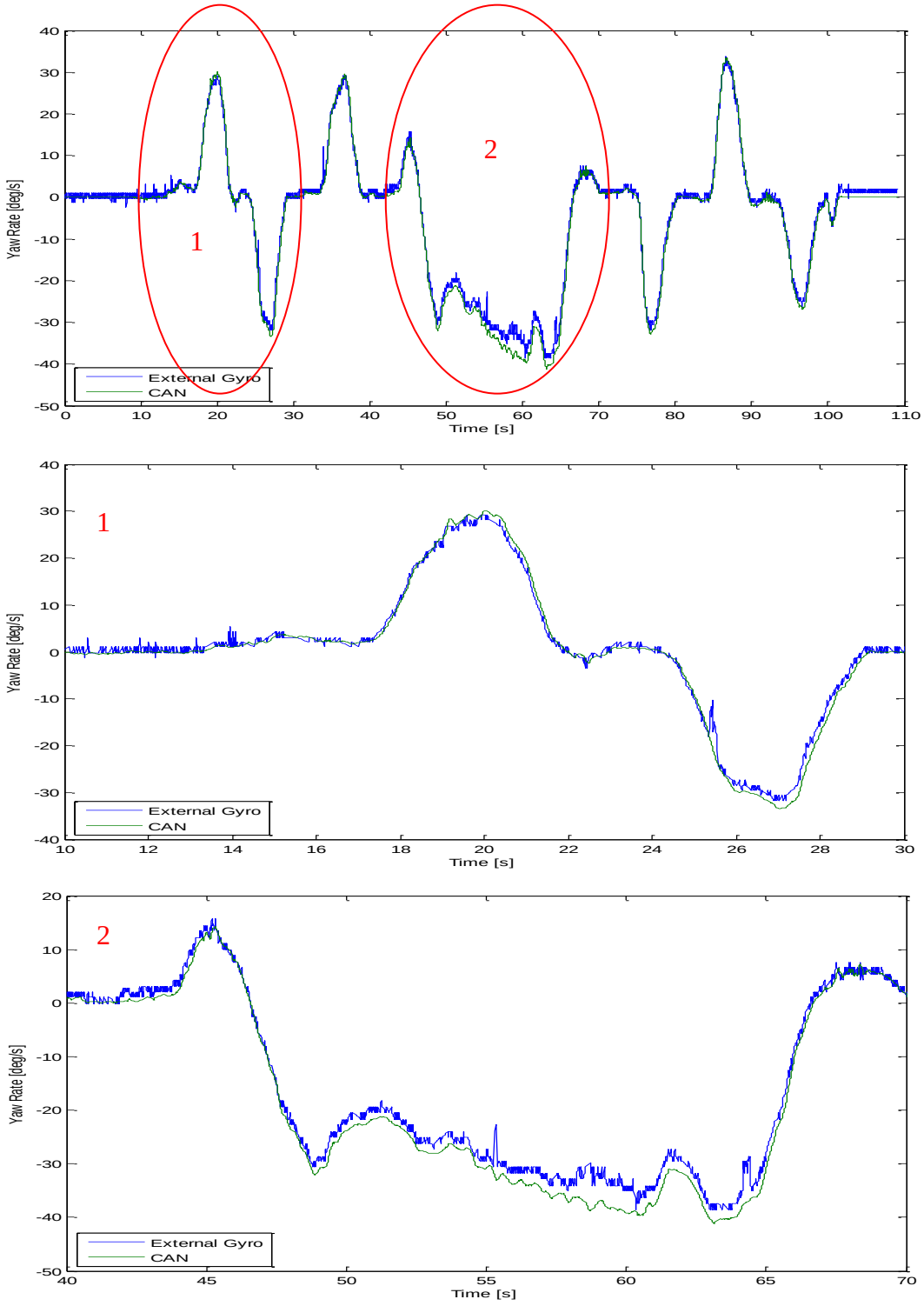

Figure C-7 Comparison of external gyro yaw rate and CAN yaw rate signal

The external sensors (data logger accelerometer and gyro), were verified against equivelent signals taken for the vehicle Can BUS to ensure correct calibration and functionality Figure C-6 and Figure C-7 .

C.7 Data post processing and presentation

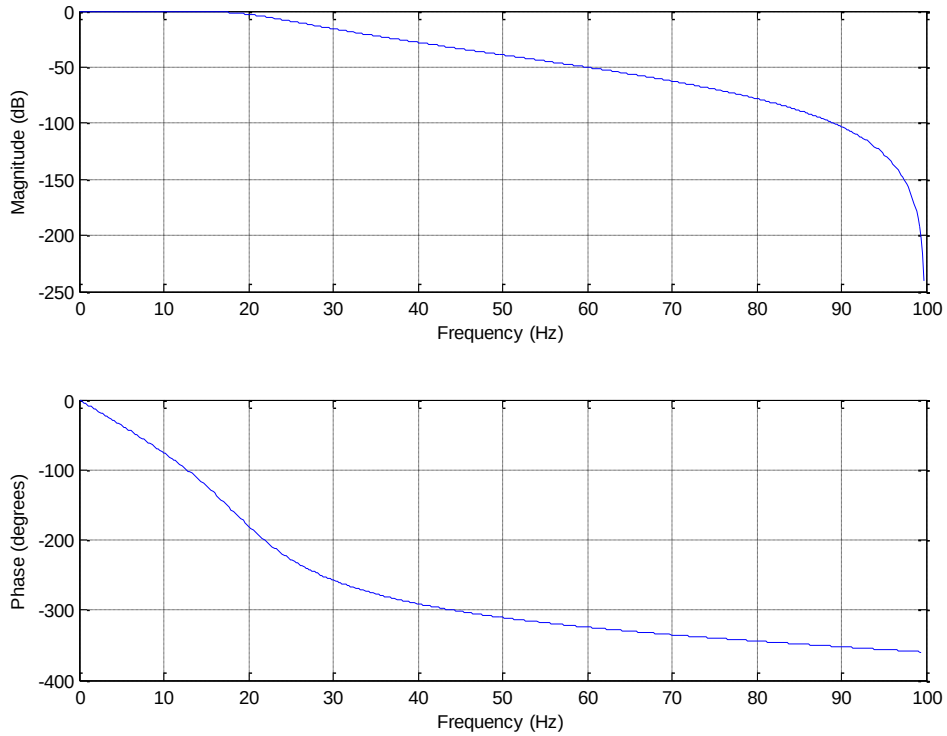

Figure C-8 Characteristics of 2nd order 20Hz low pass filter applied to logged data

C.8 Vehicle Testing

C.8.1 Steady State Tests

The following test will be carried out as close as possible in accordance with BS 4138:2004 and based on the Bruntingthorpe runway being 60.043m in width, circuit sizes may need scaling if this differs.

Data to be logged	Sensor	Logging rate [Hz]
Vehicle Speed	CAN	100
Lateral Acceleration	CAN	100
Steering Wheel Angle	CAN	100
Yaw Velocity	CAN	100
Longitudinal Acceleration	CAN	100
Vehicle Roll Angle	External gyro (integration of roll velocity)	100

Table C-4 Steady state test data requirements

Before any testing takes place, ensure that data logger and sensors are functioning correctly, carry out a brief test run and download data.

C.8.2 Circular Path Testing

1. Lay out 15m radius circle (15m at vehicle centre line, 14.2m to inner cones) on flattest section of track.

2. Warm up the vehicle; bring tyres and engine up to normal operating temperature

3. Obtain static sensor readings; remain stationary for 3 seconds on flat ground with steering wheel straight ahead whilst logging data.

4. Enter the circuit turning clockwise, drive as slow as possible for one lap to obtain data for the theoretical Ackerman steering angle.

5. Increase speed so that lateral acceleration is 0.5m/s2, hold steady state for 3 seconds to obtain data.

6. Keep repeating step 4 at 0.5 m/s2 intervals until steady state can no longer be obtained.

7. Download and label data

8. Repeat steps 3 – 7 travelling anti-clockwise.

9. Stop and allow tyres to cool.

10. Repeat steps 3 – 9, 3 times in total to ensure repeatability of results.

11. Repeat steps 1 – 10 for circuit diameters of 20, 25 and 30m if possible and time permitting.

C.8.3 Transient

The following test will be carried out as close as possible in accordance with ISO 7401:2003.

Data to be logged	Sensor	Logging rate [Hz]
Vehicle Speed	CAN	100
Lateral Acceleration	CAN	100
Steering Wheel Angle	CAN	100
Yaw Velocity	CAN	100
Longitudinal Acceleration	CAN	100
Vehicle Roll Angle	External gyro (integration of roll velocity)	100

Table C-5 Transient test data requirements

Before any testing takes place, ensure that data logger and sensors are functioning correctly, carry out a brief test run and download data.

C.8.4 Step Steer

1. Carry out a preliminary run to asses steering angles and speeds needed to obtain correct lateral acceleration levels (2, 4, 6 m/s2), record steer angles and speed for later use (speed should be 100 Km/h although other multiples of 20 Km/h may be used).

2. Set out marker at either end of the straight section to indicate turn in point (one for left turn one for right) ensure there is enough room after marker to achieve steady state cornering.

3. Drive at previously determined set speed along straight section (constant throttle and steering position) when turn in point is reached apply pre determined steer angle as fast as possible (keeping throttle constant), hold steer angle until steady state is reached.

4. Repeat test in other direction.

5. Download and label data.

6. Repeat steps 3 - 5 for all targeted lateral accelerations.

7. Carry out all sets of tests 3 times to ensure repeatability of results.

C.8.5 Single Sinusoidal Input

1. Set up two markers on the straight section one to indicate turn in point for a left initial steer and one for a right initial steer.

2. Drive towards marker at 100 Km/h (other 20 Km/h increments can also be used), when test initiation point is reached carry out a sinusoidal steer input with 90 degrees amplitude at 0.5 Hz frequency (initial turn left)

3. Repeat step 2 with initial turn right.

4. Download data.

5. Repeat steps 2 – 4 at 1 Hz frequency.

6. Carry out all sets of tests 3 times to ensure repeatability of results.